Series in BioEngineering

Fan-Gang Tseng
Tuhin Subhra Santra *Editors*

Essentials of Single-Cell Analysis

Concepts, Applications and Future Prospects

Springer

Series in BioEngineering

More information about this series at http://www.springer.com/series/10358

Fan-Gang Tseng · Tuhin Subhra Santra
Editors

Essentials of Single-Cell Analysis

Concepts, Applications and Future Prospects

Springer

Editors
Fan-Gang Tseng
National Tsing Hua University
Hsinchu
Taiwan

Tuhin Subhra Santra
National Tsing Hua University
Hsinchu
Taiwan

ISSN 2196-8861 ISSN 2196-887X (electronic)
Series in BioEngineering
ISBN 978-3-662-49116-4 ISBN 978-3-662-49118-8 (eBook)
DOI 10.1007/978-3-662-49118-8

Library of Congress Control Number: 2015958544

Printed on acid-free paper

This Springer imprint is published by SpringerNature
The registered company is Springer-Verlag GmbH Berlin Heidelberg

Preface

Cells play a significant role in our daily lives. However the intercellular interactions, intracellular behaviors, and environmental responses of cellular organelles are still not fully understood and the ensemble-averaged measurement of millions of cells together is not able to provide detailed information at the single-cell level. For example, the genome, epigenome, and transcriptome analyses of bulk cell populations are informative, however, they cannot reveal the heterogeneity and molecular dynamics within a certain cell population. Also, these analyses cannot provide any information about an underrepresented cell subpopulation that could have a differential or crucial function in a specific biological context, such as stem cells or tumor-initiating cells. In contrast, single cell sequencing (SCS) is able to empirically infer the driver mutations and map the sequential mutation events during cancer development. The integration of genomics and transcriptomics in single cancer cells will also provide valuable information about the functional consequences of mutations and the copy number variations in these cells. In the past few years, significant advances have been made in isolation of single cells, whole-genome or whole-transcriptome amplification and genome-wide analysis platforms, which not only allow high resolution genome and transcriptome analysis, but also have the potential to reveal the epigenome map of the target single cells. Undoubtedly, these novel approaches will produce profound health benefits, such as a more efficient treatment strategy for patients affected by genetic disorders, which can be realized at the single-cell level.

Apart from the considerable power of single-cell analysis (SCA), the huge amounts of data generated from the SCA process have emerged as a challenging issue. In recent years, bioinformatics techniques have been employed to study the "big data" from large ensembles of single cell data. Thus interestingly, some unresolved questions in the past can be answered now thanks to the unique information obtained from single-cell analysis, such as whether any two single cells are really the same if we are able to measure adequate parameters with sufficient accuracy. Are there two cells which have similar biological functions and predictable outcomes when treated with the same drugs or environmental factors?

SCA, without doubt, is an efficient and valuable approach to understand the fundamental biology in embryonic development, to provide detailed knowledge of the cell lineage trees in higher organisms, to dissect the tumor heterogeneity and disease, etc.

To analyze the cellular function, SCA can be performed by combining capillary electrophoresis (CE) with laser-induced fluorescence (LIF) detection, electrochemical detection (ED), flow cytometry or mass spectrometry, etc. Recently, with the development of microelectromechanical systems (MEMS) technology and its integration with chemical engineering, biomedical engineering, chemistry, material science, and life science, Bio-MEMS (sometimes considered synonymous with lab-on-a-chip (LOC) or micro total analysis systems (μTAS)) has emerged as a powerful tool for more complex manipulations of chemical and biological agents in micro/nano fluidic environments. Micro/nanofluidic devices with the power to manipulate and detect bio-samples, reagents, or biomolecules at the micro/nanoscale can well fulfill the requirements of single-cell analysis. Thus, they are not only useful for cell manipulation, isolation, separation, and lysis, but are also able to easily control the biochemical, electrical, and mechanical parameters in SCA with precisely controlled dosage, spatial resolution, or temporal pace.

This book includes 15 chapters, covering a wide spectrum of the essential aspects of single-cell analysis. Contributed by experts in their own fields, these chapters provide technical tips based on valuable experience and knowledge. Potential problems and challenges as well as possible solutions are also discussed with an emphasis on the future prospects. "Single-Cell Behavioral Assays for Heterogeneity Studies" describes single cell behavioral assay for heterogeneity study using single cell isolation and tracking to investigate cell proliferation, differentiation, and lineage. There are two platforms being discussed that include the cell migration platform to measure cell motility, deformation, and invasiveness and the cell–cell interaction platform to study the alteration of cell behaviors caused by reciprocal interactions among cells. "Systems Biology in Single Cells" presents single-cell analysis in systems biology. It covers technologies that enable the isolation of individual cells in a form that accommodates systomics studies, the biological methods deployed on such isolated cells to generate system-level information, and the bioinformatics technique that is specifically directed toward single-cell studies. "Electroporation for Single-Cell Analysis" introduces advanced single cell electroporation techniques for cellular delivery and analysis, which might be potentially applicable to cell therapy, clinical diagnosis, drug screening, etc. "Microinjection for Single-Cell Analysis" is devoted to the single cell microinjection technique. The basic knowledge of this technique, its advantages and disadvantages, its development and applications, its basic instrumentation, and modifications are discussed thoroughly in this chapter. "Optical Tools for Single-Cell Manipulation and Analysis" demonstrates the optical tools for single-cell analysis ranging from optical trapping systems which provide a contact-free technique for manipulation of micron-scale objects, through to a selection of different optically-mediated cell membrane disruption methods available for lysis and/or delivery of material. "Optoelectrokinetic Manipulation for Cell Analysis" explores two newly developed optoelectrokinetic techniques termed rapid

electrokinetic patterning (REP) and optoelectronic tweezers (OETs). Both the fundamental knowledge and their applications in cell-related research are covered in this chapter. "Continuous Micro-/Nanofluidic Devices for Single-Cell Analysis" discusses continuous micro/nanofluidic devices for single-cell analysis in two parts. The first part presents state-of-the-art techniques developed to handle single cells, including counting, sorting, positioning, and culturing. The second part describes the manipulation techniques combined with other stimulating and sensing techniques for the observation and characterization of single cells. "Single-Cell Mechanical Properties: Label-Free Biomarkers for Cell Status Evaluation" emphasizes the microfluidic approaches including microfluidic constriction channels, microfluidic optical stretchers, and microfluidic hydrodynamic stretchers, which are being developed as next-generation, automated, and high-throughput techniques for characterization of the mechanical properties of single cells. "Cytometry of Single-Cells for Biology and Biomedicine" presents flow cytometry, scanning image cytometry, and microfluidic cytometry with fluorescent probes used for single-cell analysis in biology and biomedicine. It also discusses the advantages of combining different approaches in integrated instruments that could perform both flow cytometry and image analysis on single cells as well as examining the internal contents of each single cell. "Single-Cell Genomics and Epigenomics" discusses the role of single-cell analysis in genomics and epigenomics, where it describes the major technological developments achieved in single cell "omics," the technical challenges to overcome, the potential applications, as well as future developments and breakthroughs. "Single-Cell Metabolomics" focuses on the single cell metabolomics in systems biology, where the recent improvement of analytical tools to unravel single cell metabolomics and their specificity, the limitations and challenges alongside the future prospects are discussed. "Applications of Cell-Based Drug Delivery Systems: Use of Single Cell Assay" presents different types of cell-based drug delivery systems to facilitate treatments for infectious and noninfectious diseases. Potential and limitations of single cell assay in this type of drug delivery systems is reviewed along with the clinical aspects. "Applications of Single Cell Sequencing in Cancer" describes the methodologies of single cell sequencing, as well as its existing and potential applications in reconstructing the evolutionary history of cancer progression and in profiling cancer transcriptome. "Single-Cell Characterization of Microalgal Lipid Contents with Confocal Raman Microscopy" highlights the recent advances in confocal Raman microscopy and its application in single cell characterization of microalgal lipid contents, which demonstrates cell-to-cell variation in structural features of expressed lipids among the screened *C. reinhardtii* mutants. "Single Differentiated Neurons from Pluripotent Embryonic Stem Cells: Motor Protein Modeling and Neurodegenerative Disease" illustrates how cross-field techniques, including the use of P19 neurons, single-cell DNA delivery devices, microchannel platforms, and kymograph data analysis for physical modeling, can enable the characterization of fundamental properties of neurodegenerative disease mechanisms.

We hope this book can be enjoyable reading material and at the same time a useful resource for scientists in academia and professionals in industry working on different aspects of SCA.

Fan-Gang Tseng
Tuhin Subhra Santra

Contents

Single-Cell Behavioral Assays for Heterogeneity Studies

Yu-Chih Chen, Patrick Ingram, Yi Luan and Euisik Yoon

Abstract Cell heterogeneity is an emerging challenge in cell biology and cancer therapies. Each cell in heterogeneous populations has its own unique behavior, and thus responds differently to the same reagent or drug, making analysis or treatment difficult and complicated. Therefore, it is important to understand the heterogeneity characteristics of cells in phenotypic behavior assays. Although conventional fluorescence-activated cell sorting can separate cells based on markers, most assays simply present the average behavior in a batch of cells sorted by markers. It is important to have a capability to fully characterize individual cell behaviors in a miniaturized, high-throughput platform, distinguishing their heterogeneity and tracking their responses over time. This chapter introduces the technological innovations enabling these assays and the associated biological experiments, including (1) single-cell isolation and tracking schemes to investigate the cell proliferation, cell differentiation and lineage, (2) cell migration platforms to measure cell motility, deformation, and invasiveness, and (3) cell–cell interaction platforms to study the alteration of cell behaviors caused by reciprocal interactions among cells.

Keywords Single cell · Behavioral assay · Cellular heterogeneity · Hydrodynamic capture · Suspension culture · Cell isolation · Cell migration · Chemotaxis · Cell–cell interaction · High throughput

1 Introduction

The cell is a fundamental building block of our body. To probe the properties of this basic unit, there are two different methodologies: One is genotypic analysis, in which we typically analyze genomes, DNA methylations, and mRNA expressions using micro-arrays, RTq-PCR, or even next-generation sequencing (NGS); and the

Y.-C. Chen · P. Ingram · Y. Luan · E. Yoon (✉)
University of Michigan, Ann Arbor, USA
e-mail: esyoon@umich.edu

F.-G. Tseng and T.S. Santra (eds.), *Essentials of Single-Cell Analysis*,
Series in BioEngineering, DOI 10.1007/978-3-662-49118-8_1

other is phenotypic (behavioral) analysis, in which we study viability, migration, proliferation rates, cytokine secretions, and protein activities. One key advantage of genotypic analysis is that it can be done without any in vitro cell culture, which may alter the properties of primary samples. Since the genotypic analysis is basically to measure markers in molecular biology, the mechanism can be interpreted directly based on the measurements. Although the genotypic analysis has many merits, the expression of the same biomarker may be different for different diseases or even different patients. For example, let us illustrate the limitation of genotypic analyses in cancer cells. There is considerable evidence that supports the presence of cancer stem-like cells (CSCs), which are only a small subset of cells but retain the ability to initiate new tumors or metastasize [1–4]. However, due to the heterogeneity and plasticity of CSCs, (1) the markers for "stem-ness" are not consistent within subtypes of a specific cancer or across different types of cancer; (2) current markers enrich in CSCs but also include non-stem tumor cells; and (3) it is unclear whether these markers can identify the same or separate CSC populations [5–7]. Compared to the complicated marker-based analyses, the behavior-based phenotypic assays are relatively straightforward and are not limited by the availability of given markers. The malignancy of a cancer sample can be estimated using the results from drug screening and metastasis assays regardless of whether it has a given CSC marker or not, allowing for marker-free assays. In this chapter, we discuss phenotypic assays examining cell behaviors.

Conventionally, behavioral assays can be performed using either in vivo mouse models or dish-based assays. The mouse model can closely mimic physiological processes in vivo, but it has drawbacks of long assay time (can easily go up to weeks) and high cost. Although it can be a good tool for late stage validation, it is impractical to perform large-scale screening in the early stage of research. Compared to mouse in vivo experiments, dish-based assays have advantages of low cost and short turnaround time (typically a few days). Using automatic systems, high-throughput drug/stimulus screening can be easily performed. However, dish-based assays suffer from two issues: (1) The condition in a dish is quite different from the in vivo environment, so the result is less physiologically relevant. (2) Dish-based assays are designed for a large number of cells, so it is difficult and unreliable to perform single-cell assays. There is a fundamental trade-off between physiological relevance and throughput (Fig. 1). In vivo models are physiologically relevant but low throughput, while dish-based assays are high throughput but less physiologically accurate.

Microfluidic assays can provide a solution to this fundamental dilemma. Using miniaturized microfluidic devices, more experiments can be done using less cells and reagents than conventional dish-based assays. Meanwhile, better microenvironment control can be achieved in miniaturized microchambers, so that the microfluidic assays can be physiologically closer to in vivo conditions. In addition to higher throughput and better microenvironmental control, the use of microfluidics enables reliable single-cell assays, which are critical for understanding cell heterogeneity. In this chapter, we introduce various microfluidic devices developed for single-cell behavioral assays, providing four key advantages as illustrated in Fig. 2: (1) ability to

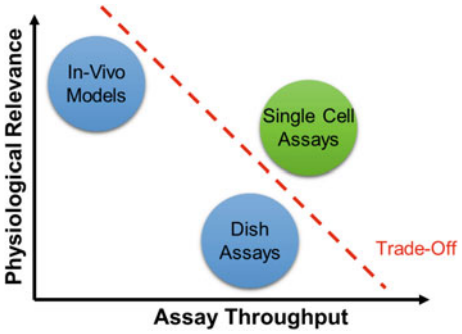

Fig. 1 Comparison between in-vivo models and dish-based assays in terms of physiological relevance and assay throughput. The single-cell microfluidic approach is expected to achieve better performance in both aspects than dish assays

Fig. 2 Four key advantages of microfluidic single cell platforms

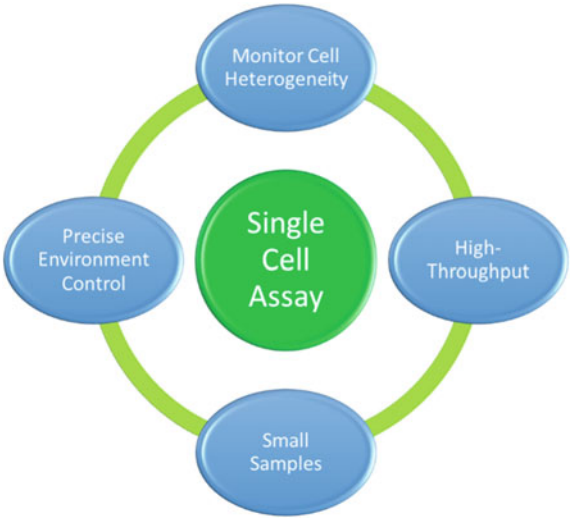

monitor and track individual cells, (2) control of various microenvironments on-chip for emulation of bioprocesses, (3) accommodation of high-throughput screening, and (4) capability of handling small amount of cells and reagents.

2 Single Cell Isolation and Tracking

2.1 Non-microfluidic Single Cell Experiments

To study cell behaviors, Petri dish culture has been used for more than 100 years. Cells can be cultured in this simple device, and various assays can be performed in a dish to test and verify hypotheses in cellular biology. Although this conventional

tool has advantages of simplicity and robustness, it is limited in its capability to study and analyze single cell heterogeneity. The dish-based method collects data from the average over a large number of cells with an underlying assumption that all cells are identical. However, new discoveries in biology support the existence of heterogeneity within a cell population, meaning that measuring the average behavior only reflects a part of the fact, while cellular heterogeneity may be more important to understand the holistic behavior of cells. Some early trials in single-cell assays still used Petri dish by applying serial dilution to achieve very low concentrations of cells to monitor single-cell behaviors [8]. As the cells are sparse in a dish, each cell can be considered isolated from one another and can be treated as noninteracting single cells. However, there are limitations, including the difficulty to monitor the same cells over time in a large dish, labor intensiveness, and low throughput. In addition, cells typically need autocrine (signal to itself) signaling to survive, so diluting cells in such a low concentration can lead to poor viability, especially for primary samples. To characterize the behavior of each individual cell reliably at high throughput, microfluidics can be an ideal platform to provide precise cell positioning and isolation. We review the recent engineering innovations and platforms to achieve single cell tracking in this section.

2.2 *Hydrodynamic Cell Capture Scheme*

In order to precisely position single cells, hydrodynamic capture has been widely used, utilizing differences in hydrodynamic resistance in microfluidic channels by optimizing the paths. This method can be implemented without using any external pumps, valves, or other complicated instruments [9–12]. As demonstrated in Fig. 3, the scheme utilizes the hydrodynamic resistance difference between the two paths: path A (or the central path) and path B (or the serpentine path) [10]. The

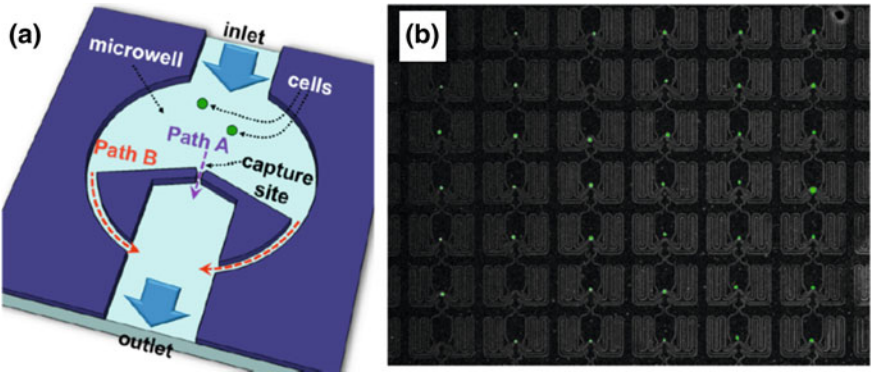

Fig. 3 Hydrodynamic cell capture scheme. **a** Schematic diagram of a unit microwell with hydrodynamic capture scheme. **b** Photograph of captured single green-fluorescent PC3 cells in microwell array. (Figure reprinted with permission from Ref. [10]. Copyright 2011, American Institute of Physics)

hydrodynamic resistance of circular and rectangular channels can be calculated as Eqs. (1) and (2), where μ is the viscosity, L is the channel length, r is the radius of the channel, w is the channel width, and h is the channel height. In the beginning, the central path has lower resistance, so the cells are likely to take this path and get captured. Once the central path is blocked by a captured cell, its flow resistance becomes much larger than the serpentine path. After that, the next coming cells flow to the serpentine path. As many microwells are connected in series, the cells flowing through serpentine path can be captured in the microwells in the downstream. A successful design should obey three guidelines. (1) The flow resistance of central path needs to be lower than the serpentine path by a factor of 2–10. (2) The central path is narrow enough to be blocked by a captured cell. Typically, the opening of the path is designed to be slightly smaller than the size of a target cell, so the cell can block the path as a plug. (3) The flow resistance in the serpentine path should not be too large. Otherwise, the slow flow rate may cause cell adhesion and clogging in the serpentine channel. The absolute flow resistance should be determined by the experimental conditions, including the properties of the cell, the surface treatment of the microfluidic device, and the flow rate.

$$R = \frac{8\,\mu L}{\pi r^4} \tag{1}$$

$$R = \frac{12\,\mu L}{wh^3\left(1 - 0.63{}^{h}/_{w}\right)}, \text{ when } w > h \tag{2}$$

From simple modeling and flow dynamic simulations, the capture efficiency of a given design can be estimated [10]. For one microwell, the cell that flows through path A is captured, while the cell that flows through path B is lost. Given that the cells are uniformly dispersed in the solution, the capture efficiency can be predicted by the flow rate ratio between the two paths. Since the flow rate is inversely proportional to the flow resistance, the flow rate ratio between paths A and B can be calculated based on the geometries of two paths as shown in Eq. 3. Q is the volumetric flow rate, R is the flow resistance, and a and b represent the paths A and B. The capture efficiency is calculated based on the flow rate ratio (Eq. 4). Various designs were tested based on this equation, and the experiment results match well with the estimation by calculation and COMSOL simulation [10]. Following the guidelines and the capture efficiency equation, the hydrodynamic capture schemes can be designed and optimized easily.

$$\frac{Q_b}{Q_a} = \left(\frac{R_a}{R_b}\right) \tag{3}$$

$$\text{Capture Efficiency} = \frac{Q_a}{Q_a + Q_b} = \left(\frac{1}{1 + \frac{Q_b}{Q_a}}\right) \tag{4}$$

2.3 Cell Isolation and Confinement of Cell Movement

After capturing single cells, cells may need to be confined or isolated for various reasons. Isolation is typically introduced for controlling the culture condition inside the microwell. For example, two cells can be co-cultured in a microwell by valve operation. The microwell is isolated to (1) preserve the secreted signaling proteins inside the microwell for interaction and (2) avoid the contamination of the signals from the cells upstream. The techniques for cell isolation and confinement are introduced in this section. One of the most prevailing isolation methods is using pneumatic valves. As shown in Fig. 4a, when the valve is pushed down, the cell inside the microwell is isolated [13]. The sealing quality can be tested using food dye. Although valves are widely used in microfluidics, they have two limitations. (1) The pneumatic valves are sensitive to channel geometry [14, 15]. Channel height and width and shape need to be carefully designed to guarantee complete sealing. (2) The valve needs to be continually connected to the pump (or constant pressure source) during the entire isolation process; otherwise, the pressure, and thus the cell isolation, will be released. Due to these limitations, alternative isolation schemes were reported. One of the trials was to block the microfluidic channel using bubbles generated by electrolysis [16]. As shown in Fig. 4b, bubbles can be generated to isolate the cell culture chambers, and the generated bubble can be easily removed by diffusion through air-permeable PDMS. The electrolytic bubble isolation has fewer design constraints compared to pneumatic valves, and its actuation circuit can be implemented compactly using commercial ICs. Another approach is to isolate the chamber using two phases between oil and water [17]. The oil can be pumped into the parallel channels (Fig. 4c). As oil and water are immiscible, the culture microenvironments can be isolated.

There are applications that may not need complete isolation of microwells, for which simple migration-blocking patterns can be used to restrict the cell inside a confined area. Adherent cells can migrate away from the initial captured position. The movement makes it difficult to track individual cells. More importantly, the cell migration from one microwell to another can introduce interference between neighboring cells and skew the experimental results. The confinement can be obtained using either physical barriers (walls/trenches) or selective chemical coating [18–22]. Figure 4d shows an example of using 5 μm height SU-8 wall as the barrier. To enhance the restriction capability, pluronic copolymer (F-108) as an anti-fouling material was coated on the SU-8 in order to repel cells and other proteins critical for cell adherence [23–25]. The coating can successfully restrict the cell migration, even after long-term culture [26].

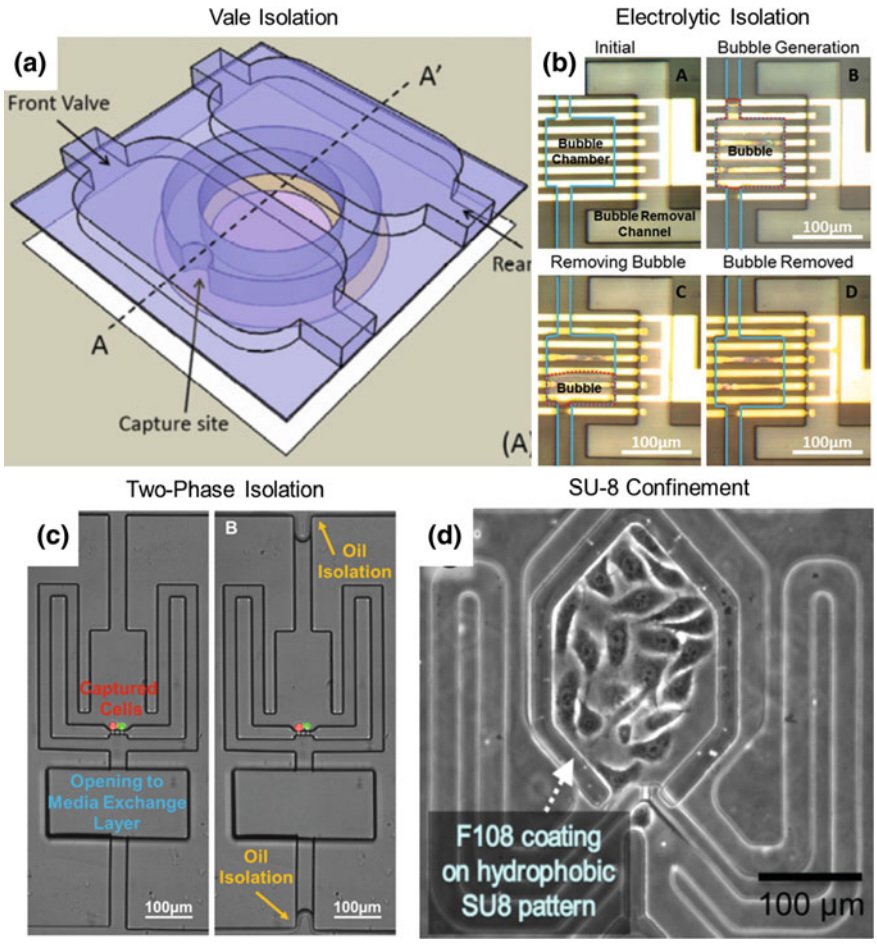

Fig. 4 Designs for cell isolation and movement confinement. **a** Schematic diagram of cell capturing and isolation operation in the array chip (Figure reproduced from Ref. [13]). **b** Electrolytic bubble generation and removal for cell isolation (Figure reproduced from Ref. [16]). **c** Two-phase isolation of cell culture chamber (Figure reproduced from Ref. [17]). d. SU-8 wall for cell movement confinement (Figure reprinted with permission from Ref. [26]. Copyright 2014, American Institute of Physics)

2.4 Surface Treatment for Suspension Culture

There are two basic approaches in cell culture; adherent cell culture (cell adheres on the substrate) and suspension cell culture (cell floats in the culture media). Typically, the bacteria and yeast are cultured in suspension, and the mammalian cells are cultured on the adherent substrate. For most mammalian cells, adhesion to the ECM is essential in maintaining homeostasis. Loss of anchorage leads to

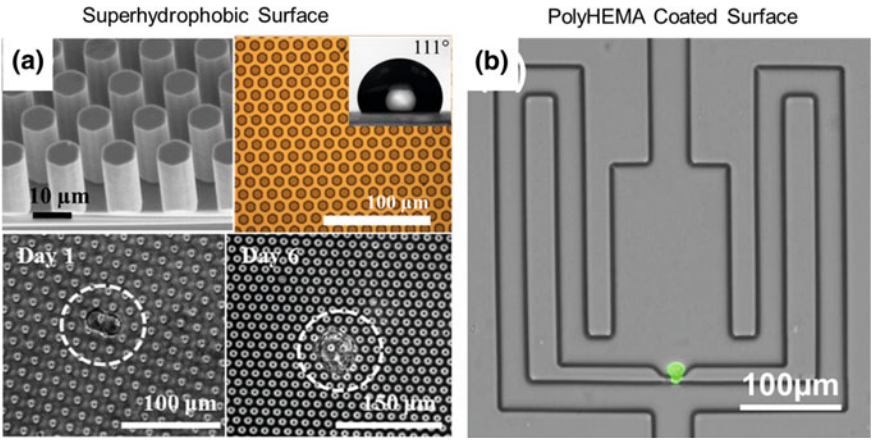

Fig. 5 Surface modifications for suspension cell culture. **a** Superhydrophobic surface by novel topological pattern (Figure reproduced from Ref. [32]). **b** PolyHEMA coated surface incorporated in a hydrodynamic cell capture platform(Figure reproduced from Ref. [37])

anoikis, a kind of programmed cell death [27]. However, suspension culture provides two major advantages over adherent culture. First, suspension-cultured primary cells better preserve its original attributes, while the adherent-cultured ones can easily change its characteristics expressed in vivo. In addition, the survival and growth of a single cell in suspension culture can indicate the stemness of a cell [28–30]. Due to the importance of single-cell suspension culture, researchers previously tried to load one tumor cell per non-adherent plate using serial dilution. As described in 2.1, this approach is labor-intensive and unreliable. The situation is even worse for suspension culture, because the cell can be easily lost when changing media. The hanging droplet method was introduced to mitigate this problem; however, it has the same problem of unreliable serial dilution for single-cell assay [31]. Here, we introduced two surface modification methods facilitating single cell suspension culture: patterned superhydrophobic surface and polyHEMA coating.

Figure 5a illustrates the topographically patterned superhydrophobic surfaces for suspension cell culture [32]. Superhydrophobic surfaces have been used for anti-biofouling applications in the past [33–35], because its surface prevents cells from adhering. The same characteristics can also be used for non-adherent mammalian cell culture. The hydrophobicity can be created by minimizing the surface area in contact with the media. As the cells interact with the surface via focal adhesion, the minimized contact area can significantly reduce the formation of focal adhesions. Using the high aspect ratio deep reactive-ion etching (DRIE) on silicon wafers, the novel topology with superhydrophobicity can be fabricated. Among different patterns, the honeycomb structures can avoid the Cassie-Baxter to Wenzel state transitions [36], so the cell can be suspension-cultured on this patterned surface for days. The patterned surface can also be incorporated with the hydrodynamic capture scheme for single-cell assay. Although the superhydrophobic surface

successfully facilitates long-term suspension culture, it has several disadvantages, including the expensive DRIE process and the interference of patterns with optical microscopy. An alternative to this topographical approach is coating poly (2-hydroxyethyl methacrylate) (polyHEMA) on the surface. PolyHEMA can absorb water to become a hydrogel, and it has many hanging, long chains, so cells cannot easily attach to its surface. PolyHEMA has been used for suspension culture by the biology community for more than 30 years and has proved to be biocompatible. Conventional coating technology is to simply place PolyHEMA ethanol solution on a Petri dish and evaporate ethanol. However, this primitive process creates a thick and rough surface, so the coated polyHEMA can cause leakage and/or may block the channel when incorporated in microfluidic devices. To overcome these issues, spin coating and reflow process was used, and the surface proved to be non-adherent for cell culture and provided good imaging quality [37]. The suspension single cell culture has been demonstrated on polyHEMA surface for 28 days (Fig. 5b).

2.5 Monitoring Single Cell Behavior and Drug Response

After positioning and confining single cells, various assays can be done at single-cell level. Here, we introduce two cell behavior assays and two drug screening studies. Figure 6a demonstrates single cell tumor sphere assays [37]. As mentioned in the previous section, adhesion to ECM is critical for survival of normal mammalian cells. However, cancer stem-like cells can survive and grow in suspension environments. Using polyHEMA coating to a hydrodynamic cell-capture microfluidic platform, development from a single cell to a tumor sphere can be observed in suspension culture. Figure 6b illustrates single cell protease activity assays [38]. Protease activity is important in modulating microenvironments and thus affecting the pathogenesis of cancer, inflammatory, and vascular diseases. To probe single-cell protease activity, cells were trapped and isolated in the microwells. The FRET-based sensing substrate, which becomes brighter when being cleaved by protease, was used to measure protease activity. As the volume trapped with a cell is small, high sensitivity can be achieved. Using this platform, hundreds of single-cell activities can be simultaneously measured [38]. The results clearly demonstrate the heterogeneity of single cells within a population.

Drug screening is one of the most widely used bioassays, and it can be performed at single-cell level to understand heterogeneity among cells. Figure 6c illustrates a microfluidic platform designed for probing the drug response of single *Escherichia coli* to investigate the difference between drug-sensitive and drug-resistant strains [39]. Single *E. coli* was loaded into the microwell, and four different drug concentrations can be tested in one experiment. The proliferation and phenotype changes of *E. coli* in each microwell can be recorded for analysis. The drug response of cancer cells has been investigated at single-cell level [26]. The platform positions cells using hydrodynamic capture and confines its migration by SU-8 wall. PC3 (prostate cancer) cells are classified into three different clonal phenotypes: namely holo-,

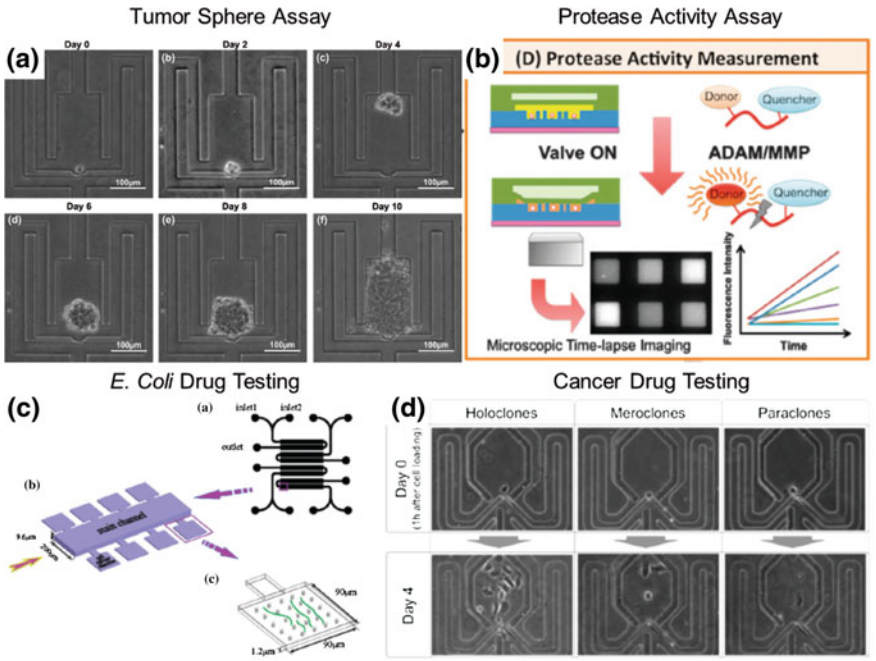

Fig. 6 The platforms for monitoring single cell behaviors and drug response: **a** Single cell tumor sphere assay (Figure reproduced from Ref. [37]), **b** single cell protease activity assay (Figure reproduced from Ref. [38] with permission from The Royal Society of Chemistry), **c** drug testing for *E. coli* (Figure reproduced from Ref. [39] with permission from The Royal Society of Chemistry), and **d** drug testing for cancer cells (Figure reprinted with permission from Ref. [26]. Copyright 2014, American Institute of Physics)

mero-, and paraclones, and the cell morphology can be easily identified using conventional optical microscopy (Fig. 6d). Different proliferation rates and drug responses were measured among different phenotypes. Paraclone, which is quiescent, is most drug resistant, matching well with the hypothesis that quiescent phenotype cells are more drug resistant. This experiment correlates different behaviors (or drug responsiveness) of various cell phenotypes from clonal culture from single cells, demonstrating unique values of single cell drug assay.

2.6 *Cell Lineage Studies*

In addition to tracking single cells, microfluidic tools can also allow for following the lineage of cells. 150 years ago, lineage of pea plants was first studied to understand the heredity of organisms. In the past, only changes in DNA were considered inheritable; yet recently, evidence shows that genetically identical cells can express distinct behaviors. The changes regulated by epigenetics are crucial for numerous biological questions, including development of embryonic cells and pathology of cancer. As in

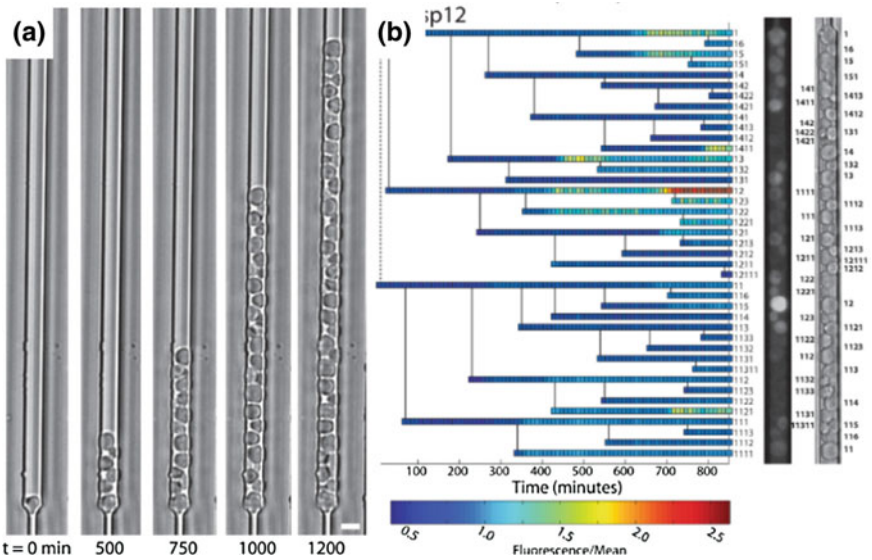

Fig. 7 Lineage tracking of yeasts by limiting their proliferated cells in a line. **a** The images of isolated yeasts in the microfluidic channel at different time points and **b** the measurement of individual yeast fluorescent intensity for lineage tracking. (Figure reproduced from Ref. [40])

the lineage study of peas, investigating the pedigree of single cells requires long-term monitoring and collecting data from many generations. Without reliable cell positioning and confinement, it is difficult to track the development of a clone, especially for non-adherent bacteria and yeasts. One example of previous studies is illustrated in Fig. 7. Single parental bacteria were first seeded in a narrow channel using hydrodynamic capture scheme [40]. The captured cells are geometrically constrained, so the divided cells form a line without changing the order. As the order of cells implies the family tree of a clone, the pedigree of cells can be recorded. The regulation of one specific protein can be monitored using the reporter, which reflects the expression of target protein by fluorescent intensity. Using this method, different regulation patterns of several genes were observed. Though this approach only applies to non-adherent bacteria and yeasts rather than adherent mammalian cells, the same concept can be applied to other studies.

3 Single Cell Migration Assays

3.1 Non-microfluidic Migration Assays

Cell migration is a critical physiological process in angiogenesis, cancer metastasis, wound healing, inflammation, and embryogenesis. Although it is critical in maintaining the operation of a human body, cancer cells also utilize migration capability

to metastasize. Researchers have noticed cell migration in various regions of a body since the late nineteenth century. Dr. Arnold was the first to report that monocyte migrates into the damaged tissue in 1873 [41]. As it is difficult to monitor cell migration in vivo, in vitro methods were introduced to study cell migration before the development of microfluidics. Two widely used non-microfluidic approaches are Boyden chamber assays and wound healing assays [42, 43]. In Boyden chamber assays, cells are loaded on top of a porous membrane. Some cells can invade through the membrane to the other side. At the endpoint of the assays, the number of penetrated cells can be quantified as the migration capability of the sample. For wound healing assays, cells are removed from a small section to create a blank (no cell) region surrounded by a cell monolayer. Within 1–2 days, cells gradually migrate to cover the blank region as healing the wound. The area of uncovered blank region is measured. The smaller the blank region is, the more motile the cells are. These assays have been widely used for decades and are still prevailing now; however, there are limitations and challenges. One of the biggest issues in wound healing assays is the irreproducibility of removing (scratching) cells on a cell monolayer. Also, chemoattraction cannot be studied using this method. On the other hand, Boyden chamber assays can allow for studying the average migration capability, but cannot track the migration process. It only reports the endpoint results. More importantly, it is infeasible to track single cells in these assays, while cellular heterogeneity is one of the most important challenges in oncology. In this section, we introduce various microfluidic-based migration platforms for tracking single-cell migration.

3.2 Positioning of Single Cells

Compared to dish-based assays, one of the advantages of microfluidic approaches is the capability to precisely control the microenvironments, including the initial position of cells, the geometry of migration channels, the extracellular matrix (ECM) concentration and composition, and the gradients of chemicals or other stimuli. Here, we start with the positioning of cells. There are three strategies for patterning cells: laminar flows, geometric restrictions, and hydrodynamic captures. The Reynolds number in microfluidic channels is typically lower than 10, so media loading operates in a laminar flow regime, meaning that the fluid flows without significant lateral mixing [44]. Using this property, cells can be selectively patterned inside a microfluidic channel. As shown in Fig. 8a [45], cells were first loaded into the channel and grew to a monolayer. The laminar flow of Trypsin-EDTA in the central and right channels can precisely trypsinize the cells on those regions. Then, the cell migration toward the right (blank substrate) can be monitored. The second strategy is to pattern cells using the geometric restriction of ECM gel or narrow migration channels. The collagen scaffold was cured before cell loading, so the cells would stay in the channel initially [46]. Then, the cells can migrate into the collagen scaffold. Another example (Fig. 8b) is to restrict cell

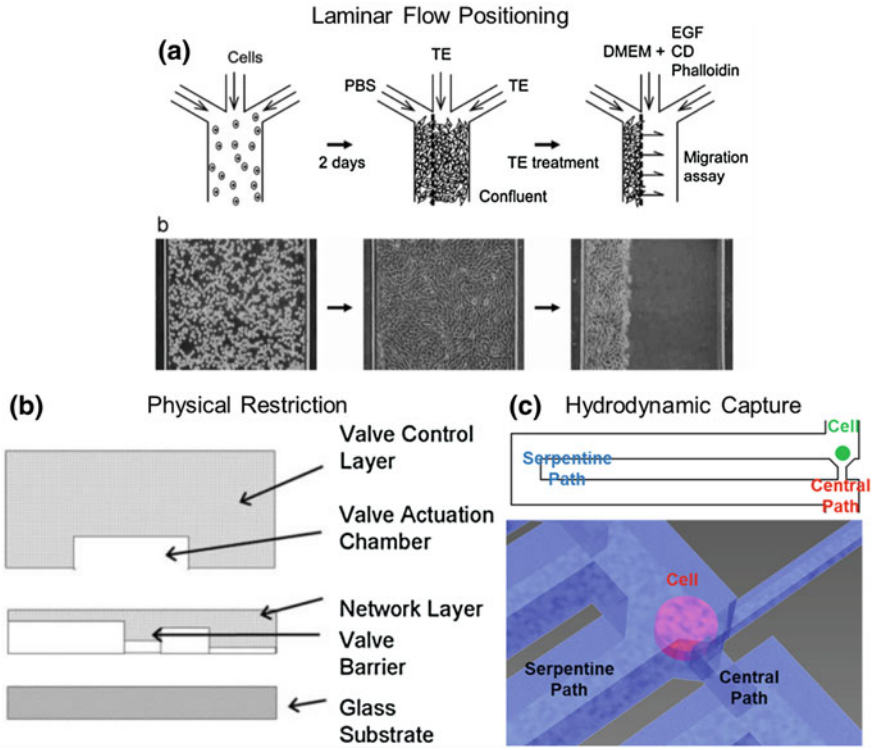

Fig. 8 Cell positioning schemes for migration studies: **a** Position of cells using a laminar flow (Reprinted from Ref. [45], Copyright 2007, with permission from Elsevier), **b** position of cells by physical barrier (Figure reproduced from Ref. [47] with permission from The Royal Society of Chemistry), and **c** hydrodynamic capture scheme (Figure reproduced from Ref. [48])

positions by a thinner channel (3 or 10 μm). Since mammalian cells are typically around 10–20 μm in diameter, the cells will be blocked and stay in the cell loading channel [47]. Once adhered, the cells become thinner, so they can migrate through the barrier. The last approach is hydrodynamic capture. As described in Sect. 2.2, single cells can be positioned using hydrodynamic capture. To incorporate the capture site right next to the entrance of the migration channels, two flow paths are implemented as Fig. 8c [48]. The long serpentine path has a higher flow resistance initially, so the cells tend to follow through the central path. Once a cell is captured at the central path, it blocks the flow as a cellular valve. Then, the next coming cell will flow through the serpentine path and get captured in the downstream. For single-cell studies, the hydrodynamic capture scheme can give a better control of initial cell position, and it is easier to track the movement of the isolated single cells. However, the hydrodynamic scheme needs more engineering optimization for a given cell type, and may not be ideal for the studies on collective cell migration.

3.3 Generation of Gradients of Chemo and Other Signals

After positioning cells, the next question to ask is how to apply stimuli to induce cell response. Of all, chemicals are the most widely used regulating signals for cells. The response to chemicals is critical for getting nutrients such as glucose and the regulation of cells such as cytokines. Chemotaxis refers to the movement of cells when exposing to certain chemicals. Cells can either be attracted or repelled by the chemical. Given the importance of chemotaxis, conventional wound healing assay is unable to be chemogradient, while it is relatively easy for microfluidics. Due to the nature of laminar flows in most operational regimes of microfluidic devices, chemical transportation is dominated by diffusion rather than convection or turbulence. Using this property, a stable chemogradient can be easily generated in a microfluidic channel or chamber. Figure 9a illustrates the generation of chemical gradients in a cell migration channel [48]. Culture media with chemoattractant flows on the right side and the media without chemoattractant flows on the left side, which will determine the fixed concentration at the ends of migration channels. According to Fick's Law of diffusion, diffusive flux is proportional to the concentration gradient (spatial derivative of concentration). In the steady state, each portion of the channel should have the same influx and outflux of chemoattractants, so the spatial derivative of chemical concentration should be the same throughout the whole migration channel. This results in a stable linear concentration along the migration channel. The generated chemical profile was confirmed by simulations and experiments [48]. The same principle can be used for generating concentration gradients in a microfluidic chamber (Fig. 9b) [49]. The solutions with ($C=C_0$) and without ($C=0$) chemicals continuously flow in the right (source) and left (sink) channels, respectively. In the steady state, the influx of the chemical generates a gradient inside the reservoir for either 2D or 3D migration assays. Moreover, nonlinear gradients can be generated by changing the geometry of the cell culture chamber and the openings (Fig. 9c) [50].

Though chemotaxis is one of the mostly studied phenomena in cell migration, gradients also play an important role in cell regulation. The stiffness of the substrate is known to regulate cell adhesion and movement. As the substrate thickness can correlate with the concentration of ECM or hydrogel, the stiffness gradient can be created from the concentration gradient of ECM as described in the previous work [51]. The other way to regulate the substrate stiffness is to make PDMS microposts on the substrates. If the microposts are taller and thinner, they have smaller spring constant and are considered softer. Different micropost geometries can be made to generate a stiffness gradient (Fig. 9d) [52]. Electrotaxis is more important in neuronal cells in guidance and wound healing. The E-field (either AC or DC) can be applied by placing electrode nearby cell migration chambers/channels for electrotaxis [53, 54].

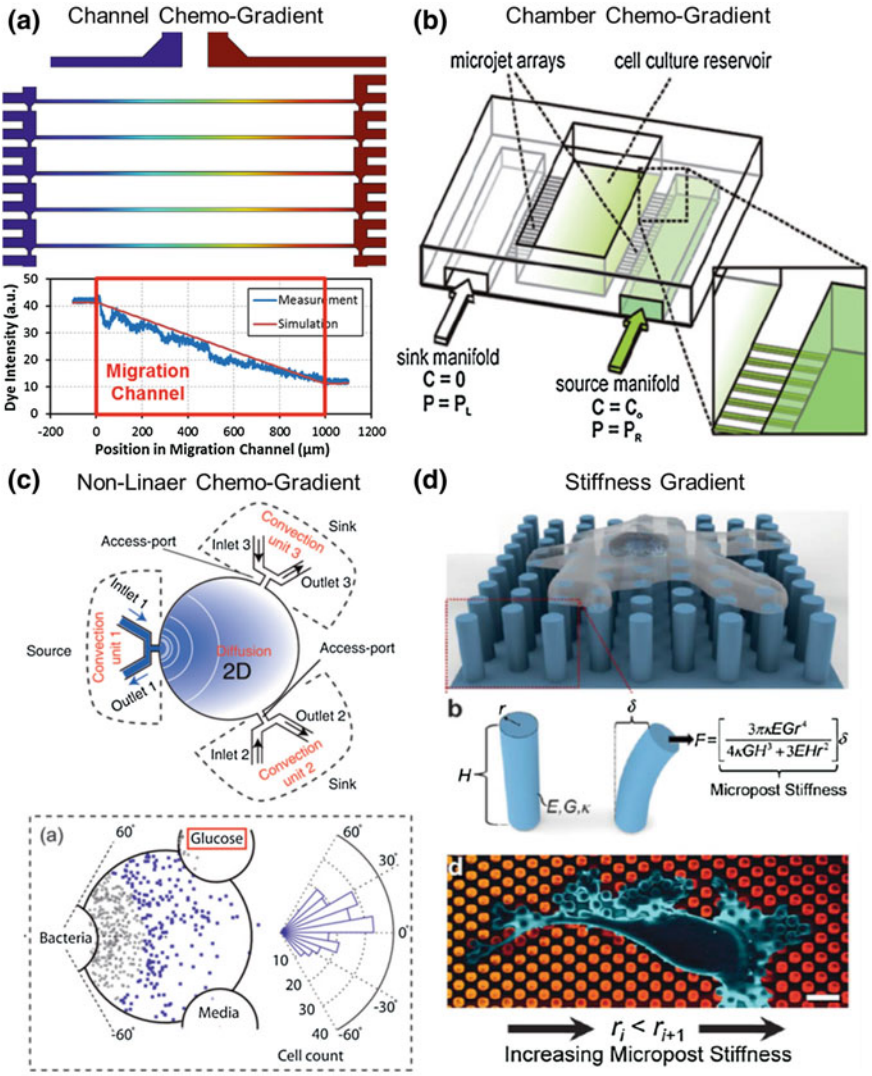

Fig. 9 The gradients generation for testing cell responses: **a** Chemogradient generated in a migration channel (Figure reproduced from Ref. [48]), **b** chemogradient generated in a microfluidic chamber (Figure reproduced from Ref. [49] with permission from The Royal Society of Chemistry), **c** nonlinear chemogradient generated in a microfluidic chamber (Figure reproduced from Ref. [50] with permission from The Royal Society of Chemistry), and **d** Stiffness gradient generated on a substrate (Figure reproduced from Ref. [52] with permission from The Royal Society of Chemistry)

3.4 1D Migration Assays in Narrow Channels

1D migration assays give a simple but useful model for studying cell migration by monitoring linear migration of cells a migratory channel. In addition to motility, deformation capability of cells can also be screened, which is important in cancer invasion. The process of Epithelial–Mesenchymal Transition (EMT), which is known to contribute to cancer metastasis, will not only make cancer cells motile, but also deformable. Using microfabrication, the migration channels can be varied (5–20 μm) to comparable size cells and the cell movement under geometric confinement can be studied. As it is difficult to monitor (or image) the cancer extravasation into blood vessels or lymphatic capillaries in vivo, in vitro micro-channel experiments provide a good alternative for observing cancer invasion process. Generally, the narrower the channel becomes, the more difficult the cancer cells can path through [55]. However, the cell deformability can be skewed (enhanced or suppressed) by drug, by regulating the cytoskeleton or the stiffness of cells and/or nuclei. In addition to external stimuli, the internal regulation of cells such as EMT and Rho proteins can also affect cell the motility in a narrow channel [56]. Although the motility of rhoC-low cells is comparable to that of wild-type cells, its capability of penetrating narrow channel is significantly degraded [48]. Thus, this regulation can be a potential drug target. The efficacy of metastasis-inhibiting drugs can be easily screened using 1D cell migration platforms.

Depending on applications, many different migration channel designs have been reported. Most channel designs are purely based on engineering optimization. The geometry is optimized to best distinguish the motility of cells of interest, but the size is not related to any specific geometries in in vivo models. Some designs specifically emulated the geometry of certain tissue for studying cell migration in that tissue (e.g., mimicking a lymphatic capillary for studying invasion of cancer cells) [48]. Other works created novel geometries to answer specific questions. As an example, Fig. 10a illustrates a novel tree-like structure consisting of two channels with different geometries, allowing for studying preference of cells when choosing their migration path [57]. The goal is to study the decision making of migrating cells, when experiencing different channel geometries and orientations. Another interesting example is the diode channel design (Fig. 10b) [58]. Cells in the channel prefer to move forward rather than backward like a diode (electrical component), showing asymmetrical behavior. Although 1D migration channels are different from in vivo conditions, it is still a useful tool for studying cell migration as well as cell deformation.

3.5 2D Migration Assays on Plane Substrate

2D migration assays monitor the movement of adherent cells on a plane substrate. Compared to simplified 1D migration assays, 2D planar migration assays provide

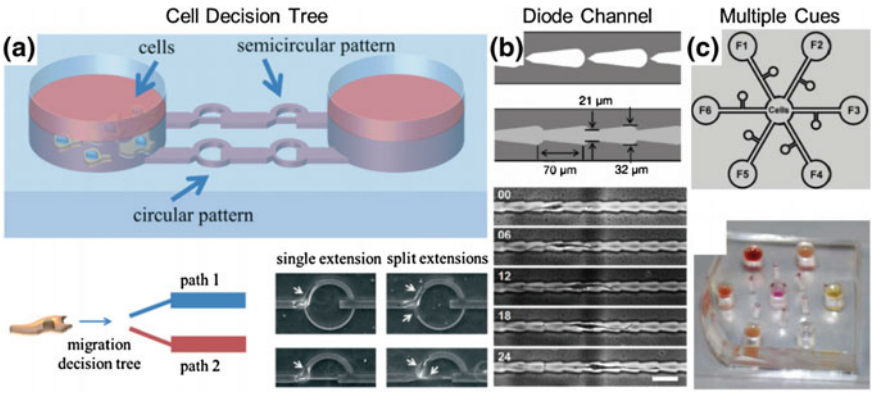

Fig. 10 **a** Schematic of cell decision tree (Figure reproduced from Ref. [57] with permission from The Royal Society of Chemistry), **b** schematic of a diode channel and asymmetric cell migration (Figure reproduced from Ref. [58] with permission from The Royal Society of Chemistry), and **c** 2D cell migration platform comparing the chemoattraction of 6 different signals (Figure reproduced from Ref. [59] with permission from The Royal Society of Chemistry)

one more degree of freedom for cell movement. As there are no geometric limitations (such as narrow migration channels), the results only reflect the chemotaxis without complicating with cell deformability. While 1D platforms can only screen one chemoattractant/stimulus at a time, 2D designs grant the capability of testing two or more stimuli simultaneously. With the additional degree of freedom, the 2D platforms can examine: (1) the competition of two different signals and, more interestingly, (2) the synergistic and antagonistic effect between two signals in one experiment. The capability to use multiple stimuli is critical for studying complicated in vivo environments, since many different cytokines typically coexist inside an actual tissue. Figure 10c shows the design of a 2D migration platform, which can compare the chemo-attraction of mesenchymal stem/stromal cells (MSCs) using 6 different cytokines in an assay [59]. Though the 2D migration platforms provide the advantage of giving one more degree of freedom, tracking an individual cell on a 2D plane is complicated. Environment chambers and time-lapse imaging systems are typically used to track the movement of each cell. The automatic analysis is also necessary to handle large quantity of time lapsed data.

3.6 3D Migration Assays

There are two types of 3D cell migration environments: migration in media or migration in ECM. Due to the different natures of physiological processes between the two, studies of bacteria and sperm chemotaxis typically observe migration in the

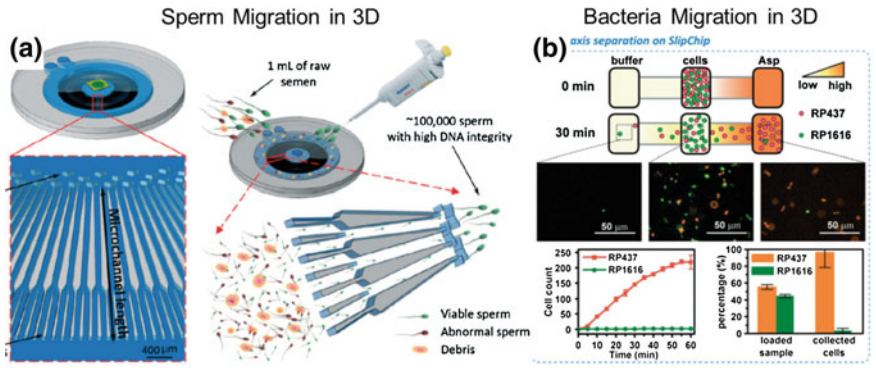

Fig. 11 3D migration platforms in media: **a** Separation of sperms (Figure reproduced from Ref. [61] with permission from The Royal Society of Chemistry); **b** Separation of bacteria (Figure reproduced from Ref. [63] with permission from The Royal Society of Chemistry)

media, while studies of cancer and stem cell migration typically use an ECM-based system [60]. The separation of sperms is one of the critical steps in assisted reproductive technologies. Since sperms are known to be heterogeneous, the healthy and motile ones are preferred for in vitro fertilization. Compared to conventional centrifugation-based sperm separation, which suffers from contamination of nonmotile and damaged sperms, microfluidics can emulate more natural selection processes [61]. As shown in Fig. 11a, sperms are injected into an outer ring of the device. After 15 min, some sperms can swim to the outlet (inner circle) for harvesting. The selected sperms were found to have better DNA integrity. The chemotaxis of bacteria is important for understanding the pathogenesis of bacterial infection and food corruption. Recently, microorganisms can be engineered to degrade some pollutants [62]. Enriching the ones that move toward pollution sources can increase the efficacy. As shown in Fig. 11b, two subpopulations of *E. coli* can be separated by their different responses to a chemogradient, demonstrating the feasibility of separating bacteria based on chemotaxis [63].

ECM-based 3D migration platforms are attractive because they can better mimic the microenvironment in vivo. Although 1D and 2D migration platforms can be used to study cell deformation and chemotaxis, their cell movement on glass/PDMS is artificial. Compared to glass (Young's modulus: 50–90 GPa, depending on impurities) or PDMS (Young's modulus: 500 MPa), ECM (Young's modulus: 50–5000 Pa, depending on tissues) is much softer by orders of magnitudes [64]. The environmental stiffness is especially important for cancer. Tissue stiffening is one of the important characteristics of tumor, and the rigid tissue is favorable for tumorigenesis. Using different hydrogel curing time, the stiffness gradient can be generated inside the microfluidic environment, and chemogradient can also be generated in the orthogonal direction [65]. Thus, the synergistic effect between mechanical and chemical cues can be investigated. In addition to stiffness, ECM itself provides biophysical signals for cells. Using cell–ECM adhesion, receptors can recognize different kinds of ECMs, and the cytoskeleton is regulated based on

that. To model cancer metastases in different tissues, the ECM concentration and composition of certain tissues can be used in 3D migration platforms [66]. Another capability of the ECM-based platforms is to study the ECM proteolysis mediated by metalloproteinases (MMPs). Since ECM is a barrier for cells to invade, degradation of ECM is critical for cancer invasion. The secretion and inhibitor of these MMPs can also be studied in the migration platforms [67, 68]. In stem cell-related studies, the mechanical and chemical environments for culturing stem cells need to be precisely controlled; otherwise the stem cells may differentiate to undesired cell types [69, 70]. The 3D ECM provides a more ideal environment than the 2D models, but tracking single cells is even more challenging in 3D. As the cells may not be on the same focal plane, automatic 3-axis imaging systems or con-focal microscopes are needed to monitor the position of single cells.

3.7 Motility-Based Cell Separation

So far, we have introduced many different migration platforms; however, most platforms are endpoint assays, meaning that after monitoring migration behavior on-chip, the cells are disposed with the device. Although single-cell heterogeneity can be reported, no more downstream analysis can be done between motile and nonmotile cells. The downstream analysis is critical for understanding the different regulations between cells with different motilities. The treatment targeting some critical regulation pathways can be developed based on this information. Recently, it was reported that highly motile cells are more EMT-like compared to nonmotile cells, indicating that as in many other aspects, the motility of cells is heterogeneous even in a given cell line [71]. Another work demonstrated the enrichment of highly motile subpopulation of cells using a microfluidic platform [48]. The harvested highly motile cells express EMT-like phenotype under scanning electron microscope (SEM) and preserve the elevated motility for a few days. More interestingly, different gene expressions in RhoC and its regulating pathway were found between highly motile and nonmotile cells. These works have demonstrated the feasibility of motility-based mammalian cell separation. More downstream analysis on the motile and nonmotile phenotypes can decipher the mystery of migration regulation.

4 Cell–Cell Interaction

4.1 Conventional Non-microfluidic Cell–Cell Interaction Studies

Although isolated single-cell assays allows for monitoring and tracking heterogeneity even in the same cell lines or phenotypes, each individual cells in vivo

interacts with many other cells around either by juxtacrine (contact-based interaction) or paracrine (secretion based interaction) signaling, or both. Using these signaling pathways, cells can concert their behaviors for healthy operation of body. Many diseases, including cancer, can result from the malfunction of certain communication mechanisms. In the early studies of cell–cell interactions, conditioned media was used to model interaction signals. For example, to study the effect of macrophages on cancer cells, we can add the cultured media from the dish of macrophage (macrophage-conditioned media) to the dish culturing cancer cells. Assuming the macrophages secrete the signaling proteins in the media, these signaling proteins can affect cancer cells. This assay can also be performed using the transwell. Using a porous membrane separating two cell types in culture, they can interact with each other through secreted proteins without physical contact. These approaches only consider paracrine-based signaling.

For studying the juxtacrine signaling, two cells have been simply mixed together in a dish for interaction. After the assay, two cell types can be sorted using the known markers for further analysis. However, this simple, conventional approach suffers from nonuniform spatial distribution of two cell types. In certain regions, one cell may be surrounded by a large number of the other type, while others may aggregate with the same type of cells in another region, meaning that it is difficult to precisely control the cell microenvironment in the dish. More importantly, these approaches typically use millions of cells for an assay, and lack the capability to track single cells for studying cell heterogeneity. In this section, we review the recent microfluidic platforms developed for cell–cell interaction studies.

4.2 Cell Pairing Schemes

Cells can be positioned using the similar techniques discussed in the previous section. However, the key difference between strategies for cell pairing is whether to load cells sequentially or simultaneously. Here, we introduce both types of schemes. Figure 12a illustrates the design of deformability-based microfluidic cell pairing schemes [72]. First, one type of cell population (green cells)is captured at the single-cell sites using hydrodynamic capture. Then, pressure is applied to deform the captured cells, so they are transferred into the larger traps. Using the same protocol, the second cell population (red cells) is transferred inside the larger traps with the first cell type. Figure 12b shows another approach for cell pairing by combining pneumatic valving and hydrodynamic capture. Initially, all the valves are in a neutral position (half open), and the first group of cells (red cells) are introduced and captured at the capture site at single cell resolution [13, 73]. Then, the captured cells are loaded into each microwell by lifting up the front valve. After that, the front valve returns to the neutral position for capturing the second cell group (green cells). The same sequential procedure (cell capture and loading) is repeated. After pairing the cells in each microwell, two valves (front and back) are closed to induce cell–cell interaction. For media refreshment, both valves are open

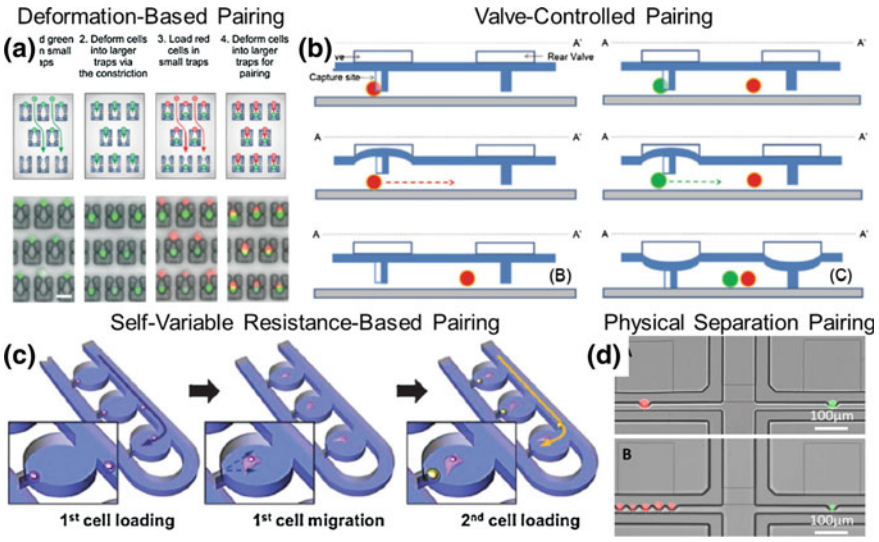

Fig. 12 Cell-pairing platforms: **a** Deformation-based cell pairing (Figure reproduced from Ref. [72] with permission from The Royal Society of Chemistry), **b** valve-controlled cell pairing (Figure reproduced from Ref. [13]), **c** self-variable resistance-based cell pairing (Figure reproduced from Ref. [74] with permission from The Royal Society of Chemistry), and **d** cell pairing using physical separation (Figure reproduced from Ref. [16])

in half (neutral position), only flowing media but holding the cells inside the microwells. Figure 12c shows a valveless pairing scheme. An optimized 3 μm width gap was designed for hydrodynamic capture of single cells [74]. The first cell type is loaded and trapped at the capture site. After incubation, the loaded cells adhere and migrate away from the gap. Then, the second cell type is loaded into chambers in the same way. In this manner, both cells are paired in a chamber.

Although the sequential loading processes provide an elegant solution for cell pairing, it will be much simpler if we can load cells in pair simultaneously. One simple method is loading a mixture of two cell populations in a large array of microwells and pairing the cells statistically. [75]. According to the Poisson distribution, some microwells capture a pair of cells by chance. Although the pairing rate is low, having a large array of thousands of microwells, we can have enough number of pairing cells. Another approach is to combine the two: hydrodynamic capture and probability-based pairing [16], as shown in Fig. 12d. One cell type is loaded on the left side and the other cell type on the right side. While two cell types are loaded at the same time, the physical separation guarantees independent cell loading and hydrodynamic cell capture on the two sides. This approach can only allow the paracrine-based signaling interaction. If we make two capture sites in one microwell and load two cell types simultaneously, mixed together in half and half, then by chance some chambers can capture a pair of cells [17].

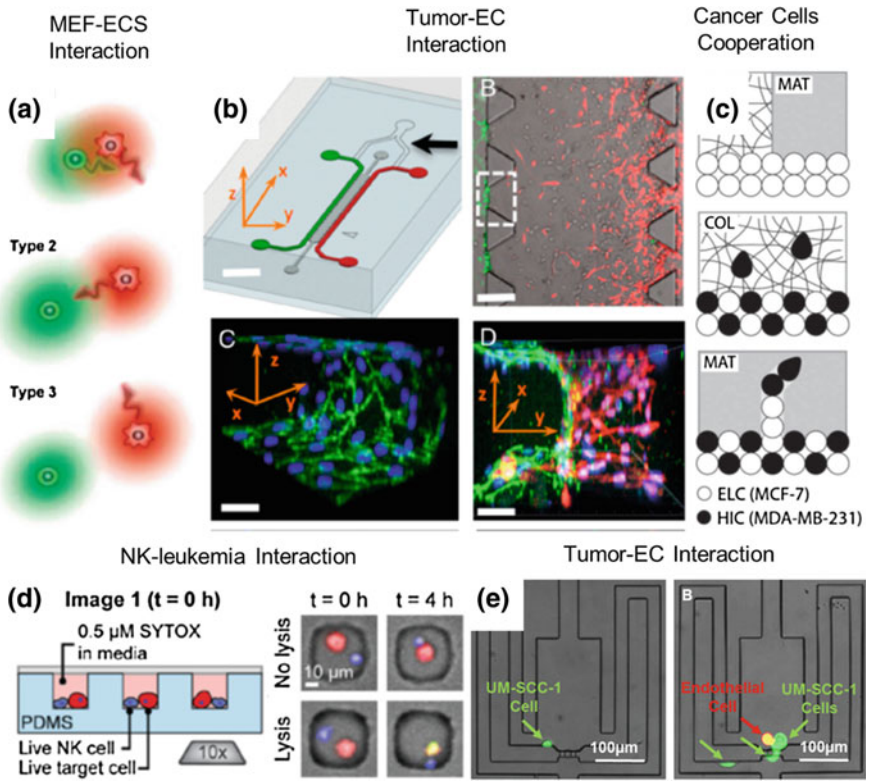

Fig. 13 Cell–cell interaction platforms: **a** Interaction between mouse embryonic fibroblasts (MEF) and mouse embryonic stem cells (mESC) (Figure reproduced from Ref. [74] with permission from The Royal Society of Chemistry), **b** interaction between tumor cells and endothelial cells (EC) for investigating tumor cell intravasation and endothelial barrier function (Figure reproduced from Ref. [76] with permission from The Royal Society of Chemistry), **c** corporation between two different breast cancer cell lines in invasion (Figure reproduced from Ref. [77] with permission from The Royal Society of Chemistry), **d** interaction between nature killer (NK) cells and leukemia cells (Figure reproduced from Ref. [75] with permission from The Royal Society of Chemistry), and **e** interaction between head and neck cancer and EC (Figure reproduced from Ref. [17])

4.3 Cell Migration Induced by Cell–Cell Interaction

The cell migration induced by cell–cell interaction can be categorized into two classes: attraction between two cell types and cooperation of cells for invasion. Figure 13a provides a good example of the former [74]. One mouse embryonic fibroblast (MEF) and one mouse embryonic stem cell (mESC) are paired inside a chamber. The motility of mECS can be enhanced by basic fibroblast growth factor (bFGF) and vascular endothelial growth factor (VEGF) secreted by the MEF. The experiments show that when two cells are close enough in the beginning, either

mECS goes after the MEF or the MEF moves toward mECS, demonstrating the attraction between two cells. Figure 13b demonstrates the interaction between tumor cells and endothelial cells for investigating tumor cell intravasation and endothelial barrier function [76]. The Fig. 13c shows the cooperation between two breast cancer cell lines (MCF-7 and MDA-MB-231) in invasion [77]. The mono-cultured MCF-7 is a low-motility cell line. However, when co-culturing with motile MDA-MB-231, which can serve as the leading cell in invasion, MCF-7 can join the invasion into the ECM scaffold. This work demonstrates the interactions between heterogeneous cancer cells that are critical for cooperation in invasion.

4.4 Other Cell–Cell Interaction Assays

In addition to the cell migrations induced by cell–cell interaction, other interactions including enhancement of cell proliferation and immuno-response can also be performed on-chip. An interesting example is the interaction between natural killer (NK) cells and leukemia cells (Fig. 13d). Using microwell loading, a pair of cells is trapped in a small microwell, so the cytolytic effect caused by NK cells can be quantified. The experiment validates that the isolated NK cell can kill the target cell independently [75]. Figure 13e shows the interaction between UM-SCC-1 (head and neck cancer cells) and endothelial cells (ECs). Secreted cytokines from ECs can boost the growth of UM-SCC-1 cells [17]. Using two-phase isolation, the cells are trapped inside the culture chamber, and proliferation enhancement has been clearly observed. In addition to these two examples, other interactions were also performed in microfluidic chips [17, 75]. With the capability of precise cell pairing, microfluidic platforms are ideal for cell–cell interaction studies at single-cell resolution.

5 Challenges and Future Opportunities

5.1 Use of Patient Samples and PDX

Although various single cell behavioral assays have been developed using microfluidic platforms, a majority of them still use cell lines for demonstration of feasibility studies. Using primary cells will better emulate actual cell behavior in vivo [78]. However, the use of primary samples is challenging for three reasons. (1) It is difficult to acquire, store, and transport primary cells. (2) Primary cells are naturally less robust; culturing in vitro is fundamentally problematic, let alone doing single-cell assays. (3) They are more heterogeneous, so the ideal culture conditions can vary from cancer to cancer and from patient to patient. Determining the culture conditions can be difficult and even controversial. In cancer research, the development of patient-derived xenograft (PDX) can be a solution to this problem [79]. PDX

is generated from implanting primary patient tumor into an immuno deficient mouse. While the property of primary tumor can be maintained by in vivo culture, primary cells can be stored and amplified for microfluidic assays. Meanwhile, the number of vendors that provide various types of primary samples and culture media has increased over time. In spite of the challenges, it is expected that more primary samples will be used in microfluidic single-cell assays in the future.

5.2 Use of Small Sample for Single-Cell Assays

One key advantage of single-cell assays is the capability to generate meaningful data using a small number of cells, and this merit is especially valuable when we handle rare samples. In the past decades, the development of microfluidics enables single-cell assays. However, typically, tens of thousands cells need to be loaded into microfluidic chips for an assay, suggesting that most samples are wasted and not efficiently used. When a syringe pump is used for cell loading, the dead volume in the syringe and in a connecting tube can be easily up to hundreds of μL. A significant portion of samples (cells) are lost in the dead volume. For example, if we would like to assay circulating tumor cells (CTCs), which have a great potential for diagnosis and precision medicine for treatment [80], the number of available cells are very small, typically less than 10 cells/mL in a patient blood. Using conventional dish-based approaches, such as western blot and qRT-PCR, it is difficult to generate meaningful data, because the large volume dilutes the concentration of proteins and mRNA from the cells. Although microfluidics can analyze a smaller number or even single cells, the volume (mL) of the CTC samples is too large to be loaded in most microfluidic platforms. For example, the C1™ Single-Cell Auto Prep System (Fluidigm) can only load 3μL into its microfluidic chip. Given a cell concentration of 10 cells/mL, almost no cell can be loaded for analysis of CTCs. Centrifuge can help to increase the cell density, but the majority of cells would be lost in the centrifuging process for three reasons [81]: (1) Reducing the volume from mL to μL is fundamentally challenging; (2) when the number of cells is really small (10–50 cells), cells cannot aggregate well into a solid pellet; and (3) Fragile primary samples cannot endure high centrifuging force (typically should be lower than 100–300 relative centrifugal force (RCF)). To resolve this problem, robust and efficient microfluidic interfaces should be developed. Such advances in small sample preparation are promising both for research and clinical applications.

5.3 Cell Retrieval for Downstream Analysis

Compared to conventional dish-based assays, which report only the average behavior, microfluidic platforms enable monitoring individual cell behaviors [10].

However, most existing microfluidic assays are endpoint assays. The behavior can be measured, but cells with different behaviors cannot be retrieved for further analysis. Although some on-chip analysis can be performed [82, 83], off-chip tools can usually provide higher multiplexing capability up to 96 mRNA (Fluidigm, C1, Biomark), 32 proteins (Fluidigm, CyTOF), or even next-generation sequencing (NGS) for single-cell analysis. Thus, the capability to retrieve target single cells for off-chip analyses is critical. Conventional cell detachment approaches, such as trypsinization and PNIPAAm-based detachment [84], have poor spatial resolution. Although there are a few publications and commercially available tools, such as PALM CombiSystem, capillary vacuum, localized trypsinization, and ultrasound-induced cavitation [85–89], these methods can only apply to open substrate but not to enclosed microfluidic chambers. Thus, it is difficult to correlate the single-cell behavior and its genomic profiles, gene expressions, and proteins. Understanding of molecular biology is critical for therapeutics and the lack of downstream analysis capability severely limits the value of on-chip behavioral assays. This problem should be solved by implementing robust cell retrieval capability from microfluidic platforms and/or integrating on-chip single-cell analysis capabilities.

References

1. Zhang M, Behbod F, Atkinson RL et al (2008) Identification of tumor-initiating cells in a p53-null mouse model of breast cancer. Cancer Res 68:4674–4682
2. Reya T, Morrison SJ, Clarke MF et al (2001) Stem cells, cancer, and cancer stem cells. Nature 414:105–111
3. Visvader JE (2009) Keeping abreast of the mammary epithelial hierarchy and breast tumorigenesis. Genes Dev 23:2563–2577
4. Zhou J, Zhang Y (2008) Cancer stem cells: Models, mechanisms and implications for improved treatment. Cell Cycle 7:1360–1370
5. Chen R, Nishimura MC, Bumbaca SM et al (2010) A hierarchy of self-renewing tumor-initiating cell types in glioblastoma. Cancer Cell 17:362–375
6. Croker AK, Goodale D, Chu J et al (2009) High aldehyde dehydrogenase and expression of cancer stem cell markers selects for breast cancer cells with enhanced malignant and metastatic ability. J Cell Mol Med 13:2236–2252
7. Prestegarden L, Svendsen A, Wang J et al (2010) Glioma cell populations grouped by different cell type markers drive brain tumor growth. Cancer Res 70:4274–4279
8. Louis SA, Rietze RL, Deleyrolle L et al (2008) Enumeration of neural stem and progenitor cells in the neural colony-forming cell assay. Stem Cells 26:988–996
9. Tan WH, Takeuchi S (2007) A trap-and-release integrated microfluidic system for dynamic microarray applications. Proc Natl Acad Sci USA 104:1146–1151
10. Chung J, Kim YJ, Yoon E (2011) Highly-efficient single-cell capture in microfluidic array chips using different hydrodynamic guiding structures. Appl Phys Lett 98:123701
11. Frimat JP, Becker M, Chiang YY et al (2011) A microfluidic array with cellular valving for single cell co-culture. Lab Chip 11:231–237
12. Chen YC, Cheng YH, Kim HS et al (2014) Paired single cell co-culture microenvironments isolated by two-phase flow with continuous nutrient renewal. Lab Chip 14:2941–2947

13. Kim YJ, Bersano-Begey T, Lou X et al (2009) Microfluidic array chip for analysis of pairwise cell interaction by temporal stimulation of secreted factors using chamber isolation. Paper presented at the 13th international conference on miniaturized systems for chemistry and life sciences (MicroTAS 2009). International Convention Center, Korea, November 2009
14. Fordyce PM, Diaz-Botia CA, DeRisi JL et al (2012) Systematic characterization of feature dimensions and closing pressures for microfluidic valves produced via photoresist reflow. Lab Chip 12(21):4287–4295
15. Chiu SH, Liu CH (2009) An air-bubble-actuated micropump for on-chip blood transportation. Lab Chip 9:1524–1533
16. Chen YC, Ingram PN, Yoon E (2014) Electrolytic valving isolation of cell co-culture microenvironment with controlled cell pairing ratios. Analyst 139(24):6371–6378
17. Chen YC, Cheng YH, Kim HS et al (2014) Paired single cell co-culture microenvironments isolated by two-phase flow with continuous nutrient renewal. Lab Chip 14:2941–2947
18. Brunette D (1986) Spreading and orientation of epithelial cells on grooved substrata. Exp Cell Res 167(1):203–217
19. Oakley C, Brunette D (1995) Response of single, pairs, and clusters of epithelial cells to substratum topography. Biochem Cell Biol 73(7–8):473–489
20. Chen C, Mrksich M, Huang S et al (1998) Micropatterned surfaces for control of cell shape, position, and function. Biotechnol Prog 14(3):356–363
21. Nelson C, Raghavan S, Tan J et al (2003) Degradation of micropatterned surfaces by cell-dependent and-independent processes. Langmuir 19(5):1493–1499
22. Jiang X, Bruzewicz D, Wong A et al (2004) Directing cell migration with asymmetric micropatterns. Proc Natl Acad Sci 102(4):975–978
23. Fan CTY, Takayama S, Meyhofer E et al (2008) Electrically programmable surfaces for configurable patterning of cells. Adv Mater 20(8):1418–1423
24. Liu V, Jastromb W, Bhatia S (2002) Engineering protein and cell adhesivity using PEO-terminated triblock polymers. J Biomed Mater Res 60(1):126–134
25. Fan C, Kurabayashi K, Meyhofer E (2006) Protein pattern assembly by active control of a triblock copolymer monolayer. Nano Lett 6(12):2763–2767
26. Chung J, Ingram PN, Bersano-Begey T et al (2014) Traceable clonal culture and chemodrug assay of heterogeneous prostate carcinoma PC3 cells in microfluidic single cell array chips. Biomicrofluidics 8(064103)
27. Mehlen P, Puisieux A (2006) Metastasis: a question of life or death. Nat Rev Cancer 6(6):449–458
28. Singh S, Clarke I, Terasaki M et al (2003) Identification of a cancer stem cell in human brain tumors. Cancer Res 3(63):5821
29. Dontu G, Wicha M (2005) Survival of mammary stem cells in suspension culture: implications for stem cell biology and neoplasia. J Mammary Gland Biol Neoplasia 10(1):75–86
30. Dontu G, Abdallah W, Foley J et al (2003) In vitro propagation and transcriptional profiling of human mammary stem/progenitor cells. Genes Dev 17:1253–1270
31. Tung YC, Hsiao AY, Allen SG et al (2010) High-throughput 3D spheroid culture and drug testing using a 384 hanging drop array. Analyst 136(3):473–478
32. Ingram P, Im M, McDermott S et al (2011) Spheroid cell culture on PDMS hydrophobic surfaces and integration into microfluidic devices. Paper presented at the 15th international conference on miniaturized systems for chemistry and life sciences (MicroTAS 2011). Washington State Convention Center, Seattle, October 2011
33. Park YB, Kang MS, Choi YK (2010) Antibacterial surface with cylindrical nanoshell array. Paper presented at the 14th international conference on miniaturized systems for chemistry and life sciences (MicroTAS 2010), Martinplaza, the Netherlands
34. Im H, Park YB, Suk J et al (2010) A hemocompatible array cylindrical nanoshell with a reduced effective blood contact area. Paper presented at the 14th international conference on miniaturized systems for chemistry and life sciences (MicroTAS 2010), Martinplaza, the Netherlands, October 2010

35. Schumacher JF, Carman ML, Estes TG et al (2007) Engineered antifouling microtopographies– effect of feature size, geometry, and roughness on settlement of zoospores of the green alga Ulva. Biofouling 23(1):55–62
36. Baxter A, Cassie S (1944) Wettability of porous surfaces. Trans Faraday Soc 40:546–551
37. Chen YC, Ingram P, Lou X et al (2012) Single cell suspension culture using PolyHEMA coating for Anoikis assay and sphere formation. Paper presented at the 16th international conference on miniaturized systems for chemistry and life sciences (MicroTAS 2012). Washington State Convention Center, Okinawa, November 2012
38. Wu L, Claas AM, Sarkar A et al (2015) High-throughput protease activity cytometry reveals dose-dependent heterogeneity in PMA-mediated ADAM17 activation. Integr Biol 7:513–524
39. Jiang X, Kang Y, Pan X et al (2014) Studies of the drug resistance response of sensitive and drug-resistant strains in a microfluidic system. Integr Biol 6(2):143–151
40. Rowat AC, Bird JC, Agresti JJ et al (2009) Tracking lineages of single cells in lines using a microfluidic device. Proc Natl Acad Sci USA 106(43):18149–18154
41. Cavaillon JM (2011) The historical milestones in the understanding of leukocyte biology initiated by Elie Metchnikoff. J Leukoc Biol 90(3):413–424
42. Rodriguez LG, Wu X, Guan JL (2005) Wound-healing assay. Methods Mol Biol 294:23–29
43. Chen HC (2005) Methods Mol Biol 294:15–22
44. Squires TM, Quake SR (2005) Microfluidics: fluid physics at the nanoliter scale. Modern Phys 77(3):977–1026
45. Nie FQ, Yamada M, Kobayashi J et al (2007) On-chip cell migration assay using microfluidic channels. Biomaterials 28(27):4017–4022
46. Chung S, Sudo R, Mack PJ et al (2009) Cell migration into scaffolds under co-culture conditions in a microfluidic platform. Lab Chip 9(2):269–275
47. Irimia D, Charras G, Agrawal N et al (2007) Polar stimulation and constrained cell migration in microfluidic channels. Lab Chip 7(12):1783–1790
48. Chen YC, Allen SG, Ingram PN et al (2015) Single-cell migration chip for chemotaxis-based microfluidic selection of heterogeneous cell populations. Sci Rep 5:9980
49. Keenan TM, Frevert CW, Wu A et al (2010) A new method for studying gradient-induced neutrophil desensitization based on an open microfluidic chamber. Lab Chip 10(1):116–122
50. Atencia J, Morrow J, Locascio LE (2009) The microfluidic palette: a diffusive gradient generator with spatio-temporal control. Lab Chip 9:2707–2714
51. Zaari N, Rajagopalan P, Kim SK et al (2004) Photopolymerization in microfluidic gradient generators: microscale control of substrate compliance to manipulate cell response. Adv Mater 16(23–24):2133–2137
52. Sochol RD, Higa AT, Janairo RRR et al (2011) Unidirectional mechanical cellular stimuli via micropost array gradients. Soft Matter 7:4606–4609
53. Cortese B, Palamà IE, D'Amone S et al (2014) Influence of electrotaxis on cell behavior. Integr Biol 6(9):817–830
54. Banks TA, Luckman PSB, Frith JE et al (2015) Effects of electric fields on human mesenchymal stem cell behaviour and morphology using a novel multichannel device. Integr Biol 7:693–712
55. Tong Z, Balzer EM, Dallas MR et al (2012) Chemotaxis of cell populations through confined spaces at single-cell resolution. PLoS ONE 7(1):e29211
56. Gallego-Perez D, Higuita-Castro N, Denning L et al (2012) Microfabricated mimics of in vivo structural cues for the study of guided tumor cell migration. Lab Chip 12(21):4424–4432
57. Mak M, Erickson D (2014) Mechanical decision trees for investigating and modulating single-cell cancer invasion dynamics. Lab Chip 14(5):964–971
58. Ko YG, Co CC, Ho CC (2013) Gradient-free directional cell migration in continuous microchannels. Soft Matter 9:2467–2474
59. Mendelson A, Cheung Y, Paluch K (2013) Competitive stem cell recruitment by multiple cytotactic cues. Lab Chip 13(6):1156–1164
60. Ahmed T, Shimizu TS, Stocker R (2010) Microfluidics for bacterial chemotaxis. Integr Biol 2:604–629

61. Nosrati R, Vollmer M, Eamer L et al (2014) Rapid selection of sperm with high DNA integrity. Lab Chip 14:1142–1150
62. Pandey G, Jain RK (2002) Bacterial chemotaxis toward environmental pollutants: role in bioremediation. Appl Environ Microbiol 68(12):5789–5795
63. Shen C, Xu P, Huang Z et al (2014) Bacterial chemotaxis on SlipChip. Lab Chip 14(16):3074–3080
64. Polacheck WJ, Li R, Uzel SG et al (2013) Microfluidic platforms for mechanobiology. Lab Chip 13(12):2252–2267
65. García S, Sunyer R, Olivares A et al (2015) Generation of stable orthogonal gradients of chemical concentration and substrate stiffness in a microfluidic device. Lab Chip 15:2606–2614
66. Barnet LE, Dandley EC, Jansen LE et al (2015) A cell–ECM screening method to predict breast cancer metastasis. Integr Biol 7(2):198–212
67. Pathak A, Kumar S (2012) Independent regulation of tumor cell migration by matrix stiffness and confinement. Proc Natl Acad Sci 109(26):10334–10339
68. Kim HD, Peyton SR (2012) Bio-inspired materials for parsing matrix physicochemical control of cell migration: a review. Integr Biol 4(1):37–52
69. Liu SQ, Tay R, Khan M et al (2010) Synthetic hydrogels for controlled stem cell differentiation. Soft Matter 6(1):67–81
70. Lee-Thedieck C, Spatz JP (2014) Biophysical regulation of hematopoietic stem cells. Biomater Sci 2(11):1548–1561
71. Wong IY, Javaid S, Wong EA et al (2014) Collective and individual migration following the epithelial–mesenchymal transition. Nat Mater 13:1063–1071
72. Dura B, Liu Y, Voldman J (2014) Deformability-based microfluidic cell pairing and fusion. Lab Chip 14(15):2783–2790
73. Ingram P, Kim YJ, Bersano-Begey T et al (2010) Microfluidic assay to compare secretion vs. contact based cell-cell interactions using dynamic isolation control. Paper presented at the 14th international conference on miniaturized systems for chemistry and life sciences (MicroTAS 2010), Martinplaza, the Netherlands, October 2010
74. Hong S, Pan Q, Lee LP (2012) Single-cell level co-culture platform for intercellular communication. Integr Biol 4(4):374–380
75. Yamanaka YJ, Berger CT, Sips M et al (2012) Single-cell analysis of the dynamics and functional outcomes of interactions between human natural killer cells and target cells. Integr Biol 4(10):1175–1184
76. Zervantonakis IK, Hughes-Alford SK, Charest JL et al (2012) Three-dimensional microfluidic model for tumor cell intravasation and endothelial barrier function. Proc Natl Acad Sci 109 (34):13515–13520
77. Shin Y, Han S, Chung E et al (2014) Intratumoral phenotypic heterogeneity as an encourager of cancer invasion. Integr Biol 6(7):654–661
78. Pan C, Kumar C, Bohl S et al (2009) Comparative proteomic phenotyping of cell lines and primary cells to assess preservation of cell type-specific functions. Mol Cell Proteomics 8 (3):443–450
79. Marangoni E, Vincent-Salomon A, Auger N et al (2007) A new model of patient tumor-derived breast cancer xenografts for preclinical assays. Clin Cancer Res 13 (13):3989–3998
80. Cristofanilli M, Hayes DF, Budd GT et al (2005) Circulating tumor cells: a novel prognostic factor for newly diagnosed metastatic breast cancer. J Clin Oncol 23(7):1420–1430
81. Wong JW (2009) Centrifugal recovery of embryonic stem cells for regenerative medicine bioprocessing. Doctoral dissertation, UCL (University College London)
82. Lu Y, Chen JJ, Mu L et al (2013) High-throughput secretomic analysis of single cells to assess functional cellular heterogeneity. Anal Chem 85(4):2548–2556
83. Jang K, Ngo HTT, Tanaka Y (2011) Development of a microfluidic platform for single-cell secretion analysis using a direct photoactive cell-attaching method. Anal Sci 27(10):973

84. Canavan HE, Cheng X, Graham DJ et al (2005) Cell sheet detachment affects the extracellular matrix: a surface science study comparing thermal liftoff, enzymatic, and mechanical methods. J Biomed Mater Res A 75(1):1–13
85. Kimio S, Kyoko K, Toshiyuki T et al (2013) Proceedings of MicroTAS, pp 100–102
86. Sada T, Fujigaya T, Niidome Y et al (2011) Near-IR laser-triggered target cell collection using a carbon nanotube-based cell-cultured substrate. ACS Nano 5(6):4414–4421
87. Baac HW, Ok JG, Maxwell A et al (2012) Carbon-nanotube optoacoustic lens for focused ultrasound generation and high-precision targeted therapy. Sci Rep 2:989
88. Dobes NC, Dhopeshwarkar R, Henley WH et al (2013) Laser-based directed release of array elements for efficient collection into targeted microwells. Analyst 138(3):831–838
89. Kudo LC, Vi N, Ma Z et al (2012) Novel Cell and Tissue Acquisition System (CTAS): microdissection of live and frozen brain tissues. PLoS ONE 7(7):e41564

Systems Biology in Single Cells

Macdara Glynn, Damien King and Jens Ducrée

Abstract From the beginning of the twenty-first century, there has been a shift towards studying biological processes using a holistic rather than a reductionist scientific paradigm thus establishing the approach now named "systems biology" or "systomics". This method of biological investigation represents a synergy where life sciences, systems engineering, and information technology examine the interactions between biological pathways, rather than solely focusing on individual pathways in an isolated manner. To date, systems biology has often studied population averages rather than individual characteristics of cells which might display a significant spread. However, as a single cell is the smallest operational biological unit that encompasses all metabolites necessary for maintaining a viable living entity, the application of systems biology approaches to the study of distinct cells is fast becoming a goal of many research groups. In this chapter we will describe some of the technologies that enable the isolation of individual cells in a form that accommodates systomics studies, the biological methods that are then deployed on such isolated cells to generate system-level information, and finally describe some of the bioinformatics that is specifically directed towards single-cell studies.

Keywords Systems level biology · Microfluidic lab-on-a-chip · Single cell analysis · Integrated biology · Single cell optical detection

1 What Is Systems Biology?

As it is the case with many emergent scientific disciplines, in its early days a generally agreed definition or understanding of the goals and boundaries of systems biology was rather elusive. Westerhoff and Alberghina [1] compare this poor definition of identity to that experienced by molecular biology in its embryonic

M. Glynn · D. King · J. Ducrée (✉)
Biomedical Diagnostics Institute, Dublin City University, Dublin 9, Glasnevin, Ireland
e-mail: jens.ducree@dcu.ie

F.-G. Tseng and T.S. Santra (eds.), *Essentials of Single-Cell Analysis*,
Series in BioEngineering, DOI 10.1007/978-3-662-49118-8_2

period where it was considered a nexus of crystallography, theoretical biology and chemistry. However, systems biology has, in the last number of years, come to represent a scientific paradigm where emergent properties and functionalities of living entities are examined from a perspective that encompasses a repertoire of often disparate biological pathways (Fig. 1). The interplay between these pathways is studied using high throughput and quantitative experimental strategies that allow the biological system to operate in its intact state, and data is then used to generate predictive mathematical models that can be queried to pose new biological questions. Crucially, systems biology represents a field where multiple disciplines including biochemistry, information technology, molecular biology, mathematics, physics and systems engineering must operate in close harmony in order to address the questions posed. Although all these disciplines have been around for some decades, their integration towards a common endpoint is relatively new [1].

Due to its ability to design, record and model vast amounts of data, many investigations of systems biology operate at the large-scale "-omics" level—i.e. genomics, proteomics and metabolomics [3]. This helps to recognise emergent phenotypes that may otherwise be too subtle to be identified without combining the big and quantitative data sets generated, with the mathematical modelling capabilities used in these studies [2]. Combining these individual "-omics" through systems biology can then lead to a higher level modelling of the "interactome".

1.1 Systems Biology at the Single Cell Level

Many studies (at both systems level, and at the classical, single-pathway level) have produced their data based on signals obtained from a large cohort of cells—termed either "population-level studies" or "bulk assays". However, such multi-cellular studies may not always identify minute changes that take place at the single cell level, particularly when the fate of a single cell within a population represents a low-frequency occurrence that results in the single cell presenting a phenotype distinct from the population (Fig. 2a). When measured at the population level, rare single-cell phenotypes can be lost to background noise in the data. This is shown by Tay et al. where they demonstrated the activation of cellular pathways in response to tumour-necrosis factor (TNF-α) over a concentration range covering four orders of magnitude.

By examining a large number of cells at the single-cell level using a systems biology approach, the heterogeneous nature of TNF-activation across the population was examined. It was found that cells may activate TNF-αdigitally, and critically, a small subset of cells were shown to activate on a lower dose exposure [4]—this was in contrast to population-based studies [5]. Alternatively, in cases where a treatment will generate more frequent but polarising phenotypes, a population-level study may suggest that the response is lower but distributed in all cells, rather than showing that distinct subpopulations emerge (Fig. 2b). For example, the response of the well-studied "defender of the genome" protein, p53, to irradiation occurs strongly in

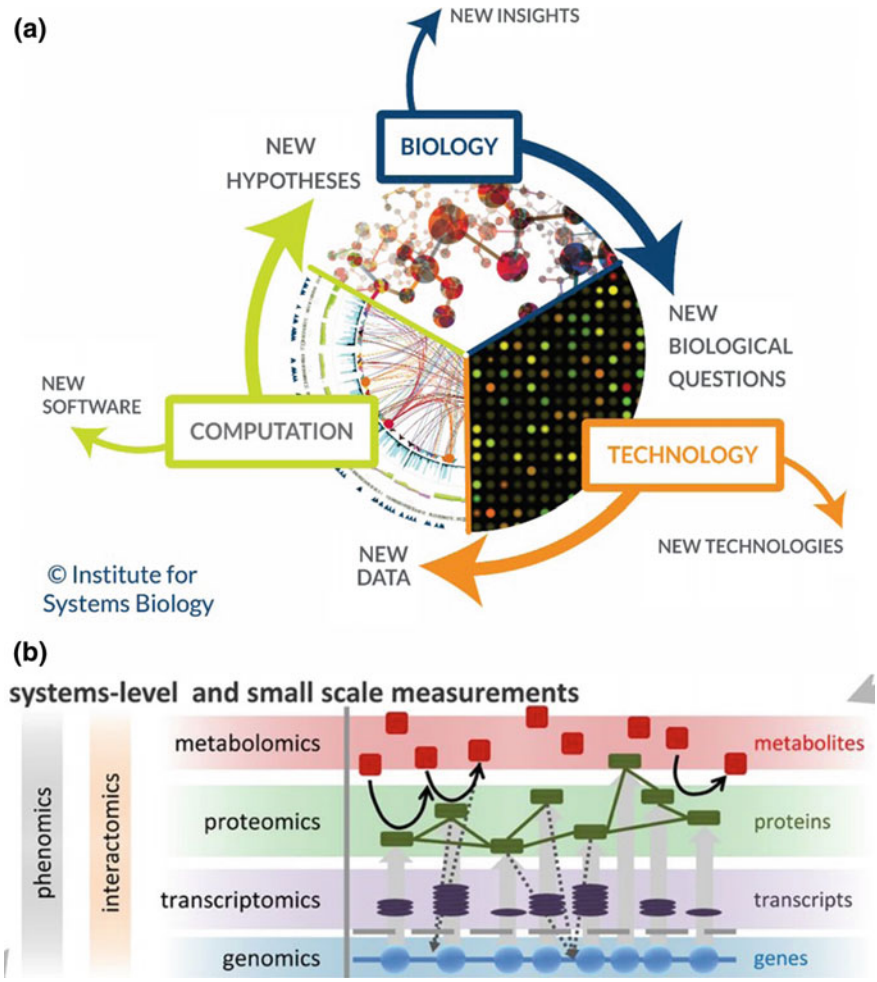

Fig. 1 Overview of the multidisciplinary and integrative nature of systems biology. **a** The innovation engine as demonstrated by the Institute for Systems Biology. **b** A visualisation of the interactions between various—omics as shown by Mast et al. [2]. Both show multi-aspect biological experiments are designed and executed using biochemical, molecular and cellular techniques. High throughput and multi-parameter technological systems (often optical-based) monitor the progress of the experiment in real-time and record data. These large and multi-dimensional datasets are mathematically analysed to identify dependencies and interactions between the biological parameters examined, and models are generated. These models are then refined and adapted as new biological questions are identified and experimentally examined. (**a**) Reprinted with permission from the Institute for Systems Biology. (**b**) Reprinted with permission from Ref. [2]. Copyright 2014 The Rockefeller University Press

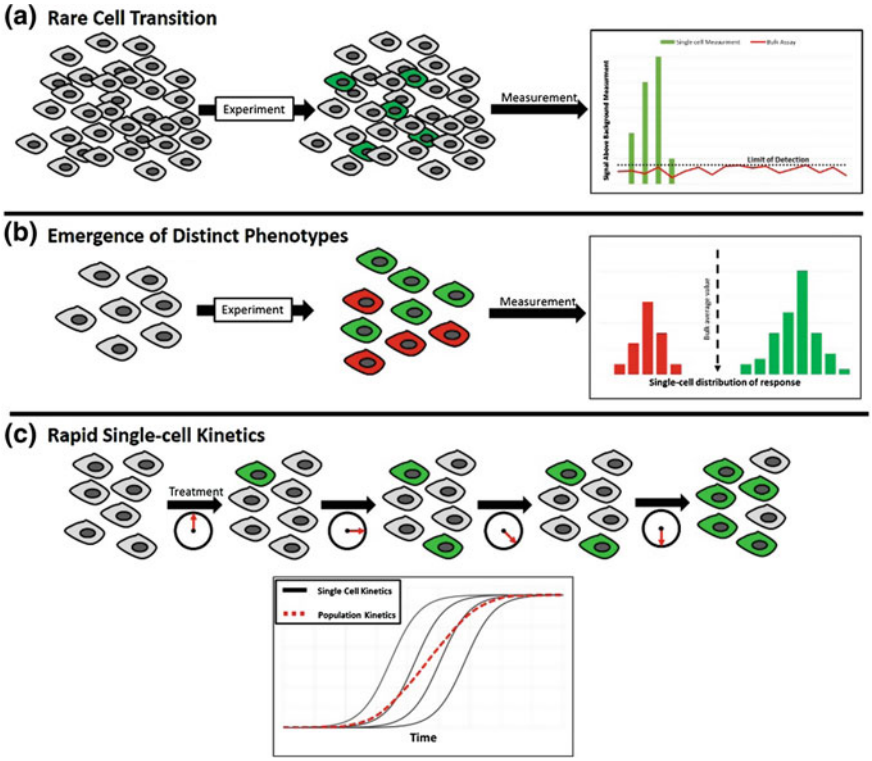

Fig. 2 Population-based bulk systems biology versus single-cell systems biology. **a** Rare cellular transitions in a large background will often not generate sufficient signal above the bulk background to be quantifiable, or even detectable. When each cell is measured individually and compared to the background, the same experiment can identify a small number of cells undergoing transition. **b** In cases were cells can transition to one of a number of phenotypes, single-cell studies can identify such bimodal distributions. **c** Rapid cellular transitions that are slow to spread through a population can be misinterpreted when examined at a population level

a sub-group of treated cells, but, if at all, only at a low level (if at all) in the other cells [6]. If examined at a population level, this dual-phenotype is not observed, and it rather appears that all cells equally respond at a lower intensity.

As a final example of the benefit of single-cell studies over population studies in systems biology, one may examine the effect of rapid, time-dependent phenotypic transitions (or gene activations) that occur at the single cell level but spread in time through the population (Fig. 2c). When examined individually, it is clear in these experiments that, when activated, the transition is rapid on a per-cell level. However, if one were to observe the bulk transition at the population level (by, for example, monitoring the production of an associated soluble and detectable factor in the culture media), it would appear that the overall transition kinetics were slow and gradual, rather than rapid but digital at the cellular level [7].

In this chapter, a number of technologies will be presented that enable systems biology to be studied on cell-by-cell basis. The chapter will be sectioned into methods of isolating or tracking single cells, the strategies of biological systems experiments used on isolated cells, and the methods of high-throughput optical monitoring of these experiments. Although these headings are used for the sake of convenience, it should be remembered that amalgamation of all these disparate disciplines into a single workflow is required to fully leverage the analytical power of systems biology.

2 Standing Out from the Crowd—Working with Single Cells

The resolution of data that can be generated on a single-cell level in a systems biology study is limited (to a first approximation) by the reliability and consistency of the instrumentation. Unlike many other single-cell level methods (such as fixed-cell immunofluorescence), the technologies used in systems biology often require cells to be maintained as viable and actively metabolising, thus allowing interaction between events in seemingly distinct and those in other cellular pathways in response to experimental conditions. Furthermore, these technologies will need to present single cells in a framework where high-speed and multi-channel optical and chemical detectors can maintain contact and record data in real-time.

Broadly speaking, there are three approaches ensuring this spatio-temporal resolution of data. Each displays specific advantages depending on the sensitivity of the cell of interest to its environment, or depending on the cellular output under investigation. In the first approach, cells can be maintained in co-culture within a population, but optical systems are employed to target a particular cell of interest and track the cell throughout the length of the experiment. This is useful, for example, when a cell is sensitive to low population density in its neighbourhood and can be lost through a process called anoikis—a type apoptotic response to the absence of cell–matrix interactions. In such cases, tracking the cell while it is maintained in a population is favourable.

In the second approach, technology is employed to physically capture or otherwise select and segregate single cells from a wider population where they can be treated and monitored, often with high levels of minute control over the surrounding environment. For example, when the secretion of soluble constituents from a single cell represents an impact factor, this approach allows the cell to be confined to a defined environment where a change in the local concentration of the soluble factor can be directly attributed to the contained cell.

The third approach is related to the second and involves processing a large population of cells through a multi-optic detection locus. Critically, even though the input sample is a bulk population, the resolution occurs at a cell-by-cell level. Flow cytometers and cell sorting devices are commonly used for such studies. However,

instruments such as the Amnis ImageStream [8] has integrated the single cell and multi-optical capabilities of a flow cytometer with a high-speed fluorescent microscope to provide a large amount of fluorescent and molecular localisation data at single-cell resolution. Although high depth cellular data can be produced and examined using a systems biology approach, each cell is only examined at a given, potentially random point in time as it flows through the detection locus; hence, kinetic data and time-dependent dynamic interactions within a specific cell are lost.

2.1 *Tracking and Monitoring Selected Cells in a Wider Population*

Microscopic monitoring of individual cells within a population throughout the duration of an entire experiment (generally also requiring that multi-channel optical systems can record data simultaneously) remains challenging. Only a few microscope setups offer a combination of high-resolution micro-displacement stages with controlling software that can recognise and track mobile targeted cells (often undergoing significant morphological change). These instruments have greatly enhanced the ability of systems biology to operate at the single-cell level. Long-term monitoring of single cell experiments—often continuing for more than 24 h—commonly requires vibration-free conditions for the setup.

There are a number of proprietary software packages that implement cell tracking which share a similar strategy. First, the operator places a region-of-interest (ROI) around the target cell. An algorithm then determines the centre of the cell, and establishes a set of features for tracking the translocation of the centre of a cell and its morphological change along subsequent frames. Upon larger movement beyond the starting position, the micron-scale resolution stage is repositioned to home on the new location of the cell. As long as the stage facilitates micron-level adjustments, a cell can be reliably tracked. In addition to such X-Y stage displacement, most modern systems also allow fine tuning of the Z-axis for investigating cells suspended above the focal plane. Sub-micron adjustment of the Z-axis even allows the selection of vertical optical slices, thus enabling spatio-temporal 4D recording of the cells for rendering and modelling (Fig. 3).

Although more challenging, such 4D tracking has revealed dynamic intra-cellular interactions leading to unexpected cellular motions. For example, using such a microscopic system, Kaczmarczyk et al. demonstrated that, when expression of the centromeric protein CENP-W is knocked down, consequent effects on the mitotic spindle brings about a rolling motion in cells that are attempting to undergo mitosis [9]. Using a similar system, but following a strategy where single cells were monitored after an on-instrument, time-controlled chemical treatment, Yivgi-Ohana et al. developed a novel tool to study progression of the highly complex apoptotic cellular system in real-time in living cells [10].

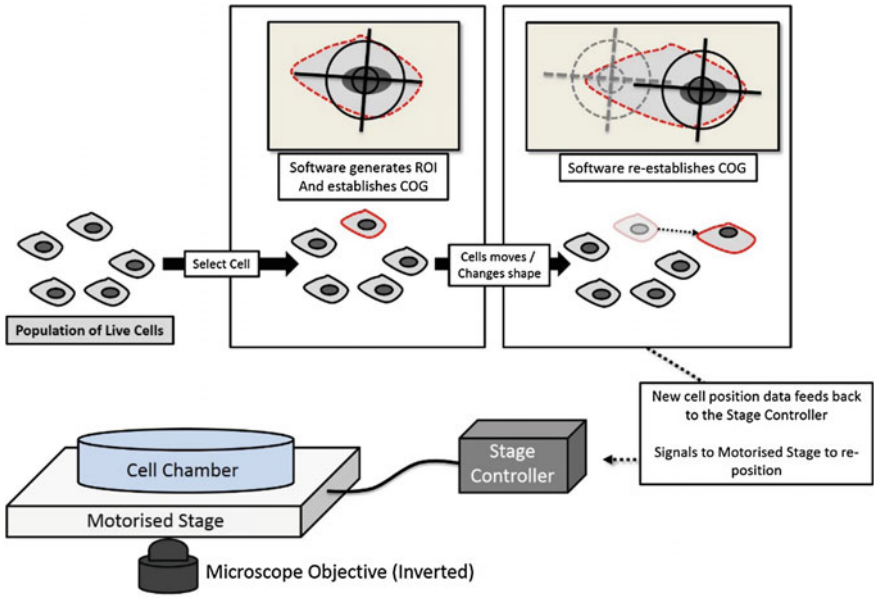

Fig. 3 Tracking of individual cells from a population of live culturing cells using a live-cell imaging microscopic platform with a high-resolution micro-displacement motorised stage

2.2 Segregating and Isolation of Single Cells from a Population

For cells that are stable when examined in isolation, it can be confined to a geometrically and chemically well-defined environment. This way the operator can re-visit the same cell repeatedly and ensure (with suitable in situ sensors) that measured changes to the environment are due specifically to the presence of the captured cell. Furthermore, the interdisciplinary collaboration between biology, microfluidics and microfabrication has leveraged high-throughput interrogation of individual cells. This is a significant advancement from classical, laborious methods such as micro-manipulation where individual cells had to be identified and hand-picked by an operator. Microfluidic single-cell isolation systems use a number of distinct strategies, some of which will be described here.

As the depth of microfluidic systems can be precisely chosen to avoid vertical stacking of cells, fine z-axis control of associated optical or other detection hardware is not as critical as it is with 4D microscopy. Moreover, strict laminarity of flow is imposed by the micro-confinement, thus offering well-defined, convection-diffusion conditions for imposing spatio-temporally stable concentration profiles and shear rates. This allows a high level of physic–chemical control and reagent exposure [11]. In free-flow microfluidic convection-diffusion systems featuring with interconnected channels and chamber [12], physic–chemical gradients

can even be generated, e.g. to establish different concentrations of a chemical stimulus at a subcellular resolution where either side of a single cell is exposed to a distinct chemistry [13]; or a temperature gradient applies between across an embryo [14]. In both these examples, the microfluidic system also permitted real-time optical monitoring of the living cells using fluorescent markers. Other microfluidic strategies enabled the generation of concentration gradients that could be applied to microfluidic test chambers in order to facilitate the effect on individual cells. These concentration profiles were imposed using a set of inputs where chemicals of a defined concentration. The chemicals were pumped through a network of interconnected serpentine channels that merged at the experimental chamber to expose cells to a concentration gradient and allowed chemotaxis of individual cells within this gradient to be monitored optically [12].

In addition to subcellular resolution, the capacity of microfluidic systems to integrate a comprehensive array of distinct test environments to a single chip permits high throughput and high fidelity systems-biology experiments. Many more recent microfluidic platforms isolated and examined a large number of individual cells on a small-footprint "chip" that could be manufactured in a cost-efficient fashion, either in bulk by a manufacturer or even made to order in the laboratory of the research group. Researchers have used a diverse assortment of microfluidic architectures to allow such high-throughput single-cell isolation, ranging from passive filtering to active bio-physical methods, some of which will be described below.

Various microfluidic chip technologies provide methods for individual cell capture, as well as rapid exchange of reagents and optical observation of the response of the captured cells to these reagents over time. Single cells can be arrayed by passage of a population through a series of physical barriers with geometries that can only retain a single cell. Rowat et al. developed a syringe-driven microfluidic chip comprised of a number of yeast capture channels in which single cells from a population can resolve. This occurs as a cell travels to the end of the chamber where it is plugs into a fluidic constriction. The resulting increase of the flow resistance to divert subsequent cells to other trapping sites increases the probability of subsequent cells of entering a bypass channel, thus making it very likely that a single cell occupies the capture channel.

Using in situ fluorescent microscopy on live cells, the researchers were then able to follow multiple phenotypic variations in the progeny of the captured cells as these were constrained to grow in a line along the chamber [15]. Wu et al. elegantly produced a microfluidic chip with the capability of trapping single cells in a 70-pl enclosure using actuated soft-polymer valves to close off a microfluidic channel, thus generating the reaction chamber. The actuation of the valves is reversible and individually controlled, and so allows random exchange of media and reagents by the operator [16]. As the chamber is hydrodynamically sealed, this device can monitor the media surrounding the captured cell for the efflux of metabolic targets in real time; Cai et al. used this functionality to monitor the protein expression in yeast cells at the single molecule level in real-time [17].

Another microfluidic architecture designed to isolate single cells for systems level investigations uses post-like barriers specifically shaped to accommodate a maximum of one cell as a population of cells travel through the micro channel. For efficient capture, the number of barriers exceeds the expected count of incoming cells. This ensures that there is a barrier available for each cell of interest. As the population progresses through the array, they occupy the available capture loci, but if a cell encounters an occupied barrier the structure is designed such that it will continue travelling until an empty post is encountered. When the population is fully resolved, cells are arrayed at well-defined positions throughout an experiment, even under changing physic–chemical conditions.

DiCarlo et al. built such a single cell isolating structure using flow through arrayed suspended obstacles [7]. Cells and chemical components were introduced to the array using a syringe and the overall structure used branched delivery channels to ensure a high uniformity of flow across the chip. Streamlines carry cells to the capture obstacles which consist of two layers of cup-shaped trapping sites—40 and 2 μm. The larger gap serves as the primary fluidic conduit to carry cells to the trap, and once resolved to the trap, a cell blocks the smaller, 2-μm gap to thus throttle the flow through this constriction. As a result, subsequent cells are diverted towards empty traps located further downstream to eventually induce a single-cell occupancy distribution. By incorporating the chip onto a fluorescent microscope, the group monitored individual membrane-bound and cytosolic carboxylesterase concentrations in live cells in a number of cell lines at single cell resolution, and also examined inhibition of these enzymes using NDGA [18].

Burger et al. further developed the post-like barrier architecture by integrating them onto a rotating chip. This "lab-on-a-disc" operates in a hydrostatic, "stopped-flow" regime to eliminate the need for self-sealing valves to re-direct flow when a cell occupies a trap. Under rotationally induced artificial gravity, cells sediment along straight radial lines until trapped by an empty obstacle termed "V-cup" in their path. Such an innovation notably increases the number of traps with single-cell occupancy. Interestingly, the group also combined the microfluidic chip with a customised "optical tweezers" module. Following distribution and live-cell fluorescent analysis of a cell population, the group could select individual cells of interest from the array and relocate them to a separate reaction chamber on the chip. In the future, such array-based technology may enable systems level translational biology where, for instance, leukocytes from a patient sample can be pre-selected and screened based on membrane markers and fluorescent imaging; from here rare cells can be further individually isolated and removed from the array for subsequent testing [19].

Microfluidic optical tweezers were also combined with microfluidic chips by Eriksson et al. for single cell live-cell systems monitoring of the cycling of fluorescently tagged proteins (Mig1 and MSN2) between the cytosol and nucleus in *S. cerevisiae* cells as environmental glucose levels were adjusted. Here, the tweezers arrayed individual cells in a spatial pattern within a rapidly adjustable chemical gradient. The cycling kinetics of proteins of interest was then monitored in real-time as the gradient was manipulated [20].

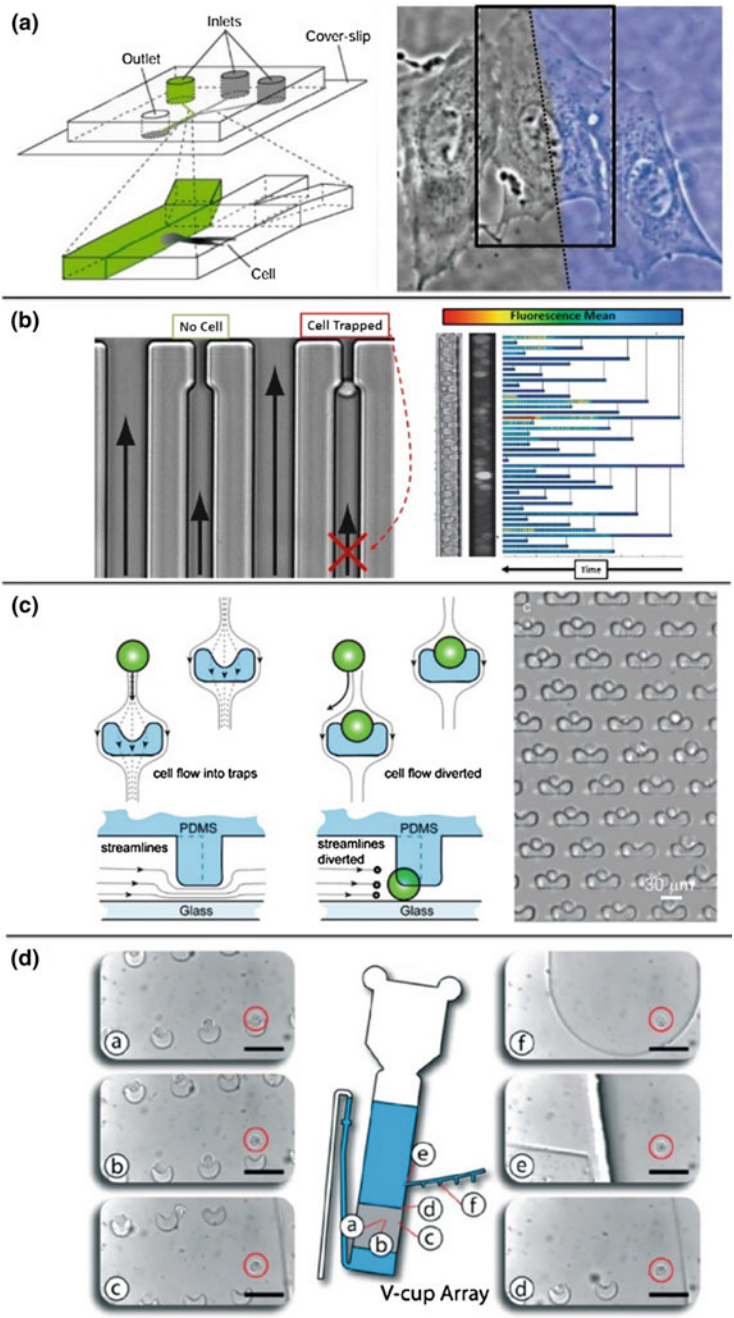
(a)
Inlets
Cover-slip
Outlet
Cell
(b)
No Cell
Cell Trapped
Fluorescence Mean
Time
(c)
cell flow into traps
cell flow diverted
PDMS
streamlines
Glass
PDMS
streamlines diverted
Glass
30 μm
(d)
a
b
c
d
e
f
V-cup Array

◀ **Fig. 4** Examples of microfluidic techniques and strategies used for either segregation of individual cells from a population or chemical treatment of cells at resolutions applicable to systems-level single-cell studies. **a** Demonstration of the minute control of chemical diffusion achieved by Takayama et al. allowing barrier-free chemical gradients to be generated at a subcellular resolution where either side of a single cell is exposed to a different chemistry. The microfluidic architecture is shown on the *left* and an image of the fluidic barrier (*hatched line*) over a single bovine capillary endothelial cell (outlined with a *black box*) is shown on the *right*. **b** Single-cell yeast capture as performed by Rowat et al. in which fluidic streamlines carry a cell to the end of a channel where it blocks an outlet and minimises the probability of further cells entering the channel (*left*). Progeny of the captured cell are confined such that each can be individually monitored in real-time for metabolic events as changes to the environment are induced (*right*) [15]. **c** Flow through arrayed suspended obstacles by DiCarlo et al. designed to direct cells to traps where they (similar to b) block a fluidic outlet thus minimising the chance of further cells resolving to an occupied trap. While in the traps, surrounding chemistry can easily be adjusted and live imaging of the cells used to monitor systems level outputs. **d** An adaptation of arrayed obstacles by Burger et al. but carried out on a centrifugal chip under stagnant-flow conditions without the need to control and valve fluidic streamlines. Circled a-f labels indicate the journey of a selected individual cell as it is picked up from its capture trap and relocated to a reaction chamber on the chip for further analysis. (**a**) Reprinted by permission from Macmillan Publishers Ltd: Ref. [13], Copyright 2001. (**b**) Reprinted with permission from Ref. [15], Copyright 2009 National Academy of Sciences, USA. (**c**) Reprinted with permission from DiCarlo et al. Ref. [7]. Copyright 2006 American Chemical Society. (**d**) Reprinted with permission from Ref. [19] Copyright 2015 Royal Society of Chemistry

Another strategy for single cell isolation and reaction monitoring in high throughput involves the use of droplet microfluidics. Here, cells are suspended in an aqueous solution or medium which is then suspended in an immiscible hydrophobic carrier liquid (generally a silicone-based oil). This way the droplets act like reaction chambers to define the physic-chemical microenvironment of each cell. The droplet can then be shuttled and directed along pathways as required using pressure fields imposed by pumps and flows through intersecting channels. Importantly, this architecture allows further chemistries or reagents to be specifically delivered to individual droplets by merging with additional droplets carrying the desired reagent.

Many systems have been developed in which droplet-based microfluidics has leveraged continuous and extremely high-throughput experimentation. Konry et al. used droplet microfluidics to monitor micro-size remodelling of the cytoskeleton and microtubule polymerization in dendritic cells at the immunological synapse formed between co-encapsulated pairs of live dendritic cells and CD4 + T cells in droplets [21]. Other groups have also integrated high-throughput droplet sorting on chip-based systems, e.g. to remove empty droplets or to select droplets containing cells of interest based on the presence of a particular fluorescent marker [22]. These strategies are shown in Fig. 4.

3 Biological Systems Used for Single Cell Systems Biology

In addition to the selection of an appropriate method of identifying and/or isolating single cells for use in systems level studies, the types of biological assays and chemistries that are to be incorporated to the study need to be taken into account to avoid compromising the quality of data. Non systems-level experiments may be considered to offer more freedom to apply well established bioassays to cell studies as these often investigate pathways at fixed points in time or even in fixed cells that are no longer alive and thus ceased to metabolise. For real-time, multi-parameter systems investigations, particularly in single cells, assays must be selected where the chemistry used to adjust or monitor the experimental environment must not interfere with the continuous output generated by the experimental cell in an uncontrollable way.

A number of strategies exist for such studies, and are frequently designed to allow a molecular switch within a cell to be activated at a specific experimental point in time. This can then coincide with the activation of multi-channel, real-time monitoring of diverse cellular events such as dynamic expression of genes of interest, physical re-structuring or movements of the cell, bio-physical reactions of the cell, or secretion of molecules into the surrounding environment—to name but a few. These experimental designs can become quite complex and can require highly multidisciplinary collaboration. For example, stable transfection and cloning of new cell lines may be required to enable the cells to switch characteristic molecular pathways in a time-dependent manner, while high-resolution real-time microscopy is then required to follow the multi-point data emerging from these cells over time. When developing novel experiments and platforms, partnering with researchers carrying competence with the design engineering of microfluidic architectures (or other methods of single-cell resolution data acquisition) is required to tailor the test-platform to the targeted outputs of the research.

3.1 Quantitatively Monitoring the Fate of Single Cells Through Time: Example of Protein-based Systems Experimentation

Classical protein investigations in bulk and/or fixed time-point studies often involve the labelling of target proteins with an antibody carrying a fluorescent marker, or alternatively by using cells genetically modified to express a fusion version of the protein of interest with green fluorescent protein (GFP) (or one of its derivatives) expressed at the N- or C-terminal. These events are then either imaged at a given point in time (for example in chemically fixed cells), or measured in the bulk sample. Yet, in systems-level studies, these techniques are less powerful as phenotypical changes in response to the protein of interest are difficult to elucidate as the entire pool of the protein is constantly labelled. Recently, a novel type of

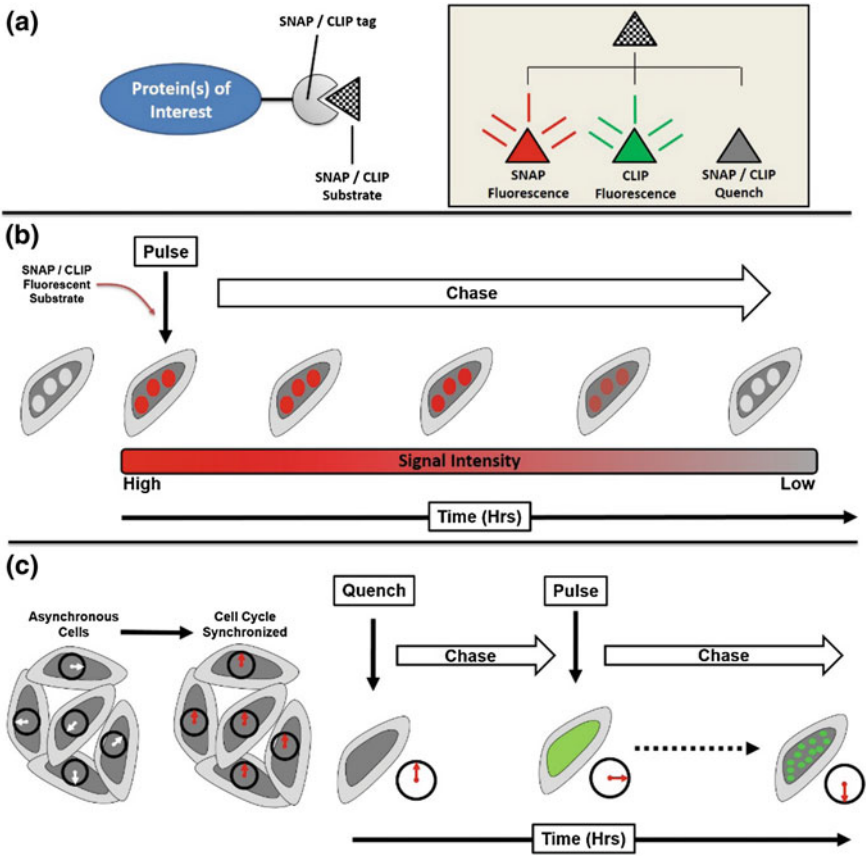

Fig. 5 The use of SNAP /CLIP tagging strategy to follow the dynamic fate of proteins in a single cell over long time scales. **a** SNAP/CLIP tagged protein of interest represented schematically. The various forms of the binding substrate are shown in the *greyed box*. **b** Experimental representation of a Pulse-Chase single cell investigation. Here, a protein of interest is monitored as the pool of protein in the cells at a point in time is fluorescently labelled and the diminishing fluorescence is measured over time in a single cell (to investigate protein turnover) or across cell generations (to investigate physical inheritability of the protein). **c** Experimental representation of a Quench-Chase-Pulse single cell investigation. Cell cycles in a population are synchronised (or the position in the cell cycle is otherwise measured for single cells) and the current pool of the protein of interest is quenched. The protein expressed in a selected window is fluorescently labelled, and the fate of this pool is monitored in time

molecular tag has been developed that can be biologically cloned onto a protein of interest and expressed (either stably or transiently) in a cell line. This tag (called SNAP-tag) provides a powerful tool for monitoring and tracking protein dynamics and half-life within living cells over longer intervals.

SNAP (Fig. 5a) is a genetically encoded protein derived from the human DNA repair enzyme O6-alkylguanine-DNA alkyl transferase (hAGT), and acts as a

suicide enzyme protein fusion tag that catalyses its own covalent binding to benzylguanine (BG), and its fluorescent derivatives [23]. Unlike most GFP-based fluorescent proteins; SNAP is therefore not, in itself, fluorescent but it can bind, under given experimental conditions, to a number of cell-permeable chemical derivatives that provide signals that can be followed in real time. More recently, a second tag similar to SNAP which uses distinct binding chemistry has become available, called CLIP-tag. Employing SNAP and CLIP in conjunction has allowed simultaneous labelling of two proteins of interest in the same cell, and concurrently follow the dynamic fates of them in real-time. There are two primary modes of use for SNAP/CLIP that are used in single cell systems level studies—Pulse-Chase labelling (Fig. 5b), and Quench-Chase-Pulse labelling (Fig. 5c).

In SNAP, Pulse-Chase labelling of live cells, protein(s) of interest are expressed in the cell with the SNAP tag expressed. At a specific time in the experiment, a fluorescent substrate is added to the cell medium that will bind the current pool of SNAP-tagged protein in the cell, thus rendering them detectable by real-time fluorescent microscopy. When the cells are exposed to the substrate for a defined, short interval, only the pool of protein that was present during exposure will be labelled, while fluorescence is absent on new protein that is expressed after removal of the substrate. This way changes in location, kinetics and turnover of this labelled pool of protein can be recorded without interference from any newly expressed protein expressed at a later stage.

As well as monitoring the turnover of a specific pool of a protein of interest in a cell, SNAP Pulse-Chase also allows tracking of the labelled pool of a given protein of interest to be followed through cellular generations, either by real-time monitoring in long-term experiments, or at fixed time-points in the pulsed cell and in its progeny. The SNAP tag method has proven invaluable in studying the highly complex biochemical system found at chromosomal centromeres. Using SNAP/CLIP Pulse-Chase strategies, Prendergast et al. [24]. and Bodor et al. [25] demonstrated the dynamic nature of the multi-faceted mechanism of centromere inheritance by characterising a number of the centromeric proteins as either physically inherited by daughter cells (such as CENP-A/Histone H.3), or non-inherited (such as CENP-T and CENP-W).

By additional use of an irreversible SNAP/CLIP substrate that is non-fluorescent, a Quench-Chase-Pulse labelling strategy can also be utilised. This allows serial labelling of SNAP-tagged proteins of interest, thus resolving when pools of a protein were expressed in a cell. At the beginning of an experiment, the cell is transiently exposed to the non-fluorescent substrate, known as the quench. This prevents the detection of the current pool of SNAP-protein in the cell. Following an experimentally selected interval (chase), the cells are then transiently exposed to the fluorescent substrate which will label only the protein pool that has been expressed since the end of the quench. When researchers couple this technique with the examination of individual cells in which the phase in the cell cycle is known, or the cell(s) have been synchronised prior to the quench, the timing of protein activity (loading, foci formation, co-localisation with other proteins) within a cell can be elucidated with great precision.

3.2 *Quantitatively Monitoring the Fate of Single Cells: Example of mRNA-Based Systems Experimentation*

The detection and monitoring of specific mRNAs in individual cells proves to be challenging, even if performed at a single target level. One of the more common methods of such investigations is the modification or adaption of an mRNA binding protein to generate a fluorescent signal upon binding to the specific mRNA of interest, thus allowing localisation of the mRNA species. However, this method is limited by the specificity of the binding protein for the targeted mRNA, often leading to inaccurate results. This can be overcome by a so-called MS2 system by modifying the gene for the mRNA of interest to co-transcribe an additional sequence known as the MS2 binding sequence (MBS). When an RNA binding protein (MCP) that specifically targets this sequence is modified to carry a fluorescent signal, the mRNA of interest can be measured in real time.

However, due to limitations arising from the number of fluorescent versions of the MCP protein, simultaneous monitoring is restricted to 3–4 mRNAs in a single cell, thus precluding the systems researcher to perform a comprehensive analysis of a large family of mRNAs simultaneously in a single cell. Another mRNA tracking method uses fluorescent in situ hybridisation (FISH) whereby an ssDNA probe with complimentary sequence can fluorescently label the mRNA of interest. The specificity of FISH probes to targeted mRNA is high, but generally restricted to two colours. Therefore, FISH is less amenable to multi-parameter systems biology that would require a larger number of mRNAs to be monitored simultaneously.

Recent developments by Lubeck et al. [26] have modified the FISH method to allow monitoring of up to 35 mRNAs. As opposed to the MS2 system, the cells must be fixed. However, the number of mRNAs that can be visualised simultaneously provides an experimental paradigm where multiple time-points are isolated and processed to allow the construction of a systems level kinetic model of gene expression. The method developed is an exemplary case for the interdisciplinary collaboration as key prerequisite of systems biology. The strategy necessitates application of technologically advanced Super-Resolution Microscopy (SRM) which can measure optical events emitted from features as small as 10–20 nm, and a number of photo-switchable fluorophore pairs that can be detected using SRM. Rather than using a single colour throughout the length of the ssDNA probe, barcodes based on three out of seven available colours are positioned along the probe at a resolution detectable by SRM. This allows biological experimentation in which a large number of specifically identifiable probes can be multiplexed in the same cell to follow the expression of a collection of genes related to a particular biological question through FISH hybridisation. Finally, due to the large amount of 3-dimensional (or 4-dimensional if time was included) data that must be processed to generate a model of the spatial arrangement of the targeted genes in the cell, an imaging method called stochastic optical reconstruction microscopy (STORM) is employed to analyse the data. As a proof of principle, the strategy profiled 32 mRNAs involved in the stress response of 60 individual *S. Cerevisiae* cells when exposed to stress-inducing

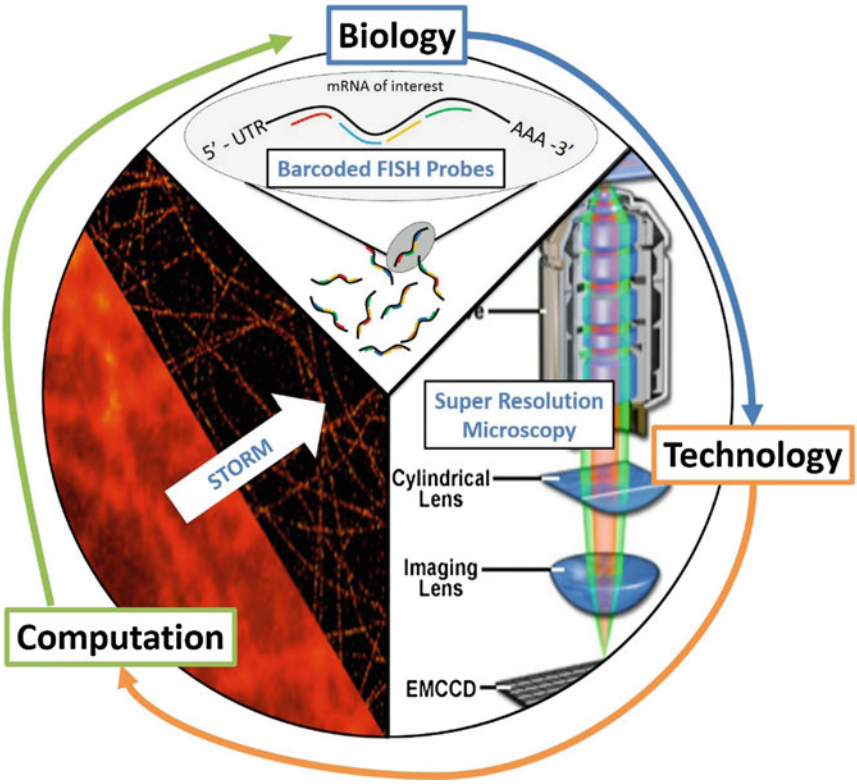

Fig. 6 Multiple modelling of mRNA transcripts as demonstrated by Lubeck et al., but displayed as an exemplary paradigm for the multi-disciplinary nature inherent to successful single cell systems biology. Biological questions are addressed by integrating new chemistries that are detectable using application of high-end technology. Novel computational strategies are devised to model the data acquired from the technology, which shows quantifiable data that loops back to inform new biological questions

concentrations of calcium. Intriguingly, should another colour be added to the barcode palate, in theory up to 792 mRNAs could be concurrently tracked in a single cell (Fig. 6).

4 Optical Detection and Imaging Systems for Single Cell Biology Systems

The final stage concerning single cells for use in systems level studies is a reliable detection/readout method for the resulting outputs of the single cell study. Taking advantage of the optical transparency of cells, light microscopy uniquely provides

non-invasive, 3D imaging of the cell interior. Moreover, specific cellular constituents, such as proteins, nucleic acids, and lipids, can be detected. Developments in the area of lens-based microscopy during the past 15 years have provided methods for investigating life at the subcellular level, discerning details below a quarter of a micrometre [27].

In addition to microscopic-based methods, various flow cytometry, image cytometry, and haematology instruments are also available for analysing cell populations [28, 29]. Typically, a platform is specifically adapted to the field of application, such as immunology, cancer biology, or microbiology. Ideally, these platforms should enhance the understanding of systems biology, across various physiological conditions.

4.1 Lens-Based Microscopic Methods for Single Cell Biology Systems

Numerous concepts have been utilised to "push and break the diffraction barrier" by reducing the focal spot size on lens-based microscopy systems. Single-point systems such as confocal microscopy, 4Pi microscopy and stimulated emission depletion (STED) methods have all become highly utilised in the area of single-cell biology systems. Parallelised systems combining numerous microscopic techniques have also emerged under the general term of reversible saturable, optically linear fluorescence transitions (RESOLFT), which can consist of systems based on STED, ground state depletion (GSD) microscopy, saturated pattern excitation microscopy (SPEM), saturated structured illumination microscopy (SSIM), photo activatable localization microscopy(PALM) and stochastic optical reconstruction microscopy (STORM). A comprehensive review of all of the above microscopic techniques has been presented by Hell [29]. The schemes are illustrated in Fig. 7 and comparisons of single-cell-resolution techniques are outlined in Fig. 8a.

Numerous applications using variations of the microscopy methods described above have been reported in recent years. Rust et al. have reported a high-resolution fluorescence microscopy technique based on STORM principles and the use of photo-switchable fluorophores [30]. The system reports an imaging resolution of 20 nm, which would be ideally suited for imaging single cells and sub-regions of single cells. Dempsey et al. have further evaluated photo-switchable fluorophores and defined a low cross talk, four colour super-resolution imaging system that can be used for single cell biology systems [31]. Schermelleh et al. have presented a comprehensive guide to super-resolution fluorescence microscopy and examples of the capability of such systems in the area of single cell biology systems are illustrated in Fig. 8b [32].

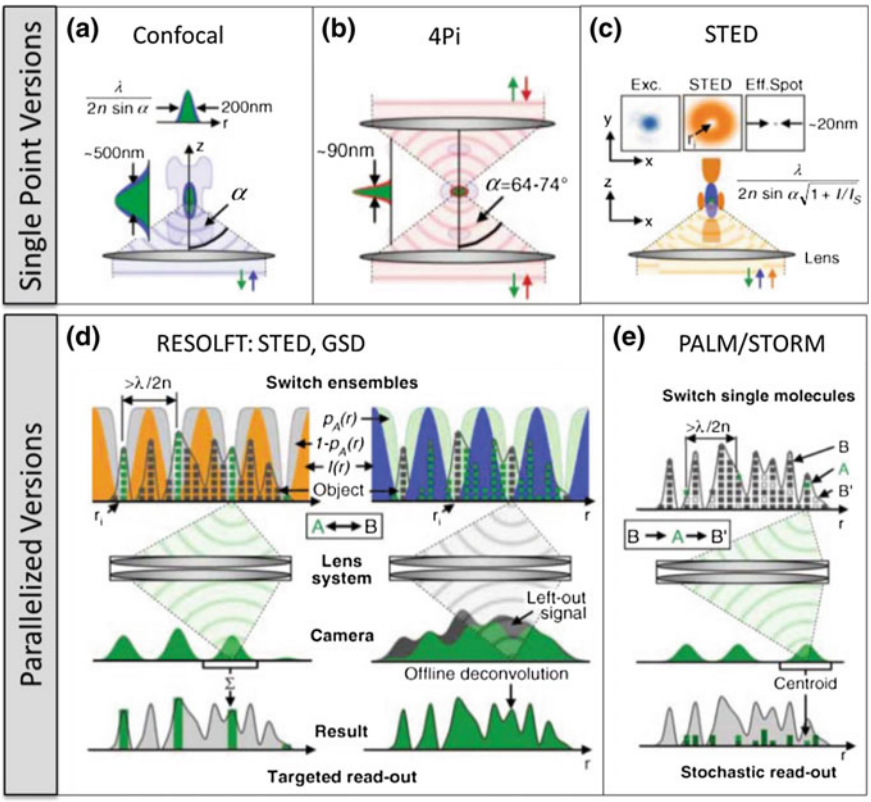

Fig. 7 Fluorescence nanoscopy schemes: single-point scanning (*upper row*) and parallelised versions (*lower row*). **a** Confocal microscopy. **b** By combining the wave front caps of two opposing lenses, 4Pi microscopy produces a narrower spot along the z-axis and hence an improved z resolution of 80–150 nm. **c** A typical single-point scanning STED microscope. **d** RESOLFT principle, corresponding to a parallelized STED, GSD, or photo-switching approach (on the *left*) and to the SPEM concept (on the *right*). **e** PALM and STORM read out the fluorophore molecules stochastically; the molecules must be switchable. From Hell et al. Ref. [27]. Adapted with permission from AAAS

4.2 *Cytometry-Based Methods for Single Cell Biology Systems*

Whilst they have found numerous applications in cell population analysis, ideal cytometry methods for single cell biology methods would incorporate imaging techniques (to obtain information on cell morphology) and absolute cell counts (similar to haematology systems).

Kantor et al. have reported a system where, in contrast to standard flow cytometry methods, the laser scans over stationary cells rather than cells flowing past the laser by using disposable capillary arrays instead of cytometry tubes or

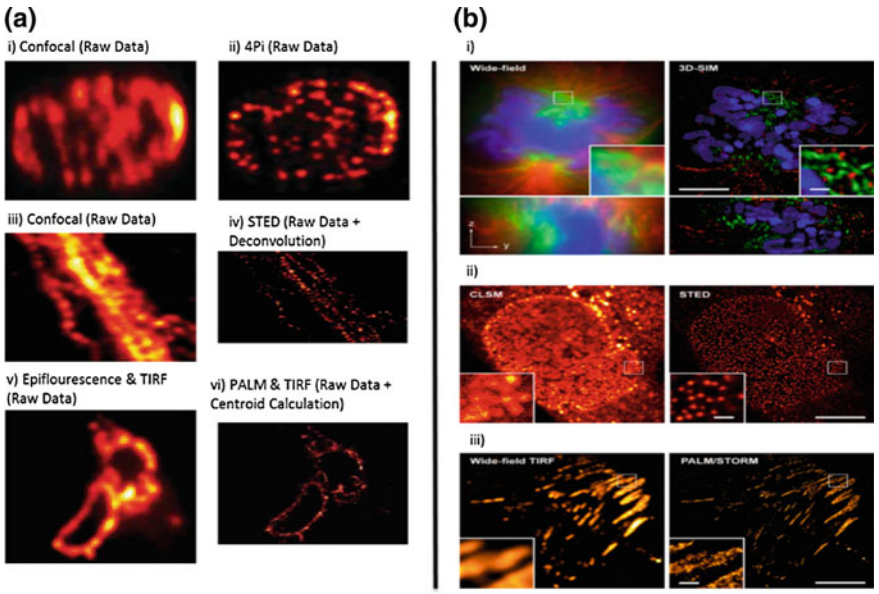

Fig. 8 **a** Comparison of single point and parallelised microscopy imaging for single cell biology systems. Images of microtubules in a neuron recorded with (i) confocal microscopy and (ii) 4Pi axial microscopy. Neurofilamentsin human neuroblatoma recorded with (iii) confocal microscopy and (iv) STED with nonlinear deconvolution. (v) Epifluorescence and (vi) PALM with centroid calculation, recording of a cryo prepared section from a mammalian cell (both images were recorded with a TIRF setup). **b** Super-resolution microscopy of biological samples. (i) Conventional wide-field image (*left*) and 3D-SIM image of a mouse C2C12 prometaphase cell stained with primary antibodies against lamin B and tubulin, and secondary antibodies conjugated to Alexa 488 (*green*) and Alexa 594 (*red*), respectively. Nuclear chromatin was stained with DAPI (*blue*). The bottom panel shows the respective orthogonal cross sections. (ii) HeLa cell stained with primary antibodies against the nuclear pore complex protein Nup153 and secondary antibodies conjugated with ATTO647 N. (iii) TdEosFP-paxillin expressed in a Hep G2 cell to label adhesion complexes at the lower surface. *Bars* 5 µm (insets, 0.5 µm). (**a**) From Hell et al. Ref. [27]. Adapted with permission from AAAS. (**b**) Reprinted from Ref. [32] Copyright 2010 The Rockefeller University Press

microscope slides [33]. A small cylindrical laser beam is scanned through the capillary in one direction while the capillary is translated relative to the optical detection system in a second, orthogonal direction. By scanning a predetermined volume for each capillary, absolute cell counts are obtained directly. In this respect, the system operates similar to haematology analysers [29], but different from laser scanning systems that focus on high-throughput screening [34], cell morphology [35], or rare cell [36] applications.

Over the past years numerous imaging cytometry systems have emerged, which integrate high-resolution microscopy imaging features into a flow cytometry instrument [8, 37] obtained from an imaging cytometry system is illustrated in Fig. 9, along with combinatorial imaging and fluorescence testing at single cell

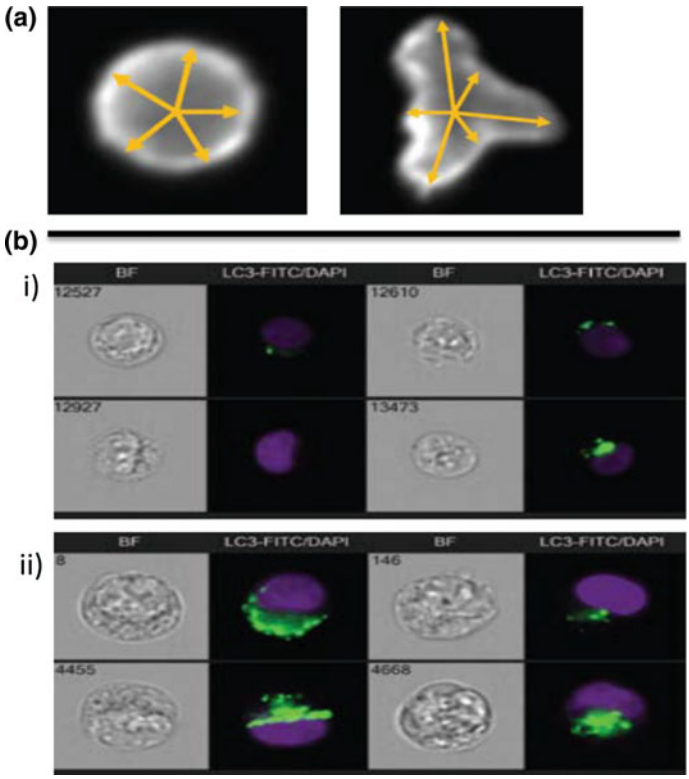

Fig. 9 **a** Cell morphology images for single primary monocytes having undergone drug treatment. **b** Representative bright-field images and merged florescence images for K562 cells in (i) control state and (ii) treated with etoposide to induce autophagy. Copyright Amnis Corporation, Seattle, WA, U.S.A Ref. [37]

resolution. Such systems can play a key role in single-cell biology systems as they can isolate single cells within a population whilst operating in a similar manner to a standard flow cytometer.

5 Conclusions and Outlook

The breadth of information produced in a modern biological science research laboratory is quite overwhelming when compared to that produced as recently as 10 years ago. Super-high throughput instrumentation, smart auto-targeting microscopy stages, imaging platforms capable of highly multiplexed optical investigations, and novel chemistries have all contributed to placing a vast amount of data into the hands of a researcher from even a single experiment. The age of "Big Data"

has certainly transformed the landscape of biology and applied medicine. It has brought it from a point where the identification of a single gene or epigenetic marker could send waves of excitement throughout the community, to where a complex assembly of interdependent cellular events can be elucidated by a single researcher; and where an entire genome can be sequenced overnight. It is rare that a researcher (or group) will have the full complement of staff with the necessary skills to (a) efficiently design a novel and massive throughput experiment, (b) develop novel instruments to carry out the experiment, and (c) mathematically analyse the considerable amount of data that ensues. The systems biology community has provided a framework whereby affiliation between groups with these skills can meet with a common goal, rather than each group seeking to acquire the skills in-house. This has allowed biological progress to keep up with the rapid expansion of capabilities in the mathematical and engineering sciences.

Single cell studies represent an area where systems biology can be applauded as a prime enabling strategy to advance cell biology to a new level. Single cell investigations have existed before the systems approach, and conversely systems biology has successfully been applied to multi-cellular studies. However, by illuminating and quantifying the rare but highly complex biochemical events that occur within an individual cell in a large population, combining the two has allowed new insights into the genesis of cellular diseases such as cancer. Population-based studies will often miss or marginalise important rare events, while non-systems level studies can focus too minutely on components of a defective biochemical system and hence miss the subtlety that leads to disease. Not all studies will require a systems level approach, or single cell resolution, but those that do now have the tools and framework to help steer biology and medicine to new and exciting insights.

References

1. Westerhoff HV, Alberghina L (2005) Systems biology: did we know it all along? Anonymous Syst Biol Springer:3–9
2. Mast FD, Ratushny AV, Aitchison JD (2014) Systems cell biology. J Cell Biol 206(6):695–706. doi:10.1083/jcb.201405027
3. Short B (2009) Cell biologists expand their networks. J Cell Biol 186(3):305–311. doi:10.1083/jcb.200907093
4. Tay S, Hughey JJ, Lee TK et al (2010) Single-cell NF-[kgr] B dynamics reveal digital activation and analogue information processing. Nature 466(7303):267–271
5. Cheong R, Bergmann A, Werner SL et al (2006) Transient Ikappa B kinase activity mediates temporal NF-kappaB dynamics in response to a wide range of tumor necrosis factor-alpha doses. J Biol Chem 281(5):2945–2950. M510085200 [pii]
6. Lahav G, Rosenfeld N, Sigal A et al (2004) Dynamics of the p53-Mdm2 feedback loop in individual cells. Nat Genet 36(2):147–150
7. Di Carlo D, Wu LY, Lee LP (2006) Dynamic single cell culture array. Lab Chip 6(11):1445–1449

8. Bonetta L (2005) Flow cytometry smaller and better. Nat Methods 2(10):785–795. doi:10.1038/nmeth1005-785
9. Kaczmarczyk A, Sullivan KF (2014) CENP-W plays a role in maintaining bipolar spindle structure. PLoS One 9(10):e106464. doi:10.1371/journal.pone.0106464
10. Yivgi-Ohana N, Eifer M, Addadi Y et al (2011) Utilizing mitochondrial events as biomarkers for imaging apoptosis. Cell Death Dis 2(6):e166. doi:10.1038/cddis.2011.47
11. Breslauer DN, Lee PJ, Lee LP (2006) Microfluidics-based systems biology. Mol Biosyst 2(2):97–112. doi:10.1039/B515632G
12. Lee PJ, Hung PJ, Rao VM et al (2006) Nanoliter scale microbioreactor array for quantitative cell biology. Biotechnol Bioeng 94(1):5–14
13. Takayama S, Ostuni E, LeDuc P et al (2001) Subcellular positioning of small molecules. Nature 411(6841):1016. doi:10.1038/35082637
14. Lucchetta EM, Lee JH, Fu LA et al (2005) Dynamics of drosophila embryonic patterning network perturbed in space and time using microfluidics. Nature 434(7037):1134–1138
15. Rowat AC, Bird JC, Agresti JJ et al (2009) Tracking lineages of single cells in lines using a microfluidic device. Proc Natl Acad Sci U S A 106(43):18149–18154. doi:10.1073/pnas.0903163106
16. Wu H, Wheeler A, Zare RN (2004) Chemical cytometry on a picoliter-scale integrated microfluidic chip. Proc Natl Acad Sci U S A 101(35):12809–12813. doi:10.1073/pnas.0405299101
17. Cai L, Friedman N, Xie XS (2006) Stochastic protein expression in individual cells at the single molecule level. Nature 440(7082):358–362
18. Di Carlo D, Aghdam N, Lee LP (2006) Single-cell enzyme concentrations, kinetics, and inhibition analysis using high-density hydrodynamic cell isolation arrays. Anal Chem 78(14):4925–4930
19. Burger R, Kurzbuch D, Gorkin R et al (2015) An integrated centrifugo-opto-microfluidic platform for arraying, analysis, identification and manipulation of individual cells. Lab Chip 15(2):378–381
20. Eriksson E, Sott K, Lundqvist F et al (2010) A microfluidic device for reversible environmental changes around single cells using optical tweezers for cell selection and positioning. Lab Chip 10(5):617–625
21. Konry T, Golberg A, Yarmush M (2013) Live single cell functional phenotyping in droplet nano-liter reactors. Sci Rep:3. doi:10.1038/srep03179
22. Mazutis L, Gilbert J, Ung WL et al (2013) Single-cell analysis and sorting using droplet-based microfluidics. Nat Protoc 8(5):870–891
23. Gautier A, Juillerat A, Heinis C et al (2008) An engineered protein tag for multiprotein labeling in living cells. Chem Biol 15(2):128–136
24. Prendergast L, Van Vuuren C, Kaczmarczyk A et al (2011) Premitotic assembly of human CENPs-T and-W switches centromeric chromatin to a mitotic state. PLoS Biol 9(6):e1001082
25. Bodor DL, Valente LP, Mata JF et al (2013) Assembly in G1 phase and long-term stability are unique intrinsic features of CENP-A nucleosomes. Mol Biol Cell 24(7):923–932. doi:10.1091/mbc.E13-01-0034
26. Lubeck E, Cai L (2012) Single-cell systems biology by super-resolution imaging and combinatorial labeling. Nat Methods 9(7):743–748
27. Hell SW (2007) Far-field optical nanoscopy. Science 316(5828):1153–1158. 316/5828/1153 [pii]
28. Shapiro HM (2005) Practical flow cytometry. Wiley, Hoboken
29. Groner W, Simson E (1995) Practical guide to modern hematology analyzers. Wiley, England
30. Rust MJ, Bates M, Zhuang X (2006) Sub-diffraction-limit imaging by stochastic optical reconstruction microscopy (STORM). Nat Methods 3(10):793–796
31. Dempsey GT, Vaughan JC, Chen KH et al (2011) Evaluation of fluorophores for optimal performance in localization-based super-resolution imaging. Nat Methods 8(12):1027–1036
32. Schermelleh L, Heintzmann R, Leonhardt H (2010) A guide to super-resolution fluorescence microscopy. J Cell Biol 190(2):165–175. doi:10.1083/jcb.201002018

33. Kantor AB, Alters SE, Cheal K et al (2004) Immune systems biology: immunoprofiling of cells and molecules. Biotechniques 36(3):520–525
34. Zuck P, Lao Z, Skwish S et al (1999) Ligand-receptor binding measured by laser-scanning imaging. Proc Natl Acad Sci U S A 96(20):11122–11127
35. Kamentsky LA (2000) Laser scanning cytometry. Methods Cell Biol 2001(63):51–88
36. Tibbe AG, de Grooth BG, Greve J et al (1999) Optical tracking and detection of immuno magnetically selected and aligned cells. Nat Biotechnol 17(12):1210–1213
37. Amnis Corporation, Seattle, WA, U.S.A. https://www.amnis.com/documents/brochures/ISX-MKII%20Brochure_Final_Web.pdf

Electroporation for Single-Cell Analysis

Tuhin Subhra Santra and Fan-Gang Tseng

Abstract Single-cell analysis is a powerful technique to understand cell to cell or cell to environment behaviors. It can provide detailed information of cell proliferation, differentiation, and different responses to external stimuli and intracellular reactions. For single cell analysis, electroporation or electropermeabilization is an efficient and fast method, where high external electric field is applied on cell membrane to form transient membrane pores to deliver ions or molecules in or out of the cell. Conventional electroporation or bulk electroporation (BEP) is performed in a batch mode with millions of cells in suspension, which can only provide an average value. Since the last decade, microfabricated devices have been developed to perform single cell electroporation, where electric field is only intense on a single cell, resulting in high transfection efficiency with high cell viability compared to BEP. Single cell analysis using electroporation technique can be performed with microfabricated electrode arrays, carbon fiber microelectrodes, micropipettes or electrolyte-filled capillaries-based devices. Recently developed nanofabricated electrodes can realize localized single cell electroporation for delivery of different molecules with high transfection efficiency and high cell viability. Thus, single cell electroporation technique opens up the new window for the manipulation of genomics, proteomics, trascriptomics, metabolomics, or fluxomics at single cell level. This chapter emphasizes the recent advancement of electroporation technique

T.S. Santra
California Nano System Institute, University of California at Los Angeles, Los Angeles, USA

T.S. Santra (✉) · F.-G. Tseng
Department of Engineering and System Science, National Tsing Hua University, Hsinchu, Taiwan
e-mail: santra.tuhin@gmail.com

F.-G. Tseng
Institute of Nano Engineering and Microsystems, National Tsing Hua University, Hsinchu, Taiwan

F.-G. Tseng (✉)
Division of Mechanics, Research Center for Applied Sciences, Academia Sinica, Taipei, Taiwan
e-mail: fangang@ess.nthu.edu.tw

F.-G. Tseng and T.S. Santra (eds.), *Essentials of Single-Cell Analysis*,
Series in BioEngineering, DOI 10.1007/978-3-662-49118-8_3

for cellular delivery and the analysis method which might be potentially applicable for biological research and therapeutic applications.

Keywords Bulk electroporation (BEP) · Single cell electroporation (SCEP) · Localized single cell electroporation (LSCEP) · Electroporation parameters · Single cell intracellular delivery · Single cell extracellular delivery · Transfection efficiency · Cell viability

1 Introduction

Cell is the fundamental building block of life and it always plays a significant role by coordinating with each other to perform systematic functions in living creatures. However, the behaviors of cell to cell or cell to the environment with their organelles and their intracellular physical/biochemical/biological effects are still unknown. Thus, single cell analysis is of great interest to analyze cell to cell behavior with different kinds of disease such as cancer metastasis or drug response of tumor cells [1–4], whereas the bulk measurement with millions of cells can only provide averaged data with low sensitivity [5, 6]. Many transfection techniques have been developed including viral vectors [7, 8], chemical methods such as calcium phosphate or basic proteins [9], and physical methods including particle bombardment [10], microinjection [11], sonoporation [12] and lipid mediated entry into cells [13]. However most of these techniques are bulk measurement of a large number of cells except microinjection technique. In contrast, electroporation technique is an efficient and fast method, where high external electric field is applied on the cell membrane causing the increase of electrical permeability and conductivity due to structural change of the cell membrane and resulting in the formation of transient hydrophilic membrane pores from initially formed hydrophobic pores [14–20]. The transient hydrophilic membrane pores are able to deliver different kinds of cargos such as drugs, antibodies, DNA, RNA, dyes, oligonucleotides from outside to inside of the cell [14, 15, 21–23] or intracellular biochemical compounds from inside to outside of the cell [24, 25]. Due to different intracellular and extracellular conductivities, cell membrane acts as a capacitor to store electrical charge [26]. This difference is called transmembrane potential (TMP), which can be expressed by Schwan's equation as

$$\mathrm{TMP} = \phi_i - \phi_e = 1.5\, rE_0 \cos\theta$$

where $\varphi_i - \varphi_e$ is the potential difference between intracellular and extracellular membrane, r is the radius of the cell, E_0 is the strength of the applied electric field and θ is the angle between direction of electric field and the selected point of the cell surface [27, 28]. The first concept of discharge of the static electric field on the

skin was studied in 1754 [29]. Later in 1898, Fuller et al. reported that multiple high voltage discharge has bacterial effect on water sample [30]. The effect of electric field on living cells (i.e., in vitro reversible and irreversible electrical breakdown of cell bilayer lipid membrane) has been studied during 1900s–1970s [16, 31–39]. Later, first custom-built electroporation chamber was developed by Neumann et al. in 1982 to study gene transfer on murine cell [40].

The electroporation technique offers several advantages in comparison with conventional gene transfer technique such as technical simplicity, ease of handling with greater reproducibility, high transfection efficiency when compared with $CaCl_2$ and PEG-mediated chemical transformation. Through tuning the electrical parameters, the position and size of the electropores can be controlled; therefore the leakage of the cytosolic components can be minimized. The size of the affected membrane area and the delivery rate of DNA/RNA into cells can also be controlled [14, 15, 41–48]. In bulk electroporation (BEP) or conventional electroporation, where two large electrodes produce a homogeneous electric field surrounding the suspension of millions of cells together, resulting in the elucidation of cellular function with an average value. Moreover, due to the larger surface area of electrodes, BEP requires higher voltage and thus during the experiment it can generate local PH variation, electric field distortion, sample contamination, higher thermal effect, which will increase the cell toxicity and decrease the cell viability [49–51]. Since the last decade, due to the rapid progress of micro/nanotechnologies, electroporation can be performed at single cell level with micro/nanofabricated devices (named single cell electroporation (SCEP)), where an inhomogeneous electric field is intense on a single cell, resulting in high transfection efficiency with high cell viability compared to BEP [52–55]. Micro/nanofluidic devices with microscale electrodes promote faster heat dissipation and minimize heat generation [56]. Moreover, in the last couple of years, another advanced technique called localized single cell electroporation (LSCEP) has been developed, using this technique the electric field can be localized on the desired area (by using nanoelectrodes) of the single cell, resulting in very precise formation of transient membrane pores to deliver ions or molecules in or out of the cell with high transfection efficiency and high cell viability compared to SCEP or BEP [15, 43, 47, 48, 57–63]. LSCEP also can be performed using Atomic Force Microscopy (AFM) [64], nanochannel-based ion transportation [65], or nanofountain probe electroporation [66], instead of using nanoelectrodes. The LSCEP technique has some promising features such as low voltage and low power requirement, low toxic effect due to negligible ion and bubble generation, small sample volume, and negligible heat generation. These features are essential to achieve high transfection efficiency with high cell viability, making LSCEP potentially applicable for various biological research and therapeutic applications. Thus, LSCEP can provide better understanding of intracellular and extracellular delivery with more precise cellular analysis compared to SCEP or BEP.

2 Electric Field Effect on Cell Membrane

One of the most promising approaches to control electroporation efficiency is to vary the parameters of external electric field such as field strength, pulse duration, number of pulses, time between two pulses, etc. The geometrical shape of the cell is important to induce transmembrane potential (TMP) to permeabilize ions or molecules in or out of the cell. Biological systems are mainly heterogeneous from electrical point of view [67, 68]. When short and intense electric field pulses are applied across the cell membrane, the conductivity of cell cytoplasm and extracellular medium is several orders of magnitude higher than cell membrane, as a result the membrane acts as the dielectric material or like a charging capacitor. This dielectric discontinuity affects the electric field distribution. Thus, the lipid vesicle with electric field acting like charging capacitor has extremely short charging time (microsecond).

To consider cell shape as a sphere with volume V, then the total current flows through this small volume must be equal to the net flow of charges or equal to the rate of decrease of charge within volume V. Thus, it can be expressed as

$$I = \int_S J \cdot \mathrm{d}s \tag{1}$$

$$= -\frac{\partial}{\partial t}\int_V \rho \mathrm{d}V \tag{2}$$

This is nothing but the principle of conservation of charge.

To use the divergence theorem, the equation

$$\int_S A \cdot n\mathrm{d}s = \int_V \nabla \cdot A\mathrm{d}V$$

can be written as

$$\int_V \nabla \cdot J\mathrm{d}V = \int_V \frac{\partial \rho}{\partial t}\mathrm{d}V \tag{3}$$

where J is the current density and ρ is the volume charge density. Now equation [3] becomes

$$\int_V \left(\nabla \cdot J + \frac{\partial \rho}{\partial t}\right) \mathrm{d}V = 0 \tag{4}$$

Since equation [4] must be true irrespective of the volume and it can be written as

$$\nabla \cdot J + \frac{\partial \rho}{\partial t} = 0 \tag{5}$$

This is the equation of continuity, which is nothing but the principle of conservation of charge where steady current involves $\frac{\partial \rho}{\partial t} = 0$ and if charges are not generated into the cell during application of the electric field pulses, then $\nabla \cdot J = 0$. Now electric field is the gradient of electric potential, then Maxwell equation becomes $\Delta^2 \psi = 0$, where Ψ denotes the electrical potential. If the conductivity of the cytoplasm and the external medium is several orders of magnitude higher than the cell membrane, then $\Delta \Psi_E$, the field-induced TMP can be written as:

$$\Delta \psi_E = 1.5 a_{\text{cell}} E_e \cos\theta \tag{6}$$

where a_{cell} is the outer radius of the cell, E_e is the applied electric field strength and θ is the angle between field line and normal to the point of interest at the membrane which can either be 0° or 180° [69–72]. Under the ideal experimental conditions like electric field, pulse width, pulse duration, number of pulses, and removal of external electric field for resealing of the cell membrane and rearrangement of the membrane protein can preserve the cell viability. If the cell is not spherical, for example, if it is considered as an ellipsoid-like structure, then Eq. (6) may not be the right explanation. But for any practical purpose, this equation can be used to evaluate the field-induced TMP. After the application of external electric field, the TMP-induced within very short charging time (microsecond range) can be expressed as [18, 73–75].

$$\Delta \psi_E(t) = 1.5 a_{\text{cell}} E_e \cos\theta (1 - \exp .(-t/\tau)) \tag{7}$$

Here τ is the charging time which depends on the dielectric properties of the cell membrane. If we consider membrane as a pure dielectric, then τ can be written as

$$\tau = a_{\text{cell}} C_{\text{memb.}} (\lambda_{\text{int.}} + 2\lambda_{\text{out}}) / (2\lambda_{\text{int.}} \lambda_{\text{out}}) \tag{8}$$

This is calculated on the order of microseconds, where $\lambda_{\text{int.}}$ and λ_{out} is the conductivity of intracellular (cell cytoplasm) and extracellular medium. $C_{\text{memb.}}$ is the membrane capacitance per unit area and a_{cell} is the radius of the cell. The charging time can be measured experimentally by fluorescence video [76]. The field-induced

TMP and charging time (τ) can be evaluated by using AC electric field with frequency less than 1 MHz and rectangular electric pulses longer than 1 μs.

The potential difference ($\Delta\psi$) across the cell membrane consists of natural ($\Delta\psi_0$) and field-induced TMP ($\Delta\psi_E$). Thus, the total potential difference across the cell membrane can be expressed as

$$\Delta\psi = \Delta\psi_0 + \Delta\psi_E \tag{9}$$

The natural membrane potential is metabolically maintained in living cell membrane to provide power to the cell or to transmit signal. Typically it is −40 to −60 mV, whereas the potential of the outside surface of the cell membrane is taken to be zero [18, 77, 78]. Golzio et al. [79], experimentally showed the fluorescence uptake of CHO-K1 cell, which was correlated with Eqs. (6) and (9).

After the application of a short and intense electric field, cell membrane acts as a charging capacitor, because of its dielectric behavior. When total membrane potential ($\Delta\psi$) exceeds a threshold value, transient hydrophilic pores can be generated to transport ions or molecules from outside to inside of the cell. Typically ($\Delta\psi$) varies from 0.2 to 1 V. Figure 1 shows the electric field distribution within a cell, where the induced TMP is higher at the poles and lower at the equator.

The essential features of electroporation include (a) application of short electric pulse (b) charging of lipid bilayer membrane (c) structural rearrangement of the cell membrane resulting in reorientation of phospholipids (d) transitions to water-filled membrane structures, which can perforate the membrane ("aqueous pathways" or "hydrophilic pores") and (e) increase in molecular and ionic transportation [17, 80–83]. During the charging of the membrane as a capacitor, positive and negative charges will accumulate at the poles facing anode and cathode, respectively.

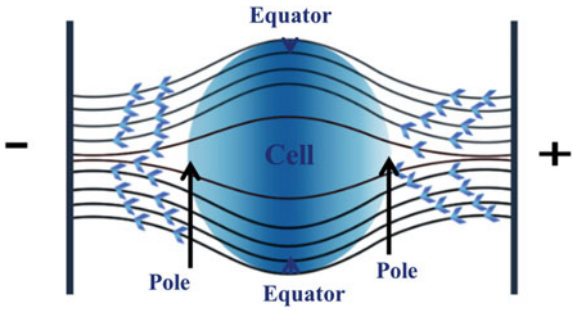

Fig. 1 Electric field distribution within a cell where field-induced TMP is higher at the poles and lower at the equator

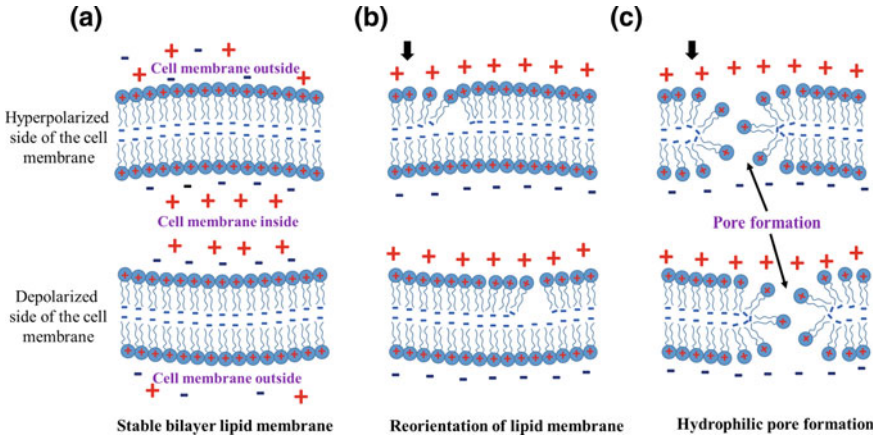

Fig. 2 Reorientation of phospholipids in depolarized and hyperpolarized sides of a bilayer lipid membrane under a threshold electric field. The arrows in (**b**) and (**c**) indicate the directions of the applied electric field. Figure has been redrawn from Refs. [83–87]. **a** Without electric field, **b** with electric field, **c** sustained electric field

Generally, the pole close to the cathode is depolarized ($\theta + \pi$) while the pole close to the anode is hyperpolarized ($\theta = 0$). Figure 2 shows the reorientation of the phospholipids within cell membrane to form transient membrane pores due to the threshold electric field for both depolarized and hyperpolarized membrane.

The total potential ($\Delta\psi$) is higher at hyperpolarized pole due to negative natural ($\Delta\psi_0$) potential and thus electroporation initiates at the pole facing anode instead of the pole facing cathode, as a result the transient pore formation starts at anode. Figure 2a shows the stable hyperpolarized or depolarized side of the lipid bilayer membrane without the application of an external electric field. Whereas Fig. 2b shows the reorientation of phospholipids due to the application of an external electric field (total potential must reach the membrane threshold potential) and it can be seen that the reorientation has a greater impact on the hyperpolarized side of the membrane (at anode). Figure 2c shows the formation of hydrophilic membrane pores due to the application of a sustained electric field [87]. By maintaining the threshold voltage with an external electric field, the pore size and the number of pores can be maintained. However, pore size depends upon the electric field strength, number of pulses, duration of pulses, surface tension of the cell membrane and induced transmembrane potential [43–46]. It has been reported that pores with higher density and smaller size were created at anode side, while pores with lower density and larger size were created at cathode and equator position of the cell (see Fig. 1). However, with altered polarities after each experiment, the density and size of the pores can be maintained at poles to improve delivery efficiency and cell viability [78, 88, 89].

3 Bulk Electroporation, Single Cell Electroporation and Localized Single Cell Electroporation

3.1 Conventional or Bulk Electroporation (BEP)

In bulk electroporation or electropermeabilization, where a high external electric field (KV cm^{-1}) with short pulses is applied to the suspension of millions of cells inside a cuvette embedded with large electrodes in different shapes and sizes. These electrodes are mainly fabricated with alumina (Al), platinum (Pt), graphite or stainless steel, depending upon experimental conditions and cuvettes. Due to the high inhomogeneous electric field, induced membrane potential can easily overcome the threshold value, resulting in the formation of transient hydrophilic pores to transport ions or molecules in or out of the cell. Figure 3a shows the cuvette with suspensions of millions of cells in between two electrodes with large surface area. In Fig. 3b, cells are suspended inside the cuvette and metal electrodes are incorporated from outside to inside of the cuvette. The gap between two metal electrodes is generally in the millimeter to centimeter range.

This conventional electroporation technique is used widely with controllable electrical parameters to achieve high transfection efficiency with high cell viability [90]. However, due to the large gap between two electrodes with large surface area, higher external electric field causes field distortion, local pH variation and heat generation, resulting in low efficiency with low cell viability.

3.2 Single Cell Electroporation (SCEP)

Single cell electroporation (SCEP), where a homogeneous electric field is applied to the single cell with microscale electrodes and the distance between two electrodes is

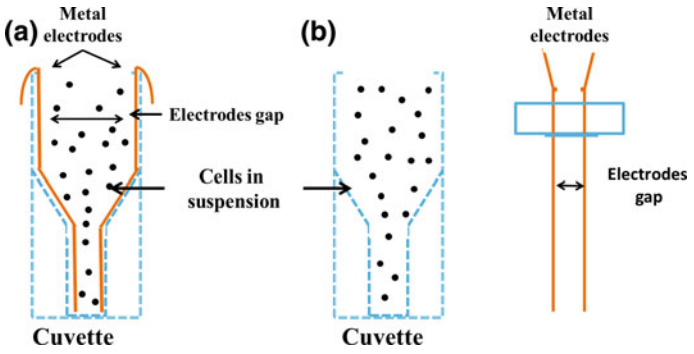

Fig. 3 Bulk electroporation or conventional electroporation apparatus (**a**) cross sectional view of the cuvette with two built-in metal electrodes, where millions of cells are suspended in between (**b**) metal electrodes can be introduced from outside to inside of the cuvette. Permission to reprint obtained from MDPI Publisher Ltd [15]

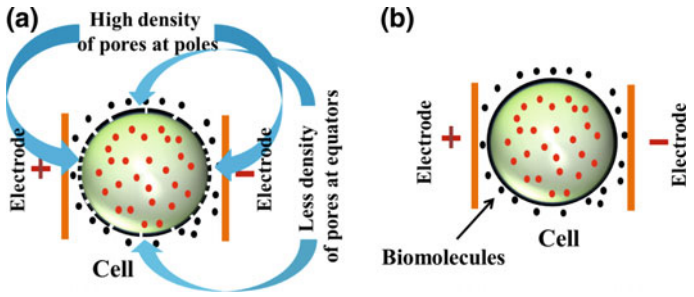

Fig. 4 Single cell electroporation (SCEP) (**a**) formation of pores and molecular delivery from outside to inside of the cell due to the application of an external electric field (**b**) cell membranes resealing and successful molecular delivery into the single cell after withdrawing the external electric field. Permission to reprint obtained from MDPI Publisher Ltd [15]

almost similar to the dimension of a single cell. Microfabrication technique has been used to fabricate microscale electrodes with different metals. Due to the small electrode gap with uniform electric field distribution, pH variation and bubble generation can be reduced to achieve higher efficiency with high cell viability for SCEP compared to bulk electroporation.

Figure 4a shows an overview of SCEP, where the electrodes are just positioned outside the cell membrane to produce homogeneous electric field with lower external voltage applied. Due to the application of external electric field, membrane potential surpasses the threshold value to create transient hydrophilic membrane pores to deliver ions or molecules from outside to inside of the cell. Figure 1 shows the detailed electric field distribution on a single cell, where field strength is higher at poles and lower at equator, resulting in the formation of higher density of pores at poles and lower density of pores at equator. Thus, for SCEP, the transfection efficiency and cell viability depends upon the external electric field strength, pulse width, number of pulses and duration of pulses. However, for SCEP, the electric field distribution is more uniform compared to BEP (in BEP, the distance between two electrodes are in millimeter to centimeter range, resulting in an inhomogeneous electric field). Figure 4b shows, after withdrawing the external electric field, cell membrane can reseal and ions or molecules can successfully be delivered from outside to inside of the cell.

3.3 Localized Single Cell Electroporation (LSCEP)

In recent years, advanced nanofabrication techniques can reduce electrode size and gap between two electrodes to nanoscale level. Thus, with the application of an external electric field, a homogeneous and intense electric field generates at the localized region of the single cell, resulting in the formation of the transient membrane pore to deliver biomolecules precisely from outside to inside of the cell.

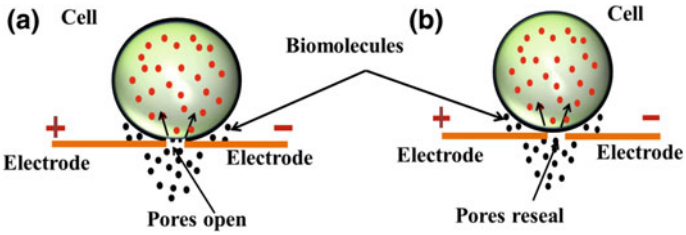

Fig. 5 Localized single cell electroporation (LSCEP) (**a**) during electroporation, transient membrane pores open at localized region of the single cell and biomolecules can be delivered from outside to inside of the single cell (**b**) after electroporation cell membrane reseals again and biomolecules enters inside the single cell successfully. Permission to reprint obtained from MDPI Publisher Ltd [15]

This process is known as localized single cell electroporation (LSCEP). Due to the very small gap between the two electrodes, local pH variation and field distortion can be reduced effectively as a result LSCEP can provide lower toxicity and higher cell viability compared to SCEP or BEP process.

The LSCEP devices can achieve spatial, temporal and qualitative dosage control during electroporation process, which is potentially useful for biological research and therapeutic applications. Figure 5a shows the formation of transient pores and the biomolecular delivery at localized region of the single cell during the LSCEP process with nanoelectrodes and nanoscale gap between two electrodes. Figure 5b shows membrane resealing and successful biomolecular delivery during the LSCEP process. The SCEP and LSCEP techniques can potentially manipulate cell to cell variation to study their heterogeneity characteristics and molecular dynamics. Thus, micro/nanofluidic devices for SCEP or LSCEEP, integrated with various analytical systems such as dielectrophoresis (DEP), electroosmosis and electrophoresis can potentially be beneficial for single cell analysis.

4 Electroporation Parameters

Highly efficient electroporation can be achieved by tuning various parameters, such as pulse parameters, cellular factor, physiochemical factor, structure of the micro/nanofluidic devices, electrode materials, electrode shape and size, buffer type, molecular concentration, size of the cell, electrode polarity, etc.

4.1 Pulse Parameters

To achieve successful gene delivery into living cells with high transfection efficiency and high cell viability, pulse parameters such as field strength, pulse

duration, pulse shape, number of pulses and time between two pulses are important. By applying proper electric pulses, smaller molecules can enter into cells through diffusion after electropermeabilization (short pulses with higher applied voltage), while larger biomolecules such as DNA can enter into cells through the electriphoretically driven process (long pulses with lower applied voltage) [91, 92]. It has been reported that cellular organelles can be electroporated without membrane permeabilization by applying higher voltage with shorter pulses (nanosecond) [24]. The affected area of cell membrane permeabilization can be controlled with short pulses with strong electric field, where diffusion takes place through the membrane permeabilization area [93, 94]. The degree of permeabilization can be controlled with pulse duration and number of pulses, the longer the pulse, the greater the perturbation of the membrane in a given area [44]. The longer pulse with lower applied voltage enhances transfection efficiency with high cell viability [95].

4.2 Cellular Factors

The cellular factors and parameters are critical for electroporation. The transformation efficiency can be influenced by cell density, cell diameter, growth phase of the cells, cell rigidity, etc. For most cells, the growth period in which higher transformation success can be achieved is early log to mid-log phase [96]. If total potential difference is proportional to cell size, cells with larger size are more sensitive to field strengths than those with smaller size [97]. Detection of a specific effect of the electroporated antibody on some cellular functions depends on many variables. These include the concentration and affinity of the introduced antibody for its target; whether the function of the target molecule will be inhibited by the binding of the antibody; the absolute intracellular concentration of the target molecule, etc. [98].

4.3 Physiochemical Factors

The physiochemical phenomena occurring during the tissue development stage mainly include transportation and consumption of nutrients and oxygen, mechanical loading of tissue or cells, generation of waste by cells, chemomachanical phenomena (swelling), electromechanical phenomena (piezoelectricity), osmotic phenomena (transport through cell membrane) or electrochemical phenomena (Debye length). During cell culture, it has the tendency to proliferate, colonize homogeneously in porous scaffolds and synthesized extracellular matrixes [99]. Also it has been reported that different molecular interactions occur during cell culture, where oxygen molecules make the major contribution to tissue growth particularly for osteoarticular system [100–102].

4.4 Electrode Shape and Electrode Material

The electrode material used for electroporation can be gold (Au), alumina (Al), platinum (Pt), graphite, stainless steel, indium tin oxide (ITO), etc. By using micro/nanofabrication technique, electrodes are generally positioned in parallel with microfluidic channel, where cells flow through the channel and electric fields are homogeneously distributed in-between the electrodes. Thus, field distribution is depending upon the size and shape of the electrode. Different shapes of the electrodes and distance between two electrodes can lead to different electric fields and therefore affect the electroporation efficiency. For BEP, due to the larger gap between electrodes, fields are distributed inhomogeneously, whereas for SCEP, electric field is distributed homogeneously due to the microscale gap between electrodes. For localized single cell electroporation (LSCEP), the fabricated electrodes are at nanoscale level to intensify electric field precisely at localized area of the single cell. However, some literatures suggested LSCEP without nanoelectrodes [65]. The electrode material can affect the electroporation efficiency and cell viability. The different electrode materials have different conductivity, thus to overcome threshold membrane potential, the voltage requirement is different for each material. Again every material has different level of toxicity, which influences the cell viability after the electroporation experiment.

4.5 Buffer

The buffer also influences the electroporation efficiency. Generally, different buffers have different conductivity, permeability, and osmolarity. The ionic strength of the buffer solution can directly affect the cell membrane as a resistance, so as to affect the pulse duration and number of pulses. During electroporation, cell swelling was observed due to various osmolarities of the buffer solution [103]. To achieve highly efficient electroporation, buffer conductivity can be varied and it depends upon the cell type.

5 Analysis of Single Cell Intracellular and Extracellular Delivery

Analysis of intracellular and extracellular delivery using different electroporation techniques such as flow-through elctroperation, droplet microfluidics, optofluidics-based microfluidics and localized single cell electroporation are discussed in below.

5.1 Flow-Through Electroporation Technique with Fluidic Channel Geometry Variation

Micro/nanofluidic devices with different channel geometries provide a key platform to analyze the genomics, proteomics, transcriptomics, fluxomics and metabolomics of a given cell population. The devices permit the correlation of phenogenomic and physical properties of a priori identified cells, obtained through biomarkers and video observation with genomic transcription and translation [104]. These devices in micro/nanofluidic environment can perform cell selection, confinement, intracellular delivery, cell lysis from the perspective of an individual cell. Single cell electroporation using micro/nano fluidic devices have advantages, such as small sample size, high separation efficiency, combination with sensitivity measurement method. The first microfluidic device for single-cell trapping and analysis was reported by Huang et al. [105]. To fabricate this device, the top and bottom n^+ polysilicon (0.5 μm thick) layers were 900 μm apart as transparent electrode material for microscopic view. Another 1 μm thick transparent silicon nitride membrane acts as an insulating layer in the middle of this device (see Fig. 6a) and thus two chambers form on top and bottom of this layer. Then a hole with diameter ranging from 2 to 10 μm was fabricated on the middle layer by using reactive ion etching technique and finally all layers were cascaded together using NEA 121 (Norland Products) as an adhesive. The individual cells flow through the inlet into the top chamber and molecules flow into bottom chamber in such a way that, bottom chamber pressure should be lower compared to the top chamber. Thus, cell can be trapped in the hole of the insulating layer due to the pressure difference between the top and bottom chambers (the hole should be smaller than the trapped cell). When the cell was trapped, an external voltage was applied (0–120 V) between the bottom and top electrodes. The electroporation and resealing process can be followed in time via impedance measurement as the cell plugs the hole (strongly changing the impedance). To test this device, different electroporation behaviors of human prostate adenocarcinoma and hepatocyte cell were studied. Later, the authors replaced the n^+ polysilicon with Ag/AgCl electrode [106], because the polysilicon electrode can hinder the precise characterization of electrical properties of the cell membrane. Using their method, it was possible to combine the impedance measurement with optical measurement by staining human prostate cell with YOYO-1 (cell membrane impermeable DNA stain) [56].

The flow-through electroporation technique with fluidic channel geometry variation based on constant voltage has been well developed [107–109]. Wang et al. [83, 103, 110] proposed a flow-through device for high throughput electrical lysis of bacterial cells based on continuous DC voltage.

The device was fabricated with polydimethylsiloxane (PDMS) using soft lithographic process. Figure 6b shows channel geometric variation-based microfluidic single cell device using electroporation technique, where sample reservoir and receiving reservoir were filled with phosphate buffered saline (PBS). The cells were loaded on sample reservoir with 10^6 cells/ml concentration and during

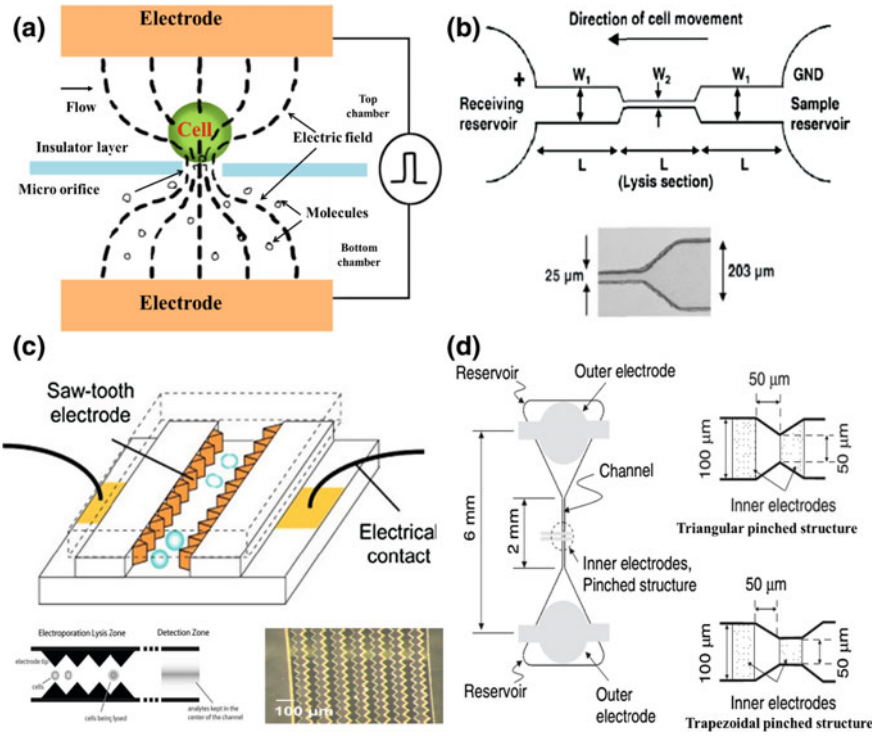

Fig. 6 Channel geometry variation for single cell electroporation (**a**) microfluidic SCEP with cell trapping device. Figure has been redrawn with reference [105] (**b**) flow-through device with high throughput electrical cell lysis. Reprinted from Ref. [83], Copyright 2006, with permission from Elsevier (**c**) schematic diagram of saw-tooth microelectrode-based device for single cell lysis. Reproduced from Ref. [111] by permission of The Royal Society of Chemistry (**d**) schematic diagram of triangular and trapezoidal pinched structure for on-chip single cell lysis. Permission to reprint obtained from the Japan Society of Applied Physics (JSAP) [112]

experiment both reservoirs contained 30 µl solutions. The platinum electrodes were placed in two reservoirs, where positive electrode was in receiving reservoir and the negative electrode was in sample reservoir. By applying a high external electric field, cells were moved from the sample reservoir to the receiving reservoir through lysis section and the geometry variation affects electrical field amplification and finally the cell lysis. The dimension of cell lysis section was 25 µm to avoid cell clogging and ensure stable performance. This section has higher electric field strength (because of narrow section) compared to reservoirs and thus it can overcome easily the threshold value for cell lysis. The cell viability in sample and receiving reservoirs after the cell lysis experiment were measured using plate count. The cell lysis rate can vary due to the changes of length and width of the two reservoirs and lysis section. Nearly 100 % cell lysis could be achieved when 1000–1500 V/cm electric field was applied. Lu et al. [111] demonstrated microfluidic

device for single cell lysis prior to subcellular analysis. Figure 6c shows the schematic diagram of the fabricated saw-tooth micro electrode-based device. Dielectrophoresis (DEP) phenomena were observed as a consequence of the saw-tooth shapes of the micro electrodes and the resulting nonuniform electric field. The cells flowed through in-between the saw-tooth micro electrodes and the external electric field was applied to each electrode through electrical contact. The HT-29 cells were electroporated under the conditions within the intermediate frequency range (1–100 kHz). When treated at 5 kHz, 6 V, 28 % cells were lysed and approximately 81 % cells were ghost cells, while for 10 kHz, 8.5 V, 74 % cells were lysed and 71 % cells were ghost cells. The higher fraction of lysed cells and ghost cells indicated that the majority of the cells were dead after electroporation process. The lower frequency can provide a higher percentage of ghost cells and a lower percentage of lysed cells, suggesting that this condition was gentler and perhaps more suitable for selective lysis of plasma membrane. Ikeda et al. [112] proposed on-chip single cell lysis for extracting intracellular material. Figure 6d shows schematic view of the single cell lysis device using electroporation technique with triangular and trapezoidal pinched structure. The microfluidic chip contains pinched-channel structure with two pairs of electrodes. The outer electrodes were located at the end of the channel and it can generate electroosmotic (EOF) flow in fluidic device, while inner electrodes were positioned at the center of the channels to generate electric field for electroporation. The pinched structure was used to capture the cells in-between inner electrodes. When external voltage was applied on outer electrodes, the generated EOF flow drive the cells across the pinched structure and cells were lysed by shear forces at the triangular pinched structure. When voltage was applied on both outer and inner electrodes, the DC voltage at outer electrodes caused flow movement, while AC voltage at inner electrodes generated a gradient electric field surrounding the captured cell, resulting in cell lysis. The inner trapezoidal pinched structure can break the zucchini protoplast cells with diameter 40–85 μm at 10 Vpp or less at 1 MHz frequency.

5.2 Droplet Microfluidics-Based Electroporation

Droplet microfluidics offer significant advantages to perform high throughput screening by reducing the volume and increasing the sensitivity of assays. This technique prevents undesirable interactions between reactants and solid surface to facilitate the rapid manipulation by separating the reactant from fluid. Droplets can encapsulate cells, DNA, dyes, particles or molecules in the inner aqueous phase [113]. Recently, droplet microfluidic has wide applications in biotechnology such as animal cell growth encapsulated droplet in picoliter range with high cell viability [114]. Lu et al. [115] first proposed droplet microfluidic-based electroporation technique where yeast cell is encapsulated into the droplet. Later Brouze et al. [116] reported high throughput screening of single mammalian cell. Zhan et al. [117] demonstrated electroporation of cells in microfluidic droplet. Figure 7a shows the

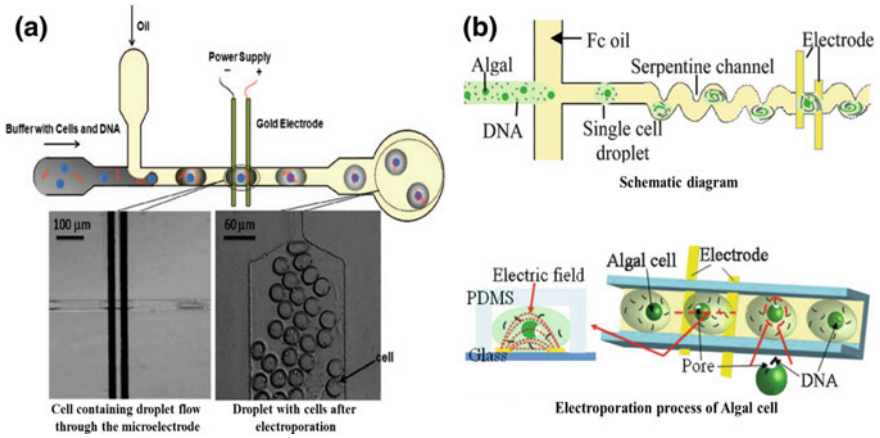

Fig. 7 Droplet microfluidics for cellular analysis (**a**) droplet microfluidics for electroporation. Cell containing droplet flow through in between two microelectrodes (*left bottom*) and exit from reservoir of the system, where droplet with encapsulated cells collected after electroporation (*right bottom*). Reprinted with the permission from Ref. [117]. Copyright 2009 American Chemical Society (**b**) schematic diagram of droplet with algal cell for electroporation. Reproduced from Ref. [118] by permission of The Royal Society of Chemistry

layout and droplet microfluidic-based electroporation device, which was fabricated with PDMS by standard lithographic process. To start droplet microfluidic electroporation process, initially Chinese hamster ovary (CHO) cells were encapsulated into aqueous droplet in oil. Then cell containing droplets flowed through the channel (see Fig. 7a) and passed through the top of the electrode pair (25 µm wide electrode with 20 µm distance between two electrodes). When constant voltage was applied between the pair of electrodes, the electric current run through the conducting buffer droplet and electroporated CHO cells.

The duration and intensity of the electroporation are defined by the velocity (1.38–8.86 m/min) and dimensions of the droplets (60–386 µm in the length). Using this device, EGFP was successfully delivered into CHO cells with 11 % transfection rate at 5.8 V applied voltage. The percentage of the cell death was only 11 % when voltage was not applied, indicating that the contact with oil compromised the cell viability. When the applied voltage was increased from 4.7 to 7.1 V, the viability of cells dropped from ~68 to ~14 %. Another droplet microfluidic-based electroporation device for efficient transformation was reported by Qu et al. [118], this device was fabricated by PDMS using standard lithographic process. Figure 7b shows schematic view of droplet microfluidic electroporation device. Two types of green microalgae, wall-less mutant and wild-type *Chlamydomonas reinhardtii,* were used for this experiment. Cells of wild-type plant have cell wall and cell membrane, whereas animal cells only have the cell membrane, so they can be easily transformed at lower electric field strength either by a bulk or a microfluidic process. For electroporation experiment, initially algal cell and DNA were encapsulated into the aqueous droplet.

Then the droplet with cells flows in a continuous oil phase across serpentine channel with five pairs of microelectrodes biased with constant voltage to transfect cells. The achievable transformation efficiency and cell viability were 8.14×10^{-4} and 81 % with DNA/algal cell ratio of 1000. The authors claim that this microfluidic chip can provide 1600 times higher efficiency compared to bulk electroporation process. The wild-type cell with the cell wall and membrane layers also exhibited 200 times higher efficiency compared to bulk process. Thus, droplet microfluidic electroporation is potentially useful for high efficient transformation of algal cells as well as other microorganisms, which is difficult to achieve by conventional electroporation process.

5.3 Optofluidic-Based Microfluidic Electroporation

Light is a special kind of energy carried by an electromagnetic wave in both temporal and spatial domains. The highest energy density created by optical methods is not possible with any other actuation mechanism in microfluidics. In recent years, optofluidic technology has been widely applied in microfluidics and biomedical systems for detection and analysis [119–121]. Using patterned light fields, micro/nano-size objects such as particles or cells can be trapped, guided, and sorted in microfluidics and this system can produce very less toxicity with high cell viability during experiment. Thus, optofluidic-based microfluidic electroporation attracts increasing interest. Choudhury et al. [122] reported continuous flow single cell electroporation using ultrafast laser with optofluidic device. The device was designed with continuous flow and allowed the selection of target cells within a population for electroporation by the selective application of radiation pressure of light emanating from a NIR waveguide. Using this device, author successfully delivered CdTe quantum dots into HL-60 cell. Lee et al. [123] demonstrated optically induced electroporation method for gene transfection by using microfluidic platform. Chang et al. [124] presented optically induced electroporation on a microfluidic platform for replacing culture medium and electroporation buffer in a seamless fashion. The device avoids cell losses and cell damage during manual operation in traditional centrifuge system therefore it is suitable for handling small and rare cell population. Valley et al. [125] proposed light-induced parallel single cell elelctroporation with microfluidic device.

Figure 8 shows the schematic view of light-induced microfluidic-based electroporation device and it consists of two glass substrates coated with Indium Tin Oxide (ITO) layer. A photosensitive layer was coated on bottom ITO layer and a chamber was formed between these ITO layers by using SU-8 spacer (see Fig. 8b). Then solution containing cells were filled into the chamber. When AC voltage was applied between these ITO layers without light illumination, electric field can concentrate on highly resistive photoconductive layer. Due to light illumination, the resistance can decrease rapidly on the illumination spot and electric field can increase sharply on that liquid layer, resulting in single cell electroporation (cell must be present on the illumination spot, see Fig. 8b). The optical power density

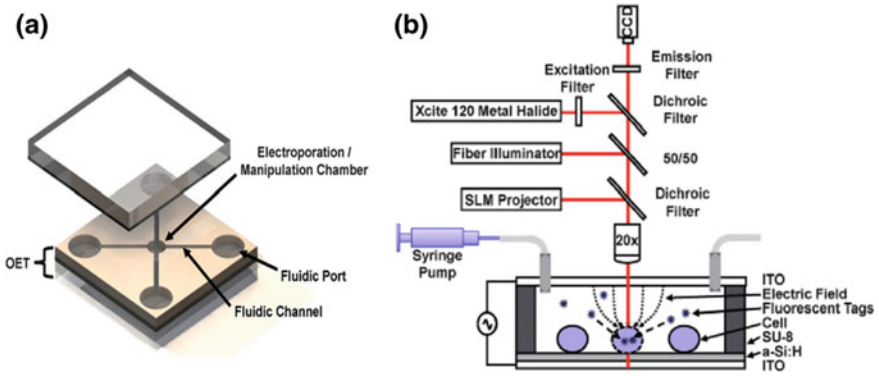

Fig. 8 Schematic diagram of the light-induced electroporation device (**a**) device layout with microfluidic channel for electroporation where optoelectronic tweezers and electroporation are coupled through a change in device bias (**b**) cross section of the device where experimental setup and mechanism of light-induced electroporation are demonstrated. Reproduced from Ref. [125] by permission of The Royal Society of Chemistry

(1 W/cm) was supplied by a standard projector. Using this device, author successfully showed that, 0.2 kV/cm^{-1} AC electric field with 100 kHz frequency can produce dielectrophoretic force to manipulate and trap HeLa cell in a predefined position. The optimal field was 1.4–2.3 kV/cm^{-1} to maintain the cell viability.

5.4 *Localized Single Cell Electroporation*

Micro/nano fluidic devices have the ability for high throughput delivery into a single cell with controllable doses. The dose control as well as high selectivity, high transfection efficiency and high cell viability are important for biological research and therapeutic applications. The devices with nanoscale dimension such as nanoelectrode [43, 47, 57], nanostraw [58], atomic force microscopy (AFM) with nano-size tip [64], nanochannel [65], nanofountain probe [66] and nanowires [126] can selectively and precisely deliver biomolecules into single cell. Due to the nanoscale dimension, very high electric field focuses at the local region of single cell membrane to form transient pores to delivery biomolecules in or out of the cell, whereas the remaining area of the membrane is unaffected. Thus, molecules can be delivered selectively and precisely through the local area of single cell membrane with high transfection efficiency and high cell viability. Nawarathna et al. [64] reported an efficient and fast method for selective and localized single cell electroporation by using AFM technique. The AFM tip acts as a nanoelectrode to focus the electric field at localized region of the single cell. Figure 9a shows the schematic diagram and spatial distribution of electric field in the vicinity of the cell that is being electroporated and SEM image of the modified AFM tip for electroporation experiment. To fabricate the AFM tip, 20 nm thick SiO_2 layer was deposited on top

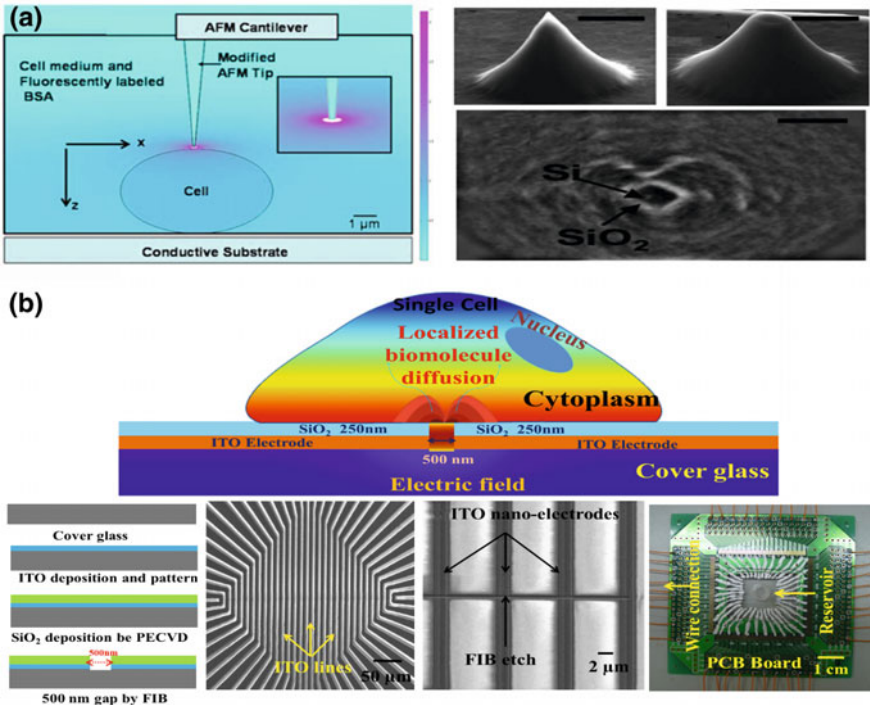

Fig. 9 Localized single cell electroporation (**a**) schematic diagram and spatial distribution of the electric field at cell membrane-tip interface and SEM image with modified AFM tip (20 nm thick SiO_2 layer). The machined AFM tip was fabricated by Focused Ion Beam (FIB) with 0.5 μm end diameter. Reprinted with permission from Ref. [63]. Copyright 2008, American Institute of Physics (**b**) schematic diagram of localized single cell nanoelectroporation (*up*), and the fabrication process step, SEM image of nanoelectrodes and final fabricated nanoelectrode-based transparent chip (*down*). Reproduced from Ref. [57] by permission of The Royal Society of Chemistry

of the conventional boron doped silicon tip. Then, Focused Ion Beam (FIB) was used for machining purpose until the bare silicon of the tip was exposed. Finally the diameter of the tip was 0.5 μm for localized electroporation experiment with rat fibroblast cells *(Rattus norvegicus).* For this experiment, initially cells were mixed with electroporation buffer and FITC labeled BSA medium, then a drop of the mixture was transferred on ITO coated glass slide.

Then modified AFM tip was approached toward the single cell membrane. When distance between tip and cell membrane was 200 nm, voltage was applied (1 Vpp, 0.5 Hz between the tip and the ITO substrate) for electroporation experiment. Due to external voltage application, electric field at the cell membrane is intense, resulting in the formation of transient hydrophilic pores to deliver molecules from outside to inside of the cell. This technique can be used to electroporate cells in a cell friendly environment such as cell culture disk with high cell viability. Santra et al. [43, 57] demonstrated localized single cell nanoelectroporation using

nanoelectrode chip. Figure 9b shows schematic diagram of localized single cell nanoelectroporation and the fabrication process step, SEM image of nanoelectrodes and final fabricated localized single cell nanoelectroporation chip. To fabricate nanoelectrode, ITO film was deposited on top of the glass substrate and patterned by wet chemical etching. Then dielectric passivation layer (SiO_2) was deposited on top of the patterned ITO layer and FIB technique was used to form ITO nanoelectrodes. The gap between two nanoelectrodes was 500 nm. When voltage was applied (4–10 Vpp, square wave positive pulse) on the nanoelectrodes, electric field in-between the nanoelectrodes is intense, resulting in the formation of localized transient membrane pores (those cells seeded on top of the nanoelectrodes) to deliver molecules from outside to inside of the cell. The deposited passivation layer on the chip surface not only performed key roles in reducing harmful reactions between nanoelectrodes, but also reduced the resistive heating effect on the membrane surface, resulting in the reduction of cell toxicity. The author used this method to successfully deliver dyes, Quantum Dots (QDs), plasmids into different cancer cells with high delivery rate (90 %) and high cell viability (80–95 %). This device might have potential applications for single cell studies and therapeutic research. Khine et al. [127] proposed a PDMS-based microfluidic chip for selectively immobilizing and locally electroporating single cells. Figure 10a shows the layout of the chip and cell, where two wide inlet channels on left and right side were used for cell input and output. One of the Ag/AgCl electrodes was connected with one of these main channels and the other was connected to the small channel where cell was trapped. These two electrodes connected with an amplifier (PC-ONE Patch clamp, Dagan) to provide the voltage and measure the current. By applying negative pressure into the small channel, a cell was pulled laterally into the channel and it can act as a high resistance component in this system. When a cell was trapped into the small channel, the cell extends to a tail-like structure. And due to its viscoelastic nature, the cell can retain its original shape after the negative pressure was removed. After a cell was trapped into the channel, a current–voltage program written in LabVIEW was run to input a sequence of pulses (at 0.1 V intervals from 0.1 to 1.0 V) while recording the current at a sampling rate of 10 kHz. The average transmembrane potential (TMP) for HeLa cells was 0.51 ± 0.13 V. The cell membrane permeability was measured by the characteristic "jumps" in current due to cell resistance drop and by the use of fluorescent microcopy (Calcein AM or trypan blue delivery). Jokilaakso et al. [126] demonstrated ultra-localized single cell electroporation using silicon nanowires. In this device, the cell was positioned and lysed on silicon nanowires and nanoribbon biological field effect transistors. Figure 10b shows the schematic view of the device. The magnetic beads were used to optimize speed and control the movement of cells. The HT-29 cancer cells were positioned on top of the transistors by manipulating magnetic beads using external magnetic fields. The fringing electric field was generated directly on the device surface to disrupt the cell membrane, leading to cell lysis or irreversible electroporation with lower applied voltage. The HT-29 cell lysis was performed by applying 600–900 mVpp, 10 MHz across the transistor channel and the bulk substrate. This simple method for releasing biological component from the single

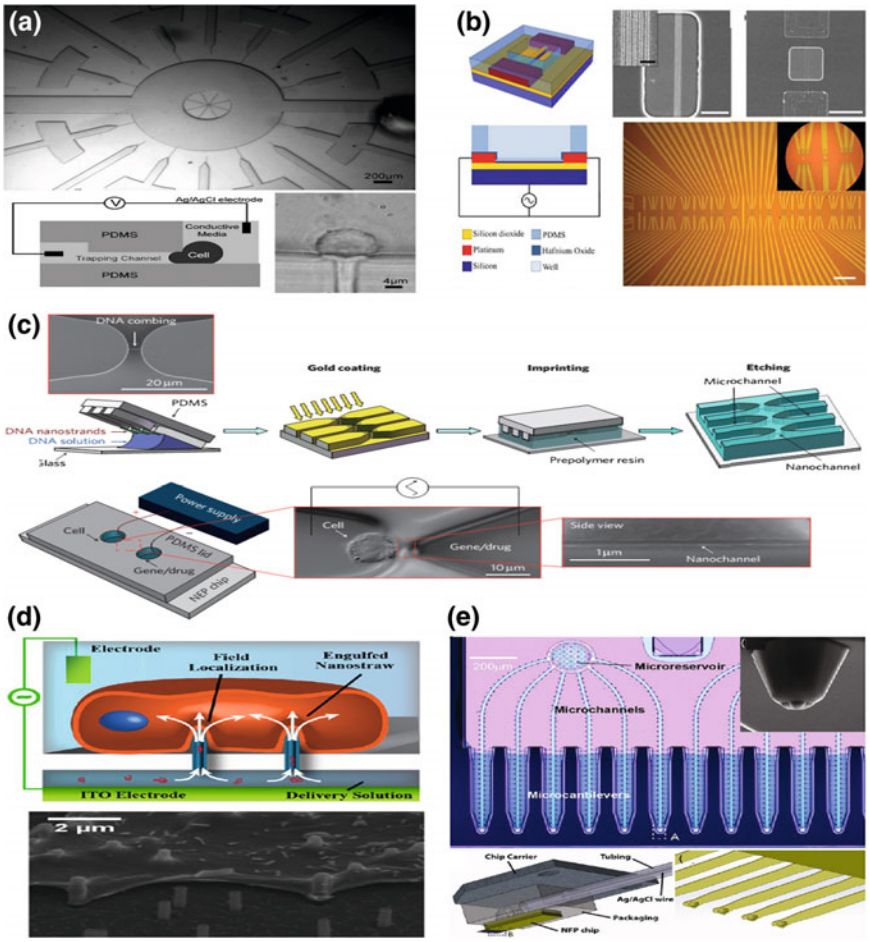

Fig. 10 Localized single cell electroporation (**a**) schematic view of an array of narrow lateral channels for cell trapping and localized single cell electroporation. Reproduced from Ref. [127] by permission of The Royal Society of Chemistry (**b**) Silicon field effect device with silicon nanowires and silicon nanoribbons. Reproduced from Ref. [126] by permission of The Royal Society of Chemistry (**c**) Apparatus and operation of the nanochannel electroporation device. Reprinted by permission from Macmillan Publishers Ltd: Ref. [65], copyright 2011 (**d**) Nanostraw electroporation system. Reprinted with the permission from Ref. [58]. Copyright 2013 American Chemical Society (**e**) Nanofountain probe chip and packaging for single cell electroporation. Reprinted with the permission from Ref. [66]. Copyright 2013 American Chemical Society

cell can reduce the impact on molecular stability from thermal, chemical, or mechanical degradation. The device might be useful for localized single cell lysis on a biosensing platform. Boukany et al. [65] proposed nanochannel electroporation for precise bimolecular delivery into single live cell.

Figure 10c shows the schematic view and operation of the nanochannel electroporation device. The device was fabricated with a simple and low-cost DNA

combing and imprinting (DCI) method, which can be used to form a sealed array of laterally ordered nanochannels interconnected to microchannels. The device consists of two microchannels connected by one nanochannel (90 nm in diameter at the center). The single cell can be loaded at one side of the microchannel–nanochannel junction by using optical tweezers and transfection agents were loaded to the other side of the junction. An electrode was placed in each microchannel reservoir and voltage was applied with pulses varying between 150 and 350 V, which depends upon the needs. Due to high voltage application, an intense electric field was generated throughout the nanaochannel and a very small area of single cell membrane was permeabilized to deliver transfection agent precisely into single cell through an electrophoretically driven process. This device can easily deliver dyes, Quantum Dots (QDs), plasmids with high transfection efficiency and high cell viability. The dose control was achieved by adjusting pulse duration and number of pulses, voltage and agent concentration, etc. The device has the ability for special, temporal and qualitative dose control and it can be used for high throughput delivery applications. Xie et al. [58] proposed a nanostraw electroporation system for efficient intracellular delivery and transfection. The alumina-based nanostraw was fabricated with 250 nm in diameter and 1.5 μm in height, and the density of nanostraw was 0.2 straws/μm^2, which was roughly 10–50 straws/cell. The nanostraw membrane was integrated between a polydimethylsiloxane (PDMS) microfluidic channel and a second PDMS layer with a cell culture well. Figure 10d shows schematic view of nanostraw-based nanoelectroporation system, where an ITO coated glass underneath the PDMS microfluidic channel can serve as the bottom electrode and a Pt electrode placed into the cell culture well serves as top electrode. The nanaostraw has close contact with cell membrane but it cannot penetrate into the cell due to the large diameter. When voltage was applied between Pt electrode and ITO, an intense electric field was generated and passed through each nanostraw. Thus, nanoelectroporation was achieved at the contact between nanostraw and cell membrane and biomolecules delivered through the nanostraw into electroporated cells, which was regulated by controlling the solution composition in the microfluidic channel. The device achieved highly efficient dye delivery (>95 %) and plasmid transfection (~81 %) into Chinese hamster ovary cells (CHO), as well as Human Embryonic Kidney (HEK) 293T cells (plasmid transfection ~67 %), all with high cell viability (>98 %). This uniform nanostraw electroporation system with spatial and temporal dosage control can serve as a powerful and reliable platform for high-throughput intracellular delivery and transfection. Kang et al. [66] presented localized single cell nanoelectroporation using nanofountain probe. Figure 10e shows the schematic view of a nanofountain probe chip for localized single cell electroporation. The nanofountain probe is a microfabricated chip consists of an array of cantilevers connected with two independent microreservoirs through sealed microchannels. The bimolecular solution was stored in the microreservoirs and loaded into the microchannels by using capillary force or an externally applied pressure. The nanomanipulator (Inject Man NI 2, Eppendorf, Germany) was used to control three-dimensional displacement of the nanofountain probes with step size resolution of 40 nm. When applying a voltage between the

nanofountain probe and ground electrode (cell was positioned on top of the ground electrode), an intense electric field was generated at the probe tip (tip was in close contact with cell membrane) and cell membrane was permeabilized to deliver biomolecules precisely into the cell through the tip. The system successfully deliver biomolecules (applied voltage 15–30 V) into HeLa cell with high transfection efficiency (>95 %) and high cell viability (92 %). The device has the advantages for targeted transfection such as single cell selectivity, high transfection efficiency, dosage control and high cell viability.

6 Conclusions

Electroporation technique is an efficient and fast method for cellular delivery and analysis. The conventional or bulk electroporation (BEP) technique processing millions of cells together cannot provide detailed information of cell proliferation, differentiation, and different responses to external stimuli and intracellular reactions. As a powerful technique to elucidate the cellular function, single cell electroporation (SCEP) provides various advantages compared to BEP, such as ease of handling, low power consumption, low toxicity, small sample volume, lower contamination rate, high transfection rate and high cell viability. Micro/nanofluidic devices with the power to manipulate and detect samples at micro/nanoscale can well fulfill the requirement of SCEP. In recent years, more studies require single cell analysis with spatial, temporal and qualitative dosages control, thus localized single cell electroporation (LSCEP) for precise molecular delivery and analysis with high transfection efficiency and high cell viability becomes a frontier research area. This chapter well summarized different electroporation techniques such as BEP, SCEP and LSCEP for single cell analysis, their future prospects and limitations are also elaborated.

Acknowledgments The authors greatly appreciate the financial support from National Science Council (NSC) of Taiwan ROC through National Nanotechnology and Nanoscience Program under Contract no. NSC 101-2221-E-007-032-MY3, 102-2321-B-007-006 and 103-2321-B-007-004.

References

1. Valastyan S, Weinberg RA (2011) Tumor metastasis: molecular insights and evolving paradigms. Cell 147(2):275–292
2. Fidler IJ, Kripke ML (1977) Metastasis results from preexisting variant cells within a malignant tumor. Science 197:893–895
3. Sharma SV, Lee DY, Li B et al (2010) A chromatin-mediated reversible drug-tolerant state in cancer cell subpopulations. Cell 141:69–80
4. Cohen AA, Geva-Zatorsky N, Eden E et al (2008) Dynamic proteomics of individual cancer cells in response to a drug. Science 322:1511–516

5. Yuan TL, Wulf G, Burga L et al (2011) Cell-to-cell variability in PI3 K protein level regulates PI3 K-AKT pathway activity in cell populations. Curr Biol 21:173–183
6. Loo LH, Lin HJ, Singh DK et al (2009) Heterogeneity in the physiological states and pharmacological responses of differentiating 3T3-L1 preadipocytes. J Cell Biol 187:375–384
7. Yin LH, Fu SQ, Nanakorn T et al (1998) Results of retroviral and adenoviral approaches to cancer gene therapy. Stem Cells 16(S2):247–250
8. Wu SC, Huang GYL, Liu JH (2002) Production of retrovirus and adenovirus vectors for gene therapy: A comparative study using microcarrier and stationary cell culture. Bitechnol Prog 18:617–622
9. Schmid RM, Weidenbach H, Draenert GF et al (1997) Liposome mediated gene transfer into the rat oesophagus. Gut 41:549–556
10. O'Brien JA, Lummis SCR (2006) Biolistic transfection of neuronal cultures using a hand—held gene gun. Nat Protoc 1:977–981
11. Capecchi MR (1980) High efficiency transformation by direct microinjection of DNA into cultured mammalian cells. Cell 22:479–488
12. Ohta S, Suzuki K, Ogino Y et al (2008) Gene transduction by sonoporation. Dev Growth Differ 50(6):517–520
13. Ewert KK, Ahmad A, Bouxsein NF et al (2008) Non-viral gene delivery with cationic liposome-DNA complexes. Methods Mol Biol 433:159–175
14. Prasanna GL, Panda T (1997) Electroporation: basic principles, practical considerations and application in molecular biology. Bioprocess Eng 16:261–264
15. Santra TS, Tseng F-G (2013) Recent trends on micro/nanofluidic single cell electroporation. Micromachines 4:333–356
16. Zimmermann U, Pilwat G, Friemann F (1974) Dielectric breakdown of cell membrane. Biophys J 14:881–899
17. Weaver JC, Chizmadzhev YA (1996) Theory of electroporation: A review. Bioelectrochem Bioenerg 41:135–160
18. Teissie J, Golzio M, Rols MP (2005) Mechanism of cell membrane electropermeabilization: a minireview of our present (lack of?) knowledge. Biochim Biophys Acta 1724:270–280
19. Escoffre JM, Porter T, Wasungu L et al (2009) What is (still not) known of the mechanism by which electroporation mediates gene transfer and expression in cells and tissues. Mol Biotechnol 41:286–295
20. Neu WK, Neu JC (2009) Theory of electroporation. In: Efimov IR, Kroll MW, Tchou PJ (eds) Cardiac bioelectric therapy. Springer, New York, pp 133–134
21. Ho SY, Mittal GS, Cross JD (1997) Effect of high electric field pulses on the activity of selected enzymes. J Food Eng 31:69–84
22. Serpersu EH, Tsong TY, Kinosita K (1985) Reversible and irreversible modification of erythrocyte membrane permeability by electric field. Biochim Biophys Acta 812:779–785
23. Tsong TY, Kinosita K (1985) Use of voltage pulses for the pore opening and drug loading and the subsequent resealing of red blood cells. Bibl Haematol 51:108–114
24. Schoenbach KH, Beebe SJ, Buescher ES (2001) Intracellular effect of ultrashort electrical pulses. Bioelectromagnetics 22:440–448
25. Chen N, Schoenbach KH, Kolb JF et al (2004) Leukemic cell intracellular responses to nanosecond electric fields. Biochem Biophys Res Commun 317:421–427
26. DeBruin KA, Krassowska W (1999) Modeling electroporation in a single cell. I. Effects of field strength and rest potential. Biophys J 77(3):1213–1224
27. DeBruin KA, Krassowska W (1999) Modeling electroporation in a single cell. II. Effects of ionic concentrations. Biophys J 77(3):1225–1233
28. Movahed S, Li D (2011) Microfluidics cell electroporation. Microfluid Nanofluid 10:703–734
29. Nollet JA (1754) Researches Sur Les Causes Particulieres Des Phenomenes Electriques (in French). In: Guerin CHL, Delatour LF (eds) Paris, France
30. Fuller GW (1998) Report on the investigations into the purification of the Ohio river water at Lauisville Kentucky. D. Van Nostrand Company, New York

31. Rockwell AD (1903) The medical and surgical uses of electricity: including the X-Ray, Finsen light, vibratory therapeutics, and high frequency currents. E.B. Treat & Company, New York
32. Frankenhaueuser B, Widen L (1956) Anode break excitation in desheated frog nerve. J Physiol 131:243–247
33. Stampfli R, Willi M (1957) Membrane potential of a Ranvier node measured after electrical destruction of its membrane. Experimentia 13:297–298
34. Doevenspeck H (1961) Influencing cells and cell walls by electrostatic impulses. Fleishwirtshaft 13:986–987
35. Coster HGL (1965) A quantitative analysis of the voltage-current relationship of fixed charge membranes and the associated property of "punch through". Biophys J 5:669–586
36. Sale AJH, Hamilton WA (1967) Effects of high electric fields on microorganisms I. killing of bacteria and yeasts. Biochim Biophys Acta 148:781–788
37. Sale AJH, Hamilton WA (1968) Effect of high electric fields onmicroorganisms II. lysis of erythrocytes and protoplasts. Biochim Biophys Acta 163:37–43
38. Pohl HA, Crane JS (1971) Dielectrophoresis of cells. Biophys J 11:711–727
39. Crowley JM (1973) Electrical breakdown of bimolecular lipid membranes as an electromechanical Instability. Biophys J 13:711–714
40. Neumann E, Schaefer-Ridder M, Wang Y et al (1982) Gene transfer into mouse lyoma cells by electroporation in high electric fields. J EMBO 1(7):841–845
41. Miller EM, Nickoloff JA (1995) Escherichia coli electrotransformation. In: Nickoloff JA (ed) electroporation protocols for microorganisms. Humana Press, Totowa, New Jersey, pp 105–114
42. Withers HL (1995) Direct plasmid transfer between bacterial species and electrocuring. In: Nickoloff JA (ed) Electroporation protocols for microorganisms. Humana Press, Totowa, New Jersey, pp 47–54
43. Santra TS, Chang H-Y, Wang P-C et al (2013) Tuning nano electric field to affect restrictive membrane area on localized single cell nano-electroporation. Appl Phys Lett 103:233701
44. Lundqvist JA, Sahlin F, Aberg MA et al (1998) Altering the biochemical state of individual cultured cells and organelles with ultra-microelectrodes. Proc Natl Acad Sci 95(18):10356–10360
45. Zhao X, Zhang M, Yang R (2010) Control of pore radius regulation for electroporation-based drug delivery. Commun Nonlinear Sci Numer Simul 15(5):1400–1407
46. Yoo JS, Won N, Kim HB, Bang J et al (2010) In vivo imaging of cancer cells with electroporation of quantum dots and multispectral imaging. J Appl Phys 107:124702
47. Chen S-C, Santra TS, Chang C-J et al (2012) Delivery of molecules into cells using localized single cell electroporation on ITO micro-electrode based transparent chip. Biomed Microdevices 14(5):811–817
48. Santra TS, Wang P-C, Tseng F-G (2013) Electroporation based drug delivery and its applications. In: Takahata K (ed) Advances in micro/nano electromechanical systems and fabrication technologies. In Tech, Rijeka, pp 61–98
49. Kim K, Kim JA, Lee S-G et al (2012) Seeing the electroporative uptake of cell-membrane impermeable fluorescent molecules and nanoparticles. Nanoscale 4:5051–5058
50. Valero A, Merino F, Wolbers F et al (2005) Apoptotic cell death dynamics of HL60 cells studied using a microfluidic cell trap device. Lab Chip 5:49–55
51. Kim JA, Cho K, Shin MS et al (2008) A novel electroporation method using a capillary and wire-type electrode. Biosens Bioelectron 23:1353–1360
52. Lee WG, Demirci U, Khademhosseini A (2009) Microscale electroporation: challenges and perspectives for clinical applications. Integr Biol 1:242–251
53. Ionescu-Zanetti C, Baltz A, Khine M (2008) Electrophoresis-assisted single-cell electroporation for efficient intracellular delivery. Biomed Microdevices 10:113–116
54. Sowinski S, Jolly C, Berninghausen O et al (2008) Membrane nanotubes physically connect T cells over long distances presenting a novel route for HIV-1 transmission. Nat Cell Biol 10:211–219

55. Wang S, Zhang X, Wang W et al (2009) Semicontinuous flow electroporation chip for high-throughput transfection on mammalian cells. Anal Chem 81:4414–4421
56. Huang Y, Rubinsky B (2003) Flow-through micro-electroporation chip for high efficiency single-cell genetic manipulation. Sens Actuators A 104(3):205–212
57. Santra TS, Chang H-Y, Wang P-C et al (2014) Impact of pulse duration on localized single-cell nano-electroporation. Analyst 139(23):6249–6258
58. Xie X, Xu AM, Ortiz SL et al (2013) Nanostraw-electroporation system for highly efficient intracellular delivery and transfection. ACS Nano 7(5):4351–4358
59. Xie C, Lin Z, Hanson L et al (2012) Intracellular recording of action potentials by nanopillar electroporation. Nat Nanotechnol 7:185–190
60. Santra TS, Kar S, Borana J et al (2014) Nanolocalized single cell membrane nano-electroporation. IEEE Nanatechnol Mag 8(1):30–34
61. Santra TS, Borana J, Wang P-C et al (2014) Nanoelectroporation and controllable intracellular delivery into localized single cell with high transfection rate and cell viability. In: The 27th international conference on Micro Electro Mechanical Systems (IEEE-MEMS), San Francisco, CA, pp 865–868, 26–30 Jan 2014. doi:10.1109/MEMSYS.2014.6765778
62. Santra TS, Wang P-C, Tseng F-G (2013) Nano-intensified electric field for multilocalized single cell electroporation. In: The 17th international conference on miniaturized systems for chemistry and life sciences (μ-TAS-2013), Freiburg, Germany pp 1036–1038, 27–31 Oct 2013. 978-0-9798064-6-9/J.1TAS 20 13/$20© 13CBMS-OOO 1
63. Santra TS, Chiu C, Agarwal N et al (2013) Nanofocused electric field for localized single cell nanoelectroporation with membrane reversibility. In: 8th annual IEEE international conference on Noano/Micro Engineered and Molecular Systems (IEEE-NEMS), Suzhou, China, pp 961–964, 7th–10th April 2013. doi:10.1109/NEMS.2013.6559882
64. Nawarathna D, Unal K, Wickramasinghe HK (2008) Localized electroporation and molecular delivery into single living cells by atomic force microscopy. Appl Phys Lett 93:153111
65. Boukany PE, Morss A, Liao W-C et al (2011) Nanochannel electroporation delivers precise amounts of biomolecules into living cells. Nat Nanotechnol 6:747–754
66. Kang W, Yavari F, Jolandan MM et al (2013) Nanofountain probe electroporation (NFP-E) of single cells. Nano Lett 13(6):2448–2457
67. Polk C, Postow E (eds) (1996) CRC Handbook of biological effects of electromagnetic fields, 2nd edn. CRC, Boca Ratom
68. Gift EA, Weaver JC (1995) Observation of extremely heterogeneous electroporative uptake which changes with electric field pulse amplitude in saccharomyces cerevisiae. Biochim Biophys Acta 1234:52–56
69. Tsong TY, Tsong TT, Kingsley E et al (1976) Relaxation phenomena in human erythrocyte suspensions. Biophys J 16:1091–1104
70. Linder P, Neumann E, Rosenheck K (1977) Kinetics of permeability changes induced by electric impulses in chromaffin granules. J Membr Biol 32:231–254
71. Cole KS (1972) Membranes, ions and impulses. University of California Press, Berkeley
72. Pauly H, Schwan WP (1966) Dielectric properties and ion mobility in erythrocytes. Biophys J 6:621–639
73. Neumann E, Sowers AE, Jordan CA (1989) Electroporation and electrofusion in cell biology. Plenum, New York
74. Chang DC, Chassy BM, Saunders JA et al (1992) Guide to electroporation and electrofusion. Academic Press, San Diego
75. Kotnik T, Bobanovic F, Miklavcic D (1997) Sensitivity of transmembrane voltage induced by applied electric fields—a theoretical analysis. Bioelectrochem Bioenerg 43:285–291
76. Lojewska Z, Farkas D, Ehrenberg B et al (1989) Analysis of the effect and membrane conductance on the amplitude and kinetics of membrane potentials induced by externally applied electric fields. Biophys J 56:121–128
77. Barrau C, Teissie J, Gabriel B (2004) Osmotically induced membrane tension facilitates the triggering of living cell electropermeabilization. Bioelectrochemistry 63:327–332

78. Geng T, Lu C (2013) Microfluidic electroporation for cellular analysis and delivery. Lab Chip 13:3803–3821
79. Golzio M, Teissie J, Rols MP (2002) Direct visualization at the single-cell level of electrically mediated gene delivery. Proc Natl Acad Sci USA 99:1292–1297
80. Weaver JC (2000) Electroporation of cell and tissues. IEEE Trans Plasma Sci 28(1):24–33
81. Hibino M, Itoh H, JrK K (1993) Time courses of cell electroporation as revealed by submicrosecond imaging of transmembrane potential. Biophys J 64:1789–1800
82. Kinosita K, Tsong TY (1977) Formation and resealing of pores of controlled sizes in human erythrocyte-membrane. Nature 268:438–441
83. Wang H-Y, Bhunia AK, Lu C (2006) A microfluidic flow-through device for high throughput electrical lysis of bacterial cells based on continuous dc voltage. Biosens Bioelectron 22(5):582–588
84. Moldovan D, Pinisetty D, Devireddy RV (2007) Molecular dynamics simulation of pore growth in lipid bilayer membranes in the presence of edge-active agents. Appl Phys Lett 91:204104
85. Hu Q, Viswanadham S, Joshi RP et al (2006) Simulations of transient membrane behaviour in cells subjected to a high-intensity ultra-short electric pulse. Phys Rev E 71:031914
86. Hu Q, Shidhara V, Joshi RP et al (2006) Molecular dynamics analysis of high electric pulse effects on bilayer membranes containing DPPC and DPPS. IEEE Trans Plasma Sci 34:1405–1411
87. Morshed BI, Shams M, Mussivand T (2013) Electrical lysis: dynamics revisited and advances in on-chip operation. Crit Rev™ Biomed Eng 41(1):37–50
88. Rebersek M, Faurie C, Kanduser M et al (2007) Electroporator with automatic change of electric field direction improves gene electrotransfer in-vitro. Biomed Eng Online 6:25
89. Wang J, Zhan Y, Ugaz VM et al (2010) Vortex-assisted DNA delivery. Lab Chip 10:2057–2061
90. Canatella PJ, Karr JF, Petros JA et al (2001) Quantitative study of electroporation-mediated molecular uptake and cell viability. Biophys J 80:755–764
91. Klenchin VA, Sukharev SI, Serov SM et al (1991) Electrically induced DNA uptake by cells is a fast process involving DNA electrophoresis. Biophys J 60:804–811
92. Sukharev SI, Klenchin VA, Serov SM et al (1992) Electroporation and electrophoretic DNA transfer into cells: the effect of DNA interaction with electropores. Biophys J 63:1320–1327
93. Gabriel B, Teissie J (1997) Direct observation in the millisecond time range of fluorescent molecule asymmetrical interaction with the electropermeabilized cell membrane. Biophys J 73:2630–2637
94. Kanduser M, Miklavcic D, Pavlin M (2009) Mechanisms involved in gene electrotransfer using high- and low-voltage pulses—an in vitro study. Bioelectrochemistry 74:265–271
95. Stroh T, Erben U, Kuhl AA et al (2010) Combined pulse electroporation—a novel strategy for highly efficient transfection of human and mouse cells. PLoS ONE 5:e9488
96. Tryfona T, Bustard MT (2006) Enhancement of biomolecule transport by electroporation: A review of theory and practical application to transformation of corynebacterium. Biotechnol Bioeng 93(3):413–423
97. Teissie J, Eynard N, Gabriel B et al (1999) Electropermeabilization of cell membranes. Adv Drug Deliv Rev 35:3–19
98. Nickoloff JA (ed) (1995) Methods in molecular Biology, Animal cell electroporation and electrofusion protocols, vol 48. Humana press Inc., Totowa. ISBN-10 / ASIN: 089603304X, ISBN-13 / EAN: 9780896033047
99. Vafai K (ed) (2011) Porous media, Applications in biological systems and biotechnology. CRC Press, Taylor and Francis group, Boca Raton
100. Lanza R, Langer R, Vacanti JP (2002) Principle of tissue engineering, 2nd edn. Academic Press, London, UK
101. Tuncay OC, Ho D, Barker MK (1994) Oxygentension regulates osteoblast function. Am J Orthod Dentofac Orthop 105:457–463

102. Arnett T, Gibbons D, Utting J et al (2003) Hypoxia is a major stimulator of osteoclast formation and bone resorption. J Cell Physiol 196:2–8
103. Wang HY, Lu C (2006) High-throughput and real-time study of single cell electroporation using microfluidics: effects of medium osmolarity. Biotechnol Bioeng 95(6):1116–1125
104. Dykstra B, Ramunas J, Kent D et al (2006) High-resolution video monitoring of hematopoietic stem cells cultured in single-cell arrays identifies new features of self-renewal. Proc Natl Acad Sci USA 103(21):8185–8190
105. Huang Y, Rubinsky B (1999) Micro-electroporation: Improving the efficiency and understanding of electrical permeabilization of cells. Biomed Microdevices 2:145–150
106. Huang Y, Rubinsky B (2001) Microfabricated electroporation chip for single cell membrane permeabilization. Sens Actuators 89:242–249
107. Geng T, Zhan Y, Wang J et al (2011) Transfection of cells using flow-through electroporation based on constant voltage. Nat Protoc 6(8):1192–1208
108. Bao N, Zhan Y, Lu C (2008) Microfluidic electroporative flow cytometry for studying single-cell biomechanics. Anal Chem 80(20):7714–7719
109. Bao N, Wang J, Lu C (2008) Microfluidic electroporation for selective release of intracellular molecules at the single-cell level. Electrophoresis 29(14):2939–2944
110. Wang HY, Lu C (2006) Electroporation of mammalian cells in a microfluidic channel with geometric variation. Anal Chem 78(14):5158–5164
111. Lu H, Schmidt MA, Jensen KF (2005) A microfluidic electroporation device for cell lysis. Lab Chip 5:23–29
112. Ikeda N, Tanaka N, Yanagida Y et al (2007) On-chip single cell lysis for extracting intracellular material. Jpn J Appl Phys 46(9B):6410–6414
113. Koster S, Angile FE, Duan H et al (2008) Drop-based microfluidic devices for encapsulation of single cells. Lab Chip 8:1110–1115
114. He M, Edgar JS, Jeffries GDM et al (2005) Selective encapsulation of single cells and subcellular organelles into picoliter- and femtoliter-volume droplets. Anal Chem 77:1539–1544
115. Luo C, Yang X, Fu Q et al (2006) Picoliter-volume aqueous droplets in oil: Electrochemical detection and yeast cell electroporation. Electrophoresis 27:1977–1983
116. Brouzes E, Medkova M, Savenelli N et al (2009) Droplet microfluidic technology for single cell high throughput screening. Proc Natl Acad Sci 106(34):14195–14200
117. Zhan Y, Wang J, Bao N et al (2009) Electroporation of cells in microfluidic droplets. Anal Chem 81:2027–2031
118. Qu B, Eu Y-J, Jeong W-J et al (2012) Droplet electroporation in microfluidics for efficient cell transformation with or without cell wall removal. Lab Chip 12:4483–4488
119. Brennan D, Justice J, Corbett B et al (2009) Emerging optofluidic technologies for point-of-care genetic analysis systems: a review. Anal Bioanal Chem 395(3):621–636
120. Ramser K, Hanstorp D (2010) Optical manipulation for single-cell studies. J Biophotonics 3 (4):187–206
121. Lin Y-H, Leea G-B (2009) An optically induced cell lysis device using dielectrophoresis. Appl Phys Lett 94:033901
122. Choudhury D, Maestro LM, Ramsay WT et al (2012) Continuous flow single cell electroporation in an ultrafast laser inscribed optofluidic device. In: International conference on fiber optics and photonics © OSA 2012, 978-1-55752-959-0/13/$31.00 ©2013 Optical Society of America
123. Lee Y-H, Wang C-H, Lee G-B (2013) Different optical images for optically-induced electroporation of multiple gene transfection. In: MEMS 2013, Taipei, Taiwan, 20–24 Jan 2013, 978-1-4673-5655-8/13/$31.00 ©2013 IEEE
124. Chang C-J, Lu M-Y, Lee G-B (2014) A continuous optically-induced cell electroporation device with on-chip medium exchange mechanism. In: MEMS 2014, San Francisco, CA, USA, 26–30 Jan 2014, 978-1-4799-3509-3/14/$31.00 ©2014 IEEE
125. Valley JK, Neale S, Hsu H-Y et al (2009) Parallel single-cell light-induced electroporation and dielectrophoretic manipulation. Lab Chip 9(12):1714–1720

126. Jokilaakso N, Salm E, Chen A et al (2013) Ultra-localized single cell electroporation using silicon nanowires. Lab Chip 13:336–339
127. Khine M, Lau A, Ionescu-Zanetti C et al (2005) A single cell electroporation chip. Lab Chip 5:38–43

Microinjection for Single-Cell Analysis

Muniesh Muthaiyan Shanmugam and Tuhin Subhra Santra

Abstract The mere existence of life, from unicellular organisms to well-organized multicellular organisms, pathological conditions and death, has always fascinated human beings and demanded understanding of biological systems over several centuries. Further, an efficient treatment strategy for genetic disorders requires understanding of pathological conditions at the single-cell level. Numerous experimental methodologies have been developed over several decades to facilitate our understanding of cellular functions, by modulating the molecular pathways. Needle microinjection is one of them and it is widely used to modulate cellular functions by introducing foreign cargo into the cell. Microinjection is a method that can directly deliver a precise amount of foreign cargo either into the cytoplasm or the nucleus of a single cell using micropipettes. It is considered a gold standard method of direct cargo delivery. After introduction of this technique in the early 1900s, numerous modifications were made to improve its efficiency and it was applied to a wide variety of fields from scientific research to clinical therapy. This chapter is intended to provide a basic knowledge of the microinjection technique, its advantages and disadvantages, its development, the basic instrumentation required along with a basic protocol, and its uses collected extensively from numerous literatures up-to-date. Further, several modifications that have been carried out to improve the basic instrumentation setup, in order to increase the efficiency and rate of microin-

M.M. Shanmugam (✉)
Institute of Molecular and Cellular Biology, National Tsing Hua University, Hsinchu, Taiwan
e-mail: shanmugambms@gmail.com; s100080881@m100.nthu.edu.tw

T.S. Santra
Department of Engineering and System Science, National Tsing Hua University, Hsinchu, Taiwan

T.S. Santra
California Nano Systems Institute, University of California at Los Angeles, Los Angeles, USA

M.M. Shanmugam
Department of Life Science, National Tsing Hua University, Room no. 506 W, Life Science Building I, Hsinchu, Taiwan

F.-G. Tseng and T.S. Santra (eds.), *Essentials of Single-Cell Analysis*, Series in BioEngineering, DOI 10.1007/978-3-662-49118-8_4

jection by the addition of semi-automated and automated computerized systems, are also discussed. Finally, this chapter provides a gateway to explore advanced understanding of microinjection for single-cell analysis.

Keywords Microinjection · Single-cell microinjection · Needle microinjection · Nuclear injection · Microneedle · Sperm injection

1 General Introduction

Understanding of biological phenomena at the single-cell level gained importance upon the discovery of various genetic disorders, e.g., cancer, neurodegenerative disorders, metabolic syndromes, etc. In order to facilitate our study, various techniques were discovered and microinjection is one of them for single-cell analysis. Its inception was in the early 1900s [1, 2], and the microinjection technique has undergone several modifications to increase its specificity, efficiency, and outcome [3, 4]. Ions, DNA, RNA, proteins, enzymes, antibodies, sperm, nanoparticles, metabolites, cellular organelles, and various co-injection markers can be successfully transduced into a single cell using the needle microinjection technique [5]. Although various methods are available for transduction of foreign cargos [6, 7], either into a single cell or a population of cells, needle microinjection is widely used for its unique applications, such as injection of large biomolecules/cells such as injection of sperm DNA into oocytes [8, 9]. The transduction efficiency of microinjection is theoretically 100 %, but the limitations of this technique lie in the number of cells that can be microinjected in a given time, unnoticed obstruction of the microinjection needle, severe cytotoxicity of the injected foreign cargo, etc.; however, several control tests can be performed for the evaluation of efficiency of the technique [10]. The success rate not only relies on more cells being injected, but it also depends on the subcellular location of the microinjection and the nature of the biomaterials being microinjected. Commonly, microinjection can be carried out in two subcellular locations, one being the nucleus (e.g., DNA or plasmids) and the other being the cytoplasm (e.g., proteins or RNA).

As may be anticipated, microinjection at the microscale level requires extensive instrumentation when compared to other transduction techniques for precise subcellular delivery and for a precise amount of cargo delivery. A basic instrumentation setup for single-cell microinjection requires the following:

1. An inverted microscope with a *Differential Interference Contrast* (DIC) function enabled for microinjection of unstained cells.
2. A micropipette or microneedles for insertion into a single cell and to deliver the cargo.
3. A needle puller to make the microneedles of the desired size and shape.
4. A micromanipulator in order to position the microneedles.

5. An injection system to create a positive pressure for injection of materials into the cells and a negative pressure development to overcome the capillary force and for immobilization of the suspended cells.
6. An injection chamber to maintain survival conditions for the cells [2, 4].

In order to enhance the efficiency and comfort of the microinjection technique, numerous modifications have been developed in the basic apparatus units mentioned above. For example, microneedles are replaced by ultra-high-throughput microfluidic microinjection platforms to increase the rate of cells being microinjected per minute [11, 12], an automated micromanipulation system instead of a manual system [13, 14], etc. Further, a new type of single-cell microinjection has been developed based on the concept of atomic-force microscopy with specialized microinjection probes [15, 16].

This chapter is intended to provide a basic knowledge of the single-cell microinjection technique along with a briefing of all available methods for transduction, a history of microinjection and its development, and further extends toward providing details about the instrumentation needed for microinjection. The chapter will also explain all the available modifications within the instrumentation, the fabrication of micropipettes, the basic protocol for microinjection, and potential applications with their limitations.

2 Physical and Chemical Methods for Transduction of Foreign Cargo

Over several decades, scientists have developed various techniques for transduction of foreign cargo into a living cell. One of these techniques is needle microinjection. This section will provide a brief introduction to other techniques developed for transduction, along with their advantages and disadvantages. In general, the methodologies available for transduction can be classified into the following [12]:

1. Viral-mediated delivery.
2. Chemical-mediated delivery.
3. Physical delivery

   I. Direct delivery

      (a) Microinjection
      (b) Bombardment
      (c) Magnetofection

   II. Physical membrane poration

      (a) Electroporation
      (b) Sonoporation
      (c) Optoinjection

2.1 Viral-Mediated Delivery

Viruses have been studied and developed as potential vectors for transduction of foreign biomolecules, such as RNA and DNA, into host cells or tissues. Here a gene of interest is cloned into a virus, which is replication-defective and allowed to infect the host cell or organism. Viruses possess several unique properties, such as the capacity to bypass cellular barriers (refer to Sect. 6), integrating viral genome into the host cell to have latent infection or expression, gene delivery into a variety of tissues in an organism for long-time gene therapy applications, creation of stable transgenic cell lines, etc. Several researches have shown that viral properties can be turned into an effective means of gene delivery in the host cell or organisms [17]. Many different types of viruses have been employed for the purpose of gene delivery, such as Retrovirus, Adenoviruses, Adeno-associated viruses, Herpes viruses, Baculoviruses, etc. [17–21]. However, the use of viral vectors also has disadvantages, such as induction of immune response in organisms, induction of cancer [22], etc.

2.2 Chemical-Mediated Delivery

Various chemicals, such as calcium phosphate or DEAE-dextran, can help to precipitate or bind the DNA or cloned plasmid onto the surface of host cells, resulting in an efficient uptake of DNA into the cells. Lipid/liposome-mediated transduction can envelop the DNA in small liposomes and deliver the DNA to the cytosol, where these particles can overcome the lipid bilayer barrier. Chemical-mediated gene delivery has been proven to be more cost-effective, simpler, and more frequently applied for different types of cell lines in scientific research. However, the disadvantage of this methodology is the cytotoxicity to the cells caused by the chemicals, especially to primary cells, which are highly sensitive to adverse chemical concentrations or conditions [3, 6]. Further, various standardizations have to be carried out to achieve high transduction efficiency in a particular cell line.

2.3 Physical Delivery

All those methods that use a physical force to deliver the cargo into the cell come under this classification. Physical methods of gene delivery can involve either direct delivery of cargo into the cell (microinjection, bombardment, and magnetofection) or just the use of physical force to create an insertion or pores in plasma membrane, so that the DNA or particle in the environment can diffuse through the membrane pores (electroporation, sonoporation, and optoinjection) [12].

2.3.1 Microinjection

This involves direct insertion of a microneedle into a subcellular location and injection of a calculated amount of cargo into the cell [2, 13, 14, 23]. Needle microinjection has been described in great detail throughout this chapter.

2.3.2 Bombardment

This method involves needle-free delivery of nucleic acid biomolecules that are coated onto a metal particle and projected at high velocities toward the target cells [24, 25]. Bombardment has gained more popularity in relation to gene delivery to various superficial tissues [26, 27]. The disadvantages are that bombardment is not an effective gene delivery method into deeper tissues in an organism, and this technique causes excessive tissue damage, resulting in inflammatory reactions with unpredictable outcome [28].

2.3.3 Magnetofection

Magnetofection does not involve direct gene delivery. This technique enhances the rate of introduction of viral and nonviral carriers or other particles to the host cell surfaces with the help of magnetic nanoparticles upon application of a magnetic field [29–31]. This technique can be combined with other methods of gene delivery to enhance the transduction rate.

2.3.4 Electroporation

Electroporation involves the application of an electric field in order to generate nano-sized pores in the cell membrane, thereby producing an entry point for biomolecules or particles to diffuse into the cytosol from the medium [32–34] (for more information about electroporation refer to Chap. 3).

2.3.5 Sonoporation

The high intensity of focused ultrasound is used to produce a shear force in the extracellular fluid. The shear force has the capacity to induce pores in the cell membrane, resulting in the delivery of DNA, drugs, or other nanoparticles into the cell. Unlike electroporation, the physical force responsible for pore formation in sonoporation is the physical movement of fluid [35, 36]. Sonoporation has gained popularity in clinical applications, because noninvasive ultrasound technique is already in use for diagnosis and therapy [37]. However, this technique is limited by the nonavailability of a proper method to control the localization of energy and the entry of cargo molecules into the cells [38].

2.3.6 Optoinjection

Optoinjection makes use of laser irradiation in order to create membrane pores that facilitate the entry of DNA or other cargo into the cytosol from the extracellular fluid [39–41]. The greatest advantage of this technique is that less damage is caused to the cellular membrane. Although various experiments and modifications have been carried out in recent years [42, 43], the technique of optoinjection is very young and requires further investigation to transfer the technology to a wide variety of applications and practices.

3 Advantages

The technique of microinjection is becoming more popular every day, because of its unique advantages. Needle microinjection requires excellent technical expertise, yet it is widely used for its unique and critical advantages, which are listed below:

- Transfection-challenged cells, such as primary cell cultures, neuronal cell lines, primary neuronal cells, etc., can be successfully transduced with foreign cargo, because needle microinjection involves direct insertion and delivery of cargos.
- A precise amount of cargo can be delivered into each cell.
- Theoretically, the transduction rate of needle microinjection is 100 % and it is possible to attain such a high transduction rate with excellent technical expertise and automation. A report shows that upon automation, higher success rates of 90 % for cytoplasmic microinjection and 85 % for nuclear microinjection had been achieved [13].
- It has ability to track the fate of a single stem and progenitor cell in a tissue at single-cell level [44].
- The technique of needle microinjection completely depends on the control of pressure to deliver the cargo, thus making the delivery of cargo independent of factors such as the charge of cargos and the chemical nature of cargos (hydrophobic, hydrophilic, etc.) [44].
- It enables the delivery of multiple cargos at the same time, such as a pool of genes or different types of proteins involved in the same signal pathway, etc. [44]. This provides the greatest advantage of being able to study the interplay of various factors or protein–protein interaction within a single cell.
- As microinjection of proteins into a cell overcomes the extensive cellular protein synthesis and export mechanisms, various cellular responses from the microinjected protein can be observed immediately. This is very helpful for studying the function of a protein accurately. Further, this also reduces the time lag between the delivery of a gene and transcription and translation to a protein [44].

4 Disadvantages

There may be no technique that has no disadvantages. The microinjection technique has a handful of disadvantages. However, its unique advantages have always outweighed the disadvantages and kept the technique alive for over a century. It is always better to understand the disadvantages of any technique, with its limitations, for successful applications. The followings are some of the disadvantages of the needle microinjection technique:

- Needle microinjection requires laborious and expensive instruments made for high precision and accuracy.
- Successful microinjection requires not only expertise in the technique of microinjection, but also a good understanding of cell and tissue behavior, expertise in cell culture, and an excellent experimental design and standardization.
- Although theoretically the transduction rate of microinjected cells is 100 %, it requires technical expertise to differentiate a blocked microneedle from an unblocked microneedle, standardization of the amount of cargo being microinjected for survival of the microinjected cells, etc.
- One of the major disadvantages is the number of cells that can be microinjected at a given time. Although various microfluidic devices and automation are being studied in detail, the number of cells that can be microinjected remains fewer when compared to other methods of transduction (refer Sect. 2).
- When manipulating a single cell in a tissue or cultured tissue section, only tissue samples with lumen or a tissue cavity or an assessable surface on the tissue can be successfully microinjected and manipulated for in vivo studies, because cells exposed to the luminal side can be reached by the microinjection needle for microinjection without causing extensive tissue damage. Microinjection of a single target cell, except for cells in the periphery of the tissue, in a tissue without lumen can result in extensive tissue damage [44].
- This technique needs a coinjection marker and maintenance of the control group to identify the microinjected cell and to prove that the observed effect is due to the microinjected test cargo and not because of the microinjection procedure [44].

5 Brief History of Microinjection

The concept of microsurgery of a single cell was proposed by a French biologist, Félix Dujardin, in 1835 [4] and the technique of microinjection was first successfully performed by M.A. Barber in 1911 [2]. M.A. Barber explains the inoculation of bacteria and other substances into eukaryotic living cells (plant cells, fungi, algae, and unicellular eukaryotes) along with a detailed introduction of the basic instrumentation design (Fig. 1 shows the first microinjection instrumentation setup and describes its functional parts) [2]. Following M.A. Barber, several scientists

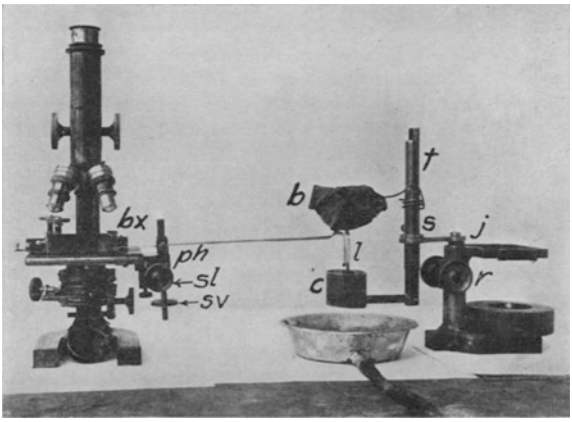

Fig. 1 Microinjection setup by M.A. Barber. The first unit contains a compound microscope and micromanipulator along with a micropipette holder '*ph,*' whereas '*sl*' and '*sv*' represent the screw that can provide up-and-down and lateral movement to the pipette, respectively. This unit will help to visualize the living cell and to perform the act of penetration of the microneedle into the cell. The second unit is equivalent to a modern-day microinjector system to regulate the injection pressure. This unit consists of a brass metal cup '*c*,' which contains cold water, attached to a brass tube '*t*,' along with a rubber bag '*b*,' which contains hot water and is connected to '*t*' with a wire. This setup is connected to a simple dissection microscope through sleeve '*s*,' while '*r*' represents the screw to move '*t*' up and down and '*j*' allows '*t*' to swing aside. With the help of '*b*,' '*c,*' and '*l*' (which is the pipette region in room temperature) the expansion of mercury is controlled, so that sufficient pressure is created to inject the cargo into the host cell. More information about the microinjection system and different versions of the system developed by M.A. Barber is given in Korzh and Strähle (2002) [46]. Reprinted from Barber [2] by permission of Oxford University Press

microinjected foreign substances into cells in order to study the cytomatrix [45]. Half a century later, the technique of microinjection underwent enormous development, which is evident from the large increase in the number of citations in the 1990s when compared to the early 1900s. Since then, various biological and nonbiological samples have been successfully microinjected into different cell types in an attempt to understand cellular functions. Furthermore, the technique of microinjection itself has been improved to increase its efficiency along with automated instrumentation, so that the technique can be adapted to a wide variety of biological samples in the early twenty-first century.

It is fascinating that M.A. Barber used the temperature-dependent expansion property of metal mercury to generate sufficient injection force for needle microinjection. By the late 1960s and early 1970s, various experiments of needle microinjection of radioactive substances for labeling Golgi apparatus in amoeba [47], the injection of heterologous cytoplasmic homogenates from one strain of amoeba to other [48], and injection of bovine gamma globulin into mouse zygote [49] provided initial clues about the growing microinjection technique for studying various subcellular phenomena. Following this success, a variety of cargo molecules, including biological molecules, such as DNA, RNA, subcellular organelles, mitochondria,

kappa particles, etc., were tested for successful microinjection and delivery into a wide range of study models such as *Paramecium* [50, 51], *Xenopus* egg [52], and isolated mammalian somatic cells [53, 54]. As a gold-standard technique for physical and direct introduction of a foreign substance into an individual cell, the microinjection technique was applied for the production of transgenic animals in the 1980s [55–59]. Further, this technique was used to study cellular functions such as gene expression, molecular regulation of cellular pathways, identification of protein kinases, and inhibitors [60], understanding of the cell cycle [61], the function of membrane channels and ion [62]; understanding the fate of protein inside the cell and the process of intracellular degradation [63], the cytoskeleton and membrane dynamics [64–66]; identification of oncogene and cancer pathways [67, 68], etc. Apart from plant and animal research studies, needle microinjection gained clinical importance upon application of the technique to treat different infertility problems among human beings. The initial microinjection of spermatozoa of hamsters and humans into hamster eggs, intracytoplasmic sperm injection (ICSI), was performed and resulted in the successful development of male pronuclei [69]. Later studies were conducted to enable understanding of the behavior of sperm nuclei upon microinjection in a variety of species [8, 70–72]. Following extraordinary success in animal studies, ICSI was applied to human beings and finally developed as a treatment strategy for a variety of infertility problems [9, 73–76].

Over the last decade, not only have various scientific discoveries been made by applying needle microinjection, but also a dramatic modification has been made to microinjection instrumentation to increase the efficiency and compatibility for a wide variety of needs and applications [3, 5]. Semi-automation has been introduced to increase the efficiency of microinjection from a few cells per hour to several hundred cells per hour by an expert technician. Apart from automation, research and development of microfluidic devices has improved the efficiency from low-throughput to high-throughput injection of close to 1000 cells per hour [11, 12]. Further, the technique has been modified so that it can be adapted to different types of cells and even cultured tissues at the single-cell level in recent years [44, 77].

The important role played by the single-cell microinjection technique can be understood from the wide-ranging applications from cellular research to clinical use and also from recent developments for increasing the efficiency of this technique. This gold-standard technique of single-cell microinjection, indeed, has an excellent future, which will be explored in the upcoming decades.

6 Basic Structure of a Cell and Cellular Barriers for Foreign Cargo

Cells have evolved into different sizes, shapes, and structures with a variety of cellular pathways and immune barrier mechanisms for efficient survival. Cells are considered to be basic structural and functional units of an organism. All living cells

or organisms can be divided into two classes: prokaryotes and eukaryotes [78]. Unlike prokaryotes, a typical eukaryotic cell has a nucleus, enveloping the genome in the form of DNA with nuclear membrane. Cytoplasm surrounds the nucleus. Cellular organelles (vesicles, vacuoles, endoplasmic reticulum, mitochondria, Golgi apparatus, endosomes, chloroplast, autophagosomes, etc.) float in an organized manner in cytoplasm. Plasma membrane forms a cell boundary enveloping cytoplasm. Unlike animal cells, a subtle difference can be observed in a plant cell, which is covered by a thick cell wall [78, 79]. (Refer to Chap. 1 for more information on single-cell behavior.)

All existing complex unicellular and multicellular organisms are presumed to have evolved from the first cell, a ribonucleic acid (RNA) enveloped by phospholipids [80]. During the initial stages of evolution, enhanced sharing or lateral transfer of essential biomolecules between the evolving ancestral cells (progenotes) [81] increased the rate of survival along with increased evolution [82]. As the ancestral cells evolved into diverse species, they developed highly compartmentalized cellular structures as barriers for acceptance of disadvantaged biomolecules [82, 83]. Such barriers protected the species from pathogenic and invading microorganisms. Thus cellular barriers are formed, which provide a great obstacle for transduction of foreign cargos as follows [82, 84, 85]:

- Extracellular matrix: An extracellular matrix is developed by biomolecules secreted by the cell itself. Some of the important functions include providing three-dimensional support for cellular organization, cell migration, cell-to-cell communication, etc. An extracellular matrix also provides a very harsh environment with extreme pH and the presence of protease and nucleases, which form a protective barrier for the cell. However, these barriers are incapable of providing effective protection for the cell. In a multicellular organism, long-term administration of DNA to pregnant mice resulted in the association of administered DNA in the fetus [86]. Indeed, various studies show that the existence of nucleases is known to reduce the half-life of DNA as a result of degradation [87].
- Plasma membrane: Plasma membrane, which forms the cellular boundary, is made up of phospholipid bilayer. The main function is being a good physical barrier for a variety of biomolecules and small molecules. It also helps with cell-to-cell communications, maintenance of the internal environment of the cell, etc. Most small molecules and ions can diffuse through the plasma membrane, but the rate of diffusion is unique to a particular molecule [88]. Large biomolecules have to be transported into the cell by a specific mechanism called ‘endocytosis.’ Depending upon the pathway involved for endocytosis, the fate of endocytosed foreign cargo is varied [89–94].
- Cytoplasm: Cytoplasm is a viscous mass of fluid between the nucleus and plasma membrane, where cellular organelles carry out their cellular processes to meet the survival standard. The cytoplasm is infiltrated with a cytoskeleton

network mesh and it is very crowded with numerous biomolecules (for example: ~100 mg/ml of protein) [84]. The crowded cytoplasm limits the diffusion of large biomolecules. However, the movement of proteins, vesicles, and other membrane organelles within a cell cytoplasm is highly organized by specific cellular pathways [95, 96]. Indeed, it was shown in several studies that the microinjected beads or vesicles move several hundred times more slowly in cytoplasm than in aqueous solutions [84, 97, 98].

- Nuclear membrane: One of the most efficient barriers is a nuclear membrane, as it is made up of a double lipid bilayer, whose intermembrane space is continuous with endoplasmic reticulum (ER). The transport across the membrane is highly regulated at the nuclear pore by nuclear pore complex (NPC). The diameter of the nuclear pore is in the range of 30–40 nm [99]. Small biomolecules, ~40 kDa, have the ability to diffuse passively. However, larger biomolecules need a special signal sequence in order to be transported across the nuclear pore. Various evidences show that biomolecules as large as 25–50 MDa can be transported across the nuclear pore by large conformational changes in the NPC, upon the existence of appropriate cellular signals [84, 100–102].

Although barriers exist at various levels of cellular entry, the technique of needle microinjection has an advantage in overcoming these barriers, because it involves penetration of the microneedle into the cytoplasm or nucleus. However, it is important that the subcellular location of the microinjection is carefully chosen for an error-free experiment. The choice of subcellular location for microinjection depends on the research study being conducted. However, there are several proteins, such as plasma membrane bound growth factors, tyrosine kinase receptors, acidic fibroblast growth factors, etc., which are known to translocate to the nucleus to carry out their cellular functions [103, 104]. Such proteins and RNA (for transport studies) can be microinjected into the nucleus, depending upon the cellular aspect being studied. Literatures provide clues for appropriate selection of subcellular location for microinjection. For example, plasmid DNA microinjected into the cytoplasm did not make any significant movement and was found at the microinjection site. Further, only 20-bp-long oligonucleotides and DNA fragments of less than 250 bp are known to diffuse into the nucleus from cytoplasm, while the mobility of larger plasmids is severely prohibited with diffusion rates much slower for larger DNA fragments [105–107]. Along with diffusion barriers for DNA molecules, degradation of DNA in cytoplasm is yet another fate [108], although cytoplasm acts as a barrier and DNA expression is known to be better in dividing cells than in nondividing cells (DNA has better access to the nucleus upon disintegration of the nuclear envelope during cell division) by lipid-mediated transfection method [109]. A study had shown successful nuclear entry of cytoplasmically microinjected DNA for myotubes [106] and the kinetics of DNA uptake into the nucleus is much slower with the involvement of a large amount of friction [110].

7 Types of Cargos for Microinjection

As the technique developed, researchers microinjected a wide variety of cargos for scientific studies. The following Table 1 summarizes the variety of cargos that were microinjected from the literature:

Table 1 Table summarizes the cargos microinjected into varieties of host for differential research and clinical studies from the literature

Cargos	Host cells	Explanation	References
Microorganisms, mercury etc.	Fungal cells, algae, rotifers, *Paramecium*, plant cells, cultured living animal cells	Development and standardization of needle microinjection technique	[2, 111]
Colored solution, oil drops, etc.	Sea urchin eggs, oocytes of a variety of species	In order to understand the structure and physiological role of cytoplasm, protoplasm and cytomatrix	[45, 112, 113]
Cytoplasmic content	*Amoebae* *Paramecium*	To study the inheritance property of cellular contents	[48, 51, 114]
Radioactive sugar molecules	*Amoebae*	To study and label the Golgi apparatus. To study the protein fate	[47]
Cellular organelle	*Paramecium*	To study organelle-induced resistance for chemical substance	[50]
Proteins, peptides, antibodies	Oocytes, neurons, cultured cell, and primary cell lines	To understand the function of a protein/transduction of larger biomolecules and cells highly sensitive to toxic chemical transduction methods	[61, 67, 68, 115–120]
Naked DNA, plasmid DNA, linear DNA, cDNA, etc.	Oocytes, neurons, cultured cell, protoplast, and primary cell lines	To understand the function of an expressed protein and to study DNA mobility and to cells highly sensitive to toxic chemical transduction methods	[54–59, 77, 106]
mRNA, interfering RNAs, etc.	Primary cultured cell lines, other unicellular eukaryotes, oocytes, etc.	To understand RNA transport, function of protein, etc., to cells that cannot uptake larger biomolecules and cells highly sensitive to toxic chemical transduction methods	[52, 114]
Antisense oligonucleotide	Cultured cells	For silencing the expression of genes and to cells highly sensitive to toxic chemical transduction methods	[105]

(continued)

Table 1 (continued)

Cargos	Host cells	Explanation	References
Sperm, pronuclei, etc.	Human egg, oocyte of various species	In vitro fertilization/clinical treatment	[8, 9, 69–76]
Nanoparticles	Cultured cells, primary cell lines, tissue, etc.	Toxicity studies, label cells, and for studying development	[121–123]

8 Types of Host Samples for Microinjection

While microinjection can be adopted and performed in many types of eukaryotes, the host cell sample can be broadly classified into two different types. The classification is based on differences in the application of the microinjection technique or cell growth property (refer to Fig. 2). Cultured cells and tissue can be classified into wide varieties based on differential factors. But this chapter will stick with the following types, for a microinjection perspective in order to attain a basic understanding of the microinjection technique (refer to a basic cell culture book for more information [124]). The groups are

1. Adherent cells, and
2. Suspension cells.

8.1 Adherent Cells

Cultured cells that require a substrate to attach-to and grow are called 'adherent cells.' Although these cells can move around the attached surface to perform physiological functions, they are nonmotile at a given time point. Microinjection of adherent cells does not require a holding pipette. Examples of adherent cells include neuronal cells, heart cells, kidney cells, or any cells that require an extracellular matrix and form a 3D organization to create a tissue or an organ.

8.2 Suspension Cells

Suspension cells do not require any substrate to attach-to and grow. These cells float around the cultured media. Examples of suspension cells include blood cells, oocytes, some eukaryotic single-cell organisms, etc. As suspension cells float around the media, they need to be immobilized using a holding pipette for microinjection.

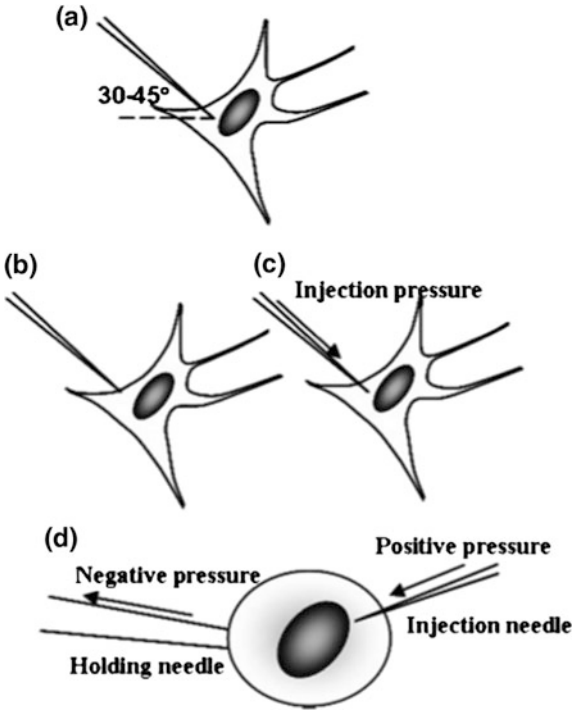

Fig. 2 Microinjection into adherent cell and suspension cell. **a** An adherent cell with an injection needle that is at a more optimized angle for microinjection. As adherent cells attach-to the surface of the cultured plate or coverslip, they spread out on the surface to form discrete boundaries and shapes depending upon the cell type. **b** Pictorial representation of a needle just before microinjection placed on the surface of the cell membrane. **c** Pictorial representation of injection of foreign cargo after cellular penetration. **d** A suspension cell being held by a holding pipette with a negative pressure and an injection needle with a positive pressure performing microinjection. As suspension cells do not require any surface to attach-to and grow, they are generally round in shape. Reproduced from Zhang and Yu [5] by permission of John Wiley & Sons Ltd.

9 Basic Instrumentation for Needle Microinjection

Microinjection at the microscale level demands extensive and expensive instruments to carry out the technique with ease. This section of the chapter will discuss the basic instrumentation requirements for performing microinjection and also explains the latest high-throughput modifications available in different parts of instruments. The high-throughput modifications increase the efficiency and success rate of the technique. The followings are the main instrumental requirements for needle microinjection:

9.1 Microscope

One of the most important pieces of equipment for microinjection is a microscope, which is used to visualize the cells and micropipettes and to perform microinjection. An inverted microscope is highly recommended as it provides sufficient workspace above the microscope stage, whereas an upright microscope does not provide sufficient workspace with microneedles. The recommended magnification for the microinjection of a cell is ~400×, especially if nuclear microinjection is involved. However, some authors feel comfortable with ~200× for cytoplasmic microinjection [4]. In order to understand the depth of the microneedles and the cell, the microscope should be equipped with a differential interference contrast (DIC)/Nomarski facility or a phase contrast facility. This system not only helps us to understand the depth of the field and spatial arrangement of microsubstances in the field, but it can also help us to visualize changes after successful microinjection. For a basic injection setup, a visible light source should be sufficient; however, for the use of a fluorescent coinjection marker or fluorescent tagged proteins, the microscope should have a mercury lamp or other fluorescent light source with an appropriate filter for visualization of microinjected cells [3–5]. Example microscopes include the IMT-2 research microscope from Olympus [4] and the Axiovert-200 microscope from Zeiss [44]. Further, care is to be taken to prevent any vibrations of the microscope or the microneedle attached to the micromanipulator. Any vibrations can affect the visualization and penetration of the microneedle into the cell. However, vibrations can be prevented by mounting the microscope on an anti-vibration platform.

9.2 Micromanipulator

A micromanipulator is a device that carries the needle holder (the needle holder holds the micropipette, which is connected to the microinjector) at the desired angle in respect to the cell surface and allows three-dimensional movement of the microneedle tip. The three-way movement of the tip includes front and back, up-and-down, and lateral movement away from the microscope and close to the microscope (Fig. 3). This device is used to position the needle tip appropriately, in respect to the cell, and it also helps to penetrate the cell by moving the needle down against the cell surface. In a manual micromanipulator, the device is fitted with several screws and levers, which can be adjusted to make microdisplacements of the microneedle, for example, the Integra™ micromanipulation system from Nikon.

However, for semi-automated micromanipulators, a joystick instrument is used to move the needle into position for microinjection and a click of a button can perform

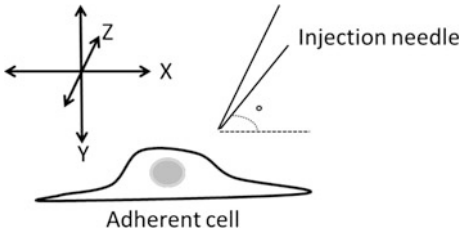

Fig. 3 The direction of the movement of the needle in all three axes and the angle of the needle in respect to the cell surface. The *z-axis* represents the *front* and *back* movement, the *y-axis* the *up*-and-*down* movement, and the *x-axis* the *lateral* movement away and toward the microscope

the microinjection according to the set program. Examples include the TransferMan® 4r micromanipulator and the Injectman NI2 micromanipulator from Eppondorf. For completely automated instruments, a robotic system guides the micromanipulator to position the needle for microinjection and carries out the microinjection process as programmed. Refer to Fig. 4 in order to understand the needle movement during microinjection for manual and semi-automated or automated systems.

9.3 Microinjector

A microinjector is an instrument that can control and maintain the necessary pressure requirements and perform controlled injection of a calibrated amount of fluid or cargo into the cell. It controls the pressure using compressed air or compressed nitrogen gas. The compressor pump for creating the compressed air may be a separate unit or it may be integrated into the microinjector. Various different kinds of pressure have to be applied or controlled by the microinjector system. A simple capillary tube is known to exert a pressure called 'capillary force' on any solution into which the capillary tube is immersed. In microinjection, the micropipette dipped into the cell culture medium or other solution should not suck the surrounding medium and dilute the injection material. In order to prevent the action of capillary force, a base or compensation pressure has to be applied to the solution in the microneedle [4]. To perform the injection of a set amount of cargo into the cell, injection pressure has to be applied to the solution inside the microneedle. Further, on blockage of the needle an increased pressure has to be applied to clear the clogged needle. So by controlling and applying pressure at various levels, the microinjector can be calibrated to inject the precise amount of cargo into the host cell. Manual microinjectors can be custom-made in several ways, such as that described in Barber [2] (Fig. 1), and a well-regulated syringe can be used to maintain the compensation pressure and produce sufficient injection pressure, as shown by Gueroussov et al.

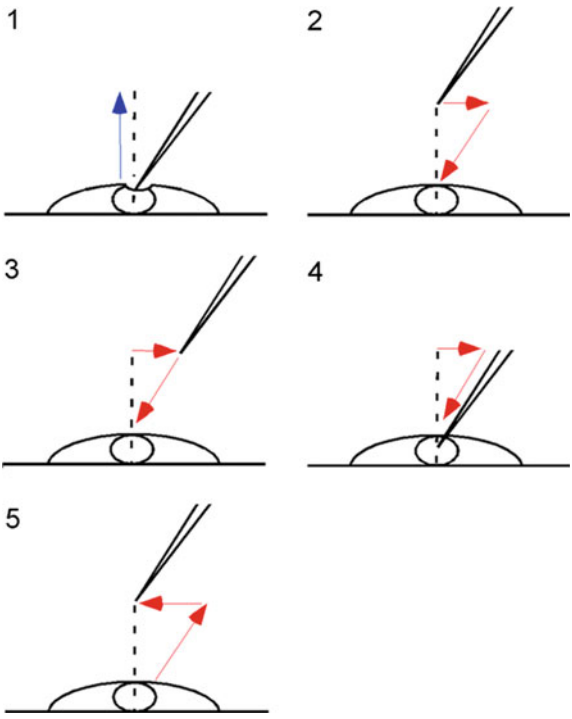

Fig. 4 Schematic representation of the movement of the needle during microinjection. (1) Manual movement of the needle by a technician indicated by a *blue arrow*. (2–5) Movement of the needle by an automatic injection system indicated by *red arrows* in several steps. Reprinted from Lappe-Siefke et al. [125], Copyright 2008, with permission from Elsevier

[126] (Fig. 5). The disadvantage of the manual system is that there is no precise pressure control, resulting in uncontrollable cargo delivery.

There are two types of microinjector system: (a) a constant flow system and (b) a pulse flow system. In the former system, a constant amount of pressure is applied, resulting in a continuous flow of injection material out of the microneedle. This system is disadvantageous as the amount of cargo injected depends upon the duration for which the needle remains penetrated in the cell, resulting in nonreproducibility. Highly reproducible experiments can only be obtained by repeated practice. An example of a constant flow system is World Precision Instruments' Pneumatic PicoPump PV830. The pulse flow system can produce pressure only for a programmed amount of time, resulting in a flow of injection material for a set amount of time. This system can microinject roughly the same amount of cargo into all cells and is highly advantageous, producing reproducible data [127]. An example of a pulse flow microinjector system is Femtojet® from Eppendorf.

Some research articles provide precise pressure values for microinjection [115, 128]. However, pressure values have to be calibrated or standardized for a particular

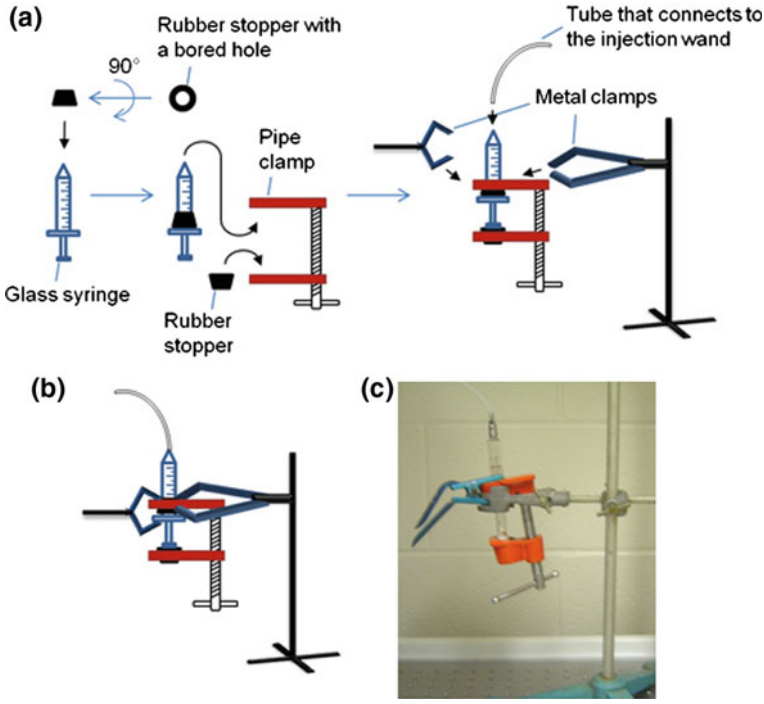

Fig. 5 Syringe-regulated microinjector. **a** Step-by-step assembly of syringe regulator. **b** Pictorial diagram of assembled syringe regulator. **c** Actual picture of syringe regulator. Reprinted from Gueroussov et al. [126] with permission obtained from JoVE

needle with a particular tip opening size, in order to microinject the precise amount of cargo.

9.4 Needle, Needle Puller, and Its High-Throughput Modifications

Although capillaries of different materials are available, such as borosilicate glass capillaries, aluminosilicate glass capillaries, quartz, etc., borosilicate glass capillaries are most widely used for needle microinjection. In order to make an injection needle or holding pipette, a glass capillary obtained from any company has to be pulled at a certain speed, with timed heating and cooling. Variation in any of the above-mentioned factors will result in varieties of different sizes and shapes of needles [129]. Through precise control of these physical factors, needles of appropriate size and shape can be obtained in a highly reproducible manner. A needle puller is an instrument that can be used to make an injection needle

mechanically. Examples include the P-97 Micropipette puller (Sutter Instruments) and the PMP102 Micropipette puller (MicroData Instruments *Inc.*). The tip of the injection needle or holding pipette is sealed at the time of pulling and needs to be broken for a microinjection experiment (refer to Sects. 10.1.3 and 10.1.4 for more information). Commonly, the borosilicate glass capillary, with an outer diameter of 1.0 mm and an inner diameter ranging from 0.5 to 0.75 mm, is used for microinjection, but a wide range of capillaries are available and can be used for experimentation. After needle preparation, the inner diameter ranges from 3 to 5 μm, whereas a holding pipette has a bigger inner diameter of around 10–20 μm. Apart from lab-made needles, commercial microneedles are also available, for example, the Femtotips I and Femtotips II from Eppendorf. The injection needle used by Barber [2] was pulled by his own hands, which requires several months of training. However, to make the needle-pulling procedure highly reproducible and comfortable, a variety of mechanical instruments have been developed.

The introduction of various upgrades in instrumentation and automation resulted in increase of both efficiency and the number of cells being microinjected, from a few hundred cells to 1000 cells per hour. Microneedles have been replaced by microfluidic devices aided by automated cell deduction and microinjection. In most of the microfluidic devices, the needle is made stationary, whereas the cells are mobilized and impinged by the needle from delivering cargo, unlike the traditional microinjection technique, where the needle is constantly mobilized and the cells are immobilized [12]. Adamo and Jensen [11] introduced a microfluidic device, where a cell is mobilized in a microchannel, then captured by a microneedle for injection, and finally collected in a reservoir. The movement of the cell and its capture toward the microneedle is controlled by two valves (Fig. 6a). This microfluidic device can achieve a microinjection rate of 3600 cells per hour [11, 12]. Another device was designed by Zhang et al. [130]. The device consisted of several injection units, where the cells were captured via negative aspiration flow resulting in the penetration of the microneedles and injection of the cargo, followed by the release of cells by positive aspiration flow (Fig. 6b, c). However, the poration efficiency was $\sim$15 %, which dictates further development in order to acquire greater advantage for the device [130]. Yet, another injection device was provided by Adamo et al. [131], where a jet of injection fluid was generated by a piezoelectric membrane that can penetrate into the cell to deliver the cargo (Fig. 6d). This device can deliver cargo at up to 1000 cells per minute, but further evaluation is needed to calculate the efficiency of the microinjection [131].

Apart from the introduction of microfluidic devices, microneedles made with specialized materials have been used successfully to perform microinjection, for example, a silicon microchip nanoinjector with a solid, electrically conductive lance [132], a nanoinjector made of carbon nanotubes attached with an atomic-force microscopy (AFM) probe [133, 134], and a modified AFM probe with nanofluidics [135]. As DNA is negatively charged, it can be adsorbed to the surface of the positively charged lance. On penetrating the cell, the negatively charged lance can be made to release the DNA into the cell. The use of a lance has shown several advantages over conventional needle microinjection, such as increased integration

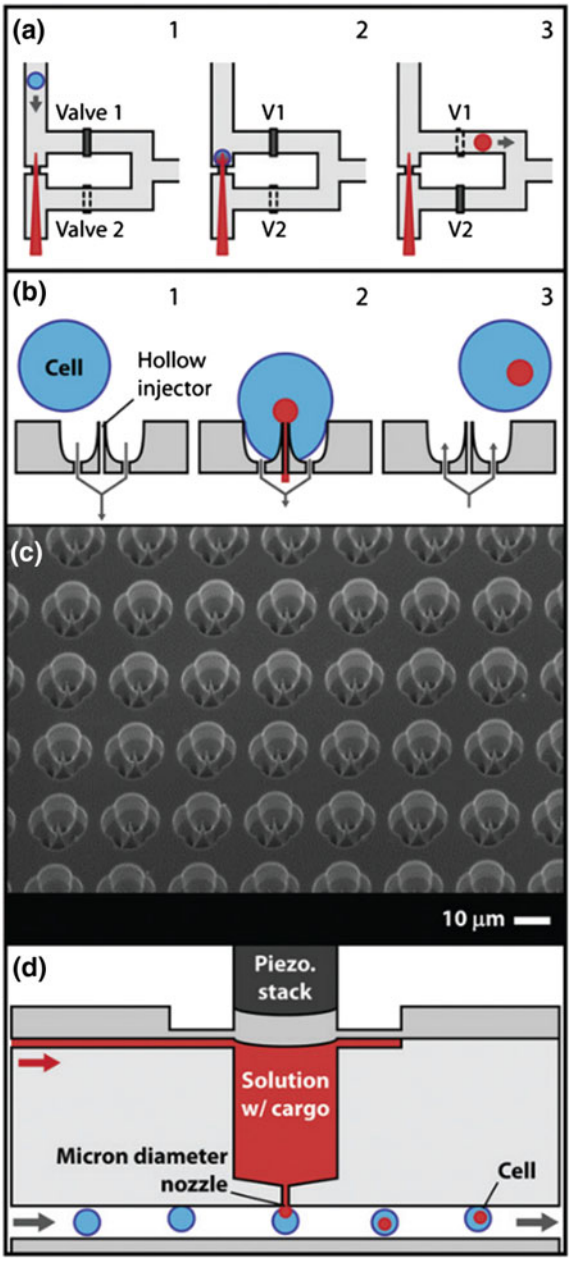

Fig. 6 High-throughput microfluidic devices and their concepts. **a** Microfluidic device introduced in Adamo and Jensen [11]. **b** Methodology of microinjection of cells in ultra-high-throughput (UHT) microinjection device introduced in Zhang et al. [130], where *1* shows the cell moving toward the injection needle, *2* shows the cell impinging the microneedle, and *3* shows the removal of cells from the microfluidic device and Valve V1 and V2 controlling the movement of the cell inside the device shown in (**a**). **c** SEM image of UHT capture site from Zhang et al. [130]. **d** Schematic representation of jet injection system introduced in Adamo et al. [131], where the pressure generated by the piezoelectric element is used to inject the cargo solution into the cell. Reprinted from Meacham et al. [12], with permission from SAGE publications. Copyright © 2014

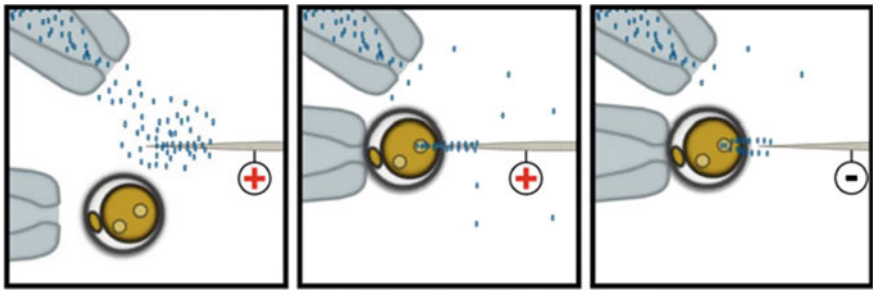

Fig. 7 Schematic representation of microinjection using a lance. From *left* to *right*—shows the step-by-step procedure for microinjection using a lance. First, the lance is positively charged to adsorb the negatively charged DNA molecules; then the lance is injected into the zygote followed by charging the lance to negative thereby releasing the adsorbed DNA inside the cell. Reprinted from Aten et al. [132], with kind permission from Springer Science+Business Media

of injected DNA, injection of DNA without any fluid, and increased success rate of the progression of injected zygotes to transgenic pups (Fig. 7) [132]. A carbon nanotube with an AFM tip has been able to carry cargo attached to nanotubes by a disulfide-based linker. Upon microinjection, reduction of the disulfide-based linker results in the release of cargo into the cell (Fig. 8) [133]. Further, AFM tips designed with nanochannels can successfully deliver cargo into the cell (Fig. 9) [135]. AFM tip-based microinjection has shown better interaction between the cell and AFM nanoneedle probes for precise cargo delivery into the cell.

9.5 Perfusion and Injection Chamber

A perfusion chamber is a small box-like apparatus caging the microscope stage, where microinjection will be performed. As injection of hundreds of cells requires a considerable time, proper maintenance of growth conditions such as CO_2 atmospheric concentration (in order to maintain the pH), humidity and sterility (to prevent contamination from other microorganisms), etc. is needed to ensure the survival of the cells. A perfusion chamber can be fitted with appropriate gas cylinders and a control system to regulate the percentage of atmospheric concentration of gases. The problem of pH maintenance can also be solved by supplementing the cell growth media with HEPES pH 7.4. Further modifications in the microscope stage are available, specifically for microinjection of the cells to maintain an appropriate temperature in order to ensure the survival of the cells. Thus, the modified microscope stage is called the 'injection chamber.' The main function of injection and perfusion chambers is to maintain appropriate survival conditions for host cells. However, with an experienced technician, or with the help of an automated injection system, several cells can be microinjected in a short time. This will limit the exposure of cells to adverse environmental conditions. Therefore,

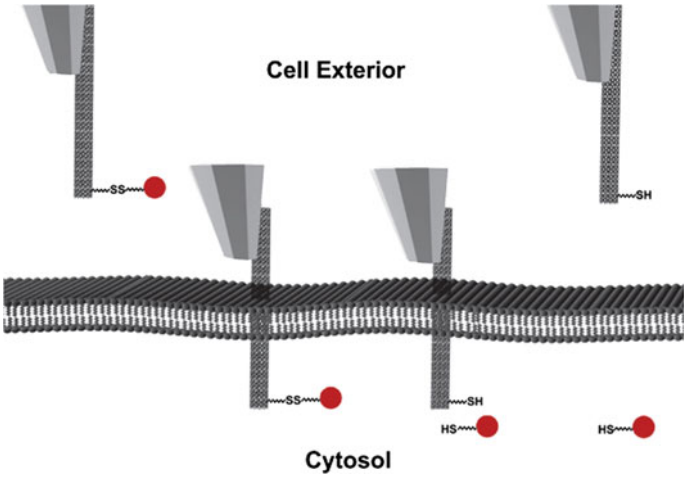

Fig. 8 Schematic representation of microinjection using a Multiwalled Carbon Nanotube-AFM tip. The figure shows the step-by-step process of penetration of the AFM tip, which carries cargo attached to the carbon nanotube by a disulfide linker. After penetration inside the cell, the cargo is released upon reduction of the disulfide bond. Reprinted with permission from Chen et al. [133], Copyright (2007) National Academy of Sciences, U.S.A.

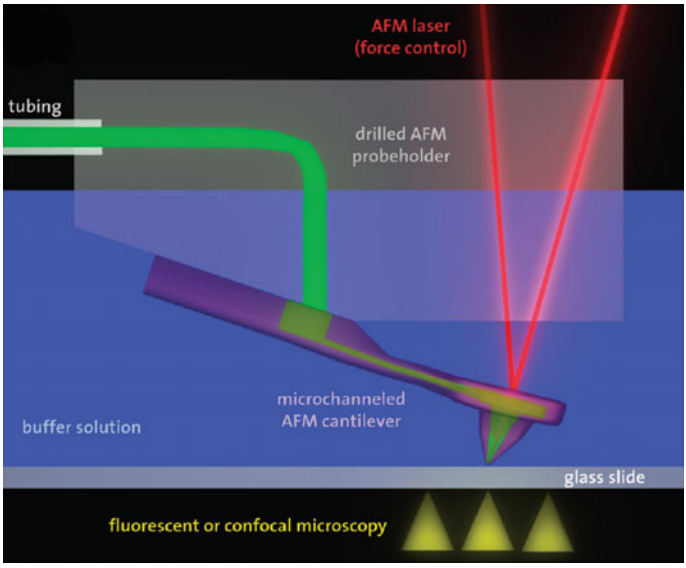

Fig. 9 Schematic representation of microchanneled cantilever chip fixed to a drilled AFM probe holder. This system can be operated both in air and immersed in a buffer solution. The injection solution passes through the microchannel and is released into the cell upon insertion into the cell. The use of appropriate microscopy can help to visualize the injected substrate in the cell. Reprinted with the permission from Meister et al. [135]. Copyright 2009 American Chemical Society

the injection or perfusion chamber can be sacrificed [4], but sacrificing these chambers is not recommended.

9.6 Semi-automated and Automated Systems for Needle Microinjection

The microinjection technique can be instrumentalized at various stages, such as with (1) a manual system, (2) a semi-automated system, and (3) an automated system. A manual microinjection system requires several months of practice. However, only a few hundred cells can be microinjected at a given time. In order to overcome these difficulties in a manual injection system, technological upgrades have been made, resulting in semi-automated and automated systems that can increase the efficiency and rate of microinjection.

There are only a few technological differences between the above-mentioned systems, but the final output of the experiment is greatly increased by increasing automation. In a manual microinjection system, the micromanipulator is operated completely manually by the technician. This requires greater technical skills, in order not to damage the cell or the microneedle. Also, manipulating the position of the needle for microinjection of several cells in a field requires a considerable amount of time and thus limits the number of cells being microinjected at a given time. In a modern-day manual microinjection, the injection pressure and the amount of material injected are controlled mechanically. However, this unit can also be manualized, resulting in a demand for greater technical skills (refer to Fig. 1 to understand a completely manual system). In semi-automated instruments, an initial calibration is made to guide the needle for injection into the cell [136]. Once calibrated, the needle can be used to inject several thousand cells. The calibration needs to be changed only when the needle is changed or for a new microinjection experiment. Further, the injection needle can be moved precisely from cell to cell with the help of a joystick controller by a technician. Thus, microinjection using semi-automated instruments increases the efficiency of the injection, along with decreased cellular damage.

Further improvements were made by the integration of robotic systems with microinjection systems. As a result, the location of the cells can be recognized by the robotic system. This involves initial calibration of the needle along with marking the location of adherent cells or the coordinates of the position of the cells. Later, the robotic system can automatically microinject all the marked cells [13]. Because adherent cells grow on a surface and do not have a uniform shape, various methods and programs are being developed in order to facilitate the identification of adherent cells [14, 23, 137, 138].

To use semi-automated and automated systems for microinjection, all the cells in the cultured dish should be in the same focal plane or on a flat surface. Further, automations are being made to increase the efficiency of the microinjection of

oocytes of different species such as mouse, zebrafish, embryo of fruit fly, and protoplast, resulting in increased efficiency of up to several times [14, 139, 140]. Care is to be taken to identify a clogged needle as early as possible. Otherwise, an unidentified clogged needle may perform microinjection of many cells in an automated system, which may mislead the analysis of the results.

10 Brief Protocol

A microinjection experiment can be divided into two stages: (1) preparation of all the items needed for the microinjection and (2) the act of performing the microinjection experiment. It is important to carry out both stages of the experiment with utmost care.

10.1 Preparation of Items for Microinjection

For efficient application of the microinjection technique, the samples (host cells and cargos), instruments, and other materials should be prepared based on previously described protocols from the literature. Some of the important procedures include the following:

10.1.1 Cargo Sample Preparation

As previously discussed in Sect. 7, a wide variety of chemical substances and biomolecules have been efficiently microinjected in various studies. It is highly recommended that cargos for microinjection should be prepared in an appropriate way, so that the cargo can be accepted by the host cell. The most commonly used cargo biomolecules include DNA, RNA, peptides, proteins, and sperm.

DNA and RNA (nucleic acids): Purified nucleic acid (either DNA or RNA) is generally dissolved with an injection buffer (140 mM KCl and 10 mM HEPES, pH 7.4 for mammalian cells) [126] at an appropriate concentration and loaded into the micropipette. Injection buffer generally mimics the intracellular conditions with appropriate ion concentrations and pH. For most of the experiments, it is advisable to standardize the cargo concentration (between 10 ng/μl and 500 ng/μl, depending upon the experimental design) for that particular cargo and the host cell. It is important to understand that neither overdosage nor a very low amount of cargo will produce scientifically sound data. Note that contamination of a cargo sample with ethanol, used for purification of nucleic acid, may be toxic for host cells. Along with the cargo sample, it is a common practice to mix fluorescent or colored dye particles such as Oregon Green 488(OG)-conjugated 70 kDa dextran (1 mg/ml) [126] or Dextran Texas red [4] in order to identify the microinjected cells. Kits are

available on the market, from companies such as Invitrogen, Qiagen, etc., to prepare pure DNA or in vitro synthesis of RNA followed by purification. Further, as soon as the microinjection mixture is prepared, it is highly recommended to centrifuge the mixture at 16,000 g for 20–30 min at 4 °C and load the supernatant into microneedles for microinjection. This process will pellet down the potential particulate matter that can block the micropipette [44, 126].

Peptides and protein cargos: When preparing peptide or protein cargos for microinjection, it is important to use an appropriate buffer that can maintain the cargo in a functionally and structurally active state so that an appropriate response can be observed in the host cell, for example, recombinant caspases were suspended in a 'caspase active buffer—20 mM PIPES, 100 mM NaCl, 10 mM DTT, 1 mM EDTA, 0.1 % CHAPS, 10 % sucrose with pH 7.2' [4], whereas Aβ peptides were diluted in phosphate-buffered saline for microinjection [120]. Thus, it is important to understand the nature of the peptide or protein from the existing literature in order to microinject a functionally active protein cargo. Further, it is also necessary to standardize the concentration of protein to prevent toxicity to the host cells. As mentioned for nucleic acid biomolecules, the microinjection mixture should always contain fluorescent dye (coinjection marker) to identify the microinjected cells. Further, centrifugation of the microinjection mixture prior to microinjection, to pellet down the particulate debris, is also essential.

Sperm for ICSI: Sperm samples from male mice are collected from a dissected-out cauda epididymis structure of the testicles. The epididymis is suspended in HEPES–CZB buffer and teased into fine pieces, to suspend the spermatozoa in the buffer. The sample should be diluted using HEPES–CZB buffer and mixed with an equal volume of polyvinylpyrrolidone saline. The prepared sample can be stored for up to 3 h at a cooler temperature, 18 °C, until microinjection [8]. For clinical purposes, the semen samples will be collected from male partners or donors. The spermatozoa were incubated with T6 medium and then exposed to an electric field of 1250 V/cm for 2.5 ms (in order to increase the acrosome-reacted spermatozoa). This was followed by a wash and incubation again in T6 medium with 3.5 mmol/L of pentoxifylline until microinjection [9].

10.1.2 Host Cell Preparation

The basic procedure for the preparation of most common host cells is discussed below (refer to Sects. 7 and 8 for different kinds of host cells); these include cultured cell lines, cultured tissue, oocyte for ICSI, and plant protoplast.

Cultured cell lines: Generally, a well-spread monolayer is highly amenable to microinjection. In order to achieve a well-spread monolayer of cells, fibronectin can be coated on the culture dish prior to cell seeding. Further, cellular confluency of 70–90 % should be achieved at the time of the microinjection experiment. Depending upon the purpose of the study, the cells can be seeded on a coverslip or in a cell culture dish for at least 24 h prior to the microinjection experiment. Proper maintenance of the CO_2 concentration in the injection environment is necessary to

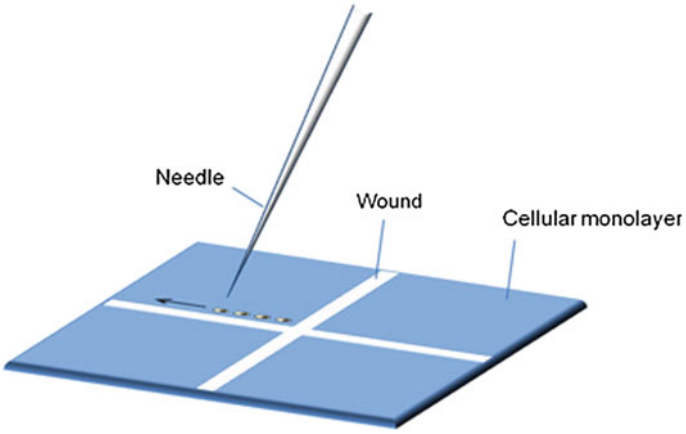

Fig. 10 Monolayer of cultured cells wounded by marking a cross across the cell monolayer with a 200 µl tip. This marking help us to perform an ordered microinjection array as shown and can be used for quick identification of microinjected cells for further analysis. Figure reprinted from Gueroussov et al. (2010) with kind permission from JoVE [126]

maintain an appropriate pH of the culture media or the media must be supplemented with 10 mM HEPES pH 7.4 to resist the change in pH. Finally, injection should be carried out in an injection chamber fitted with a microscope to maintain the survival temperature. In order to identity the microinjected cells or for a proper microinjection array, the cell monolayer can be wounded using a sterile 200 µl plastic pipette tip as shown in Fig. 10 [126].

Cultured tissues: The animal tissues for culturing and microinjection should be obtained in an appropriate way and should be maintained in survival conditions, as described elsewhere. A brief description of the preparation of animal tissue taken from Wong et al. [44] is as follows (Fig. 11). Dissected tissue is washed and maintained in Tyrode's solution, and then embedded in 3 % agarose type XI dissolved in phosphate-buffered saline and sliced with a vibratome, followed by removal of the agarose around the tissue sections. The sliced tissue section is placed in a Petri dish containing slice culture medium (SCM) and incubated until microinjection. For microinjection, the tissue section is placed in a Petri dish containing pre-warmed CO_2-independent microinjection medium (CIMM). Then a custom-made grid is placed above the tissue, so that the nylon threads that make the grid remain perpendicular to the surface being microinjected and parallel to the microneedle. After microinjection of several single cells into the tissue section, the tissue is cultured in SCM. During all the tissue processing steps, it is very important to maintain the tissue in survival conditions as described by Wong et al. [44] or elsewhere, depending upon the tissue used and the purpose of the experiment.

Oocyte for ICSI: Oocytes of mammalian animals, such as mice, for microinjection are generally collected by flushing out the oviduct or by sacrificing the female animal following superovulation by administration of chorionic gonadotropin

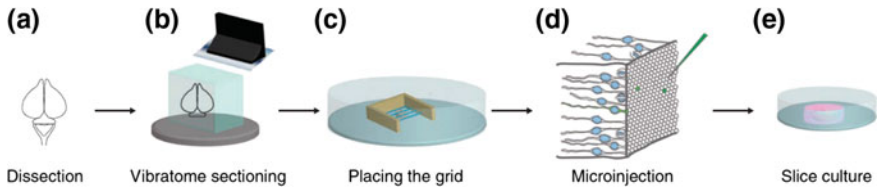

Fig. 11 *Pictorial flowchart* of the steps involved in microinjection of cultured tissue section. **a** Dissected brain tissue. **b** The embedded tissue is sectioned in a vibratome. **c** Tissue section arrangement in a petri dish with custom-made grid. **d** Microinjection of individual cells along the injection surface of the tissue. **e** Culture of injected tissue section. Reprinted by permission from Macmillan Publishers Ltd: Wong et al. [44], copyright 2014

hormone [128, 141], whereas in human beings an ultrasound-guided probe is used to reach the ovarian follicle and the superovulated oocytes are sucked out by a trained and licensed physician. Oocytes of mice are collected in collection medium (MEM/PVP) containing milrinone (M) [128]. The oocyte is freed from cumulus cells by repeated sucking and releasing of the oocyte–cumulus complex in either the collection medium or CZB medium and cultured in an appropriate culture medium, such as CZB medium, until microinjection [8, 128, 141]. Human oocytes were transferred to M2 medium containing 1 mg/ml of hyaluronidase for 1 min and pipetted up and down to remove the cumulus cells followed by washing with M16 medium containing human serum albumin prior to the microinjection procedure [142]. In order to microinject the oocyte, the chamber slide is prepared containing a drop (around 5 µl) of MEM/PVP+M close to a drop (around 0.5 µl) of injection material or spermatozoa and covered with mineral oil. Prior to microinjection, transfer the oocytes to the MEM/PVP+M drop and then perform the microinjection procedure (Fig. 12 shows a chamber slide being prepared for microinjection) [8, 128]. A vast amount of literature is available to explain the isolation of oocytes from different organisms for microinjection. It is important to adopt appropriate buffers and media for isolation and culturing of oocytes from different species, as described elsewhere.

Plant protoplast: Protoplast can be isolated from different kinds of plant tissues, depending upon the purpose of the experiment and by adopting different methods [143–145]. It has been reported that freshly isolated protoplast was not suitable for microinjection [146]. Thus culturing protoplast for 2–7 days prior to microinjection in Linsmaier and Skoog medium containing 1-naphthaleneacetic acid, 6-benzylaminopurine, and glucose is recommended [146].

10.1.3 Microneedle Preparation

Micropipettes are made from borosilicate glass capillary (commonly the outer diameter is 1.0 mm with an inner diameter of 0.75 or 0.5 mm) using a mechanical needle-pulling machine (refer to Sect. 9.4 for more information about the

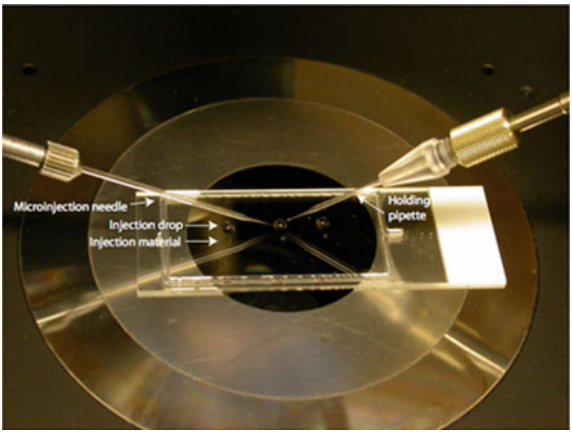

Fig. 12 Chamber slide prepared for microinjection, where the three sets of injection drop (containing oocytes) and injection material drop (containing injection material) are covered by mineral oil which fills the chamber. On the *right side* is a holding pipette to immobilize the oocyte, while on the *left side* is the injection needle. Figure reprinted from Stein and Schindler (2011) with kind permission from JoVE [128]

fabrication of microinjection pipettes and holding pipettes). The resulting injection pipette can have an outer diameter of ~7 μm and an inner diameter of ~5 μm. However, holding micropipettes have a relatively larger inner diameter of ~10 μm. At the time of micropipette fabrication, the tip of the pipette is sealed and has to be broken for microinjection either by touching/hitting/tapping the pipette tip against a capillary tube/holding pipette or by dragging it along the edge of a hard surface of a glass coverslip which is placed perpendicular to the injection pipette tip. Care is to be taken to avoid breaking the tip into a larger internal diameter, which can cause extensive cellular damage. However, a very small internal diameter will result in clogging the micropipette tip. A holding pipette is pulled in a similar way to an injection pipette. But after pulling, the holding pipette is broken or cut to a diameter of ~80–120 μm and the tip of the holding pipette is fire-polished using a micro-forge [8, 9, 128, 147].

10.1.4 Loading the Sample into the Microneedle

Prior to microinjection, the injection needle can be loaded with the injection sample from the back end of the needle using GELoader tips (item # 022351656; Eppendorf) or using a custom-made syringe tip from a 1 ml clinical syringe. Custom-made syringe tips are made by heating the middle part of the plastic cylinder of a 1 ml syringe without the plunger. On heating, the middle part of the

cylinder will melt and start to collapse. Then, the ends of the cylinder are pulled apart so that the cylinder becomes very thin (do not pull too much as it might break the syringe cylinder into two pieces). Let the plastic cylinder cool and harden. The syringe cylinder is cut at an appropriately thin point, resulting in making a fine tip that can be inserted into the back of the microneedle. A few microliters of the sample can be loaded into the injection needle. The loaded sample solution at the back of the microneedle will be drawn to the needle tip by capillary force and gravity within few seconds to minutes when placed vertically or at a 45° angle to the ground. The loaded injection needle can be fitted onto the adaptor, which can be connected to the micromanipulator [44, 126]. The needle tip can be broken prior to microinjection as mentioned above in Sect. 10.1.3. Alternatively, in the case of ICSI or microinjection of oocyte with biomolecules, the injection needle is attached to the micromanipulator and broken prior to sucking a single spermatozoon or injection material from the injection material drop, thereby loading the needle with a single spermatozoon or other biomolecules.

10.2 Microinjection Procedure

1. Prepare the microinjection needle and hold the pipette (if necessary) as mentioned above in Sects. 10.1.3 and 10.1.4, and attach it to the micromanipulator.
2. In the inverted microscope, adjust the micromanipulator to focus the microinjection needle using a combination of 10× and 40× objective, so that the microinjection needle tip is at the center of the field when visualized using the 40× objective.
3. Raise the injection needle above the focal plane and place the Petri dish containing the cultured cells or tissue or chamber slide containing the oocyte and injecting material on the microscope stage.
4. Focus the cells on the wounded region or cultured tissue section or oocytes with a lower magnification objective of 10×.
5. The magnification is increased to the 40× objective and the injection needle is lowered to visualize the needle clearly and adjusted to stay just above the cultured cells or perpendicular to the cultured tissue sections or close to the oocyte.
6. The needle is lowered further to puncture the cultured cells [126] (Fig. 13) or gently touched on the surface of the cultured tissue where the cell is needed to be microinjected [44] (Fig. 14) or suck hold the oocyte with the holding pipette and try to puncture the oocyte with the injection needle filled with injection material [8, 71, 128] (Fig. 15).
7. Perform the injection where the injection is controlled using the microinjection system. Observe all noticeable changes that happen inside the cell upon microinjection and this is very clear through a phase-contrast microscope.

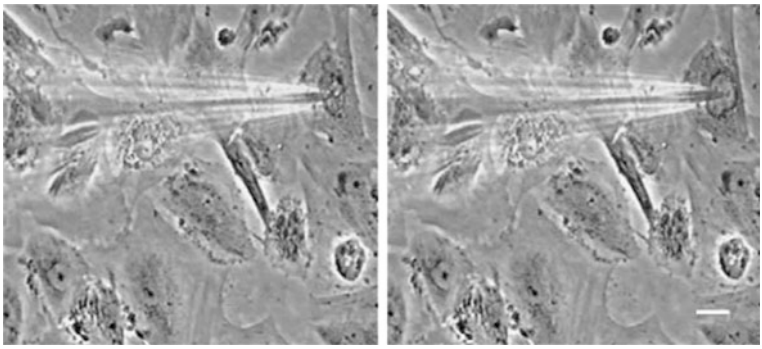

Fig. 13 Microinjection of adherent cells. The figure on the *left* shows the needle before penetration into the adherent cells and the figure on the *right* shows the needle after penetration. Scale bar 20 µm. Figure reprinted from Viigipuu and Kallio (2004) with kind permission from Altern. To Lab Anim [10]

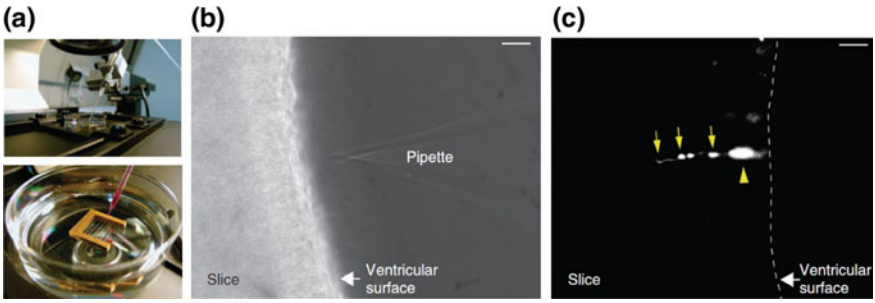

Fig. 14 Microinjection into a single cell on a tissue section. **a** Shows the microinjection setup with the host tissue sample, above, and the Petri dish containing the host tissue section and a grid placed above it, below. **b** Phase-contrast image of tissue showing the ventricular surface and the injection pipette. **c** Shows successful microinjection of a single cell; the *arrowhead* shows the cell body and the *arrows* show the cellular processes. Scale bar 10 µm. Reprinted by permission from Macmillan Publishers Ltd: Wong et al. [44], copyright 2014

Commonly, the injection volume is around 5–10 picoliters. Further, a single needle can be used to microinject several individual cells until the needle blocks or the experiment ends.

8. After microinjection, the microneedle is removed from the monolayer of cultured cells or moved laterally away from the cultured tissue section or removed from the oocyte.
9. The microinjected cells are incubated appropriately and used for further analysis.

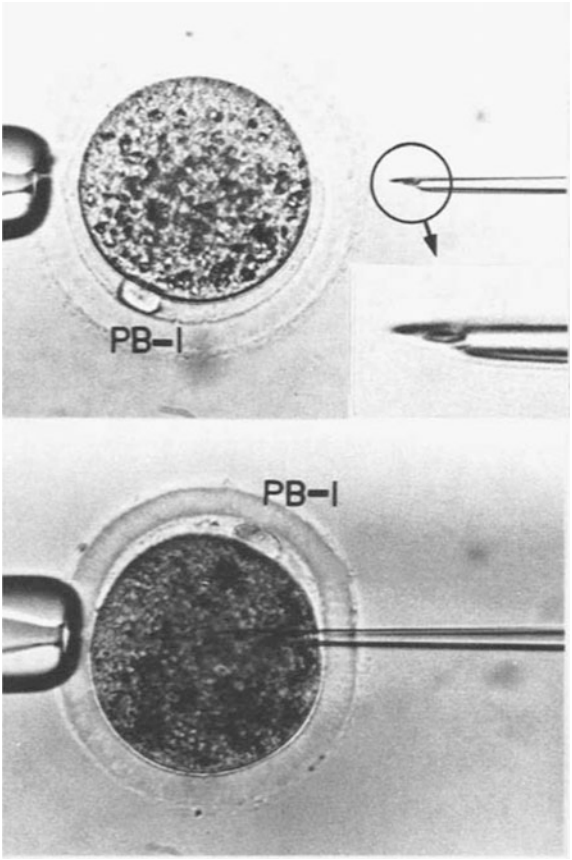

Fig. 15 Microinjection of a rabbit oocyte. The *top image* shows an oocyte immobilized by a holding pipette, which contains a polar body I (PB-I) and shows the magnified tip of the injection needle, magnification 415×. The *bottom image* shows the injection of spermatozoon. Reproduced from Iritani et al. [71] by permission of John Wiley & Sons Ltd.

11 Important Troubleshooting

As the technique of microinjection requires extreme technical expertise, several critical steps to overcome the technical obstacles are always appreciated. This section concentrates only on troubles related to the microinjection procedure. However, as mentioned earlier, the host cell has to be maintained in good condition before and after microinjection. Further, a quality control examination for oocyte should be performed for a successful experiment, as described elsewhere. The followings are some useful tips for successful troubleshooting: (Table 2).

Table 2 Table summarizes the expected technical troubles in microinjection procedure, its causes, and solutions to solve the technical difficulties

Trouble	Cause	Troubleshooting
• No visible change inside host cell upon microinjection • Very low or no outflow of fluorescent coinjection marker	• The needle did not penetrate the cell or it penetrated too much to punch through the cell • The needle is clogged	• Try to understand the difference in the focal plane between the cell and the needle tip in the phase-contrast microscopy, to successfully penetrate the cell • Increase the pressure to unclog the needle • Always centrifuge the injection solution to pellet down the particulate matter • Place the tip of the needle in the media or solution to prevent it from drying • Raise the needle above the media and dip it again, the clogged particle may be released from the tip because of the rinsing effect developed by this action • Rub the tip on a hard coverslip glass surface to unclog it or break the needle a little more • Change to a new microneedle [44, 126]
• Lot of fluorescent coinjection marker outflow • The cell is inflated or busting on microinjection or too much visible cellular damage	• Too high pressure • The needle is broken more, resulting in bigger external and internal diameter	• Decrease the pressure of the injection [4] • Change to a new microinjection needle [44]
• Only a few microinjected cells survived after the microinjection experiment	• The pipette tip is not of optimal shape and size • Microinjection conditions are not optimal • Cellular damage is extensive resulting in cell death • Concentration of the cargo is toxic to the cells • Injection environment is not maintained properly to buffer the pH of media • Insufficient experimental skills, especially in oocyte microinjection	• Optimize the shape and size of the microneedle tip by standardizing the needle pulling • Standardize the microinjection condition for optimized cargo delivery • Avoid causing extensive cellular damage to the cell, especially oocytes, by hitting the nucleus or organization of the spindle cytoskeleton network [8, 128] • Standardize the amount of cargo being microinjected

(continued)

Table 2 (continued)

Trouble	Cause	Troubleshooting
	• Cells located near the cut surface of the tissue sections are microinjected	• Perform a quality control test such as a penetration test, injection test or survival test, etc. [10] • Maintain proper CO_2 concentration in the injection chamber to maintain the pH of the media or add appropriate buffering agents to the media • Repeat the experiment and practice until your success or survival rate is 50 % [128] • Do not microinject the cells near the cut surface, microinject at least ~40 μm away from the tissue cut surface [44]
• Tissue section pops out of agarose embedding	• Agarose is not homogenous	• On adding tissue to the agarose for embedding, mix the agarose without damaging the tissue to form a homogenous agarose mixture before the agarose solidifies [44]

12 Microinjection for Single-Cell Analysis

This section of the chapter will provide some examples from literatures, to help readers to understand how the techniques of microinjection can be applied to study scientific queries.

Gueroussov et al. [126] employed the technique of single-cell microinjection to study the nuclear export kinetics of mRNA in mammalian cells. Here, mRNA and cloned plasmid DNA were microinjected at concentrations of 200 and 50–200 μg/ml along with Oregon Green 488 (OG)-conjugated 70 kDA dextran (1 mg/ml), respectively. An inverted microscope with a dry 40× extra-long working distance phase objective along with a three-axis hanging joystick micromanipulator device (NT-88-V3MSH, Narishige) was used for microinjection. Upon microinjection of several single cells into a culture dish or coverslip, the cells were fixed and probed with fluorescent FISH probe for analysis of the amount of mRNA export from the nucleus to the cytoplasm. This manuscript states that the microinjection technique is more suitable for analysis of mRNA export between the subcellular components than other transfection methods, because direct microinjection triggers the mRNA export rapidly, unlike other transfection methods that take several hours. It is also mentioned that individual cell-to-cell variations observed in their mRNA quantification were greater and might have resulted from

inconsistencies in the needle flow rate, which is a potential disadvantage of the microinjection technique.

Zhang et al. [115] attempted to provide evidences for the neuroprotective role of androgen and estrogen hormones on amyloid $\beta_{1\text{-}42}$ induced toxicity. Further, they also show that transcriptional activity, following estrogen receptor and androgen receptor activation, is necessary for the neuroprotective role. Microinjections were performed in 11-day primary fetal cortical cultured neurons with Eppendorf Microinjector 5246 using Burleigh Micromanipulator MIS-5000. Microneedle tip diameter was around 0.5 μm pulled from 1.0 mm outer diameter and 0.5 mm inner diameter thin-walled glass capillaries (borosilicate with filament MTW100F-4; World Precision Instruments) with a Flaming/Brown micropipette puller (model P-87; Sutter Instruments). The injection pressure of 100 hPa and the compensation pressure of 50 hPa for an injection time of 0.1 s resulted in an injection volume of 25 pl. Amyloid $\beta_{1\text{-}42}$ was injected at a concentration of 10 nM, cDNAs at 30 ng/ml and heat shock protein at 5 μg/ml with a coinjection fluorescent marker dye Dextran Texas Red at 100 μg/ml into the cytoplasmic region of neurons. Three independent trials with around 200 neurons per trial for an experiment were performed.

Feramisco et al. [67] employed the microinjection technique to show the oncogenic property of oncogenic human ras protein. In their experiments, protein at a concentration of 100–800 μg/ml is injected into ∼35–40 individual cells (REF-52, NIH3T3 and ATCC 1571) and examined for the proliferation capacity of quiescent cells. The proliferation capacity is attained only on injection of oncogenic protein, and not on injection of proto-oncogenic protein or in uninjected cells (Fig. 16).

Masani et al. [77] attempted to create nonchimeric transgenic callus from the protoplast of oil palm plants using PEG-mediated transformation and DNA microinjection. The DNA cassette was diluted to a concentration of 100 ng/μl and mixed to a ratio of 100:1 with Lucifer yellow CH dilithium salt. The microinjection was performed using a Leica DM LFS upright microscope. Application of microinjection to protoplast has the advantage of increased efficiency, unlike particle bombardment and *Agrobacterium*-mediated transformations. Further, microinjection can be used to create a stable single copy of integrated transgenic lines in plants.

Taverna et al. [148] attempted to manipulate the fate of a single neuronal progenitor cell in an organotropic tissue slice using the technique of microinjection. The balance of apical progenitor proliferation versus differentiation was significantly changed upon microinjection of NS-5 prol poly-A^+ RNA. Thus, the fate of a single cell in a tissue was successfully changed. The technique of microinjection into a single cell in a tissue can be used to study various developmental aspects and the function of various proteins in cellular differentiation (Fig. 17).

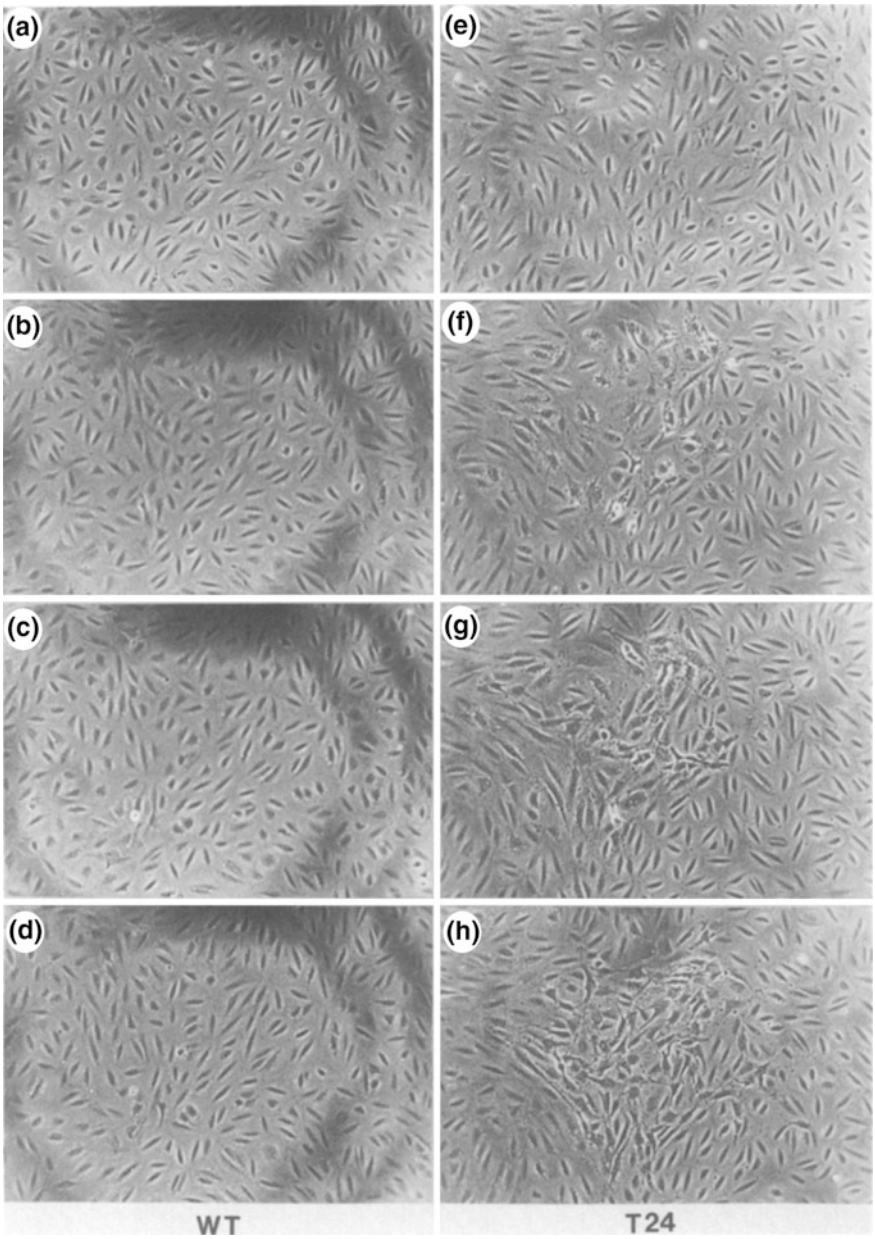

Fig. 16 Microinjection of mutant H-*ras* protein shows oncogenic property in REF-52 cells. **a**–**d** Cells at the center of the field were microinjected with 5×10^6 molecules/cell of proto-oncogenic form of H-*ras* protein and does not show any proliferation of quiescent cells post-microinjection. **e**–**h** Cells microinjected with 8×10^6 molecules/cell of oncogenic H-*ras* protein (T24) show cell proliferation indicating the oncogenic property of mutant oncogenic H-*ras* protein. Cells were imaged at 10× objective lens with phase-contrast microscopy at 30 min. (**a**, **e**), 4 h (**b**, **f**), 12 h (**c**, **g**) and 20 h (**d**, **h**) post-injection. Reprinted from Feramisco et al. [67], Copyright 1984, with permission from Elsevier

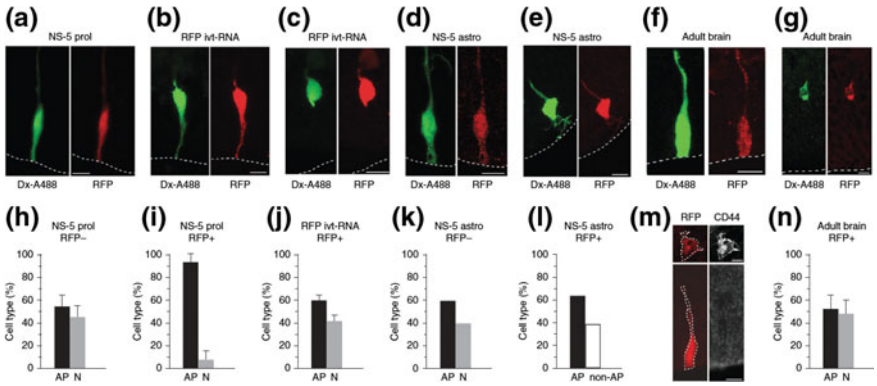

Fig. 17 Microinjection of exogenous mRNA into a single cell on a tissue section changed cell differentiation fate. **a**, **h,** and **i** Poly-A^+ RNA from proliferating NS-5 cells (NS-5 prol) were microinjected into E13.5 hindbrain single apical progenitor cell in a tissue section along with in vitro transcribed red fluorescent protein (RFP) mRNAs (1 %). Dextran-3-A488 (*green*) is a co-injection marker to identify the microinjected cells, whereas RFP mRNAs were used to indicate the microinjected cells that translate the exogenous poly-A^+ RNA. Post-microinjection of 24 h has changed the balance of proliferation of apical progenitor versus differentiation resulting in less neurons (**i**) when compared to control (**h**, cells that did not translate the exogenous RNAs). **c**, **b,** and **j** Microinjection of another control, in vitro transcribed RFP ivt-RNA (which lacks NS-5 proliferating poly-A^+ RNA) did not change the cell fate balance. **d**, **e**, **k**, **l**, and **m** Further, microinjection of poly-A^+ RNA from NS-5 cells differentiated to astrocytes (NS-5 astro) into apical progenitor (AP) cell resulted in AP cells that lost apical progenitor like morphological features and differentiated into cells with astrocytes like morphology, with early astrocytes marker CD44. **f**, **g,** and **n** Finally, microinjection of poly-A^+ RNA from adult brain did not produce any effect in the cell fate. Reprinted by permission from Macmillan Publishers Ltd: Taverna et al. [148], copyright 2011

13 Uses

The uses of the microinjection technique are widespread; apart from applications in scientific research it has been successfully applied in ICSI clinical practice to treat various causes of infertility. The uses of microinjection can be divided into two categories, i.e., research uses and clinical uses.

13.1 Research Applications and Uses

The needle microinjection technique is a gold-standard technique for the introduction of membrane impermeable foreign cargos into a living cell. The technique has an inherent capacity to bypass all the cellular barriers (refer to Sect. 6). It is also

an excellent method for studying the changes and responses of a single cell after the introduction of cargo molecules. As a versatile technique in cellular biology, this technique has been applied to study various aspects of cellular function in scientific research. Several research findings, where the technique of microinjection was successfully employed, have been mentioned and cited throughout this chapter. The followings are some of the important research applications and uses:

- Used in transport studies of biomolecules between different subcellular locations, such as from nucleus to cytoplasm or from cytoplasm to nucleus [126].
- Used for labeling a particular cell (neural stem cells) and tracking the fate of a progenitor cell [44].
- To study the structure of cellular components such as protoplast, cytoplasm, etc. by microinjection of foreign chemicals.
- Used to understand the protein synthesis, maturation pathways, and transport to plasma membrane by microinjection of radioactive substances [47, 63].
- Used to study cytoskeleton dynamics by injecting purified cytoskeletal proteins [64–66].
- Used to study the properties of subcellular substances, by injection of a subcellular substance from one cell to another [50, 51].
- To create transgenic organisms in a variety of species such as mouse, *C. elegans*, fruit fly, and zebrafish by microinjection of engineered DNA into the oocyte or gonads of appropriate organisms [55, 56, 149–151].
- To study the function of various proteins such as kinases, phosphatases, membrane protein, and ion channels by injecting either DNA or purified protein into a single cell [60–62].
- To study the early-stage development of an embryo and cell cycle [61].
- To study the cell death pathway, apoptosis, neurodegenerative disease mechanisms, etc. [4].
- To understand pathways involved in cancer and to study oncoproteins in detail [67, 68].
- Microneedles have been used to create injury in organisms and study wound healing mechanisms and development [152].

13.2 Clinical Applications and Uses

Several decades after the introduction of the microinjection technique to biological research, and the subsequent addition of several technical developments by translational medicine, the technique of microinjection of sperm to oocyte was transferred to a clinical treatment strategy, which resulted in successful pregnancies [9]. Following initial success, developments were applied to increase the success rate of treatment. ICSI has been a treatment of choice for several forms of explained and unexplained infertility problems among couples worldwide. Various statistical data show that several hundreds of thousands of couples undergo an ICSI procedure

every year in order to have a child [153]. The problem of infertility is also linked to various psychological problems and ICSI has played a critical role in attenuating those social and psychological problems related to infertility [154]. Apart from its application in ICSI, the needle microinjection technique has been employed in tissue engineering and biomolecule delivery such as DNA vaccine into individual cells in localized areas of target tissue in human beings for therapy and vaccination [38]. Depending on the delivery region and purpose of the clinical treatment, several modifications have been made in the microneedle in order to maximize the clinical outcome [155, 156]. Vaccine administration using microneedles has been studied in various animal models for several virus types, including influenza, hepatitis B, Japanese encephalitis, and bacteria, anthrax. Further, successful human trials have been reported for the influenza virus and the technique is being adapted into a routine administration procedure [156–158].

14 Conclusion

This chapter provides an overview of the needle microinjection technique, its history, and the basic instrumentation needed, along with recent advancements and its applications in scientific research as well as in clinical therapy. As mentioned earlier, a successful microinjection experiment not only comes from the use of the latest automation technology or from the microinjection of many cells, but also from careful understanding of the technique with better experimental planning and practice to attain expertise. This chapter can be considered as a basic source for understanding the technique, a gateway to understand the advanced materials and research findings in relation to needle microinjection. From this chapter, every researcher can gain a complete understanding of their experimental needs for microinjection and successfully start their research. Apart from the above-mentioned applications of needle microinjection in single cells, it can be applied at the organismal level for the generation of transgenic animals, such as the microinjection of *C. elegans* [149], zebrafish embryos [150], and *Drosophila* embryos [151]. Further, as one of the assisted reproductive techniques, needle microinjection has provided mental satisfaction to couples with infertility problems and developed hope for millions of couples who undergo various kinds of psychological stress as a result of infertility [154]. Thus it can be said that the application of a particular technique and its development is limited only by the applicants' imagination. Needle microinjection, being a gold-standard technique for direct delivery of foreign cargo at the cellular level, can only be expected to undergo more and more development and be applied to a wide variety of fields in the years to come.

References

1. Feramisco J, Perona R, Lacal JE (1999) Needle microinjection: a brief history. In: Microinjection, pp 9–15
2. Barber M (1911) A technic for the inoculation of bacteria and other substances into living cells. J Infect Dis 8:348–360
3. Zhang Y, Yu L-C (2008) Microinjection as a tool of mechanical delivery. Curr Opin Biotechnol 19:506–510. doi:10.1016/j.copbio.2008.07.005
4. Zhang Y, LeBlanc AC (2002) Microinjections to study the specific role of proapoptotic proteins in neurons. In: Apoptosis Techniques and Protocols. Springer, New York, pp 83–106
5. Zhang Y, Yu L-C (2008) Single-cell microinjection technology in cell biology. BioEssays 30:606–610. doi:10.1002/bies.20759
6. Colosimo A, Goncz KK, Holmes AR et al (2000) Transfer and expression of foreign genes in mammalian cells. Biotechniques 29:314–331
7. Dokka S, Rojanasakul Y (2000) Novel non-endocytic delivery of antisense oligonucleotides. Adv Drug Deliv Rev 44:35–49. doi:10.1016/S0169-409X(00)00082-X
8. Kimura Y, Yanagimachi R (1995) Intracytoplasmic sperm injection in the mouse. Biol Reprod 52:709–720. doi:10.1095/biolreprod52.4.709
9. Palermo G, Joris H, Devroey P, Van Steirteghem AC (1992) Pregnancies after intracytoplasmic injection of single spermatozoon into an oocyte. Lancet 340:17–18. doi:10.1016/0140-6736(92)92425-F
10. Viigipuu K, Kallio P (2004) Microinjection of living adherent cells by using a semi-automatic microinjection system. Altern Lab Anim 32(4):417–423
11. Adamo A, Jensen KF (2008) Microfluidic based single cell microinjection. Lab Chip. doi:10.1039/b803212b
12. Meacham JM, Durvasula K, Degertekin FL, Fedorov AG (2014) Physical methods for intracellular delivery: practical aspects from laboratory use to industrial-scale processing. J Lab Autom 19:1–18. doi:10.1177/2211068213494388
13. Pepperkok R, Schneider C, Philipson L, Ansorge W (1988) Single cell assay with an automated microinjection system capillary. Exp Cell Res 178:369–376
14. Matsuoka H, Komazaki T, Mukai Y et al (2005) High throughput easy microinjection with a single-cell manipulation supporting robot. J Biotechnol 116:185–194. doi:10.1016/j.jbiotec.2004.10.010
15. Katarzyna J (2012) AFM based single cell microinjection: technological developements, Biological experiments and biophysical analysis of probe indentation
16. Cuerrier CM, Lebel R, Grandbois M (2007) Single cell transfection using plasmid decorated AFM probes. Biochem Biophys Res Commun 355:632–636. doi:10.1016/j.bbrc.2007.01.190
17. Kay MA, Glorioso JC, Naldini L (2001) Viral vectors for gene therapy : the art of turning infectious. Nature 7:33–40. doi:10.1038/83324
18. Zhang X, Godbey WT (2006) Viral vectors for gene delivery in tissue engineering. Adv Drug Deliv Rev 58:515–534. doi:10.1016/j.addr.2006.03.006
19. Robbins PD, Ghivizzani SC (1998) Viral vectors for gene therapy. Pharmacol Ther 80:35–47. doi:10.1016/S0163-7258(98)00020-5
20. Casper D, Engstrom SJ, Mirchandani GR et al (2002) Enhanced vascularization and survival of neural transplants with ex vivo angiogenic gene transfer. Cell Transplant 11:331–349
21. Condreay JP, Witherspoon SM, Clay WC, Kost TA (1999) Transient and stable gene expression in mammalian cells transduced with a recombinant baculovirus vector. Proc Natl Acad Sci U S A 96:127–132. doi:10.1073/pnas.96.1.127
22. Thomas CE, Ehrhardt A, Kay MA (2003) Progress and problems with the use of viral vectors for gene therapy. Nat Rev Genet 4:346–358. doi:10.1038/nrg1066

23. Truong HH, de Sonneville J, Ghotra VPS et al (2012) Automated microinjection of cell-polymer suspensions in 3D ECM scaffolds for high-throughput quantitative cancer invasion screens. Biomaterials 33:181–188. doi:10.1016/j.biomaterials.2011.09.049
24. Sanford JC, Klein TM, Wolf ED, Allen N (1987) Delivery of substances into cells and tissues using a particle bombardment process. Part Sci Technol 5:27–37. doi:10.1080/02726358708904533
25. Yang NS, Burkholder J, Roberts B et al (1990) In vivo and in vitro gene transfer to mammalian somatic cells by particle bombardment. Proc Natl Acad Sci U S A 87:9568–9572. doi:10.1073/pnas.87.24.9568
26. Udvardi A, Kufferath I, Grutsch H et al (1999) Uptake of exogenous DNA via the skin. J Mol Med (Berl) 77:744–750. doi:10.1007/s001099900048
27. Zelenin AV, Kolesnikov VA, Tarasenko OA et al (1997) Bacterial beta-galactosidase and human dystrophin genes are expressed in mouse skeletal muscle fibers after ballistic transfection. FEBS Lett 414:319–322. doi:10.1016/s0014-5793(97)01019-3
28. Sohn RL, Murray MT, Schwarz K et al (2001) In-vivo particle mediated delivery of mRNA to mammalian tissues: ballistic and biologic effects. Wound Repair Regen 9:287–296. doi:10.1046/j.1524-475X.2001.00287.x
29. Plank C, Schillinger U, Scherer F et al (2003) The magnetofection method: using magnetic force to enhance gene delivery. Biol Chem 384:737–747. doi:10.1515/BC.2003.082
30. Scherer F, Anton M, Schillinger U et al (2002) Magnetofection-enhancing and targeting gene delivery by magnetic force in vitro and in vivo. Gene Ther 102–109. doi: 10.1038/sj/gt/3301624
31. Plank C, Zelphati O, Mykhaylyk O (2011) Magnetically enhanced nucleic acid delivery. Ten years of magnetofection-progress and prospects. Adv Drug Deliv Rev 63:1300–1331. doi:10.1016/j.addr.2011.08.002
32. Santra TS, Tseng FG (2013) Recent trends on micro/nanofluidic single cell electroporation. Micromachines 4:333–356. doi:10.3390/mi4030333
33. Chen SC, Santra TS, Chang CJ et al (2012) Delivery of molecules into cells using localized single cell electroporation on ITO micro-electrode based transparent chip. Biomed Microdevices 14:811–817. doi:10.1007/s10544-012-9660-9
34. Santra TS, Wang PC, Chang HY, Tseng FG (2013) Tuning nano electric field to affect restrictive membrane area on localized single cell nano-electroporation. Appl Phys Lett. doi:10.1063/1.4833535
35. Frenkel V, Li KCP (2006) Potential role of pulsed-high intensity focused ultrasound in gene therapy. Future Oncol 2:111–119. doi:10.2217/14796694.2.1.111
36. Newman CMH, Bettinger T (2007) Gene therapy progress and prospects: ultrasound for gene transfer. Gene Ther 14:465–475. doi:10.1038/sj.gt.3302925
37. Ter Haar G (2007) Therapeutic applications of ultrasound. Prog Biophys Mol Biol 93:111–129. doi:10.1016/j.pbiomolbio.2006.07.005
38. Mellott AJ, Forrest ML, Detamore MS (2013) Physical non-viral gene delivery methods for tissue engineering. Ann Biomed Eng 41:446–468. doi:10.1007/s10439-012-0678-1
39. Palumbo G, Caruso M, Crescenzi E et al (1996) Targeted gene transfer in eucaryotic cells by dye-assisted laser optoporation. J Photochem Photobiol B Biol 36:41–46. doi:10.1016/S1011-1344(96)07335-6
40. Zeira E, Manevitch A, Khatchatouriants A et al (2003) Femtosecond infrared laser—an efficient and safe in vivo gene delivery system for prolonged expression. Mol Ther 8:342–350. doi:10.1016/S1525-0016(03)00184-9
41. Tao W, Wilkinson J, Stanbridge EJ, Berns MW (1987) Direct gene transfer into human cultured cells facilitated by laser micropuncture of the cell membrane. Proc Natl Acad Sci U S A 84:4180–4184. doi:10.1073/pnas.84.12.4180
42. Ogura M, Sato S, Nakanishi K et al (2004) In vivo targeted gene transfer in skin by the use of laser-induced stress waves. Lasers Surg Med 34:242–248. doi:10.1002/lsm.20024
43. Shirahata Y, Ohkohchi N, Itagak H, Satomi S (2001) New technique for gene transfection using laser irradiation. J Investig Med 49:184–190

44. Wong FK, Haffner C, Huttner WB, Taverna E (2014) Microinjection of membrane-impermeable molecules into single neural stem cells in brain tissue. Nat Protoc 9:1170–1182. doi:10.1038/nprot.2014.074
45. Porter KR (1984) The cytomatrix: a short history of its study. J Cell Biol. doi:10.1083/jcb.99.1.3s
46. Korzh V, Strähle U (2002) Marshall Barber and the century of microinjection: from cloning of bacteria to cloning of everything. Differentiation 70:221–226. doi:10.1046/j.1432-0436.2002.700601.x
47. Flickinger CJ (1974) Radioactive labeling of the Golgi apparatus by micro-injection of individual amebae. Exp Cell Res. doi:10.1016/0014-4827(74)90262-6
48. Jeon KW, Lorch IJ, Moran JF et al (1967) Cytoplasmic inheritance in amoebae: modification of response to antiserum by micro-injection of heterologous cytoplasmic homogenates. Exp Cell Res 46:615–619. doi:10.1016/0014-4827(67)90392-8
49. Lin TP (1966) Microinjection of mouse eggs. Science 151:333–337. doi:10.1126/science.151.3708.333
50. Knowles J (1974) An improved microinjection technique in Paramecium aurelia: transfer of mitochondria conferring erythromycin-resistance. Exp Cell Res 88:79–87
51. Koizumi S (1974) Microinjection and transfer of cytoplasm in Paramecium. Experiments on the transfer of kappa particles into cells at different stages. Exp Cell Res. doi:10.1016/0014-4827(74)90619-3
52. Gurdon JB, Lane CD, Woodland HR, Marbaix G (1971) Use of frog eggs and oocytes for the study of messenger RNA and its translation in living cells. Nature 233:177–182. doi:10.1038/233177a0
53. Graessmann A, Graessmann M (1971) The formation of melanin in muscle cells after direct transfer of RNA from Harding-Passeg melanoma cells. Hoppe-Seyler's Z Physiol Chem 352:527–532
54. Capecchi MR (1980) High efficiency transformation by direct microinjection of DNA into cultured mammalian cells. Cell. doi:10.1016/0092-8674(80)90358-X
55. Harbers K, Jähner D, Jaenisch R (1981) Microinjection of cloned retroviral genomes into mouse zygotes: integration and expression in the animal. Nature 293:540–542. doi:10.1038/293540a0
56. Gordon JW, Scangos GA, Plotkin DJ et al (1980) Genetic transformation of mouse embryos by microinjection of purified DNA. Proc Natl Acad Sci U S A 77:7380–7384. doi:10.1073/pnas.77.12.7380
57. Costantini F, Lacy E (1981) Introduction of a rabbit beta-globin gene into the mouse germ line. Nature 294:92–94
58. Lacy E, Roberts S, Evans EP et al (1983) A foreign beta-globin gene in transgenic mice: integration at abnormal chromosomal positions and expression in inappropriate tissues. Cell 34:343–358. doi:10.1016/0092-8674(83)90369-0
59. Gordon JW, Ruddle FH (1981) Integration and stable germ line transmission of genes injected into mouse pronuclei. Science 214:1244–1246. doi:10.1126/science.6272397
60. Wang J, Liu XJ (2004) Progesterone inhibits protein kinase A (PKA) in Xenopus oocytes: demonstration of endogenous PKA activities using an expressed substrate. J Cell Sci 117:5107–5116. doi:10.1242/jcs.01383
61. Maller JL, Koontz JW (1980) Induction of cell division in amphibian oocytes by insulin. J Cell Biol 87:309–316. doi:10.1016/0012-1606(81)90262-1
62. Stühmer W, Ruppersberg JP, Schröter KH et al (1989) Molecular basis of functional diversity of voltage-gated potassium channels in mammalian brain. EMBO J 8:3235–3244
63. Stacey DW, Allfrey VG (1977) Evidence for the autophagy of microinjected proteins in HeLa cells. J Cell Biol. doi:10.1083/jcb.75.3.807
64. Kozma R, Ahmed S, Best A, Lim L (1995) The Ras-related protein Cdc42Hs and bradykinin promote formation of peripheral actin microspikes and filopodia in Swiss 3T3 fibroblasts. Mol Cell Biol 15:1942–1952

65. Scheer U, Hinssen H, Franke WW, Jockusch BM (1984) Microinjection of actin-binding proteins and actin antibodies demonstrates involvement of nuclear actin in transcription of lampbrush chromosomes. Cell 39:111–122. doi:10.1016/0092-8674(84)90196-X
66. Ridley AJ, Paterson HF, Johnston CL et al (1992) The small GTP-binding protein rac regulates growth factor-induced membrane ruffling. Cell. doi:10.1016/0962-8924(92)90174-L
67. Feramisco JR, Gross M, Kamata T et al (1984) Microinjection of the oncogene form of the human H-ras (T-24) protein results in rapid proliferation of quiescent cells. Cell 38:109–117. doi:10.1016/0092-8674(84)90531-2
68. Bar-Sagi D, Feramisco JR (1985) Microinjection of the ras oncogene protein into PC12 cells induces morphological differentiation. Cell. doi:10.1016/0092-8674(85)90280-6
69. Uehara T, Yanagamachi R (1976) Microsurgical ingection of spermatozoa into hamster eggs with subsequent transformation of sperm nuclei into male pronuclei. Biol Reprod 470:467–470
70. Uehara T, Yanagimachi R (1977) Behavior of nuclei of testicular, caput and cauda epididymal spermatozoa injected into hamster eggs. Biol Reprod 16:315–321. doi:10.1095/biolreprod16.3.315
71. Iritani A, Utsumi K, Miyake M et al (1988) In vitro fertilization by a routine method and by micromanipulation. Ann N Y Acad Sci 541:583–590
72. Goto K, Kinoshita A, Takuma Y, Ogawa K (1990) Fertilisation of bovine oocytes by the injection of immobilised, killed spermatozoa. Vet Rec 127:517–520
73. Van Steirteghem AC, Nagy Z, Joris H et al (1993) High fertilization and implantation rates after intracytoplasmic sperm injection. Hum Reprod 8:1061–1066. doi:10.1097/00006254-199402000-00020
74. Palermo G, Joris H, Derde MP et al (1993) Sperm characteristics and outcome of human assisted fertilization by subzonal insemination and intracytoplasmic sperm injection. Fertil Steril 59:826–835. doi:10.1071/RD9940085
75. Fishel S, Timson J, Lisi F et al (1994) Micro-assisted fertilization in patients who have failed subzonal insemination. Hum Reprod 9:501–505
76. Tournaye H, Devroey P, Liu J et al (1994) Microsurgical epididymal sperm aspiration and intracytoplasmic sperm injection: a new effective approach to infertility as a result of congenital bilateral absence of the vas deferens. Fertil Steril 61:1045–1051. doi:10.1016/0020-7292(95)90216-3
77. Masani MYA, Noll GA, Parveez GKA et al (2014) Efficient transformation of oil palm protoplasts by PEG-mediated transfection and DNA microinjection. PLoS ONE. doi:10.1371/journal.pone.0096831
78. Lodish H, Berk A, Kaiser CA et al (2013) Molecular cell biology, 7th edn. W.H. Freeman and company, New York
79. Karp G (2008) Cell and molecular biology: concepts and experiments. Wiley, New York
80. Cooper G (2000) The cell: a molecular approach, 2nd edn. Sinauer Associates, Sunderland (MA)
81. Woese C (1998) The universal ancestor. Proc Natl Acad Sci U S A 95:6854–6859
82. Belting M, Sandgren S, Wittrup A (2005) Nuclear delivery of macromolecules: barriers and carriers. Adv Drug Deliv Rev. doi:10.1016/j.addr.2004.10.004
83. Woese CR (2002) On the evolution of cells. Proc Natl Acad Sci U S A 99:8742–8747. doi:10.1073/pnas.132266999
84. Lechardeur D, Verkman AS, Lukacs GL (2005) Intracellular routing of plasmid DNA during non-viral gene transfer. Adv Drug Deliv Rev. doi:10.1016/j.addr.2004.12.008
85. Lechardeur D, Lukacs GL (2002) Intracellular barriers to non-viral gene transfer. Curr Gene Ther 2:183–194. doi:10.2174/1566523024605609
86. Schubbert R, Hohlweg U, Renz D, Doerfler W (1998) On the fate of orally ingested foreign DNA in mice: chromosomal association and placental transmission to the fetus. Mol Gen Genet 259:569–576. doi:10.1007/s004380050850

87. Hashida M, Mahato RI, Kawabata K et al (1996) Pharmacokinetics and targeted delivery of proteins and genes. J Control Release 41:91–97. doi:10.1016/0168-3659(96)01360-0
88. Jain MK, Wagner RC (1980) Introduction to biological membranes. Wiley, New York
89. Conner SD, Schmid SL (2003) Regulated portals of entry into the cell. Nature 422:37–44. doi:10.1038/nature01451
90. Swanson JA, Watts C (1995) Macropinocytosis. Trends Cell Biol 5:424–428. doi:10.1016/S0962-8924(00)89101-1
91. Pelkmans L, Helenius A (2002) Endocytosis via caveolae. Traffic 3:311–320. doi:10.1034/j.1600-0854.2002.30501.x
92. Aderem A, Underhill DM (1999) Mechanisms of phagocytosis in macrophages. Annu Rev Immunol 17:593–623. doi:10.1146/annurev.immunol.17.1.593
93. Schmid SL (1997) Clathrin-coated vesicle formation and protein sorting: an integrated process. Annu Rev Biochem 66:511–548. doi:10.1146/annurev.biochem.66.1.511
94. Hafez IM, Maurer N, Cullis PR (2001) On the mechanism whereby cationic lipids promote intracellular delivery of polynucleic acids. Gene Ther 8:1188–1196. doi:10.1038/sj.gt.3301506
95. Klopfenstein DR, Vale RD, Rogers SL (2000) Motor protein receptors: moonlighting on other jobs. Cell 103:537–540
96. Rogers SL, Gelfand VI (2000) Membrane trafficking, organelle transport, and the cytoskeleton. Curr Opin Cell Biol 12:57–62. doi:10.1016/S0955-0674(99)00057-5
97. Burke NV, Han W, Li D et al (1997) Neuronal peptide release is limited by secretory granule mobility. Neuron 19:1095–1102. doi:10.1016/S0896-6273(00)80400-6
98. Steyer JA, Horstmann H, Almers W (1997) Transport, docking and exocytosis of single secretory granules in live chromaffin cells. Nature 388:474–478. doi:10.1038/41329
99. Panté N, Kann M (2002) Nuclear pore complex is able to transport macromolecules with diameters of about 39 nm. Mol Biol Cell 13:425–434. doi:10.1091/mbc.01-06-0308
100. Talcott B, Moore MS (1999) Getting across the nuclear pore complex. Trends Cell Biol 9:312–318. doi:10.1016/S0962-8924(99)01608-6
101. Harel A, Forbes DJ (2001) Welcome to the nucleus: Can I take your coat? Nat Cell Biol 3:E267–E269. doi:10.1038/ncb1201-e267
102. Kuersten S, Ohno M, Mattaj IW (2001) Nucleocytoplasmic transport: ran, beta and beyond. Trends Cell Biol 11:497–503. doi:10.1016/S0962-8924(01)02144-4
103. Olsnes S, Klingenberg O, Wiedłocha A (2003) Transport of exogenous growth factors and cytokines to the cytosol and to the nucleus. Physiol Rev 83:163–182. doi:10.1152/physrev.00021.2002
104. Keresztes M, Boonstra J, Gfs N (1999) Import(ance) of growth factors in (to) the nucleus. 145:421–424
105. Leonetti JP, Mechti N, Degols G et al (1991) Intracellular distribution of microinjected antisense oligonucleotides. Proc Natl Acad Sci U S A 88:2702–2706. doi:10.1073/pnas.88.7.2702
106. Dowty ME, Williams P, Zhang G et al (1995) Plasmid DNA entry into postmitotic nuclei of primary rat myotubes. Proc Natl Acad Sci U S A 92:4572–4576. doi:10.1073/pnas.92.10.4572
107. Lukacs GL, Haggie P, Seksek O et al (2000) Size-dependent DNA mobility in cytoplasm and nucleus. J Biol Chem 275:1625–1629. doi:10.1074/jbc.275.3.1625
108. Lechardeur D, Sohn KJ, Haardt M et al (1999) Metabolic instability of plasmid DNA in the cytosol: a potential barrier to gene transfer. Gene Ther 6:482–497. doi:10.1038/sj.gt.3300867
109. Mortimer I, Tam P, MacLachlan I et al (1999) Cationic lipid-mediated transfection of cells in culture requires mitotic activity. Gene Ther 6:403–411. doi:10.1038/sj.gt.3300837
110. Salman H, Zbaida D, Rabin Y et al (2001) Kinetics and mechanism of DNA uptake into the cell nucleus. Proc Natl Acad Sci U S A 98:7247–7252. doi:10.1073/pnas.121067698
111. Chambers R, Fell HB (1931) Micro-operations on cells in tissue cultures. Proc R Soc B Biol Sci 109:380–403. doi:10.1098/rspb.1931.0090
112. Kopac MJ (1938) The Devaux effect at oil-protoplasm interfaces. Biol Bull 75:372

113. Chambers R (1940) The micromanipulation of living cells. In the cell and protoplasm. Am Assoc Adv Sci Sci Press 14:20–30
114. Hawkins SE (1969) Transmission of cytoplasmic determinants in amoebae by microinjection of RNA-containing fractions. Nature 224:1127–1129
115. Zhang Y, Champagne N, Beitel LK et al (2004) Estrogen and androgen protection of human neurons against intracellular amyloid beta1-42 toxicity through heat shock protein 70. J Neurosci 24:5315–5321. doi:10.1523/JNEUROSCI.0913-04.2004
116. Zhang Y, Hong Y, Bounhar Y et al (2003) P75 neurotrophin receptor protects primary cultures of human neurons against extracellular amyloid beta peptide cytotoxicity. J Neurosci 23:7385–7394. doi:23/19/7385 [pii]
117. Zhang Y, Goodyer C, LeBlanc A (2000) Selective and protracted apoptosis in human primary neurons microinjected with active caspase-3, -6, -7, and -8. J Neurosci 20:8384–8389. doi:20/22/8384 [pii]
118. Bounhar Y, Zhang Y, Goodyer CG, LeBlanc A (2001) Prion protein protects human neurons against bax-mediated apoptosis. J Biol Chem 276:39145–39149. doi:10.1074/jbc.C100443200
119. Zhang Y, Tounekti O, Akerman B et al (2001) 17-beta-estradiol induces an inhibitor of active caspases. J Neurosci 21:RC176. doi:20015731 [pii]
120. Zhang Y, McLaughlin R, Goodyer C, LeBlanc A (2002) Selective cytotoxicity of intracellular amyloid β peptide1-42 through p53 and Bax in cultured primary human neurons. J Cell Biol 156:519–529. doi:10.1083/jcb.200110119
121. Slotkin JR, Chakrabarti L, Hai ND et al (2007) In vivo quantum dot labeling of mammalian stem and progenitor cells. Dev Dyn 236:3393–3401. doi:10.1002/dvdy.21235
122. Candeloro P, Tirinato L, Malara N et al (2011) Nanoparticle microinjection and Raman spectroscopy as tools for nanotoxicology studies. Analyst 136:4402. doi:10.1039/c1an15313g
123. Ehrenberg M, McGrath JL (2005) Binding between particles and proteins in extracts: Implications for microrheology and toxicity. Acta Biomater. doi:10.1016/j.actbio.2005.02.002
124. Freshney RI (2011) Culture of animal cells: a manual of basic technique and specialized applictions, 6th edn.
125. Lappe-Siefke C, Maas C, Kneussel M (2008) Microinjection into cultured hippocampal neurons: a straightforward approach for controlled cellular delivery of nucleic acids, peptides and antibodies. J Neurosci Methods 175:88–95. doi:10.1016/j.jneumeth.2008.08.004
126. Gueroussov S, Tarnawsky SP, Cui XA et al (2010) Analysis of mRNA nuclear export kinetics in mammalian cells by microinjection. J Vis Exp. doi:10.3791/2387
127. Goldman RD, Spector DL (2004) Live cell imaging: a laboratory manual. Cold Spring Harbor Laboratory Press, New York
128. Stein P, Schindler K (2011) Mouse oocyte microinjection, maturation and ploidy assessment. J Vis Exp. doi:10.3791/2851
129. Miller DFB, Holtzman SL, Kaufman TC (2002) Customized microinjection glass capillary needles for P-element transformations in Drosophila melanogaster. Biotechniques 33:366–375
130. Zhang Y, Ballas CB, Rao MP (2012) Towards ultrahigh throughput microinjection: MEMS-based massively-parallelized mechanoporation. Proc Annu Int Conf IEEE Eng Med Biol Soc EMBS 594–597. doi:10.1109/EMBC.2012.6346001
131. Adamo A, Roushdy O, Dokov R et al (2013) Microfluidic jet injection for delivering macromolecules into cells. J Micromech Microeng 29:997–1003. doi:10.1088/0960-1317/23/3/035026
132. Aten QT, Jensen BD, Tamowski S et al (2012) Nanoinjection: pronuclear DNA delivery using a charged lance. Transgenic Res. doi:10.1007/s11248-012-9610-6
133. Chen X, Kis A, Zettl A, Bertozzi CR (2007) A cell nanoinjector based on carbon nanotubes. Proc Natl Acad Sci U S A. doi:10.1073/pnas.0700567104

134. Yum K, Wang N, Yu M-F (2010) Nanoneedle: a multifunctional tool for biological studies in living cells. Nanoscale. doi:10.1039/b9nr00231f
135. Meister A, Gabi M, Behr P et al (2009) FluidFM: combining atomic force microscopy and nanofluidics in a universal liquid delivery system for single cell applications and beyond. Nano Lett. doi:10.1021/nl901384x
136. Lacal JC, Perona R, Feramisco J (1999) Microinjection. Springer
137. Becattini G, Mattos LS, Caldwell DG (2013) A visual targeting system for the microinjection of unstained adherent cells. Comput Biol Med. doi:10.1016/j.compbiomed.2012.11.015
138. Wang W, Sun Y, Zhang M et al (2008) A system for high-speed microinjection of adherent cells. Rev Sci Instrum. doi:10.1063/1.3006000
139. Wang W, Liu X, Gelinas D et al (2007) A fully automated robotic system for microinjection of zebrafish embryos. PLoS ONE. doi:10.1371/journal.pone.0000862
140. Xie Y, Sun D, Liu C et al (2010) A force control approach to a robot-assisted cell microinjection system. Int J Rob Res 29:1222–1232. doi:10.1177/0278364909354325
141. Duselis AR, Vrana PB (2007) Retrieval of mouse oocytes. J Vis Exp 185. doi:10.3791/185
142. Palermo G, Joris H, Devroey P, Van Steirteghem AC (1992) Induction of acrosome reaction in human spermatozoa used for subzonal insemination. Hum Reprod 7:248–254
143. Gregory DW, Cocking EC (1965) The large-scale isolation of protoplasts from immature tomato fruit. J Cell Biol 24(1):143–146
144. Power JB, Cocking EC (1970) Isolation of leaf protoplasts: macromolecule uptake and growth substance response. J Exp Bot 21:64–70. doi:10.1093/jxb/21.1.64
145. From P, Avena THE, By A (1965) Protoplasts from the *Avena coleoptile*. Proc Natl Acad Sci U S A 54:56–64
146. Morikawa H, Yamada Y (1985) Capillary microinjection into protoplasts and intranuclear localization of injected materials. 26:229–236
147. Stein P, Svoboda P (2006) Microinjection of dsRNA into mouse oocytes and early embryos. CSH Protoc. doi:10.1101/pdb.prot4511
148. Taverna E, Haffner C, Pepperkok R, Huttner WB (2011) A new approach to manipulate the fate of single neural stem cells in tissue. Nat Neurosci 15:329–337. doi:10.1038/nn.3008
149. Evans T (2006) Transformation and microinjection. WormBook 1–15. doi:10.1895/wormbook.1.108.1
150. Xu Q (1999) Microinjection into zebrafish embryos. Methods Mol Biol 127:125–132. doi:10.1385/1-59259-678-9:125
151. Ringrose L (2009) Transgenesis in Drosophila melanogaster. Methods Mol Biol 561:3–19. doi:10.1007/978-1-60327-019-9_1
152. Juarez MT, Patterson RA, Li W, McGinnis W (2013) Microinjection wound assay and in vivo localization of epidermal wound response reporters in Drosophila embryos. J Vis Exp e50750. doi:10.3791/50750
153. Devroey P, Van Steirteghem A (2004) A review of ten years experience of ICSI. Hum Reprod Update 10:19–28. doi:10.1093/humupd/dmh004
154. Cousineau TM, Domar AD (2007) Psychological impact of infertility. Best Pract Res Clin Obstet Gynaecol 21:293–308. doi:10.1016/j.bpobgyn.2006.12.003
155. Prausnitz MR (2004) Microneedles for transdermal drug delivery. Adv Drug Deliv Rev 56:581–587. doi:10.1016/j.addr.2003.10.023
156. Prausnitz MR, Langer R (2008) Transdermal drug delivery. Nat Biotechnol 26:1261–1268. doi:10.1038/nbt.1504
157. Prausnitz MR, Mikszta JA, Cormier M, Andrianov AK (2009) Microneedle-based vaccines, pp 369–393
158. Laurent PE, Bonnet S, Alchas P et al (2007) Evaluation of the clinical performance of a new intradermal vaccine administration technique and associated delivery system. Vaccine 25:8833–8842. doi:10.1016/j.vaccine.2007.10.020

Optical Tools for Single-Cell Manipulation and Analysis

Duncan Casey and Jayne Dooley

Abstract Experiments on individual cells require a range of extremely precise tools to permit their selection, manipulation, stimulation and analysis. This is further complicated by the cells' sensitivity to their environment, meaning that such tools must also be very gentle (or at least very localised) to minimise the generation of artefacts. Optical tools provide ideal performance in a number of such roles, exhibiting high spatial and temporal selectivity while causing minimal non-specific effects. This chapter focuses upon the optical tools that have been developed for these purposes, ranging from optical trapping systems which provide a contact-free technique for the manipulation of micron-scale objects, through to a selection of the different optically mediated cell membrane disruption methods available for lysis and/or delivery of material.

Keywords Optical trapping · Single-cell manipulation · Single-cell poration and transfection · Spatial light modulators · Optical poration · Optical physics theory

Optical trapping techniques provide the means to manipulate matter at approximately a 1–100 μm scale, without requiring direct contact with the cell [1]. The use of infrared wavelengths minimises the amount of light absorbed by biological targets, while a range of light-sculpting approaches are available to generate a wide array of complex beams which can be dynamically modified. This means that cells (or microstructured probes) can be directly manipulated, either to build arrays or to perform mechanical measurements of the properties of the cell membrane.

However, to modulate or measure processes occurring beyond the cell membrane, a mechanism of controlled membrane rupture must be utilised. These can either be destructive, for selective lysis experiments, or reversible, to allow the introduction of material to stimulate responses with minimal disruption to the cell. Both approaches feature a range of modalities: for example, lysis can be induced by

D. Casey (✉) · J. Dooley
Engineering and Technology Research Institute, Liverpool John Moores University, Liverpool L3 3AF, UK
e-mail: D.R.Casey@ljmu.ac.uk

F.-G. Tseng and T.S. Santra (eds.), *Essentials of Single-Cell Analysis*, Series in BioEngineering, DOI 10.1007/978-3-662-49118-8_5

direct plasma formation using high-energy pulsed lasers to induce catastrophic damage to anything within a defined radius [2], or can be combined with electrical fields to provide lysis with single-cell resolution [3]. Similarly, photoporation can be accomplished directly with very high precision (although conditions must be finely tuned to minimise cell disruption), or in combination with materials with specific absorption characteristics to deliver similar effects using much longer wavelengths and commensurately lower cell damage [4].

The theories underpinning these techniques will be discussed, and illuminated using examples of recent research to provide first-hand examples of their successful application. The advantages and disadvantages of each approach will be comprehensively debated, and directions of promising research will be presented to give insight into the tools and techniques likely to be available in the future.

1 Introduction

The traditional tools of biochemistry, based around the measurement of the ensemble behaviour of tens or hundreds of thousands of cells, have served faithfully for decades and provided deep insights into the structure and function of many of the proteins and pathways that underpin biological functions. However, by their nature they provide limited resolution: such averaged measurements, necessary to generate the masses and concentrations of sample required for meaningful measurements, cannot identify outliers from the main population and are unsuitable for the analysis of rare cell types. This is of particular importance in the case of circulating tumour cells, widely believed to be the vectors responsible for cancer metastases but present at such vanishingly low concentrations in blood as to be almost invisible [5]. However, it has been demonstrated that stochastic behaviour in protein transcription and regulation makes a substantial contribution to (and may even dominate) cellular responses to a number of stimuli and stresses [6]. In order to fully probe these effects, a new range of tools are under development: tools which combine the extraordinary sensitivity and precision required to provide single-cell or even single-molecule resolution, with the throughput necessary to identify quantitative differences between outliers and the median behaviour of a cell population.

Optical platforms provide the ideal basis for this new generation of tools. Coupled with advances in microscopy techniques, particularly in the field of super-resolution microscopy, optical systems provide a view into the inner workings of the cell in unprecedented detail. These microscopy techniques require a textbook of their own right to do them justice and so are beyond the scope of this review, but as a starting point the interested reader is directed to a recent overview of the topic by Godin et al. [7].

1.1 Typical Sample Volumes

The development of tools to precisely handle and measure low volumes of biological material has been at the forefront of life science research almost since its inception. A typical mammalian cell has an internal volume of measured in tens of picolitres (1 picolitre = 10^{-15} m^3), surrounded by a membrane of detergent and protein that is rarely more than two molecules thick. This miniscule envelope contains a system of dazzling complexity: the ~23,000 genes in your DNA each code for a protein that may be modified in a variety of ways post-transcription, leading to hundreds of thousands of potential forms, expressed at concentration levels spanning some six orders of magnitude. For example, membrane proteins (those studded throughout or somehow affiliated with the detergent bilayer that maintains cellular compartmentalisation) make up some 27 % of the human genome and the majority of active drug targets [8], despite being constrained within a vanishingly small total volume.

In order to generate workable volumes, cell biology has often focused upon the generation of clonal colonies of cells: cells bred from a single progenitor which should be genetically identical. Similarly, feeding and starvation cycles have been developed which coordinate the growth phases of cells within a culture, providing some measure of metabolic alignment between neighbouring cells. Despite these methods, wide disparities in responses to stimuli are observed amongst cells in many studies. Some of this will inevitably be statistical: delivery of bulk stimulus to a bulk population of cells will lead to a distribution of effective dosages, leading to a range of responses. However, more fundamental stochastic effects are observed in the studies of cellular metabolism, effects which are transmitted throughout the cell [9]: it is hypothesised that these heterogeneities may contribute to a number of phenomena observed at the phenotypic level, such as antibiotic or chemotherapeutic drug resistance.

1.2 Early Single-Cell Approaches

In order to probe these single-cell phenomena, a range of single-cell techniques were developed. Microinjection techniques were an early approach: using precisely controlled pressures across micropipettes, skilled researchers could isolate, manipulate and inject material into individual cells of interest. Most famously, these techniques were applied to in vitro fertilisation: while the first human birth was recorded in the late 1970s [10], this was achieved using relatively crude co-incubation techniques and the first successful microinjection of human sperm was not performed in humans for another 15 years [11].

While undoubtedly a powerful tool, microinjection is challenging to apply to smaller cells, which are much harder to manipulate and experience commensurately greater damage during injection. Extensive discussion of the field of microinjection

is available in Chap. 4, while detailed protocols are available from Zhang [12] and a comprehensive review of the history and development of the application of the technique to in vitro fertilisation is provided by Neri et al. [13].

To ameliorate these issues, research into contact-free techniques has been pursued. A number of approaches have used microfluidic flow systems to sort and capture cells into corrals. Although almost infinitely configurable, such techniques can only be applied to bloodborne or artificially detached cells which have been released from their native culture, as the targets must be free-floating in suspension. A number of innovative approaches have been developed to minimise the disruption to the target cell's surface during detachment [14], but these still necessitate the removal of the cell from its surroundings upon which it depends for a constant stream of signals that maintain or modulate its growth cycles and function. What is required for the study of epithelial tissue, then, is a platform that can provide spatial resolution by delivering the experiment to the target cell, not vice versa. Optical tools provide the perfect mechanism to do so, providing a gentle, sterile and contact-free system to manipulate micron-scale objects in three dimensions, or alternatively by delivering powerful pulses of light to disrupt the membranes of specific cells of interest, allowing direct access to their contents one cell at a time.

2 Optical Trapping

Optical trapping (sometimes referred to as optical tweezers) is a technique based around the combination of light's classical and quantum mechanical properties. Quantum mechanics dictates that a photon has a momentum linked to its wavelength by Eq. 1. As light is scattered by a dielectric particle, there must therefore be an associated momentum transfer.

$$p = \frac{\lambda}{h} = mc \tag{1}$$

Conservation of momentum requires that every action has an equal and opposite reaction, meaning that as a photon is scattered away from its incident path, a force acts on the scattering object to force it back in the opposite direction. If targeted by a Gaussian beam like a laser, this has the effect of driving the target away from the light source along the centre of the incident beam. The photon intensity is highest in the centre of the beam, meaning that less light is scattered around the edges: the net effect is that the target is trapped and pulled back towards the centre, but flung forwards through photon pressure. This phenomenon is exactly the one used by the IKAROS project in their recent demonstration of solar sail technology, using sunlight upon a 20 m-diameter gold sail to assist in driving a small satellite from Earth to Venus [15].

While this presents an interesting effect, in this form it is of limited use as a propulsion system: on Earth, these effects of light are normally negligible next to

gravity and air resistance. However, by using a tightly focused beam, the region of maximum intensity can be restricted into a small three-dimensional space, the beam waist—discussed in detail, along with the mechanics of the trapping force, in Sect. 2.2. This creates a far more useful tool, a trap in all three planes, and one that can overcome the Brownian forces experienced by objects of approximately cellular diameters and densities in solution and restricting them within the focal volume. This force directing particles back to the beam waist can be precisely calculated or measured, meaning that objects so captured can be not only be precisely manipulated but also used as pico-Newton- or femto-Newton-sensitive force probes for investigating the topography and mechanical behaviour of microscale biological structures.

Practically, this can be achieved using a high numerical aperture (NA) objective lens fitted to an inverted microscope, meaning that in the apparatus' simplest form the microscope's focal range provides z-axis control, while trapped objects may be moved relative to their surroundings by the use of a motorised stage. This configuration allows the imaging of the trapped particle utilising the same apparatus used to maintain its position. Remarkably little power is required to exhibit effective trapping: a 5 mW continuous-wave Helium–Neon (HeNe) source emitting at 633 nm may be effectively used to trap polystyrene beads of 5–10 μm diameter in a safe and visually very impressive demonstration of the technique. However, it is important to remember that within the focal volume, photon intensities can be intense: the HeNe laser in the above example would, if focused to a relatively easily achieved 5 μm diameter spot, reach an intensity of some 2.5×10^8 W/m^2, or some 200,000 times more intense than sunlight at the Earth's surface. As a result, a number of effects may be observed in some samples due to heating or direct photon damage, and it is typically wise to choose a laser wavelength that features a low or negligible extinction coefficient in the target material.

2.1 History and Development

Modern optical trapping has developed as a result of the work undertaken by Ashkin in the 1970s during his experiments exploring the nature of radiation pressure [16]. He observed the effects of the scattering and gradient forces which act on a small refractive particle in a beam of light. Light exerts a force on all objects that refract or reflect light due to the change of the incident photons' momentum, which is transferred when they collide with or are diverted by a target, as described in Sect. 2. However, for macroscopic objects, these forces are so small that they are negligible compared to others acting on the object such as air pressure or turbulence. Ashkin's breakthrough experiments came when he attempted the manipulation of micron-sized particles in liquids and gases using a continuous-wave, visible laser in order to observe their effects.

His initial experiments used microscopic transparent latex spheres freely suspended in water. An argon laser was focused horizontally through a glass cell and

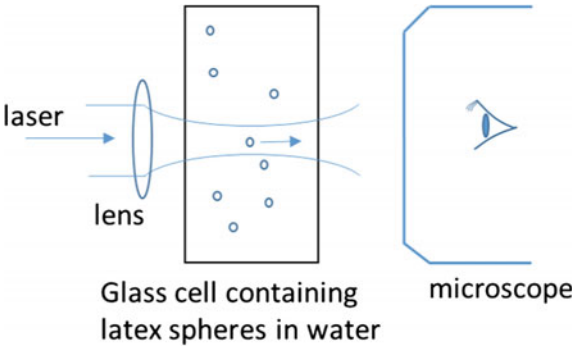

Fig. 1 Schematic cross section of Ashkin's experiment set-up during the discovery of optical trapping [16]

manipulated to focus on single spheres. A schematic cross section through the experiment set-up is shown in Fig. 1.

The effects of the laser on the sphere were observed with a microscope. As the beam hit a sphere off-centre the sphere was observed being drawn into the beam axis whilst simultaneously being accelerated in the direction of light from the beam. It moved in this direction until it hits the cell wall where it then remained trapped in the laser beam. If the beam was blocked then the sphere moved away, randomly driven by Brownian motion. More powerful lasers are required as the diameter of the spheres increased relative to that of the beam. By introducing a second beam operating in the opposing direction, Ashkin was able to produce what he termed 'a stable optical well', as shown in the sketch in Fig. 2.

Light can cause temperature gradients across the medium surrounding the particle under investigation. These temperature gradients can produce thermal forces much larger than the radiation pressure, obscuring its effects. This had historically been a limiting factor in exploring the phenomenon. However, Ashkin eliminated these obscuring effects in his experiments through using particles and surrounding medium with low refractive indices, i.e. relatively transparent materials, which minimised the absorption of photons.

Ashkin's experiments initially focused on manipulation of particles ranging in diameter from 0.59 to 2.68 μm as the traps appeared to be most stable in this range. However, results from his experiments suggested that tuneable lasers could selectively accelerate, trap or separate larger particles including single molecules [17].

Further exploration has resulted in the development of optical trap instrumentation enabling the trapping and manipulation of single molecules with nanometre precision along with measurement of the forces acting on the particles. It is this

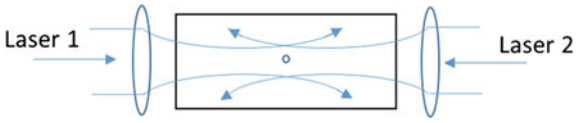

Fig. 2 Plan view of a 'stable optical well', as described by Ashkin [16]

ability for precise measurement that has led to the use of optical traps in biological applications [18].

2.2 Theory and Optical Physics

When light hits an object, some of the light will be reflected by the object and some of it will be refracted. The amount refracted or reflected will depend upon the refractive index of the object. This change in direction of the photons also changes their momentum: the magnitude of the effective forces exerted on the light rays will depend upon the size of the object, the wavelength of the light and the refractive index of the medium. This change in momentum leads to an equal and opposite force in the opposing direction, back towards the centre of the incident beam. For microscopic particles, these forces can be significant enough to move the particle. Optical tweezers, as optical traps used in biological applications are often referred, consist of a single laser beam strongly focused through a lens. Infrared trapping beams are commonly used for biological processes as tissue is effectively transparent at these wavelengths meaning little is absorbed by the tissue, minimising optical damage [17].

As the laser beam passes through the microscope lens, the rays converge to a focal point. However, each ray is refracted at the surface of the particle, resulting in the change of path and momentum as shown in the schematic in Fig. 3. In return the rays of light exert an equal and opposite force on the particle, effectively pulling it to the centre of the beam and towards its focal point, as shown. The off-axis components of these forces cancel each other out resulting in a restoring force F directed towards the focal point of the laser beam.

The scattering (or pushing) force is a result of the light reflecting off the target particle and acts in the direction of the light propagation and is proportional to the light's intensity as shown in Fig. 4. It is the balancing of the reflecting and refracting forces that facilitates trapping of the particle [19].

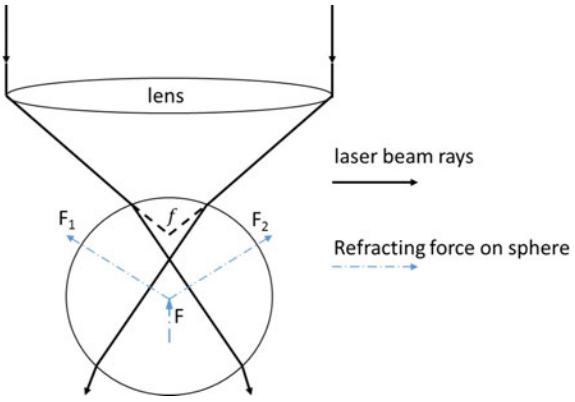

Fig. 3 Refracting forces on a particle in an optical trap

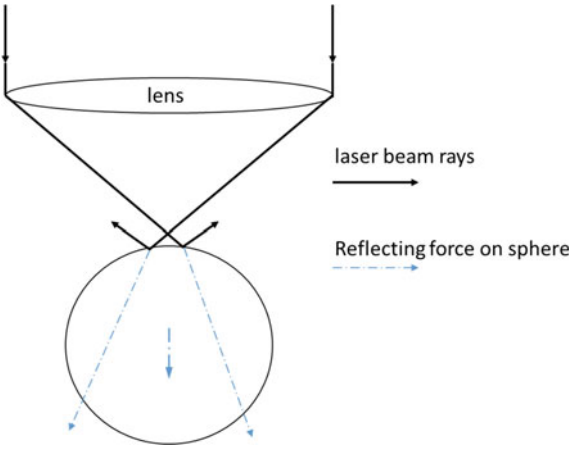

Fig. 4 Reflecting forces on a particle in an optical trap

As the size of the particle changes relative to the laser wavelength, the trapping regime also changes. The interaction between light and particles can be explained by two different theories, Rayleigh or Mie, depending upon the particle size. The Rayleigh theory relates to particles which are much smaller than the wavelength of the incident light. As the particle size approaches that of the light wavelength then the interaction becomes more complicated and can be determined using the Mie theory [20]. Biological applications usually require manipulation of particles in the Mie regime.

The change in direction of the laser beam rays due to refraction at the particle surface will depend upon its angle of incidence along with the refractive indices of the particle and the surrounding medium. This change in direction can be determined using Snell's law (Eq. 2, [18]), which states that where n_1 and n_2 are the refractive indices of the particle and of the surrounding medium (generally air, water or oil) respectively, θ_1 is the angle of incidence of the ray with respect to line perpendicular to the particle surface and θ_2 is the angle with respect to the same line at which the ray propagates within the sphere their relationship can be characterised thus:

$$\mathrm{NA} = n_1 \sin\theta_1 = n_2 \sin\theta_2 \tag{2}$$

In order to trap a particle, the forces that produce scattering of the particles, such as those due to reflection, must be overcome. To overcome this, the trap requires a high trapping force which in turn requires a microscope with a high numerical aperture (NA). The numerical aperture of the lens describes its ability to gather the light from the beam, but essentially dictates the focal length of the lens and thus its maximum working distance. Also, in order to obtain a trapping beam with a high convergence angle, the input aperture needs to be adequately filled by the beam.

Optical traps are characterised as having a dimensionless quality factor, Q. The quality factor depends upon the type of trap, the NA of the microscope lens and the

target particle size. Ashkin has suggested that Q can be as high as 0.3 for trapping forces acting perpendicular to the direction of the laser beam. The trapping force, F, can be determined from Eq. 3 where P is the incident power of the laser beam and $\frac{n_1 P}{c}$ is the incident momentum per second in a medium of refractive index n_1.

$$F = Q\left(\frac{n_1 P}{c}\right) \tag{3}$$

If particles, such as micron-sized polystyrene beads can be attached to single molecules then by manipulating the bead and hence the molecule using an optical trap, the forces acting on the molecule can be determined. Through this, biological interactions can be investigated if the bead is attached to, for example, a DNA molecule [18].

2.2.1 Spatial Light Modulators

Spatial light modulators (SLMs) are screens or masks which can manipulate the shape of light as it is reflected, refracted or passed through the device. They come with varying degrees of sophistication: an overhead projector is a spatial light modulator, as is a cinema projector. However, those based upon remotely addressable screens can display rapidly updating patterns, allowing the shaping of incident light into complex arrangements. In optical trapping applications, the screens can be used to generate holographic patterns of concentric rings, effectively a sinusoidal wave in two dimensions. These diffract light into the Fourier transform of the display, providing a highly focused point of illumination which makes an excellent optical trap.

These screens can be mechanically, optically or electronically controlled to alter their patterns, providing dynamic control over the properties of the transmitted or reflected light. This means that arrays of traps can be created and individually controlled, or that a range of alternative trap geometries can be explored to induce or alleviate the effects of optical aberrations. Early devices were based upon relatively slow-updating nematic liquid crystal displays [21]. In order to maintain several traps at once, multiple holograms had to be calculated and spatially multiplexed simultaneously, which led to a high computational cost. More rapidly updating systems such as ferroelectric liquid crystal systems with millisecond response times mean that a range of much simpler holograms can be generated and overlaid temporally rather than spatially [22]. A similar effect can be achieved with mechanically actuated mirrors, but the very rapid switching of an SLM means that many more traps can be implemented and controlled, while the system's outputs are infinitely more flexible than a mirror of fixed geometry.

A system developed in laboratories at Imperial College utilised this technique to generate up to 24 individually addressable traps based on a single ferroelectric SLM [23]. This approach used each of the red–green–blue colour channels in 8 bit-planes

to generate an individual trap, as the SLM output was by its nature monochrome making the intensities equal. By interlacing these relatively simple holograms onto the SLM at 60 Hz, each trap could be manipulated without interfering with the others, and by programming the system in OpenGL the entire process could be conducted using a graphical processing unit designed for gaming, thus minimising data transfer across the system and the load upon the controlling computer's CPU. This system was driven through a point-and-click interface written in the LabVIEW programming environment, but more intuitive and flexible systems have been developed such as the multi-touch platform pioneered at the University of Bristol which allows trapping control using an interface similar to an Android or Apple tablet [24].

2.3 *Practical Implementation*

The installation of a single optical trap on an inverted microscope is a remarkably straightforward exercise, and effective trapping can be achieved at low powers (≈5 mW) making the system a powerful demonstration of optical physics for the classroom or outreach activities as well as a tool in research. A comprehensive guide to the construction of such a system and its optimisation for force measurement is provided by [25], while the theory behind such measurements is discussed in Sect. 2.4.2. For simple trapping, however, all that is required is a laser source, some form of alignment mirror system such as a periscope arrangement and a beam expander to fill the back aperture of a high numerical aperture microscope objective (see Fig. 5, below). A steering lens or mirror arrangement may be fitted to the path to provide a measure of additional control over a trapped object, but is not essential.

More complex systems with more traps can be produced through the use of either a beam splitter to produce a dual-trap system, or the introduction of an SLM after or instead of the alignment mirrors to generate multiple, individually addressable holographic traps. An alternative technique was also recently developed, using multiple static microlenses to create a geometric pattern of stable traps, allowing the assembly of an optically confined microarray of individual cells without the use of complex optics or software [26].

A trapping system even simpler than that described in Fig. 5 can be produced using a tapered optical fibre to produce the tight focal volume required. Such a fine point can be relatively simply produced using chemical etching or microforge apparatus such as that manufactured by the Narashige Group (Japan), used routinely for the production of micropipettes. These shaped fibres produce a trap at a defined distance from their point that may be simply steered by moving the fibre itself using a micromanipulator or piezoelectric stage, allowing the rapid organisation of microscopic objects at angles and geometries that are not always available using conventional optical tweezers [27]. More recently, unusual behaviour has been observed showing the ability of these systems to trap multiple objects

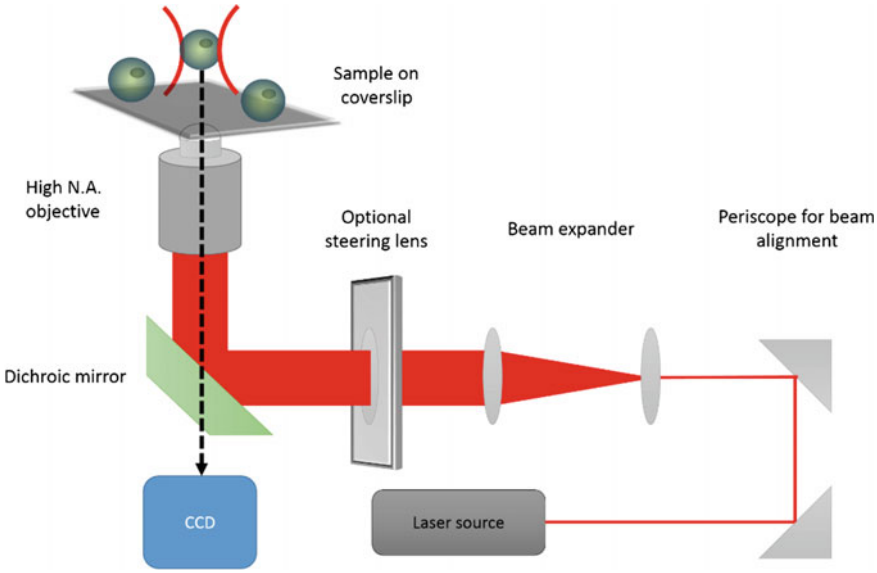

Fig. 5 Schematic of a simple single-trap system built into an inverted microscope. Trapping of 5–10 μm polystyrene particles can be easily achieved with laser powers as low as 5 mW. N.A.: Numerical aperture; CCD: charge-coupled diode; digital camera. The captured image is shown using the black dashed arrow

end-to-end, providing a regular spacing in one or two dimensions, controlled by the cone angle of the tip [28, 29]. This relatively simple set-up provides lower spatial precision than a conventional system, but provides a range of analogous and sometime complementary characteristics that may be explored for limited investment of time or resources.

2.3.1 Effects of Trapping on Biological Systems and Structures

When designing an optical trapping system, it is vital to consider the effects of the incident light upon what are often extremely delicate samples. Photons absorbed by the sample are very likely to release their energy as heat, and the tightly confined focal volumes mean that light intensities can easily reach levels in excess of 10^9 W m^{-2}, even when using low laser powers such as those outlined above. As such, even a small extinction coefficient in the sample will lead to rapid heating and damage.

In order to minimise this, it is normal to use micron-scale wavelengths when applying optical trapping for the study of biological systems. In this window, absorbance by most biological tissue is almost zero, meaning that samples can in theory be handled indefinitely without ill-effect. Such wavelengths are conveniently accessible using Nd:YAG (neodymium-doped yttrium aluminium garnet) and

Yb-fibre lasers, which are commonplace in trapping systems both for this reason and because they can provide high power densities capable of maintaining multiple traps simultaneously. However, even at these wavelengths heating has been observed in cell-sized vesicles [30]; while the majority of cells and their components may be unaffected, some cell types, metalloproteins and organelles exhibit different absorption spectra to the median. These tissues will be selectively heated and thus damaged by the trapping beam, although the average temperature profile of the target may only rise by a degree or two. Optical trapping has also been observed to cause changes in cellular behaviour, inhibiting growth and division in bacteria even at low powers [31]. Such effects must be carefully considered when assessing the applicability of trapping techniques to an experimental problem.

2.3.2 Safety

Safety must be a prime consideration when building or using trapping systems, particularly bespoke or home-built instruments which may lack the safety features and robustness of off-the-shelf models. Micron-scale wavelengths such as the Nd:YAG's primary output at 1064 nm are in the infrared, and as such are invisible to human vision. This means that a user working on a poorly-aligned or -shielded system will have little or no indication of exposure unless beam visualising cameras or other tools are available.

The majority of trapping lasers in research use are Class 4, meaning that they are capable of causing significant damage to exposed tissue, and may cause permanent and catastrophic eye damage even from indirect reflections. As a result, the most significant risks are experienced during assembly and alignment, when the beam is imperfectly positioned and beam tubes and other shielding are likely to have been removed to improve access to the instrument. Alignment must be conducted at the lowest possible laser power visible through the available imaging equipment, and users must wear goggles suitable for filtering the wavelengths and powers at hand, as well as removing all reflective items from their person such as rings, watches, etc. Practically, a major source of risk can be eliminated if the system can be aligned by using the microscope backlight rather than the laser itself: this light should propagate down the same path as the laser if no sample is present on the stage to block its path, and the white light sources generally used (typically filament bulbs or LEDs) pose little or no risk, particularly when compared to the laser systems. Once assembled, trapping systems should be interlocked and key switched to prevent unauthorised use or access to the beam path.

Beams which are diffracted using an SLM or other technique must dump unwanted energy into a specialist beam dump to prevent unwanted reflections and heat build-up. Similarly, it is good practice to for a beam stopper or other shield above the plane of the microscope stage, as trapping beams will typically be entering from underneath the sample and otherwise unwanted reflections may cause injury.

2.4 Applications in Single-Cell Studies

2.4.1 Cell Manipulation

The most obvious application for optical trapping in single-cell studies lies in the manipulation of the cells themselves. Optical traps provide a gentle, sterile and contact-free method to arrange cells within a chip or microfluidic system, isolating them by dragging them through a labyrinth or narrow channel for independent analysis [32], or arranging them into arrays for parallel screening. Most cells are too large to be wholly trapped (typical mammalian cells have diameters in excess of 20 μm, while a typical trap focus is below 2 μm), although bacteria and viruses can be effectively captured [33]. However, one or more traps can be effectively used to capture a region of membrane in a detached cell, which normally provides sufficient purchase to move it through solution. Alternatively, silica or polystyrene beads which trap strongly due to their strong scattering of light can be functionalised with a biochemical handle such as an antibody or biotin, which may be used as an anchor point for cells engineered to express a membrane associated avidin protein [34].

However, the majority of optical traps are based around infrared lasers, which operate at wavelengths at which the cytosol is essentially transparent. This means that organelles with different optical properties such as mitochondria may be trapped and handled while within the cell body [35], while in small systems such as zebrafish embryos, cells and other small objects may be moved and probed in vivo [36].

2.4.2 Single-Cell Force Measurements

The precise and contact-free trapping mechanism afforded by optical tweezing provides the idea tool for the quantitative measurement of membrane stiffness and environment viscosity, in a manner similar to atomic force microscopy (AFM) but with several major advantages. Most obviously, the optical trapping techniques offer the opportunity to measure in three dimensions, as opposed to AFM which measures almost exclusively in the z-direction. A micron-scale sphere or other probe can be captured and the magnitude and rate of its Brownian motion analysed in real time (or close to it), which when coupled with information about the trapping force, can give great insight into the environment of the probe and the barriers and heterogeneities within it. One valuable property of optical traps is that the trapping force obeys Hooke's Law, i.e. the restorative force increases linearly with distance as the particle strays or is pushed from the centre of the trap. This makes the calculation of the resistance exerted by the target object relatively simple to calculate.

Currently, such data are best acquired through the use of a quadrant detector [37], which provides extremely fast response rates and nanometre resolution by breaking the region of interest into four separate zones, effectively quadrupling the

frame rate and providing extremely high sensitivity to movements of an object around the centre point where the four quadrants meet. Particle tracking algorithms can then follow the probe, typically a high refractive index and/or albedo particle such as silica, through its random walk about the focal volume and identify any deviations from the norm. Although this approach is only really applicable in the x and y directions on a typical inverted microscope, as the combination of short focal distance and non-linear response in the z direction (in which a particle typically experiences the weakest trapping forces) limits its applicability, for most viscosity measurements the environment can be considered isotropic. In membrane (or other microstructure) rigidity or elastic modulus measurements, this weakness can be ameliorated by approaching the target from all angles: unlike AFM, an optical probe can be brought into contact with the object of study from any side. An important practical note to remember, however, is that binding between many probe materials and biological structures is commonplace, and that optical trapping requires a defined scattering edge to operate effectively. As such, care must be taken to 'block' the probe's surface, either by way of material choice or through the use of some agent like bovine serine albumen.

This and related techniques have been successfully applied in investigations including the measurement of kinesin stepping [38, 39], and analysis of the mechanical properties of membrane lipids in giant vesicles, where the response of the trapped particles could be directly measured as a function of membrane composition and the protein content of the surrounding medium [40].

A more direct approach to measuring the structural properties of biological microsystems has been developed in the laboratories of Jesper Glückstad, who has utilised two-photon polymerisation techniques to develop a range of microprobes with a designed, three-dimensional structure comprising three or more handles connected by a chassis attached to a probe tip. The rigid body of the $\sim$40 μm tools, combined with the additional stability conferred through the application of multiple traps, may be manipulated in all axes to provide direct force measurements. However, the group has also incorporated a microscopic waveguide into their designs, permitting the same tool to be used for spectroscopic analysis of the target at extremely high precision and in a plane orthogonal to normal microscope geometry [41] (Fig. 6).

The binding of microtools to biological materials can itself be utilised, however. Coupling biological polymers to silica or polystyrene beads provides a handle or handles by which their spring constants or affinities for a target can be measured. The pico- or femto-Newton forces applied through trapping can, with care, be used to pull individual proteins from membranes or ligands from receptors in such a way as to resolve individual events within the unbinding process. Typically, many such recordings are required to statistically eliminate the inevitable noise resulting from thermal fluctuations, but the technique is nonetheless a powerful one. In an intriguing recent demonstration, such tools were linked to force feedback controllers allowing the user to experience a physical measure of the resistance felt by the trap as interpreted by the system software [42].

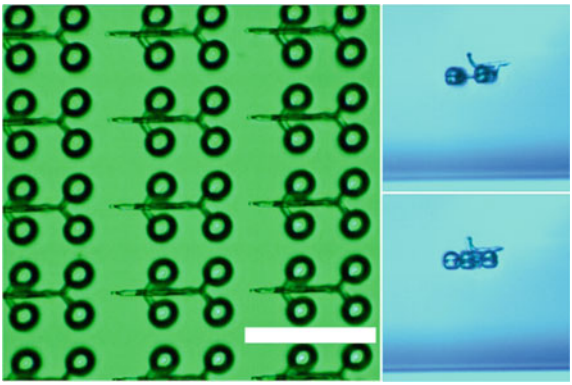

Fig. 6 Optically-guided probes created by two-photon polymerisation on glass. Each may be manipulated in true 3D by gripping each bead with an individually addressable optical trap, providing the means for both direct force measurements and, through the incorporation of a waveguide into the probe tip, the ability to introduce light to a sample in the x-y plane (scale bar = 40 μm). The inset pictures show side-view image of these probes being manipulated in solution [41]. Figure used with permission from the Optical Society of America

2.4.3 Sub-cellular Sampling and Biopsy

As alluded to in the chapter introduction and elsewhere within this book, in the ideal case it should be possible to repeatedly monitor and quantify the individual responses of large numbers of cells from a population, while causing minimum perturbation to those specimens in the process. Through this approach, it will be possible to build up a solid statistical model of both the bulk tissue response and the heterogeneity of reaction amongst cells to a given stimulus. This is of critical importance in the study and treatment of diseases showing high resistance to treatment or persistent relapses, implying some reservoir of infection or 'stem-cell'-like behaviour that complicates treatment [43].

Again, optical tools provide the ideal combination of precision and lightness of touch to repeatedly and non-destructively sample specific regions of a cell—particularly its surface, the home of >30 % of its presently druggable targets [44]. Tools for sub-cellular sampling have typically revolved around delicate microinjection or electrowetting techniques requiring a direct puncture of the cell membrane using a piezoelectric actuator [45]. However, we have recently published a protocol in collaboration with the University of Natural Resources and Life Sciences in Vienna, Austria utilising optically trapped, micron-diameter probes surrounded by a fusogenic detergent bilayer to directly extract functional protein from the membrane of a cell and deposit it into a supported planar membrane for analysis [46]. This technique samples using detergent solubilisation techniques alone, meaning that an intact membrane is present at all times and repeated samples could be removed without damaging the cell.

This and other techniques promise the first genuinely scalable single-cell measures of heterogeneity of response: information which will help identify the differences between high- and low-responding cells under treatment. Such approaches can and must be simply and rapidly automated to provide huge data sets from each individual cell of study across a broad population. This is of value in situations where rare cells can be of crucial importance, such as leukaemia and circulating tumour cells in cancer metastases, but also in such cases as bacterial resistance to therapy where rapidly changing phenotype amongst a small population of cells can determine the outcome of a broadly applied treatment.

Sampling and measurement approaches are insufficient to conquer such issues alone, however. The volumes of data generated using these and related approaches are such that in practice, as much thought and preparation must be applied to its management and analysis as is devoted to its initial generation.

2.5 Alternative Beam Profiles

While simple trapping systems described above can provide a useful tool, they are limited by a number of factors such as their short working distances and the fixed position of the trap generated. It is possible to shift the centre of a trapping beam using manual controls such as a steering lens or adjustable mirrors, although early designs simply maintained a static trap and used the movement of the microscope stage to achieve relative motion. Similarly, multiple individually addressable traps can be generated using a beam splitter and mirrors in a 4-f arrangement [47]. However, manual control of traps is extremely cumbersome in real experiments, particularly ones in which cells or samples must be moved through a complex environment. As such, the development of optical components which allow the rapid and automated sculpting of an incident laser beam greatly expanded the applicability of optical trapping to micromanipulation experiments. Early approaches centred upon the use of fast-scanning lasers, directed through actuated mirrors which shared the beam between a number of sites, and relying on the fluid viscosity of the medium to retain target localisation between cycles [48]. However, there is a limit to how rapidly such a system can scan and as such a limit on the number of stable traps that can be generated, and a more elegant solution was presented by the development of spatial light modulators.

2.5.1 Bessel Beams and Related Wave Masks

One of the major limitations of optical trapping as a technique comes from the relatively short working distances available (generally below 250 μm). Optical trapping depends upon an extremely narrow focal volume to generate its forces, with a typical diameter of only 1–2 wavelengths of light: the spread of a Gaussian light source, typically characterised by the Rayleigh range Z_R which denotes the

distance over which the beam area doubles, depends upon the wavelength λ and the beam waist radius w_0 according to Eq. 4 [49].

$$Z_R = \frac{\pi w_0^2}{\lambda} \tag{4}$$

It can therefore be seen that maintaining a tight focus in a situation where $\lambda \approx w_0$ requires a tight cone angle, thus a high numerical aperture lens and a commensurately short working distance. These high numerical aperture lenses normally require water or oil immersion and thus thermal contact with the target coverslip or chip. This can lead to serious experimental issues, as these distances are often incompatible with cell culture or microfluidic assemblies. Similarly, thermal gradients through the objective assembly can generate optical aberrations which may distort the traps or forces produced, although they can in some cases be avoided by allowing the entire microscope to reach thermal equilibrium. However, the wavelengths used for trapping are normally invisible to the human eye and filtered out by the microscope optics, meaning that identifying and ameliorating such aberrations can be a frustrating and time-consuming task.

One approach that has been developed to extend the range of trapping effects is through the use of Bessel (or at least approximations of Bessel) beams, light shaped to form a series of concentric rings which are effectively non-diffracting over the range of normal microscopy experiments [50]. Although these structures possess no beam waist and thus cannot form a true three-dimensional trap, they can be used to direct material in a given direction across relatively long ranges, corral objects with a defined long axis such as many bacteria and also have applications in trapping low-refractive-index materials which would be repelled by a normal Gaussian trap, sequestering them in the dark regions between light rings (Fig. 7).

Fig. 7 A typical Bessel beam profile. The white regions (indicating laser beam) show negligible diffraction over the working range of a microscope, meaning they can be used over longer distances than a normal Gaussian trap

The scope and complexity of the field is beyond the scope of a broad, practical guide such as this, but the interested reader is directed to comprehensive reviews elsewhere [51, 52]. However, a related approach using interfering plane waves has been recently developed that allows the generation of long-range trapping forces: the first demonstration of a genuine tractor beam. This approach allows micron-scale spheres to be directed via control of the incident wave's polarisation rather than gradient forces normally used for trapping, greatly extending its effective range [53].

3 Optoporation and Optically Controlled Cell Lysis

Experiments to manipulate and sample cells are extremely valuable in watching their response to stimuli, either in terms of their cell-level structural and motile behaviour or even in the expression of markers at a molecular level. However, for truly quantitative studies, such observations must be tied to a known dose of said stimulus and this is another area in which traditional techniques are weak. In normal biochemical experiments from drug-receptor binding assays to genetic modification, payloads are dissolved or dispersed throughout the bulk cell medium to a known concentration. This payload is then taken up by the cells: either passively via diffusive processes governed broadly by Overton's Rule [54, 55]; actively in the case of specific nutrients or biomimetic substances such as the chronic myeloid leukaemia drug imatinib [56]; using delivery vectors such as cationic lipids or polymers to trigger endocytosis [57] or finally via direct disruption of the membrane through applied voltage, ultrasound or heating [58]. Each of these approaches is generally successful when applied in the correct context, but each delivers a distribution of material to the target cells based upon their position within the well or culture dish, the chemistry of payload and state of the cell at the time of administration. As a result, biochemical dose–response data are famously noisy, and all information is lost about the cell heterogeneity that contributes a substantial proportion of the effect.

Optical tools, either alone or in combination with other modalities, provide a complementary technique to these studies. In general, the high photon flux required means that optical techniques operate at the low-throughput, single-cell level, but in doing so provide a level of precision, control and quantitation far in excess of that available to traditional experiments. Optical cell poration typically operates via one of two mechanisms: either a short-duration pulsed laser is used to generate free electrons at the cell surface which create a localised plasma whose shockwave can mechanically disrupt nearby membranes; alternatively a continuous-wave (CW) system may be used to cause sufficient heating to destabilise the hydrophobic bonds between lipids within a defined volume, triggering defect formation. The narrow three-dimensional focal volume of an optical trapping system makes it the ideal CW photoporation system, turning the cell manipulation tool developed earlier in the chapter into an all-purpose single-cell biology workstation.

Both pulsed and CW approaches have advantages and disadvantages, and both are capable of causing significant damage to the target membrane and wider cell if intensity or exposure time is too great. These destructive effects are also of value, however, permitting the approach to be utilised as a selective lysis tool, rupturing individual cells of interest to allow the analysis of their contents or even therapeutically as a precision ablation tool.

As with other topics in this chapter, an in-depth analysis of optically mediated membrane disruption and its applications could fill a textbook in its own right and so this should only be taken as an introduction to the topic. The interested reader is, however, directed to the review of Stevenson et al. for a concise, thorough review of the state of the field [59].

3.1 Pulsed Laser Poration

The poration of a cell membrane and its subsequent transfection using laser light was originally demonstrated by Tsukakoshi et al. [60]: their use of a nanosecond-pulsed UV laser ($\lambda = 355$ nm) was the first to generate microscopically observable membrane holes which would heal over the course of 1–2 s after the cessation of the light pulse. Their technique showed relatively low success rates of DNA transfection, but these were ameliorated by a throughput of thousands of cells per minute, meaning that the technique could be used to generate statistically valid populations of test subjects. However, the reported success rates were strongly coupled to the portion of cell illuminated: cytoplasmic irradiation showed <1 % efficacy, whilst nuclear targeting yielded ≈10 % transfection under ideal conditions. This was one of the first indications of the mechanisms underpinning the heterogeneity of response described in Sect. 1: the region of the cell that a penetrating payload encounters may have a strong influence upon the degree of response it triggers. Such information is irretrievably lost in bulk studies.

The high extinction coefficients experienced by short-wavelength light in biological tissue means that extremely low-powered lasers can induce effective poration, with powers as low as 0.3 mW sufficient to induce observable defects [61]. However, the lipids of the cell membrane are nearly transparent in UV and visible wavelengths, meaning that the absorption must be elsewhere in the cell. The majority of biological macromolecules such as proteins or DNA will strongly absorb in these regions, but this in itself poses a problem: the energies of the photons involved are of the order of chemical bonds, meaning they are sufficient to trigger substantial photochemistry which is likely to irreparably damage the affected proteins or nucleic acids. This strong absorbance also means that cells other than those on the surface closest to the laser are difficult or impossible to target, and certainly may not be probed without causing catastrophic damage to any intervening tissue.

Two-photon effects can ameliorate some of these shortcomings, however. Under the right conditions, two identical photons can sum their energies to form one of

twice the energy (and thus half the wavelength) [62]. This effect requires very high light intensities from pulsed laser sources, as the two photons must arrive at the chromophore at almost precisely the same instant and in phase with each other. This means that the effective absorption coefficients observed are both non-linear and many orders of magnitude below those experienced using normal illumination. However, the effect means that pulsed infrared lasers may be used to achieve similar effects to UV sources, eliminating many of the off-target problems and providing scope for investigations through several layers of cells, as photons arriving individually or in regions of lower intensity (outside the focal volume) experience little or no interactions with the tissue through which they pass. Such a technique is routinely applied to selectively excite short-wavelength-absorbing fluorophores in tissue without interacting with those around it [63]; photoporation requires significantly higher intensities but proceeds via the same process.

Different pulse intensities and durations trigger different effects: femtosecond-pulses will typically generate micron or sub-micron scale pores within an individual cell, which can be targeted with remarkable precision. In an elegant recent demonstration, Waleed et al. utilised the difference in focal length of two different laser wavelengths through the same optics to deliver optoporation pulses precisely to the membrane of a target cell, using an optically trapped microbead as a gunsight and subsequently as a delivery vehicle for plasmids once the pore had been established (Fig. 8; [64]).

Longer duration pulses of the order of picoseconds or nanoseconds will generate bubbles whose shockwave can lyse, damage or porate many cells across a range of ≈100 μm. The effects of these bubbles decrease with distance from the laser focus, meaning that different degrees of disruption can be inflicted upon a range of cells in the same chamber [2, 65].

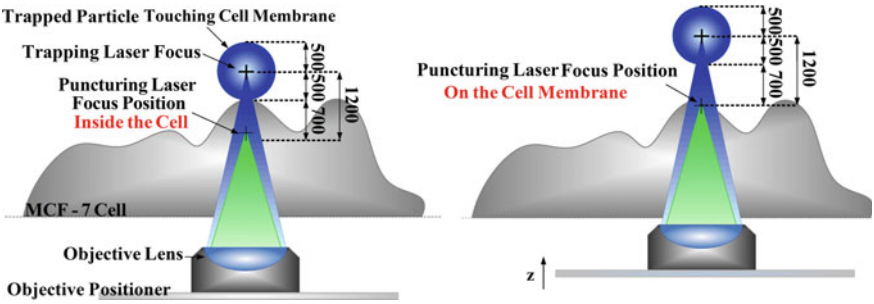

Fig. 8 Waleed et al. used the intrinsic difference in focal lengths of two different laser wavelengths to provide extremely precise targeting of a cell membrane by means of an optically trapped microbead [64]. The bead was held in a λ = 1064 nm trapping beam (*blue*), which was found by calculation and measurement to have a focal length of 1.2 μm longer than a pulsed poration beam of λ = 800 nm (shown in *green*). Precise alignment of the other optical components meant that the bead could be used as a sight for the poration pulse, while functionalisation of the bead with plasmids meant it could be used to directly deliver nucleic acid through the pore created. Figure used with permission of the Optical Society of America

3.1.1 Secondary Target Pulsed Laser Techniques

An alternative approach to using two-photon absorption to avoid cell damage comes from the use of secondary targets in the cell culture medium, materials which strongly absorb infrared wavelengths and transduce the laser energy into another form. This is typically an optothermal approach, although plasma formation using the right conditions. These materials can either be incorporated into the cell chamber structure itself, or can be introduced in the form or micro- or nanoparticles that offer opportunities for precision delivery via an alternative (ideally orthogonal) manipulation strategy. Care must be taken to ensure that the target material does not itself induce artefacts in the cells under study, and materials which are not wholly biocompatible and/or biodegradable are likely to accumulate over repeated treatments, exacerbating effects, but used carefully this tool can provide a pathway to the poration of even the most sensitive of cells and membranes.

Arita et al. have demonstrated this technique using an optical trap to isolate an individual gold nanoparticle, triggering its laser-induced breakdown with a nanosecond laser pulse at a different wavelength using some three orders of magnitude less energy than that required to achieve the same effect in water alone [4]. Fan et al. have demonstrated that a similar effect can be mediated by a thin layer of amorphous silicon irradiated using an infrared source with microsecond pulses [66], while Wu et al. have recently expanded the utility of the technique by making it possible to apply secondary target techniques to large numbers of cells in batches of $\sim$100,000 over the course of approximately a minute [67]. In this experiment, the researchers developed a multi-layer cell culture and poration chip incorporating micron-scale regions of TiO_2 only 100 nm thick. This titanium dioxide film absorbs the nanosecond-duration, λ = 532 nm pulses applied to generate cavitation microbubbles in the manner described above, which in turn create membrane pores of around 3 μm in diameter allowing the introduction to the target cells of relatively large biomolecules. This provides a substantial improvement over previous techniques to increase throughput, which relied upon moving the cells through a laser focus via microfluidic flow focusing and thus required that the cells were detached from their native culture before treatment [68].

3.2 Continuous-Wave Poration and Lysis

In contrast to pulsed laser sources, the intensity of CW lasers is typically many orders of magnitude lower and so lasers of infrared wavelengths are insufficient to generate the same plasmas. As a result, CW lasers almost always operate via an optothermal mechanism with a secondary target, similar to that described above. As in the case of pulsed systems, orthogonal target steering methods can be used to selectively porate or lyse cells of interest. Gu et al. recently demonstrated this technique using iron-doped carbon nanoparticles which could be localised in target regions by application of a small magnet, before irradiation with an infrared

source [69]. Optoelectronic tweezers are a variation on this theme, using focused, low-intensity CW light to facilitate precisely controlled dielectrophoresis. Such techniques are well covered elsewhere in this book and will not be covered further here, although research by the groups of Jon Cooper and Steven Neale in Glasgow have recently demonstrated that such a platform can be utilised to electroporate cells selecting both spatially and for cell morphology, based upon the 'electrochemical shadow' that the cells cast upon the amorphous silicon surface [3, 70]. Amorphous silicon layers can be used to directly facilitate optoporation, however: the microsecond-pulse experiments of Fan et al. [66, 71] and continuous-wave experiments in our own laboratories [72] have demonstrated that hot-spot generation upon infrared irradiation of thin-layer silicon is sufficient to cause single- or even sub-cellular poration (see Fig. 9, below).

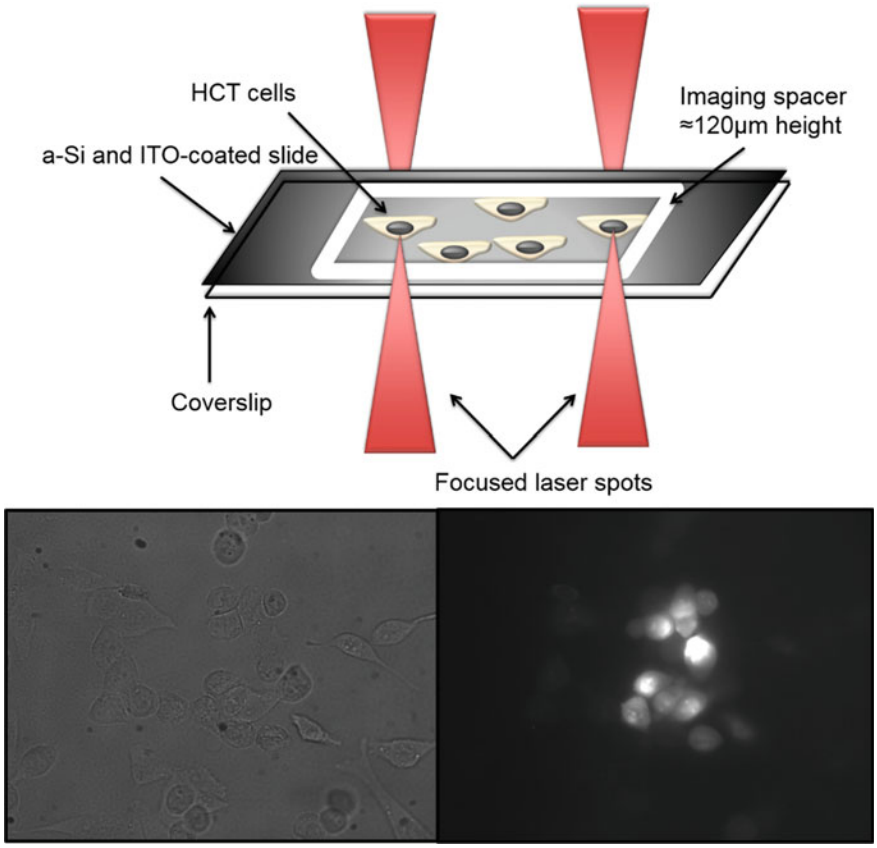

Fig. 9 (*Above*) a schematic of the experimental apparatus used in our laboratories for continuous-wave optoporation (λ = 1064 nm). HCT116 cells [73] were cultured directly onto thin-layer amorphous silicon and assembled into a closed chip, then inverted so as to hang pendant. (*Below*) Bright-field and fluorescence images showing selective poration of HCT cells, illustrated using propidium iodide [72]

If tissue lysis or ablation is the aim, CW sources become the method of choice: infrared lasers with powers of 5–50 W are routinely used in medicine for highly localised tumour ablation, particularly in cases where small tumours are scattered across a region of tissue, as is often the case in secondary cancers such as small hepatocellular carcinoma [74]. In such cases, the technique's applicability is greatly strengthened by the surgeon's ability to steer the light using a flexible, narrow fibre-optic cable and the light's relatively short penetration length of around 12–15 mm, minimising damage to healthy tissue.

4 Conclusions

Optical tools provide an almost universal tool for single-cell biology experiments, although what is gained in flexibility and precision is often lost in throughput. The sterile, contact-free manipulation techniques provided by optical trapping allows extremely gentle spatial control in three dimensions between multiple microscopic objects simultaneously, while coupling trapping with either coaxial high intensity sources or the introduction of carefully chosen secondary targets allows the delivery of specific payloads to a specific cell or cells, all with sub-micron accuracy.

At present, such techniques are generally confined to the research laboratory as throughput is too low and optical path lengths through tissue too short to be of immediate clinical significance. However, tissue ablation through fibre-coupled lasers, a process requiring less finesse of power and exposure time, is already a routine surgical tool, and as control systems develop in line with endoscopic delivery tools it is likely that optical manipulations and payload delivery platforms will become increasingly important in medicine as well as fundamental research.

References

1. Bowman RW, Padgett MJ (2013) Optical trapping and binding. Rep Prog Phys 76:026401. doi:10.1088/0034-4885/76/2/026401
2. Quinto-Su PA, Lai H-H, Yoon HH, Sims CE, Allbritton NL, Venugopalan V (2008) Examination of laser microbeam cell lysis in a PDMS microfluidic channel using time-resolved imaging. Lab Chip 8:408–414. doi:10.1039/b715708h
3. Kremer C, Witte C, Neale SL, Reboud J, Barrett MP, Cooper JM (2014) Shape-Dependent optoelectronic cell lysis. Angew Chem 126:861–865. doi:10.1002/ange.201307751
4. Arita Y, Ploschner M, Antkowiak M, Gunn-Moore F, Dholakia K (2014) Single cell transfection by laser-induced breakdown of an optically trapped gold nanoparticle. In: Heisterkamp A, Herman PR, Meunier M, Nolte S (eds) Proceedings of SPIE. SPIE, p 897203
5. Willison KR, Klug DR (2013) Quantitative single cell and single molecule proteomics for clinical studies. Curr Opin Biotechnol 24:745–751. doi:10.1016/j.copbio.2013.06.001
6. Raj A, van Oudenaarden A (2008) Nature, nurture, or chance: stochastic gene expression and its consequences. Cell 135:216–226. doi:10.1016/j.cell.2008.09.050
7. Godin AG, Lounis B, Cognet L (2014) Super-resolution microscopy approaches for live cell imaging. Biophys J 107:1777–1784. doi:10.1016/j.bpj.2014.08.028

8. Almén MS, Nordström KJV, Fredriksson R, Schiöth HB (2009) Mapping the human membrane proteome: a majority of the human membrane proteins can be classified according to function and evolutionary origin. BMC Biol 7:50. doi:10.1186/1741-7007-7-50
9. Kiviet DJ, Nghe P, Walker N, Boulineau S, Sunderlikova V, Tans SJ (2014) Stochasticity of metabolism and growth at the single-cell level. Nature 514:376–379. doi:10.1038/nature13582
10. Steptoe PC, Edwards RG (1978) Birth after the reimplantation of a human embryo. Lancet 2:366
11. Palermo G, Joris H, Derde MP, Camus M, Devroey P, Van Steirteghem A (1993) Sperm characteristics and outcome of human assisted fertilization by subzonal insemination and intracytoplasmic sperm injection. Fertil Steril 59:826–835. doi:10.1071/RD9940085
12. Zhang Y (2007) Microinjection technique and protocol to single cells. Protoc Exch. doi:10.1038/nprot.2007.487
13. Neri QV, Lee B, Rosenwaks Z, Machaca K, Palermo GD (2014) Understanding fertilization through intracytoplasmic sperm injection (ICSI). Cell Calcium 55:24–37. doi:10.1016/j.ceca.2013.10.006
14. Salazar GTA, Wang Y, Young G, Bachman M, Sims CE, Li GP, Allbritton NL (2007) Micropallet arrays for the separation of single, adherent cells. Anal Chem 79:682–687. doi:10.1021/ac0615706
15. Tsuda Y, Mori O, Funase R, Sawada H, Yamamoto T, Saiki T, Endo T, Yonekura K, Hoshino H, Kawaguchi J (2012) Achievement of IKAROS—Japanese deep space solar sail demonstration mission. Acta Astronaut 82:183–188. doi:10.1016/j.actaastro.2012.03.032
16. Ashkin A (1970) Acceleration and trapping of particles by radiation pressure. Phys Rev Lett 24:156–159. doi:10.1103/PhysRevLett.24.156
17. Ashkin A (1992) Forces of a single-beam gradient laser trap on a dielectric sphere in the ray optics regime. Biophys J 61:569–582
18. Williams MC (2002) Optical tweezers: measuring piconewton forces. In: Schwille P (ed) Biophysics Textbook Online. Biophysical Society, Bethesda, pp 1–14
19. Neuman KC, Block SM (2004) Optical trapping. Rev Sci Instrum 75:2787–2809. doi:10.1063/1.1785844
20. Neuman KC, Block SM (2004) Optical trapping. Rev Sci Instrum 75:2787–2809. doi:10.1063/1.1785844
21. Armitage D, Thackara JL, Eades WD (1989) Photoaddressed liquid crystal spatial light modulators. Appl Opt 28:4763–4771. doi:10.1364/AO.28.004763
22. Mao CC, Johnson KM, Turner R, Jared D, Doroski D (1992) Applications of binary and analog hydrogenated amorphous-silicon ferroelectric liquid-crystal optically addressed spatial light modulators. Appl Opt 31:3908–3916. doi:10.1364/AO.31.003908
23. Lanigan PMP, Munro I, Grace EJ, Casey D, Phillips J, Klug DR, Ces O, Neil MAA (2012) Dynamical hologram generation for high speed optical trapping of smart droplet microtools. Biomed Opt Express 3:1609–1619. doi:10.1364/BOE.3.001609
24. Grieve JA, Ulcinas A, Subramanian S, Gibson GM, Padgett MJ, Carberry DM, Miles MJ (2009) Hands-on with optical tweezers: a multitouch interface for holographic optical trapping. Opt Express 17:3595–3602. doi:10.1364/OE.17.003595
25. Lee WM, Reece PJ, Marchington RF, Metzger NK, Dholakia K (2007) Construction and calibration of an optical trap on a fluorescence optical microscope. Nat Protoc 2:3226–3238. doi:10.1038/nprot.2007.446
26. Werner M, Merenda F, Piguet J, Salathé R-P, Vogel H (2011) Microfluidic array cytometer based on refractive optical tweezers for parallel trapping, imaging and sorting of individual cells. Lab Chip 11:2432–2439. doi:10.1039/c1lc20181f
27. Hu Z, Wang J, Liang J (2004) Manipulation and arrangement of biological and dielectric particles by a lensed fiber probe. Opt Express 12:4123–4128. doi:10.1364/OPEX.12.004123
28. Mohanty SK, Mohanty KS, Berns MW (2008) Organization of microscale objects using a microfabricated optical fiber. Opt Lett 33:2155–2157. doi:10.1364/OL.33.002155

29. Liang P-B, Lei J-J, Liu Z-H, Zhang Y, Yuan L-B (2014) A study of multi-trapping of tapered-tip single fiber optical tweezers. Chin Phys B 23:088702. doi:10.1088/1674-1056/23/8/088702
30. Liu Y, Cheng DK, Sonek GJ, Berns MW, Chapman CF, Tromberg BJ (1995) Evidence for localized cell heating induced by infrared optical tweezers. Biophys J 68:2137–2144. doi:10.1016/S0006-3495(95)80396-6
31. Ayano S, Wakamoto Y, Yamashita S, Yasuda K (2006) Quantitative measurement of damage caused by 1064-nm wavelength optical trapping of Escherichia coli cells using on-chip single cell cultivation system. Biochem Biophys Res Commun 350:678–684. doi:10.1016/j.bbrc.2006.09.115
32. Xie C, Chen D, Li Y (2005) Raman sorting and identification of single living micro-organisms with optical tweezers. Opt Lett 30:1800. doi:10.1364/OL.30.001800
33. Ashkin A, Dziedzic JM (1987) Optical trapping and manipulation of viruses and bacteria. Science 235:1517–1520. doi:10.1126/science.3547653
34. Neuman KC, Nagy A (2008) Single-molecule force spectroscopy: optical tweezers, magnetic tweezers and atomic force microscopy. Nat Methods 5:491–505. doi:10.1038/NMETH.1218
35. López-Quesada C, Fontaine A-S, Farré A, Joseph M, Selva J, Egea G, Ludevid MD, Martín-Badosa E, Montes-Usategui M (2014) Artificially-induced organelles are optimal targets for optical trapping experiments in living cells. Biomed Opt Express 5:1993–2008. doi:10.1364/BOE.5.001993
36. Schroder BW, Johnson BM, Garrity DM, Dasi LP, Krapf D (2014) Force spectroscopy in the bloodstream of live embryonic zebrafish with optical tweezers. In: Frontiers in optics 2014. OSA, Washington, D.C., p FTu1F.5
37. Simmons RM, Finer JT, Chu S, Spudich JA (1996) Quantitative measurements of force and displacement using an optical trap. Biophys J 70:1813–1822. doi:10.1016/S0006-3495(96)79746-1
38. Svoboda K, Schmidt CF, Schnapp BJ, Block SM (1993) Direct observation of kinesin stepping by optical trapping interferometry. Nature 365:721–727. doi:10.1038/365721a0
39. Nicholas MP, Rao L, Gennerich A (2014) An improved optical tweezers assay for measuring the force generation of single kinesin molecules. Methods Mol Biol 1136:171–246. doi:10.1007/978-1-4939-0329-0_10
40. Kato N, Ishijima A, Inaba T, Nomura F, Takeda S, Takiguchi K (2015) Effects of lipid composition and solution conditions on the mechanical properties of membrane vesicles. Membranes (Basel) 5:22–47. doi:10.3390/membranes5010022
41. Villangca M, Bañas A, Palima D, Glückstad J (2014) Dynamic diffraction-limited light-coupling of 3D-maneuvered wave-guided optical waveguides. Opt Express 22:17880–17889. doi:10.1364/OE.22.017880
42. Pacoret C, Bowman R, Gibson G, Haliyo S, Carberry D, Bergander A, Régnier S, Padgett M (2009) Touching the microworld with force-feedback optical tweezers. Opt Express 17:10259–10264. doi:10.1364/OE.17.010259
43. Jordan CT, Guzman ML, Noble M (2006) Cancer stem cells. N Engl J Med 355:1253–1261. doi:10.1056/NEJMra061808
44. Rucevic M, Hixson D, Josic D (2011) Mammalian plasma membrane proteins as potential biomarkers and drug targets. Electrophoresis 32:1549–1564. doi:10.1002/elps.201100212
45. Actis P, Maalouf MM, Kim HJ, Lohith A, Vilozny B, Seger RA, Pourmand N (2014) Compartmental genomics in living cells revealed by single-cell nanobiopsy. ACS Nano 8:546–553. doi:10.1021/nn405097u
46. Schrems A, Phillips J, Casey DR, Wylie D, Novakova M, Sleytr UB, Klug D, Neil MAA, Schuster B, Ces O (2014) The grab-and-drop protocol: a novel strategy for membrane protein isolation and reconstitution from single cells. Analyst 139:3296–3304. doi:10.1039/c4an00059e
47. Fällman E, Axner O (1997) Design for fully steerable dual-trap optical tweezers. Appl Opt 36:2107–2113. doi:10.1364/AO.36.002107

48. Molloy JE (1998) Optical chopsticks: digital synthesis of multiple optical traps. In: Wilson L, Tran P (eds) Methods in cell biology. Elsevier B.V., New York pp 205–216
49. Svelto O (2010) Principles of lasers, 5th edn. Princ lasers. doi:10.1007/978-1-4419-1302-9
50. Durnin J, Miceli J, Eberly JH (1987) Diffraction-free beams. Phys Rev Lett 58:1499–1501. doi:10.1103/PhysRevLett.58.1499
51. McGloin D, Dholakia K (2005) Bessel beams: diffraction in a new light. Contemp Phys 46:15–28. doi:10.1080/0010751042000275259
52. Woerdemann M, Alpmann C, Esseling M, Denz C (2013) Advanced optical trapping by complex beam shaping. Laser Photonics Rev 7:839–854. doi:10.1002/lpor.201200058
53. Brzobohatý O, Karásek V, Šiler M, Chvátal L, Čižmár T, Zemánek P (2013) Experimental demonstration of optical transport, sorting and self-arrangement using a "tractor beam". Nat Photonics 7:1–5. doi:10.1038/nphoton.2012.332
54. Overton CE (1899) On the general osmotic properties of the cell, their probable origin, and their significance for physiology. Vierteljahrsschr Naturforsch Ges Zurich 44:88–135
55. Al-Awqati Q (1999) One hundred years of membrane permeability: does Overton still rule? Nat Cell Biol 1:E201–E202
56. Gottesman MM, Fojo T, Bates SE (2002) Multidrug resistance in cancer: role of ATP-dependent transporters. Nat Rev Cancer 2:48–58. doi:10.1038/nrc706
57. Samal SK, Dash M, Van Vlierberghe S, Kaplan DL, Chiellini E, van Blitterswijk C, Moroni L, Dubruel P (2012) Cationic polymers and their therapeutic potential. Chem Soc Rev 41:7147–7194. doi:10.1039/c2cs35094g
58. Kalli C, Teoh WC, Leen E (2014) Introduction of Genes via Sonoporation and Electroporation. In: Grimm S (ed) Advances in experimental medicine and biology anticancer genes. Springer, London, pp 231–254
59. Stevenson DJ, Gunn-Moore FJ, Campbell P, Dholakia K (2010) Single cell optical transfection. J R Soc Interface 7:863–871. doi:10.1098/rsif.2009.0463
60. Tsukakoshi M, Kurata S, Nomiya Y, Ikawa Y, Kasuya T (1984) A novel method of DNA transfection by laser microbeam cell surgery. Appl Phys B Photophysics Laser Chem 35:135–140. doi:10.1007/BF00697702
61. Paterson L, Agate B, Comrie M, Ferguson R, Lake TK, Morris JE, Carruthers AE, Brown CTA, Sibbett W, Bryant PE, Gunn-Moore F, Riches AC, Dholakia K (2005) Photoporation and cell transfection using a violet diode laser. Opt Express 13:595. doi:10.1364/OPEX.13.000595
62. Franken PA, Hill AE, Peters CW, Weinreich G (1961) Generation of optical harmonics. Phys Rev Lett 7:118–119. doi:10.1103/PhysRevLett.7.118
63. Denk W, Strickler JH, Webb WW (1990) Two-photon laser scanning fluorescence microscopy. Science 248:73–76. doi:10.1126/science.2321027
64. Waleed M, Hwang S-U, Kim J-D, Shabbir I, Shin S-M, Lee Y-G (2013) Single-cell optoporation and transfection using femtosecond laser and optical tweezers. Biomed Opt Express 4:1533–1547. doi:10.1364/BOE.4.001533
65. Venugopalan V, Guerra A, Nahen K, Vogel A (2002) Role of laser-induced plasma formation in pulsed cellular microsurgery and micromanipulation. Phys Rev Lett 88:078103. doi:10.1103/PhysRevLett.88.078103
66. Fan Q, Hu W, Ohta AT (2015) Efficient single-cell poration by microsecond laser pulses. Lab Chip 15:581–588. doi:10.1039/C4LC00943F
67. Wu Y-C, Wu T-H, Clemens DL, Lee B-Y, Wen X, Horwitz MA, Teitell MA, Chiou P-Y (2015) Massively parallel delivery of large cargo into mammalian cells with light pulses. Nat Methods 1–8. doi:10.1038/nmeth.3357
68. Marchington RF, Arita Y, Tsampoula X, Gunn-Moore FJ, Dholakia K (2010) Optical injection of mammalian cells using a microfluidic platform. Biomed Opt Express 1:527. doi:10.1364/BOE.1.000527
69. Gu L, Koymen AR, Mohanty SK (2014) Crystalline magnetic carbon nanoparticle assisted photothermal delivery into cells using CW near-infrared laser beam. Sci Rep 4:5106. doi:10.1038/srep05106

70. Witte C, Kremer C, Chanasakulniyom M, Reboud J, Wilson R, Cooper JM, Neale SL (2014) Spatially selecting a single cell for lysis using light-induced electric fields. Small. doi:10.1002/smll.201400247
71. Fan Q, Hu W, Ohta AT (2013) Light-induced microbubble poration of localized cells. In: Proceedings annual international conference of the IEEE on Engineering in Medicine and Biology Society (EMBS). IEEE, pp 4482–4485
72. Casey D, Wylie D, Gallo J, Dent M, Salehi-Reyhani A, Wilson R, Brooks N, Long N, Willison K, Klug D, Neil M, Neale SL, Cooper J, Ces O (2015) A novel, all-optical tool for controllable and non-destructive poration of cells with single-micron resolution. In: Optics in the life sciences. OSA, Washington, D.C., p BW1A.5. doi:10.1364/BODA.2015.BW1A.5
73. Brattain MG, Fine WD, Khaled FM, Thompson J, Brattain DE (1981) Heterogeneity of malignant cells from a human colonic carcinoma. Cancer Res 41:1751–1756
74. Pacella CM, Francica G, Di Costanzo GG (2011) Laser ablation for small hepatocellular carcinoma. Radiol Res Pract 2011:595–627. doi:10.1155/2011/595627

Optoelectrokinetic Manipulation for Cell Analysis

Han-Sheng Chuang, Hu-Yao Ku, Fu-Tsun Li, Aloke Kumar, Jhih-Cheng Wang and Kuan-Chih Wang

Abstract Rapid advancement of microfluidic technology in the recent years has opened a new era for biological diagnostics. The demands for fast response, multi-functionality, non-invasiveness, and programmability boost the developments in many fields, such as tissue engineering, cell analysis, and molecular biology. For this trend, an appropriate manipulation tool is pivotal to the success of all applications. In this chapter, we explore two newly developed optoelectrokinetic techniques, termed rapid electrokinetic patterning (REP) and optoelectronic tweezers (OETs), from the fundamental principles to their applications in cell-related research. Details about fabrications, setups, and assessments are also thoroughly discussed. Both techniques are enabled by a deliberate integration of light and electric fields, therefore imparting them the unique abilities to dynamically manipulate biological targets. Unlike some well-adopted techniques, such as dielectrophoresis (DEP), REP and OETs feature high flexibility in manipulation. Their repertoire of manipulation includes, but not limited to, micro/nano concentration, sorting, translation, single particle trapping, and patterning. By combining with optoelectrowetting (OEW), a cross-scale platform suitable for multiple purposes can be even achieved. The multi-functionality endows the optoelectrokinetic manipulation the potential to further extend the cell analysis in all aspects.

Keywords REP · OETs · Optoelectrokinetics · Particle · Cell · Microfluidics

H.-S. Chuang (✉) · H.-Y. Ku · F.-T. Li · K.-C. Wang
Department of Biomedical Engineering, National Cheng Kung University, Tainan, Taiwan
e-mail: oswaldchuang@mail.ncku.edu.tw

H.-S. Chuang
Medical Device Innovation Center, National Cheng Kung University, Tainan, Taiwan

A. Kumar
Mechanical Engineering, University of Alberta, Edmonton, AB, Canada

J.-C. Wang
Department of Urology, Chimei Medical Center, Tainan, Taiwan

F.-G. Tseng and T.S. Santra (eds.), *Essentials of Single-Cell Analysis*,
Series in BioEngineering, DOI 10.1007/978-3-662-49118-8_6

1 Introduction

Single-cell analysis (SCA) is a useful measure to understanding the specific expressions of individual cells against different stimuli. In a multicellular model, those influences are difficult to address because the measurements of the individual cellular response are lost in the bulk average. Therefore, SCA provides a valuable insight to its assembly phenotypes. To date, SCA has been broadly adopted in many research fields, such as tissue engineering, regenerative medicine [1, 2] and microarrays [3–5], due to an easy-to-understand framework of system. Distinct from model animals, however, the tiny size of single cells forms a major barrier for researchers who are involved in the cell-related work.

To tackle the problem, a wide variety of devices capable of handling micro-/nano-sized matters have been proposed over the past decades [6–15]. Among them, the flow cytometer [6] was first developed and has eventually turned out to be a successful platform well known as fluorescence activated cell sorter (FACS) [7]. In the device, cells are hydrodynamically focused by sheath flow. The focused single-cell stream is then counted and sorted in the downstream channels. High efficiency and high throughput make FACS a popular device in the modern clinical uses.

For versatile manipulation, the spotlight is drawn to dielectrophoresis (DEP). DEP is a phenomenon showing migration of dielectric particles in a nonuniform electric field. When the polarizability of particles is higher than that of surrounding medium, particles tend to move toward the field intensity maxima, which is termed positive DEP (pDEP); whereas, negative DEP (nDEP) causes particles to move away from the field intensity maxima. The behavior endows DEP the potential in the selective manipulation of viruses, bacteria, cells and other submicron biological particles based on their spatial, dielectric and shape properties [10–13, 15]. Considerable studies [9, 11, 12] have proven DEP to be an innovative technique in cell analyses and processing. However, the flexibility is limited by the fixed electrode layout.

For higher resolution in control, optical tweezers (OTs), developed since 1986 [8], do not have a higher degree of freedom than DEP. Rather it has a higher resolution. The mechanism relies on light that is highly focused in a colloidal suspension, and the focal point will create an energy trap, pulling particles into it. Using spatial light modulators (SLM), the phase of the light beam can also be altered and complex trapping geometries can be created including multiple trapping sites. In addition, a scanning mirror (a galvanized mirror) can also achieve the same effect of programmable control. With a galvanized mirror, Castelain et al. [14] reported that removing a yeast cell from adhesion required forces of 1–10 pN under the laser power of up to 127 mW. Meanwhile, the photo-damage on cells was found negligible during the 5-h trapping due to the use of near IR wavelength (810 nm) and a short period of laser exposure (1 Hz). Lately, Zhong et al. [16] further applied the technique to live animals. They trapped in vivo red blood cells with a 168-mW IR laser (1064 nm) in the capillary of a live mouse's ear to demonstrate capillary

blockage and clearance of a clogged blood vessel. Sophisticated cell level research is therefore carried out with the addressable and noninvasive measure.

Traditional techniques such as OTs or DEPs utilize either electric fields or light waves for micro/nano scale manipulation. In contrast, recently invented optoelectrokinetic techniques simultaneously use light illumination and electric fields for manipulation of matter at the micro/nano scale. The special combination allows them to inherit the properties from both electrokinetic and optical techniques. Therefore, the optoelectrokinetic techniques are capable of trapping biological particles not only by size but also by dielectric properties through light patterns. This unique characteristic draws tremendous attention from the public and makes it a promising tool in the biological applications. Herein two optoelectrokinetic techniques, REP and OETs, will be thoroughly discussed. The configurations of both REP and OETs are shown in Fig. 1. Noted that REP can be operated in other configurations as well. For example Kumar et al. [17] and Chuang et al. [18] utilized REP in a setup where the electrodes were interdigitated instead of being uniform and parallel.

Rapid electrokinetic patterning (REP) was first proposed by Williams et al. in 2008 [19]. The simplest REP device is composed of two parallel uniform electrodes with a focused laser beam impinging on one of the electrodes. The laser is suitably chosen so that it can selectively heat the illuminated region of the electrode surface. Such localized heating generates strong electrothermal flows in the device and in conjunction with other electrokinetic forces, REP can lead to the trapping of micro/nano scale objects near the electrode surface. The repertoire of particle manipulation that has been developed so far includes micro/nanoparticle concentration, translation, sorting and patterning [19–23]. Especially, the technique has achieved trapping of all sorts of material, including polystyrene (PS) beads, quantum dots (QDs), gold nanoparticles (NPs), carbon nanotubes (CNTs) and biological cells. Therefore, REP is considered to have strong potential in advancing the future biological research.

Optoelectronic tweezers (OETs) were officially introduced to the scientific community in 2005 [24]. The typical OET device is composed of two parallel

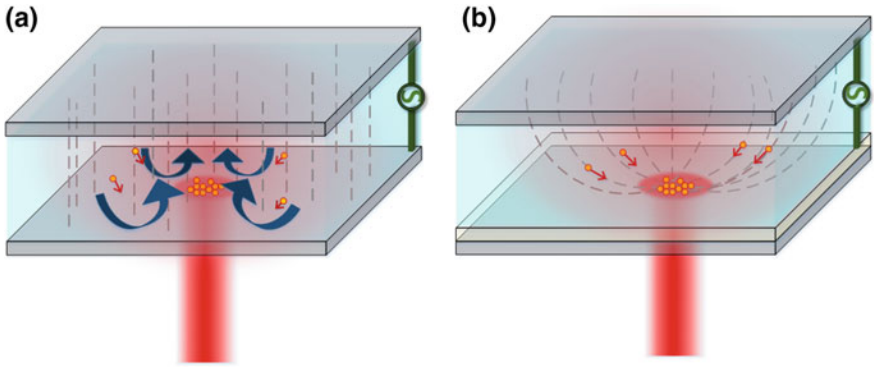

Fig. 1 Configurations of **a** REP and **b** OET microchips. The dashed lines show the electric field lines. The red cylinders represent the light patterns inducing the virtual electrodes. The blue arrows represent the fluid vortices. The tiny yellow circles are the micro particles

Table 1 Experimental parameters for cell manipulation

Parameters	OETs	REP
Electric field	1–3 kV/cm	1–3 kV/cm
Operational frequency	100 kHz–1 MHz	1–200 kHz and 1–5 MHz
Light intensity	100 mW/cm^2–100 W/cm^2	<100 W/cm^2
Conductivity of medium	<10 mS/m	<100 mS/m
Particle size	1 μm[a]–100 μm	10 nm–100 μm
Applications	Massively parallel manipulation, single particle trapping, sorting, patterning, cell electroporation/lysis, etc.	Rapid aggregation, multiple/single particle trapping, sorting, patterning, biological particle manipulation, parallel manipulation etc.
P.S.	Visible light	Visible light—IR[b]

[a]Nanoparticles can be manipulated with other light-induced effects, such as LACEO
[b]The optimal wavelength is dependent on the material of substrate used

featureless electrodes and driven by light and an electric field simultaneously. Especially, there is a photoconductive layer coated on one of the electrodes to convert the optical energy into the electrical energy. This configuration allows the illuminated regions to act as 'virtual electrodes' and thus DEP forces can be generated in the device. Accordingly, target particles will be trapped or repelled away from the maxima depending on their pDEP or nDEP response. To date, the technique has shown wide applications in cell processing, including sorting [24, 25], patterning [24, 26], parallel manipulation [24, 26, 27], etc. Limited by the nature of DEP, however, OETs are less capable of controlling matter at the nanoscale. A comparison showing the empirical parameters used for cell applications in REP and OETs is shown in Table 1.

In the following article, we will start with the main principles and detailed characterizations of the both techniques, followed by their applications in cell analyses. Eventually, some unsolved challenges and future work will be discussed in the last section.

2 Materials and Device Configurations

2.1 The REP System

2.1.1 Microchip Fabrication

Here we describe fabrication of the REP microchip. The microchip is composed of two parallel plate electrodes separated with a spacer. To induce a strong REP effect, the electric field is suggested to be at least 1 kV/cm. An example of fabrication is

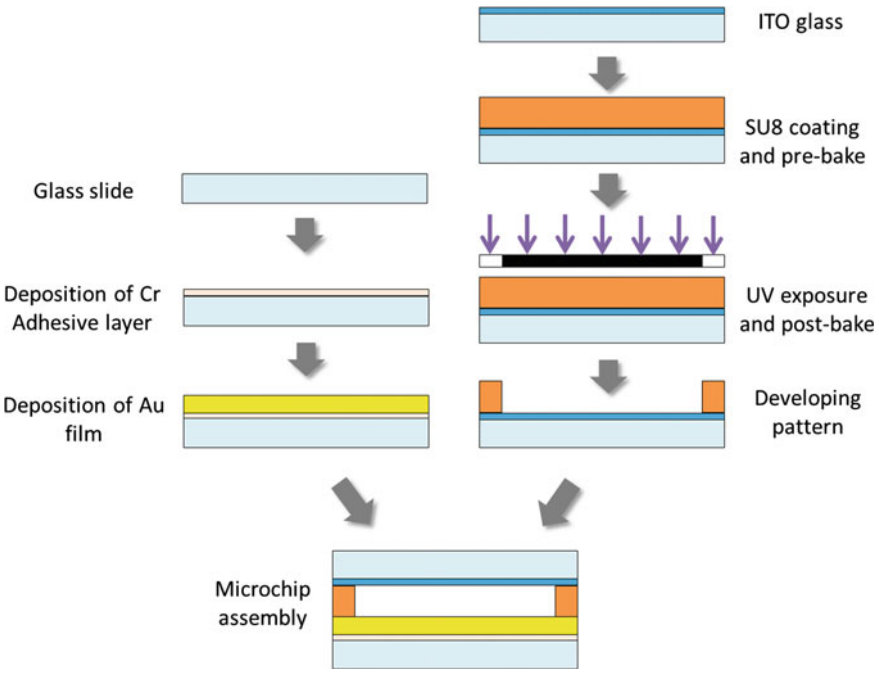

Fig. 2 Fabrication procedure of the REP microchip

demonstrated in Fig. 2. To facilitate the observation, one of the electrodes is made of indium tin oxide (ITO) glass. The other electrode is a plain glass slide coated with a 150-nm gold film. Under the gold film lays a 25-nm adhesive layer made of chromium. Both layers are deposited on the slide by an E-beam evaporator in a cleanroom. A negative photoresist (SU8-2025, Microchem), treated as a spacer, is then coated on the ITO glass by a spinner, followed by the standard photolithographic process. Eventually, the microchip is assembled by placing the ITO glass on the top of the gold electrode. Noted that other materials can be chosen as electrodes and the reader can refer to the detailed review of REP by Kumar et al. [28].

2.1.2 System Setup

Figure 3 shows the schematic of the REP system setup. Before operation, a microchip is fixed on a holder with edges of ITO glass and gold electrode connected to the power amplifier. A function generator is used to provide a sinusoidal signal to the power amplifier. A tunable solid-state IR laser beam (1064 nm) is directed to the bottom of the microchip and focused by an 4.6× objective lens on the back of the gold electrode. A motorized mirror is set up in the light path to steer the laser beam

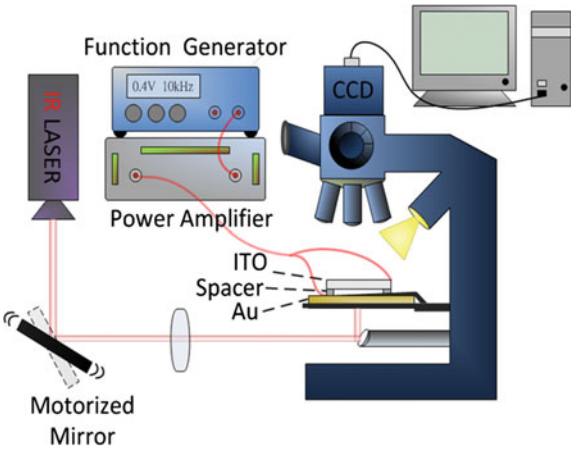

Fig. 3 Schematic of the experimental REP system. (Reprinted with permission from [20]. Copyright 2014 Royal Society of Chemistry.)

over the entire microchip for programmable particle trapping. Above the microchip, an upright fluorescent microscope equipped with an objective lens, a filter cube and a fast CMOS camera is used to visualize and record the particle manipulation.

To evaluate the temperature distribution of the microchip in the presence of illumination and an electric field, an IR coated microscope coupled with an IR camera is used in place of the upright microscope. When operating the system, the electric field is usually applied first, followed by the laser illumination. The measurement starts after the temperature becomes stable.

2.2 The OET System

2.2.1 Microchip Fabrication

Figure 4 illustrates the fabrication procedure of the OET microchip. Similar to the REP counterpart, the OET microchip is composed of two parallel plate electrodes separated with a spacer. To obtain light-induced reactions, one of the ITO glasses is deposited with 1-μm hydrogenated amorphous silicon (a-Si:H) using plasma enhanced chemical vapor deposition (PECVD). Subsequently, on the top of a-Si:H, a thin film (20 nm) of silicon dioxide (SiO_2) is coated as a protective layer. Notably, the insulating layer, SiO_2, needs to increase its thickness to 100 nm when the function of OEW is incorporated into the system. In this situation, the surfaces of both the substrates will require an additional thin hydrophobic layer (Teflon AF1600, Dupont). On the plain ITO glass, the negative photoresist (SU8-2025) is used to fabricate a spacer (<50 μm) with the standard photolithography. Similarly, the use of the ITO glass substrate can allow better optical access. Eventually, the OET microchip is complete by bonding the two ITO substrates.

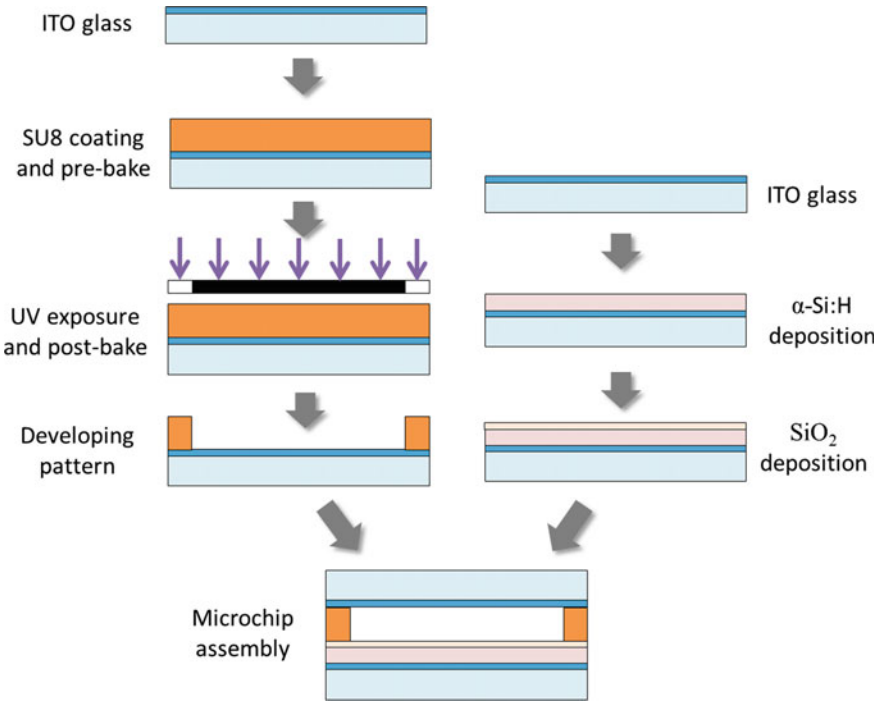

Fig. 4 Fabrication procedure of the OET microchip

2.2.2 System Setup

By sandwiching a colloidal suspension in the OET microchip in the presence of light and an electric field, the OET effect can be carried out. An equivalent RC circuit is usually employed to elucidate the frequency-related response. The microchip is placed under a fluorescent microscope equipped with a camera. The steering beam is illuminated at the photoconductive layer while the observation window is from the other side of the microchip. The electric field is generated from a power amplifier with the AC signal supplied by a function generator. A wide variety of visible light sources can be used for the particle manipulation on the OET microchip as long as the photoconductive layer is energized. For example, a green solid-state laser (532 nm) beam, with a maximum power of 150 mW, is used to induce the "virtual electrodes". For addressable beam steering or variable light patterns, a SLM device is incorporated into the light path. The incident light is linearly polarized in space according to the designed pattern and gray level, and then passes through another analyzer to filter the unwanted portions. When all the optical components are properly aligned, only the desired pattern will be bright leaving the rest to be dark. Subsequently, an objective lens underneath the microchip is used to shrink the pattern and project it onto the photoconductor.

Alternatively, the light source can also be replaced with broadband illumination such as a DMD projector. More detailed setup can be referred to the prior studies [24, 26, 29].

3 Principles of the Optoelectrokinetic Techniques

3.1 Rapid Electrokinetic Patterning (REP)

3.1.1 Light-Induced Electrothermal (ET) Flow

ET flow is an electrohydrodynamic motion of a fluid generated by the simultaneous application of an AC electric field and a heat source. The heat source induced temperature gradient results in a nonuniform distribution of electrical conductivity and permittivity in the fluid bulk. It, in turn, produces an electrical body force (f_e) to drive the fluid element and then forms a convective vortex. The time-averaged expression for this electrothermal body force is [30]

$$\langle f_e \rangle = 1/2Re\left[\frac{\sigma_m \varepsilon_m(\alpha-\beta)}{\sigma_m + i\omega\varepsilon_m}(\nabla T \cdot E)E^* - 1/2\varepsilon_m \alpha |E|^2 \nabla T\right] \quad (1)$$

where * indicates complex conjugate and Re refers to the real part of expression; for an AC signal of frequency ω, E is the electric field; σ_m and ε_m are the conductivity and permittivity of fluid, respectively; β and α are $(1/\sigma_m)(\partial\sigma_m/\partial T)$ and $(1/\varepsilon_m)(\partial\sigma_m/\partial T)$, respectively. The equation indicates that a temperature gradient is more important than an absolute temperature in the electrothermal flow. The first term in Eq. (1) represents the Coulomb force and the second term represents the dielectric force.

When the heat source is generated from a focused light beam as shown in Fig. 5, ET flow will drive the fluid toward the center of the illumination, forming a toroidal flow

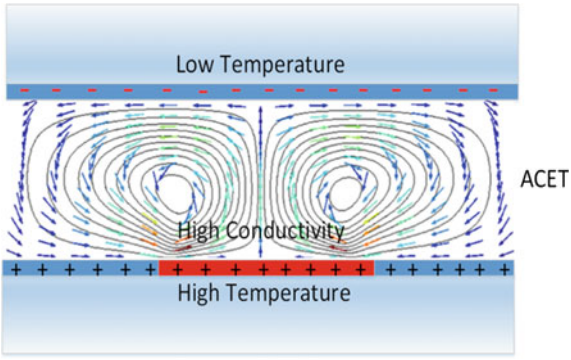

Fig. 5 Optoelectrokinetically induced ACET flow. The *arrows* indicate the flow direction. The *red color* stands for the illuminated region. (Reprinted with permission from [20]. Copyright 2014 Royal Society of Chemistry.)

[17, 31]. Meanwhile, suspended particles will be brought to the center via the fluid drag (F_{drag}). The location of concentrated particles can thus be dynamically altered with the illuminated spot. A high light intensity (i.e., a high temperature gradient) enhances the ET flow, whereas an increased AC frequency diminishes the effect due to the declined Coulomb force in Eq. (1). In practice, ET flow can be considered negligible when the applied frequency exceeds the cut-off threshold ($>f_H$) [17].

3.1.2 Induced Polarization of Colloids

The prior studies have stated that dielectric colloids in an electric field will experience induced polarization. Polarizability is a measure of the charges bound within the dielectric material to respond to an applied field. Among numerous polarization mechanisms, Maxwell–Wagner interfacial polarization and Ionic double layer polarization are considered to be the dominant mechanisms at the current frequency regime (1 Kh–10 MHz). Since the polarization involves the movement of ions, which takes a finite amount of time to migrate from one pole to another, both mechanisms exhibit their own characteristic frequency responses.

Maxwell–Wagner (MW) interfacial polarization refers to the polarization of the surface charge at the interface of dielectric material in the presence of an electric field. The effective polarizability of particles due to the MW polarization can be described by the Clausius–Mossotti (CM) factor, f_{CM}. The phenomenon is well known as dielectrophoresis (DEP), which will attract particles toward the field intensity maxima when $f_{CM} > 0$ (i.e., pDEP) and repel particles away from the maxima when $f_{CM} < 0$ (i.e., nDEP). At $f_{CM} = 0$, particles will lose track of the electric field. The cross-over threshold is hence termed as relaxation frequency.

When a dielectric solid is in contact with a liquid, the surface of the solid will acquire an electric charge due to dissociation of the chemical group or adsorption of molecules from the solution. Accordingly, a very thin layer of opposite ions in the liquid will be attracted by the charge and migrate to the surface of the solid, forming an electric double layer (EDL). When EDL is in an electric field, ionic double layer polarization (*a.k.a.*, EDL polarization) will take shape in order to respond to the field, thus polarizing the solid. Compared with the MW polarization, the migration of the ions due to the EDL polarization is slower and dependent on the size of particle. In other words, the induced ions will need to take longer time to migrate from one pole to another on a large particle rather than a small particle. The relaxation herein is also known as α dispersion, which occurs at lower frequencies than the MW relaxation frequencies.

3.1.3 Combinative Effect of Electrohydrodynamics and Electrokinetics

With a deliberate combination of the electrohydrodynamics and electrokinetics, particles can be aggregated rapidly. The particle aggregation exhibits a dynamic

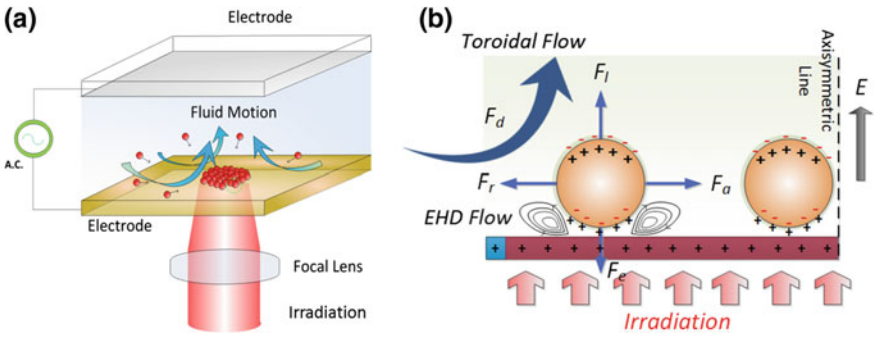

Fig. 6 **a** Illustration of the optoelectrokinetic trapping system. **b** Model illustrating the particle–particle/electrode interactions in a local viewpoint. (Reprinted with permission from [20]. Copyright 2014 Royal Society of Chemistry.)

balance of multiple force interactions. All forces are simplified to four types as illustrated in Fig. 6. F_l denotes a lift force capable of moving particles away from the bottom electrode. The lift force is a comprehensive performance of several complex phenomena: (i) the bulk electrothermal vortex, (ii) hydrodynamic lift when a particle is close to a wall, (iii) the disruption of bulk flow in particle aggregates, and (iv) localized, particle–electrode induced hydrodynamic flow. Particle–particle repulsive electrokinetic interactions (i.e., the dipole–dipole repulsive force) may also lift particles if the particle aggregation becomes more compact, generating instability within the aggregation.

Prior study [17] showed that the bulk electrothermal flow is the major contributor to F_l and declines with frequency, so the force reaches the maximum at low frequencies ($<f_L$) but becomes negligible when exceeding the upper limit frequency ($>f_H$). F_a denotes the particle–particle attraction, which is dominated by the local electrohydrodynamic (EHD) flow at low frequencies ($<f_L$) [32, 33]. Although the electric field seems to be uniform between the two electrodes of the optoelectric device, the local electric fields adjacent to particles are distorted by the particle itself inducing the nonuniform fields for local EHD flow. The tiny vortices bring particles toward each other and levitate them slightly above the surface of electrode [34].

F_r and F_e denote the particle–particle repulsion and the particle–electrode adhesion, respectively. The induced dipoles form repulsion between particles when particles are perpendicular to the electric field, but turn to attraction when particles are aligned in parallel with the electric field regardless of frequency [35]. These phenomena elucidate why particles repel each other but are attracted to the surface of the electrode in the presence of electric fields. Since F_e decays rapidly with distance, trapped particles stay near the bottom surface. Instead of adhesion, particles levitate slightly above the surface due to the local EHD flow.

All the three forces, F_a, F_r, and F_e, at the low frequency domain ($<f_L$), are subjected to the EDL polarization. Similar to the electroosmotic flow, the EDL induced forces peak at low frequencies but diminishes when the frequency is over

f_L. When the EDL polarization exceeds its relaxation frequencies, the MW induced forces will dominate.

In the transitional phase ($f_L \sim f_M$), F_a, F_r, and F_e decline significantly due to the transition from EDL polarization to MW polarization. Since the ET flow induced force (F_l) declines slower than the MW induced particle–electrode adhesion (F_e), particles cannot be trapped firmly on the electrode. The provisional imbalance accounts for the disappearance of particle aggregation during the frequency period.

When the frequency is between f_M and f_H, however, the electrothermal flow is constantly declining, leaving F_r to drop below F_e. The reversal relationship between F_l and F_e hence allows particle to reaggregate. Unlike the trapping at low frequencies, the reaggregation is loose and weak due to lack of the local EHD induced attraction (F_a) and weak ET flow. Notably, the gravity will turn out to be significant as particle size is larger than 10 μm. Eventually, the optoelectrokinetic trapping is terminated due to extinction of ET flow when the frequency is over f_H.

Taking all the electrohydrodynamic and electrokinetic effects into consideration, the possible scenarios of particle behavior and frequency in the REP device are verified in the experiments (Fig. 7). At low frequencies ($< f_L$), particles are brought to the illuminated spot by the toroidal electrothermal flow (Fig. 7a) and then form a compact cluster by the particle–particle attraction resulting from the local EHD flow (Fig. 7d).

At the transitional phase ($f_L \sim f_M$), effective particle trapping temporarily disappears due to the diminishing EDL polarization and the MW relaxation frequency (Fig. 7e) even though the global ET flow remains effective (Fig. 7b).

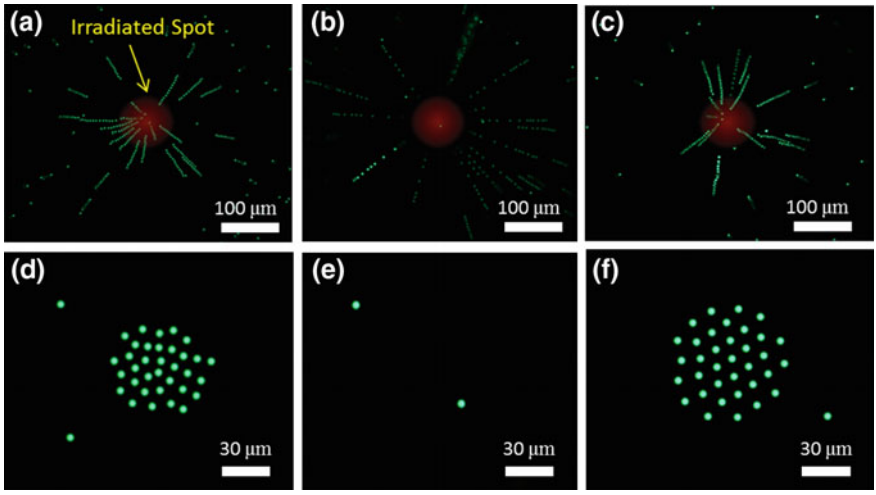

Fig. 7 Multiple exposures of 5-μm particle trajectories at **a** 5 kHz, **b** 100 kHz and **c** 1 MHz, and their close-ups at **d** 5 kHz, **e** 100 kHz and **f** 1 MHz. (Reprinted with permission from [20]. Copyright 2014 Royal Society of Chemistry.)

When the frequency enters the interval $f_M \sim f_H$, particles slowly reaggregate to form a cluster (Fig. 7c). However, the cluster structure in this frequency domain is usually less dense due to lack of the particle–particle attractive force (F_a) to resist the repulsive force (F_r) (Fig. 7f). In addition, the declining electrothermal flow accounts for the slow response.

When the frequency exceeds the upper limit ($>f_H$), toroidal flow becomes negligible, resulting in no optoelectrokinetic trapping. Consequently, the result suggests the optimal range of optoelectrokinetic trapping to be the low frequencies ($<f_L$) rather than the frequency interval between f_M and f_H.

3.2 *Optoelectronic Tweezers (OETs)*

3.2.1 Light-Induced Dielectrophoresis (LDEP)

Distinct from REP, OET is an optoelectrokinetic technique that harnesses particles by converting optical energy into mechanical motion. The solar-cell material, a-Si:H, is considered a photoconductor sensitive to the visible spectrum [36]. The photoconductor is arranged between the insulating and conductive layers serving as a binary gate in the presence of AC electric fields. The use of such a photoconductive layer in the OET microchip enables the creation of "virtual electrodes" with any visible light sources.

To understand the formation of the virtual electrodes, the microchip can be simplified to an equivalent circuit as shown in Fig. 8a. When the device is in a dark environment, the photoconductor has a high impedance to shield most of the electric field, resulting in a very small voltage drop in the medium. When the photoconductor is illuminated by a focused light source, however, the impedance of the photoconductor will drop significantly. This significant change shifts the major

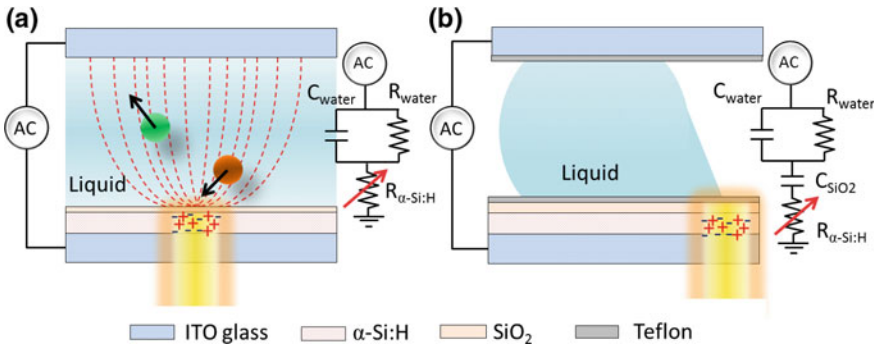

Fig. 8 Equivalent circuits of OETs and OEW. **a** Diagram of the device operating in OET modality (f > 100 kHz). **b** Diagram of the device operating in OEW modality (valid for frequencies, $f < 100$ kHz)

voltage drop from the photoconductor to the medium, thus creating virtual electrodes on the surface of the photoconductive layer. Once the virtual electrodes are formed, DEP will dominate the colloidal behavior.

However, the technique is subjected to some limitations: (1) the requirement of low conductive medium, and (2) an alternating current (AC) power supply. The use of a low conductive medium ensures most of the voltage drop will be across the medium when the photoconductor turns out to be more conductive due to illumination. As a result, OETs are not capable of dealing with biological buffers. Noted that the use of AC power supply is necessary in the RC circuit. Accordingly, direct current (DC) DEP will not work in the device driven by LDEP.

In addition to LDEP, another light-actuated phenomenon, OEW, can also be induced on a similar microchip at a lower frequency regime. Unlike LDEP that is focused on micro-/nano-sized particles, OEW highlights aqueous droplet actuation. As shown in Fig. 8b, the OEW microchip has thicker insulating layer and additional hydrophobic coatings (Teflon) on both substrates as compared with the OET microchip. Therefore, the insulator must be considered in the equivalent circuit.

When OEW is in effect, similar principle can be applied to interpret the formation of "virtual electrodes". Rather than impedance switching between the medium and the photoconductor, however, the impedance is altered between the photoconductor and the insulator. The photoconductor and the insulator must be comparable in order to induce the optical switching effect. Notably, the medium can be a high conductive buffer since it is not involved in the effect.

For the droplet actuation, OEW alters the surface energy of the substrate under an aqueous droplet by modulating an external electric field with a light source. Charges induced by the electric potential are accumulated on both sides of the insulator. The droplet hence changes its geometric profile in response to the new energy state.

Since OETs and OEW are driven by similar principles, a combination of both techniques on the same microchip is likely to benefit cell analysis that requires cross-scale manipulation (submicrons to millimeters). In such an integrated system, a colloidal droplet is sandwiched in an OEW microchip. For the macroscale preparation, the droplet is processed by OEW at low frequencies (100 Hz–1 kHz). For the microscale preparation, the colloids are manipulated with OETs at high frequencies (>10 kHz).

3.2.2 Light-Actuated AC Electroosmosis (LACEO)

Although the major operational principle of OETs is dependent on DEP, there still exist other mechanisms that can be induced by modulating the frequency and light intensity (see Fig. 9). According to Jamshidi et al.'s study [37], LACEO and ET flow may outperform DEP at low frequencies and high light intensity, respectively. However, the induction of strong ET flow requires power of nearly 100 W/cm^2, which is out of the practical ranges used for trapping. Therefore, ET flow is

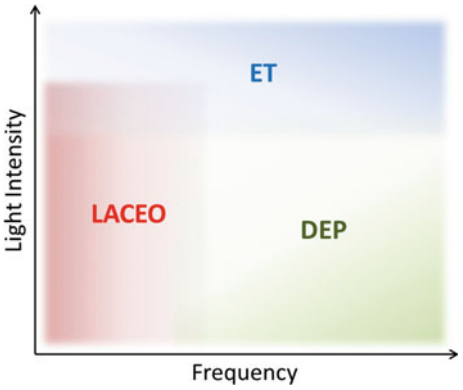

Fig. 9 OET operational regimes as a function of optical power and frequency

typically not a factor that will alter the operations. In contrast, LACEO becomes more significant as the frequency is lower than several tens of kilo-Hertz.

LACEO can induce bulk flow to move toward the center of the virtual electrode (illuminated spot) due to the imbalanced ionic gradients on the photoconductive surface. The vortices then drag colloids into the recirculating flow. For most polystyrene particles, they experience strong LACEO flow at frequencies near 10 kHz [38]. When the frequency is between 10 and 100 kHz, suspended particles will undergo transitional effects mixed with light-induced DEP and LACEO. Since both the mechanisms are also functions of particle size, size-based particle sorting can be achieved by carefully tuning the frequency [39].

4 Assessments of the Optoelectrokinetic Techniques

4.1 Characterizations of REP

4.1.1 System Assessments

Successful particle trapping with REP requires light illumination and an electric field being applied simultaneously. The illuminated spot will form a "virtual electrode" to trap suspended particles. A temperature gradient generated from the focused laser beam will result in an ET flow dragging particles toward the region of illumination. Figures 10a, b show the temperature distributions before and after light illumination measured by a microscopic IR camera. The temperature maintains uniformly at 32 °C with only an electric field applied (16.5 V_{pp} at 5 kHz) when the room temperature is 28 °C. In contrast, a normal distribution peaking at nearly 39 °C emerges after illumination with a laser intensity of 69 W/cm^2.

An investigation of the flow field in the device with a three-dimensional particle tracking velocimetry (3D PTV) is shown in Fig. 10c. For a point heat source, the vortices results in a toroidal flow. The radial velocity shows significant acceleration

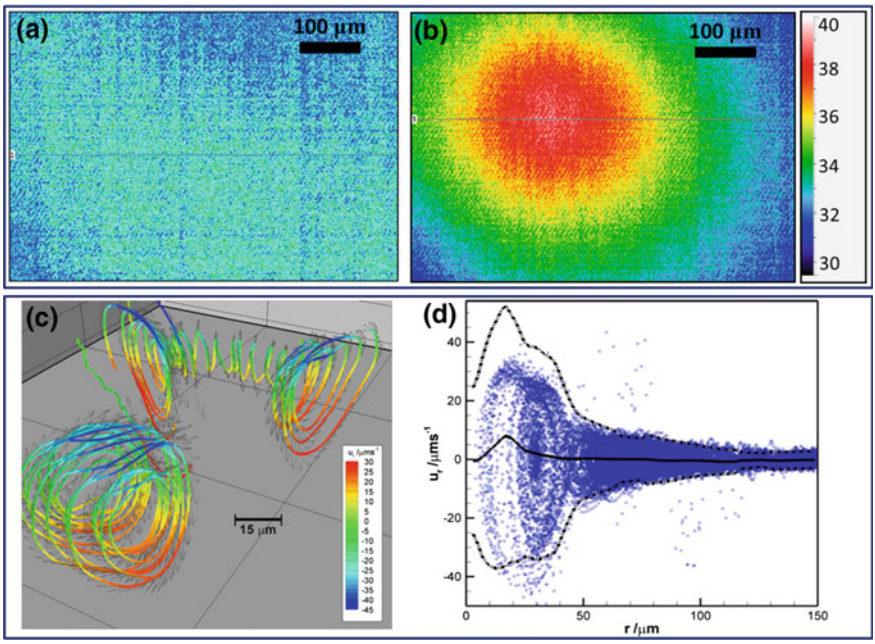

Fig. 10 Temperature distributions **a** with and **b** without laser illumination. The temperature scale is in celsius. (Reprinted with permission from [20]. Copyright 2014 Royal Society of Chemistry.) **c** Three-dimensional particle trajectories and corresponding velocity vectors in the vortex center. Color represents the radial velocity component. The optical axis (not shown) lies centrally. **d** Radial velocity component versus radius. (Reprinted with permission from [31]. Copyright 2009 Springer.)

as approaching the illuminated spot and turns nearly stagnant at the center in response to the drag forces acting on particles at different locations. This velocity profile can therefore be applied to calculate the effect of fluid transport in different microfluidic applications involving with REP.

The prior studies have shown that REP is subjected to laser intensity, voltage, and frequency. Figure 11a shows the optoelectrokinetic behavior of particles is in response to different frequencies. Frequencies ranging from 5 kHz to 5 MHz were investigated. All particles appear to experience distinct responses at different frequency domains as predicted in the previous model. The frequency domains vary with particle size as well. The observed responses are divided into four zones, including strong trapping, no trapping with vortices, weak trapping, and no trapping without vortices.

In general, between 1 kHz and f_L (the green solid line), a dense cluster is achieved. Below 1 kHz, bubbles are formed, signifying electrolysis due to Faradaic reactions. Accordingly, the minimal frequency investigated is chosen to be 5 kHz in the study. Between the green solid line and the red dotted line ($f_L \sim f_M$), no particles are firmly trapped. When the frequency is over the red dotted line ($>f_M$) but

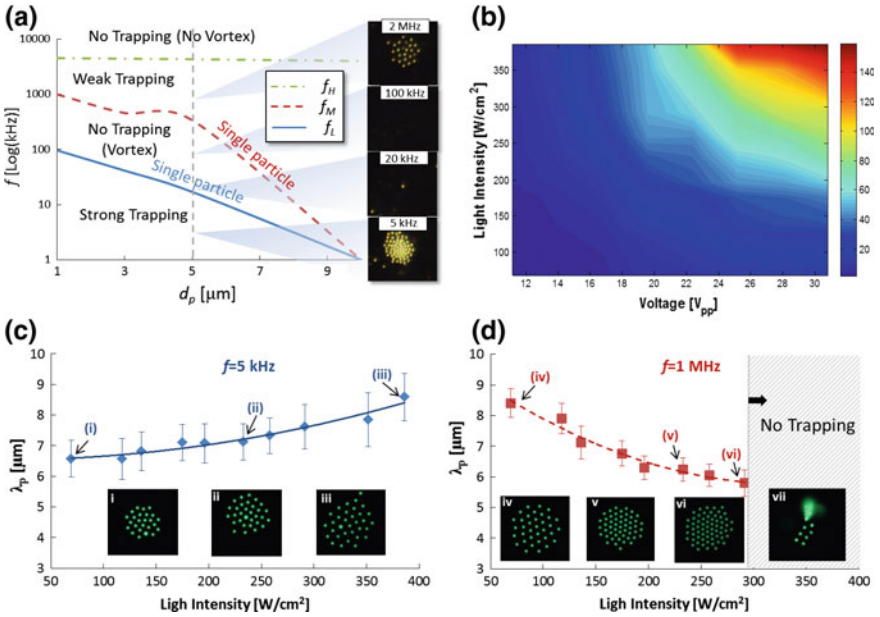

Fig. 11 Characterizations of the optoelectrokinetic trapping. **a** Behavior of particles varies with frequency and particle size. **b** Surface contour of concentration efficiency of 5-μm particles as a function of laser intensity and voltage. The color bar represents the CE index. **c** Mean distance between 5-μm particles with respect to light intensity at 5 kHz (n = 3). The error bars represent standard deviations. **d** Mean distance between 5-μm particles with respect to light intensity at 1 MHz (n = 3). The error bars represent standard deviations. The aggregation collapses when the light intensity exceeds 291 W/cm^2. (Reprinted with permission from [20]. Copyright 2014 Royal Society of Chemistry.)

remains below the upper limit ($<f_H$), a loose cluster reappears. ET flow disappears when the frequency exceeds the upper limit ($>f_H$). No effective aggregation was ever observed beyond the upper limit. As mentioned previously, gravity contributes additional effect to F_e in larger particles, resulting in 10 μm particles to be trapped at all frequencies. The right insets of Fig. 11a show the actual particle images of 5 μm particles captured at 5, 20, 100 kHz, and 2 MHz. A good agreement with the prediction validates the hypothetical model.

Wang et al. [20] made additional novel observations regarding REP: (1) single particle trapping, (2) smallest nanoparticle trapped by REP, and (3) reaggregation at high frequencies. The single particle trapping occurs near the two transitional boundaries (i.e., f_L and f_M). Notably, particles tend to detach from a cluster when approaching f_L but reaggregates when approaching f_M. Therefore, the single particle trapping can be achieved by carefully tuning the frequency near the two critical values. REP has been proven not only powerful in microparticle trapping but also in nanoparticle trapping. A clump of 22 nm polystyrene particles was reported to be successfully aggregated in this study [21]. This size is the smallest reported particle size on which REP has been demonstrated to date.

Additionally, in an early attempt to trap other nano-sized materials, such as gold nanoparticles and quantum dots (CdSe), excellent aggregation is observed as well, showing the potential applications at the nanoscale. The reaggregation behavior at high frequencies is also observed (Fig. 11a). In our model this behavior is likely a result of reduced hydrodynamic lift (F_l) due to the declining ET flow. A simple test by switching off either electric fields or laser resulted in dispersion of particles, confirming the necessity of applying laser and electric fields simultaneously. The test implies that the optoelectrokinetic trapping remains effective in the high frequency domain. However, the trapping progressively weakens as the frequency approaches the upper limit (f_H).

In addition to the frequency, the particle trapping is also a function of voltage and laser intensity (Fig. 11b). An evaluation was implemented with 5 μm polystyrene particles prepared in a concentration of 3.7×10^8 count/mL, 1064 nm IR laser, 5 kHz and 0.3 mS/m medium. To facilitate the assessment of particle trapping, concentration efficiency (CE) is introduced. The CE index is defined as the number of particles aggregated within the illuminated spot in a second. A high CE value means a large aggregate in a short period of time and vice versa. When the laser intensity is elevated, the CE index increases accordingly. The increase usually comes along with strong toroidal flow. Similarly, the CE index increases as the voltage is elevated as well. The toroidal flow is subjected to the modulated electric field. The strong vortices promote the particle aggregation by bringing more particles to the center of illumination rapidly. However, high voltages may cause electrolysis and electric breakdown while high laser intensity usually causes overheat.

Light intensity affects not only the CE index but also the mean distance (λ_p) between particles. In the trapping zone at low frequencies ($< f_L$), λ_p increases with the light intensity (Fig. 11c). Since conductivity is proportional to temperature, high light intensity suppresses the particle–particle attraction due to dwindling local EHD flow, repelling particles from each other. Compared with the EDL induced repulsive force, the electrothermal flow is insignificant.

Whereas, λ_p decreases with the light intensity in the trapping zone between f_M and f_H (Fig. 11d). When the light intensity is over 291 W/cm^2, however, all particles collapse to the center as shown in the inset (vii) of Fig. 11d. Unlike the dominant attraction at low frequencies, no significant particle–particle attraction appears in this frequency regime.

Nevertheless, the electrothermal flow is comparable with the MW induced repulsive force and turns more influential as the light intensity is elevated. The enhanced drag then contributes to the compact particle aggregation. Although the laser intensity induces toroidal flow—greater hydrodynamic drag to compact and lift particles, the hydrodynamic lift (F_l) may surpass the adhesive force (F_e) and remove particles from the surface at higher laser power.

4.1.2 Repertoire of Particle Manipulation

The REP microchip has demonstrated versatile particle manipulation with an addressable illumination device. Several manipulation capabilities, including micro/nanoparticle concentration, translation, single particle capturing, sorting, and patterning, have been achieved by modulating frequency, path of illumination, and voltage [18, 19, 21–23]. The demonstrations show that the technique is not only excellent in dynamic concentration but also useful in other applications such as single-cell manipulation and self-assembly.

Several representative manipulation capabilities are depicted in Fig. 12. Figure 12a shows no trapping when the laser illumination and electric fields are not simultaneously applied. In other words, only an electric field or a laser beam acting on the microchip is incapable of producing successful trapping. However, when both laser illumination and electric fields are applied simultaneously, particles can be rapidly concentrated within the illuminated spot as shown in Fig. 12b. The comparison proves that REP is a result of synergistic action of light and electric fields [19, 22].

The extent of cluster can be altered by either increasing the laser intensity or the size of the illuminated spot. For translation, the trapped site is changed by simply moving the illuminated spot. Figure 12c shows a transient status of a cluster translating from an old spot to a new one. Figure 12d shows the successful trapping of 5-μm single particle at 17 kHz. As demonstrated previously, single particle trapping can be realized at transitional frequencies (f_L and f_M). Despite disturbance from the vortex, most single particles remain trapped stably.

Figure 12e, f show a realization of size-dependent sorting based on the frequency modulation. A mixture of 1 and 5 μm particle suspension was initially concentrated at a low frequency of 5 kHz. When the frequency was gradually elevated to 36 kHz, 5 μm particles first reached their relaxation threshold. Subsequently, 5 μm particles were released from the cluster while 1 μm particles remained trapped. The simple demonstration reveals insight to sort particles by size. Nevertheless, frequency modulation can be used to sort particle by type as well [23].

When intentionally a short duration of a voltage rise or drop, such as on-off the power or coupling the input signal with a DC shift, the trapped particles will be irreversibly stuck to the surface of electrode. By performing this operation with a careful arrangement, special patterns can be achieved. Two types of operation are implemented in Fig. 12g. Clusters of 5-μm particles are assembled step by step to form a letter “L” at 5 kHz. Similarly, single 5-μm particles are assembled step by step to form the same letter “L” at 17 kHz. The ability to pattern single particles shows the potential of the technique for bottom-up manufacturing.

An attempt to aggregate nanoparticles is also achieved successfully with the optoelectrokinetic technique as shown in Fig. 12i. 22-nm fluorescent polystyrene particles are suspended in DI water, making a conductivity of 0.3 mS/m. A cluster rapidly takes shape after a laser beam and an electric field of 16.5 V_{pp} at 5 kHz are applied on the microchip simultaneously. Switching off either the electric field or the laser removed the cluster, implying a typical response of REP. The above

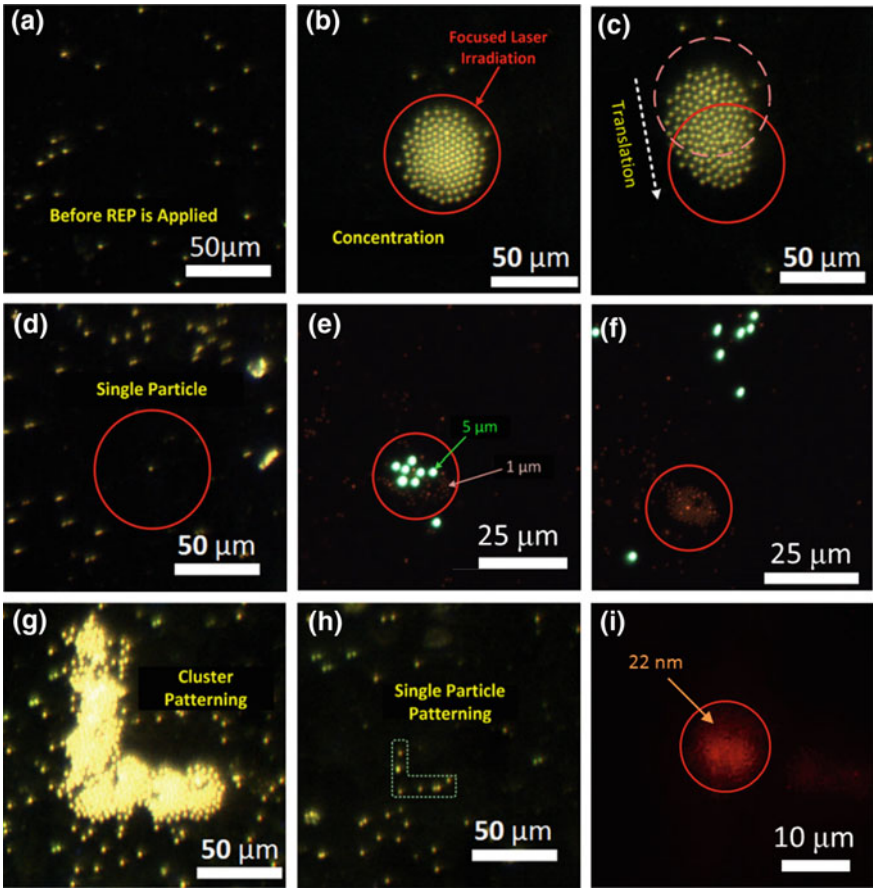

Fig. 12 Repertoire of particle manipulation with the optoelectrokinetic technique: **a** no trapping in the initial state, **b** microparticle aggregation at 5 kHz, **c** translation at 5 kHz, **d** single particle manipulation (d_p = 5 μm) at 17 kHz, **e** 1 and 5-μm particles trapped simultaneously at 5 kHz, **f** sorting by size at 36 kHz, **g** patterning with clusters, **h** patterning with single particles, and **i** nanoparticle aggregation at 5 kHz and 16.5 V_{pp}. (Reprinted with permission from [20]. Copyright 2014 Royal Society of Chemistry.)

manipulation capabilities therefore lead to the realization of all-in-one bead-based bioassays. More detailed information regarding the sorting, patterning, and nanoparticle concentration can also be referred to the prior literature [19, 22, 23, 40].

4.2 Characterizations of OETs

4.2.1 System Assessments

The photoconductive layer, a-Si:H, is the cornerstone of the OET microchip. Assessments of the photoconductor in response to light illumination aid the understanding of the device. The photovoltaic effect allows a semiconductor to absorb the incident light energy and excite free electrons to form electron-hole pairs. The movement of electrons therefore creates current and decreases impedance. In principle, higher light intensity, especially at a wavelength that matches the energy gap, promotes the conductivity.

Figure 13a exhibits the relationship between the photoconductivity and the incident light intensity. The result shows that the photoconductivity proportionally increases with the light intensity. Under the ambient lighting conditions and a 100-V_{rms} voltage, the photoconductivity of a-Si:H is measured to be on the order of 10^{-8} S/cm. However, the photoconductivity will elevate by 80 times under illumination intensity of 65 mW/cm^2 [41]. In addition, the OET force decreases as the spacer gets thicker due to the dwindling field intensity gradient [42]. In practice, the thickness is usually chosen to be less than 100 μm to achieve better operations. This trend is the same as REP because both techniques require the application of electric fields.

As mentioned previously, the OET and OEW microchips have very similar configurations, yet different driving mechanisms. As a result, cross-scale manipulation of aqueous droplets and micro/nano-sized particles can be achieved by simply modulating the electrical frequency on the same platform. To this end, an OEW microchip is usually used for this purpose [25]. Figure 13b is an illustration elucidating the operational regimes between OEW and OETs, where Z_l, Z_d, Z_{di}, and

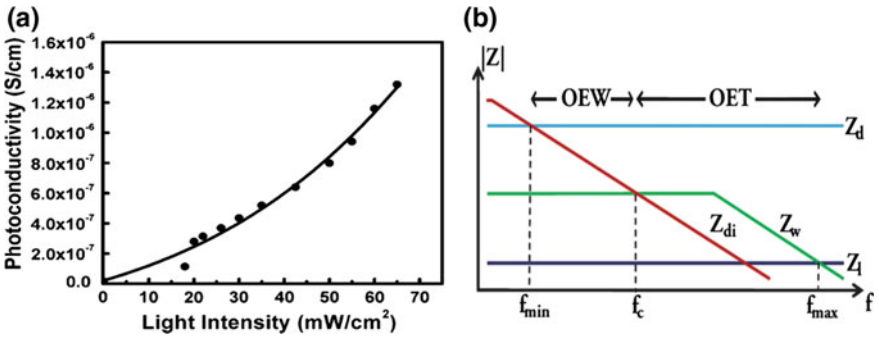

Fig. 13 **a** Photoconductivity of undoped a-Si:H as a function of light intensity. Reprinted with permission from [41]. Copyright 2003 Elsevier.) **b** Graphical depiction (not to scale) of the frequency response of device showing impedance of a-Si:H in the light and dark states. OEW occurs between f_{min} and f_c, while OET occurs between f_c and f_{max}. (Reprinted with permission from [25]. Copyright 2011 Royal Society of Chemistry.)

Z_w represent the impedance of a-Si:H in the light and dark states, the impedance of the liquid and dielectric layers, respectively. For the OEW-dominant regime, Z_d is comparable with Z_{di} in the dark, but turns to be relatively low under illumination. When the major voltage drop is within the insulator, the electrowetting on dielectric (EWOD) effect will take place, resulting in bulk droplet actuation.

Below f_{min}, however, Z_{di} is much higher than Z_l and consumes the entire voltage drop. Accordingly, the impedance change of the photoconductor between the bright and the dark has no effect on the droplet. In addition, when the frequency exceeds a critical threshold at f_c, the impedance of water surpasses that of the insulator and enters the OET-dominant regime. Subsequently, the switching effect falls between the photoconductor and the droplet. When the major voltage drop is within the water, DEP will take place. As the frequency keeps running higher than another critical threshold at f_{max}, Z_w will be much lower than Z_d, eliminating the optical switching effect.

An experimental measurement identifying the force variations between EW and DEP shows that the empirically optimal frequency peaks at 10–20 kHz for electrowetting and at 100–200 kHz for DEP. The cross-talking region (20–100 kHz) which mixes with OEW and OET effects should be therefore avoided.

4.2.2 Repertoire of Particle Manipulation

With an addressable illumination device, such as a DMD or a SLM panel, OETs can achieve a variety of manipulation capabilities. Particularly, OETs require only 100,000 times lesser optical intensity than conventional optical tweezers [24], such that makes this technique an ideal candidate for biological applications.

A demonstration of massively parallel manipulation with 15,000 virtual electrodes over 1.3×1.0 mm^2 area is shown in Fig. 14a. A red-emitting diode (625 nm) of 1-mW output power coupled with a 10x objective and a 1,024 × 768 pixels digital micromirror modulator are used. 4.5 μm polystyrene particles experiencing nDEP are trapped in the dark holes and translated with the pattern. Similar to DEP, the forces are subjected to the particle size. In other words, the trapping forces will drop significantly as the particle size shrinks from microscale to nanoscale. Considering the Brownian motion turns to be serious for nano-sized particles, the pure OET forces will not be feasible for trapping particles with size less than 1 μm. However, by carefully harnessing other electrohydrodynamic mechanisms (LACEO or ACET) with different frequencies, it is still likely to manipulate nano-sized particles [43].

Since DEP is subjected to particle sizes, dielectric properties, and electric field gradients, DEP is usually considered a very powerful tool for particle sorting to date. Moreover, OETs accompanying with virtual electrodes can be used for particle sorting with self-actuating sources. This self-actuation allows OETs to process a small amount of samples. Because of the unique characteristic, OETs can deal with complicated situations that require multitude capabilities.

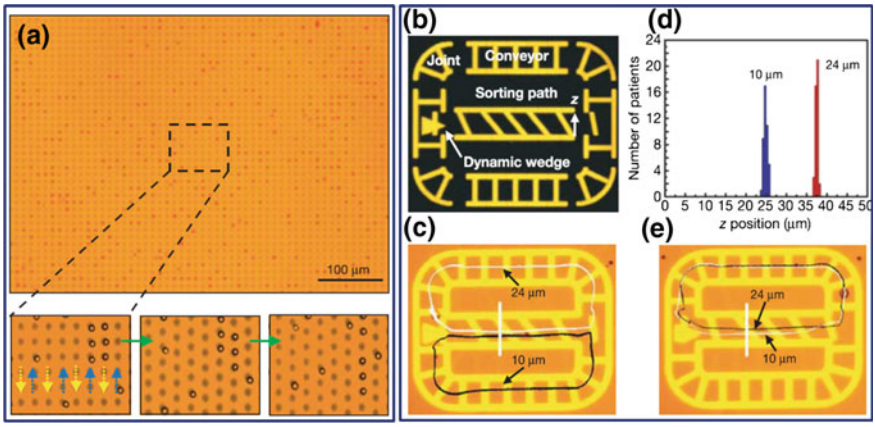

Fig. 14 **a** Massively parallel manipulation of single particles. 15,000 particle traps are created across a 1.3 mm × 1.0 mm area. **b** Integration of virtual components, including an optical sorter path, conveyors, joints and a wedge. The motion of different components is synchronized. **c**, **e** Two polystyrene particles with sizes of 10 and 24 mm pass through the sorter path and are fractionated in the z direction owing to the asymmetrical optical patterns. The particle trajectories can be switched at the end of the sorter path by the optical wedge. **d** Optical sorting repeatability test. (Reprinted with permission from [24]. Copyright 2005 Nature.)

Figure 15 is an example showing how live and dead cells can be separated by their dielectric properties other than their sizes. In principle, dead cells show no response to the OET stimulation due to porous membranes while live cells show nDEP. By dynamically generating concentric light patterns to confine live cells to the center part of the patterns, live and dead cells are separated. Sorting with other materials can be achieved in the same fashion as well.

Although the nature of DEP restricts the performance of OETs on nano-sized targets, Jamshidi et al. proved that OETs still have limited controls of some long semiconducting and metallic nanowires [44]. In their study, several tens of nanometers wide and 5-μm long nanowires were trapped and translated under 100 W/cm^2 HeNe laser with a voltage of 20 V (Fig. 16a), reaching a maximum speed of about 135 μm/s. Large-scale assembly of nanowires was also achieved by using a digital micromirror device. Figure 16b shows the formation of a 5 × 5 array of single silver nanowires that are individually addressed in real time. The vertically aligned nanowire array has rising applications for solar energy conversion, thermoelectric cooling and vertical field-effect transistor.

In addition, a new effort [45] attempting to trap gold nanoparticles seems to show a breakthrough to the size limitation. With a small temperature increase (<0.1 °C) and a strong electric field gradient (∇E^2) up to 10^{16}–10^{17} V^2/m^3, they stated to trap gold nanoparticles with sizes ranging from 60 to 250 nm. Trapping, translation and patterning were demonstrated. Meanwhile, it was also found that the gold nanoparticles tend to keep a certain distance between each other when there is only the electric field applied. The repulsive forces are considered originated from

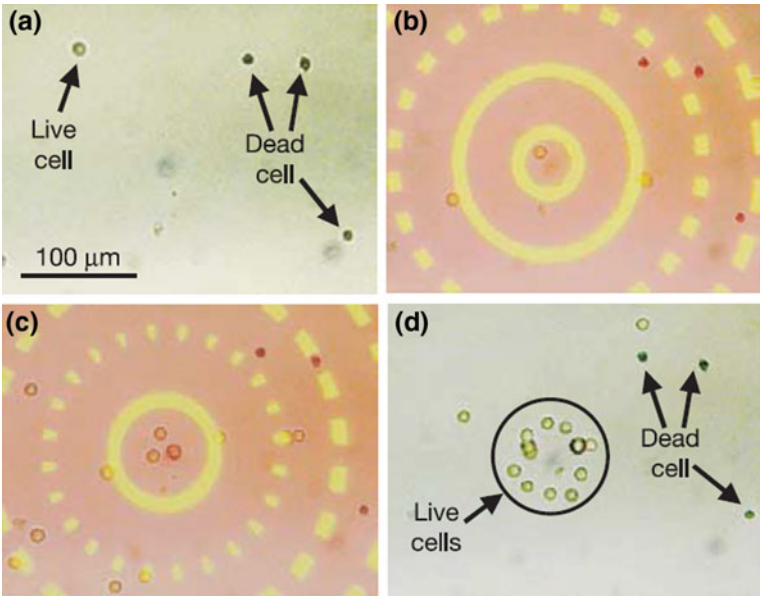

Fig. 15 Selective collection of live cells from a mixture of live and dead cells. **a** Randomly positioned cells before OET. **b–c** Cell sorting. The live cells experience positive OET, trapping them in the bright areas, and pulling the live cells into the pattern's center. The dead cells (stained with Trypan *blue dye*) leak out through the *dark gaps* and are not collected. The optical pattern has a *yellowish color*, while weak background scattered light results in a *pinkish hue* in the non-patterned areas. **d** Sorted cells. (Reprinted with permission from [24]. Copyright 2005 Nature.)

the Columbic force due to negative zeta potential (−70 mV) and induced dipole–dipole interactions. A higher voltage will increase the distance between particles. As a result, both the electric field and illumination are necessary for the successful particle trapping.

In contrast to trapping nanoparticles with a raw OET microchip, Ota et al. [46] attempted coating a very thin layer of supported lipid bilayer (SLB) on the photoconductor to tether gold nanoparticles to the surface of the substrate. The tethered nanoparticles are therefore able to resist the interferences from the Brownian motion. This surface treatment allows OETs to manipulate more nanoparticles in a stable way. Figure 16c shows the schematic of the configuration and a pattern formed by hundreds of 60-nm gold nanoparticles.

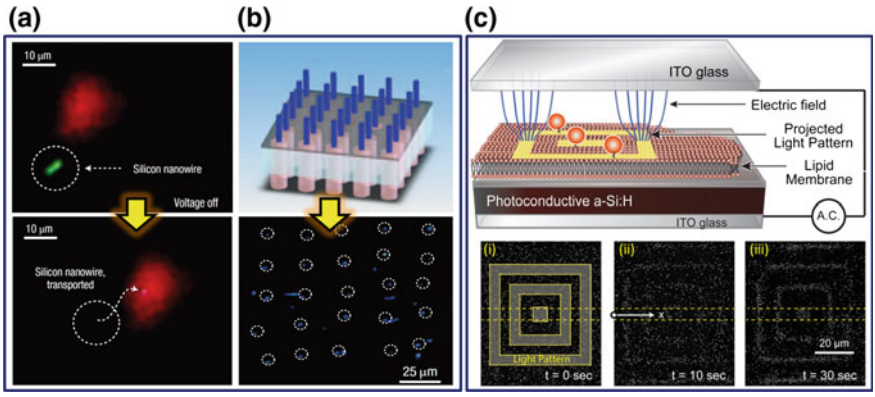

Fig. 16 **a** OET trapping and translation of a single 100-nm diameter and 5 μm long nanowire. (Reproduced from [44]) **b** Trapping and transport of a 5 × 5 *silver* nanowire array. The nanowires are vertically aligned in the laser trap. (Reprinted with permission from [44]. Copyright 2008 Nature.) **c** Optoelectronic tweezers integrated with a supported lipid bilayer (SLB). Insets (i)–(iii) are the time-sequence images (B/W inverted for visualization) of the gold nanoparticles, showing that they were successfully trapped into the projected light patterns. (Reprinted with permission from [46]. Copyright 2013 American Chemical Society.)

5 Applications of Cell Analysis

5.1 Cell Preparations and Analysis

In addition to the well-defined polystyrene particles, gold nanoparticles/carbon nanotubes used in the preliminary studies and cells feature more morphological variety, biophysical uncertainty and biomechanical complexity. However, it is also the cellular multitude that allows a variety of manipulation and analysis to be realized. In the OET microchip, cells can perform a multitude of parameters, including electrorotation, rotation of cell wheel, collisions of cells and the 3D pearl chain effect [47]. The behavior is typically indicative of the physiological states of single cells. A careful analysis of these parameters may lead to useful information used for cell preparations or cell morbidity analysis. In addition to the fundamental capabilities of translating single and multiple cells [24, 42] or sorting live and dead cells [24, 42], advanced functions contributing to more cell preparations and cell analyses have been constantly developed in the recent years [25, 48].

Cellular membrane allows cells to selectively take up signaling ions, proteins or genetic transfection from the extracellular fluid. Electroporation is a common technique used for introduction of such exogenous molecules across the membrane into cells [49]. The temporary permeation of the cellular membrane requires a "proper electric field" to depolarize the bi-lipid layer. As a result, the temporary formation of pores on the membrane will reseal after the electric field is removed. In contrast, a much higher electric field will irreversibly damage the cellular membrane to result in cell lysis.

Contrary to the electroporation, cell lysis is an essential way to extract the intracellular contents, such as DNA and proteins, into the extracellular medium. Taking advantage of OETs, selective electroporation and cell lysis can be realized. As shown in Fig. 17a, an OET-based device was proposed [27, 50, 51] to selectively lyse or electroporate cells. In the conventional OET mode, a living fibroblast cell stained with a green dye is positioned before illumination (Fig. 17b). When a light-induced high electric field (>2.2 kV/cm) is imposed on the cell, the cell membrane and nucleus are ruptured (Fig. 17c, d). A red dye penetrating into the cell nucleus proves the irreversible damage of the cell membrane due to the operation (Fig. 17e).

Similarly, when a lower electric field of 1.5 kV/cm is applied to selected HeLa cells (Fig. 17f, g), the cells remain intact in shape in the bright light mode (Fig. 17h). In the fluorescent mode, however, the electroporated cells express red fluorescence, implying a change of the membrane porosity. Through the maneuver, the OET technique can aid the study of the cell–cell signaling and interactions.

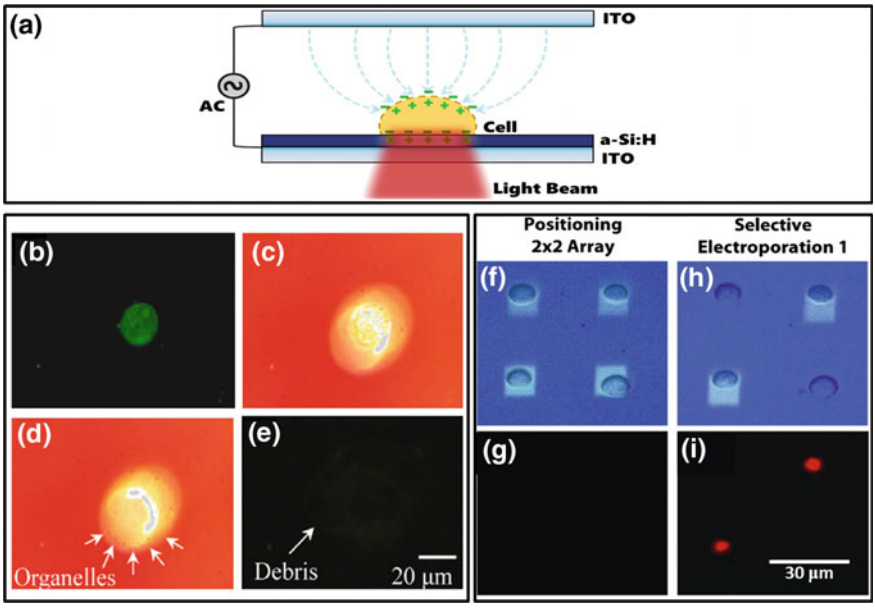

Fig. 17 *Top block*: **a** Configuration of the light-induced cell electroporation/lysis with OETs. *Lower left block*: **b** Fluorescent image of a fibroblast cell in the OET device before illumination. **c**–**d** The cell is illuminated by light and then organelles are spread out due to the rupture of the membrane. **e** The extracellular dye penetrates into the cell nucleus to cause *red fluorescence* after the disruption. (Reprinted with permission from [50]. Copyright 2009 American Institute of Physics.) *Lower right block*: **f** and **h** shows bright field image of cells and optical pattern. *Bottom row* **g** and **i** shows the corresponding PI dye fluorescence. (Reprinted with permission from [51]. Copyright 2009 Royal Society of Chemistry.)

More recently, Huang et al. [48] presented a total solution using an OET integrated microfluidic platform for multistep single-cell sample preparation and extraction (Fig. 18a, e). On this platform, a mixture of cells is introduced into an active OET manipulation chamber. Cells with desired optical signatures such as sizes, shapes, and fluorescent colors detected under a microscope can be selectively trapped and transported by light beams into small chambers for isolation. Cells and fluid in these chambers can be cut by airflows to form droplets that can be transported and extracted out of the chip for downstream single-cell analysis using commercial instruments.

A small fraction of HeLa cells stained with Calcein AM were experimentally extracted from unstained HeLa cells on the proposed platform and analyzed with a RT-qPCR for beta-actin mRNA. The result showed that a single-cell sample eventually required at least 31 thermal cycles to be detected.

5.2 Cell Patterning

The ability to arrange cells into desired patterns has potential benefits for biological investigations and applications, such as microarrays [3–5], tissue engineering [1, 52, 53], and regenerative medicine [1, 2]. By patterning hexagonal electrodes on a substrate, some researchers [52] have successfully assembled hepatocytes (HepG2) and human umbilical vein endothelial cells (HUVECs) to mimic the lobular morphology of real liver tissue using DEP.

Similarly, the same group later achieved dynamic cell patterning with an OET device [26]. In their device an organic photoconductive material (TiOPc) rather than a-Si:H was used, such that the complicated microfabrication was simplified. Since the hepatocyte HepG2 shows nDEP on the organic OET microchip, a dark pattern is generated to position the cells. In Fig. 19a, b, a planar liver structure is projected on the photoconductor and then a branch-like pattern composed of the liver cells takes shape in 10s. The preliminary work reveals a possibility to grow functional cells in a more efficient way.

Later, Yang et al. [54] demonstrated trapping single hepatocytes in a 3 × 3 light array generated from a laser diffracted pattern (Figs. 19c, e). To investigate the biocompatibility of the TiOPc surface, HepG2 cells were cultured on the microchip for up to 72 h. The result showed no significant differences between the TiOPc and glass surfaces in cell morphology and growth. In addition, the HepG2 cells remained alive and covered more than 80 % of the observed TiOPc surface after 72 h (Fig. 19).

Lately, REP also shows some promising capabilities in cell manipulation based on a different optoelectrokinetic mechanism. In Li et al.'s study [55], the intestinal endothelial cells of rat (IEC-18) were initially harvested from a culture disk and then resuspended in an isotonic medium adjusted by D-Mannitol and phosphate buffered saline (PBS). The resuspended cells were used for manipulation in the REP microchip. To facilitate cell adhesion and growth, the gold surface of the microchip

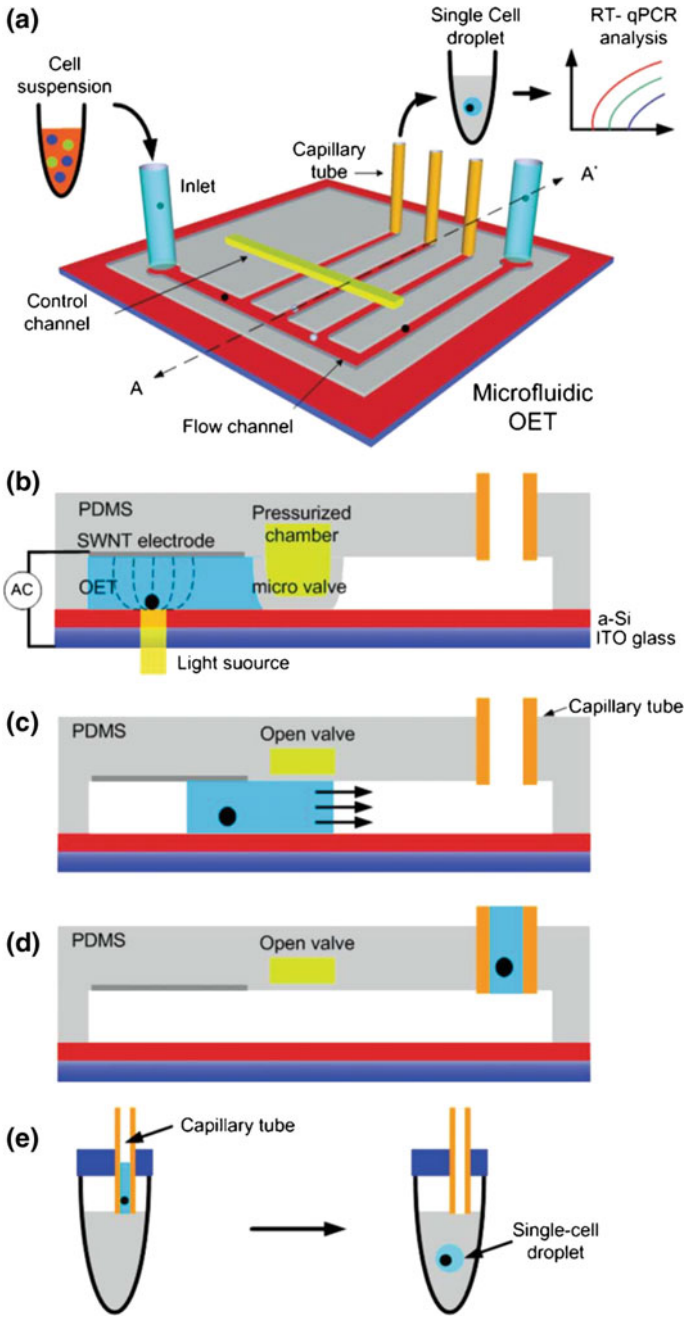
(a)
Cell suspension
Inlet
Capillary tube
Single Cell droplet
RT- qPCR analysis
A`
Control channel
A
Flow channel
Microfluidic OET
(b)
PDMS
SWNT electrode
Pressurized chamber
AC
OET
micro valve
a-Si
ITO glass
Light suource
(c)
PDMS
Open valve
Capillary tube
(d)
PDMS
Open valve
(e)
Capillary tube
Single-cell droplet

◀ **Fig. 18** **a** Schematic of the OET integrated microfluidic platform and the procedure of preparing single-cell samples for analysis. **b–d** The side view of the A–A' cross section. **b** The SWNT electrode enables OET integration with multilayer PDMS microfluidics. Cell manipulation in OET is achieved by light-induced DEP forces on a photoconductive surface. Droplet generation is achieved by flowing air into the main channel after target cells are moved into the isolation chambers. **c** The elastomeric PDMS membrane valve controls fluid flows on the chip. When the valve opens, droplets with cells are pushed by airflows to pass the valve. **d** A nano-liter droplet can be stored in a capillary tube. **e** The cell in the droplet can be transferred to a PCR tube by the capillary tube. (Reprinted with permission from [48]. Copyright 2013 Royal Society of Chemistry.)

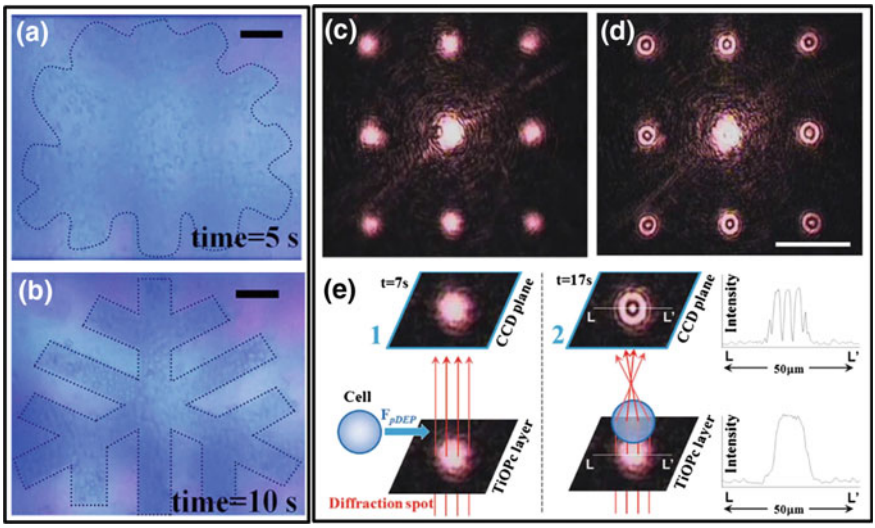

Fig. 19 **a**, **b** Real-time image recording for our liver-cell patterning demonstration by using light-driven optoelectronic manipulation. The scale bar is 100 μm [26]. **c**, **d** The laser diffraction pattern generates virtual electrode spots on the TiOPc substrate. Nine HepG2 cells are attracted toward each spot center due to the pDEP force (**c** and **d**) are recorded at 0 and 26s, respectively. **e** The images on the TiOPc layer surface and the CCD plane and the related light intensity analyses for square 1 and square 2. (Reprinted with permission from [54]. Copyright 2013 Royal Society of Chemistry.)

was coated with a thin layer of poly-L-lysine as shown in Fig. 20a. An AC voltage as low as 3 V_{pp} at 5 kHz was applied to migrate the cells. Evidence suggests that cells tend to reaggregate to simulate their original biological environment after seeding on a culture disk [56]. By activating a short duration of negative DC bias ($\sim$0.5 V), the aggregated cells would adhere to the surface (Fig. 20b->Fig. 20c). Cell viability tests showed that the cell growth and survivorship after REP operations were nearly identical to the control group. The patterned cells were later grown in a culture medium separately. The aggregated endothelial cells indeed showed a better growth state than individual cells because the clustering morphology mimics the real biological environment. Other studies involving shear

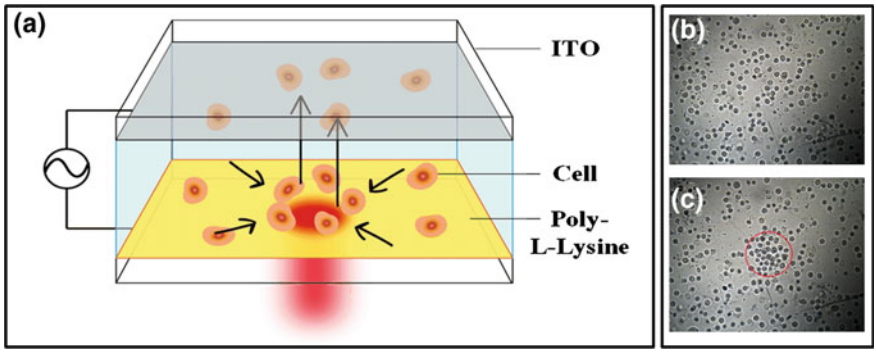

Fig. 20 **a** Configuration of a modified REP microchip used to migrate and aggregate cells. **b**, **c** By simultaneously activating the microchip with light and an electric field, formation of cell cluster is progressively observed in the region of illumination

stress induced from the electrohydrodynamic flow can be investigated by REP as well.

5.3 Bacterial Manipulation

A cell-based bioassay is an analytical method that assesses concentration and biological activity of chemicals/bio-molecules in a sample using microorganisms such as viruses, bacteria and fungi. Fast and precise on-chip manipulation of microorganisms aids in the development of high-performance bioassay systems. By employing the optoelectrokinetic tool, REP, Kwon et al. [57] demonstrated aggregation, patterning, translation, trapping and size-based separation of microorganisms. Three types of bacterium were investigated, including *Shewanella oneidensis* (*S. oneidensis*) MR-1, *Saccharomyces cerevisiae* (*S. cerevisiae*) and *Staphylococcus aureus* (*S. aureus*). In Fig. 21, aggregation, patterning and translation of the assembly is implemented with *S. oneidensis* MR-1. The experimental conditions are 16.9 V_{pp} at 17.3 kHz and 30 mW in the laser intensity.

In addition, REP was also used to achieve size-based separation of *S. cerevisiae* ($\sim$5 μm) and *S. aureus* ($\sim$1 μm). The principle for the cell separation lies in the relaxation frequency of particles which is associated with their size. At a low frequency of 17.5 kHz and 10 V_{pp}, both *S. cerevisiae* and *S. aureus* are trapped simultaneously (Fig. 22a). When the frequency is elevated to 38.9 kHz, *S. cerevisiae* is swept away by the vortex due to its larger size. Most of the bacteria showed viable under the experimental conditions during the entire operations. The demonstration with the microorganisms strengthens the essential role of REP in the biotechnology and provides an insight to more future REP-enabled on-chip bioassays.

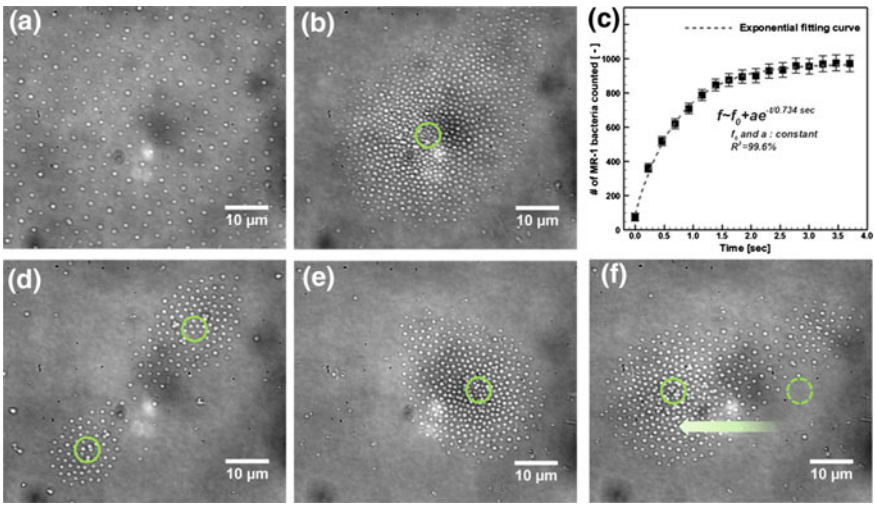

Fig. 21 Manipulation of *S. Oneidensis* MR-1 by REP technique. *Red-dots* in the figure represent the locations of a focused laser beam on the bottom ITO electrode surface, and their size corresponds to the actual diameter of the laser beam (1.3–1.5 mm in diameter). **a** A random distribution of MR-1 bacteria on the electrode when only a uniform AC electric field is applied to the chip. **b** Aggregation of *S. Oneidensis* MR-1 by REP technique. The applied electrical signal is 17.8 V_{pp} at 18.69 kHz and the laser power is 20 mW. **c** The change of the number of MR-1 bacteria in the assembly along with a time after optoelectrokinetic technique is applied to the chip. **d** Patterning of the *S. Oneidensis* MR-1 using two laser illuminations under an electric field. The applied electrical frequency and voltage is 17.32 kHz and 16.9 V_{pp}, and the laser power is 30 mW. **e–f** Translation of the *S. Oneidensis* MR-1 assembly by the movement of a laser beam. The provided frequency, voltage and laser power is 18.69 kHz, 13.8 V_{pp} and 20 mW, respectively. The *blue-dot* reflects the location and actual size of the beam before the movement and the *arrow* represents the direction of the laser movement. All of above images were taken from the *bottom view*. (Reprinted with permission from [57]. Copyright 2012 Royal Society of Chemistry.)

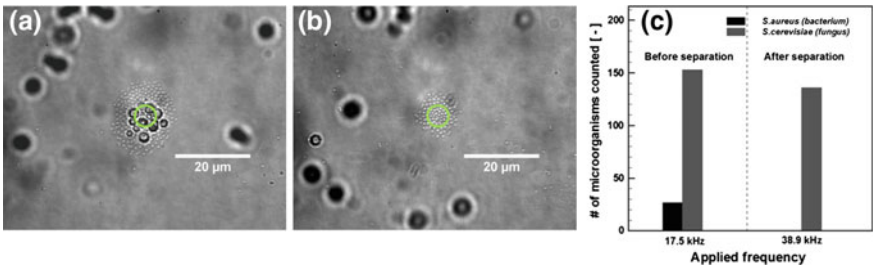

Fig. 22 Size-based separation of *S. aureus* and *S. cerevisiae* (larger cells) by REP technique. **a** Initialization of the aggregation consisting of *S. aureus* and *S. cerevisiae* before the separation. The applied frequency and voltage is 17.5 kHz and 10.07 V_{pp}, respectively and the laser power is 20 mW. **b** Separation of *S. aureus* from the aggregation. As the frequency is increased from 17.5 to 38.9 kHz, only the *S. aureus* cells remain in the aggregation. **c** Size-based separation efficiency. Cell counts were calculated from **a** and **b**. (Reprinted with permission from [57]. Copyright 2012 Royal Society of Chemistry.)

5.4 Bead-Based Immunoassays

Highly sensitive diagnostics are critical to early detection of diseases and play a pivotal role in today's health care. However, poor signal due to low-abundance of pathogens in clinical samples poses a major barrier in the detections. Concentration of target molecules or cells is a widely used measure to tackle the difficulty. Using bead-based immunoassays, specific targets of interest can be detected [58, 59]. Bead-based immunoassays, as opposed to conventional bioassays, feature not only simplicity but also flexibility and high efficiency [58, 60–63].

An in situ biosignal enhancement system was realized by the integrated use of REP and a bead-based FRET fluorescence immunoassay (Fig. 23). A proof-of-concept [20] demonstration utilizing biotin-streptavidin binding reaction was implemented to assess the optoelectrokinetically enabled bead-based signal enhancement. The result proved that the fluorescent signal was effectively improved by at least two orders of magnitude down to 3.87 nM as compared to an ELISA reader. Before the signal saturated, the fluorescent intensity constantly elevated when the functionalized particles were concentrated over time.

A practical immunoassay was conducted with lipocalin 1 (LCN1). LCN1 is one of the biomarkers in tear drops of patients with diabetic retinopathy. To achieve an in situ diagnosis, FRET was used to prevent the conventional wash procedure. In the design, FRET signal was obtained by evoking the immune effect to form a sandwich-structured immunocomplex including a dye-labeled antibody, the QD-conjugated antibody. Although nonspecific binding due to QD adsorption on

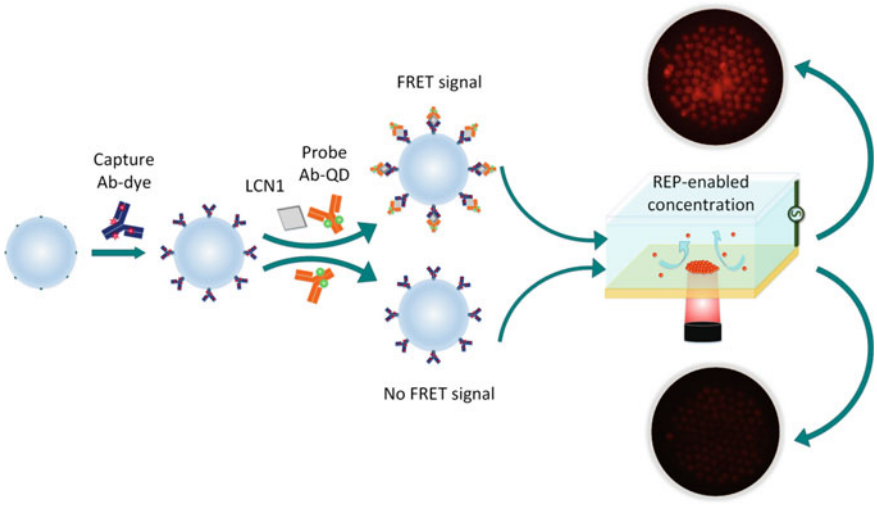

Fig. 23 Schematic of the REP-enabled bead-based FRET fluorescence immunoassay. Dispersed biomarker LCN1 is initially collected by the functionalized particles and then concentrated by REP. The concentrated particles with LCN1 show significant fluorescent signal

particles was observed, the fluorescent intensity remained lower than the signal of interest. Attempts to mitigate the QD-conjugated antibody adsorption with smaller carrier particles showed a good improvement and will be used to replace the current particles in the future research. The successful signal enhancement of the dilute biomarker, LCN1, enables the concept of rapid and noninvasive diagnostics of diabetic retinopathy through tear drops. Moreover, the technique also provides a valuable insight to detecting other diseases in the early stage.

6 Challenges and Future Developments

6.1 Low Conductivity of the Medium

Cells need to be cultured in an isotonic buffer which contains high concentration of free ions. Moreover, plasma extracted from human bodies is also measured to be very high conductive. Accordingly, the optoelectrokinetic techniques driven by electric fields are unable to deal with most biological fluids. A high conductive medium usually causes air bubbles, Joule heating, electrolysis and reduce the effective voltage during operations. Because of the fundamental limitations, the biological buffer needs to be replaced with a low conductive medium (<100 mS/m) to be used in the optoelectric devices. The replacement therefore incurs labor intensive wash cycles and an inaccurately cellular environment. Some effort [64, 65] has been attempted to prevent the formation of air bubbles and surface damage. However, both the REP and OETs still suffer from reduced optoelectrokinetic effects in a high conductive medium. A breakthrough to improve the low efficiency remains underway.

6.2 Multi-Scale Manipulation

The growing demand for point-of-care (POC) diagnosis has motivated the rapid growth of the lab on a chip (LoC) market. Considering the complexity, diversity, and multitasking nature of the technology, the quest for a versatile platform capable of handling multiple targets across different length scales has risen in the scientific field in the recent years. Unfortunately, the rapid progress in the micro/nanofluidics over the past decade has not fully overcome the operational gaps of macroscale to microscale and microscale to nanoscale regimes. Until now, the emergence of the optoelectrokinetic techniques provides a possible solution to bridge the gaps. An integration of REP and OEW [18, 66] or OETs and OEW [25] have demonstrated the cross-scale manipulation between droplets and particles. Although such a system remains under development, it has shown the potential to proceed with bioassays from sample preparation to final diagnosis all on the same platform.

7 Conclusion

Single-cell analysis (SCA) has opened a new field that allows investigations of cellular processes and identifications of biophysical mechanisms, with complementary approaches in mechanics (forces), optics (photonics), electrodynamics (charge transport) and thermodynamics (energies). Meanwhile, considerable effort is contributed to the development of unconventional tools for efficient and precise cell controls. Among the newly developed technologies, the emergence of the optoelectrokinetic techniques, REP and OETs, has drawn numerous attention from the scientific community due to their unique characteristics of non-invasiveness, flexible dynamics, and programmability. The techniques enable the realization of SCA with an all-optical method on a microchip. Both REP and OETs are capable of performing trapping, translation sorting and patterning on cells. Particularly, the combination of electric fields and light illumination enables them to achieve massively parallel processing, yet limits the conductivity of the medium used to be less than 100 mS/m. To show the potential of the optoelectrokinetic techniques in the cell applications, several examples associate with cell preparation and analysis, cell patterning, bacteria manipulation, and immunoassay are discussed in the article. As compared with the whole-animal studies, SCA has opened a new era for biological diagnostics. With the advancement of the novel optoelectrokinetic tools, one can envision a comprehensive cell analysis to be carried out on a single microchip in the near future.

Acknowledgements This work was supported by the Ministry of Science and Technology under the grant number 103-2221-E-006-172-MY2 and partially supported by the Future Star Award from the College of Engineering at National Cheng Kung University. The authors would also like to thank the grant CMNCKU10405 from the Chimei Medical Center. A. Kumar would like to acknowledge the support of Canada Research Chair program.

References

1. Khetani SR, Bhatia SN (2008) Microscale culture of human liver cells for drug development. Nat Biotechnol 26:120–126
2. Smith C (2007) Tools for drug discovery: tools of the trade. Nature 446:219–222
3. Fernandes TG, Kwon SJ, Bale SS, Lee MY, Diogo MM, Clark DS, Cabral JM, Dordick JS (2010) Three-dimensional cell culture microarray for high-throughput studies of stem cell fate. Biotechnol Bioeng 106:106–118
4. Flaim CJ, Chien S, Bhatia SN (2005) An extracellular matrix microarray for probing cellular differentiation. Nat Methods 2:119–125
5. Wheeler DB, Carpenter AE, Sabatini DM (2005) Cell microarrays and RNA interference chip away at gene function. Nat Genet 37:S25–S30
6. Fulwyler M (1965) Electronic separation of biological cells by volume. Science 150:910–911
7. Julius M, Masuda T, Herzenberg L (1972) Demonstration that antigen-binding cells are precursors of antibody-producing cells after purification with a fluorescence-activated cell sorter. Proc Natl Acad Sci USA 69:1934–1938

8. Ashikin A, Dziedzic JM, Bjorkholm JE, Chu S (1986) Observation of a single beam gradient force optical trap for dielectric particles. Opt Letts 11:288–290
9. Doh I, Cho YH (2005) A continuous cell separation chip using hydrodynamic dielectrophoresis (DEP) process. Sens Actuators, A 121:59–65
10. Hu X, Bessette PH, Qian J, Meinhart CD, Daugherty PS, Soh HT (2005) Marker-specific sorting of rare cells using dielectrophoresis. Proc Natl Acad Sci USA 102:15757–15761
11. Thomas RS, Morgan H, Green NG (2009) Negative DEP traps for single cell immobilisation. Lab Chip 9:1534–1540
12. Peitz I, van Leeuwen R (2010) Single-cell bacteria growth monitoring by automated DEP-facilitated image analysis. Lab Chip 10:2944–2951
13. Valero A, Braschler T, Demierre N, Renaud P (2010) A miniaturized continuous dielectrophoretic cell sorter and its applications. Biomicrofluidics 4:022807
14. Castelain M, Rouxhet PG, Pignon F, Magnin A, Piau J-M (2012) Single-cell adhesion probed in-situ using optical tweezers: a case study with *Saccharomyces cerevisiae*. J Appl Phys 111:114701
15. Chuang HS, Chung TY, Li Y (2014) Compact and tunable size-based dielectrophoretic flow fractionation. J Micromech Microeng 24:125016
16. Zhong MC, Wei XB, Zhou JH, Wang ZQ, Li YM (2013) Trapping red blood cells in living animals using optical tweezers. Nat Commun 4:1768
17. Kumar A, Williams SJ, Wereley ST (2009) Experiments on opto-electrically generated microfluidic vortices. Microfluid Nanofluid 6:637–646
18. Kumar A, Chuang HS, Wereley ST (2010) Dynamic manipulation by light and electric fields: micrometer particles to microliter droplets. Langmuir 26:7656–7660
19. Williams SJ, Kumar A, Wereley ST (2008) Electrokinetic patterning of colloidal particles with optical landscapes. Lab Chip 8:1879–1882
20. Wang KC, Kumar A, Williams SJ, Green NC, Kim KC, Chuang HS (2014) An optoelectrokinetic technique for programmable particle manipulation and bead-based biosignal enhancement. Lab Chip 14:3958–3967
21. Williams SJ, Kumar A, Green NG, Wereley ST (2009) A simple, optically induced electrokinetic method to concentrate and pattern nanoparticles. Nanoscale 1:133–137
22. Kumar A, Kwon JS, Williams SJ, Green NG, Yip N, Wereley ST (2010) Optically modulated electrokinetic manipulation and concentration of colloidal particles near an electrode surface. Langmuir 26:5262–5272
23. Williams SJ, Kumar A, Green NG, Wereley ST (2010) Optically induced electrokinetic concentration and sorting of colloids. J Micromech Microeng 20:015022
24. Chiou PY, Ohta AT, Wu MC (2005) Massively parallel manipulation of single cells and microparticles using optical images. Nature 436:370–372
25. Valley JK, NingPei S, Jamshidi A, Hsu H-Y, Wu MC (2011) A unified platform for optoelectrowetting and optoelectronic tweezers. Lab Chip 11:1292–1297
26. Yang SM, Yu TM, Huang HP, Ku MY, Hsu L, Liu CH (2010) Dynamic manipulation and patterning of microparticles and cells by using TiOPc-based optoelectronic dielectrophoresis. Opt Lett 35:1959–1961
27. Valley JK, Ohta AT, Hsu H-Y, Neale SL, Jamshid A, Wu MC (2009) Optoelectronic tweezers as a tool for parallel single-cell manipulation and stimulation. IEEE Trans Biomed Circ Syst 3:424–431
28. Kumar A, Williams SJ, Chuang HS, Green NG, Wereley ST (2011) Hybrid opto-electric manipulation in microfluidics—opportunities and challenges. Lab Chip 11:2135–2148
29. Hwang H, Choi YJ, Choi W, Kim SH, Jang J, Park JK (2008) Interactive manipulation of blood cells using a lens-integrated liquid crystal display based optoelectronic tweezers system. Electrophoresis 29:1203–1212
30. Green NG, Ramos A, González A, Castellanos A, Morgan H (2001) Electrothermally induced fluid flow on microelectrodes. J Electrostat 53:71–87

31. Kumar A, Cierpka C, Williams SJ, Kähler CJ, Wereley ST (2011) 3D3C velocimetry measurements of an electrothermal microvortex using wavefront deformation PTV and a single camera. Microfluid Nanofluid 10:355–365
32. Ristenpart WD, Aksay IA, Saville DA (2004) Assembly of colloidal aggregates by electrohydrodynamic flow: kinetic experiments and scaling analysis. Phys Rev E 69:021405
33. Ristenpart WD, Jiang P, Slowik MA, Punckt C, Saville DA, Aksay IA (2008) Electrodehydrodynamic flow and colloidal patterning near inhomogeneities on electrodes. Langmuir 24:12172–12180
34. Ristenpart WD, Aksay IA, Saville DA (2007) Electrohydrodynamic flow around a colloidal particle near an electrode with an oscillating potential. J Fluid Mech 575:83–109
35. Wei MT, Junio J, Ou-Yang HD (2009) Direct measurements of the frequency-dependent dielectrophoresis force. Biomicrofluidics 3:012003
36. Chiou PY, Moon H, Toshiyoshi H, Kim CJ, Wu MC (2003) Light actuation of liquid by optoelectrowetting. Sens Actuators, A Phys 104:222–228
37. Valley JK, Jamshidi A, Ohta AT, Hsu HY, Wu MC (2008) Operational regimes and physics present in optoelectronic tweezers. J Microelectromech Syst 17:342–350
38. Jamshidi A, Ohta AT, Valley JK, Hsu HY, Neale SL, Wu MC (2008) Optofluidics and optoelectronic tweezers. In: Proceedings of SPIE, MEMS, MOEMS, and micromachining III
39. Lee SH, Park HJ, Yoon JS, Kang KH (2010) Optoelectrofluidic field separation based on light-intensity gradients. Biomicrofluidics 4:034102
40. Velasco V, Williams SJ (2013) Electrokinetic concentration, patterning, and sorting of colloids with thin film heaters. J Colloid Interface Sci 394:598–603
41. Chiou PY, Moon H, Toshiyoshi H, Kim CJ, Wu MC (2003) Light actuation of liquid by optoelectrowetting. Sens Actuators, A 104:222–228
42. Ohta AT, Chiou PY, Phan HL, Sherwood SW, Yang JM, Lau ANK, Hsu HY, Jamshidi A, Wu MC (2007) Optically controlled cell discrimination and trapping using optoelectronic tweezers. IEEE J Sel Top Quantum Electron 13:235–243
43. Jamshidi A, Neale SL, Yu K, Pauzauskie PJ, Schuck PJ, Valley JK, Hsu HY, Ohta AT, Wu MC (2009) NanoPen: dynamic, low-power, and light-actuated patterning of nanoparticles. Nano Lett 9:2921–2925
44. Jamshidi A, Pauzauskie PJ, Schuck PJ, Ohta AT, Chiou PY, Chou J, Yang P, Wu MC (2008) Dynamic manipulation and separation of individual semiconducting and metallic nanowires. Nat Photonics 2:86–89
45. Jamshidi A, Hsu HY, Valley JK, Ohta AT, Neale S, Wu MC (2009) Metallic nanoparticle manipulation using optoelectronic tweezers. IEEE: Sorrento. Italy, pp 579–582
46. Ota S, Wang W, Wang Y, Yin X, Zhang X (2013) Lipid bilayer-integrated optoelectronic tweezers for nanoparticle manipulations. Nano Lett 13:2766–2770
47. Puttaswam SV, Yang SM, Sivashankarl S, Chang KW, Hsu L, Liu CH (2012) Experimental investigation of bulk response of cells on optoelectronic dielectrophoresis chip. IEEE: Kyoto, Japan
48. Huang KW, Wu YC, Lee JA, Chiou PY (2013) Microfluidic integrated optoelectronic tweezers for single-cell preparation and analysis. Lab Chip 13:3721–3727
49. He H, Chang DC, Lee YK (2007) Using a micro eletroporation chip to determine the optimal physical parameters in the uptake of biomolecules in HeLa cells. Bioelectrochem 70:363–368
50. Lin YH, Lee GB (2009) An optically induced cell lysis device using dielectrophoresis. Appl Phys Lett 94:033901
51. Valley JK, Neale S, Hsu HY, Ohta AT, Jamshidi A, Wu MC (2009) Parallel single-cell light-induced electroporation and dielectrophoretic manipulation. Lab Chip 9:1714–1720
52. Ho CT, Lin RZ, Chang WY, Chang HY, Liu CH (2006) Rapid heterogeneous liver-cell on-chip patterning via the enhanced field-induced dielectrophoresis trap. Lab Chip 6:724–734
53. Qin D, Xia Y, Whitesides GM (2010) Soft lithography for micro—and nanoscale patterning. Nat Protoc 5:491–502

54. Yang SM, Tseng SY, Chen HP, Hsu L, Liu CH (2013) Cell patterning via diffraction-induced optoelectronic dielectrophoresis force on an organic photoconductive chip. Lab Chip 13:3893–3902
55. Li FT, Chuang HS (2014) Cell patterning with a multi-functionally optoelectric device. GCBME 2014 and APCMBE 2014: Tainan, Taiwan
56. Landry J, Bernier D, Ouellet C, Goyette R, Marceau N (1985) Spheroidal aggregate culture of rat liver cells: histotypic reorganization, biomatrix deposition, and maintenance of functional activities. J Cell Biol 101:914–923
57. Kwon JS, Ravindranath SP, Kumar A, Irudayaraj J, Wereley ST (2012) Opto-electrokinetic manipulation for high-performance on-chip bioassays. Lab Chip 12:4955–4959
58. Teste B, Ali-Cherif A, Viovy JL, Malaquin L (2013) A low cost and high throughput magnetic bead-based immuno-agglutination assay in confined droplets. Lab Chip 13:2344–2349
59. Yu H-W, Jang A, Kim LH, Kim S-J, Kim IS (2011) Bead-based competitive fluorescence immunoassay for sensitive and rapid diagnosis of cyanotoxin risk in drinking water. Environ Sci Technol 45:7804–7811
60. Horejsh D, Martini F, Poccia F, Lppolito G, Caro AD, Capobianchi MR (2005) A molecular beacon, bead-based assay for the detection of nucleic acids by flow cytometry. Nucl Acids Res 33:e13
61. Miraglia S, Swartzman EE, Mellentin-Michelotti J, Evangelista L, Smith C, Gunawan II, Lohman K, Goldberg EM, Manian B, Yuan PM (1999) Homogeneous cell—and bead-based assays for high throughput screening using fluorometric microvolume assay technology. J Biomol Screen 4:193–204
62. Thompson JA, Bau HH (2010) Microfluidic, bead-based assay: theory and experiments. J Chromatogr B 878:228–236
63. Yu X, Hartmann M, Wang Q, Poetz O, Schneiderhan-Marra N, Stoll D, Kazmaier C, Joos TO (2010) mFBI: a microfluidic bead-based immunoassay for multiplexed detection of proteins from a mL sample volume. PLoS ONE 5:e13125
64. Krishnan R, Sullivan BD, Mifflin RL, Esener SC, Heller MJ (2008) Alternating current electrokinetic separation and detection of DNA nanoparticles in high-conductance solutions. Electrophoresis 29:1765–1774
65. Heller MJ, Forster AH, Tu E (2000) Active microeletronic chip devices which utilize controlled electrophoretic fields for multiplex DNA hybridization and other genomic applications. Electrophoresis 21:157–164
66. Chuang HS, Kumar A, Williams S, Wereley ST, Bhushan B (ed) (2012) Optoelectrically enabled multi-scale manipulation. In: Encyclopedia of nanotechnology. Springer, Netherlands, pp 1991–1999

Continuous Micro-/Nanofluidic Devices for Single-Cell Analysis

Chihchen Chen

Abstract Micro- and nanofluidic devices are revolutionizing the fields of single-cell analysis, and benefiting related efforts in life science research, agricultural industry, and clinical medicine. These miniaturized devices introduce much desired capabilities in accurate cell and fluid handling, and thus enable quantitative multiparameter and high-throughput approaches to analyze single cells in large numbers, advancing our understanding on how the complex normal and diseased behavior of ensembles of cells emerges from the behavior of each cell or only a few dominating rare cells. The content of this chapter is broadly divided into two parts —single-cell manipulation (SCM) and single-cell analysis (SCA). The first part of the chapter presents state-of-the-art techniques developed to handle single cells, including counting, sorting, positioning, and culturing, which are essential steps in many biological and medical assays. These manipulation techniques are frequently combined with other stimulating and sensing techniques for the observation and characterization of single cells, which are described in the second part of the chapter. Major approaches to probe either intact or lysed single cells, with a special attention on the integration of fluidics and sensor technology, are reviewed. Various operation principles are explained along with pivotal examples demonstrating their applications and perspectives. Droplet-based techniques, although very exciting, are not discussed here due to different sets of technical considerations and performance metrics involved. Techniques providing the access to the intracellular content for sampling or injection of additional compounds are not included here and are covered in Chaps. 3 and 4 of this book, respectively.

Keywords Single-cell · Microfluidic devices · Nanofluidics devices · Cell sorting · Cell manipulation · Flow focusing · Cell count · Cell culture · Cell probing · Sensors

C. Chen (✉)
Institute of Nanoengineering and Microsystems, National Tsing Hua University, Hsinchu, Taiwan
e-mail: chihchen@mx.nthu.edu.tw

F.-G. Tseng and T.S. Santra (eds.), *Essentials of Single-Cell Analysis*, Series in BioEngineering, DOI 10.1007/978-3-662-49118-8_7

1 General Introduction

The cell is the basic unit of living organisms. Studying of biological processes at the single-cell level at high throughput is important because cells are inherently variable biochemical reactors. Cellular heterogeneity, present even when genetic and environmental differences among cells are rigorously reduced, is a fundamental principle of cell biology [9, 25, 32, 43, 81]. New discoveries derived from cellular heterogeneity hold great potential to transform systems biology, regenerative medicine, and cancer biology. To understand fully the cellular specificity and complex of tissue microenvironments, it is necessary to quantify molecular and cellular behaviors at the single-cell level. Additionally, rich statistics are required both for capturing the distribution of physiological responses and for detecting rare cells with abnormal or unique phenotypes. Conventional techniques that measure the properties of large ensembles of cells or probe physiology at the cellular scale (i.e., biomarkers, microscopy, micropipettes, etc.) are not well suited for most high-throughput single-cell analyses. Recent advances in micro- and nanofluidic technologies can not only permit accurate handling of cells and small volumes of fluids, but can also perform the task with low cost, high-spatiotemporal resolution, throughput, and hence provide more statistically significant results, as illustrated by several excellent review articles [1, 2, 58, 77, 97]. Here, we review state-of-the-art micro- and nanofluidic approaches utilized for single-cell manipulation (SCM) and single-cell analysis (SCA), including advances in cell counting, sorting, positioning, high-throughput molecular readouts as well as continuous, noninvasive observation of cell behaviors over time. Droplet-based techniques are not discussed here due to different sets of technical considerations and performance metrics involved. Readers are referred to several excellent reviews [33, 46, 71].

Two commonly employed methods for single-cell analysis (SCA) are microscopy and flow cytometry. Microscopy is well suited for studying spatial localization of fluorescence within or between cells and time-dependent behaviors of either fixed or live cells [75, 91]. However, limitations of microscopy often involve throughput, multiparametric assays, and image analysis [20, 80]. On the contrary, cells in suspension can be analyzed in flow cytometry at high throughput ($\sim$100,000 cell/s). Current high-dimensional cytometry is capable of analyzing 100 unique parameters on single cells [42]. However, traditional flow cytometry suffers from several drawbacks, including expensive and non-aseptic hardware and operation, low cell viability, and inability to provide the kinetic and spatial information on the distribution of cellular or subcellular components. For example, the spatial information of the cell–cell arrangement is inevitably lost during sample preparation and it is not possible to track the same single cell over time. These two methods, although successful and well-adopted, are almost complementing to each other and are not designed for handling, manipulation, and dynamic analysis of single cells. Micro- and nanofluidic devices that are linked to conventional methods or employ different working principles provide increased benefits to SCA, as shall be seen in the following sections.

1.1 Microfluidics and Nanofluidics

Microfluidics is the field that studies and exploits the behavior of fluids confined to micrometer dimensions, such as microchannels, droplets, jets, and thin water films, etc. At this small scale, most fluids behave in nonintuitive ways because capillary forces and viscous forces that are usually negligible on a larger scale become the predominant forces. Microfluidic devices that integrate multiple procedures of cell manipulation, lysis, and detection provide enabling platforms for single-cell analysis. They confer advantages, including quantitative predictions of the fluidic environment, similar scales to the size of cells, high throughput with lower cost per assay, smaller reagents and sample consumption, and amiability to be automated and portable. These features make microfluidic devices very suitable for single-cell manipulation and analysis. For example, microfluidic technologies, capable of precise control of nutrient concentrations and the number of adjacent cells, enable the decoupling of confounding factors (e.g., environment and genotype) that can contribute to cellular heterogeneity [15].

When the fluid volume under study has a dimension less than 1 μm, it enters the realm of nanofluidics, at which scale new physical phenomena can be exploited [6, 79]. For instance, electrokinetic effects, like electroosmosis and ion polarization, are strongly exemplified, especially when concentrations of ions in the solution are low. The ability to manipulate fluids, particles, and molecules at nanometer scale provides innovative techniques to single cell analysis, such as protein separation and preconcentration [16], electrostatic trapping of submicrometer-sized particles [52].

2 Single-Cell Manipulation (SCM)

Isolating, sorting, counting, and positioning of cells are essential single-cell manipulation (SCM) steps in preparing for high-performance downstream single-cell analysis. There are currently no standardized techniques for single-cell manipulation. Microfluidic-based techniques can be broadly classified into two categories, passive and active methods, depending on whether an external force field in additional to forces generated by the flow is applied. Passive SCM devices, utilizing the intrinsic properties of cells, fluids, and device geometry for cell manipulation, are in general simpler to fabricate and operate [48]. In contrast, hybrid materials are often required to provide the additional force field in active SCM devices, in which forces such as electric or magnetic force fields may be employed for more versatile manipulation of cells. Another parameter to consider in determining the strategy for SCM is the cell type. Prokaryotes, such as bacteria, are typically smaller than eukaryotes, such as yeasts and mammalian cells. In addition, prokaryotes are in general more resilient to environmental conditions, such as temperature, osmolality, pH, and oxygen levels. In contrast, eukaryotes are more sensitive. Gentle and consistent handling of samples cannot be overemphasized for

high-quality SCA, especially when live mammalian cells are manipulated and analyzed. In the following sections, we will introduce examples and techniques to achieve SCM.

2.1 Cell Isolation

Isolation of cells of interest is commonly the first and critical step in single-cell analysis, as the volume of a typical mammalian cell is only ~4 pL, which is approximately 9 orders of magnitude smaller than common cell culture volume (~mL). Currently isolation of single cells is often achieved stochastically by serial dilutions or by using pipettes when cells are in suspension, or deterministically by using laser capture microdissection to select cells when they still remain adherent. Microfluidic devices have been developed for accurate, automatic, and unbiased isolation of single cells. For example, collecting rate tumor cells [82] and fetal cells in peripheral blood samples [47] are essential for early cancer diagnosis and prenatal screening, respectively (Fig. 1). However, detachment of cells is required for

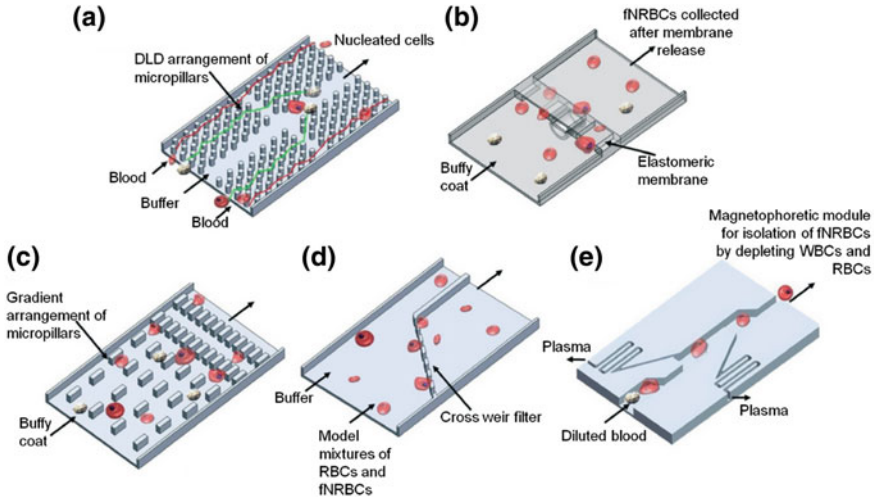

Fig. 1 Various passive microfluidic approaches for the isolation of cells. **a** Cells are separated by size using deterministic lateral displacement (DLD). Small cells tend to follow the direction of the fluid flow, whereas large cells continue to get displaced laterally by the asymmetrically placed micropillars. **b** Fetal nucleus red blood cells (fNRBCs) are concentrated at the microgap and later released after the underneath diaphragm is deflected. **c** Cells that are small and deform readily can squeeze through gaps, while others are retained. **d** Adult red blood cells (RBSs) are smaller than fNRBCs and can pass through the cross weir filter, whereas fNRBCs cannot pass and are diverted to the other collecting channel. **e** At a bifurcation, cells tend to migrate into the center of the channel of the higher flow rate, while cell-free plasma exits the branches of lower flow rates, known as the Zweifach–Fung effect. Reproduced from Ref. [47] by permission of The Royal Society of Chemistry

adherent cells biopsied from tissues or cultured within the microdevice, which may cause perturbation to the phenotype of the cell due to culture conditions and stimuli introduced during the detaching and analysis procedures.

2.2 Cell Counting

Cell counting is one of the fundamental procedures in cell biology research. It can be accomplished using optical, electrical, or magnetic means. Microscopy and flow cytometry are two of the most widely used optical techniques for single-cell analysis. The hemocytometer, originally designed for the counting of blood cells, is frequently used for assessing the concentration of various types of cells. It consists of a chamber defined by a grid-patterned bottom glass microscope slide with raised wedges that hold the top coverslip at a fixed distance off. Many disposable plastic hemocytometers have been marketed. They eliminate the need to wash for reuse of the glass hemocytometer and are especially advantageous when infectious or hazardous materials are involved.

Flow cytometry is an optical technique that is capable of counting cells at the single-cell resolution. It is also the gold standard, most widely used cell sorting technology. In flow cytometry, cells are "shot" through a capillary past an intersecting light beam, causing scattering of light; thus each cell is "read" as a signal of scattered or fluorescent light intensity by means of a light detector. To ensure that all cells pass through the same observation point and in a single-cell file, the cell suspension is injected by means of a glass capillary into a "sheath" flow, which focuses the capillary flow into a thin, single-cell wide flow. Flow cytometry is a powerful tool and can be capable of sorting of cells when equipped with a downstream sorting device that distributes the cell into different reservoirs based on the information relayed by the detector and rules determined by the user. Miniaturized flow cytometers have been successfully demonstrated [17, 18, 40, 100]. They allow for implementing microvalves, micropumps, or integrated microoptical stimulation/detection. In addition to cost reduction, major advantages of microfluidic flow cytometry include a much lower number of cells required and the potential for integration with multiple functionalities, both of which are of particular values for studying rare cells or clinical samples. The low throughput typically associated with early microfluidic flow cytometers have been greatly improved up to $\sim 10^6$ cell/s utilizing inertial effects (Fig. 2) [40]. A recent advance is the integration of inexpensive optical detectors or imaging modules [29, 99], which makes the flow cytometer much affordable and user friendly.

A Coulter counter detects cells upon their transfer through a pore, and is an electrical sensing zone method of counting cells, bacteria, and virus particles [8, 28, 62]. This method is relatively fast, real-time, label-free, viscosity-independent, and does not require large sample volumes. When an electric potential is applied across a pore contained within an insulating membrane, a transmembrane ionic current is established. When a particle less conductive than the electrolyte solution travels

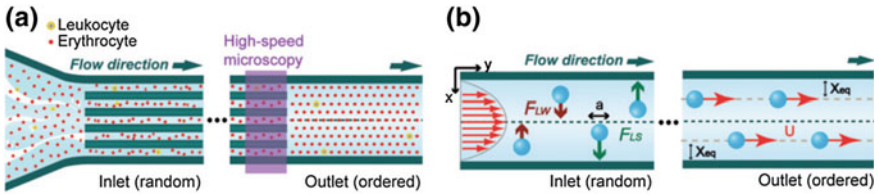

Fig. 2 A high-throughput microfluidic flow cytometer. **a** Schematics illustrate randomly distributed cells at the inlet become ordered at the downstream channel. **b** Cells are focused to specific lateral equilibrium positions, *Xeq*, where the wall effect lift force, F_{LW}, and shear-gradient lift force, F_{LS}, balance each other. Reproduced from Ref. [40] by permission of The Royal Society of Chemistry

through the pore, the same volume of the electrolyte solution is replaced by the particle, resulting a current blockade, or resistive pulse. The duration of this resistive pulse can be used to assess the surface charges carried by the particle [51], while the frequency of resistive pulses reflects the particle concentration [21, 73, 93]. Micro- and nanofluidics resistive pulse sensors advance over the traditional Coulter counter with a lower cost and a higher sensitivity. On-chip electronic sensing systems can be integrated with the fluidic network to achieve a better signal-to-noise ratio [78]. Alternatively, cells tagged with magnetic beads in the presence of abundant non-tagged cells can be counted accurately utilizing the Hall effect [44].

2.3 Cell Sorting

Microfluidic devices based on various cell sorting principles have been designed. Cells may be sorted based on biomarkers and antigens [18]. Alternatively, label-free cell separation can be achieved by exploiting intrinsic physical characteristics of the cell, such as its size [5, 19, 60, 87], deformability [30, 38], density [35], electric [10, 63, 67, 69], acoustic [27], and magnetic properties [44]. Here we introduce a few cell sorting approaches developed in recent years. Interested readers may also check out the excellent and comprehensive review papers [3, 4, 13, 31].

Capture molecules, recognizing and binding to molecules on the surface of the target cell, have been used to sort cell populations successfully for various cell types. Targeted cells are immobilized on the surface of a substrate or a magnetic bead coated with capture molecules, while the other cells are rinsed away. One of the important parameters in designing such a system is to maximize the chance of the target cell to explore the surface and hence be captured. Different approaches have been developed to achieve this goal, including incorporating micropillars [65], herringbone structures [82], or nanostructures [14, 66] inside the device, or using fibrous materials [11], etc. Antibodies have been the most popular choice as capture molecules. They can be highly sensitive and specific to targets. However, expensive

and lengthy processes associated with the antibody production hamper the biomarker discovery using antibodies. Aptamers, which can be single-stranded deoxyribonucleic acid (ssDNA) or ribonucleic acid (RNA) molecules folding into unique three-dimensional (3D) structures, can function similarly as antibodies and have the potential to accelerate the exploring appropriate biomarkers for specific cell types. Target-specific aptamers have been screened using microfluidic-based systematic evolution of ligands by exponential enrichment (SELEX) and phage display technology, which process is automated and greatly reduces the time and expertise required [36].

Endogenous physical traits of cells, independent of surface markers, provide another aspect for the sorting of cells. Cells have been sorted based on their size, deformability, density, electric, acoustic, and magnetic properties. Different dependences of various forces on cells' physical properties are exploited to drive cells differently in a designed direction or to a location where forces balance out, and hence the sorting of cells. For instance, the interaction of the lift force with Dean flow drag force leads to the focus of cells to defined size-dependent equilibrium positions inside the microfluidic channel [22]. Cancer cells and leukocytes can be separated based on differences in their sizes and electrical properties (Fig. 3) [37].

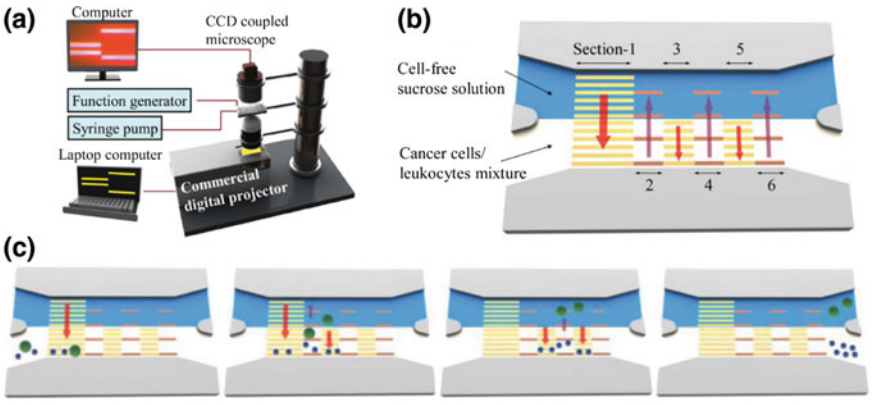

Fig. 3 Cell sorting using optically induced dielectrophoretic force (ODEP). **a** Photoconductive bottom electrodes of the microfluidic device can be reconfigured using a projector to generate programmable DEP forces. **b** Cells suspended in sucrose solution are introduced into the device featured with six sections of moving optically induced bottom electrodes. **c** Cells are lined up close to the edge of the channel in Sect. 1. Cells of larger size and higher permittivity are dragged across the boundary of two fluids by the DEP force and carried away by the cell-free sucrose solution in Sects. 2, 4, and 6, whereas other cells are pushed back toward the edge of the channel in Sects. 3 and 5. Reproduced from Ref. [37] by permission of The Royal Society of Chemistry

2.4 Cell Positioning

One of the essential steps in single-cell manipulation is moving a cell to a desired location for subsequent observation and treatments. Parameters, such as the type and number of single cells to be positioned, duration of monitoring, and target readouts, affect the decision on which approaches are suitable for achieving experimental goals. One of the pioneering papers in microfluidics, presented in 1997 by Jed Harrison's group at the University of Alberta, Canada, demonstrated the electrokinetic routing and on-chip lysing of cells [55]. Since then, a variety of alternatives have been proposed due to concerns of the high voltages involved in electrokinetic valving. Here we discuss technologies for positioning cells using hydrodynamic trapping and several others mechanisms.

In hydrodynamic trapping, cells may be delivered and positioned to stagnant or low-flow locations created in designed channel geometry or inside the induced vortex [56]. Microwells are simple cell trapping devices [72, 96]. Cells are captured by gravity into a microwell array for imaging or subsequent analysis on its content such as RNA or DNA [24, 94]. It is not easy for fluid to dislodge the trapped cell. Often repeated cell seeding procedures are employed to increase the microwell occupancy rates. Cells can be also delivered actively by fluid to the cell trap consisting of a constriction that is smaller than the size of the cell [12]. Once a cell is inside the trap, occluding the constriction, fluid is diverted and delivers cells to other unoccupied cell traps (Fig. 4) [23, 50]. Alternatively, cells may be trapped

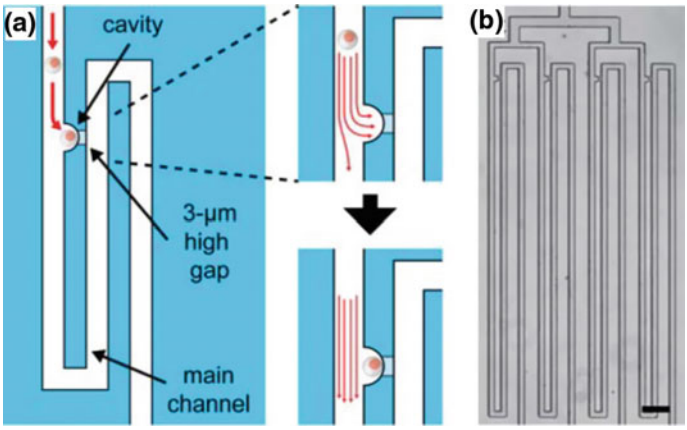

Fig. 4 A self-regulating hydrodynamic single-cell trapping device. **a** Schematic depicts a cell is delivered by the flow and trapped at the cavity connecting to a 3 μm high gap. The *top* insert illustrates the majority of the flow goes through the gap that has less fluidic resistance than the main channel. Once the cavity is occupied, the flow is redirected to deliver cells to downstream cell traps along the main channel (*bottom* insert). **b** An array of single-cell traps are incorporated in the device. Four cell traps are shown (*scale bar* is 100 μm). Reproduced from Ref. [50] by permission of The Royal Society of Chemistry

hydrodynamically within a vortex induced by modified channel geometry [39], acoustic streaming [34], or electroosmosis [59].

Arrays of trapped single cells have also been created by exploiting the differences in various properties between cells and the surrounding media. For instance, small coils fabricated using CMOS (complementary metal–oxide semiconductor) processes can trap cells labeled with magnetic beads [53]. Dielectrophoretic (DEP) traps represent an attractive solution for selectively trapping and releasing single cells; each trap is created by a set of electrodes (in a microfluidic chamber) that generate a nonuniform electric field and hence electrodynamic forces acting on the cell when the suitable electric fields, usually in AC, are applied to the electrodes [86]. However, subtle adverse effects on cells due to the typical electric fields applied in DEP limit its applicability for long-term clasp and culture of cells [41, 61].

Cells can be trapped chemically using antibodies or extracellular matrix molecules. Various techniques have been developed to pattern chemicals, biomolecules, or cells on a surface. Interested readers may check out excellent reviews [58, 74].

One recent trend to position cells is to print cells directly. Surface printing of cells has been demonstrated using a microfluidic 'pen' [45]. 3D printing of cells and biocompatible materials has shown promising progress, while advances in increased biocompatibility, print resolution and speed are needed [64].

3 Single-Cell Analysis (SCA)

Progress in microscale and nanoscale technologies is revealing new insights into single cell biology. Analysis of single cells can be monitoring a few parameters of intact cells or directly identifying its contents after cell lysis. Spatial and temporal information of a few labeled species or detectable parameters can be performed through observing intact cells, while inaccessible for labeling or complex mixture of species may be identified in cell lysate. However, separate samples are needed for each individual experimental condition if cells are to be lysed for measurements.

3.1 Intact Cells

Many assays used in molecular or cellular biology and drug development target the selection or screening of cells based on complex phenotypes or behaviors such as morphology, migration, or growth rates. Although detection of (usually fluorescent) markers for a specific gene or enzymatic activity may serve as reporters on the behavior of interest, this is a nonoptimal approach because the behavior is not screened directly, which can result in false positives or false negatives if the marker also reports on other biochemical pathways or the behavior involves many other pathways (as is often the case). Salient features of microfluidic systems, such as the

precise temporal and spatial control of the fluid and substrate at the micrometer scale allow the precise regulation and modulation of the cellular microenvironment. Many microfluidic technologies have been developed for high-throughput sorting of cells based on complex cell behaviors. Experimenters are often presented with an additional set of challenges when the measurement or question requires the interrogated sample to be kept alive.

The capability of miniaturized devices to position cells and to create well-defined physical and chemical microenvironments provides unique opportunities to study cell biology and screen drugs [95]. Different types of cells may be cocultured. In addition, large numbers of single cells may be trapped and clonally expanded. Drugs may be tested on cells grown into 3D aggregates. Mounting evidences have revealed cells in conventional monolayer culture differ from cells in 3D environment in various cellular activities such as proliferation rate, cytotoxicity and viability, cellular functions and structure, morphology and differentiation efficacy [26, 89]. 3D cell culture is potentially a powerful tool to mimic physiological tissue environment and hence confers a high degree of physiological relevance of cell-based assays and advances the quantitative modeling of biological systems from cells to organisms. Various microfluidic devices have been designed to increase uniformity and efficiency of formed 3D cell cultures, to provide better controlled cellular environment, high-throughput screening (HTS), and to simplify handling procedure [49, 54, 76, 85]. It is, however, important to note that care has to be taken while designing on-chip cell culture systems and interpreting results. Differences between experimental conditions, including the transport and spatiotemporal gradients of gases, ions, nutrients, waste products, and factors released from cells and devices, need to be carefully considered. 3D cell cultures, such as cancer spheroids and embryoid bodies, can be dissociated into single cells to characterize cellular heterogeneity and identify rare cells. Disaggregation of cells is usually accomplished by enzymatic digestions, which can be inefficient, inconsistent, and lead to cell damage. Mechanical dissociation of cells has been demonstrated using microfluidic devices incorporating constrictions to shear cell aggregates into single cells with a better consistency and cell viability (Fig. 5) [57, 70].

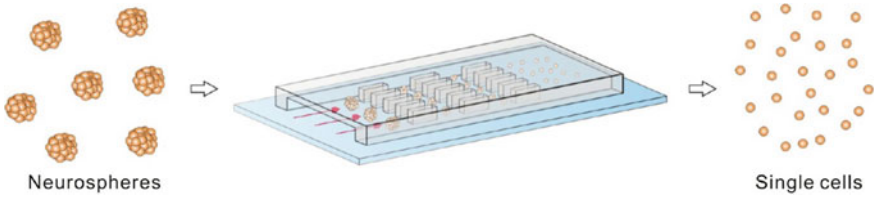

Fig. 5 Enzyme-free dissociation of neurospheres into single cells. Exogenous contamination is reduced using flow and microstructures to mechanically dissociate neurospheres with high yields of single cells and viabilities. Reprinted with the permission from ref. [57]. Copyright 2013 American Chemical Society

3.2 Cell Lysate

Breakage of a cell reveals its content for direct extraction, separation, and identification. However, standard biochemical techniques, while successful in many applications, often lyse a multitude of cells and introduce a more than a millionfold dilution of the cell content into microliter volume, risking the sensitivity and reliability of single-cell assays. High-resolution separation and high-sensitivity detection methods have been instrumental to the analysis of lysate from single cells. In general, there are two approaches to analyze single-cell lysate. One aims to integrate micro- or nanosensors with the fluidic system. The other focuses on the miniaturization of analytical chemical methods. Parameters to be considered include techniques to lyse cells, properties of target molecules, sample separation, and coupling to outside instruments, etc.

Microfluidic devices have recently proved to be very convenient and useful tools for single-cell genomics, transcriptomics, proteomics, and metabolomics [7, 88, 98]. Microfluidic devices provide a very small growth environment, comparable to the dimensions of the environment that surrounds a cell, in order to analyze cells under conditions that are similar to those that occur naturally. Also, these tools provide a controlled area for monitoring the small changes in a single cell [83, 84]. Waters et al. had demonstrated the cell lysis, polymerase chain reaction (PCR), and electrophoretic analysis of single-cell DNA on a microfluidic device in 1998 [90]. A bit more than a decade later, White et al. demonstrated high-precision reverse transcription quantitative polymerase chain reaction (RT-qPCR) assays on hundreds of single cells in parallel using a fully integrated microfluidic platform in 2011 (Fig. 6) [92]. The pace of progress has been remarkable. However, it remains technologically challenging to distinguish cell heterogeneity from the technical variation that is intrinsic to the detection method, such as PCR, when the amount of sample from a single cell is minute.

3.3 Integrated Sensors

Biochemical microsensors have been successfully demonstrated for the detection of biomolecules, chemicals, and gases with high sensitivity [68]. They can be included on-chip to characterize the molecular contents of the sample in real time. Integration techniques that are biocompatible while conserve or even improve the performance of biosensors are being developed.

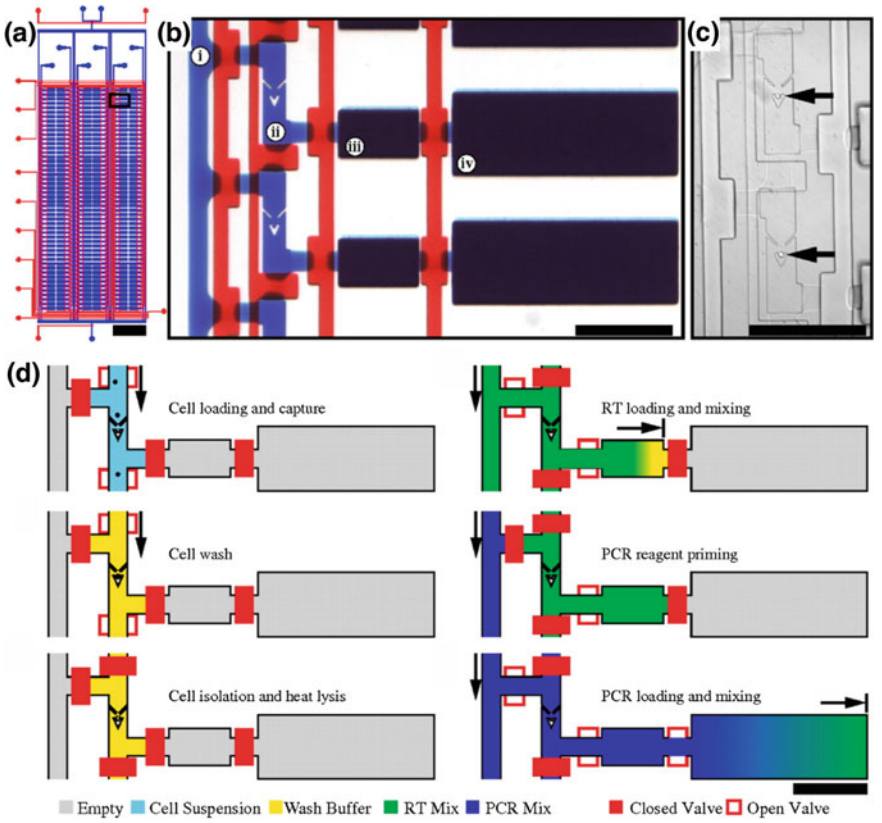

Fig. 6 Microfluidic single-cell RT-qPCR. **a** The microfluidic device contains 6 sample inputs and is capable of performing 300 RT-PCR reactions using ~20 μL of reagents (*scale bar* is 4 mm). **b** A micrograph of an array unit consisting (i) a reagent channel, (ii) a cell capture chamber, (iii) a reverse transcription (RT) chamber, and (iv) a PCR chamber (*scale bar* is 400 μm). **c** A micrograph of two-cell capture chambers with trapped cells indicated by arrows (*scale bar* is 400 μm). **d** The operation of the device. Cells in suspension are introduced into the device and captured. Extracellular RNAs are rinsed away prior to heat lysis of trapped cells. RT and PCR reagents are injected sequentially for single-cell transcriptome analysis (*scale bar* is 400 μm). (Reproduced with permission from White et al. [92])

4 Summary

Micro- and nanotechnologies enable scientists to handle and analyze single live entities (ranging from cells, embryos, to worms) at high throughput in small fluid volumes, and are revolutionizing the fields of molecular biology, biochemistry, and cell biology because they are providing a more quantitative description of cellular heterogeneity—which is crucial in understanding both physiological and patho-physiological phenomena such as differentiation, migration, reproduction and

cancer, among many others. For the same token, this ability is greatly benefitting many related efforts in biotechnology, e.g., in the development of cell analysis chips for PCR, patch clamp electrophysiology, etc. We can expect that the miniaturization trends and integration of analytical components continue to greatly advance the field of single-cell analysis.

References

1. Andersson H, Van Den Berg A (2003) Microfluidic devices for cellomics: a review. Sens Actuators B-Chem 92:315–325
2. Andersson H, Van Den Berg A (2004) Microtechnologies and nanotechnologies for single-cell analysis. Curr Opin Biotechnol 15:44–49
3. Autebert J, Coudert B, Bidard F-C et al (2012) Microfluidic: an innovative tool for efficient cell sorting. Methods 57:297–307
4. AaS Bhagat, Bow H, Hou HW et al (2010) Microfluidics for cell separation. Med Biol Eng Comput 48:999–1014
5. AaS Bhagat, Hou HW, Li LD et al (2011) Pinched flow coupled shear-modulated inertial microfluidics for high-throughput rare blood cell separation. Lab Chip 11:1870–1878
6. Bocquet L, Charlaix E (2010) Nanofluidics, from bulk to interfaces. Chem Soc Rev 39:1073–1095
7. Bontoux N, Dauphinot L, Vitalis T et al (2008) Integrating whole transcriptome assays on a lab-on-a-chip for single cell gene profiling. Lab Chip 8:443–450
8. Branton D, Deamer DW, Marziali A et al (2008) The potential and challenges of nanopore sequencing. Nat Biotechnol 26:1146–1153
9. Cai L, Friedman N, Xie XS (2006) Stochastic protein expression in individual cells at the single molecule level. Nature 440:358–362
10. Cemazar J, Miklavcic D, Kotnik T (2013) Microfluidic devices for manipulation, modification and characterization of biological cells in electric fields—a review. Informacije Midem-J Microelectron Electron Compon Mater 43:143–161
11. Chen C, Lin B-R, Wang H-K et al (2014) Paper-based immunoaffinity devices for accessible isolation and characterization of extracellular vesicles. Microfluid Nanofluid 16:849–856
12. Chen CC, Folch A (2006) A high-performance elastomeric patch clamp chip. Lab Chip 6:1338–1345
13. Chen J, Li J, Sun Y (2012) Microfluidic approaches for cancer cell detection, characterization, and separation. Lab Chip 12:1753–1767
14. Chen W, Weng S, Zhang F et al (2013) Nanoroughened surfaces for efficient capture of circulating tumor cells without using capture antibodies. ACS Nano 7:566–575
15. Chen YC, Cheng YH, Kim HS et al (2014) Paired single cell co-culture microenvironments isolated by two-phase flow with continuous nutrient renewal. Lab Chip 14:2941–2947
16. Cheow LF, Han J (2011) Continuous signal enhancement for sensitive aptamer affinity probe electrophoresis assay using electrokinetic concentration. Anal Chem 83:7086–7093
17. Cheung KC, Di Berardino M, Schade-Kampmann G et al (2010) Microfluidic Impedance-based flow cytometry. Cytometry Part A 77A:648–666
18. Cho SH, Chen CH, Tsai FS et al (2010) Human mammalian cell sorting using a highly integrated micro-fabricated fluorescence-activated cell sorter (mu FACS). Lab Chip 10:1567–1573
19. Choi Y-S, Seo K-W, Lee S-J (2011) Lateral and cross-lateral focusing of spherical particles in a square microchannel. Lab Chip 11:460–465
20. Conrad C, Gerlich DW (2010) Automated microscopy for high-content RNAi screening. J Cell Biol 188:453–461

21. Dharmasiri U, Njoroge SK, Witek MA et al (2011) High-throughput selection, enumeration, electrokinetic manipulation, and molecular profiling of low-abundance circulating tumor cells using a microfluidic system. Anal Chem 83:2301–2309
22. Di Carlo D (2009) Inertial microfluidics. Lab Chip 9:3038–3046
23. Di Carlo D, Aghdam N, Lee LP (2006) Single-cell enzyme concentrations, kinetics, and inhibition analysis using high-density hydrodynamic cell isolation arrays. Anal Chem 78:4925–4930
24. Dimov IK, Lu R, Lee EP et al (2014) Discriminating cellular heterogeneity using microwell-based RNA cytometry. Nat Commun 5:3451
25. Eldar A, Elowitz MB (2010) Functional roles for noise in genetic circuits. Nature 467: 167–173
26. Fennema E, Rivron N, Rouwkema J et al (2013) Spheroid culture as a tool for creating 3D complex tissues. Trends Biotechnol 31:108–115
27. Friend J, Yeo LY (2011) Microscale acoustofluidics: microfluidics driven via acoustics and ultrasonics. Rev Mod Phys 83:647–704
28. Garza-Licudine E, Deo D, Yu S et al (2010) Portable nanoparticle quantization using a resizable nanopore instrument—the Izon qNano (TM). In: 2010 Annual international conference of the IEEE engineering in medicine and biology society (EMBC), pp 5736–5739
29. Goda K, Ayazi A, Gossett DR et al (2012) High-throughput single-microparticle imaging flow analyzer. Proc Natl Acad Sci USA 109:11630–11635
30. Gossett DR, Tse HTK, Lee SA et al (2012) Hydrodynamic stretching of single cells for large population mechanical phenotyping. Proc Natl Acad Sci USA 109:7630–7635
31. Gossett DR, Weaver WM, Mach AJ et al (2010) Label-free cell separation and sorting in microfluidic systems. Anal Bioanal Chem 397:3249–3267
32. Graf T, Stadtfeld M (2008) Heterogeneity of embryonic and adult stem cells. Cell Stem Cell 3:480–483
33. Guo MT, Rotem A, Heyman JA et al (2012) Droplet microfluidics for high-throughput biological assays. Lab Chip 12:2146–2155
34. Hertz HM (1995) Standing-wave acoustic trap for nonintrusive positioning of microparticles. J Appl Phys 78:4845–4849
35. Hsu CH, Di Carlo D, Chen CC et al (2008) Microvortex for focusing, guiding and sorting of particles. Lab Chip 8:2128–2134
36. Huang C-J, Lin H-I, Shiesh S-C et al (2010) Integrated microfluidic system for rapid screening of CRP aptamers utilizing systematic evolution of ligands by exponential enrichment (SELEX). Biosens Bioelectron 25:1761–1766
37. Huang S-B, Wu M-H, Lin Y-H et al (2013) High-purity and label-free isolation of circulating tumor cells (CTCs) in a microfluidic platform by using optically-induced-dielectrophoretic (ODEP) force. Lab Chip 13:1371–1383
38. Hur SC, Henderson-Maclennan NK, Mccabe ERB et al (2011) Deformability-based cell classification and enrichment using inertial microfluidics. Lab Chip 11:912–920
39. Hur SC, Mach AJ, Di Carlo D (2011) High-throughput size-based rare cell enrichment using microscale vortices. Biomicrofluidics 5(2):022206
40. Hur SC, Tse HTK, Di Carlo D (2010) Sheathless inertial cell ordering for extreme throughput flow cytometry. Lab Chip 10:274–280
41. Ibey BL, Roth CC, Pakhomov AG et al (2011) Dose-dependent thresholds of 10-ns electric pulse induced plasma membrane disruption and cytotoxicity in multiple cell lines. PLoS ONE 6:e15642
42. Irish JM, Doxie DB (2014) High-dimensional single-cell cancer biology. In: Fienberg HG, Nolan GP (eds) High-dimensional single cell analysis: mass cytometry, multi-parametric flow cytometry and bioinformatic techniques, pp 1–21
43. Irish JM, Kotecha N, Nolan GP (2006) Innovation—mapping normal and cancer cell signalling networks: towards single-cell proteomics. Nat Rev Cancer 6:146–155
44. Issadore D, Chung J, Shao HL et al (2012) Ultrasensitive clinical enumeration of rare cells ex vivo using a micro-hall detector. Sci Trans Med 4:141ra92

45. Juncker D, Schmid H, Delamarche E (2005) Multipurpose microfluidic probe. Nat Mater 4:622–628
46. Kang DK, Ali MM, Zhang KX et al (2014) Droplet microfluidics for single-molecule and single-cell analysis in cancer research, diagnosis and therapy. Trac-Trends Anal Chem 58:145–153
47. Kantak C, Chang CP, Wong CC et al (2014) Lab-on-a-chip technology: impacting non-invasive prenatal diagnostics (NIPD) through miniaturisation. Lab Chip 14:841–854
48. Karimi A, Yazdi S, Ardekani AM (2013) Hydrodynamic mechanisms of cell and particle trapping in microfluidics. Biomicrofluidics 7(2):021501
49. Kim C, Lee KS, Bang JH et al (2011) 3-Dimensional cell culture for on-chip differentiation of stem cells in embryoid body. Lab Chip 11:874–882
50. Kobel S, Valero A, Latt J et al (2010) Optimization of microfluidic single cell trapping for long-term on-chip culture. Lab Chip 10:857–863
51. Kozak D, Anderson W, Vogel R et al (2012) Simultaneous size and zeta-potential measurements of individual nanoparticles in dispersion using size-tunable pore sensors. ACS Nano 6:6990–6997
52. Krishnan M, Mojarad N, Kukura P et al (2010) Geometry-induced electrostatic trapping of nanometric objects in a fluid. Nature 467:692–695
53. Lee H, Liu Y, Ham D et al (2007) Integrated cell manipulation system—CMOS/microfluidic hybrid. Lab Chip 7:331–337
54. Lee WG, Ortmann D, Hancock MJ et al (2010) A hollow sphere soft lithography approach for long-term hanging drop methods. Tissue Eng Part C-Methods 16:249–259
55. Li PCH, Harrison DJ (1997) Transport, manipulation, and reaction of biological cells on-chip using electrokinetic effects. Anal Chem 69:1564–1568
56. Lieu VH, House TA, Schwartz DT (2012) Hydrodynamic tweezers: impact of design geometry on flow and microparticle trapping. Anal Chem 84:1963–1968
57. Lin C-H, Lee D-C, Chang H-C et al (2013) Single-cell enzyme-free dissociation of neurospheres using a microfluidic chip. Anal Chem 85:11920–11928
58. Lindstrom S, Andersson-Svahn H (2010) Overview of single-cell analyses: microdevices and applications. Lab Chip 10:3363–3372
59. Liu S-J, Wei H-H, Hwang S-H et al (2010) Dynamic particle trapping, release, and sorting by microvortices on a substrate. Phys Rev E 82:026308
60. Long BR, Heller M, Beech JP et al (2008) Multidirectional sorting modes in deterministic lateral displacement devices. Phys Rev E 78:046304
61. Lu J, Barrios CA, Dickson AR et al (2012) Advancing practical usage of microtechnology: a study of the functional consequences of dielectrophoresis on neural stem cells. Integr Biol 4:1223–1236
62. Menestrina J, Yang C, Schiel M et al (2014) Charged particles modulate local ionic concentrations and cause formation of positive peaks in resistive-pulse-based detection. J Phys Chem C 118:2391–2398
63. Muratore M, Srsen V, Waterfall M et al (2012) Biomarker-free dielectrophoretic sorting of differentiating myoblast multipotent progenitor cells and their membrane analysis by Raman spectroscopy. Biomicrofluidics 6(3):034113
64. Murphy SV, Atala A (2014) 3D bioprinting of tissues and organs. Nat Biotechnol 32: 773–785
65. Nagrath S, Sequist LV, Maheswaran S et al (2007) Isolation of rare circulating tumour cells in cancer patients by microchip technology. Nature 450:1235–1239
66. Park GS, Kwon H, Kwak DW et al (2012) Full surface embedding of gold clusters on silicon nanowires for efficient capture and photothermal therapy of circulating tumor cells. Nano Lett 12:1638–1642
67. Patel S, Showers D, Vedantam P et al (2012) Microfluidic separation of live and dead yeast cells using reservoir-based dielectrophoresis. Biomicrofluidics 6(3):034102
68. Pearton SJ, Ren F, Wang YL et al (2010) Recent advances in wide bandgap semiconductor biological and gas sensors. Prog Mater Sci 55:1–59

69. Pethig R (2010) Review article-dielectrophoresis: status of the theory, technology, and applications. Biomicrofluidics 4(2):022811
70. Qiu X, De Jesus J, Pennell M et al (2015) Microfluidic device for mechanical dissociation of cancer cell aggregates into single cells. Lab Chip 15:339–350
71. Rakszewska A, Tel J, Chokkalingam V et al (2014) One drop at a time: toward droplet microfluidics as a versatile tool for single-cell analysis. Npg Asia Mater 6:e133
72. Rettig JR, Folch A (2005) Large-scale single-cell trapping and imaging using microwell arrays. Anal Chem 77:5628–5634
73. Roberts GS, Yu S, Zeng Q et al (2012) Tunable pores for measuring concentrations of synthetic and biological nanoparticle dispersions. Biosens Bioelectron 31:17–25
74. Robertus J, Browne WR, Feringa BL (2010) Dynamic control over cell adhesive properties using molecular-based surface engineering strategies. Chem Soc Rev 39:354–378
75. Rosenfeld N, Young JW, Alon U et al (2005) Gene regulation at the single-cell level. Science 307:1962–1965
76. Sakai Y, Yoshiura Y, Nakazawa K (2011) Embryoid body culture of mouse embryonic stem cells using microwell and micropatterned chips. J Biosci Bioeng 111:85–91
77. Schmid A, Kortmann H, Dittrich PS et al (2010) Chemical and biological single cell analysis. Curr Opin Biotechnol 21:12–20
78. Song YX, Yangi JD, Pan XX et al (2015) High-throughput and sensitive particle counting by a novel microfluidic differential resistive pulse sensor with multidetecting channels and a common reference channel. Electrophoresis 36:495–501
79. Sparreboom W, Van Den Berg A, Eijkel JCT (2010) Transport in nanofluidic systems: a review of theory and applications. New J Phys 12:015004
80. Spiller DG, Wood CD, Rand DA et al (2010) Measurement of single-cell dynamics. Nature 465:736–745
81. Spudich JL, Koshland DE (1976) Non-genetic individuality—chance in single cell. Nature 262:467–471
82. Stott SL, Hsu C-H, Tsukrov DI et al (2010) Isolation of circulating tumor cells using a microvortex-generating herringbone-chip. Proc Natl Acad Sci USA 107:18392–18397
83. Taylor RJ, Falconnet D, Niemisto A et al (2009) Dynamic analysis of MAPK signaling using a high-throughput microfluidic single-cell imaging platform. Proc Natl Acad Sci USA 106:3758–3763
84. Toriello NM, Douglas ES, Thaitrong N et al (2008) Integrated microfluidic bioprocessor for single-cell gene expression analysis. Proc Natl Acad Sci USA 105:20173–20178
85. Tung YC, Hsiao AY, Allen SG et al (2011) High-throughput 3D spheroid culture and drug testing using a 384 hanging drop array. Analyst 136:473–478
86. Voldman J, Gray ML, Toner M et al (2002) A microfabrication-based dynamic array cytometer. Anal Chem 74:3984–3990
87. Wang C, Jalikop SV, Hilgenfeldt S (2011) Size-sensitive sorting of microparticles through control of flow geometry. Appl Phys Lett 99:034101
88. Wang DJ, Bodovitz S (2010) Single cell analysis: the new frontier in 'omics'. Trends Biotechnol 28:281–290
89. Wang H, Pilla F, Anderson S et al (2012) A novel model of human implantation: 3D endometrium-like culture system to study attachment of human trophoblast (Jar) cell spheroids. Mol Hum Reprod 18:33–43
90. Waters LC, Jacobson SC, Kroutchinina N et al (1998) Microchip device for cell lysis, multiplex PCR amplification, and electrophoretic sizing. Anal Chem 70:158–162
91. Weinberger LS, Burnett JC, Toettcher JE et al (2005) Stochastic gene expression in a lentiviral positive-feedback loop: HIV-1 Tat fluctuations drive phenotypic diversity. Cell 122:169–182
92. White AK, Vaninsberghe M, Petriv OI et al (2011) High-throughput microfluidic single-cell RT-qPCR. Proc Natl Acad Sci USA 108:13999–14004
93. Willmott GR, Vogel R, Yu SSC et al (2010) Use of tunable nanopore blockade rates to investigate colloidal dispersions. J Phys-Condens Matter 22:454116

94. Wood DK, Weingeist DM, Bhatia SN et al (2010) Single cell trapping and DNA damage analysis using microwell arrays. Proc Natl Acad Sci USA 107:10008–10013
95. Wu M-H, Huang S-B, Lee G-B (2010) Microfluidic cell culture systems for drug research. Lab Chip 10:939–956
96. Chung Yu-Hsiang, Hsiao Yi-Hsing, Kao Wei-Lun et al (2015) Microwells support high-resolution time-lapse imaging and development of preimplanted mouse embryos. Biomicrofluidics 9(2):022407
97. Zare RN, Kim S (2010) Microfluidic platforms for single-cell analysis. In: Yarmush ML, Duncan JS, Gray ML (eds) Annu Rev Biomed Eng 12:187–201
98. Zhong JF, Chen Y, Marcus JS et al (2008) A microfluidic processor for gene expression profiling of single human embryonic stem cells. Lab Chip 8:68–74
99. Zhu HY, Mavandadi S, Coskun AF et al (2011) Optofluidic fluorescent imaging cytometry on a cell phone. Anal Chem 83:6641–6647
100. Zhuang GS, Jensen TG, Kutter JP (2012) Detection of unlabeled particles in the low micrometer size range using light scattering and hydrodynamic 3D focusing in a microfluidic system. Electrophoresis 33:1715–1722

Single-Cell Mechanical Properties: Label-Free Biomarkers for Cell Status Evaluation

Jian Chen, Song-Bin Huang, Chengcheng Xue, Beiyuan Fan, Deyong Chen, Junbo Wang and Min-Hsien Wu

Abstract The mechanical behavior of biological cells is largely determined by their cytoskeletons; abnormal cellular functions can change cytoskeletons, leading to variations in cellular mechanical properties. This chapter begins with a summary of the relationships between cellular mechanical properties and various disease processes and changes in cell states: (1) changes in stiffness of red blood cells in cytoskeletal disorders, such as malaria and sickle cell anemia; (2) increased cell deformability of invasive cancer cells, compared with benign counterparts; (3) increased stiffness of leukocytes in sepsis; and (4) decreased deformability during the stem cell differentiation process. In the following section, we discuss the well-established techniques that are being used to measure the mechanical properties of single cells, including atomic force microscopy and micropipette aspiration. Finally, we describe the microfluidic approaches—including microfluidic constriction channels, microfluidic optical stretchers, and microfluidic hydrodynamic stretchers—that are being developed as next-generation, automated, and high-throughput techniques for characterization of the mechanical properties of single cells. The advantages and limitations of each technique are compared and future research opportunities are highlighted.

Keywords Single-cell analysis · Cellular mechanics · Characterization of single-cell mechanical properties · Microfluidics

J. Chen · C. Xue · B. Fan · D. Chen · J. Wang (✉)
State Key Laboratory of Transducer Technology, Institute of Electronics, Chinese Academy of Sciences, No.19 North 4th Ring Road West, Haidian District, Beijing, People's Republic of China
e-mail: jbwang@mail.ie.ac.cn

S.-B. Huang · M.-H. Wu (✉)
Graduate Institute of Biochemical and Biomedical Engineering, Chang Gung University, No. 259, Wenhua 1st Road, Guishan District, Taoyuan City, Taiwan
e-mail: mhwu@mail.cgu.edu.tw

F.-G. Tseng and T.S. Santra (eds.), *Essentials of Single-Cell Analysis*, Series in BioEngineering, DOI 10.1007/978-3-662-49118-8_8

1 Introduction

The mechanical behavior and properties of a eukaryotic cell are largely determined by the characteristics of its cytoskeleton, an elaborate network of fibrous proteins [1, 2]. More specifically, the deformability of nucleated cells is determined by the membrane, the cytoskeletal network (actin filaments, intermediate filaments, and microtubules), and its interaction with the nucleus. Incompressible viscoelastic solids with key parameters of $E_{instantaneous}$ and $E_{equilibrium}$ are proposed to model these nucleated cells. As to the deformability of red blood cells (RBCs), it is determined by the membrane skeleton network, which is modeled as cortical shell-liquid core (or liquid drop) models [3]. Abnormal cellular functions can change cytoskeletons and lead to variations in mechanical properties of cells [4, 5].

This chapter summarizes the relationships between cellular mechanical properties and various disease processes and changes in cell states, including (1) changes in stiffness of red blood cells in cytoskeletal disorders, such as malaria and sickle cell anemia [6, 7]; (2) increased cellular deformability of invasive cancer cells, compared with benign counterparts [8–10]; (3) increased stiffness of leukocytes in sepsis [11]; and (4) decreased deformability during the stem cell differentiation process [12–14].

In the following section, we discuss the well-established techniques that are being used to measure cellular mechanical properties, including atomic force microscopy (AFM) [15–24] and micropipette aspiration [25]. In addition, we describe the emerging microfluidic approaches (e.g., constriction channels, optical stretchers, hydrodynamic stretchers) for the characterization of cellular mechanical properties [26–29].

2 Cellular Mechanical Properties with Various Cell States

2.1 Red Blood Cell Disorders

Malaria is currently one of the world's most threatening diseases, infecting about 200 million people and leading to roughly 2,000 deaths per day [30, 31]. Malaria infection is caused by a single-cell parasite of the genome of *Plasmodium* [32]; after parasite invasion, red blood cells undergo extensive structural and molecular changes during a 48-h intra-erythrocytic cycle, leading to decreases in cellular deformability and increases in cellular adhesiveness [4, 5, 33]. The changes in the mechanical properties of red blood cells after *P. falciparum* infection have been probed using micropipette aspiration [34–36], optical tweezers [33, 37, 38], and microfluidic constriction channels [39–41]. The stiffness of red blood cells with the *P. falciparum* infection is approximately nine times that of their healthy counterparts [33]; the stiffer infected red blood cells were found to irreversibly block the passage of normal red blood cells when they were forced to travel through microfluidic constriction channels [39].

Sickle cell anemia is a hereditary blood disorder where changes in the molecular structure of hemoglobin result in stiffer sickle or crescent-shaped red blood cells, giving rise to circulation problems and depriving tissues and organs of oxygenated blood [42–45]. Studies of cell mechanics using, for example, micropipette aspiration [46–51], have been performed to probe the changes in mechanical properties of sickle-shaped red blood cells; red blood cells from sickle cell anemia patients are stiffer and more viscous when compared with the healthy red blood cells [52, 53].

2.2 Tumor

Cancer is currently one of the leading causes of death worldwide, with roughly 14 million new cases and more than 8 million deaths in 2012 [54]. Cancer is a disease that results from rapid, unrestricted, and uncontrolled proliferation of abnormal cells, due to dysregulation of the cellular signaling pathways that control cell proliferation and apoptosis—generally caused by mutations in genes that express key proteins involved in these biochemical reactions [55, 56].

Cancer is also accompanied by specific changes in the mechanical properties of cells [8, 10, 57], which have been probed using micropipette aspiration [58–62], AFM [63–90], magnetic twisting cytometry [91], microfluidic optical stretchers [92, 93], microfluidic constriction channels [94–97], and microfluidic hydrodynamic stretchers [98]. Experimental findings have revealed that cellular stiffness decreases significantly with malignant transformation in a variety of cancers, including breast cancer, lung cancer, renal cancer, prostate cancer, oral cancer, and skin cancer (see Table 1).

2.3 Leukocyte Activation in Sepsis

Sepsis is a progressive, injurious, inflammatory response to overwhelming infection associated with tissue hypoperfusion and multiorgan dysfunction [99, 100]. Neutrophils are crucial components of the innate immune response during sepsis, releasing important regulatory cytokines and contributing directly to antimicrobial killing. In patients with sepsis, reprogramming of neutrophil occurs, manifested by impaired recruitment of neutrophils to sites of infection, abnormal accumulation of neutrophils to remote sites, and dysregulation of neutrophil effector responses [11, 101, 102]. Changes in neutrophil rigidity and sequestration during sepsis have also been reported, leading to neutrophil accumulation in capillary beds, particularly in the lung and liver sinusoids. The changes in the mechanical properties of neutrophils have been probed using polymeric filters [101, 103], micropipette aspiration [104–106], and microfluidic constriction channels [107–109]. The results have confirmed that leukocyte deformability decreases in patients with sepsis, and that this change negatively affects the rheological properties of whole blood.

Table 1 Key developments in the field of mechanical phenotypes of tumor cells

Cell types	Techniques and quantified parameters	Key results
Normal rat embryo fibroblasts (CREF) and CREF transfected with T24 ras oncogene (CREF T24)	Micropipette aspiration + $E_{instantaneous}$ and $E_{equilibrium}$	The CREF T24 cells were 50 % more deformable than CREF cells [62]
Two normal cells of Hu609 and HCV29 and two bladder cancerous cells of T24 and BC3726	AFM + $E_{elastic}$ (elastic modulus)	Values of $E_{elastic}$ of Hu609, HCV29, T24, and BC3726 cells (ca. 20 cells per type) were 12.9 ± 4.8, 10.0 ± 4.6, 1.0 ± 0.5, and 1.4 ± 1.0 kPa, respectively [81]
Normal hepatocytes and hepatocellular carcinoma cells (HCC)	Micropipette aspiration + $E_{instantaneous}$ and $E_{equilibrium}$	Values of $E_{instantaneous}$ and $E_{equilibrium}$ of normal hepatocyptes (n = 24) were 181 ± 34 and 131 ± 18 Pa, respectively; for HCC (n = 30) they were 219 ± 34 and 155 ± 19 Pa, respectively [60]
Breast benign cell line of MCF-10; malignant tumor cells of MCF-7, mod-MCF-7, MDA-MB-231, and mod-MDA-MB-231	Microfluidic optical stretcher + optical deformability	Optical deformabilities of MCF-10 (n = 36), MCF-7 (n = 26), mod-MCF-7 (n = 21), MDA-MB-231, and mod-MDA-MB-231 cells were 10.5 ± 0.8, 21.4 ± 1.1, 30.4 ± 1.8, 33.7 ± 1.4, and 24.4 ± 2.5, respectively [93]
Human benign reactive mesothelial cells and metastatic tumor cells in human pleural fluid samples	AFM + $E_{elastic}$	Values of $E_{elastic}$ of tumor cells (n = 8 for each patient sample) and benign mesothelial cells (n = 8 for each patient sample) were 0.53 ± 0.10 and 1.97 ± 0.70 kPa, respectively [83]
Prostate tumor cell lines of LNCaP, PC-3, and BPH	AFM + $E_{elastic}$	Values of $E_{elastic}$ of LNCaP (n = 52), PC-3 (n = 53), and BPH cells (n = 47) were 287 ± 52, 1401 ± 162, and 2797 ± 491 Pa, respectively [87]
Breast benign cell line of MCF-10A and malignant tumor cells of MCF-7	AFM + $E_{elastic}$	MCF-7 cells had a value of $E_{elastic}$ significantly lower (1.4–1.8 times) than that of MCF-10A cells [88]
Breast benign cell line of MCF-10A and malignant tumor cells of MCF-7	Microfluidic constriction channel + entry time and transit velocity	MCF-10A cells had a longer entry time than MCF-7 cells, but a comparable transit velocity [97]

(continued)

Table 1 (continued)

Cell types	Techniques and quantified parameters	Key results
Breast tumor cell line of MCF-7 and cervical tumor cell line of HeLa	AFM + $E_{elastic}$	Values of $E_{elastic}$ of MCF-7 and HeLa cells (n > 15) were within the ranges 20–30 and 100–200 kPa, respectively [89]
Prostate tumor cell lines of LNCaP and PC-3	AFM + $E_{elastic}$	Values of $E_{elastic}$ of LNCaP and PC-3 were < 2.0 and 3.0–4.5 kPa, respectively [85]
Normal squamous, metaplastic, and dysplastic cell lines of EPC2, CP-A, and CP-D	AFM + $E_{elastic}$	Values of $E_{elastic}$ of EPC2 (n = 18), CP-A (n = 10), and CP-D (n = 19) cells were 4.7, 3.1, and 2.6 kPa, respectively [90]
Breast cell lines of MCF-10, MCF-7, and MDA-MB 231; lung cell lines of A431 and A125; skin cell lines of Te354.T and MeWo; colon cell lines of Hacat and SW480; cervical cell lines of Me180 and Ms751	AFM + $E_{elastic}$	Values of $E_{elastic}$ of MCF-10 (n = 22), MCF-7 (n = 25), MDA-MB 231 (n = 35), A431 (n = 26), A125 (n = 26), Te354.T (n = 23), MeWo (n = 24), Hacat (n = 23), SW480 (n = 23), Me180 (n = 23), and Ms751 (n = 23) were 478 ± 69, 425 ± 31, 341 ± 41, 374 ± 64, 265 ± 35, 352 ± 59, 319 ± 53, 384 ± 55, 466 ± 77, 540 ± 75, and 471 ± 53 Pa, respectively [77]
Ovarian surface epithelial (OSE) cells	AFM + $E_{elastic}$	Values of $E_{elastic}$ of early and late-stage OSE cells were 1.097 ± 0.632 and 0.549 ± 0.281 kPa, respectively [75]
Metastatic B16 melanoma variants, including B16-F10, B16-BL6, and B16-F1	AFM + $E_{elastic}$	Values of $E_{elastic}$ of B16-F10, B16-BL6, and B16-F1 cells were 350.8 ± 4.8, 661.9 ± 16.5, and 727.2 ± 13.0 Pa, respectively [72]
Ovarian cell lines of IOSE, HEY, HEY A8, OVCAR-3, and OVCAR-4	AFM + $E_{elastic}$	Values of $E_{elastic}$ of IOSE (n = 55), HEY (n = 60), HEY A8 (n = 59), OVCAR-3 (n = 20), and OVCAR-4 (n = 18) cells were 2.472 ± 2.048, 0.884 ± 0.529, 0.494 ± 0.222, 0.576 ± 0.236, and 1.120 ± 0.865 kPa, respectively [71]
Brain normal human glial cells, tumor cell lines of A172 and 1321N1	Microfluidic constriction channel + entry time and transit velocity	Brain tumor cells had shorter entry time than benign counterparts [95]

2.4 Stem Cell Differentiation

Stem cells have unique capacities to regenerate functional tissues continually for the lifetime of an organism [110, 111]. Realization of the potential of stem cells for tissue engineering requires characterization of their unique biological, biochemical, and proteomic properties, which have yet to be fully elucidated [112]. Changes in mechanical properties of cells have been reported during stem cell differentiation [13, 14], as probed using micropipette aspiration [113–115], AFM [116–120], and microfluidic hydrodynamic stretchers [98]. Significant decreases in cellular deformability have been observed for differentiated stem cells, compared with their undifferentiated counterparts (see Table 2).

Table 2 Key developments in the field of mechanical phenotypes of stem cells

Cell types	Techniques and quantified parameters	Key results
Human adipose–derived adult stem cells, bone marrow–derived mesenchymal stem cells, primary chondrocytes, and osteoblasts	AFM + $E_{instantaneous}$ and $E_{equilibrium}$	Values of $E_{instantaneous}$ and $E_{equilibrium}$ of osteoblasts (n = 43), chondrocytes (n = 50), adult stem cells (n = 52), and mesenchymal stem cells (n = 67) were 6.5 ± 2.7 and 4.5 ± 2.3 kPa, 1.8 ± 1.7 and 1.0 ± 1.6 kPa, 2.5 ± 1.2 and 1.7 ± 1.1 kPa, and 3.2 ± 2.2 and 2.3 ± 2.1 kPa, respectively [116]
Human bone marrow–derived mesenchymal stem cells	Micropipette aspiration + $E_{instantaneous}$ and $E_{equilibrium}$	Values of $E_{instantaneous}$ and $E_{equilibrium}$ of human mesenchymal stem cells were 518 ± 280 and 126 ± 81 Pa, respectively [113]
Human embryonic stem cells with chondrogenical differentiation; primary articular chondrocytes	Unconfined creep cytocompression + $E_{instantaneous}$ and $E_{equilibrium}$	Values of $E_{instantaneous}$ and $E_{equilibrium}$ of human embryonic stem cells (n > 10), chondrogenically differentiated human embryonic stem cells (n > 10), and articular chondrocytes (n > 10) were 0.53 ± 0.33 and 0.37 ± 0.20 kPa, 1.83 ± 0.75 and 1.09 ± 0.44 kPa, and 1.33 ± 0.37 and 1.14 ± 0.31 kPa, respectively [121]

(continued)

Table 2 (continued)

Cell types	Techniques and quantified parameters	Key results
Human mesenchymal stem cells with adipogenesis or osteogenesis	Micropipette aspiration + $E_{instantaneous}$ and $E_{equilibrium}$	Values of $E_{instantaneous}$ and $E_{equilibrium}$ of undifferentiated human mesenchymal stem cells, stem cells with adipogenesis, and stem cells with osteogenesis were 466 ± 87 and 116 ± 15 Pa, 420 ± 52 and 87 ± 23 Pa, and 890 ± 219 and 224 ± 40 Pa, respectively [114]
Undifferentiated and early differentiating mouse embryonic stem cells	AFM + $E_{elastic}$	Values of $E_{elastic}$ of undifferentiated (n > 10) and early differentiating mouse embryonic stem cells (n > 10) were 1.49 ± 0.09 and 16.07 ± 1.48 kPa, respectively, when using a pyramidal tip, and 0.2176 ± 0.015 and 0.4473 ± 0.036 kPa, respectively, when using a spherical tip [117]
Undifferentiated and early differentiating mouse and human embryonic stem cells	Microfluidic hydrodynamic stretcher + deformability	Deformabilities of undifferentiated (n = 3535) and early differentiating mouse embryonic stem cells (n = 1046) were 1.68 and 1.54, respectively; for undifferentiated (n = 2523) and early differentiating human embryonic stem cells (n = 2283), they were 1.82 and 1.59, respectively [98]
Human mesenchymal stem cells	AFM + $E_{elastic}$	Values of $E_{elastic}$ of mesenchymal stem cells (n > 10) were 15.4 ± 1.9 kPa for the cytoplasm and 11.9 ± 2.2 kPa for the nucleus portions [118]
Human amniotic fluid stem cells and murine osteoblast (OB6) cells	AFM + $E_{elastic}$	Values of $E_{elastic}$ of human amniotic fluid stem cells were 32.9 ± 3.66 kPa for the cytoskeleton and 13.9 ± 2.25 kPa for the nucleus portions; for OB6, they were 42.8 ± 3.44 and 26.9 ± 3.41 kPa, respectively [119]

(continued)

Table 2 (continued)

Cell types	Techniques and quantified parameters	Key results
Human adipose–derived stem cells	AFM + $E_{elastic}$	Values of $E_{elastic}$ of live (n > 10) and dead human adipose–derived stem cells (n > 10) were 1.27 and 18.61 kPa, respectively [120]
Bone marrow–derived human mesenchymal stem cells with differentiation toward smooth muscle cells	Micropipette aspiration + $E_{instantaneous}$ and $E_{equilibrium}$	Values of $E_{instantaneous}$ and $E_{equilibrium}$ of differentiating stem cells toward smooth muscle cells were 622.9 ± 114.2 and 144.3 ± 11.6 Pa, respectively—significantly higher than those values of undifferentiated stem cells [115]

3 Established Approaches for Quantifying Cellular Mechanical Properties

3.1 AFM

Because of increasing interest in the characterization of cellular mechanical properties, several approaches have been developed (Fig. 1) to quantify the intrinsic mechanical properties of individual cells [5, 122–124]. Among them, AFM has been proven to be a valuable tool for probing individual cellular surfaces at specific locations to measure the localized elasticity (Fig. 1a). Typically, a pyramidal or spherical probe tip attached to a flexible cantilever is pressed into the cellular surface for a set distance and then the deflection of the cantilever is measured using a laser beam, with mathematical models used to estimate the stiffness of the probed surface [15–24, 125].

Upon changing the external conditions, the change in elasticity of a cell membrane, quantified using AFM, is much greater than the change in the morphology of the cell, based on the following four factors [74, 88, 126, 127]. The first is the depth of indentation. For small indentation depths, histograms of the relative values of the Young's modulus describe regions rich in the network of actin filaments; for large indentation depths, however, the modulus represents the stiffness of the whole cell, typically accompanied by a decrease in its value (see Fig. 2a, b). The second factor is the effect of the substrate used for cell attachment, potentially leading to different Young's moduli for cells originating from the same tumor type (see Fig. 2c). The third parameter is the load rate, which can lead to significant differences in modulus after fitting with the Hertz model (see Fig. 2d). The fourth factor is linked to the

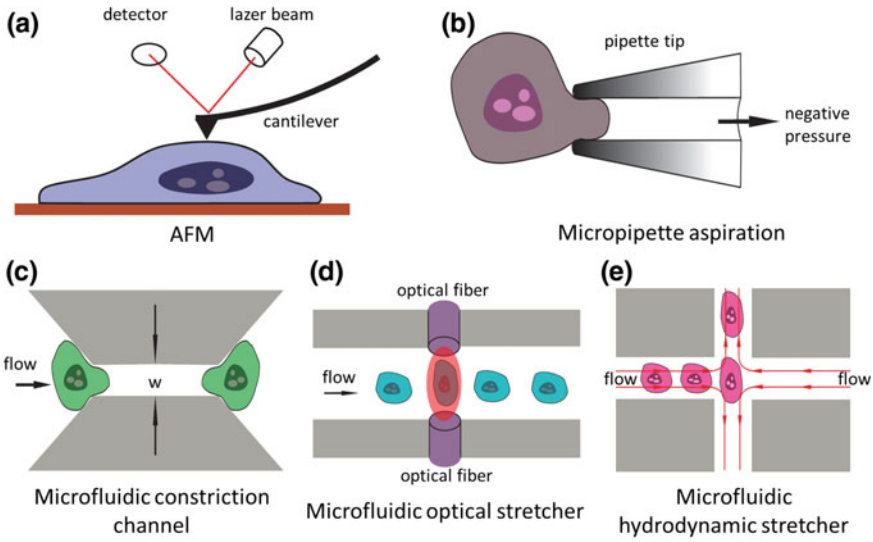

Fig. 1 Techniques enabling characterization of the mechanical properties of single cells. **a** AFM, where a sharp tip at the free end of a flexible cantilever generates a local deformation on the cell surface, an indicator of the cellular mechanical properties. **b** Micropipette aspiration, where a cell is deformed by applying suction through a micropipette placed on the surface of the cell to infer the cellular elastic responses, based on recorded geometrical changes. **c** A microfluidic constriction channel, where differences in hydraulic pressure squeeze cells through a channel having a small cross-sectional area, with the cell's transit time recorded as an indicator of its mechanical properties. **d** A microfluidic optical stretcher, where a two-beam laser trap is formed to serially deform single suspended cells, under optically induced surface forces, to measure mechanical properties of single cells. **e** A microfluidic hydrodynamic stretcher, where the cell under measurement is exposed to fluid stresses and the corresponding deformations are collected as stiffness indicators

position and time of the cell poking event, because the force curves, recorded at constant positions, usually manifest a narrow histogram that may not reflect the stiffness of a whole cell (see Fig. 2e, f).

3.2 Micropipette Aspiration

Micropipette aspiration is a well-established technique that enables determination of cellular mechanical properties through aspiration of the surface of a cell into a small glass tube with the leading edge of its surface tracked (see Fig. 1b). Interpretation of the measured data, using basic continuum models, leads to values for a cell's elastic and viscous properties. In particular, based on the equivalent model (e.g., a liquid surrounded by an elastic cortical shell), neutrophils were found to have a cortical surface tension of approximately 30 pN/μm and a viscosity on the order of 100 Pa s. On the other hand, chondrocytes and endothelial cells behave as homogeneous elastic solids with quantified elastic moduli on the order of 500 Pa [25].

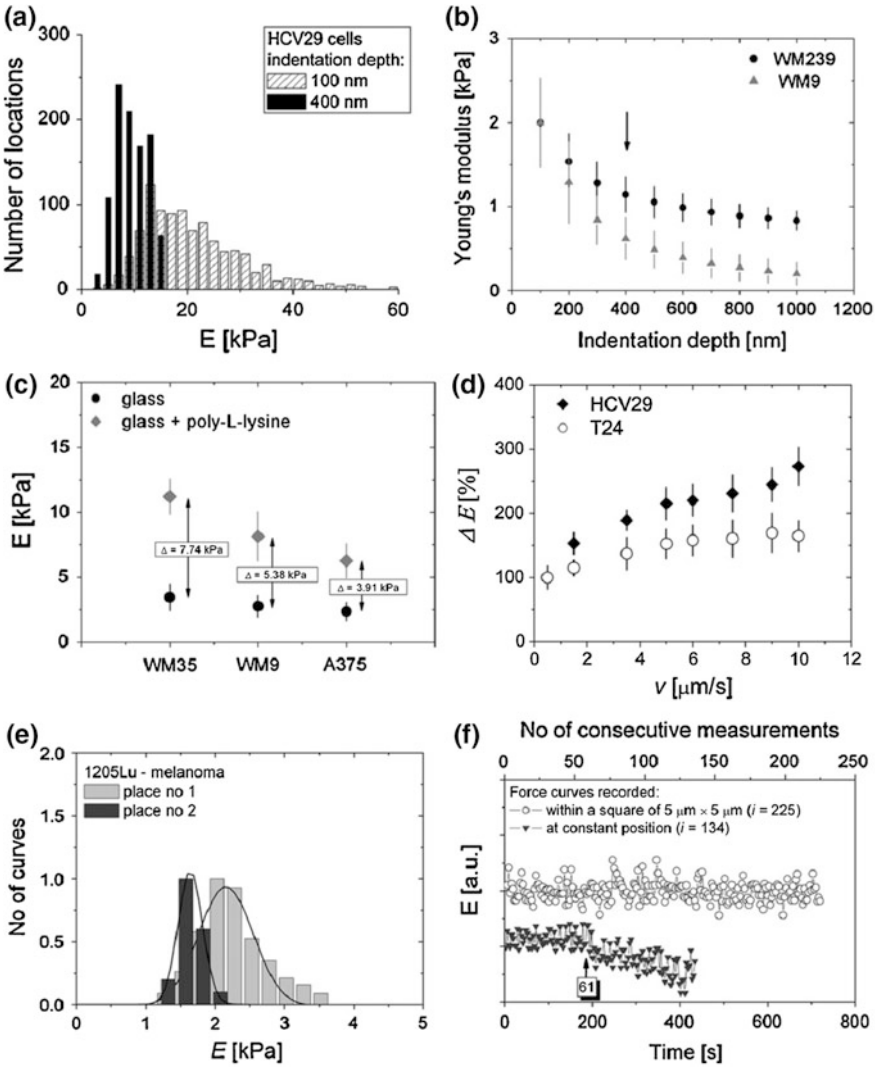

Fig. 2 Factors influencing the mechanical properties of single cells probed using AFM. **a** Young's moduli determined at tip indentation depths of 100 and 400 nm (nonmalignant HCV29 bladder cell). **b** Young's moduli determined as a function of tip indentation depth [human melanoma cell lines: WM239 (skin) and WM9 (lymph node metastasis)]. **c** Influence of surface properties on Young's modulus, quantified using AFM (WM35-primary melanoma, and two metastatic cell lines: WM9 and A375). **d** Changes in Young's modulus as a function of the tip scanning rate (nonmalignant and malignant human bladder cells). **e** Effect of the relative positions of cell poking on cellular Young's modulus (melanoma 1205Lu). **f** Effect of repeated cell poking on the quantification of Young's modulus (nonmalignant and malignant human bladder cells). Reproduced with permission from ref. [74]. Copyright 2012, Elsevier Ltd

Compared with AFM, micropipette aspiration deforms a cell in a more global manner, leading to more accurate characterization of cellular mechanical properties. Although precise, this technique requires skilled manual operation and proceeds with very low throughput (<1 cell/10 min) [4]. To address this issue, an automated micropipette aspiration setup was recently proposed where a micromanipulator, a motorized translation stage, and a custom-built pressure system to position a micropipette were controlled with real-time visual feedback to accurately measure cell deformations online. This system still suffers, however, from the issue of low throughput, with the mechanical properties reported from only approximately 30 cells for each cell type [128, 129].

4 Emerging Microfluidic Tools for Characterization of Cellular Mechanical Properties

Microfluidics is a science and technology related to the processing and manipulation of small volumes of fluids (from 10^{-9} to 10^{-18} l) in channels having dimensions on the scale of tens of micrometers [130–132]. The micrometer-scale dimensions of the devices match well with the size of a typical biological cell, making microfluidics an ideal platform for cell studies [133–137]. More specifically, microfluidics has been used for characterizing biochemical (e.g., gene and protein) and/or biophysical (mechanical and electrical) properties of cells at the single-cell level [138–144].

In the field of microfluidics-based characterization of cellular mechanical properties, three major approaches have been developed so far [26–29]: microfluidic constriction channels [39–41, 94–97, 145–162] (see Fig. 1d), microfluidic optical stretchers [92, 93, 163, 164] (see Fig. 1e), and microfluidic hydrodynamic stretchers [98] (see Fig. 1f). Compared with conventional techniques, these microfluidic approaches display significantly higher throughput, enabling the collection of data from large numbers of cells.

4.1 Microfluidic Constriction Channel

The microfluidic constriction channel is designed to operate by evaluating the transition process as cells pass through microchannels having cross-sectional areas smaller than the dimensions of a single cell (see Fig. 3). An attractive feature of this technique is the ability to achieve higher throughput than those of conventional approaches (e.g., micropipette aspiration) for cellular mechanical characterization (up to ca. 1 cell/s). This technique was first used to evaluate the mechanical properties of red blood cells [39–41, 145–152, 165], and then further expanded to study the deformability of white blood cells [153] and tumor cells [94–97, 154].

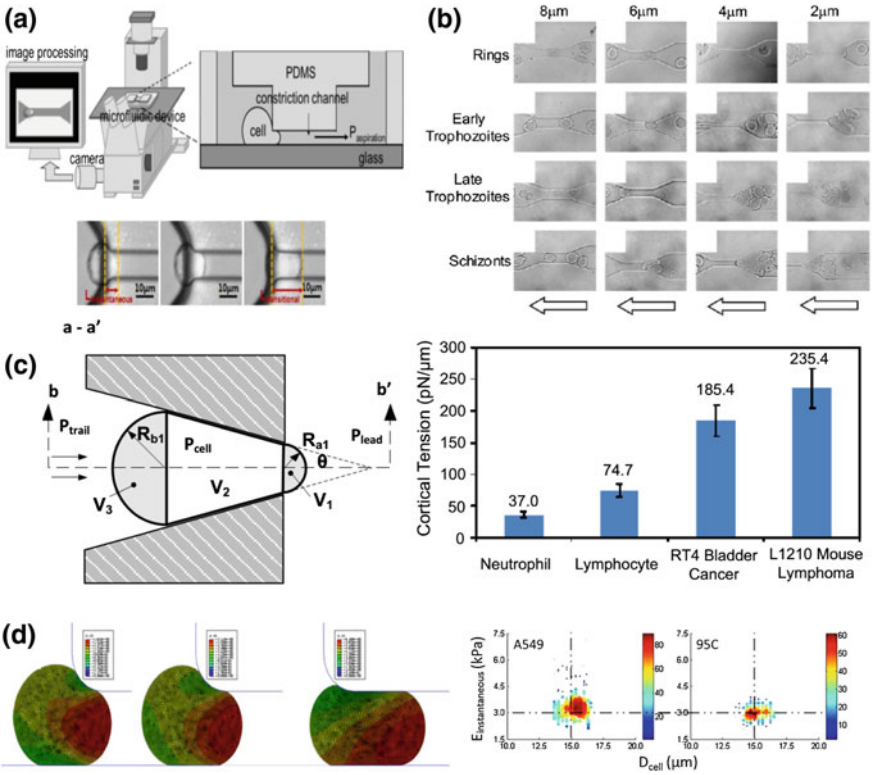

Fig. 3 Experimental setup and key application results of microfluidic constriction channels used for the characterization of cellular mechanical properties. **a** Schematic and raw experimental images of a microfluidic constriction channel for the characterization of cellular mechanical properties, where hydraulic pressure differences squeeze cells through a channel having a small cross-sectional area, with the cell transit time recorded as an indicator of the mechanical properties. Reproduced with permission from ref. [157]. Copyright 2014, Elsevier Ltd. **b** Four sequences of video images recorded during four stages of malaria-infected red blood cells (early ring stage, early trophozoite, late trophozoite, schizont) passing through constriction channels. Ring-stage-infected erythrocytes retained much of the structural characteristics of normal erythrocytes and could pass through all constricted channels. Early trophozoite and late trophozoite-infected cells passed through the larger (8 and 6 μm) channels, but eventually blocked the smaller (4 and 2 μm) channels. Schizont-stage-infected erythrocytes blocked all but the 8 μm channel. The arrows indicate the direction of flow. Reproduced with permission from ref. [39]. Copyright 2003, the National Academy of Sciences of the USA. **c** Models of the cellular entry process into the constriction channel, enabling quantification of the cortical tensions of blood cells and tumor. Reproduced with permission from ref. [158]. Copyright 2012, Royal Society of Chemistry. **d** Numerical simulations of the cellular entry process into the constriction channel, using a cellular viscoelastic model, rather than a liquid droplet model, and taking cellular friction with constriction channel walls into consideration, enabling quantification of the instantaneous Young's moduli of single cells. Reproduced with permission from ref. [157]. Copyright 2014, Elsevier Ltd

Initially, the cellular entry time and transit velocity through the constriction channel were used as biophysical markers to evaluate the cellular mechanical properties. These parameters cannot reflect the intrinsic cellular mechanical properties because they are highly dependent on the cellular sizes. To tackle this issue, several groups have modeled the cellular entry process into the constriction channel, with the purpose of translating cell-dependent mechanical biomarkers into size-independent parameters [155–159].

Lim et al. modeled the cellular entry process into the constriction channel using numerical simulations, suggesting that the cell entry time depends strongly on the cortical stiffness [159]. Ma et al. simplified the cellular entry process and quantified the cortical tension of blood and tumor cells as the first reported use of the constriction channel design to characterize size-independent mechanical properties [158, 160]. Chen et al. used numerical simulations to model the cellular entry process into the constriction channel, employing a cellular viscoelastic model, rather than a liquid droplet model, thereby enabling the quantification of the instantaneous Young's moduli of single cells [157]. In addition, because small constriction channels are prone to clogging, constriction channels with adjustable cross-sectional areas have also been proposed to address the clogging issue to a certain extent [161, 162].

4.2 Microfluidic Optical Stretcher

In an optical stretcher, a two-beam laser trap is used to serially deform single suspended cells, through optically induced surface forces, and, thereby, measure the mechanical properties of single cells (see Fig. 4). This technique has been integrated with microfluidic channels and operates on spherically symmetrical cells in suspension [92, 93, 163, 164]. It was first used to classify MCF-10, MCF-7, and mod-MCF-7 cells, revealing a fivefold increase in deformability for cancer cells relative to benign counterparts [92, 93].

Furthermore, the microfluidic optical stretcher has been used to quantify acute leukemia cells during differentiation therapy, revealing significant softening of neutrophils during the differentiation process [163]. In addition, the compliance of cells from cell lines and primary samples of healthy donors and cancer patients has been measured using the microfluidic optical stretcher, revealing that cancer cells were 3.5 times more compliant than cells from healthy donors [164].

The microfluidic optical stretcher does, however, have two significant limitations. First, its throughput remains at approximately 1 cell/min, and it cannot be improved significantly. This limitation is due to the trade-off between higher optical forces and increased optical power leading to significant heating of the measured cells. Second, the quantified cellular deformability is not an intrinsic biomechanical marker because it depends on the cellular size and the characterization conditions.

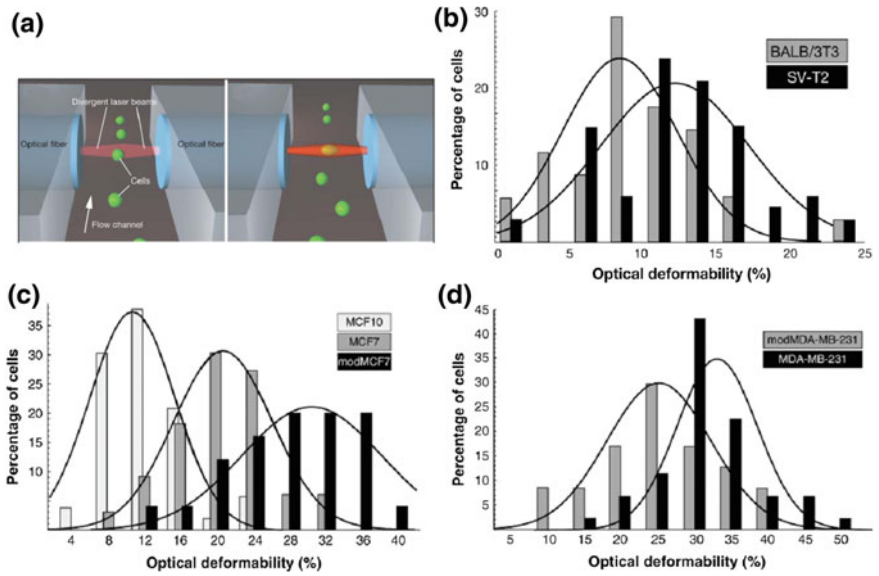

Fig. 4 Experimental setup of and key results from microfluidic optical stretchers used for the characterization of cellular mechanical properties. **a** Schematic representation of a microfluidic optical stretcher; a two-beam laser trap is used to serially deform a single suspended cell, through optically induced surface forces, to measure the mechanical properties of the cell. **b** The optical deformability of malignantly transformed SV-T2 fibroblasts is significantly higher than that of normal BALB/3T3 fibroblasts ($OD_{BALB/3T3}$ = 8.4 ± 1.0; $OD_{SV\text{-}T2}$ = 11.7 ± 1.1). **c** Optical deformabilities of three populations of MCF cell lines: $OD_{MCF\text{-}10}$ = 10.5 ± 0.8; $OD_{MCF\text{-}7}$ = 21.4 ± 1.1; $OD_{modMCF\text{-}7}$ = 30.4 ± 1.8. **d** Two populations of MDA-MB-231 cell lines are clearly distinguishable in the histograms of the measured optical deformability ($OD_{MDA\text{-}MB\text{-}231}$ = 33.7 ± 1.4; $OD_{modMDA\text{-}MB\text{-}231}$ = 24. 4 ± 2.5). Reproduced with permission from ref. [93]. Copyright 2005, Biophysical Society

4.3 Microfluidic Hydrodynamic Stretcher

In a microfluidic hydrodynamic stretcher, fluid stresses are generated by elaborately designing channel geometries, which are used to deform single cells. The rigidity of RBCs has been investigated using shear flow in narrowing channels [166] and extensional flow in hyperbolic converging channels [167]. Recently, inertial focusing is used to deliver cells uniformly to a stretching extensional flow, where cells are deformed at high strain rates, while a high-speed camera records images that can be used to extract biophysical parameters (see Fig. 5) [98]. Unlike the techniques discussed above, this approach is capable of ultrahigh throughput (ca. 1000 cells/s). It has been used to quantify native populations of leukocytes and malignant cells in pleural effusions; the experimental deformability data can be used to predict disease states in patients with cancer or immune activation, with a sensitivity of 91 % and a specificity of 86 %.

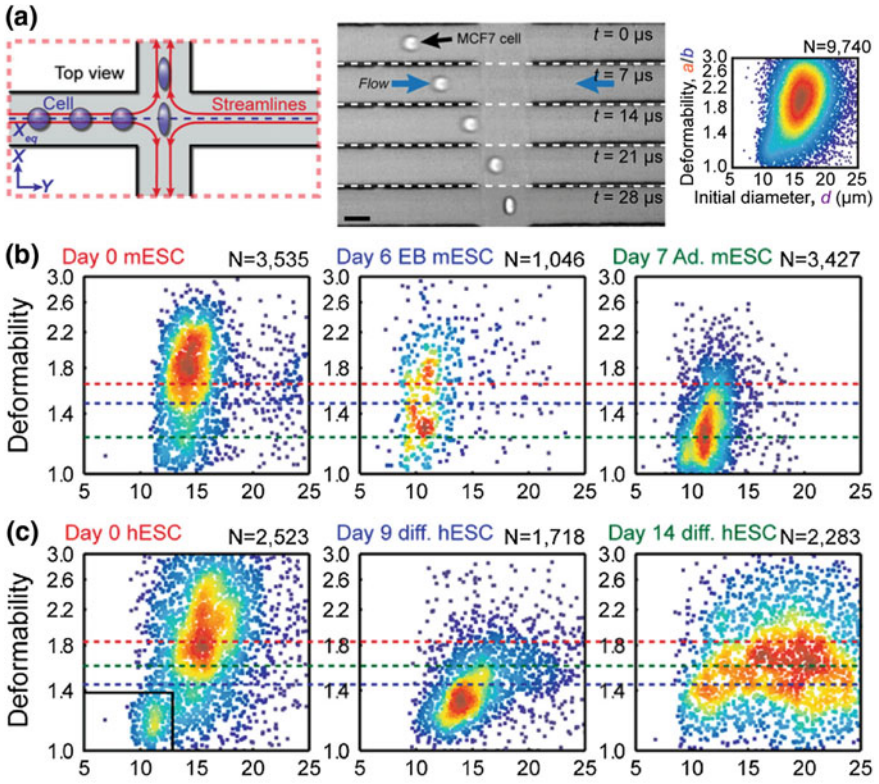

Fig. 5 Experimental setup of and key results from microfluidic hydrodynamic stretchers used for characterization of cellular mechanical properties. **a** Schematic representation, raw experimental images, and quantified deformability of the microfluidic hydrodynamic stretcher for characterization of cellular mechanical properties, where single cells under measurement are exposed to fluid stresses and the corresponding deformations are collected as stiffness indicators. **b**, **c** Decreased deformability has been correlated with increased stem cell pluripotency for **b** mouse embryonic stem cells and **c** human embryonic stem cells. Reproduced with permission from ref. [98]. Copyright 2012, the National Academy of Sciences of the USA

5 Conclusion

Various proof-of-concept approaches have been developed for the characterization of the mechanical properties of single cells, enabling correlations to be made between cellular mechanical properties and cellular biophysical statuses. Nevertheless, to convince the wider cell biology and clinical communities of the merits of cellular biophysical biomarkers, much research effort remains to be exerted in the development of both equipment and applications.

For conventional approaches (e.g., AFM and micropipette aspiration) capable of collecting size-independent intrinsic biophysical markers (e.g., instantaneous and

equilibrium Young's moduli), the issue of low throughout (ca. 1 cell per 10 min) without the capability of collecting statistically significant data remains problematic. For microfluidic approaches enabling high-throughput characterization of the biomechanical properties of single cells (ca. 1000 cells/s), the collected parameters remain dependent on the cell size and experimental conditions (e.g., pressure drop, channel geometry). Thus, further technical developments remain necessary to enable characterization of the intrinsic biophysical properties of single cells in a high-throughput manner.

Furthermore, the correlations between biophysical markers and the biochemical properties of single cells should be explored further. It is possible to design experiments to characterize both cellular biophysical (e.g., Young's modulus) and biochemical markers, including genetic and protein information, simultaneously, potentially revealing correlations between these biophysical and biochemical markers. This process should also provide a comprehensive understanding of cellular status at the single-cell level, paving the foundation for further studies of cell biology.

Acknowledgment We thank the National Basic Research Program of China (973 Program, Grant No. 2014CB744600), the National Natural Science Foundation of China (Grant Nos. 61201077, 61431019 and 81261120561), the National High Technology Research and Development Program of China (863 Program, Grant No. 2014AA093408), and the Beijing NOVA Program of Science and Technology for financial support.

References

1. Ethier CR, Simmons CA (2007) Introductory biomechanics: from cells to organisms. Cambridge texts in biomedical engineering, vol xiii. Cambridge University Press, Cambridge, 511 p, [16] p. of plates
2. Fletcher DA, Mullins RD (2010) Cell mechanics and the cytoskeleton. Nature 463 (7280):485–492
3. Lim CT, Zhou EH, Quek ST (2006) Mechanical models for living cells—a review. J Biomech 39(2):195–216
4. Di Carlo D (2012) A mechanical biomarker of cell state in medicine. J Lab Autom 17(1):32–42
5. Lee GYH, Lim CT (2007) Biomechanics approaches to studying human diseases. Trends Biotechnol 25(3):111–118
6. Diez-Silva M et al (2010) Shape and biomechanical characteristics of human red blood cells in health and disease. MRS Bull 35(5):382–388
7. Lim CT, Li A (2011) Mechanopathology of red blood cell diseases—Why mechanics matters. Theor Appl Mech Lett 1(1):014000
8. Suresh S (2007) Biomechanics and biophysics of cancer cells. Acta Biomater 3(4):413–438
9. Katira P, Bonnecaze RT, Zaman MH (2013) Modeling the mechanics of cancer: effect of changes in cellular and extra-cellular mechanical properties. Front Oncol 3:145
10. Zhang W et al (2013) A brief review of the biophysical hallmarks of metastatic cancer cells. Cancer Hallm 1(2–3):59–66
11. Kovach MA, Standiford TJ (2012) The function of neutrophils in sepsis. Curr Opin Infect Dis 25(3):321–327

12. Keefer CL, Desai JP (2011) Mechanical phenotyping of stem cells. Theriogenology 75 (8):1426–1430
13. Li D et al (2011) Role of mechanical factors in fate decisions of stem cells. Regenerative Med 6(2):229–240
14. Discher DE, Mooney DJ, Zandstra PW (2009) Growth factors, matrices, and forces combine and control stem cells. Science 324(5935):1673–1677
15. Lehenkari PP et al (2000) Adapting atomic force microscopy for cell biology. Ultramicroscopy 82(1–4):289–295
16. Charras GT, Horton MA (2002) Single cell mechanotransduction and its modulation analyzed by atomic force microscope indentation. Biophys J 82(6):2970–2981
17. Radmacher M (2002) Measuring the elastic properties of living cells by the atomic force microscope. Methods Cell Biol 68:67–90
18. Alonso JL, Goldmann WH (2003) Feeling the forces: atomic force microscopy in cell biology. Life Sci 72(23):2553–2560
19. Costa KD (2003) Single-cell elastography: probing for disease with the atomic force microscope. Dis Markers 19(2–3):139–154
20. Costa KD (2006) Imaging and probing cell mechanical properties with the atomic force microscope. Methods Mol Biol 319:331–361
21. Kuznetsova TG et al (2007) Atomic force microscopy probing of cell elasticity. Micron 38 (8):824–833
22. Lekka M, Laidler P (2009) Applicability of AFM in cancer detection. Nat Nanotechnol 4 (2):72
23. Kirmizis D, Logothetidis S (2010) Atomic force microscopy probing in the measurement of cell mechanics. Int J Nanomed 5:137–145
24. Shi X et al (2012) Living cell study at the single-molecule and single-cell levels by atomic force microscopy. Nanomedicine 7(10):1625–1637
25. Hochmuth RM (2000) Micropipette aspiration of living cells. J Biomech 33(1):15–22
26. Kim DH et al (2009) Microengineered platforms for cell mechanobiology. Annu Rev Biomed Eng 11:203–233
27. Zheng Y, Sun Y (2011) Microfluidic devices for mechanical characterisation of single cells in suspension. Micro Nano Lett 6(5):327–331
28. Mao X, Huang TJ (2012) Exploiting mechanical biomarkers in microfluidics. Lab Chip 12 (20):4006–4009
29. Zheng Y et al (2013) Recent advances in microfluidic techniques for single-cell biophysical characterization. Lab Chip 13(13):2464–2483
30. White NJ et al (2014) Malaria. Lancet 383(9918):723–735
31. Grayson M (2012) Malaria. Nature 484(7395):1
32. Miller LH et al (2002) The pathogenic basis of malaria. Nature 415(6872):673–679
33. Suresh S et al (2005) Connections between single-cell biomechanics and human disease states: gastrointestinal cancer and malaria. Acta Biomater 1(1):15–30
34. Nash GB et al (1989) Abnormalities in the mechanical properties of red blood cells caused by Plasmodium falciparum. Blood 74(2):855–861
35. Paulitschke M, Nash GB (1993) Membrane rigidity of red blood cells parasitized by different strains of Plasmodium falciparum. J Lab Clin Med 122(5):581–589
36. Glenister FK et al (2002) Contribution of parasite proteins to altered mechanical properties of malaria-infected red blood cells. Blood 99(3):1060–1063
37. Mills JP et al (2004) Nonlinear elastic and viscoelastic deformation of the human red blood cell with optical tweezers. Mech Chem Biosyst 1(3):169–180
38. Bambardekar K et al (2008) Measuring erythrocyte deformability with fluorescence, fluid forces, and optical trapping. J Biomed Opt 13(6):064021
39. Shelby JP et al (2003) A microfluidic model for single-cell capillary obstruction by Plasmodium falciparum infected erythrocytes. Proc Natl Acad Sci USA 100(25):14618–14622

40. Handayani S et al (2009) High deformability of Plasmodium vivax-infected red blood cells under microfluidic conditions. J Infect Dis 199(3):445–450
41. Bow H et al (2011) A microfabricated deformability-based flow cytometer with application to malaria. Lab Chip 11(6):1065–1073
42. Rees DC, Williams TN, Gladwin MT (2010) Sickle-cell disease. Lancet 376(9757):2018–2031
43. Cancado RD (2012) Sickle cell disease: looking back but towards the future. Rev Bras Hematol Hemoter 34(3):175–177
44. Darlison MW, Modell B (2013) Sickle-cell disorders: limits of descriptive epidemiology. Lancet 381(9861):98–99
45. Fottrell E, Osrin D (2013) Sickle cell anaemia in a changing world. PLoS Med 10(7): e1001483
46. Evans E, Mohandas N, Leung A (1984) Static and dynamic rigidities of normal and sickle erythrocytes. Major influence of cell hemoglobin concentration. J Clin Invest 73(2):477–488
47. Nash GB, Johnson CS, Meiselman HJ (1984) Mechanical properties of oxygenated red blood cells in sickle cell (HbSS) disease. Blood 63(1):73–82
48. Nash GB, Johnson CS, Meiselman HJ (1986) Influence of oxygen tension on the viscoelastic behavior of red blood cells in sickle cell disease. Blood 67(1):110–118
49. Evans EA, Mohandas N (1987) Membrane-associated sickle hemoglobin: a major determinant of sickle erythrocyte rigidity. Blood 70(5):1443–1449
50. Itoh T, Chien S, Usami S (1992) Deformability measurements on individual sickle cells using a new system with pO2 and temperature control. Blood 79(8):2141–2147
51. Itoh T, Chien S, Usami S (1995) Effects of hemoglobin concentration on deformability of individual sickle cells after deoxygenation. Blood 85(8):2245–2253
52. Barabino GA, Platt MO, Kaul DK (2010) Sickle cell biomechanics. Annu Rev Biomed Eng 12:345–367
53. Ballas SK, Mohandas N (2004) Sickle red cell microrheology and sickle blood rheology. Microcirculation 11(2):209–225
54. Ferlay J et al (2015) Cancer incidence and mortality worldwide: Sources, methods and major patterns in GLOBOCAN 2012. Int J Cancer 136(5):E359–E386
55. Ruddon RW (2007) Cancer biology, vol xiv, 4th ed. Oxford University Press, New York, 530 p
56. Weinberg RA (2007) The biology of cancer. Garland Science, Taylor and Francis, New York, London
57. Jonietz E (2012) Mechanics: the forces of cancer. Nature 491(7425):S56–S57
58. Ward KA et al (1991) Viscoelastic properties of transformed cells: role in tumor cell progression and metastasis formation. Biorheology 28(3–4):301–313
59. Thoumine O, Ott A (1997) Comparison of the mechanical properties of normal and transformed fibroblasts. Biorheology 34(4–5):309–326
60. Wu ZZ et al (2000) Comparison of the viscoelastic properties of normal hepatocytes and hepatocellular carcinoma cells under cytoskeletal perturbation. Biorheology 37(4):279–290
61. Zhang G et al (2002) Mechanical properties of hepatocellular carcinoma cells. World J Gastroenterol 8(2):243–246
62. Anderson K et al (1991) In vitro studies of deformation and adhesion properties of transformed cells. Cell Biophys 18(2):81–97
63. Saab MB et al (2013) Differential effect of curcumin on the nanomechanics of normal and cancerous Mammalian epithelial cells. Cell Biochem Biophys 65(3):399–411
64. Sarna M et al (2013) Nanomechanical analysis of pigmented human melanoma cells. Pigm Cell Melanoma Res 26(5):727–730
65. Andolfi L et al (2014) Investigation of adhesion and mechanical properties of human glioma cells by single cell force spectroscopy and atomic force microscopy. PLoS One 9(11): e112582
66. Liu H et al (2014) Biophysical characterization of bladder cancer cells with different metastatic potential. Cell Biochem Biophys 68(2):241–246

67. Omidvar R et al (2014) Atomic force microscope-based single cell force spectroscopy of breast cancer cell lines: an approach for evaluating cellular invasion. J Biomech 47 (13):3373–3379
68. Osmulski P et al (2014) Nanomechanical biomarkers of single circulating tumor cells for detection of castration resistant prostate cancer. Prostate 74(13):1297–1307
69. Ramos JR et al (2014) The softening of human bladder cancer cells happens at an early stage of the malignancy process. Beilstein J Nanotechnol 5:447–457
70. Rother J et al (2014) Atomic force microscopy-based microrheology reveals significant differences in the viscoelastic response between malign and benign cell lines. Open Biology 4(5):140046
71. Xu W et al (2012) Cell stiffness is a biomarker of the metastatic potential of ovarian cancer cells. PLoS One 7(10):e46609
72. Watanabe T et al (2012) Higher cell stiffness indicating lower metastatic potential in B16 melanoma cell variants and in (−)-epigallocatechin gallate-treated cells. J Cancer Res Clin Oncol 138:859–866
73. Plodinec M et al (2012) The nanomechanical signature of breast cancer. Nat Nanotechnol 7 (11):757–765
74. Lekka M et al (2012) Cancer cell recognition–mechanical phenotype. Micron 43(12):1259–1266
75. Ketene AN et al (2012) The effects of cancer progression on the viscoelasticity of ovarian cell cytoskeleton structures. Nanomedicine 8(1):93–102
76. Bastatas L et al (2012) AFM nano-mechanics and calcium dynamics of prostate cancer cells with distinct metastatic potential. Biochim Biophys Acta 1820(7):1111–1120
77. Jonas O, Mierke CT, Kas JA (2011) Invasive cancer cell lines exhibit biomechanical properties that are distinct from their noninvasive counterparts. Soft Matter 7(24):11488–11495
78. Cross SE et al (2011) Green tea extract selectively targets nanomechanics of live metastatic cancer cells. Nanotechnology 22(21):215101
79. Wang J et al (2009) Atomic force microscope study of tumor cell membranes following treatment with anti-cancer drugs. Biosens Bioelectron 25(4):721–727
80. Iyer S et al (2009) Atomic force microscopy detects differences in the surface brush of normal and cancerous cells. Nat Nanotechnol 4(6):389–393
81. Lekka M et al (1999) Elasticity of normal and cancerous human bladder cells studied by scanning force microscopy. Eur Biophys J 28(4):312–316
82. Lekka M et al (2001) The effect of chitosan on stiffness and glycolytic activity of human bladder cells. Biochim Biophys Acta 1540(2):127–136
83. Cross SE et al (2007) Nanomechanical analysis of cells from cancer patients. Nat Nanotechnol 2(12):780–783
84. Cross SE et al (2008) AFM-based analysis of human metastatic cancer cells. Nanotechnology 19(38):384003
85. Docheva D et al (2010) Effect of collagen I and fibronectin on the adhesion, elasticity and cytoskeletal organization of prostate cancer cells. Biochem Biophys Res Commun 402 (2):361–366
86. Tang X et al (2014) A mechanically-induced colon cancer cell population shows increased metastatic potential. Molecular Cancer 13:131
87. Faria EC et al (2008) Measurement of elastic properties of prostate cancer cells using AFM. Analyst 133(11):1498–1500
88. Li QS et al (2008) AFM indentation study of breast cancer cells. Biochem Biophys Res Commun 374(4):609–613
89. Leporatti S et al (2009) Cytomechanical and topological investigation of MCF-7 cells by scanning force microscopy. Nanotechnology 20(5):055103
90. Fuhrmann A et al (2011) AFM stiffness nanotomography of normal, metaplastic and dysplastic human esophageal cells. Phys Biol 8(1):015007

91. Coughlin MF et al (2013) Cytoskeletal stiffness, friction, and fluidity of cancer cell lines with different metastatic potential. Clin Exp Metastas 30(3):237–250
92. Lincoln B et al (2004) Deformability-based flow cytometry. Cytometry Part A 59A(2):203–209
93. Guck J et al (2005) Optical deformability as an inherent cell marker for testing malignant transformation and metastatic competence. Biophys J 88(5):3689–3698
94. Mak M, Erickson D (2013) A serial micropipette microfluidic device with applications to cancer cell repeated deformation studies. Integr Biology 5(11):1374–1384
95. Khan ZS, Vanapalli SA (2013) Probing the mechanical properties of brain cancer cells using a microfluidic cell squeezer device. Biomicrofluidics 7(1):11806
96. Byun S et al (2013) Characterizing deformability and surface friction of cancer cells. Proc Natl Acad Sci 110(19):7580–7585
97. Hou HW et al (2009) Deformability study of breast cancer cells using microfluidics. Biomed Microdevices 11(3):557–564
98. Gossett DR et al (2012) Hydrodynamic stretching of single cells for large population mechanical phenotyping. Proc Natl Acad Sci USA 109(20):7630–7635
99. Hotchkiss RS, Karl IE (2003) The pathophysiology and treatment of sepsis. N Engl J Med 348(2):138–150
100. Bone RC (1991) The pathogenesis of sepsis. Ann Intern Med 115(6):457–469
101. Yodice PC et al (1997) Neutrophil rheologic changes in septic shock. Am J Respir Crit Care Med 155(1):38–42
102. Alves-Filho JC et al (2008) The role of neutrophils in severe sepsis. Shock 30(Suppl 1):3–9
103. Worthen GS et al (1989) Mechanics of stimulated neutrophils: cell stiffening induces retention in capillaries. Science 245(4914):183–186
104. Poschl JM, Ruef P, Linderkamp O (2005) Deformability of passive and activated neutrophils in children with Gram-negative septicemia. Scand J Clin Lab Invest 65(4):333–339
105. Skoutelis AT et al (2000) Neutrophil deformability in patients with sepsis, septic shock, and adult respiratory distress syndrome. Crit Care Med 28(7):2355–2359
106. Linderkamp O et al (1998) Passive deformability of mature, immature, and active neutrophils in healthy and septicemic neonates. Pediatr Res 44(6):946–950
107. Inoue Y et al (2006) A neutrophil elastase inhibitor, sivelestat, improves leukocyte deformability in patients with acute lung injury. J Trauma 60(5):936–943
108. Nishino M et al (2005) Serial changes in leukocyte deformability and whole blood rheology in patients with sepsis or trauma. J Trauma 59(6):1425–1431
109. Tanaka H et al (2001) Granulocyte colony-stimulating factor (G-CSF) stiffens leukocytes but attenuates inflammatory response without lung injury in septic patients. J Trauma 51 (6):1110–1116
110. Lovell-Badge R (2001) The future for stem cell research. Nature 414(6859):88–91
111. Krupalnik V, Hanna JH (2014) Stem cells: The quest for the perfect reprogrammed cell. Nature 511(7508):160–162
112. Chamberlain JS (2006) Stem-cell biology: a move in the right direction. Nature 444 (7119):552–553
113. Tan SC et al (2008) Viscoelastic behaviour of human mesenchymal stem cells. BMC Cell Biology 9:40
114. Yu H et al (2010) Mechanical behavior of human mesenchymal stem cells during adipogenic and osteogenic differentiation. Biochem Biophys Res Commun 393(1):150–155
115. Khani MM et al (2014) Evaluation of mechanical properties of human mesenchymal stem cells during differentiation to smooth muscle cells. Ann Biomed Eng 42(7):1373–1380
116. Darling EM et al (2008) Viscoelastic properties of human mesenchymally-derived stem cells and primary osteoblasts, chondrocytes, and adipocytes. J Biomech 41(2):454–464
117. Pillarisetti A et al (2011) Mechanical phenotyping of mouse embryonic stem cells: increase in stiffness with differentiation. Cell Reprogram 13(4):371–380
118. Ruiz JP et al (2012) The effect of nicotine on the mechanical properties of mesenchymal stem cells. Cell Health Cytoskelet 4:29–35

119. Aryaei A, Jayasuriya AC (2013) Mechanical properties of human amniotic fluid stem cells using nanoindentation. J Biomech 46(9):1524–1530
120. Hu K, Zhao F, Wang Q (2013) Mechanical characterization of living and dead undifferentiated human adipose-derived stem cells by using atomic force microscopy. Proc Inst Mech Eng [H]: J Eng Med 227(12):1319–1323
121. Ofek G et al (2009) Mechanical characterization of differentiated human embryonic stem cells. J Biomech Eng 131(6):061011
122. Van Vliet KJ, Bao G, Suresh S (2003) The biomechanics toolbox: experimental approaches for living cells and biomolecules. Acta Mater 51(19):5881–5905
123. Lim CT et al (2006) Experimental techniques for single cell and single molecule biomechanics. Mater Sci Eng, C 26(8):1278–1288
124. Addae-Mensah KA, Wikswo JP (2008) Measurement techniques for cellular biomechanics in vitro. Exp Biol Med 233(7):792–809
125. Guo Q et al (2012) Characterization of cell elasticity correlated with cell morphology by atomic force microscope. J Biomech 45(2):304–309
126. Pogoda K et al (2012) Depth-sensing analysis of cytoskeleton organization based on AFM data. Eur Biophys J 41(1):79–87
127. Lekka M et al (2012) Cancer cell detection in tissue sections using AFM. Arch Biochem Biophys 518(2):151–156
128. Shojaei-Baghini E et al (2013) Mechanical characterization of benign and malignant urothelial cells from voided urine. Appl Phys Lett 102(12):123704
129. Shojaei-Baghini E, Zheng Y, Sun Y (2013) Automated micropipette aspiration of single cells. Ann Biomed Eng 41(6):1208–1216
130. Wootton RC, Demello AJ (2010) Microfluidics: exploiting elephants in the room. Nature 464 (7290):839–840
131. Whitesides GM (2006) The origins and the future of microfluidics. Nature 442(7101):368–373
132. Squires TM, Quake SR (2005) Microfluidics: fluid physics at the nanoliter scale. Rev Mod Phys 77(3):977
133. Sackmann EK, Fulton AL, Beebe DJ (2014) The present and future role of microfluidics in biomedical research. Nature 507(7491):181–189
134. El-Ali J, Sorger PK, Jensen KF (2006) Cells on chips. Nature 442(7101):403–411
135. Meyvantsson I, Beebe DJ (2008) Cell culture models in microfluidic systems. Annu Rev Anal Chem 1:423–449
136. Paguirigan AL, Beebe DJ (2008) Microfluidics meet cell biology: bridging the gap by validation and application of microscale techniques for cell biological assays. BioEssays 30 (9):811–821
137. Velve-Casquillas G et al (2010) Microfluidic tools for cell biological research. Nano Today 5(1):28–47
138. Thompson AM et al (2014) Microfluidics for single-cell genetic analysis. Lab Chip 14(17):3135–3142
139. Yin H, Marshall D (2012) Microfluidics for single cell analysis. Curr Opin Biotechnol 23(1):110–119
140. Lecault V et al (2012) Microfluidic single cell analysis: from promise to practice. Curr Opin Chem Biol 16(3–4):381–390
141. Ryan D, Ren K, Wu H (2011) Single-cell assays. Biomicrofluidics 5(2):21501
142. Zare RN, Kim S (2010) Microfluidic platforms for single-cell analysis. Annu Rev Biomed Eng 12:187–201
143. Sims CE, Allbritton NL (2007) Analysis of single mammalian cells on-chip. Lab Chip 7(4):423–440
144. Di Carlo D, Lee LP (2006) Dynamic single-cell analysis for quantitative biology. Anal Chem 78(23):7918–7925
145. Quinn DJ et al (2011) Combined simulation and experimental study of large deformation of red blood cells in microfluidic systems. Ann Biomed Eng 39(3):1041–1050

146. Diez-Silva M et al (2012) Pf155/RESA protein influences the dynamic microcirculatory behavior of ring-stage Plasmodium falciparum infected red blood cells. Sci Rep 2:614
147. Zheng Y et al (2012) High-throughput biophysical measurement of human red blood cells. Lab Chip 12(14):2560–2567
148. Huang S et al (2013) Dynamic deformability of Plasmodium falciparum-infected erythrocytes exposed to artesunate in vitro. Integr Biol 5(2):414–422
149. Wu T, Feng JJ (2013) Simulation of malaria-infected red blood cells in microfluidic channels: passage and blockage. Biomicrofluidics 7(4):44115
150. Zheng Y et al (2013) Electrical measurement of red blood cell deformability on a microfluidic device. Lab Chip 13(16):3275–3283
151. Zheng Y et al (2014) Characterization of red blood cell deformability change during blood storage. Lab Chip 14(3):577–583
152. Myrand-Lapierre M-E et al (2015) Multiplexed fluidic plunger mechanism for the measurement of red blood cell deformability. Lab Chip 15(1):159–167
153. Rosenbluth MJ, Lam WA, Fletcher DA (2008) Analyzing cell mechanics in hematologic diseases with microfluidic biophysical flow cytometry. Lab Chip 8(7):1062–1070
154. Chen J et al (2011) Classification of cell types using a microfluidic device for mechanical and electrical measurement on single cells. Lab Chip 11(18):3174–3181
155. Lee LM, Liu AP (2015) A microfluidic pipette array for mechanophenotyping of cancer cells and mechanical gating of mechanosensitive channels. Lab Chip 15(1):264–273
156. Tsai CH et al (2014) A new dimensionless index for evaluating cell stiffness-based deformability in microchannel. IEEE Trans Bio-Med Eng 61(4):1187–1195
157. Luo YN et al (2014) A constriction channel based microfluidic system enabling continuous characterization of cellular instantaneous Young's modulus. Sens Actuators B: Chem 202:1183–1189
158. Guo Q, Park S, Ma H (2012) Microfluidic micropipette aspiration for measuring the deformability of single cells. Lab Chip 12(15):2687–2695
159. Leong FY et al (2011) Modeling cell entry into a micro-channel. Biomech Model Mechanobiol 10(5):755–766
160. Guo Q et al (2012) Microfluidic biomechanical assay for red blood cells parasitized by Plasmodium falciparum. Lab Chip 12(6):1143–1150
161. Beattie W et al (2014) Clog-free cell filtration using resettable cell traps. Lab Chip 14 (15):2657–2665
162. Huang SB et al (2014) A clogging-free microfluidic platform with an incorporated pneumatically-driven membrane-based active valve enabling specific membrane capacitance and cytoplasm conductivity characterization of single cells. Sens Actuators B: Chem 190:928–936
163. Lautenschlager F et al (2009) The regulatory role of cell mechanics for migration of differentiating myeloid cells. Proc Natl Acad Sci USA 106(37):15696–15701
164. Remmerbach TW et al (2009) Oral cancer diagnosis by mechanical phenotyping. Cancer Res 69(5):1728–1732
165. Chen B, Guo F, Xiang H (2011) Visualization study of motion and deformation of red blood cells in a microchannel with straight, divergent and convergent sections. J Biol Phys 37 (4):429–440
166. Forsyth AM et al (2010) The dynamic behavior of chemically "stiffened" red blood cells in microchannel flows. Microvasc Res 80(1):37–43
167. Lee SS et al (2009) Extensional flow-based assessment of red blood cell deformability using hyperbolic converging microchannel. Biomed Microdevices 11(5):1021–1027

Cytometry of Single Cells for Biology and Biomedicine

James F. Leary

Abstract Flow and image cytometry are mature single-cell analysis technologies that have been developed over the past 50 years. Fluorescence has been the primary mode of generating single-cell signals. There are now hundreds of different color fluorescent probes linked to thousands of different molecules including antibodies, ligands, and other molecules. Increasingly sophisticated commercial flow cytometry instruments measure multiple colors (e.g., 17 or more colors per cell) of fluorescence per single cell. Often these fluorescent labels are being used to identify combinations of biomarkers in many human diseases. Recently, microfluidic systems have shown the advantage of either reexamining the same cells at different time points or capturing and treating those cells and measuring their response. These microfluidic structures can combine flow and imaging technologies in the same structure. Other technologies such as PCR can be added to these multifaceted microfluidic structures. The microfluidic devices can be built to provide low-cost, point-of-care medicine. Making multiple correlated measurements per cell is extremely powerful leading to very large amounts of data of high dimensionality. Recently, bioinformatics techniques are being employed to study "big data" from large ensembles of single-cell data. This is leading to questions whether any two single cells are really ever the same if you are able to measure enough parameters at sufficient accuracy? When are two cells similar enough to have similar biology, functions and predictable outcomes when challenged with drugs and/or environmental factors? Single-cell analyses provide us with the tools to answer these intriguing questions.

Keywords Flow cytometry · Image cytometry · Single-cell analysis · Microfluidic cytometry · Multiparameter · Fluorescence

J.F. Leary (✉)
Purdue University, West Lafayette, IN 47907, USA
e-mail: jfleary@purdue.edu

F.-G. Tseng and T.S. Santra (eds.), *Essentials of Single-Cell Analysis*,
Series in BioEngineering, DOI 10.1007/978-3-662-49118-8_9

1 What Is Cytometry and Why Is It Important?

"Cytometry" whether done by flow or scanning image involves making quantitative measurements on single cells. This is important because it allows detection of single cells with properties differing from their neighbors. "Bulk" cell measurements involve measuring properties of a collection of cells which may be heterogeneous. Single-cell properties, unless they are dominant subpopulations, may be completely lost or otherwise averaged by their relative frequency in the total cell population.

In flow cytometry the cell populations are made into a single-cell suspension and run individually past one or more light sources (usually lasers) at speeds from a few hundred cells/sec up to throughput rates of more than 100,000 cells/sec. Scanning image cytometry usually deals with cells attached to surfaces and potentially in contact with each other. To perform single-cell analysis in the case of attached cells, the cell "sheet" must first be separated into single-cell images by a process known as "segmentation." Another important difference between flow cytometry and image cytometry is that in flow cytometry the cells are typically exposed to laser light for only a few microseconds during which fluorescent probes on these cells are not photobleached as they typically are in image cytometry. On the other hand, image cytometry preserves the tissue architecture of the sheet of cells of different types—something very important to pathologists diagnosing diseases on the basis of the positions of cells worth respect to each other in a tissue biopsy.

Why is cytometry of single cells important to biology and medicine? In cell biology it is important to make measurements at single-cell level, typically on the basis of several different molecular properties as labeled by fluorescent probes, to distinguish not only between different cell types but even between cells of the same type under different conditions such as different stages of the cell cycle or whether these cells are healthy or undergoing apoptosis or necrosis. In medicine, it is important to distinguish between diseased cells (e.g., infected or cancer cells) and normal cells at the single-cell level. Otherwise, the presence of diseased cells will be masked by the properties of normal cells which are usually present in much higher numbers. For example, one of the major advances in diagnosis and treatment of leukemias and lymphomas in medicine was the discovery, using cell surface "biomarker" molecules, where there were actually many different types of lymphoma and leukemia which could not be seen based on morphology but could be seen on the basic of immunophenotyping these tumors on the basis of their different expressions of biomarkers. Then a specific treatment could be developed that was highly effective for that particular cancer type. In many cases, the treatment itself involved using antibodies to target therapies to the lymphoma or leukemia cell types (e.g., rituximab monoclonal antibody therapies to non-Hodgkin's lymphoma patients, the first FDA-approved monoclonal antibody therapy). Now there are more than 20 FDA-approved monoclonal antibody therapies for different types of cancer. These therapies are, in general, much more effective than conventional chemotherapeutic drugs and also make huge difference in quality of life to patients.

2 Basic Elements of Cytometry of Single Cells

"Cytometry" literally means measurement of individual cells. It can be accomplished by a variety of techniques, but there are two principal approaches. The first, "flow cytometry," is a "zero resolution" technique whereby single cells flow past excitation sources and the total fluorescence of each color is collected for each cell without capture of images. The second basic approach is to process images of cells on a surface, and process the images to obtain measurable properties of single cells. There also exist hybrid approaches that capture images of cells as they flow past excitation sources.

2.1 Flow Cytometry

"Flow cytometry" involves processing a cell suspension of single cells one cell at a time past one or more light sources. In simplest terms, a flow cytometer by analogy can be thought of as a fluorescence microscope whereby the cells are flowing past the light source rather than being static on a slide (Fig. 1).

In practice, commercially available flow cytometers for single-cell analysis vary from the simple (usually, 2–3 colors of fluorescence with a single excitation source) to the very complicated (e.g., five lasers with 18 colors of fluorescence). If there are multiple spatially separated light sources, as with the five lasers, 18-color fluorescence for example, then the flow cytometer is essentially making very fast and sophisticated time-resolved fluorescence measurements. Fluorescent probes on these cells can be excited at different wavelengths by each laser and their fluorescence collected on different photosensors after passing through optical filters

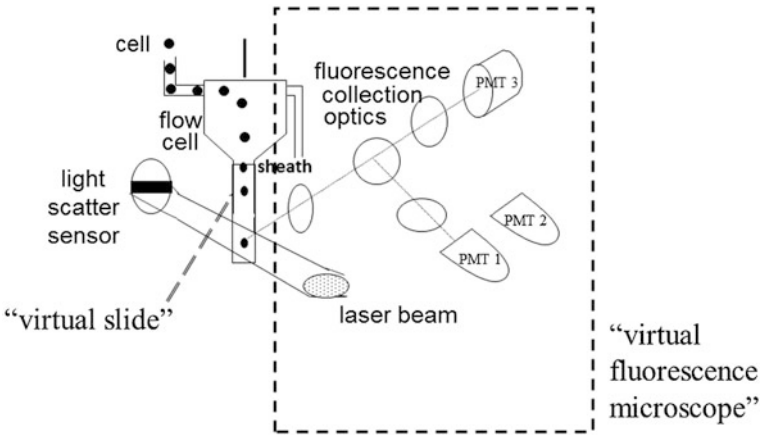

Fig. 1 A flow cytometer is really just another form of a fluorescence microscope

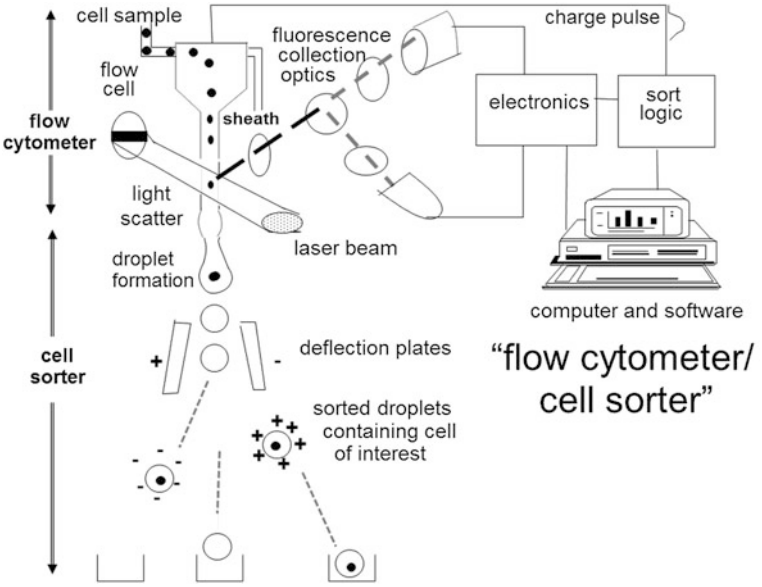

Fig. 2 A flow cytometer/cell sorter is a two-stage system, whereupon the first "flow cytometer" stage is followed by a secondary stage system that allows "sorting" of single cells based on the properties measured in the first stage using a variation of ink-jet printing technology

of fluorescence collection systems that can spectrally separate colors onto different photodetectors. A "cell sorter" is a flow cytometer with a secondary stage of processing based on ink-jet printing whereby cells that are individually measured in the first stage flow cytometer can be individually separated inside individual liquid droplets in the secondary "cell sorting" stage (Fig. 2).

Cell sorting can be thought of as a high-speed micromanipulation of single cells accomplished by electrostatically manipulating the droplets containing these cells at very high speeds. In microfluidic or lab-on-a-chip cytometry systems the cell separation can be done by a variety of techniques including direct cell manipulation through use of valve structures or even by optical trapping methods.

2.2 Scanning Image Cytometry

In scanning image cytometry, the cells are attached to a surface and may, or may not, be spatially separated into single cells. If connected to each other in a cell sheet, then the image processing system must find a way of not only exciting individual cells (usually through a slit or spot of light that is smaller than individual cells) but also must separate the cells using image analysis software "segmentation" algorithms. This is much harder to accomplish. Hence, image cytometry systems are

inherently slower (and more complicated) than flow cytometry systems but can also contain additional information not available to flow cytometry systems such as cell size and shape and the positional relationships between the different cells that can reveal tissue architecture. This tissue architecture information is destroyed in the process of preparing single-cell suspension for flow cytometry.

2.3 Microfluidic Cytometry

There is currently a renaissance going on in the development of new "microfluidic cytometry" whereby flow cytometers are being miniaturized into very small and portable devices. For examples of microfluidic cytometry developed as portable devices for point-of-care, see these references [1, 2]. This will change the paradigm of cell samples being brought to large centrally located facilities with complicated instruments that must be operated by highly trained operators. Instead, the instruments are small enough to be brought to the sample, for example, as "point-of-care" devices for doctors' offices or in the field where they can be coupled with GPS chips to also record where the measurements were taken. These microfluidic cytometers can also be coupled to telecommunications technology (e.g., cell phones or satellite phone) to transmit the data back to scientists or physicians. Microfluidic cytometers can also be part of a more multipurpose "lab-on-a-chip" device that can contain other technologies such as cell imaging, and PCR amplification of cell DNA and RNA sequences.

3 Importance of Multiple, Correlated Measurements per Cell

3.1 Quantitative, Correlated Single-Cell Measurements

The acquisition of multiple, correlated measurements per cell obtained by flow or image cytometry, is extremely powerful and is yet another example of "big data" whereby many gigabytes or terabytes of data can be collected per day. Initially, each fluorescence measurement was taken as analog measurements sometimes with log amplification circuitry, converted through and analog-to-digital converter and stored at relatively low bit resolution (e.g., eight-bit (255 channels) or 10-bit (1024 channels)). Initially, this data was binned into histograms for each molecular parameter identified by a specific fluorescent color (Fig. 3). Recent progress in digital signal processing electronics has led to rapid digitization out to as much as 24-bit precision without much of any further linear or log amplification and also a considerable reduction of these electronics in terms of both size and power

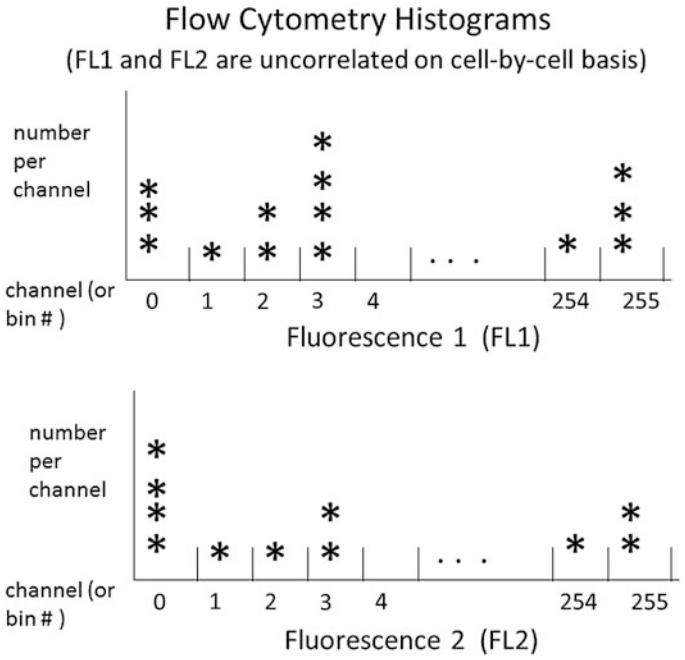

Fig. 3 Each property measured on single cells in a flow or image cytometer can be "binned" into histograms where the similarity of cells is governed by the "bit resolution" of the measurements

requirements as well as considerable reduction of cost which then permits much greater portability of these systems.

3.2 The Power of "Listmode" Data Formats for Correlated Single-Cell Measurements

It was quickly realized that data could be stored cell-by-cell in a "listmode" data file (Fig. 4), whereby the entire experiment could be replayed or reanalyzed under a variety of scenarios. The standardization of listmode file structures and header information then permitted a variety of researchers and software vendors to develop increasingly powerful software (both commercial and open-source) to analyze these data.

Initially, this data was mostly examined by manually displaying simple histograms or bivariate data displays and doing simple human pattern recognition and manual formation of various Boolean logic gates through the data. This was such a laborious process that much of the data in many experiments was only quickly and simply analyzed losing much of the advantages of collecting large and sophisticated data analysis files. But as the complexity of the data grew through a huge expansion

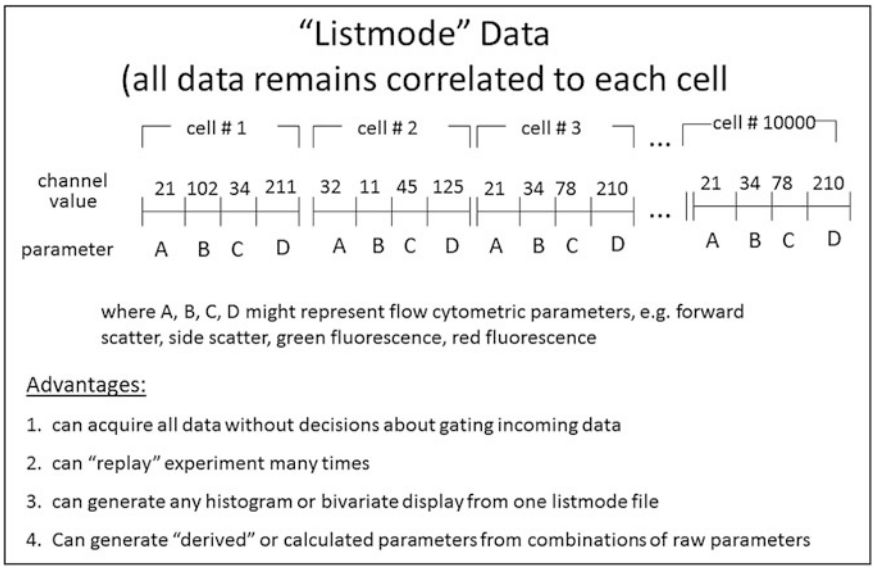

Fig. 4 If all measurements on each cell are maintained correlated to that single cell and are stored as a "list" of data points, then all possible correlations and relationships between the different measurable parameters can be explore in this "listmode" data format

of the number of commercially available fluorescent probes available (now in the thousands) and the growth in the number of colors of fluorescence collected per cell from 2 to 3 colors out to as many as 18 colors or more, as well as the speed of measurements, cytometry has now crossed into the arena of "big data." This has led to the development of automated data analysis techniques with conventional flow cytometry data analysis techniques and more recently into the arena of bioinformatics software with far more sophisticated algorithms including unsupervised data analysis techniques that have started to remove experimenters from their data in the same way as has happened with genomics data.

3.3 Analysis and Display of Cytometry Data

Cytometric data for single cells are traditionally displayed as histograms of single parameters or attempts to display higher dimensional data as a collection of two-dimensional "bivariate" displays. Early in the history of cytometry, it was appreciated that two-dimensional visualization and analysis of data could reveal relationships not visible in analyses of uncorrelated histograms as shown in Fig. 5.

What has still not been appreciated by many in the cytometry community is the fact that if relationships are hidden when data are reduced (or projected) from two dimensions onto one as in the above figure, why are relationships not hidden when

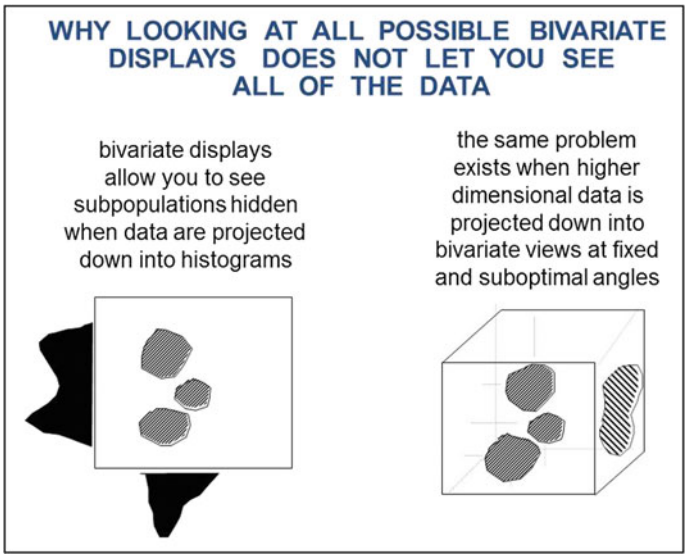

Fig. 5 Whenever higher dimensional data is viewed as a lower dimensional projection, data are projected down on top of each other and information is lost. Even dimensional reduction techniques such as principal component analysis ultimately suffer this same fate

higher dimension data are projected down onto two- or even three dimensions? You simply cannot see all of the relationships in complex multidimensional data by looking at all possible permutations of parameters taken two at a time. The reason is that these bivariate displays only allow visualization at fixed and suboptimal viewing angles. Data in higher dimensions are being projected down on top of each other in these two-dimensional data planes. Attempts to communicate this fact [3] have only been recently appreciated. Use of principal component data dimensionality reduction techniques is being used more often to better visualize higher dimensional cytometry data. But all of these dimensionality reduction techniques still suffer the same fundamental flaws and are driven by the human desire to use human pattern recognition beyond where it should be used. Fortunately, the sheer size and multidimensional complexity of the data are starting to drive the field into use of better techniques which are standard in the field of bioinformatics.

3.4 Bioinformatic Approaches to Cytometry Data for Single Cells

Due to both the growth of the number of fluorescence parameters per cell and higher single-cell throughput rates, cytometry has recently entered the age of "big data." This has led to the development of new bioinformatic approaches to data analysis [4].

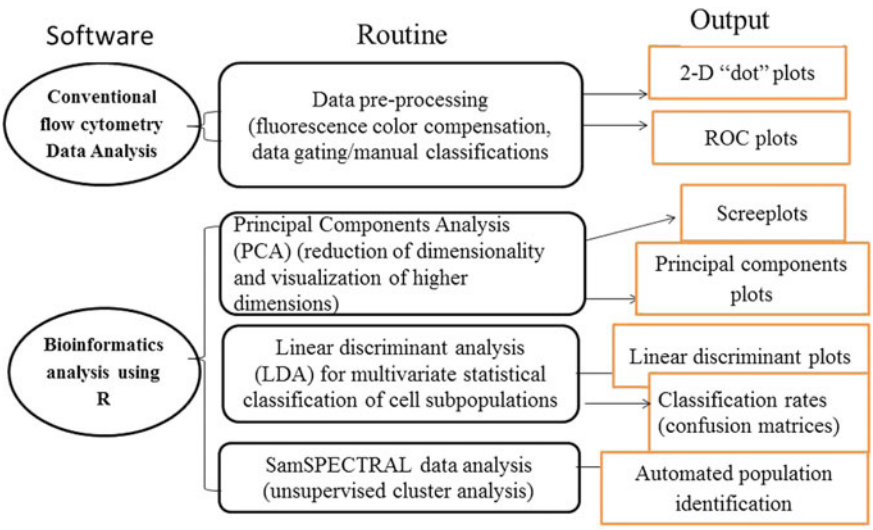

Fig. 6 Recent example from [5] showing conventional and bioinformatic techniques applied to single-cell analyses

Much of this software is freely available as open-source software routines as part of the "R" statistical package. For an example of these bioinformatic techniques applied to rare cells, see [5] in References and Fig. 6 below.

With so many fluorescence parameters per single cell, the dimensionality of the data has increased beyond the capability of human pattern recognition and manual determination of data analysis gates. Batch processing of data files, automated gating, and supervised or unsupervised clustering algorithms reveal the presence of different cell subpopulations.

3.5 Single-Cell Heterogeneity—No Two Cells Are Alike?

Interestingly, this great expansion of flow cytometric parameters per single cell has led researchers to appreciate that probably no two cells are really alike. Our desire to group different single cells into "cell subpopulations" may be overly simplistic. Similarly, our desire to group single cells into one cell subpopulation may suffer from our desire to classify cells as definitely this type of cell or that type of cells, when in fact the single cell is evolving from one type of cell to another and frequently deserves partial membership in more than one cell subpopulation in a kind of fuzzy logic, rather than crisp logic, classification system. This is pretty obvious when looking at the process of cell differentiation. Even cell populations grown from a single-cell clone tend to diverge into separate cell subpopulations when examined in detail at the single-cell level on the basis of many cellular

parameters. If true, this issue of whether any two cells are ever completely alike has many important ramifications for both biology and medicine.

4 Fluorescent Probes for Single-Cell Analyses

There are many types of fluorescent probes, based on their luminescent lifetimes, used to label single cells. Most organic fluorescent probes have fluorescent lifetimes in the range of 2–5 ns. This means that they can be excited/re-excited anywhere from 1000 to 10,000 times while flowing through an exciting light source that typically lasts from 2 to 20 microseconds or in the range of milliseconds in a microfluidic system. Indeed, this is the only reason a flow cytometer works as well as it does.

4.1 Probe Excitation and Fluorescent Emission Basics

The excitation spectrum for a given probe shows what its probability of being excited at a given wavelength, so the probe need not be excited at its excitation maximum but will be less bright when excited at wavelengths away from this maximal excitation wavelength (Fig. 7).

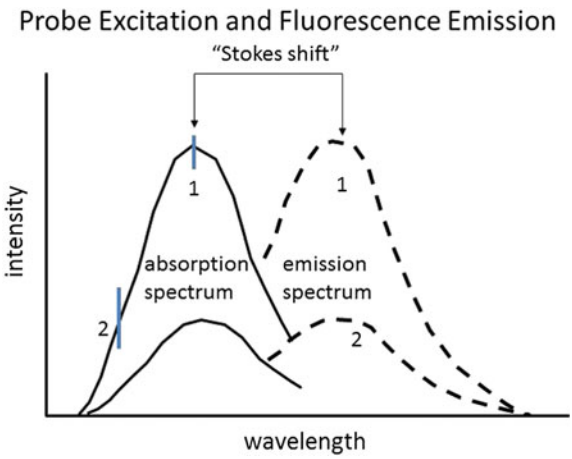

Fig. 7 A fluorescent probe can be excited anywhere within its absorption spectrum and the resulting fluorescence emission wavelength will be the same. But the fluorescence emission intensity will be proportional to the fraction of maximal absorption at the particular exciting wavelength chosen. For example, exciting the probe at *wavelength 1* will result in maximal fluorescence emission, whereas excitation at *wavelength 2* will result in proportionally less fluorescence emission intensity as shown

Delayed fluorescent probes (e.g., Europium chelate dyes) have fluorescent lifetimes roughly 10 times longer than typical organic fluorescent dyes, but that means that they are excited/re-excited 10 times less. However, if the light source is pulsed which means that background cellular fluorescence which is organic will have decayed leaving only the signal from the delayed fluorescent probe. This is of particular use when looking at a relatively small positive fluorescent signal on top of a big fluorescent background of similar wavelength. Nanocrystals (e.g., "quantum dots") have properties similar to delayed fluorescent probes. Phosphorescence and chemiluminescence are typically not used for quantitative analysis in flow cytometers but can be useful in imaging systems because they often are relatively resistance to photobleaching.

4.2 Microscopy and Lasers to Excite Probes

Early single-cell analysis was performed primarily by fluorescence microscopy in only a semi-quantitative way due to photobleaching problems. Flow cytometry was developed at several institutions around the world during the 1960s [6–11]. In 1979 researchers developed the first fluorescence microscope-based flow cytometer by flowing cells in a stream across a slide and through the focal point of the system [12]. When high-speed flow cytometry was invented, it presaged the transition of flow cytometry into the world of "big data" [for review see, 13]. Fluorescent probes can provide highly quantitative measures of molecules present in single cells including actual numbers of molecules per cells if the labeling is well understood and appropriate fluorescent standards are used. Most, but not all, flow cytometers and modern microscopes use lasers to excite single cells because the light beam spatial structure can be tightly controlled and cells flowing through these laser light patterns can be rapidly excited so that photobleaching does not occur in flow cytometers and can be minimized in scanning image cytometers if the light is rapidly pulsed.

In the early days of single-cell analysis by flow cytometry, there were relatively few commercially available fluorescent probes. Most of those probes were optimized for excitation by fluorescence microscope, in particular by the specific lines of mercury arc lamps. Interestingly, many of the early lasers used for single-cell cytometry recapitulated these lines at near UV 365 nm, 405 nm (violet), 514 nm (green) from argon-ion lasers and 568 nm (orange) from krypton-ion lasers. The exception was the 488 nm (blue) laser which was much brighter than the relatively weak blue excitation from the arc lamp. Now most of these same wavelengths have been duplicated in smaller, much less-expensive solid-state lasers and more recently in even smaller and cheaper LEDs suitable for microfluidic cytometry of single cells.

4.3 Parameters and Probes

The number of probes has grown from a small number to many thousands. A good source for a rapid overview of the range of fluorescent probes available for labeling single cells has been compiled over many years by Howard Shapiro [14]. Other sources are either published in the literature [for example, 15] or are available on the internet through probe manufacturer sites. Many of these probes are ligands that bind to single-cell receptors. Other probes intercalate into the membrane or pass through damaged membranes to identify dead or damaged cells.

5 Fluorescence Probes with Targeting Molecules to Label "Biomarkers" on Single Cells

Many of these same probes can be attached to targeting molecules that will bind to just about any molecule on or within single cells. In particular, fluorescent probes have been attached to antibodies which recognize cell surface molecules expressed during cell differentiation, frequently referred to as "biomarkers" because these molecules can be used to identify a wide range of normal and diseased cells. There are now thousands of fluorescently labeled antibodies commercially available. These fluorescent probes can also be attached to other targeting molecules such as peptides and aptamers. Sometimes, the fluorescent probes are singly or multiply integrated into microbeads or nanobeads to produce intensely bright fluorescent probes through bead surfaces which are activated with carboxyl oramine groups which allow for relatively simple chemical attachment of antibodies to these beads.

5.1 Fluorescent Antibody Labeling of Single Cells

There are many strategies for using antibodies to fluorescently label single cells for subsequent analyses. The simplest is to directly couple the fluorescent probe to the antibody and use "direct immunofluorescence." The advantages are simplicity of labeling and direct quantitation of the number of molecules on the cell if the antibodies label all of these molecules and the number of fluorescent probes per antibody is known. But it is actually not quite that simple, since the labeling of fluorescent probes on antibodies follows a Poisson distribution and will be only predictable if there are a large amount of antibodies labeling each cell such that the mean fluorescence per cell equals the mean of the Poisson distribution as shown in Fig. 8.

These means, or Poisson averaged number of fluorescent probes per antibody molecule, are usually called F/P ratios by the probe/antibody vendors. Desirable F/P ratios are in the range 3–6 fluorescent molecules per antibody. If the F/P ratio is

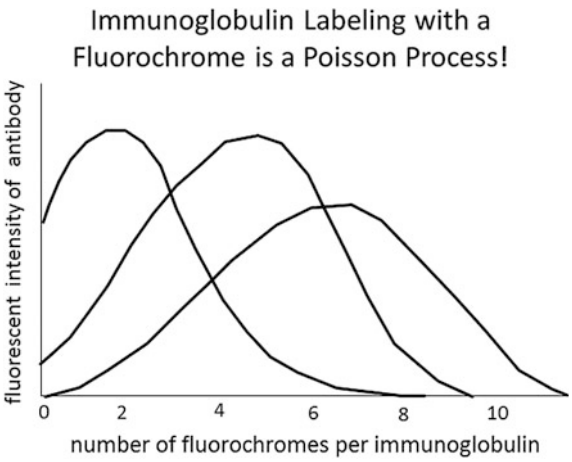

Fig. 8 The number of fluorochrome binds per immunoglobulin (Ig) is a Poisson distribution. Unlabeled Ig will outcompete labeled Ig, and Ig with large numbers of fluorochromes will become increasingly nonspecific. To obtain highest specific brightness, one should stay away from the leftmost curve, and avoid using antibody that has too many fluorochromes (typically more than about 8) per Ig. HPLC purification can also be used to eliminate the unlabeled and over-labeled species and to give a more uniform fluorescence per cell

only 1, then there will be many unlabeled antibodies which tend to outcompete the labeled antibodies leading to diminished fluorescence. If too many fluorescent molecules are attached to antibodies, then they will start binding closer to the antibody binding region of the antibody leading to less specific targeting, so very bright antibodies may also be very nonspecific antibodies!

5.2 Obtaining Quantitative Immunofluorescence on Single Cells

For antibodies to quantitatively and reproducibly label molecules on single cells, it is necessary to titrate the antibody so that the antibody is "in excess" but not too excess. If too much antibody is used, the antibody becomes very nonspecific and labels cells it should not label. If insufficient antibody is used then not all antigenic sites on each single cell will be labeled and the result will be not properly proportional to the true number of molecules present on each single cell. Vendors usually express this relationship by telling the user how much antibody to use on a known number of cells of a specific type, since each cell type has a different amount of receptors for that antibody per single cell. Vendors have performed these titration experiments for known cell types but the user must do these experiments if different cell types are used. This antigen–antibody titration experiment is shown conceptually in Fig. 9.

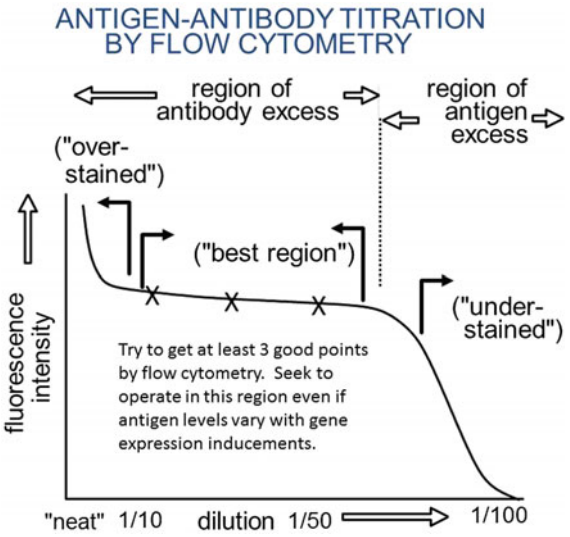

Fig. 9 Immunostaining of single cells is always a titration experiments whereby you want to be in antibody excess to saturate all antigenic sites but not be in too much excess because it will then start staining nonspecifically

5.3 Single-Cell Immunofluorescence Labeling Strategies

Once these concepts have been understood and properly used, immunofluorescence labeling of cells can be performed and single cells can be analyzed by flow cytometry or scanning image cytometry.

5.3.1 Direct Immunofluorescence Labeling of Single Cells

An example of "direct immunofluorescence" labeling of single cells, as well as a proper control, is shown in Fig. 10.

This strategy works very well in most circumstances but requires careful labeling of the antibodies to prevent the generation of subpopulations of antibodies where the fluorescent probe has changed the specificity of the antibody for its antigen. Such a situation is usually caused by fluorescent probes attaching too near the antigen combining site on the tips of the antibody. Unless the F/P ratio gets too high this is unlikely to occur. But nonspecific subpopulations can be removed by HPLC purification and some commercial vendors specifically offer this service for providing more specific antibodies.

5.3.2 Indirect Immunofluorescence Labeling of Single Cells

Sometimes, the number of receptors per single cell is too small to get a good signal. In these cases, one strategy is to amplify the signal per receptors molecule using "indirect immunofluorescence" whereby multiple secondary antibodies which bind

to the primary antibody can provide fluorescent signal amplification of typically 3–5 times as much fluorescence per receptor molecule labeled on a single cell as shown in Fig. 11 along with the proper control.

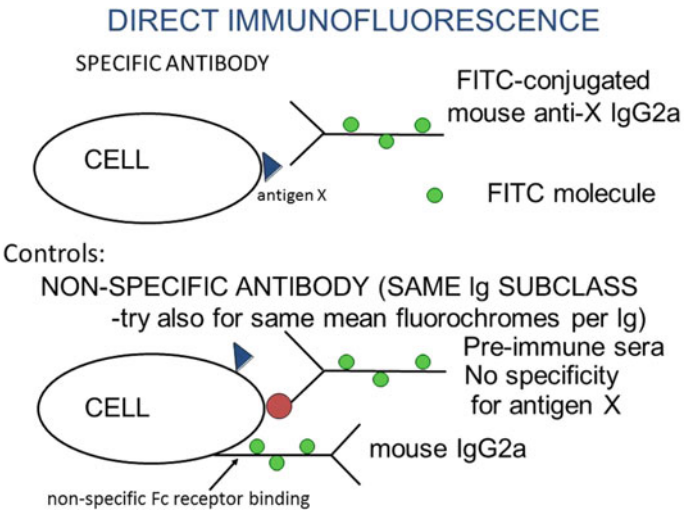

Fig. 10 "Direct immunofluorescence" attaches the fluorescent probe directly to the primary antibody which recognizes the antigen on the single cell

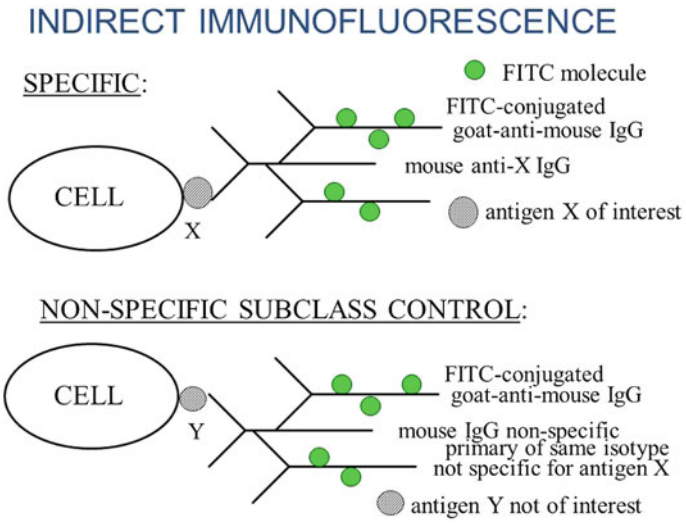

Fig. 11 If primary antibodies are recognized by two or more secondary antibodies containing a fluorescence probe, then the total fluorescence per antigenic site can be amplified

5.3.3 Biotin–Avidin Labeling of Single Cells

A different way to amplify the fluorescent signal is to use "biotin-avidin" labeling strategy. Biotin and avidin have a binding strength as great or greater than antigen and antibody binding. Antibodies can be relatively easily labeled with small biotin molecules and then subsequently recognized with avidin containing a number of fluorescent molecules. Typically, biotin–avidin labeling strategies produce 5–10 times as much fluorescent signal as direct immunofluorescence. Avidins are commercially available in a wide variety of different colors containing different fluorescent probes. Since avidin is a relatively large molecule and must align properly to bind biotin (it contains four biotin binding sites per avidin molecule), molecular "spacer arms" consisting of typically 10–14 hydrocarbon chains are typically employed as shown in Fig. 12.

5.3.4 Fluorescent Nanoparticle–Antibody Labeling of Single Cells

A fourth labeling strategy is to use fluorescent microspheres or nanospheres, usually in the size range of 200–700 nm with carboxyl (COO-) or amine (NH_2) group activated surfaces to allow antibodies to be easily coupled to them as shown in Fig. 13.

These fluorescent spheres can contain large numbers of fluorescent molecules and these fluorescent molecules are usually embedded inside the spheres leading to considerable protection from photobleaching. Immunospheres can be in many different colors and can provide the simplicity of direct immunofluorescence but

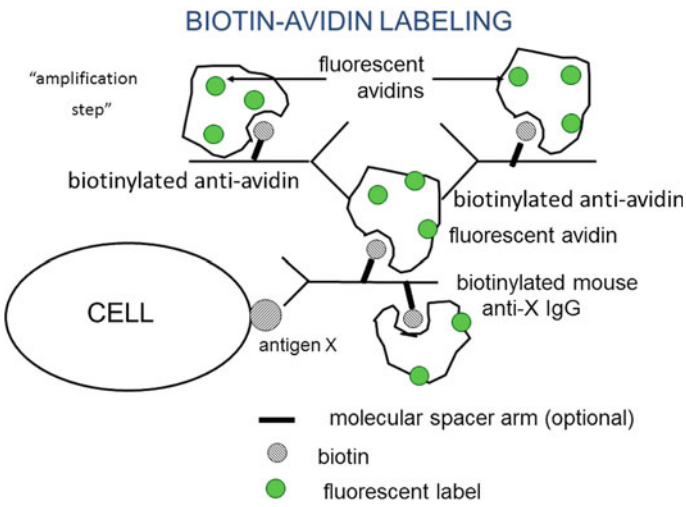

Fig. 12 If primary antibodies are "biotinylated," then avidin containing many fluorescent molecules per avidin molecule can make for much brighter staining

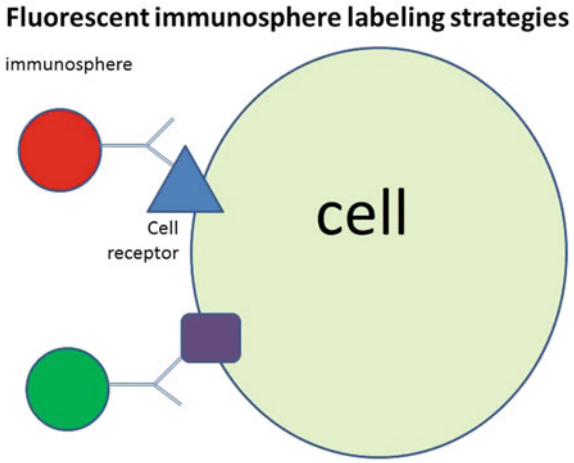

Fig. 13 "Immunospheres" are nano- or micro-sized particles containing one or more fluorescent probes in large quantities. By attaching antibodies directly to their activated surfaces they can provide a much brighter fluorescence than any of the other methods previously discussed

with fluorescent signals that may be 10–100 times stronger, or more depending on the size of the immunosphere. The best size range is about 200–700 nm reflecting a trade-off because the amount of fluorescence is proportional to the volume (cube of the diameter), whereas the amount of steric hindrance (the physical blocking of these particles on the surface of a cell) varies as the cross-sectional area of the immunospheres (the square of the diameter).

6 "Omic" Measurements at Single-Cell Level

Most biomedical proteomic measurements involve "cell-free" mass spectrometry measurements on blood serum or urine. That is not to say that such measurements are not very important and useful, but much useful and potentially important information is lost by ignoring the power of "single-cell proteomics" which is now possible by at least two avenues.

6.1 Phospho-specific Antibodies to Measure Expressed Proteins for "Single-Cell Proteomics"

The recognition that expressed proteins within a cell are usually phosphorylated led to the exciting new field of "single-cell proteomics, whereby antibodies could be generated that could distinguish between the phosphorylated and non-phosphorylated

forms of these proteins within single cells [16]. This unleashes the full power of multicolor fluorescence analysis of single cells by flow or image cytometry. The power to look at the proteomics of single cells on the basis of 10 or more specific proteins is extremely powerful, sometimes more valuable than measuring hundreds or even thousands of proteins on mixed heterogeneous populations of cells for the same reasons as described earlier in this chapter. The conventional mass spectrometry proteomics profiles on mixtures of cells represent the weight-averaged profiles based on the relative frequencies of the individual cell subpopulations present. Unless these subpopulations can otherwise be purified, the measurements on heterogeneous cell mixtures are meaningless. Adding to this problem is the fact argued earlier that perhaps no two single cells are really alike. This has very important implications for problems such as measuring the proteomics of rare circulating tumor cells in cancer patients when following them for detection of minimal residual disease. The hope is to detect aberrant dangerous new clones of cancer when their frequency is still rare and before they overwhelm the patient's immune system. Indeed, this is a frequent cause of patient death after periods of apparent remission when the dangerous clones were not detectable by "bulk cell" and other conventional methods that are not sensitive to the appearance of rare aberrant single cancer cell clones arising from mutations and development of multidrug resistance to cancer therapies.

6.2 Single-Cell Proteomic Measurements by CyTOF Analyses

Recently, a new form of hybrid flow cytometry/mass spectrometry ("CyTOF") has been developed and is now commercially available [17]. In this system the cells flow through a system similar to a flow cytometry instrument except that cells are labeled with antibodies, or other probes, containing rare earth atoms that can be distinguished by mass spectrometry. The single cells are effectively vaporized one at a time and their constituents analyzed by an integrated mass spectrometry system. Such a system provides a way to get around the problems of mass spectrometry of mixed cell populations described in the previous section. It also provides for an even greater number of labeled probes per cell than has yet been achieved by even the most sophisticated multi-laser/multicolor fluorescence systems. While commercial CyTOF instruments are now commercially available, the probes are currently expensive to manufacture.

7 Lab-on-a-Chip Measurements of Single Cells

Lab-on-a-chip approaches allow multiple measurements to be performed on single cells and can employ several technologies. One example of such an approach is a portable microfluidic blood analyzer designed and built for NASA to allow for blood cell analysis on the International Space Station [1, 2]. It consists of a chip/reader combination whereby single cells are optically examined at multiple points along a microfluidic pathway that also magnetically sorts white blood cells from red blood cells so that a pinprick of whole peripheral blood can be directly processed without the need for blood fractionation (Fig. 14).

The system uses antibody coupled superparamagnetic nanoparticles that bind to mature white blood cells, and antibody coupled quantum dot nanoparticles of different colors that bind to various white blood cell subsets important to monitor the immune status of astronauts in the microgravity of space (Fig. 15). The system uses a near UV LED as a light source and solid-state photonic sensors, all of which can be operated using a battery system.

From the preceding discussions, we can see the advantages of combining different approaches in some kind of integrated instrument that could perform both flow cytometry and image analysis on single cells as well as examining the internal contents of each single cell. While many of these systems are still under development, they will soon be commercially available. An integrated "lab-on-a-chip" approach provides many advantages. Its microfluidics system can move single cells past light, or other sources (e.g., electrical impedance), move cells to stations for individual image analysis, and then compartmentalize single cells for exploration of their internal contents both directly and indirectly (using PCR amplification) of

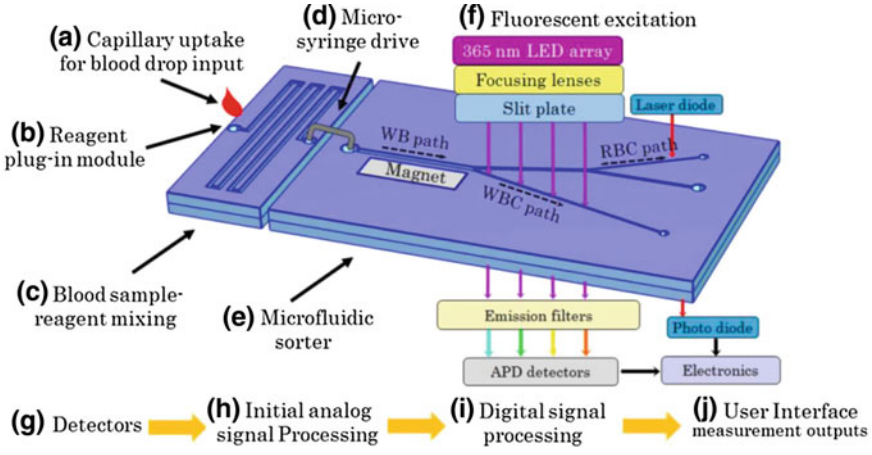

Fig. 14 Schematic of the subcomponents and processes that constitute an integrated portable microcytometer reader, reagent packs, and disposable microfluidic chip. Reprinted with permission from ref. [1]

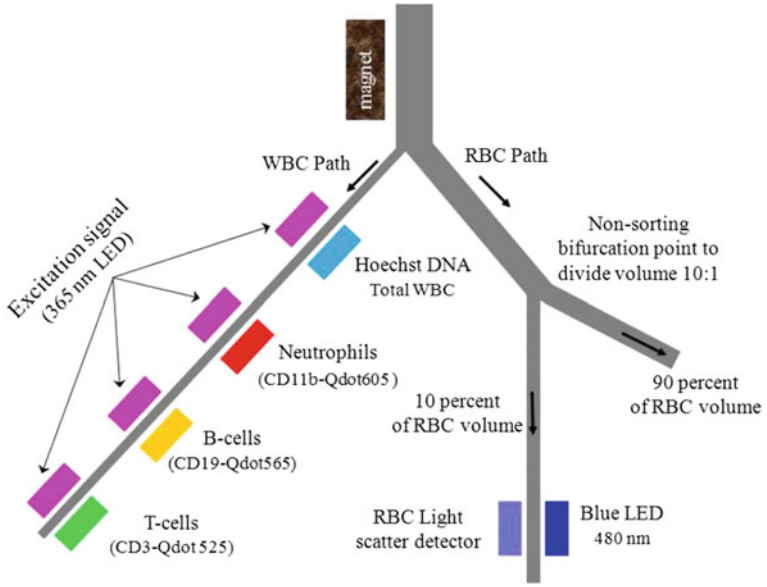

Fig. 15 Top view conceptual schematic of on-chip magnetic WBC sorting and subsequent WBC and RBC counting and classifications. Reprinted with permission from ref. [1]

some of these components. The ability of PCR to expand copies of intracellular molecules in low abundance (even single molecules copies) to detectable levels is powerful.

References

1. Grafton MMG, Maleki T, Zordan MD, Reece LM, Byrnes R, Jones A, Todd P, Leary JF (2011) Microfluidic MEMS hand-held flow cytometer. Proc SPIE 7929:79290C-1–79290C10
2. Maleki T, Fricke T, Quesenberry JT, Todd P, Leary JF (2012) Point-of-care, portable microfluidic blood analyzer system. Proc SPIE 8251:82510C-1–82510C-13
3. Leary JF, McLaughlin SR, Reece LN, Rosenblatt JI, Hokanson JA (1999) Real-time multivariate statistical classification of cells for flow cytometry and cell sorting: a data mining application for stem cell Isolation and Tumor Purging. Proc SPIE 3604:158–169
4. Aghaeepour N, Greg Finak G, The FlowCAP Consortium, The DREAM Consortium, Holger Hoos H, Mosmann TR, Brinkman R, Raphael Gottardo R, Scheuermann RH (2013) Critical assessment of automated flow cytometry data analysis techniques. Nat Meth 10(3):228–238
5. Cooper CL, Leary JF (2015) Advanced flow cytometric analysis of nanoparticle targeting to rare leukemic stem cells in peripheral human blood in a defined model system. In: Proceedings of SPIE 9328, imaging, manipulation, and analysis of biomolecules, cells, and tissues XIII, 02 Mar 2015, p 932810. doi:10.1117/12.2076043
6. Fulwyler MJ (1965) Electronic separation of biological cells by volume. Science 150:910–911
7. Kamentsky LA, Melamed MR (1967) Spectrophotometric cell sorter. Science 156:1364–1365

8. Dittrich W, Gohde W (1969) Impulse fluorometry of single cells in suspension. Z Naturforsch 24:360–361
9. Bonner WA, Hulett HR, Sweet RG, Herzenberg LA (1972) Fluorescence activated cell sorting. Rev Sci Instr 43:404–409
10. Herzenberg LA, Sweet RG, Herzenberg LA (1976) Fluorescence-activated cell sorting. Sci Am 234:108–117
11. Sweet RG (1965) High frequency recording with electrostatically deflected ink jets. Rev Sci Instr 36:131–136
12. Steen HB, Lindmo T (1979) Flow cytometry: a high-resolution instrument for everyone. Science 204(4391):403–440
13. Leary JF (2005) Ultra high speed cell sorting. Cytom Part A 67A:76–85
14. Shapiro HM (2003) Practical flow cytometry, 4th edn. Wiley-Liss, New York
15. Johnson I (1998) Review: fluorescent probes for living cells. Histochem J 30:123–140
16. Krutzik PO, Nolan GP (2003) Intracellular phospho-protein staining techniques for flow cytometry: monitoring single cell signaling events. Cytometry Part A 55A:61–70
17. Bendall SC, Simonds EF, Qiu P, Amir ED, Krutzik PO, Finck R, Bruggner RV, Melamed R, Trejo A, Ornatsky OI, Balderas RS, Plevritis SK, Sachs K, Pe'er D, Tanner SD, Nolan GP (2011) Single-cell mass cytometry of differential immune and drug responses across a human hematopoietic continuum. Science 332(6030):687–696

Single-Cell Genomics and Epigenomics

Fátima Valdés-Mora and Heather J. Lee

Abstract The cell is the fundamental unit of life, in which the blueprint of the genome is transcribed and translated into biological function. Most of our current understanding of the genome, epigenome, and transcriptome is based on analysis of millions of cells as a bulk population. These analyses are highly informative but they do not provide information about the heterogeneity and molecular dynamics that occur within a population of cells, nor any information about an underrepresented cell subpopulation that could have a differential or crucial function in a specific biological context. Thus, single cell analysis is, without doubt, an invaluable approach to understand fundamental biology in embryonic development, normal organs, and disease. Improvements in techniques for the isolation of single cells, whole genome or transcriptome amplification, and genome-wide analysis platforms have allowed high-resolution analysis of the genome and transcriptome, and also have potential to reveal the epigenome map of one cell. In particular, the rapid advances in next-generation sequencing technologies are raising new methodologies in these areas allowing sequencing of the small amounts of DNA and RNA present in single cells. The integration of the knowledge from different types of single cell "omics" datasets will revolutionize the way we understand whole-organism science and will have high impact on both basic biological research and medicine. For example, a combination of single-cell "omics" datasets will be applied to reveal important biological insights, such as: a detailed cell lineage tree in higher organisms; a deep understanding of embryonic development from one single cell onwards; and a dissection of tumor heterogeneity. Integration of genomics and transcriptomics in single cancer cells will also provide valuable

F. Valdés-Mora (✉)
Histone Variants Group. Genomics and Epigenetics Division,
Garvan Institute of Medical Research, 384 Victoria St, Darlinghurst,
NSW 2010, Australia
e-mail: f.valdesmora@garvan.org.au

H.J. Lee
Epigenetics Programme, The Babraham Institute Babraham, CB22 3AT,
Cambridgeshire, UK
e-mail: Heather.lee@babraham.ac.uk

F.-G. Tseng and T.S. Santra (eds.), *Essentials of Single-Cell Analysis*,
Series in BioEngineering, DOI 10.1007/978-3-662-49118-8_10

information about the functional consequences of mutations and copy number variations in these cells. In this chapter, we first review the major technological developments achieved in single cell "omics" as well as the technical challenges to overcome and the potential of future developments. We then describe the impact that these methods would have on normal development and disease and their potential applications. Finally, we discuss our vision of the future developments and breakthroughs of single cell "omics" with a special focus on the integration of all these methods to understand whole-organism biology.

Keywords Single cell genomics · Single cell transcriptomics · Single cell epigenomics · Next-generation sequencing technologies · Whole genome amplification methods · Whole transcriptome amplification methods

1 History of Single Cell "Omics"

Methods for genomic, transcriptomic, and epigenomic analysis (herafter on "omics") at single-cell level allow us to understand complex biological phenomena. Single-cell (SC) omics techniques ranging from isolation methods such as flow cytometry, laser capture microdissection and microfluidics to PCR-based methods and next-generation sequencing (NGS) are used to understand these processes. Although techniques for the isolation of single cells have been around for quite a while, for example fluorescence-activated cell sorting (FACS) from the 1970s and laser capture microdissection (LCM) in the 1990s, the major limitation of the study of single cell "omics" is the lack of sensitivity and the amount of starting material needed to sequence the whole genome, transcriptome or epigenome.

Single-cell transcriptomics was the first successful "omics" data obtained for single cells in 1999 [88], as the methodology for cDNA amplification based on PCR or T7 in vitro transcription followed by microarrays had been already developed. The development of SC genome and exome sequencing methods has proven to be more challenging, taking another 7 years to obtain the first genome map from a single cell [179]; Zhang et al. were able to improve the methods for amplifying chromosomes of single bacteria to produce DNA in sufficient quantity and quality to allow partial genome sequencing [179]. The technology to obtain SC epigenomes has been by far the most challenging area for single cell "omics" (with the exception of noncoding RNAs). It was not until 2013 that Hi-C [104] and DNA methylation [44, 85, 137] were first reported for single cells.

In the past 4 years there has been an exponential growth and advances in methods of isolation single cells (in particular with microfluidics), whole genome or transcriptome amplification, and genome-wide analyses platforms (primarily next-generation sequencing devices and chemistry) leading to major advances in understanding single-cell biology. For example, the amount of starting material needed has dramatically decreased from 1 microgram in 2006 to a 10 nanograms in

2015; however, at present all SC genomic approaches are still based on amplification methods.

SC omics is currently a very hot topic and with lower costs, better technology, and tools for analyses of data, this "new" field will offer huge and accurate information on single cells that will conceptually change the way we understand and study whole organisms and complex diseases.

2 Single Cell Genomics

2.1 Methods for Single Cell Genomics

The analysis of the genome of a single cell starts from the isolation of single cells from a bulk/mixed population of cells. The most prominent methods for isolation single cells as well as single nuclei are explained in detail elsewhere in this book (reviewed in [136], summarized in Fig. 1). Subsequently, the cell is lysed and its genome amplified. A diploid human cell contains approximately 7 pg of genomic DNA, thus it is still needed to amplify the DNA prior to microarray or NGS-based analyses. Current whole-genome amplification (WGA) principles are based on the multiple displacement amplification (MDA), polymerase chain reaction (PCR), or a combination of both. The amplified DNA is then ready for whole genome analyses by microarrays-based or NGS-based methods. Finally the resulting genomic information would be analyzed for the profiling of copy number variants (CNVs), full chromosome aneuploidies, structural variations (genomic deletions, amplifications), mobile element insertions, segmental loss of heterozygosity (LOH), copy neutral DNA anomalies, indels (short insertions or deletions), and base substitutions (single nucleotides polymorphisms, SNPs) [89] (Fig. 1).

2.1.1 Whole Genome Amplification Approaches

- *PCR-based methods (DOP-PCR, LA-PCR, PEP-PCR)*

A version of the polymerase chain reaction (PCR), termed degenerate oligonucleotide-primed PCR (DOP-PCR), which employs oligonucleotides of partially degenerate sequence [150], has been developed for genome mapping studies [12]. DNA is amplified using these oligos for several cycles of low annealing and extension temperature to allow many binding sites in the human genome. After these permissive conditions, the annealing temperature is increased to allow more specific priming only at the fragments now tagged with the above primer sequence (Fig. 1).

DOP-PCR generates low physical coverage of an SC genome (approximately 10 %) being its major limitation; however, it can accurately retain copy number levels during amplification, thus this WGA method has been widely used in SC

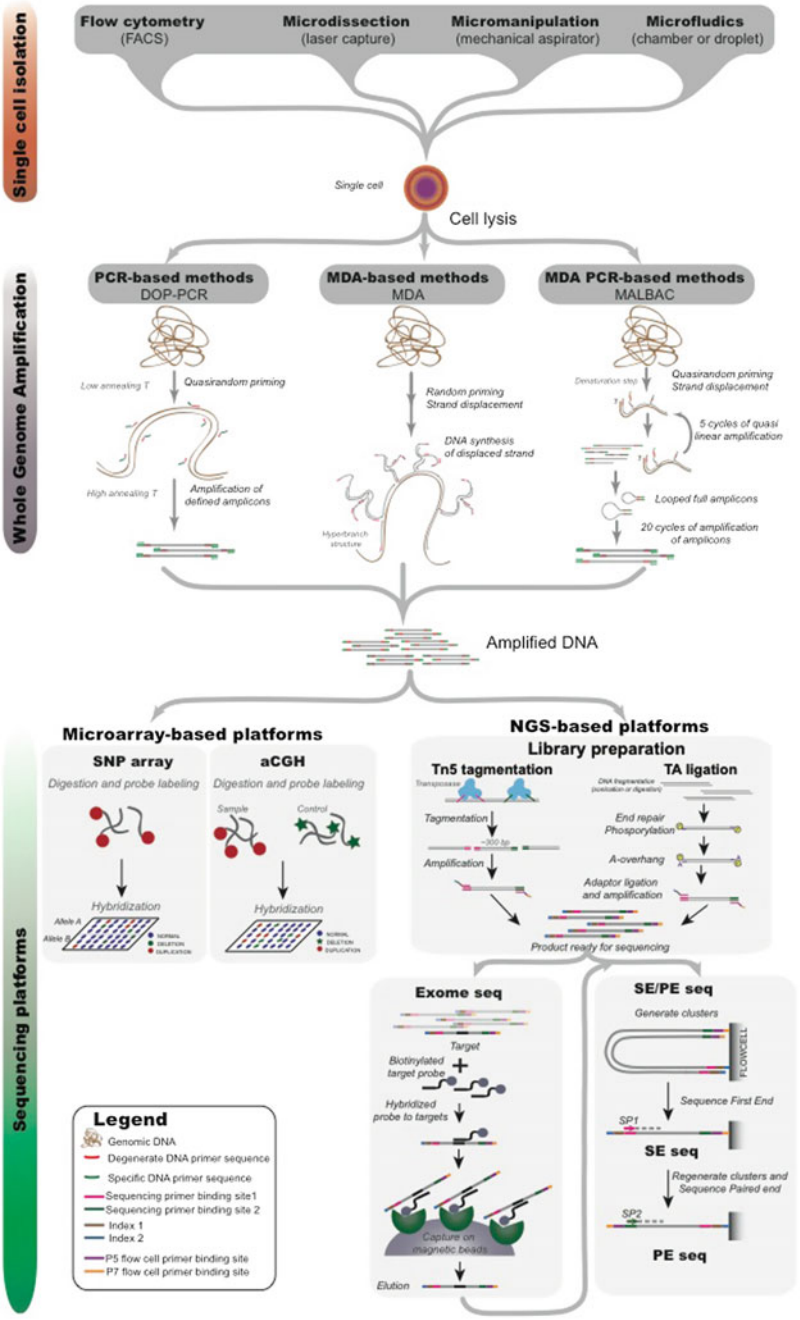

Fig. 1 Workflow for the most prominent methods discussed in this book chapter for single cell genomics, from cell isolation, whole genome amplification to sequencing

genomics for the analysis of copy number variation first in comparative genomic hybridization (CGH) arrays [166] and recently in single nucleus sequencing (SNS) [6, 106]. However, the low physical coverage of DOP-PCR in a single cell makes it a poor tool for measuring mutations at base-pair resolution.

Other PCR-based methods have been applied for WGA in SC genomics but have not been as popular as DOP-PCR. This includes primer extension preamplification (PEP)-PCR [180] and linker-adaptor (LA)-PCR [69]. In the PEP-PCR, DNA is amplified with oligos of complete degenerate sequence using permissive thermocycling with increasing annealing temperatures. In LA-PCR, DNA is sheared or digested, adaptors with universal sequence are ligated to the DNA ends, and the universal sequences are used for PCR amplification.

- *Multiple Displacement Amplification (MDA)-based methods*

MDA was the first successful amplification method used for single cell sequencing [122, 179]. This approach is based on the use of Φ29 DNA polymerase, which is highly processive and has a strong strand displacement activity [19, 20]. Using Φ29 DNA polymerase and random exonuclesase-resistant hexamers, DNA is amplified in a 30 °C isothermal reaction. When the polymerase reaches the next starting site, it displaces the newly produced DNA strand and continues its strand elongation. A cascade of strand displacement reactions results in an exponential amplification, as displaced strands become templates for the random hexamers population. This product has been termed a hyperbranched structure. To separate this structure, S1 nucleases are used to cleave the fragments at the displacements sites. The nicks on the resulting DNA fragments are repaired by DNA polymerase I. The products generated are quite large with an average length of more than 12 kb (Fig. 1).

For more than a decade, the most reliable method for amplifying a whole genome from a single cell has been MDA [139]. Compared with earlier whole-genome amplification methods that relied on PCR, MDA reduces amplification bias by three to four orders of magnitude and generates larger amplicons, therefore yielding more uniform coverage of the genome. The resulting coverage is sufficient for extensive sequencing of single bacterial cells and has made it possible to analyze the vast numbers of uncultured microbial species [73].

However, MDA has some limitations. One of its drawbacks is amplification bias, resulting in allele dropout (ADO) and high false discovery (FD) ratios. The false discovery ratio is defined as an FD heterozygous site in a homozygous sample [52, 171]. Despite the efforts of many laboratories, no reductions in the amplification bias of MDA have been reported in more than a decade since it was introduced. MDA was been unsuccessful in genotyping SNVs in diploid human genome from a single cell until a modified version of MDA was introduced in 2014 called NUC-Seq. This method uses G2/M phase of the cell cycle to duplicate the amount of starting material in a single cell from 6 pg to 12 pg, followed by limited isothermal amplification using Φ29 DNA polymerase [164]. A DNA input of four (or more) copies of each single cell genome for WGA improves physical coverage (>94 %) and reduces the ADO (approximately 10 %) and FD rates. Additionally,

limiting the MDA timeframe mitigates FP errors associated with the infidelity of the ϕ29 polymerase.

- *MDA-PCR-based methods: MALBAC*

In 2012, Zong and colleagues introduced a new technique for WGA that directly addressed the underlying causes of amplification bias by combining features of MDA and PCR [181]. Multiple annealing and looping-based amplification cycles (MALBAC) approach uses primers of eight nucleotides and a common 27-nucleotide tag to be annealed to the DNA template. The *Bacillus stearothermophilus* (*Bst*) DNA polymerase copies the DNA from the annealed primers in an isothermal strand displacement reaction, similar to MDA. However, unlike MDA, MALBAC uses repeated short cycles of primer extension followed by denaturation at 94 °C. This is a "quasilinear" amplification where the strand displacement synthesis generates partial amplicons that are subsequently denatured from the template; this generates more priming positions on the genomic DNA template to create more partial amplicons, which increases coverage of the genome with a resulting reduction of the amplification bias. Priming and extension on the partial amplicons yield complete amplicons having the MALBAC primer sequence at the 5′ end and its complementary sequence at the 3′ end. These complete amplicons form loops, due to the 27-nucleotide common sequence across all primers, and this inhibits the 3′ ends from serving as primers. The loops prevent the fragments from being copied again, and the amplification thus stays linear. After 5 cycles of the "quasilinear" amplification, the resulting DNA is amplified by 20 cycles of PCR using primers complementary to the common 27-nucleotide region (Fig. 1). MALBAC has been successfully used for the detection of single-nucleotide variants in single cells [87, 109, 181].

MALBAC is believed to have brought great improvement with respect to the other WGA methods, for example, improving the efficiency for detection of single-nucleotide variations from both alleles to 71 %, compared to only 10 % for MDA. Although the amplification bias is substantially reduced in MALBAC, there is still room for improvement as there are still 20–30 % underrepresented genomic regions that have not been accurately genotype [181]. Another limitation of MALBAC is the false positive rate for genotyping single nucleotide variants that with MALBAC is 40-fold higher than for MDA. This could be overcome by adapting the protocol to use a high-fidelity enzyme, such as Φ29 DNA polymerase, or a thermostable DNA polymerase with strong proofreading activity.

2.1.2 Sequencing Platforms

For the study of partial or nearly complete genome of single cells, two types of genome-wide sequencing platforms have been used, microarray-based platforms, where multiple areas of the genome are interrogated by fluorophore or chemiluminescence labeled probe-target hybridization; and NGS-based platforms, in which after WGA, DNA is either target-enriched or taken straight away for library

preparation and sequencing (Fig. 1). The method of choice would depend on the specific application.

- *Microarray-based platforms: SNP array and CGH array*

  – *Single-nucleotide polymorphism (SNP) array*

An SNP is a single base-pair mutation at a specific locus, usually consisting of two alleles (where the rare allele frequency is >1 %). SNPs are the most common types of genetic variation between members of the same species. Genetic variation of SNPs is found to affect human health, diseases and responses to drugs and environmental factors.

In high-density oligonucleotide SNP arrays, a very high number of probes are arrayed on a small chip, allowing to assess from hundreds of thousands to millions of SNPs simultaneously. By comparing the differential amount of hybridization of the target DNA to each of redundant probes, it is possible to determine specific homozygous and heterozygous alleles (Fig. 1). In single cells, SNP arrays have been used to provide information for single-nucleotide mutations [159], copy number variations (CNV) [71], and structural variants (like LOH or chromosome aneuploidy) [3, 31, 59, 153]. The most prominent SNP array types are available from commercial vendors like Affymetrix (i.e., Genome-Wide Human SNP Array 6.0), Illumina (i.e., HumanOmni or HumanCore BeadChips), and Fluidigm (SNP Type Assays, custom primer design for high-throughput SNP genotyping). These companies sell competing arrays and continue to offer increased coverage for detecting copy number events and SNP assays simultaneously. Assay technique for the arrays differ but the signal-intensity output from these platforms present similar analysis and interpretation problems.

The WGA method of choice used for SNP arrays in single cells is MDA [31, 59] because it gives the highest coverage and higher concordance for chromosome copy number from single cells compared to any other PCR-based methods. However, it also has limitations from the WGA approach, especially ADO (about 30–20 %) [84]. This MDA coupled with SNP mapping array has been widely in use in the clinic for preimplantation genetic diagnosis (PGD) of embryos to detect molecular disorders (Fig. 2) [3, 153, 156, 159]. Recently, MALBAC has been applied for SNP arrays [55] and has given highly accurate results for 24-chromosome aneuploidy screening (Fig. 2).

Additionally, Fan and colleagues developed a microfluidic device capable of separating and amplifying homologous copies of each chromosome from a single human metaphase cell followed by SNP arrays of the amplified DNA. This separation-improved method allowed to achieve completely deterministic, whole-genome, personal haplotypes of four individuals, including a HapMap trio with European ancestry (CEU) and an unrelated European individual with a 99.8 % accuracy for up to approximately 96 % of all assayed SNPs. Thus, this new approach has potential applications in personal genomics, single-cell genomics, and statistical genetics [31].

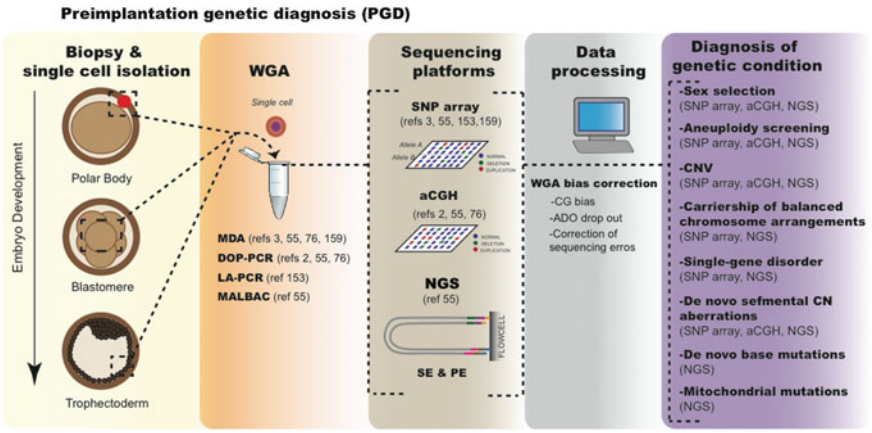

Fig. 2 Application pipeline for preimplantation genetic diagnosis. Single cell genomics has been applied for preimplantation genetic diagnosis (Figure adapted from Van de Aa et al. [156], using different approaches for WGA and different sequencing platforms dependent on the desired genetic diagnosis

- *Comparative genomic hybridization arrays (aCGH)*

aCGH technology is based on differential labeling of sample and reference DNA with fluorophores, hybridization to arrays containing oligonucleotide probes, and subsequent analysis of fluorometric signal ratios [119] (Fig. 1). As an alternative to FISH, aCGH has been successfully used for chromosomal imbalances detection in whole-genome amplified DNA products from single cells [36, 53, 76].

Different WGA methods have been used prior array hybridization: DOP-PCR, where the authors did not obtain robust results since incorrect ratios of chromosomal imbalances were sometimes observed for about eight different chromosomes [53]; MDA, this approach was able to detect aneuploidies of whole chromosomes, however, with a detection resolution of 34 Mb at best, thus it failed to demonstrate a significant improvement compared with conventional methodologies [76]; LA-PCR [36, 17] which seems to be the best WGA reliable approach for the detection of numerical genomic alterations as small as 0.1 Mb in a single cell [17]; or MALBAC [55], which gave the most accurate and reliable results for 24-chromosome aneuploidy screening.

The study of copy number alterations and chromosome imbalances using aCGH has been applied for SC studies in oncology and clinical diagnostics. Disseminated cancer cells and circulating tumor cells are extremely rare, but comprise the precursors cells of distant metastases or therapy resistant cells, aCGH has led to the identification of recurrent amplifications and deletions is these extremely underrepresented cells [17, 94, 120]. On the other hand, aCGH has been introduced as a rapid and high-resolution method for the detection of both benign and disease-causing genomic copy number variations in PGD testing, noninvasive prenatal diagnosis, and postnatal genetic diagnosis (Fig. 2) [2, 55, 76, 156].

- *NGS-based platforms: whole-exomesequencing and single-end or paired end sequencing*

With the introduction of next-generation sequencing (NGS) [99], it became feasible to characterize entire genomes for the full spectrum of genetic variants in a single experiment. NGS has a number of advantages over microarrays enabling improved resolution and accuracy in for example variant calling. First, NGS can examine every nucleotide amplified from the cell and allows genome-wide discovery of the full spectrum of DNA mutations, while microarrays-based platforms only probe for certain CNV. Second, NGS provides digital precision, with a one digital unit representing a mapped sequence read. Third, paired-end sequencing allows the identification of structural variations via read-pairs mapping discordantly to the reference genome.

SC genome sequencing has become more reliable since the introduction in 2012 of the world's first automated solution for SC genomics research, the C1™ Single-Cell Auto Prep system (Fluidigm). C1 employs an innovative microfluidic technology [90] to rapidly and automatically capture, lysis, and DNA purify and amplify for up to 96 individual cells in a single workflow. Amplified products harvested from the system are ready for downstream library preparation for whole-exome sequencing, or whole-genome sequencing [39].

DNA library preparation is a critical step for NGS. Once the genome is amplified by WGA, a standard sequencing library can be prepared. This method consists of the fragmentation of the amplified DNA into the appropriate size; the size would depend on the sequencing approach, but as a standard the desired fragment size is around 250 bp. Then sequencing-specific oligonucleotides probes (called adaptors) are ligated to both ends of the DNA fragments. The adaptors contain amplification and sequencing binding sites, which are platform and chemistry-specific and optionally could contain indexes or barcodes to allow multiplexing during sequencing. The DNA is then PCR amplified for limited cycles with the sequencing-specific oligonucleotides to amplify the ligated products. Finally these amplicons would be ready for cluster generation (the expected size would be around 350 bp).

NGS library preparation enables diverse applications, ranging from whole-genome to targeted DNA sequencing (including exome and amplicon), as well as targeted RNA and total RNA sequencing (RNA-seq). There are two main approaches for the construction of sequencing libraries for SC genomics: TA ligation [164] and Tn5 transposase and tagmentation [1]. Briefly, TA ligation library starts off by fragmenting the DNA, either by sonication or enzyme digestion, and then the fragmented DNA is blunt-ended and phosphorylated. A single 'A' nucleotide is added to the 3' ends of the fragments in preparation for ligation to an adapter that has a single-base 'T' overhang. The ligation products are purified and accurately size-selected by agarose gel electrophoresis. Size-selected DNA is purified and PCR-amplified to enrich for fragments that have adapters on both ends. The final purified product is then quantitated before cluster generation (Fig. 1). A great advance in library preparation was the introduction of a hyperactive variant

of the Tn5 transposase that mediates the fragmentation of double-stranded DNA and ligates synthetic oligonucleotides (adaptors) at both ends in a 5 min reaction [1], then a limited cycle PCR is performed to add the sequencing oligos and indexes (Fig. 1). This Tagmentation-based library approach has been commercialized by Illumina as the Nextera system and it is being mainly used for exome capture sequencing. For single cells, this Nextera system has been only used in one report so far [164], while most studies have used the traditional TA ligation method.

After library preparation, the samples are ready for sequencing. NGS is based on the spatial immobilization of millions of short DNA fragments followed by a massively parallel sequencing process providing digital information on a DNA fragment. These short sequences are then assembled and aligned to reference genomes using bioinformatics tools. NGS technologies include a number of methods that are grouped broadly as template preparation, sequencing and imaging, and data analysis (Reviewed in [99]). The unique combination of specific protocols distinguishes one technology from another and determines the type of data produced from each platform. The most popular commercially available next-generation technologies are 454 GS FLX (Roche), HiSeq 2500 (Illumina) and Ion Torrent Personal Genome Machine and the SOLiD4/5500 (Life Technologies).

- *Whole-exome sequencing*:

Target-enrichment methods allow the selection of capture genomic regions of interest from a DNA sample prior to sequencing. The sequencing from single cells of complex genomes, like the human genome, is still challenging and does not give enough coverage to study the biology of single cells. The exome represents less than 2 % of the human genome, but contains ~85 % of known disease-causing variants, making whole-exome sequencing a cost-effective alternative to whole-genome sequencing.

This method consists of the capture of exonic regions from the pool of DNA after library preparation. Library pooled fragments are denaturated and hybridized to biotinylated RNA baits. Then these exonic regions are captured with streptavidin magnetic beads to be finally eluted and ready for sequencing (Fig. 1). MALBAC [109] and MDA-based methods [52, 83, 144, 164, 171] are the WGA of choice for this approach.

Whole-exome targeted sequencing can efficiently identify SNPs, indels, LOH, and copy neutral DNA anomalies and has been extensively applied in SC cancer genomics [52, 83, 109, 144, 164, 171].

- *Single-end (SE) or paired-end (PE) whole genome sequencing*:

After library preparation the DNA can be sequenced straight away. SE sequencing involves sequencing DNA from only one end, while paired-end sequencing allows the sequencing of both ends of a fragment (Fig. 1). PE readings generate high-quality, mappable sequence data making it much more effective than single-end reading in resolving structural rearrangements such as indels or inversions [161]. It can also improve the assembly of repetitive regions. This degree of

accuracy may not be required for all experiments, however, and paired-end reads are more expensive and time-consuming to perform than single-end reads.

SC whole-genome sequencing would be the most informative approach if the coverage is deep enough and provides information for 100 % of the genome. Mainly due to limitations of the current WGA methods the sequencing of 100 % of the genome of single cells has not been possible yet neither from the human genome nor bacterium. The WGA methods used for this approach are MDA [6, 164] and MALBAC [181]. Nevertheless, advances on the technical and computational fronts keep improving every year [164, 181], suggesting that very soon we will have a complete genome sequencing of single cells.

SE or PE whole genome sequencing has been applied in single cell genomics mainly in cancer for the detection of CNVs [6, 161, 181], SNVs [181], multiple classes of DNA mutations [161], structural variants [161]. Microbial genomics has applied this methodology for the analysis of culture-independent microbes [73, 96], for understanding the genomic diversity and evolution of bacterial ecosystems [28, 96] and for the characterization of new phyla [97].

2.1.3 Limitations

The major limitations of SC genomics come from the WGA step. Starting with only two copies of DNA as input material for WGA results in a number of technical errors, including low physical coverage, nonuniform coverage, events, false positive (FP), allelic dropout (ADO), errors, and false-negative (FN) errors.

- *Low physical and nonuniform coverage*

It is often difficult to achieve high coverage breadth (nucleotide sites with at least 1X coverage) for whole-genome or exome sequencing of a single cell. However, achieving high physical coverage of the exons or genome is crucial for calling mutations at the same regions across multiple single cells. Coverage uniformity is another technical challenge with SC data, owing to the significant GC bias that occurs during WGA. This leads to deviations from the Poisson coverage distributions that are normally observed in NGS data, requiring higher coverage depths to achieve sufficient coverage in regions with low read counts (ideally 10-40X coverage).

- *False positive (FP) errors*

FP errors occur due to the infidelity of the WGA polymerase during amplification and lead to single-base-pair errors [19, 74]. These errors are most severe during the initial rounds of genome duplication because all subsequent molecules inherit the errors, making them abundant in the pool. Interestingly, most FP errors generated during MDA show a very strong bias for C > T (G > A) transitions [52], which could be mitigated by filtering or using probabilistic variant calling models.

- *Allelic dropout (ADO)*

The greatest errors in SC genomics data are ADO events, which can be found in 10 to 50 % of the mutation sites [36, 52, 74, 145, 181]. ADO occurs when one allele in a heterozygous mutation is not amplified by the polymerase, resulting in a homozygous genotype. These technical errors must be accounted for in postprocessing analysis of the data as otherwise every mutation will be reported as showing heterogeneity in the population of single cells.

Within the different WGA methods the grade of technical errors differ and have to be considered when choosing the WGA method to perform in your single cell experiment, the limitation of each particular WGA method has been already discussed in the section on WGA methods. In summary, the DOP-PCR-based WGA methods and MALBAC are ideal for copy number profiling as they generate very high FP error rates and low physical coverage, but provide uniform amplification across the genome. In contrast, MDA methods are more suitable for detection of point mutations and indels at base-pair resolution. However, owing to the high technical error rates, mutations must be detected in multiple single cells in order to distinguish real biological variants from technical errors. Furthermore, validation of individual mutations using an orthogonal technology is imperative at this stage of the sequencing technologies.

2.2 Applications and Most Relevant Breakthroughs

In 2013, single-cell sequencing was named "method of the year" in recognition of its recent impact on several scientific fields [13]. Genomic DNA sequencing of microbial genomics from single cells has multiple applications including the analysis of culture-independent microbes [73, 96], the understanding the genomic diversity and evolution of bacterial ecosystems [28, 96], and for the characterization of new phyla [97].

SC genomics has been also widely applied to understand the cellular composition of tissues by the discovery of new and rare cell types or by the reconstruction of cell lineages trees [38, 130, 175]. Embryonic development is another field that has great advances with the introduction of SC genomics, for example for the understanding of the whole developmental process and insights in genomic variation, and also for the use in diagnosis including the reasons of loss of conception or genetic disorders [2]. Another highly important field that has been impacted by SC genomics is cancer especially on understanding tumor heterogeneity and evolution and also for the analysis of circulating tumor cells [52, 106, 164]. Here we highlight the most relevant and established applications so far.

2.2.1 Microbiome Single Cell

DNA sequencing from single cells has revolutionized microbial genomics. The capture of bacterial genomes has been a long-standing challenge in microbiology research because the great majority of bacterial species cannot be readily cultivated. SC genomics has been most broadly applied to the microbial universe, where understanding the genomic diversity and evolution of bacterial ecosystems is essential for the applications ranging from understanding climate [75] to the treatment of infectious diseases [96]. The largest study so far has been carried out to sequence genomes from major uncultivated bacterial and archaeal lineages [125] using optimized high-throughput procedures [124]. Nine environmental samples, including marine, brackish, freshwater, and hydrothermal samples were used[13] and around 200 single cells were deeply sequenced. The partially assembled genomes, which range from 148 kb to 2.4 Mb, represent 29 major uncharted branches of the evolutionary tree [125]. This study revealed unexpected metabolic features, including a complete sigma factor in archaea that is similar to those in bacteria, a novel amino acid use for the opal stop codon, and an archaeal-type purine synthesis in bacteria.

Another application of bacterial single-cell genomics is the detection of hospital pathogens during those phases of their life cycle when they persist at very low levels in environmental reservoirs and can be transmitted but not detected easily. The first SC pathogen study was of a biofilm isolated from a hospital restroom sink [97, 98]. Roughly 400 amplified genomes revealed a broad range of bacteria covering 25 different genera representing environmental species, human commensals, and opportunistic human pathogens. For example, three individual amplified genomes were obtained for *Porphyromonas gingivalis*, a human pathogen whose genome was first obtained from a source outside of a human host, with the largest de novo assembly being a complete genome [98].

2.2.2 Cancer Single Cell Genomics

Several studies have sequenced and dissected cancer genomes to single-cell resolution [107, 158], with the aim of understanding tumor development and progression of the disease. Copy number landscapes of single nuclei (SNS-sequencing) from primary mammary ductal carcinomas and a paired metastatic liver tumor were generated following low-coverage sequencing. This revealed various chromosomal rearrangements, followed by distinct phases of clonal expansion during tumor evolution and metastasis; by phylogenetic analyses, they could infer common ancestors, clonal expansions and divergence of subpopulations [106]. Furthermore, Wang and colleagues developed whole-genome and exome single cell sequencing approach (NUC-seq) to sequence single normal and tumor nuclei from an estrogen-receptor-positive breast cancer and a triple-negative ductal carcinoma and found that aneuploid rearrangements occurred early in tumor evolution and remained highly stable as the tumor masses clonally expanded. Point mutations, on

the other hand, evolved gradually, generating extensive clonal diversity; they also found differences between tumor subtypes where in the triple-negative tumor cells had an increased mutation rate whereas the ER tumor cells did not [164].

Subsequent SC exome sequencing studies in bladder [83], kidney [171], and hematopoietic neoplasms [52] provided a detailed characterisation of base mutations in specific genes. Similarly, whole-genome sequencing of multiple MALBAC-amplified cells revealed a base mutation rate of a cancer cell line to be increased tenfold when compared to estimated germ-line ciphers [181].

2.2.3 Clinical Applications

SC genetic analysis is important for clinical purposes including its use in preimplantation genetic diagnosis, noninvasive prenatal diagnosis, and cancer diagnosis and prognosis using noninvasive methods by the detection of circulating tumor cells.

- *Preimplantation genetic diagnosis (PGD)*

PGD aims to help couples with heritable genetic disorders to avoid the birth of diseased offspring or the recurrence of loss of conception. Following in vitro fertilization (IVF), one or a few cells are biopsied from each human embryo for genetic testing, allowing diagnosis and selection of healthy embryos for uterine transfer [156]. SC genomics is revolutionizing PGD, as rapid SC aCGH- and SNP-array protocols have enabled the detection of inherited or even de novo DNA copy number aberrations encompassing a few megabases simultaneously across all 24 chromosomes (Fig. 2). Although these genome-wide methods are not routine in PGD practice yet, large-scale validation studies are ongoing, and in the near future they are likely to gradually replace locus- and family-specific FISH-based PGD approaches [2, 153, 159].

- *Circulating tumour cells (CTCs)*

SC genomics is also applied for studying blood-borne circulating tumor cells (CTCs) [50, 109, 144], derived from a solid tumor, to investigate the value of these rare cells for guiding diagnosis, prognosis, and treatment of the cancer [105].

Heitzer et al. used aCGH and target-enriched sequencing to profile genetic relationships between primary colorectal carcinomas, metastases and CTCs derived from the same patients [50]. Although CTCs shared a number of gains and losses with the primary tumor and/or the metastasis, unique copy number changes in CTCs as well as heterogeneity between CTCs were observed. Such results are paving the way for using CTCs as a liquid biopsy to guide clinical decision-making. On the other hand, Ni et al. [109] demonstrated that copy number aberration patterns of CTCs in different patients with the same lung cancer subtype can be extraordinarily similar, but dissimilar when compared to copy number landscapes of CTCs in patients with different lung cancer subtypes, and thus be of diagnostic significance.

3 Single Cell Transcriptomics

3.1 Methods for Single Cell Transcriptomics

Following SC isolation, transcriptome can also be studied. Methods for single-cell transcriptomics have flourished and delivered baffling new insight into the functional heterogeneity of cell populations. A single cell has approximately 10 pg of total RNA and often contains only 0.1 pg of polyadenylated RNA (mRNA). Some transcripts are thought to be expressed over several orders of magnitude, where many transcripts have low level of expression (5–20 transcript copies per cell), with more than 85 % having less than 100 copies per cell [142]. Thus it is not yet possible to directly sequence RNA molecules, so a common strategy is used to capture the SC transcriptome and relies on three major steps: RNA reverse transcription into first-strand cDNA, second-strand synthesis and cDNA amplification.

SC-reverse transcription and whole transcriptome amplification (WTA) methods have been developed and are grounded on PCR-based, MDA-based or in vitro transcription (IVT)-based amplification of reverse transcribed SC mRNA. Following WTA, the transcriptome of the retrotranscribed and amplified RNA can be analyzed by (multiplexed) RT-qPCR [43, 54, 165], microarray [50, 167], and more recently, NGS [134, 172, 173].

3.1.1 Whole Transcriptome Amplification (WTA) Approaches

Reverse transcription is the initial step in each RNA amplification method, and subsequent conversion of cDNA into amplifiable molecules. Many new amplification technologies have been developed to enable the global transcriptome sequencing, particularly PCR-based methods, IVT-based methods and Φ29 DNA polymerase-based methods.

- *PCR-based methods* (Fig. 3a):

A variety of versions of PCR-based methods have been developed for exponential amplification and sequencing of the transcriptome each offering an overview of either the 5′-end, 3′-end or even the full length of transcripts from a single cell.

- *Tang/Surani method*:

This approach was the first SC RNA-seq method reported [148, 149]. After single cell isolation and lysis, the mRNA is reverse transcribed into cDNAs using a poly (T) primer with anchor sequence and the nonreactive primers are digested by exonuclease I. Then Poly(A) tails are added to the first-strand cDNAs at the 3′ end by terminal deoxynucleotidyl transferase. Next, the second-strand cDNAs are synthesized using poly-dT primers with another anchor sequence. Then these cDNAs are evenly amplified by PCR of 20 cycles using the anchor primers. After

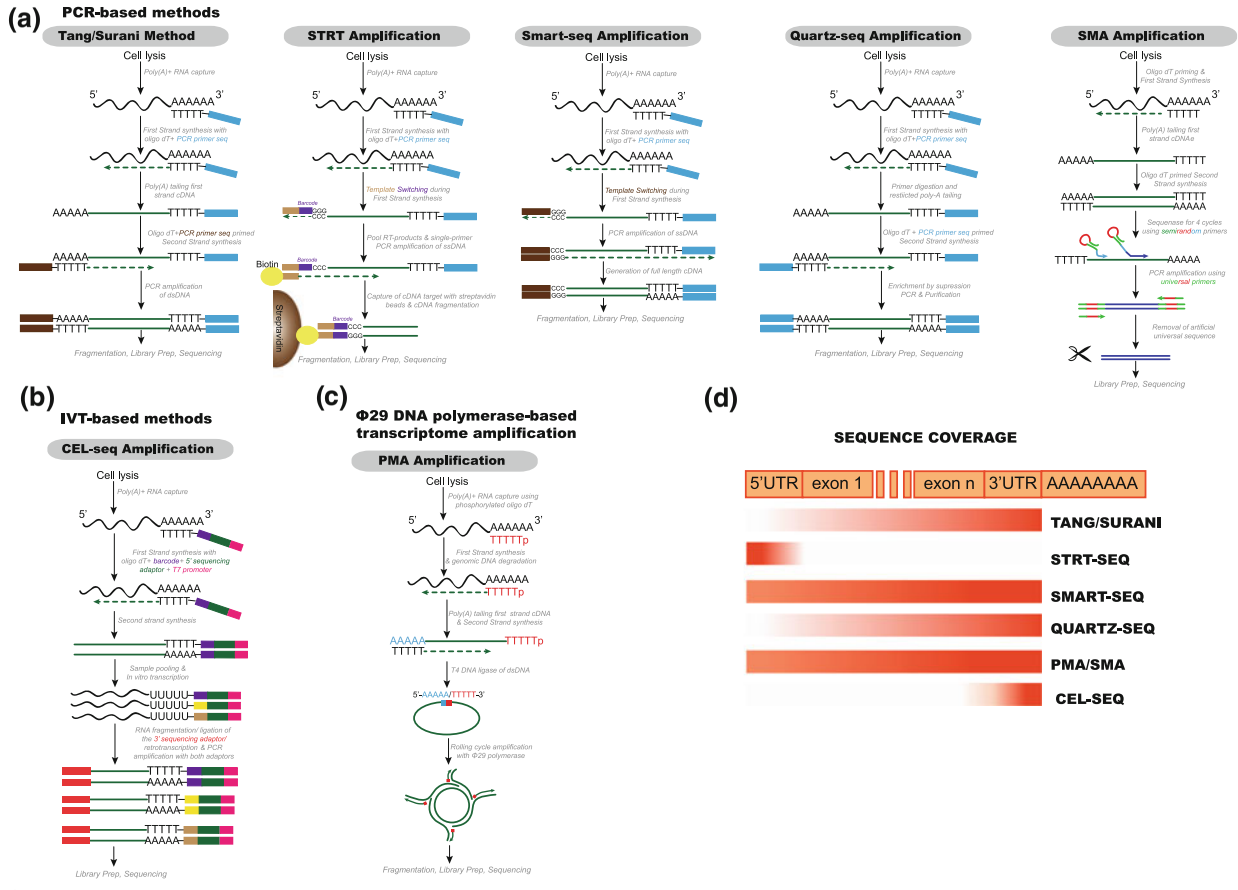

Fig. 3 **a** Detailed workflow of the current whole transcriptome amplification approaches for single cell RNA-seq based on PCR methods, **b** in vitro transcription (IVT) and **c** ϕ29 DNA polymerase. **d** Overview of the sequence coverage of a typical transcript which will be obtained by each of the currently available single-cell RNA-seq methods

purification, these cDNAs are ready to construct a sequencing library and for subsequent mRNA-Seq analysis.

This method successfully detected thousands of genes expressed in mouse oocytes, and showed increased sensitivity compared with microarrays [149]. However, this first SC mRNA-Seq experiment lacked technical controls, making it impossible to distinguish biological variation between different cells from the technical variation that is intrinsic to cDNA amplification protocols when starting with low amounts of RNA. This method also preferentially amplifies the 3′ ends of mRNAs, and hence the data could only be used to identify distal splicing events.

- *Single-cell Tagged Reverse Transcription (STRT):*

This is a highly multiplexed method for SC RNA-seq on the IlluminaPlatform that allows sequencing of a number of single cells by barcoding at an early stage of cDNA amplification at the 5′ end of the mRNAs [56, 57]. Briefly, single cells are collected in a 96-well plate, where each well contains one single cell, preloaded with lysis buffer. The first-strand cDNA is generated is by adding an oligo-dT adaptor-primer. To incorporate a cell-specific barcode, a reverse transcriptase template-switching mechanism is used [131] whereby a helper oligo directs the incorporation of a specific sequence at the 3′ end of the cDNA molecule during the first-strand synthesis. A different helper oligo is used in each well, with distinct six-base barcodes and a universal primer sequence.

After cDNA synthesis, the 96 reactions are pooled, purified, and amplified by biotin-labeled primer PCR. Cell-to-cell amplification bias is thus reduced, and the number of PCR cycles can be kept low. Then the 5′ ends of the amplified samples are captured with streptavidin beads and sequenced. From each transcript, a single read is obtained, corresponding to a template-switching site located preferentially at the 5′ end of the mRNA. This way, both single-cell detail and cell type–specific population averages are available and can be studied without the mixing of data from unrelated cell types. However, this method is not able to generate read coverage across full transcripts.

- *SMARTer or Smart-seq*:

This is a widely used method [123] that has updated versions, Smart-seq 2 [117, 118], and that promises near full-length coverage of transcripts. Retro-transcription generates full-length cDNA using oligo-dT priming, once the reverse transcription reaction reaches the 5′ end of the RNA molecule a template switching by the SMART template switching technology is performed. Briefly, the terminal transferase activity of MMLV retrotranscriptase adds a few non-templated nucleotides to the 3′ end of the cDNA. The carefully designed SMARTer II A oligo then base-pairs with these additional nucleotides, creating an extended template. The reverse transcriptase then switches templates and continues transcribing to the end of the oligonucleotide. The resulting full-length cDNA contains the complete 5′ end of the mRNA, as well as an anchor sequence that serves as a universal priming site for second-strand synthesis. The cDNA is then PCR-amplified and sequenced. Smart-seq and its variants are very popular probably due to their successful

optimization and commercialization (SMARTer Ultra Low RNA Kit for Illumina sequencing, Clontech), and because with these methods, mRNAs are highly, selectively amplified from total RNA and gDNA, and so no pre-purification of RNA is required. Compared with existing methods, Smart-Seq and its variants have improved read coverage across transcripts, which significantly enhance detailed analyses of alternative transcript isoforms and the identification of SNPs.

- *Quantitative single-cell RNA-seq (Quartz-seq)*

The WTA for Quartz-Seq consists of five main steps [128]: (1) Generation of the first-strand cDNAs from the target RNAs by reverse transcription with an reverse transcription primer, which contains oligo-dT and the suppression PCR target region sequences; (2) Primer digestion with exonuclease I; this is one of the key steps to prevent the synthesis of byproducts; (3) The addition of a poly-A tail to the 3′ ends of the first-strand cDNAs, and (4) the second-strand synthesis using a tagging primer, which prepares the substrate for subsequent amplification; (5) PCR enrichment reaction with a suppression PCR primer to ensure that a sufficient quantity of cDNA is obtained for NGS sequencing and microarray experiments.

Quartz-Seq is a simplified protocol compared with previously established methods based on the poly-A tailing reaction, as all of the steps are completed in a single PCR tube without any purification. The reproducibility and sensitivity of Quartz-Seq is higher than CEL-seq, Smart-seq and STRT. This method allows to distinguish not only different cell types but also different cell-cycle phases of the same cell type. However, it also has some limitations including GC bias, bias towards longer cDNAs compare with CEL-seq and shorter cDNAs than Smart-seq [128].

- *Semi-Random Priming and Universal PCR for mRNA Transcriptome Amplification (SMA):*

This method generates a number of overlapping, relatively short PCR constructs for each piece of sequence from any transcript through random priming and universal PCR amplification [114]. SMA method starts with a first-strand synthesis carried out using a thermostable. The single-strand cDNA, A Poly(A) tail is added to the first-strand cDNA tobe converted to the double-stranded form using an oligo dT primer. Then oligonucleotides with random 3′ sequences and a universal 5′ sequence that serves as a priming site are used for capture of the whole cDNA sequence. PCR amplification using universal primers that recognize the 5′ end of the random oligonucleotides is then performed and, once the amplicon is obtained, the oligonucleotide adapter is completely removed with a type IIs restriction enzyme, BciVI, whose recognition sequence was built into random oligonucleotides. Because of the semi-random priming, each sequence can be covered by multiple different lengths of PCR templates, and because all products are of similar length and amplified with the same primer, the amplification is not subject to the well-known biases of PCR that favor shorter fragments or certain primer sequences. This method enables an extensive and uniform coverage of any size mRNA transcript.

- *IVT (in vitro transcription)-based methods* (Fig. 3b):

IVT-based methods are characterized by linear amplification, which was originally developed for the RNA amplification from a low quantity of cells in 1990 by Dr. James Eberwine [157]. IVT-based methods have overcome the common problems of PCR-based amplification described above and do not require pre-purification of RNA (no need to remove gDNA) because in vitro transcription does not apply to gDNA. Several of the recent versions are very efficient, including the method dubbed Cell Expression by Linear amplification and sequencing (CEL-seq), which is a highly multiplexed method [49] and Massively parallel RNA single-cell sequencing (MARS-seq) [60].

- *Cell Expression by Linear amplification and sequencing (CEL-seq)*

The CEL-Seq method begins with a SC-reverse transcription reaction using a primer designed with an anchored poly-dT, a unique barcode, the 5′ sequencing adaptor, and a T7 RNA-polymerase priming site. Next, second-strand synthesis is performed and then the cDNA samples are pooled and consequently comprise sufficient template material for an IVT reaction. RNA is linearly amplified from the cDNA by T7 RNA polymerase. The cRNA is then fragmented to a size distribution appropriate for sequencing and ligated with a 3′ sequencing adaptor. The cRNA is then reverse transcribed to DNA, and the 3′-most fragments that contain both sequencing adaptors are selected for paired-end sequencing. CEL-Seq is highly strand specific and the reads mapped show an exclusively bias to the 3′ end of transcripts as a consequence of using polyT-T7 primer. However, CEL-Seq gives more reproducible, linear, and sensitive results than STRT method [49].

- *Φ29 DNA polymerase-based transcriptome amplification (PMA)* method (Fig. 3c):

PMA is based on the previously reported WGA method, MDA [122, 179], which depends on the high processivity and strand displacement properties of the Φ29 DNA polymerase that requires relatively long DNA templates (usually > 3–4 kb) for efficient amplification [114]. In this method, the double-strand cDNA is generated similarly to the SMA method, with the exemption that the priming oligo-dT is phosphorylated. The full-length double-strand DNA is then circularized using a T4 DNA ligase and amplified using Φ29 DNA polymerase and random primers. This rolling in cycle amplification ensures highly efficiency, sequence orientation, low bias and uniformity regardless the sizes of the original transcripts [63, 113]. These features facilitate amplification of cDNAs on a microfluidic platform with very small volumes, and most notably, full-length sequence coverage. However, one limitation is that the RNA has to be selected from the gDNA background (or the gDNA has to be removed using an in-tube treatment) before amplification otherwise it will be co-amplified with the RNA.

3.1.2 Sequencing Platforms

Until recently the method of choice to study gene expression of single cells was multiplexed **qRT-PCR**; however, its throughput has remained limited to several hundreds of genes even when using highly parallel microfluidic systems [168]. **Microarrays** enable SC analyses on transcriptome-wide scale [48], but compared to RNA-seq, they suffer from limited sensitivity and dynamic range. In addition, hybridization-based methods typically require larger starting amounts of RNA than the ones required for library preparation for RNA-seq. Thus, as seen previously with populations of cells, **RNA-seq** is also replacing hybridization-based methods on the SC level [148, 149]. Moreover, largely thanks to the use of microfluidics platforms for cell capture and reaction processing (C1™ Single-Cell Auto Prep system, Fluidigm) [45, 141], SC RNA-seq has now become an established, reliable and automated laboratory technique.

- *SC RNA-seq:*

Various SC RNA-seq methods now exist, each offering an overview of either the 5′ end (STRT) [56, 57], 3′ end (CEL-seq) [49] or the full length (Tang/Surani, Smart-seq (2), Quartz-Seq and SMA/PMA) [114, 117, 118, 123, 128, 148, 149] of transcripts from a single cell (Fig. 3d). After WTA, a sequencing library can be prepared from the amplified cDNA using the standard methods, TA ligation or tagmentation, as described in Sect. 2.1.2, with the exemption of CEL-seq [49], The resulting libraries from all these methods undergo paired-end sequencing (explained in Sect. 2.1.2). The extra information of a second read sequence and prior knowledge of the expected distance between each read during paired-end sequencing allows more accurate mapping, in particular when alternative splicing is of greater interest. An additional advantage of paired-end RNA-seq, that is particularly useful when sequencing cancer transcriptomes, is the opportunity to detect chimeric transcripts resulting from gene fusion events.

An in-depth SC RNA-seq analysis of a whole tissue may require the profiling of several thousands if not millions of representative individual cells. To reduce sequencing costs and increase throughput, the recent developments of STRT [57] and CEL-seq [49] methods include the incorporation of a unique cellular barcode allowing to pool the cDNA from hundreds of cells and perform library preparation and sequencing in the same tube and in a single sequencer run. Later, each read is in silico attributed to its original cell according to its barcode.

3.1.3 Limitations

Since it is not yet possible to sequence RNA directly from single cells, RNA needs to be converted to cDNA and amplified providing an indirect representation of the transcriptome. A careful assessment of all aspects of the process is required, for example, biological variability versus technical variability, the latter of which is due to loss of specific transcripts during RNA isolation and library preparation;

inclusion of different transcript classes; transcript coverage; maintenance of strand specificity and maintaining the initial transcript abundance.

- *Reverse transcription bias*

The initial step in each RNA amplification method, and subsequent conversion of cDNA into amplifiable molecules are likely key limiting factors in the detection and quantification of transcripts in single cells. It is estimated that on average only 5–25 % of mRNA-molecules are converted to amplifiable cDNA [57].

- *Limitations of WTA methods*

PCR-based amplification methods have the potential for nonlinear amplification, resulting in the distortion of the relative abundance of transcripts, causing the loss of relatively lowly expressed transcripts and the magnification of the original ratio, it tends to make the original small difference much larger. Furthermore, amplification methods also generate low coverage. The median read coverage across expressed transcripts is 53.8 % in the Quartz-Seq method, compared with 84.4 % in conventional RNA-seq [128]. IVT-based methods [49] may arguably avoid such complications through linear amplification of the transcriptome. Additionally, PCR-based amplification methods also have a sequence bias associated with GC content and/or transcript size (favoring short transcripts) with exception of the SMA [114] method, in which the PCR products are relatively short and uniformed in size. Tang et al. only obtained RNA transcripts shorter than 3 kb in single mouse blastomere cells, missing 36 % of the expressed genes [148]. As mentioned before, the majority of the WTA methods only amplifies the polyadenylated RNAs of a cell's transcript repertoire, and may be biased to the 3′ end or the 5′ end of a transcript (Fig. 3d). Full-length mRNA-characterization from a single cell can only be achieved by a few WTA-methods (Tang/Surani, Smart-seq, Smart-seq 2, Quartz-seq, SMA/PMA) (Fig. 3d). Furthermore, nanoliter-scale reactions can demonstrate benefits over microliter-scale processes [169].

- *Maintaining strand specificity information*

Given the prevalence of antisense transcription [116] it is critical to maintain the information from which genomic DNA strand a transcribed RNA molecule was coming from. This remains technically challenging [79], especially if maintaining both strand specificity and full-length transcript coverage is desired at the same time. As described above, Smart-seq [117, 118, 123] and CEL-seq [49] theoretically maintain strand specificity and full-length coverage. However, library preparation require fragmentation of either the input RNA or the resulting cDNA and the currently used SC RNA-seq protocols consider fragmentation only after transcript amplification (i.e. on the cDNA level), meaning that strand specificity is lost. However, directional information can be preserved by compromising the full-length coverage and selecting either 5′ ends by affinity purification, STRT [56, 57] or 3′ ends by selective PCR after transcript fragmentation [49].

- *Absence of spatial information*

In addition, all the methods described above fail to preserve spatial information about the transcript inside the cell because it is lysed prior to detection. However, the localization of mRNAs within subcellular compartments is a cellular strategy to regulate gene expression [93], so it would be insightful to sequence cellular transcripts while preserving their natural context. There are two recent methodologies to address this problem called, transcriptome in vivo analysis (TIVA) and fluorescent in situ RNA sequencing (FISSEQ), which will be discussed in the Sect. 5 as future perspectives.

In summary, owing to the high technical error rates that are inherent in SC RNA-seq methods, orthogonal validation is of paramount importance. Without validation, many SC studies are likely to falsely report extensive 'biological variation', when in fact they are merely observing extensive 'technical errors'.

3.2 Applications and Most Relevant Breakthroughs

SC transcriptomics is able to dissect mixed populations of cells and also allows the study of the transcriptome of rare or lowly represented cell types. Furthermore, the transcriptome of an individual cell is not fixed, but reflects the functionality of the cell, as well as its responses to acute extrinsic and intrinsic stimuli. There are a high number of applications of SC transcriptomics, these include the analysis of rare cell types, the reconstruction of cell lineage trees [154], exon usage between genetically identical cells [134], the study of the embryogenesis through the dissection of transcriptional programs in single cells [172, 173], the characterisation of transcriptional fluctuations under different external or internal conditions (cell cycle, circadian rhythms, hormone stimulation, paracrine signals, etc.) in a phenotypically homogenous population [60, 134, 135], allele-specific gene expression [147], transcriptional diversity of single cancer cells [115], etc. In this section we will further comment on the two of the most well-characterized applications: the discovery or study of different cell types (giving few examples, Fig. 4) and embryogenesis based on SC transcriptomics.

3.2.1 Identification of Different Cell Types

Individual cells differ greatly in their size, morphology, developmental origin and functional properties. Yet, our current level of understanding of cell types, their origin, evolution and diversity is in general quite poor [4]. Furthermore, there is no general agreement on the number of cell types in a mammalian body. In fact, there is no agreement on what defines a cell type, and finding such a definition must surely be one of the most important goals as we embark on large-scale SC transcriptome analysis. As a starting point, cell types can be provisionally identified as

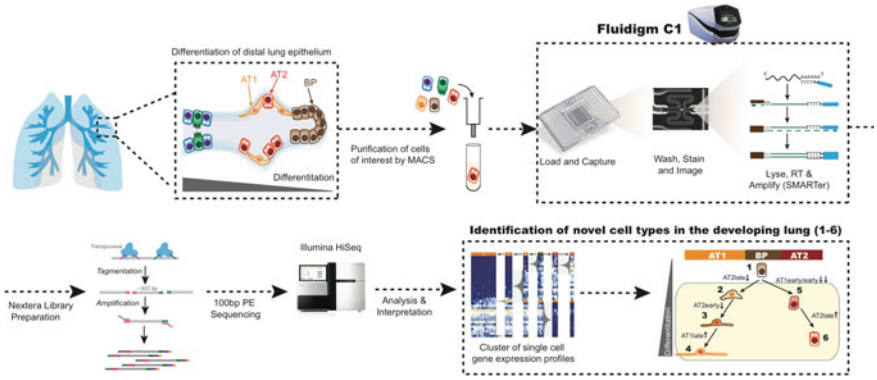

Fig. 4 Workflow of single-cell transcriptomics analysis of lung epithelial cells during development. Figure adapted by permission from Macmillan Publishers LTd: Nature [154], copyright (2014). SC transcriptomics allowed the discovery of two and three maturation intermediates in the specification processes of AT2 (cuboidal alveolar type 2) and AT1 (flat alveolar type 1) cell types from a common BP (biological progenitor)

cells for which global transcriptional states are similar. This provisional concept leads immediately to an unbiased method of cell-type discovery: collect a large, unbiased sample of cells from the tissue of interest, generate transcriptomes for each cell and use computational methods to find sets of similar cells. Established clustering and dimension-reduction methods, such as K-means, affinity propagation and hierarchical clustering, and principal component analysis, are useful starting points [40]. Comparison between these networks in normal and disease states can provide deeper mechanistic insight to the underlying effects of disease [126].

High-throughput single-cell RNA-seq (MARS-Seq) has been used for the cell-type characterization of splenic tissues in vivo [60]. The dendritic cell population represents a highly heterogeneous group that is not possible to subdivide based on cell surface markers. By modeling SC transcriptional states in dendritic cells, the authors discovered at least four different subpopulations of dendritic cells based solely on the transcriptional signature, this analysis also showed a high degree of transcriptional network organization within the dendritic cell population. These data prove SC RNA-seq as an effective tool for comprehensive cellular decomposition of complex tissues. In an independent study, SC RNA-seq of hematopoietic stem cells and seven progenitor populations enabled the identification, quantification and differential expression analysis of cell-type specific transcript isoforms, novel and unannotated splice junctions and alternative splicing events at genome-wide level. Analysis of lineage commitment events revealed a wealth of previously undetectable transcript switching and shifts altering isoform usage ratio, without appreciable changes at gene level, providing evidence of additional layers of regulation in cell fate determination [11].

The lineage hierarchy of the lung epithelium has also been studied using microfluidic SC RNA-seq [154]. The development and branching formation of the

mammalian lung has been studied by marker expression analysis and fate-mapping, however, the mechanisms that control the progression of lung progenitors along distinct lineages into mature alveolar cell types remain unknown, in part due to the limited number of lineage markers [66, 177]. The analysis of the SC RNA-seq data allowed the empirical classification of cells into distinct groups using an unbiased genome-wide approach that did not require a priori knowledge of the underlying cell types or prior purification of cell populations. The data also confirmed the basic outlines of the classical model of epithelial cell type diversity in the distal lung and led to the discovery of many novel cell type markers and transcriptional regulators that discriminate between the different populations (Fig. 4).

One major application in SC transcriptomics is the analysis of rare cell types. For example, circulating tumor cells (CTCs) can be obtained from patient blood, but typically only a few cells are isolated per blood sample and these will often be contaminated by a larger number of normal cells. SC RNA-seq could be used to differentiate between these cell types and simultaneously to obtain expression data from the tumor. In a recent elegant proof-of-principle experiment, Ramsköld et al. applied their Smart-seq method for SC RNA-seq and found differences between melanoma CTCs and primary melanocytes, giving insight into the disease [123]. Additionally, the technology allowed defining potent plasma membrane CTC biomarkers and discovering expressed coding mutations or SNPs. These proteins are thought to contribute to the invasiveness of CTCs and their ability to escape the immune system. There is great hope that RNA-seq of CTCs will aid the identification of a tumor's origin, improving the treatment of patients.

3.2.2 Embryogenesis

Embryonic development can be considered as the differentiation transition from the cellular to the whole-organism level. By definition, the early human embryo contains only rare cell types, which exist only transiently. Key questions about early development could be addressed using SC transcriptomics. SC RNA-seq studies have enabled a global analysis of early mammalian development [149, 172, 173], helping to substitute hypothesis- with discovery-driven science. All these studies relied on the poly(A) tailing protocol thus focusing on mRNA expression. New insights into early embryogenesis include, for instance, major changes in mRNA isoform abundance and defined patterns of allele-specific gene expression during murine blastomere development [147, 149]; functional modules of co-regulated genes [172], and the first lncRNA expression maps of embryonic stem cells and human preimplantation embryos [173]. RNA-seq has also the advantage of being able to use sequence polymorphisms to distinguish transcripts that are derived from each of the two parental genomes. RNA-seq will also soon improve SC analyses of subregions of the embryo, for example, the inner cell mass of murine blastocysts from which individual cells have already been analyzed via qRT-PCR and microarray [111].

4 Single Cell Epigenomics

Specialized cell types have a unique transcriptome, while sharing a common genome with every other cell in the organism. Epigenetics is defined as "both heritable changes in gene activity and expression (in the progeny of cells or of individuals) and also stable, long-term alterations in the transcriptional potential of a cell that are not necessarily heritable" (Roadmap Epigenomics project http://www.roadmapepigenomics.org). While epigenetics refers to the study of single genes or sets of genes, epigenomics refers to more global analyses of epigenetic changes across the entire genome. This involves the study of: chemical modifications to DNA, histone posttranslational modifications (HPTM), histone variants, three-dimensional chromatin conformation, nucleosome positioning and noncoding RNAs.

The epigenome is an attractive focus for single cell studies, in that it provides more cell-type specific information than the genome, and is more stable than the transcriptome. These properties may allow greater sensitivity in detecting aberrant cell types such as circulating tumor cells. Unlike the genome and transcriptome, the epigenome cannot be sequenced in a straightforward manner, making single cell epigenomics technically very challenging. Nonetheless, recent developments have allowed the first analysis of single cell epigenomics, as described below.

4.1 Single-Cell DNA Methylation

DNA methylation is perhaps the most intensely studied epigenetic modification [143]. In mammals, methylation of the 5′ carbon of cytosine (5 mC) generally occurs in the context of CpG dinucleotides, and is maintained through cell divisions by DNA methyltransferase 1 (DNMT1). While generally associated with transcriptional silencing, DNA methylation is known to have diverse functions in different biological contexts [62, 132]. An additional layer of complexity has been uncovered by the discovery that 5 mC can be oxidized by 10–11 translocation (Tet) enzymes to yield 5-hydroxymethyl cytosine (5 hmC), 5-formyl cytosine (5 fC) and 5-carboxy cytosine (5 caC) [22]. These DNA modifications are thought to be intermediaries in the removal of DNA methylation, but may have their own unique biological functions.

To study DNA methylation at high resolution, bisulfite conversion is performed. This treatment converts unmodified cytosine to uracil whereas 5mC and 5hmC are protected. One limitation of this chemistry is that the harsh bisulfite treatment causes substantial degradation of template DNA, posing a major hurdle for SC studies where starting material is minute. Thus, early attempts to study DNA methylation in single cells at high resolution were restricted to specific loci [23, 27, 64].

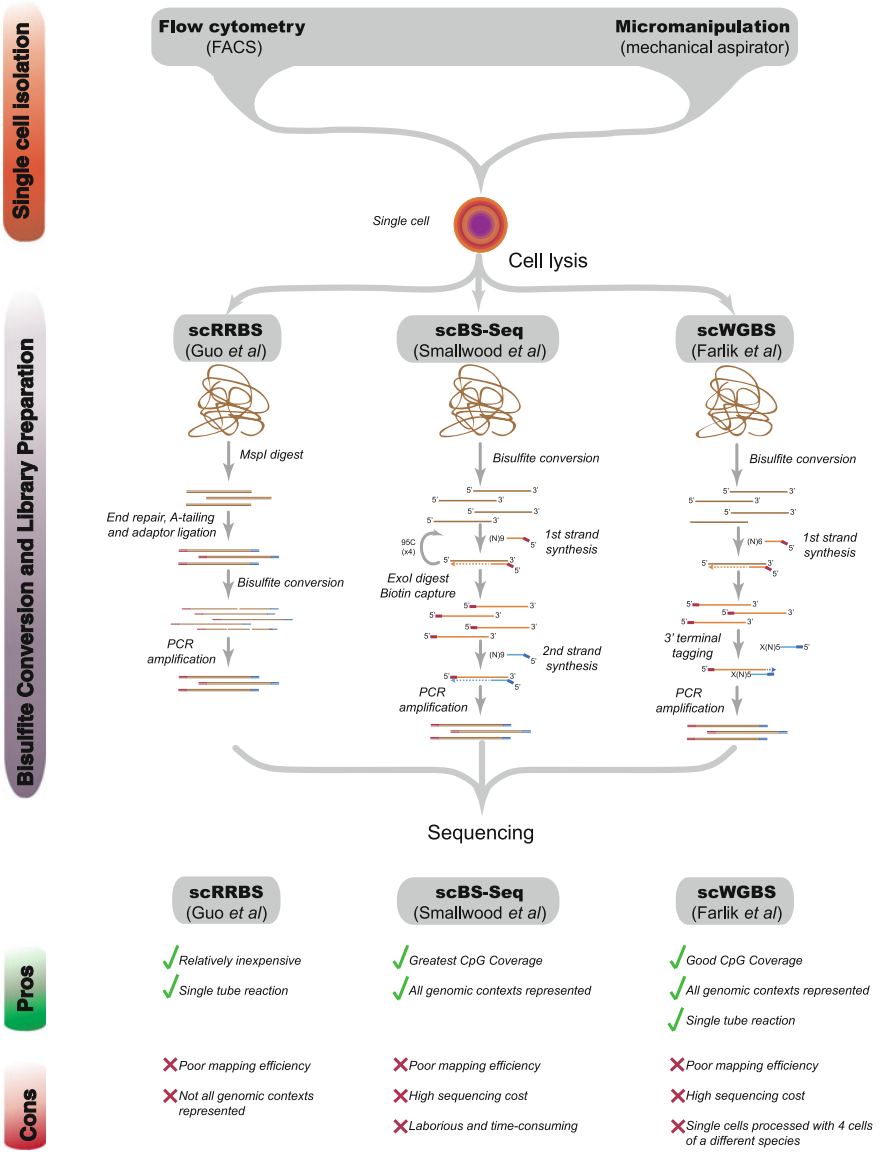

Fig. 5 Comparison of the three reported methods for analysis of the DNA methylome in single cells. The pros and cons of each approach are summarized below

Recently, several new methodologies have been developed to allow high resolution, analysis of DNA methylation at many loci in single cells (Fig. 5). These techniques are complementary and the most appropriate methodology will depend upon the biological question and experimental design.

4.1.1 Single Cell Reduced Representation Bisulfite Sequencing (ScRRBS)

In reduced representation bisulfite sequencing (RRBS) genomic DNA is first digested with a restriction enzyme, such as Msp I, which recognizes CCGG sites common in CpG islands (CGIs). The digested DNA is then subjected to library preparation for next-generation sequencing, bisulfite conversion and PCR amplification (Fig. 5). The sequencing libraries are biased towards C/G-rich sequences such as CGIs due to the nature of the Msp I enzyme, so this technique is not strictly a genome-wide approach. Since bisulfite conversion is performed following adaptor ligation, DNA degradation upon bisulfite treatment posed a significant obstacle in adapting this technique to low input amounts of DNA. Nonetheless, single-cell RRBS (scRRBS) has been achieved by adapting a single tube reaction that was previously optimized for low input amounts of DNA [137]. In scRRBS, carrier tRNA is included during the column purification step to minimize loss of material, and additional PCR cycles (a total of 47 cycles) are performed to amplify the bisulfite-converted libraries [44]. This protocol has provided information on up to 1.5 million CpG sites in the mouse genome, but is limited by a bias toward C/G-rich sequences and low library complexity that results from PCR duplication of sequences.

4.1.2 Single-Cell Bisulfite Sequencing (ScBS-Seq)

Genome-wide analysis of DNA methylation by bisulfite sequencing (BS-seq) is similar to RRBS except that the genomic DNA is fragmented randomly, typically by sonication, rather than by restriction digest. As with RRBS, the bisulfite conversion of adaptor ligated DNA fragments, results in substantial degradation and loss of library complexity. This limitation has been overcome by post-bisulfite adaptor tagging (PBAT), in which bisulfite conversion of genomic DNA is performed as the first step [101]. The sample DNA is both fragmented and single-stranded following bisulfite treatment, after which two rounds of random priming and strand extension are performed to introduce the two sequencing adaptors. This protocol was recently adapted to allow genome-wide analysis of DNA methylation in single cells [137] (Fig. 5). The first round of adaptor tagging was repeated 5 times to maximize recovery of the template DNA such that up to 48 % of CpG sites, from all types of genomic contexts, were recovered from a single mouse oocyte. While offering unbeatable CpG recovery scBS-seq is limited by low mapping efficiency and a loss of DNA strand information that results from the multiple rounds of first-strand synthesis. In a similar study, a commercially available PBAT-based kit (EpiGnome Methyl-seq kit, Illumina) has been adapted for single cell samples [33] (Fig. 5). This procedure does not repeat the first round of adaptor tagging but instead uses 3′ tagging of the first-strand synthesis products to recover as many fragments as possible. This leads to a lower recovery of CpG dinucleotides but retention of strand information.

4.2 Single Cell Chromatin Conformation

The physical arrangement of the genome in the three-dimensional space of the nucleus is known to influence gene expression in several different ways [21]. For example, regions associated with the nuclear lamina (lamina associated domains, LADs) generally contain repressed chromatin, and chromatin looping allows distal regulatory elements to contact target genes.

The classical technique used to study the arrangement of DNA in the nucleus is fluorescence in situ hybridisation (FISH). This method uses fluorescently labeled probes to map the locations of different loci of interest in individual cells. Thus, it has been possible for many years to study the three-dimensional arrangement of the genome in the nucleus, but only in a locus-specific and low-throughput manner.

To assess nuclear organization in a genome-wide manner chromatin conformation capture (3C), and its derivatives (4C and Hi-C), rely on chemical cross-linking to freeze *trans* and *cis* interactions in chromatin [18]. Restriction digest is then performed to fragment the DNA before it is diluted and the cross-linked fragments are re-ligated. PCR (3C and 4C) or sequencing library preparation (HiC) can then be employed to assess interactions between different regions of the chromatin. Recently, SC HiC has been achieved by performing the restriction digest and ligation steps in fixed nuclei [104]. SC libraries were subject to several sources of noise, but up to 30,000 contacts could be recovered from a single cell. This was sufficient to allow the structure of single-copy X chromosomes to be modeled, and to demonstrate that domains within chromosomes are maintained, while interactions between chromosomes differ between cells.

4.3 Future of Single Cell Epigenomics Methods

Further work is required to fully optimize and automate the methods described above. In addition, future studies will develop new methodologies to study other forms of epigenetic regulation in single cells including histone posttranslational modifications (HPTM), nucleosome positioning, and histone variants.

4.3.1 Optimization of Single Cell Methods for DNA Methylation

As described above, the current methodologies for single cell methylome analysis are limited by poor mapping efficiency and CpG recovery. These issues will be addressed by ongoing optimisation of these techniques. However, due to the harsh nature of bisulfite treatment, it is likely that these techniques will remain relatively inefficient and expensive in comparison to single cell transcriptomic and genomic methods. Standards for under and over conversion during bisulfite treatment also

need to be further developed to understand the technical errors involved in SC methylome analysis. To date, spiked-in unmethylated lambda DNA [44] or oligonucleotides [33], mitochondrial DNA and non-CpG methylation [137] have been used to monitor underconversion, while methylated oligonucleotides have been used as controls for over conversion [33]. While the bisulfite conversion efficiency has typically been around 98 %, standardized controls for this parameter should be developed to give confidence to measurements of single cell DNA methylation. Of course, any single cell technique will ideally be performed on a high-throughput microfluidic platform. This is an ongoing challenge for single cell analysis of DNA methylation, owing to the fact that bisulfite-converted DNA needs to be purified using magnetic beads or on-column clean-up, processes which are not easily translated to microfluidic platforms. Emerging technologies may enable scBS-seq to be performed using microfluidic devices in the future [146]. However, to date only locus-specific analysis of DNA methylation has been implemented on the Fluidigm C1 microfluidics device, with methylation specific restriction digest followed by PCR allowing multiple loci to be studied in single cells [85].

4.3.2 New Methods for Single Cell DNA Methylation

BS-seq is not able to discriminate between 5mC and 5hmC, so further treatment of the DNA is performed to study these modifications specifically. Oxidative bisulfite sequencing (oxBS-seq) can be used to measure 5mC alone [7]. The DNA is first treated with an oxidant that converts 5hmC to 5fC, so that only methylated cytosines (5mC and not 5hmC) are protected from bisulfite conversion. Tet assisted bisulfite sequencing (TAB-seq) provides an independent measure of 5hmC levels [176]. In this technique, 5hmC is first glucosylated before Tet-mediated oxidation is performed. This converts 5mC to 5caC while 5hmC is protected by the glucosyl moiety. Finally, bisulfite conversion is performed and cytosines in the sequenced libraries are indicative of 5hmC in the template DNA. The extra treatments involved in oxBS-seq and TAB-seq pose added challenges to single cell analysis. In particular, the chemical oxidation in oxBS-seq introduces further DNA damage and clean-up steps.

It may be possible to avoid these issues by applying nanopore sequencing or SMRT-seq (single-molecule real-time sequencing) technologies to epigenetic studies. Such sequencing platforms promise to be able to read 5mC and its derivatives, directly and concurrently from the untreated and unamplified DNA of a single cell. In nanopore sequencing DNA polymerases are joined to protein nanopores (such as the bacterial protein α-hemolysin) embedded in an electrically resistant lipid bilayer. A voltage is applied over the membrane as the polymerase feeds the template strand through the nanopore. In theory, modifications to the template should be evident from a unique signature in the electronic current passing through the nanopore. However, this has only been demonstrated in synthetic oligonucleotides to date [162].

Single molecule real-time sequencing (SMRT-seq) measures the kinetics of fluorescent nucleotide incorporation by individual DNA polymerases tethered to a specialized array of miniscule reaction chambers. Modifications to the template DNA strand alter the time that each nucleotide is held in complex with the polymerase, as well as the interval between incorporation of nucleotides. This has allowed detection of 5mC, 5hmC and adenine methylation (6 mA) in synthetic templates [37], 6 mA and 5mC in the *E. coli* genome [32], and glucosylated 5hmC in mouse DNA [138]. These technologies face several common challenges in epigenetic applications. In each case the signals generated by DNA modifications are influenced by the sequence context of the template molecule, and unknown modifications to the DNA may confound the sequencing read-out. Thus, both of these technologies require further development and sophisticated data analysis to confidently call epigenetic modifications to DNA. Additionally, for applications to single-cell epigenetic studies it will be necessary to optimize these approaches for very low amounts of unamplified DNA.

4.3.3 New Methods for Single Cell Analysis of HPTM

Like DNA, the histone proteins around which it is wrapped, can be chemically modified as a means of epigenetic regulation. There are many different forms of histone modifications, which are intensely studied, and have been associated with different chromatin states [5]. For example, H3K4ac is generally indicative of transcriptional activation while H3K9me is more abundant in inactive chromatin. Chromatin immunoprecipitation sequencing (ChIP-seq) is the technique typically used to study histone modifications on a genome-wide scale. Crosslinked chromatin is sheared by sonication and a specific antibody against your desired HPTM is used to pull-down the DNA-protein complexes. The specific DNA fragments containing the HPTM of choice are then purified to perform library preparation and sequencing.

ChIP-seq studies are limited by the sensitivity and specificity of the antibody in use and generally require large amounts of input DNA. Although ChIP-seq has recently been performed on as few as 1000 cells [10], this method is unlikely to be extended to single cell analysis. An interesting technique has resolved some of these limitations using DNA adenine methyltransferase identification (DamID) technology. This approach involves fusing the bacterial Dam enzyme to a protein of interest, such as a histone acetylase. When the fusion protein is in close proximity to DNA, adenine methylation (6 mA) is introduced into the DNA. This modification is not found in mammalian cells, and is not maintained through the cell cycle, providing a sensitive and temporal mark of protein-DNA interactions. If SMRT-seq technology can be developed to assess 6 mA in single cells, it may be possible to use this approach to study HPTM in individual cells. However, it is worth noting that DamID requires expression of a fusion protein, so this strategy will not be applicable to primary cell types.

4.4 Biological Insights and Future Applications

4.4.1 DNA Methylation in Embryonic Stem Cells

Techniques for SC epigenomics are still in the very early stages of development. Nonetheless, several interesting biological insights have been gained during method development. All three papers describing single cell techniques for genome-wide DNA methylation analysis use mouse embryonic stem cells (ESCs) as a model cell type. ESCs display remarkable methylome plasticity that reflects their developmental state. Addition of two inhibitors targeting Erk1/2 and Gsk3β (2i) to the culture medium returns these cells to a ground state of pluripotency [174] that is accompanied by widespread loss of DNA methylation [35, 46]. Smallwood and colleagues profiled a total of 32 single ESCs to demonstrate that DNA methylation is heterogeneous in ESCs grown in either serum-containing media or in the presence of 2i. This result is somewhat counterintuitive given that 2i ESCs are known to be relatively homogeneous at the level of transcription [92], but is consistent with previous observations that transcription and DNA methylation are uncoupled in 2i ESCs [35, 46]. Furthermore, clustering of 2i and serum ESC methylomes revealed the presence of rare "2i-like" cells in serum cultures, raising the possibility that stem cells poised for differentiation can cycle through the pluripotent ground state. A comparison of different genomic contexts in scBS-seq data demonstrated that distal regulatory elements (i.e. enhancers) had highly variable DNA methylation in ESCs. Farlik and co-authors studied ESCs in the context of short-term exposure to 2i, as well as upon induction of differentiation. They also identified enhancers as having highly dynamic DNA methylation across this spectrum of differentiation states. These observations support the hypothesis that heterogeneous DNA methylation at enhances may contribute to transcriptional heterogeneity and direct the differentiation of primed ESCs [77].

4.4.2 Future Applications

Applications for SC epigenomics will evolve as new methodologies continue to be developed, allowing many epigenetic features to be investigated in diverse contexts. To illustrate a few possibilities some applications for SC DNA methylation analysis are described below.

- *Single cell DNA methylation in early development*

The methylome undergoes two rounds of reprogramming during early mammalian development [77]. After fertilization DNA methylation is progressively lost from the genome until the blastocyst forms. At this stage specification of the inner cell mass (ICM) and trophectoderm (TE) is associated with differential DNA methylation with the TE being hypomethylated in comparison to the ICM [51]. In particular, DNA methylation at the Elf5 promoter in the ICM acts as a lineage

gate-keeper ensuring that these cells cannot trans-differentiate into the TE lineage [108]. SC epigenomics will be used to understand this and other lineage specification events in the developing embryo, and this knowledge will guide attempts to artificially direct stem cells into certain lineages for regenerative medicine applications. A second wave of global DNA demethylation is observed in the developing germ cells [133]. This is important for proper establishment of imprinted loci in the next generation, and may also ensure that epigenetic information is not conserved across generations. SC epigenomics will prove invaluable to our understanding of transgenerational epigenetic inheritance [34] and may also prove useful in assisted reproductive technology (ART) by enabling clinicians to screen for embryos with disorders in genomic imprinting [14].

- *Single cell epigenomics in cancer studies*

The epigenome is profoundly remodeled in many forms of cancer, and in some cases drugs targeting epigenetic mechanisms are already in clinical use. Thus, SC epigenomics, like SC transcriptomics and genomics, will find many applications in this field. DNA methylation has already proven useful as a biomarker for circulating tumor cells [15], owing to the fact that DNA methylation is more stable than transcriptional state. SC analysis will extend these studies by allowing minute samples to be assessed and will also reveal any heterogeneity or rare cell types present in these populations. DNA methylation can also be used as a biomarker in drug-resistant cancers [103, 140], and SC analyses will shed light on the role of DNA methylation in acquisition of drug resistance. For example, the cellular heterogeneity in cancers could be investigated before and after treatment to determine which cells are most resistant to therapy.

5 Data Analysis: Bioinformatics

SC genomics is a rapidly growing field with many new techniques emerging in the past few years. However, few bioinformatics tools specific for SC genomics analysis are available. Many current bioinformatics tools developed for bulk cell sequencing do not work well with SC sequencing data due to the inclusion of the WGA/WTA for single cells, which makes bioinformatics analysis challenging. The amplification process has two major technical problems: lower genome coverage and amplification bias. Nevertheless, as a revolutionary technology, SC sequencing will quickly be applied in many biological and medical fields, and the bioinformatics community needs to act quickly to keep pace with the expected flood of SC sequencing data.

5.1 Bioinformatics in Single-Cell Genomics

- **Algorithms for SNP calling in SC NGS**

SNPs calling algorithms for bulk cell samples have been studied extensively; among them, GATK [95], SNPdetector [178], SOAPsnp [82], and VarScan [70] are widely used. However, there is no SNP calling algorithm originally designed for SC sequencing data. Researchers have used established softwares to call SNPs in a few recently published single-cell studies. For example, Zong et al. [181] used GATK, while Xu et al. [171] used SOAPsnp to call SNPs in single cell sequencing samples. None of these methods, however, take the intrinsic properties of single-cell amplification into consideration. Base alterations, such as SNPs, can be detected in SC WGA products. However, to call accurate and reliable base substitutions in non-haploid loci, one requires the data of at least three cells to discriminate the variant from a WGA or sequencing error [52, 171, 181] and as such, detailed characterisation of extremely rare cells or subclones within populations may not be possible.

To develop a SNP calling algorithm specifically designed for SC sequencing, and to overcome the low genome coverage and high false positive rate shortcomings, several suggestions have been made [110]: (1) the algorithm should be able to distinguish true SNPs from amplification errors; and (2) the algorithm should be able to call SNPs from low-coverage sequencing.

- **Algorithms for CNV calling in SC NGS**

Currently many software packages are available for calling CNVs in bulk DNA sequencing, such as CNV-seq [170], PenCNV [163], CNAseg [58], Readdepth [100], and cn.MOPS [68]. However, few software packages and algorithms have been designed for SC CNV calling, and the impact of amplification bias on CNV calling has not been systematically investigated.

To improve the quality and accuracy of calling CNV from SC sequencing, first, we need to carefully examine the bias generated in the genome amplification process. For example, in one study of the MDA method, recurrent MDA-induced copy number biases were reported to associate with sequence repeats and proximity to chromosome ends, increased GC content, and annotated CNVs [121]. Once we know the pattern of artificial biases, we can develop algorithms to reduce the noise to call confident CNV assessment. Second, noise reduction problems also exist in other fields, such as signal processing and image processing, where noise reduction has been extensively studied, thus it is possible to employ algorithms such as wavelet and/or Fourier transformation to single cell data to reduce noise. Third, pairwise comparisons of amplified products should help to reduce the number of artificial CNVs. Fourth, allelic fractions of heterozygous SNPs or aberrantly mapping read pairs following paired-end sequencing of the WGA product [161] can be used to increase confidence in CNV measurements. Fifth, the cell cycle stage of the isolated cell must be considered, further complicating the analysis, as cells in

S-phase demonstrate a dynamic copy number profile, leading to false structural DNA-imbalance discoveries [156].

- **Analysis of structural variants in SC NGS**

The identification of the full spectrum of intra- and interchromosomal (un)balanced structural variants in a single-cell WGA product is still in poorly developed. The main difficulty is to filter true structural variants from chimeric DNA generated during WGA, as well as issues with genome coverage. Although filters have been designed to permit the detection of the structural architecture of DNA copy number variation [161], many structural variants are still missed in SC analyses.

5.2 Bioinformatics in Single-Cell Transcriptomics

Most of the bioinformatics analyses in SC transcriptomics are focused on the quantitative expression of genes, the detection of transcripts (lowly or highly expressed) and the identification of splice forms. The challenge of SC RNA bioinformatics analysis is mainly due to the bias and distortion in the WTA process: (1) amplification cannot generate full-length cDNAs; (2) transcripts are not amplified at the same ratio; and, (3) low abundant transcripts are difficult to detect.

- **Quantitative gene expression and detection of splice variants in SC RNA-seq**

The computational measurement of quantitative gene expression has been extensively studied in bulk cell sequencing analysis. Gene expression can be calculated from the number of sequencing reads mapped to a particular gene region. These approaches include two steps: mapping RNA sequencing reads to gene regions, and calculating expression levels. In the first step, many tools have been developed for sequencing read mapping, such as TopHat [151], RUM [42], BWA [81], Bowtie [72], STAR [25], etc. In the second step, reads per kilobase per million reads (RPKM) [102] and fragments per kilobase per million fragments (FPKM) [152] are commonly used to measure gene expression levels. For example, Yan et al. used BWA to align reads to a reference genome [173] to mapSC RNA sequencing reads. They selected genes with RPKM ≥ 0.1 for further analysis. Shalek et al. used Tophat1 to map reads to a reference genome, then used RSEM [80] to obtain the expression level of transcripts per million (TPM) [134].

It is usually difficult to get full-length transcripts in SC RNA sequencing, and, therefore, 3′-end biases are often generated (see Sect. 3.1.3). The FPKM/RPKM values, which are commonly used to measure gene expression levels, do not consider bias across the transcripts, and therefore, may not suitable for SC RNA sequencing in bioinformatics analysis. Furthermore, the pronounced 3′-end bias of WTA may hamper the ability to identify alternate splicing differences in single cells.

Recently several new amplification protocols have been developed, but bias still exists to a certain extent. Thus new methods are needed to generate an unbiased quantitative measure of transcript expression in SC transcriptomics analysis that consider the following:

(1) The need of new standard expression level measurement beyond RPKM/FPKM. One possible solution is to normalize expression levels by coverage lengths instead of by using full-length transcripts.
(2) To reduce amplification biases by developing new bioinformatics approaches that systematically analyze how bias is generated during amplification to discover the patterns of bias. Machine learning [47] may be a powerful tool to study the distribution of bias and to predict amplification bias.

- **Detection of lowly expressed transcripts in SC RNA-seq**

Bulk cell samples are usually sequenced at high depth to obtain low-abundance transcripts. However, in SC sequencing, the low-abundance transcripts may be undetectable due to inefficiency of the amplification approach. Even if they are detectable, the influence of technical noise and stochastic effects at these low levels may result in unreliable measurements of relative abundance within or between individual cells. For example, Picelli et al. using Smart-seq 2 found the observed variability between cells was mainly of a technical nature for low-abundance transcripts, whereas in medium- and high-abundance transcripts, variability between cells was mainly biological [117]. Thus, a major challenge in quantitative analysis of SC transcriptome data is understanding technical noise within or between the samples [91]. The inclusion of RNA spike-ins, such as those developed by the External RNA Controls Consortium (ERCC) [61], can give particular insights into the relative efficiency, detection limits, and technical noise of each amplification method [9, 65]. Furthermore, single molecule counting approaches, which incorporate a unique identifier into every molecule prior to amplification, will indicate the extent to which individual RNA molecules are amplified [67].

6 Future Perspectives and Concluding Remarks

- **Reduce or eliminate amplification methods for a satisfactory coverage and accuracy: nanopore and single molecule/real-time (SMRT) sequencing methods**

The ability to reduce [41] or even eliminate amplification of DNA or RNA before sequencing could increase the accuracy and reliability of SC analysis. Input requirements for library preparation continue to reduce, and direct library preparation from SC genomes has been demonstrated with Strand-seq methodology [29, 30]. Furthermore, the capacity to directly sequence unamplified DNA and RNA

from single cells, however, requires further innovation, though direct sequencing of single molecules is already a possibility for RNA and DNA [16, 112]. This innovation could be found with the 4th generation sequencing technologies: single molecule real-time (SMRT) sequencing from Pacific Biosciences and nanopore sequencing from Oxford Nanopore Technologies. SMRT seq is a sequencing-by-synthesis technology based on real-time imaging of fluorescently tagged nucleotides as they are synthesized along individual DNA template molecules. This technology produces considerably longer (5–20 kb) and highly accurate DNA sequences from individual unamplified molecules and can also show where methylated bases occur [26].

SMRT sequencing has proven to be ideal for small genomes but still needs some improvement in the amount of starting material and in more complex genomes in order to be applied in SC omics. Nanopore sequencing on the other hand, sequences individual DNA, methylated DNA or RNA strands as they are driven though biological nanopores by an applied electrical field. Changes in the ionic current are associated with a unique five-nucleotide DNA κ-mer and are detected as DNA molecules translocate through the nanopores at single-nucleotide precision [160]. The concept of this methodology is cutting edge being extremely precise and with no need of labeling or amplification at a low cost. However, nanopore sequencing is still in its infancy and needs a lot of improvements to be applied in complex genomes and in SC omics [8].

- **Integration of single cell genomics, transcriptomics and epigenomics**

Excitingly, methodology to analyze both the (epi)genome and transcriptome of the same cell in parallel is in development and will offer a powerful platform to analyze the exact relationship between genomic variation, regulation, and gene expression.

Recently, in a proof-of concept study, the first integrated genome and transcriptome sequencing was performed in the same cell [24]. The exciting and quasilinear amplification new strategy is able to quantify genomic DNA and mRNA from the same cell without physically separating the nucleic acids before amplification with a similar efficiency that the existing SC omics methods. In this study, the authors found that genes with high cell-to-cell variability in transcript numbers generally have lower genomic copy numbers, and vice versa, suggesting that copy number variations may drive variability in gene expression among individual cells. These findings highlight the enormous potential of integrated single cell sequencing to elucidate heterogeneity at the genome, epigenome and transcriptome level.

- **Larger and high-throughput experiments: automated cell capture and library preparation and barcoding**

Typical single-cell sequencing studies have focused on small numbers of cells (10 s–100 s) but have already demonstrated the potential to distinguish complex heterogeneity at this level, however, in order to establish powerful statistical models it is ideal the analysis of a higher number of cells especially in heterogenic samples like tumor samples [110]. The application of automated cell capture, amplification, and library preparation systems particularly those utilizing nanofluidics approaches

will dramatically increase the scale and affordability of single-cell analyses, such that much larger experiments will emerge. Currently, C1™ Single-Cell Auto Prep system (Fluidigm) enables the automation of cell isolation, DNA or RNA extraction and amplification for up to 96 individual cells in a single workflow, however, the main bottleneck of the high-throughput workflow is the library preparation that so far hasn't been automated yet. During library preparation barcoding the samples enable the samples to be pooled together in a single sequencing reaction, thus it is possible to sequence up to 25 single cells on a single-flow cell lane, allowing 200 single cells to be profiled in a single run of the Illumina HiSeq 2000/2500. Moreover, by decreasing the genomic resolution of each single-cell copy number profile (for example from 50 kb to 500 kb) it is possible to profile hundreds of cells in parallel on a single lane, or thousands on a run, making single-cell profiling economically feasible for clinical applications.

- **Live-cell or in situ visualization of locus-specific epigenetic and transcriptomic dynamics in single cells**

Currently, most SC experimental techniques provide snapshots of transcription profiles or epigenetic stages at a specific time because they depend on cell lysis, thus most persistence and hereditary information is lost and dynamics events such as transcriptional bursting or stochastic switching is overlooked. To overcome this, in situ or in vivo single cell transcriptomics and epigenetics is critical. There are two new methods for in vivo and in situ SC transcriptomics: transcriptome in vivo analysis (TIVA) and fluorescent in situ RNA sequencing (FISSEQ), respectively. TIVA is the first noninvasive approach for capturing mRNA from live single cells in their natural microenvironment. The TIVA tag enables mRNA capture from single cells in live tissue upon photoactivation. Using the TIVA tag in combination with RNA-seq is possible to obtain the transcriptome variance in tissues in vivo [86]. FISEQ allows the genome-wide profiling of gene expression in situ in fixed cells and tissues, in which RNA is converted into crosslinked cDNA amplicons and sequenced manually on a confocal microscope. Unlike traditional RNA-seq, this method enriches for context-specific transcripts over housekeeping and/or structural RNA, and it preserves the tissue architecture for RNA localization studies [78]. Recently, a new computational method called Seurat has been created to enable the spatial localization of transcripts by integrating SC RNA-seq with in situ RNA patterns in zebrafish embryo [129]. This method will be also applicable to mapping cellular localization within complex patterned tissues in diverse systems.

However, the methods to visualize chromatin modifications at the live-single cell level have been limited to visualized global level modifications. Currently there hasn't been any method developed for in vivo or in situ locus-specific or single-nucleotide level epigenetics studies. One suggestion is to used the Cas9/CRISPR system [127] in order to target specific genomic locus and couple with the FRET system [155] to achieve FRET signal when a particular modification is found at the specified locus, however, this methodology would be limited to a handful of genomic targets and it is impossible to be applied at genome-wide level.

7 Concluding Remarks

The past few years have seen rapid development of technologies and methods that permit highly detailed analysis of the genome and transcriptome of a single cell. In parallel, various observations have been made that suggest that both genomic and transcriptomic heterogeneity within an organism may have been considerably underestimated. Recently, single cell epigenomic methods have been described and have opened a new window of potential where questions about epigenetic mechanisms need to be readdressed at single cell level. Altogether, single-cell approaches now stand poised to illuminate this new layer of biological complexity during normal development and disease.

Acknowledgments FVM is a National Breast Cancer Foundation/Cure Cancer Australia Foundation Postdoctoral Training Fellow. This work is supported by National Health and Medical Research Council project grants (NHMRC 1063560). HJL supported by a grant from EU FP7 BLUEPRINT.

References

1. Adey A, Morrison HG, Asan et al (2010) Rapid, low-input, low-bias construction of shotgun fragment libraries by high-density in vitro transposition. Genome Biol 11:R119
2. Alfarawati S, Fragouli E, Colls P et al (2011) First births after preimplantation genetic diagnosis of structural chromosome abnormalities using comparative genomic hybridization and microarray analysis. Hum Reprod 26:1560–1574
3. Altarescu G, Zeevi DA, Zeligson S et al (2013) Familial haplotyping and embryo analysis for Preimplantation genetic diagnosis (PGD) using DNA microarrays: a proof of principle study. J Assist Reprod Genet 30:1595–1603
4. Arendt D (2008) The evolution of cell types in animals: emerging principles from molecular studies. Nat Rev Genet 9:868–882
5. Bannister AJ, Kouzarides T (2011) Regulation of chromatin by histone modifications. Cell Res 21:381–395
6. Baslan T, Kendall J, Rodgers L et al (2012) Genome-wide copy number analysis of single cells. Nat Protoc 7:1024–1041
7. Booth MJ, Branco MR, Ficz G et al (2012) Quantitative sequencing of 5-methylcytosine and 5-hydroxymethylcytosine at single-base resolution. Science 336:934–937
8. Branton D, Deamer DW, Marziali A et al (2008) The potential and challenges of nanopore sequencing. Nat Biotechnol 26:1146–1153
9. Brennecke P, Anders S, Kim JK et al (2013) Accounting for technical noise in single-cell RNA-seq experiments. Nat Methods 10:1093–1095
10. Brind'amour J, Liu S, Hudson M et al (2015) An ultra-low-input native ChIP-seq protocol for genome-wide profiling of rare cell populations. Nat Commun 6:6033
11. Chen L, Kostadima M, Martens JH et al (2014) Transcriptional diversity during lineage commitment of human blood progenitors. Science 345:1251033
12. Cheung VG, Nelson SF (1996) Whole genome amplification using a degenerate oligonucleotide primer allows hundreds of genotypes to be performed on less than one nanogram of genomic DNA. Proc Natl Acad Sci USA 93:14676–14679
13. Chi KR (2014) Singled out for sequencing. Nat Methods 11:13–17

14. Chiba H, Hiura H, Okae H et al (2013) DNA methylation errors in imprinting disorders and assisted reproductive technology. Pediatr Int 55:542–549
15. Chimonidou M, Strati A, Tzitzira A et al (2011) DNA methylation of tumor suppressor and metastasis suppressor genes in circulating tumor cells. Clin Chem 57:1169–1177
16. Coupland P, Chandra T, Quail M et al (2012) Direct sequencing of small genomes on the Pacific Biosciences RS without library preparation. Biotechniques 53:365–372
17. Czyz ZT, Hoffmann M, Schlimok G et al (2014) Reliable single cell array CGH for clinical samples. PLoS ONE 9:e85907
18. De Wit E, De Laat W (2012) A decade of 3C technologies: insights into nuclear organization. Genes Dev 26:11–24
19. Dean FB, Hosono S, Fang L et al (2002) Comprehensive human genome amplification using multiple displacement amplification. Proc Natl Acad Sci USA 99:5261–5266
20. Dean FB, Nelson JR, Giesler TL et al (2001) Rapid amplification of plasmid and phage DNA using Phi 29 DNA polymerase and multiply-primed rolling circle amplification. Genome Res 11:1095–1099
21. Dekker J, Marti-Renom MA, Mirny LA (2013) Exploring the three-dimensional organization of genomes: interpreting chromatin interaction data. Nat Rev Genet 14:390–403
22. Delatte B, Deplus R, Fuks F (2014) Playing TETris with DNA modifications. EMBO J 33:1198–1211
23. Denomme MM, Zhang L, Mann MR (2012) Single oocyte bisulfite mutagenesis. J Vis Exp
24. Dey SS, Kester L, Spanjaard B et al (2015) Integrated genome and transcriptome sequencing of the same cell. Nat Biotechnol
25. Dobin A, Davis CA, Schlesinger F et al (2013) STAR: ultrafast universal RNA-seq aligner. Bioinformatics 29:15–21
26. Eid J, Fehr A, Gray J et al (2009) Real-time DNA sequencing from single polymerase molecules. Science 323:133–138
27. El Hajj N, Trapphoff T, Linke M et al (2011) Limiting dilution bisulfite (pyro)sequencing reveals parent-specific methylation patterns in single early mouse embryos and bovine oocytes. Epigenetics: Off J DNA Methylation Soc 6:1176–1188
28. Engel P, Stepanauskas R, Moran NA (2014) Hidden diversity in honey bee gut symbionts detected by single-cell genomics. PLoS Genet 10:e1004596
29. Falconer E, Hills M, Naumann U et al (2012) DNA template strand sequencing of single-cells maps genomic rearrangements at high resolution. Nat Methods 9:1107–1112
30. Falconer E, Lansdorp PM (2013) Strand-seq: a unifying tool for studies of chromosome segregation. Semin Cell Dev Biol 24:643–652
31. Fan HC, Wang J, Potanina A et al (2011) Whole-genome molecular haplotyping of single cells. Nat Biotechnol 29:51–57
32. Fang G, Munera D, Friedman DI et al (2012) Genome-wide mapping of methylated adenine residues in pathogenic Escherichia coli using single-molecule real-time sequencing. Nat Biotechnol 30:1232–1239
33. Farlik M, Sheffield NC, Nuzzo A et al (2015) Single-cell DNA methylome sequencing and bioinformatic inference of epigenomic cell-state dynamics. Cell Rep
34. Ferguson-Smith AC, Patti ME (2011) You are what your dad ate. Cell Metab 13:115–117
35. Ficz G, Hore TA, Santos F et al (2013) FGF signaling inhibition in ESCs drives rapid genome-wide demethylation to the epigenetic ground state of pluripotency. Cell Stem Cell 13:351–359
36. Fiegler H, Geigl JB, Langer S et al (2007) High resolution array-CGH analysis of single cells. Nucleic Acids Res 35:e15
37. Flusberg BA, Webster DR, Lee JH et al (2010) Direct detection of DNA methylation during single-molecule, real-time sequencing. Nat Methods 7:461–465
38. Frumkin D, Wasserstrom A, Kaplan S et al (2005) Genomic variability within an organism exposes its cell lineage tree. PLoS Comput Biol 1:e50
39. Gawad C, Koh W, Quake SR (2014) Dissecting the clonal origins of childhood acute lymphoblastic leukemia by single-cell genomics. Proc Natl Acad Sci USA 111:17947–17952

40. Gehlenborg N, O'donoghue SI, Baliga NS et al (2010) Visualization of omics data for systems biology. Nature methods 7:S56-68
41. Gole J, Gore A, Richards A et al (2013) Massively parallel polymerase cloning and genome sequencing of single cells using nanoliter microwells. Nat Biotechnol 31:1126–1132
42. Grant GR, Farkas MH, Pizarro AD et al (2011) Comparative analysis of RNA-Seq alignment algorithms and the RNA-Seq unified mapper (RUM). Bioinformatics 27:2518–2528
43. Guo G, Huss M, Tong GQ et al (2010) Resolution of cell fate decisions revealed by single-cell gene expression analysis from zygote to blastocyst. Dev Cell 18:675–685
44. Guo H, Zhu P, Wu X et al (2013) Single-cell methylome landscapes of mouse embryonic stem cells and early embryos analyzed using reduced representation bisulfite sequencing. Genome Res 23:2126–2135
45. Guo MT, Rotem A, Heyman JA et al (2012) Droplet microfluidics for high-throughput biological assays. Lab Chip 12:2146–2155
46. Habibi E, Brinkman AB, Arand J et al (2013) Whole-genome bisulfite sequencing of two distinct interconvertible DNA methylomes of mouse embryonic stem cells. Cell Stem Cell 13:360–369
47. Hamelryck T (2009) Probabilistic models and machine learning in structural bioinformatics. Stat Methods Med Res 18:505–526
48. Hartmann CH, Klein CA (2006) Gene expression profiling of single cells on large-scale oligonucleotide arrays. Nucleic Acids Res 34:e143
49. Hashimshony T, Wagner F, Sher N et al (2012) CEL-Seq: single-cell RNA-Seq by multiplexed linear amplification. Cell reports 2:666–673
50. Heitzer E, Auer M, Gasch C et al (2013) Complex tumor genomes inferred from single circulating tumor cells by array-CGH and next-generation sequencing. Cancer Res 73:2965–2975
51. Hemberger M, Dean W, Reik W (2009) Epigenetic dynamics of stem cells and cell lineage commitment: digging Waddington's canal. Nat Rev Mol Cell Biol 10:526–537
52. Hou Y, Song L, Zhu P et al (2012) Single-cell exome sequencing and monoclonal evolution of a JAK2-negative myeloproliferative neoplasm. Cell 148:873–885
53. Hu DG, Webb G, Hussey N (2004) Aneuploidy detection in single cells using DNA array-based comparative genomic hybridization. Mol Hum Reprod 10:283–289
54. Huang H, Goto M, Tsunoda H et al (2014) Non-biased and efficient global amplification of a single-cell cDNA library. Nucleic Acids Res 42:e12
55. Huang J, Yan L, Fan W et al (2014) Validation of multiple annealing and looping-based amplification cycle sequencing for 24-chromosome aneuploidy screening of cleavage-stage embryos. Fertil Steril 102:1685–1691
56. Islam S, Kjallquist U, Moliner A et al (2011) Characterization of the single-cell transcriptional landscape by highly multiplex RNA-seq. Genome Res 21:1160–1167
57. Islam S, Kjallquist U, Moliner A et al (2012) Highly multiplexed and strand-specific single-cell RNA 5' end sequencing. Nat Protoc 7:813–828
58. Ivakhno S, Royce T, Cox AJ et al (2010) CNAseg–a novel framework for identification of copy number changes in cancer from second-generation sequencing data. Bioinformatics 26:3051–3058
59. Iwamoto K, Bundo M, Ueda J et al (2007) Detection of chromosomal structural alterations in single cells by SNP arrays: a systematic survey of amplification bias and optimized workflow. PLoS ONE 2:e1306
60. Jaitin DA, Kenigsberg E, Keren-Shaul H et al (2014) Massively parallel single-cell RNA-seq for marker-free decomposition of tissues into cell types. Science 343:776–779
61. Jiang L, Schlesinger F, Davis CA et al (2011) Synthetic spike-in standards for RNA-seq experiments. Genome Res 21:1543–1551
62. Jones PA (2012) Functions of DNA methylation: islands, start sites, gene bodies and beyond. Nat Rev Genet 13:484–492
63. Kang Y, Norris MH, Zarzycki-Siek J et al (2011) Transcript amplification from single bacterium for transcriptome analysis. Genome Res 21:925–935

64. Kantlehner M, Kirchner R, Hartmann P et al (2011) A high-throughput DNA methylation analysis of a single cell. Nucleic Acids Res 39:e44
65. Katayama S, Tohonen V, Linnarsson S et al (2013) SAMstrt: statistical test for differential expression in single-cell transcriptome with spike-in normalization. Bioinformatics 29:2943–2945
66. Kim CF, Jackson EL, Woolfenden AE et al (2005) Identification of bronchioalveolar stem cells in normal lung and lung cancer. Cell 121:823–835
67. Kivioja T, Vaharautio A, Karlsson K et al (2012) Counting absolute numbers of molecules using unique molecular identifiers. Nat Methods 9:72–74
68. Klambauer G, Schwarzbauer K, Mayr A et al (2012) cn.MOPS: mixture of Poissons for discovering copy number variations in next-generation sequencing data with a low false discovery rate. Nucleic Acids Res 40:e69
69. Klein CA, Schmidt-Kittler O, Schardt JA et al (1999) Comparative genomic hybridization, loss of heterozygosity, and DNA sequence analysis of single cells. Proc Natl Acad Sci USA 96:4494–4499
70. Koboldt DC, Chen K, Wylie T et al (2009) VarScan: variant detection in massively parallel sequencing of individual and pooled samples. Bioinformatics 25:2283–2285
71. Konings P, Vanneste E, Jackmaert S et al (2012) Microarray analysis of copy number variation in single cells. Nat Protoc 7:281–310
72. Langmead B, Salzberg SL (2012) Fast gapped-read alignment with Bowtie 2. Nat Methods 9:357–359
73. Lasken RS (2012) Genomic sequencing of uncultured microorganisms from single cells. Nat Rev Microbiol 10:631–640
74. Lasken RS (2007) Single-cell genomic sequencing using multiple displacement amplification. Curr Opin Microbiol 10:510–516
75. Lasken RS, Mclean JS (2014) Recent advances in genomic DNA sequencing of microbial species from single cells. Nat Rev Genet 15:577–584
76. Le Caignec C, Spits C, Sermon K et al (2006) Single-cell chromosomal imbalances detection by array CGH. Nucleic Acids Res 34:e68
77. Lee HJ, Hore TA, Reik W (2014) Reprogramming the methylome: erasing memory and creating diversity. Cell Stem Cell 14:710–719
78. Lee JH, Daugharthy ER, Scheiman J et al (2015) Fluorescent in situ sequencing (FISSEQ) of RNA for gene expression profiling in intact cells and tissues. Nat Protoc 10:442–458
79. Levin JZ, Yassour M, Adiconis X et al (2010) Comprehensive comparative analysis of strand-specific RNA sequencing methods. Nat Methods 7:709–715
80. Li B, Dewey CN (2011) RSEM: accurate transcript quantification from RNA-Seq data with or without a reference genome. BMC Bioinformatics 12:323
81. Li H, Durbin R (2009) Fast and accurate short read alignment with Burrows-Wheeler transform. Bioinformatics 25:1754–1760
82. Li R, Li Y, Fang X et al (2009) SNP detection for massively parallel whole-genome resequencing. Genome Res 19:1124–1132
83. Li Y, Xu X, Song L et al (2012) Single-cell sequencing analysis characterizes common and cell-lineage-specific mutations in a muscle-invasive bladder cancer. GigaScience 1:12
84. Ling J, Zhuang G, Tazon-Vega B et al (2009) Evaluation of genome coverage and fidelity of multiple displacement amplification from single cells by SNP array. Mol Hum Reprod 15:739–747
85. Lorthongpanich C, Cheow LF, Balu S et al (2013) Single-cell DNA-methylation analysis reveals epigenetic chimerism in preimplantation embryos. Science 341:1110–1112
86. Lovatt D, Ruble BK, Lee J et al (2014) Transcriptome in vivo analysis (TIVA) of spatially defined single cells in live tissue. Nat Methods 11:190–196
87. Lu S, Zong C, Fan W et al (2012) Probing meiotic recombination and aneuploidy of single sperm cells by whole-genome sequencing. Science 338:1627–1630
88. Luo L, Salunga RC, Guo H et al (1999) Gene expression profiles of laser-captured adjacent neuronal subtypes. Nat Med 5:117–122

89. Macaulay IC, Voet T (2014) Single cell genomics: advances and future perspectives. PLoS Genet 10:e1004126
90. Marcus JS, Anderson WF, Quake SR (2006) Microfluidic single-cell mRNA isolation and analysis. Anal Chem 78:3084–3089
91. Marinov GK, Williams BA, Mccue K et al (2014) From single-cell to cell-pool transcriptomes: stochasticity in gene expression and RNA splicing. Genome Res 24:496–510
92. Marks H, Kalkan T, Menafra R et al (2012) The transcriptional and epigenomic foundations of ground state pluripotency. Cell 149:590–604
93. Martin KC, Ephrussi A (2009) mRNA localization: gene expression in the spatial dimension. Cell 136:719–730
94. Mathiesen RR, Fjelldal R, Liestol K et al (2012) High-resolution analyses of copy number changes in disseminated tumor cells of patients with breast cancer. International journal of cancer. J Int Cancer 131:E405–E415
95. Mckenna A, Hanna M, Banks E et al (2010) The Genome Analysis Toolkit: a MapReduce framework for analyzing next-generation DNA sequencing data. Genome Res 20:1297–1303
96. Mclean JS, Lasken RS (2014) Single cell genomics of bacterial pathogens: outlook for infectious disease research. Genome Med 6:108
97. Mclean JS, Lombardo MJ, Badger JH et al (2013) Candidate phylum TM6 genome recovered from a hospital sink biofilm provides genomic insights into this uncultivated phylum. Proc Natl Acad Sci USA 110:E2390–E2399
98. Mclean JS, Lombardo MJ, Ziegler MG et al (2013) Genome of the pathogen Porphyromonas gingivalis recovered from a biofilm in a hospital sink using a high-throughput single-cell genomics platform. Genome Res 23:867–877
99. Metzker ML (2010) Sequencing technologies - the next generation. Nat Rev Genet 11:31–46
100. Miller CA, Hampton O, Coarfa C et al (2011) ReadDepth: a parallel R package for detecting copy number alterations from short sequencing reads. PLoS ONE 6:e16327
101. Miura F, Enomoto Y, Dairiki R et al (2012) Amplification-free whole-genome bisulfite sequencing by post-bisulfite adaptor tagging. Nucleic Acids Res 40:e136
102. Mortazavi A, Williams BA, Mccue K et al (2008) Mapping and quantifying mammalian transcriptomes by RNA-Seq. Nat Methods 5:621–628
103. Mulero-Navarro S, Esteller M (2008) Epigenetic biomarkers for human cancer: the time is now. Crit Rev Oncol Hematol 68:1–11
104. Nagano T, Lubling Y, Stevens TJ et al (2013) Single-cell Hi-C reveals cell-to-cell variability in chromosome structure. Nature 502:59–64
105. Navin N, Hicks J (2011) Future medical applications of single-cell sequencing in cancer. Genome Med 3:31
106. Navin N, Kendall J, Troge J et al (2011) Tumour evolution inferred by single-cell sequencing. Nature 472:90–94
107. Navin NE (2014) Cancer genomics: one cell at a time. Genome Biol 15:452
108. Ng RK, Dean W, Dawson C et al (2008) Epigenetic restriction of embryonic cell lineage fate by methylation of Elf5. Nat Cell Biol 10:1280–1290
109. Ni X, Zhuo M, Su Z et al (2013) Reproducible copy number variation patterns among single circulating tumor cells of lung cancer patients. Proc Natl Acad Sci USA 110:21083–21088
110. Ning L, Liu G, Li G et al (2014) Current challenges in the bioinformatics of single cell genomics. Front Oncol 4:7
111. Ohnishi Y, Huber W, Tsumura A et al (2014) Cell-to-cell expression variability followed by signal reinforcement progressively segregates early mouse lineages. Nat Cell Biol 16:27–37
112. Ozsolak F, Platt AR, Jones DR et al (2009) Direct RNA sequencing. Nature 461:814–818
113. Pan X (2014) Single cell analysis: from technology to biology and medicine. Single Cell Biol 3
114. Pan X, Durrett RE, Zhu H et al (2013) Two methods for full-length RNA sequencing for low quantities of cells and single cells. Proc Natl Acad Sci USA 110:594–599
115. Patel AP, Tirosh I, Trombetta JJ et al (2014) Single-cell RNA-seq highlights intratumoral heterogeneity in primary glioblastoma. Science 344:1396–1401

116. Pelechano V, Steinmetz LM (2013) Gene regulation by antisense transcription. Nat Rev Genet 14:880–893
117. Picelli S, Bjorklund AK, Faridani OR et al (2013) Smart-seq2 for sensitive full-length transcriptome profiling in single cells. Nat Methods 10:1096–1098
118. Picelli S, Faridani OR, Bjorklund AK et al (2014) Full-length RNA-seq from single cells using Smart-seq2. Nat Protoc 9:171–181
119. Pinkel D, Segraves R, Sudar D et al (1998) High resolution analysis of DNA copy number variation using comparative genomic hybridization to microarrays. Nat Genet 20:207–211
120. Polzer B, Medoro G, Pasch S et al (2014) Molecular profiling of single circulating tumor cells with diagnostic intention. EMBO Mol Med 6:1371–1386
121. Pugh TJ, Delaney AD, Farnoud N et al (2008) Impact of whole genome amplification on analysis of copy number variants. Nucleic Acids Res 36:e80
122. Raghunathan A, Ferguson HR Jr, Bornarth CJ et al (2005) Genomic DNA amplification from a single bacterium. Appl Environ Microbiol 71:3342–3347
123. Ramskold D, Luo S, Wang YC et al (2012) Full-length mRNA-Seq from single-cell levels of RNA and individual circulating tumor cells. Nat Biotechnol 30:777–782
124. Rinke C, Lee J, Nath N et al (2014) Obtaining genomes from uncultivated environmental microorganisms using FACS-based single-cell genomics. Nat Protoc 9:1038–1048
125. Rinke C, Schwientek P, Sczyrba A et al (2013) Insights into the phylogeny and coding potential of microbial dark matter. Nature 499:431–437
126. Saadatpour A, Guo G, Orkin SH et al (2014) Characterizing heterogeneity in leukemic cells using single-cell gene expression analysis. Genome Biol 15:525
127. Sander JD, Joung JK (2014) CRISPR-Cas systems for editing, regulating and targeting genomes. Nat Biotechnol 32:347–355
128. Sasagawa Y, Nikaido I, Hayashi T et al (2013) Quartz-Seq: a highly reproducible and sensitive single-cell RNA sequencing method, reveals non-genetic gene-expression heterogeneity. Genome Biol 14:R31
129. Satija R, Farrell JA, Gennert D et al. (2015) Spatial reconstruction of single-cell gene expression data. Nature Biotechnol
130. Schepers AG, Snippert HJ, Stange DE et al (2012) Lineage tracing reveals Lgr5 + stem cell activity in mouse intestinal adenomas. Science 337:730–735
131. Schmidt WM, Mueller MW (1999) CapSelect: a highly sensitive method for 5' CAP-dependent enrichment of full-length cDNA in PCR-mediated analysis of mRNAs. Nucleic Acids Res 27:e31
132. Schubeler D (2015) Function and information content of DNA methylation. Nature 517:321–326
133. Seisenberger S, Andrews S, Krueger F et al (2012) The dynamics of genome-wide DNA methylation reprogramming in mouse primordial germ cells. Mol Cell 48:849–862
134. Shalek AK, Satija R, Adiconis X et al (2013) Single-cell transcriptomics reveals bimodality in expression and splicing in immune cells. Nature 498:236–240
135. Shalek AK, Satija R, Shuga J et al (2014) Single-cell RNA-seq reveals dynamic paracrine control of cellular variation. Nature 510:363–369
136. Shapiro E, Biezuner T, Linnarsson S (2013) Single-cell sequencing-based technologies will revolutionize whole-organism science. Nat Rev Genet 14:618–630
137. Smallwood SA, Lee HJ, Angermueller C et al (2014) Single-cell genome-wide bisulfite sequencing for assessing epigenetic heterogeneity. Nat Methods 11:817–820
138. Song CX, Clark TA, Lu XY et al (2012) Sensitive and specific single-molecule sequencing of 5-hydroxymethylcytosine. Nat Methods 9:75–77
139. Spits C, Le Caignec C, De Rycke M et al (2006) Optimization and evaluation of single-cell whole-genome multiple displacement amplification. Hum Mutat 27:496–503
140. Stone A, Cowley MJ, Valdes-Mora F et al (2013) BCL-2 hypermethylation is a potential biomarker of sensitivity to antimitotic chemotherapy in endocrine-resistant breast cancer. Mol Cancer Ther 12:1874–1885

141. Streets AM, Zhang X, Cao C et al (2014) Microfluidic single-cell whole-transcriptome sequencing. Proc Natl Acad Sci USA 111:7048–7053
142. Subkhankulova T, Gilchrist MJ, Livesey FJ (2008) Modelling and measuring single cell RNA expression levels find considerable transcriptional differences among phenotypically identical cells. BMC Genom 9:268
143. Suzuki MM, Bird A (2008) DNA methylation landscapes: provocative insights from epigenomics. Nat Rev Genet 9:465–476
144. Swennenhuis JF, Reumers J, Thys K et al (2013) Efficiency of whole genome amplification of single circulating tumor cells enriched by cell search and sorted by FACS. Genome Med 5:106
145. Talseth-Palmer BA, Bowden NA, Hill A et al (2008) Whole genome amplification and its impact on CGH array profiles. BMC Res Notes 1:56
146. Tan SJ, Phan H, Gerry BM et al (2013) A microfluidic device for preparing next generation DNA sequencing libraries and for automating other laboratory protocols that require one or more column chromatography steps. PLoS ONE 8:e64084
147. Tang F, Barbacioru C, Nordman E et al (2011) Deterministic and stochastic allele specific gene expression in single mouse blastomeres. PLoS ONE 6:e21208
148. Tang F, Barbacioru C, Nordman E et al (2010) RNA-Seq analysis to capture the transcriptome landscape of a single cell. Nat Protoc 5:516–535
149. Tang F, Barbacioru C, Wang Y et al (2009) mRNA-Seq whole-transcriptome analysis of a single cell. Nat Methods 6:377–382
150. Telenius H, Carter NP, Bebb CE et al (1992) Degenerate oligonucleotide-primed PCR: general amplification of target DNA by a single degenerate primer. Genomics 13:718–725
151. Trapnell C, Pachter L, Salzberg SL (2009) TopHat: discovering splice junctions with RNA-Seq. Bioinformatics 25:1105–1111
152. Trapnell C, Williams BA, Pertea G et al (2010) Transcript assembly and quantification by RNA-Seq reveals unannotated transcripts and isoform switching during cell differentiation. Nat Biotechnol 28:511–515
153. Treff NR, Su J, Tao X et al (2010) Accurate single cell 24 chromosome aneuploidy screening using whole genome amplification and single nucleotide polymorphism microarrays. Fertil Steril 94:2017–2021
154. Treutlein B, Brownfield DG, Wu AR et al (2014) Reconstructing lineage hierarchies of the distal lung epithelium using single-cell RNA-seq. Nature 509:371–375
155. Truong K, Ikura M (2001) The use of FRET imaging microscopy to detect protein-protein interactions and protein conformational changes in vivo. Curr Opin Struct Biol 11:573–578
156. Van Der Aa N, Zamani Esteki M, Vermeesch JR et al (2013) Preimplantation genetic diagnosis guided by single-cell genomics. Genome Med 5:71
157. Van Gelder RN, Von Zastrow ME, Yool A et al (1990) Amplified RNA synthesized from limited quantities of heterogeneous cDNA. Proc Natl Acad Sci USA 87:1663–1667
158. Van Loo P, Voet T (2014) Single cell analysis of cancer genomes. Curr Opin Genet Dev 24:82–91
159. Van Uum CM, Stevens SJ, Dreesen JC et al (2012) SNP array-based copy number and genotype analyses for preimplantation genetic diagnosis of human unbalanced translocations. Eur J Hum Genet: EJHG 20:938–944
160. Venkatesan BM, Bashir R (2011) Nanopore sensors for nucleic acid analysis. Nat Nanotechnol 6:615–624
161. Voet T, Kumar P, Van Loo P et al (2013) Single-cell paired-end genome sequencing reveals structural variation per cell cycle. Nucleic Acids Res 41:6119–6138
162. Wallace EV, Stoddart D, Heron AJ et al (2010) Identification of epigenetic DNA modifications with a protein nanopore. Chem Commun (Camb) 46:8195–8197
163. Wang K, Li M, Hadley D et al (2007) PennCNV: an integrated hidden Markov model designed for high-resolution copy number variation detection in whole-genome SNP genotyping data. Genome Res 17:1665–1674

164. Wang Y, Waters J, Leung ML et al (2014) Clonal evolution in breast cancer revealed by single nucleus genome sequencing. Nature 512:155–160
165. Warren L, Bryder D, Weissman IL et al (2006) Transcription factor profiling in individual hematopoietic progenitors by digital RT-PCR. Proc Natl Acad Sci USA 103:17807–17812
166. Wells D, Sherlock JK, Handyside AH et al (1999) Detailed chromosomal and molecular genetic analysis of single cells by whole genome amplification and comparative genomic hybridisation. Nucleic Acids Res 27:1214–1218
167. Welty CJ, Coleman I, Coleman R et al (2013) Single cell transcriptomic analysis of prostate cancer cells. BMC Mol Biol 14:6
168. White AK, Vaninsberghe M, Petriv OI et al (2011) High-throughput microfluidic single-cell RT-qPCR. Proc Natl Acad Sci USA 108:13999–14004
169. Wu AR, Neff NF, Kalisky T et al (2014) Quantitative assessment of single-cell RNA-sequencing methods. Nat Methods 11:41–46
170. Xie C, Tammi MT (2009) CNV-seq, a new method to detect copy number variation using high-throughput sequencing. BMC Bioinformatics 10:80
171. Xu X, Hou Y, Yin X et al (2012) Single-cell exome sequencing reveals single-nucleotide mutation characteristics of a kidney tumor. Cell 148:886–895
172. Xue Z, Huang K, Cai C et al (2013) Genetic programs in human and mouse early embryos revealed by single-cell RNA sequencing. Nature 500:593–597
173. Yan L, Yang M, Guo H et al (2013) Single-cell RNA-Seq profiling of human preimplantation embryos and embryonic stem cells. Nat Struct Mol Biol 20:1131–1139
174. Ying QL, Wray J, Nichols J et al (2008) The ground state of embryonic stem cell self-renewal. Nature 453:519–523
175. Yona S, Kim KW, Wolf Y et al (2013) Fate mapping reveals origins and dynamics of monocytes and tissue macrophages under homeostasis. Immunity 38:79–91
176. Yu M, Hon GC, Szulwach KE et al (2012) Base-resolution analysis of 5-hydroxymethylcytosine in the mammalian genome. Cell 149:1368–1380
177. Zemke AC, Snyder JC, Brockway BL et al (2009) Molecular staging of epithelial maturation using secretory cell-specific genes as markers. Am J Respir Cell Mol Biol 40:340–348
178. Zhang J, Wheeler DA, Yakub I et al (2005) SNPdetector: a software tool for sensitive and accurate SNP detection. PLoS Comput Biol 1:e53
179. Zhang K, Martiny AC, Reppas NB et al (2006) Sequencing genomes from single cells by polymerase cloning. Nat Biotechnol 24:680–686
180. Zhang L, Cui X, Schmitt K et al (1992) Whole genome amplification from a single cell: implications for genetic analysis. Proc Natl Acad Sci USA 89:5847–5851
181. Zong C, Lu S, Chapman AR et al (2012) Genome-wide detection of single-nucleotide and copy-number variations of a single human cell. Science 338:1622–1626

Single-Cell Metabolomics

Hamidun Bunawan and Syarul Nataqain Baharum

Abstract Metabolomics, in conjunction with more conventional practises of genomics, transcriptomics and proteomics, provides a significant and holistic approach for a better understanding of the behaviour of individual cells. In a single cell, the transcription process produces mRNA which is translated into proteins, and these proteins act as biocatalysts to control metabolite biosynthesis. The study of metabolites in cellular processes is considered as a bridge that closes the gap between genotype and phenotype, and it provides a complete view on the "functionality" of each individual cell. Metabolomics is more reliable in comparison to other single-cell omics studies, as it offers a big picture on the dynamic functionality of a cell. Nevertheless, this technique is also the most problematic to quantify as the metabolome changes rapidly. The metabolome at the level of single cells is a perfect indicator of phenotypic heterogeneity, however, the techniques required to study the metabolome are relatively new. Further research is required to enhance the technique to improve the coverage of the metabolome, faster and accurate identification of metabolites, and to develop rapid non-destructive measurements. Analysis of the metabolome has to contend with the diversity of biomolecules and the grouping of different analytical platforms for complete metabolomics studies especially in single-cells metabolomics. In this chapter, the recent improvements in analytical tools to unravel single-cell metabolomics, as well as their specificity, will be described. This includes the exciting development and expansion of analytical tool technologies in metabolite analysis. These remarkable technological improvements applied to single cells have encountered several intrinsic limitations and challenges, and these major challenges will be discussed alongside the future prospects of single-cell metabolomics in systems biology.

Keywords Metabolomics · Single cell · Omics · Analytical · Systems biology

H. Bunawan · S.N. Baharum (✉)
Institute of Systems Biology, Universiti Kebangsaan Malaysia, 43600 Bangi, Selangor, Malaysia
e-mail: nataqain@ukm.edu.my

F.-G. Tseng and T.S. Santra (eds.), *Essentials of Single-Cell Analysis*, Series in BioEngineering, DOI 10.1007/978-3-662-49118-8_11

1 Introduction

Metabolomics is a developing technology that is used to assist in the biochemical analysis of the metabolome: small intracellular and extracellular molecules within a biological sample [1–3]. These molecules are involved in multiple basic intracellular processes and the physiology of the cell can be indicated by the metabolome. Metabolomics also includes the technology for sampling cells, the experimental methods used, the detection of metabolites, measuring concentrations of metabolites and interpreting the metabolomics data generated [4, 5]. Being able to detect and characterise cellular metabolites at the single-cell level, as well as to quantify their amounts, permits a variety of interesting researches including the analysis of functional heterogeneity between cells, even those which appear to have a homogeneous cell population [6, 7].

The analysis of single cells is an emergent field of research that captivates researchers from many disciplines because it provides a glimpse into the fundamental biological aspects such as evolution, cell adaptation and cell differentiation [8–10]. Metabolomics can assist in deciphering key mechanisms of cellular behaviour and contributes significantly to our understanding of metabolism. With the genetic information present in every cell and as genomics is a well-defined discipline, using DNA sequencing and bioinformatics, gene structure and function can be analysed. In cells, mRNA transcripts are produced and translated into proteins, which subsequently act as biocatalysts to control metabolite biosynthesis (Fig. 1). Understanding the final products, or metabolites, produced by this process is fundamental for gaining an insight into the metabolic functions of a particular cell. The swift development of metabolomics supplements genomic, transcriptomic and proteomic data to enable systematical research into biological systems and networks of single cells [11, 12]. Metabolomics has been demonstrated as a significant tool in

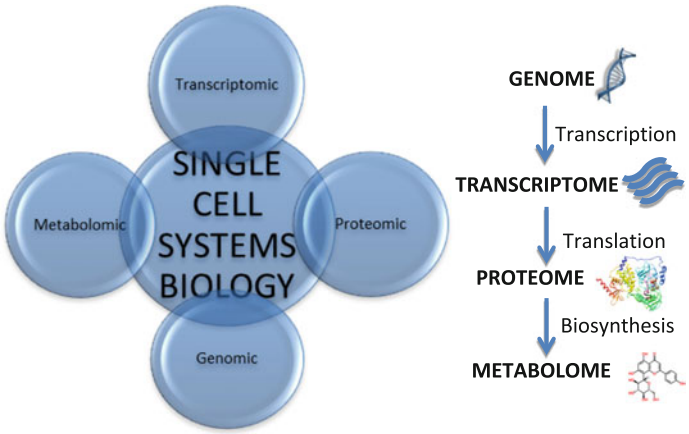

Fig. 1 Interconnection of the genome, transcriptome, proteome and metabolome within cells

anticipating and elucidating complex phenotypes in varied biological systems and has been shown as a vital method in functional genomics, illuminating individual gene functions from the comprehensive analysis of the metabolome.

Single-cell metabolomics analysis aims to help further understanding of cellular functions and to elucidate differences in single cells relative to cell populations [12–14]. One key factor is that the coordinated activities among individual cells contribute to the physiology and behaviour of multicellular organisms, and also to the organisation of ecological communities in unicellular organisms [15, 16]. Cellular variability, as well as pathological and functional heterogeneities, are integral to the development of individual biological and behavioural traits, and have important roles in the aetiology of many diseases [17, 18].

Metabolites are varied and have fundamental roles in key cellular processes. The detection, characterisation and quantification of a diverse assortment of metabolites in a single, multistage experiment are important technological objectives in single-cell metabolomics. Multiple recent advances in bioanalytical technologies for individual cell metabolome studies are available [12].

Since every single cell contributes to the product yield of the fermentation process in industrial biotechnology, it is important that lifeless, inactive or weakly active cells can be identified, as they reduce the productivity [19]. This heterogeneity is due to distinct intrinsic cell features such as age, cell cycle stage, position of the division plane, gene transfer or loss, mutations or epigenetic inheritance [19]. Therefore, single-cell related analytical techniques are required to assist in evaluating and controlling these processes. Similarly, external parameters influence cellular features due to numerous microenvironmental variations, such as the availability of carbon or other energy sources and the prevalence of stress conditions. Furthermore, in many research areas including haematology, stem cell biology, tissue engineering and cancer biology, the interpretation of data from the analysis of multiple cells can be problematic. The heterogeneity of populations and variation in dynamics within the sample is responsible for some of the difficulties in analysis and the generation of ambiguous measurements of the cell population. These emphasise the need for molecular biology methods that work at the level of the single cell [13, 20].

In this chapter, we aim to provide an overview of methodological advances in single-cell metabolomics to enable the metabolomes of every single cell in a population to be studied individually, and to elucidate information that is not obtainable from studies at the population level. Significant advances in single-cell sampling using microfluidics and nanoscale devices are discussed. The recent enhancements in sensitivity and specificity for analysis at the single-cell level using mass spectrometry, mass spectrometry imaging, capillary electrophoresis (CE) and nuclear magnetic resonance (NMR) are highlighted. The limitations and challenges of single-cell metabolomics are also discussed, as well as emerging developments within different fields aimed to illuminate the immense knowledge available upon analysis of the metabolomes of single cells.

2 Metabolomics Approach in Single-Cell Study

Single-cell metabolomics is an emerging research field with the development of new and sophisticated analytical platforms with high sensitivity and the ability to perform quantitative analyses. Advancements in mass spectrometry (MS) metabolomics for example, have made the study of metabolites at a cellular level a reality, hence increasing the unbiased characterisation of metabolites at the cellular level of biological systems [21]. Single-cell analysis mass spectrometry has been used widely and a significant numbers of other analytical approaches were developed to target very low metabolites in a cell [22]. Misra et al. [23] has summarised the recent studies in plant single cell and single-cell-type metabolomics as presented in Table 1. The studies were based on different metabolomics platforms such as GC-MS, UPLC-FT-MS, LC-ESI-MS and NMR. We have also added more information about single-cell studies on other type of samples such as microbes, algae and animals.

The first key step for single-cell metabolomics is to isolate the appropriate cells from an organism of interest. In this chapter, we highlight two small-volume separations techniques for single-cell sampling and/or manipulating of the particular cell for the metabolites analysis. Microfluidics and nanoscale devices are two common methods to retrieve single cells in a high-throughput fashion. Subsequently, analytical approaches for detecting metabolites in single cell also are discussed. In particular, mass spectrometry, MS imaging, capillary electrophoresis and nuclear magnetic resonance (NMR).

3 Technologies in Sampling Single Cells

3.1 Microfluidics

Experimental mechanisms to measure the dynamics of single cells using manual pipetting and conventional cell culture methods have restricted output and reproducibility. In addition, these are not always able to accurately alter the cellular environment in real time. Furthermore, the large volume of media required contributes to background fluorescence, inconsistency in concentration and a decrease in cell-to-cell paracrine signalling as a result of the dilution of secreted molecules [59, 60].

Microfluidic devices have significantly influenced the field of analytical chemistry since their introduction in the early 1990s. These devices provide numerous advantages over comparable bench-top instruments [61, 62]. For example, the reduction in sample size and reagent volume is a crucial advantage. It is now possible to use and manipulate volumes that are orders of magnitude lower than what was feasible a few decades ago. Another advantage specific to microfluidic devices includes the integration of multiple analytical processes onto single platforms with very little dilution, increasing the overall sensitivity of the assay (Fig. 2)

Table 1 Recent studies highlighting the analytical tools used and results obtained in single-cell and single-cell-type metabolomics

Species	Material	Analytical approach[a]	Metabolites identififed	Class of metabolites	References
Subcellular metabolomics					
Hordeum vulgare	Vacuoles from mesophyll cell protoplast	GC-MS, UPLC-FT-MS	259	Amino acids, organic acids, sugars, specialised metabolites	[24]
Single-cell metabolomics					
Torenia hybrid	Petal cell	Nano-HPLC-MS	5	Anthocyanins	[25]
Closterium acerosum	Single cell	MALDI-MS	4	Central metabolites	[26]
Pelargonium zonale	Single leaf, stem, petal cell	Nano-ESI-MS	22	Monoterpenoids	[27]
Allium cepa, Narcissus pseudonarcissus	Epidermal single cell of bulbs	AP-ESI-MS	32, 22	Specialised metabolites, oligosaccharides	[28]
Arabidopsis thaliana, Hypericum perforatum, Hypericum reflexum	Individual dark glands from petals, leaves; glandular trichomes	LDI-ToF-MS	15	Naphthodianthrones, flavonoids	[29]
Chara. australis	Vacuole and cytoplasm	CE-MS	125	Sugar phosphate, coenzyme, organic acids	[30]
Aplysia. californica *Bacillus atrophaeus* *Xenopus. laevis* *Rattus. norvegicus*	Neurons Single cells Oocyte Peripheral nervous systems	CE-ESI-MS BAMS GC-MS CE-ESI-MS	31 15 26 300	Nucleotides Amino acids, organic acids Carbohydrates, organic acids, fatty acids Amino acids, carbohydrates	[31] [32] [33] [34]
Single-cell-type metabolomics					
Dilatris pillansii	Leaf and flower secretory cavities	Cryogenic, NMR, HPLC	7	Methoxyphenylphenalenones	[35]
Eucalyptus spp.	Leaf subdermal secretory cavities	GC, GC-MS	24	Mono- and sesqui-terpenoids	[36]

(continued)

Table 1 (continued)

Species	Material	Analytical approach[a]	Metabolites identififed	Class of metabolites	References
Catharanthus roseus	Leaf epidermome	LC-ESI-MS	2	Oleanolic and ursolic acid	[37]
Picea abies	Phloem parenchyma cells	Cryogenic NMR	2	Stilbene glucosides, flavonoids	[38]
P. abies	Stone cells/sclereids	Cryogenic NMR, MS	2	Phenolic glycosides	[39]
Cucurbita maxima	Phloem latex (sieve tubes)	GC-ToF-MS, HPLC, FIE-MS	80	Amino acids, sugars	[40]
Glycine max	Root hairs	GC-MS, UPLC-QToF-MS	634	Amino acids, sugars, sugar alcohols, fatty acids, flavonoids, organic acids, nucleosides, phenolic, glucosinolates, saponins, alkaloids	[41]
Lilium longiflorum	Pollen grains	GC-ToF-MS	252	Sugars, organic acids, amino acids	[42]
Gossypium hirsutum	Fibre cells	GC-MS	86	Non-polar(sterols, alkanes) and polar (sugars, sugar alcohols, amino acids)	[43]
G. hirsutum	Fibre cells	GC-MS	27	Organic acids, amino acids, sugars	[44]
Citrus paradise	Epithelial and parenchyma cells	GC, GC-MS, UPLC-QToF-MS	28	Terpenoid, sterols, fatty acids, carotenoids, oxygen heterocyclics	[45]
A. thaliana	Guard cell and mesophyll cell protoplasts	LC-(MRM)-MS/MS	85	Phytohormones, signalling molecules, phenolics, flavonoids, amino acids	[46]
Lycopersicon hirsutum	Glandular trichomes	GC-MS	7	Terpenoids	[47]
Solanum spp	Trichomes	LC-MS	119	Terpenoid, flavonoids, fatty acids, alkaloids, acyl sugars	[48]
Solanum lycopersicum	Glandular trichomes	LC-ToF-MS	32	Acylated molecules, flavonoids, glycosides	[49]
Artemisia annua	Glandular trichomes	GC-MS	12	Mono- and sesqui-terpenoids	[50]
Cannabis sativa	Trichomes types	LC-MS, NMR	9	Cannabinoids	[51]

(continued)

Table 1 (continued)

Species	Material	Analytical approach[a]	Metabolites identififed	Class of metabolites	References
A. thaliana	Epidermal trichomes, basal/pavement cells	GC-ToF-MS	117	Amino acids, fatty acids and alcohols, alkanes, lipids N-compounds, organic acids, polyhydroxy acids, polyols, sugars, sugar conjugates, phenylpropanoids	[52]
A. thaliana	Glandular trichomes	UPLC-ESI-QToF-MS	13	Glucosinolates	[53]
Colquhounia coccinea	Peltate glandular trichomes	UPLC-MS/MS, X-ray diffraction	3	Sesqui-terpenoids (colquhounoids)	[54]
Nicotiana attenuate	Glandular trichomes	^{1}H-NMR, LC-QToF-MS	>2	Nicotine, phaseoloidin, acyl sugars, fatty acids	[55]
Ocimum basilicum	Peltate and capitate glandular trichomes	GC-MS, HPLC	15	Terpenoids, phenylpropenes	[56]
A. thaliana	Epidermal cell layer, palisade mesophyll cells, vascular bundle	MALDI-ToF-MS	18	Cell wall polysaccharides	[57]
A. thaliana	Endodermis, epidermis, columella, cortex, stele	GFP-FACS, UPLC-QToF-MS	50	Glucosinolates, phenylpropanoids, dipeptides	[58]

[a]Abbreviations: AP, atmospheric pressure; ESI, electrospray ionization; FACS, fluorescence-activated cell sorting; FIE, flow injection electrospray; FT, Fourier transform; GC, gas chromatography; HPLC, high-performance liquid chromatography; LC, liquid chromatography; LDI, matrix-free laser desorption/ionization; MALDI, matrix-assisted laser desorption/ionization; MRM, multiple reaction monitoring; MS, mass spectrometry; MS/MS, tandem mass spectrometry; NMR, nuclear magnetic resonance; QToF, quadrupole time-of-flight; ToF, time-of-flight; UPLC, ultra-performance liquid chromatography. CE, capillary electrophoresis, BAMS, bioaerosol mass spectrometry. Adapted from Ref. [23], Copyright 2014, with permission from Elsevier

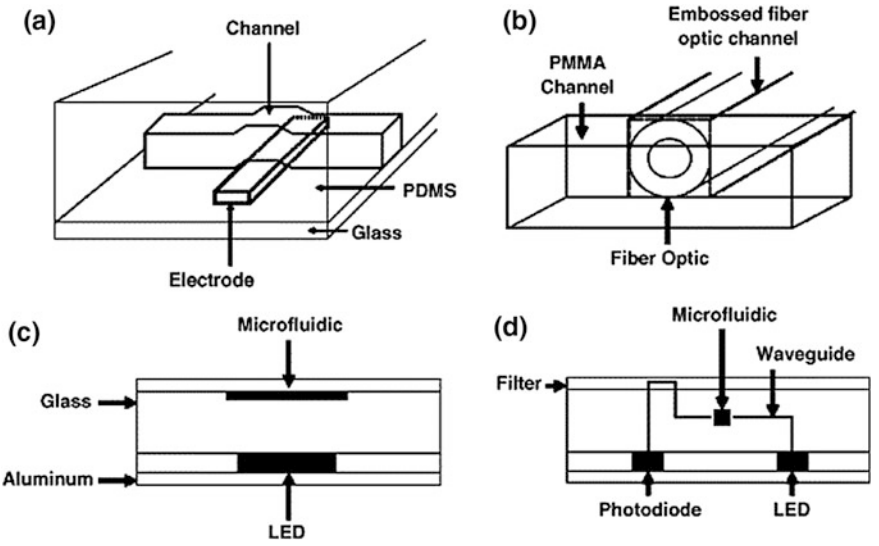

Fig. 2 Different techniques are integrated on microfluidics devices. **a** Soft polymer lithography, **b** Poly(Methylmethacrylate), **c** Complementary metal–oxide–semiconductor (CMOS) processing and **d** two-photon three-dimensional lithography. Reprinted from Ref. [64], Copyright 2007, with permission from Elsevier

[63, 64]. Furthermore, microfluidics is also useful for the observation and classification of individual cells, their stimulation within the microfluidics device, and their rapid and accurate identification.

The analysis of microbial single cells using microfluidics has shown potential in several fields including growth, strain characterisation and morphological analysis, population heterogeneity, analysis of cellular response at defined constant environmental conditions and cell-to-cell heterogeneity at specific concentration gradients [65, 66].

Microbial single cells have been analysed by four different types of simple perfusion microfluidics [65]. These can be classified by the spatial directions in which single cells can propagate, specifically 3D, 2D, 1D and 0D. Fewer cells per cultivation volume mean that the environment surrounding the single cell can be controlled more accurately. Larger 3D as well as 2D planar populations are more likely to have environmental inhomogeneity and gradients across the micro-colonies than 1D and 0D systems. In addition/as a result, the replenishment of the cultivation medium is more inefficient.

Several microfluidics technologies are available for cell culture applications, including automated antibody labelling for determining signal transduction across multiple time points in fixed cells [67–69], the study of single-cell dynamic under microfluidic gradients [70]; microfluidic perfusion of cell culture arrays [71], single-cell trap assays [72] and the isolation of single cells in microwells [73]. Recently, Kellogs et al. [74] developed and described a useful method for

single-cell analysis using microfluidics. The protocol improves accuracy and greatly increases the output, whilst enhancing existing abilities in cell and fluid manipulation. This is a significant advancement in the analysis of single cells.

3.2 Nanoscale Devices

In the past 10 years, nanobiodevice techniques have focused on establishing four main fields in biomedical applications including disease diagnostics, in vivo imaging, regenerative medicine and nanotherapy [75]. This rapid progression in nanotechnology has developed outstanding nanotools such as near-field scanning optical microscopy (NSOM), optical fiber nanosensors, nanowire-based field effect transistors (FETs), scanning ion conductance microscopy (SICM) and atomic force microscopy (AFM) at the nanoscale level [76]. Recent new advances in these technologies have promised new discoveries that could help to reveal the nanostructure of cellular organelles, spatial biomolecules organisation and biochemical reactions at nanodomains. Two different types of nanofabrication technologies have been established: (1) top–down nanotechnology, (2) bottom-up nanotechnologies. Top-down nanotechnologies involve a combination of electron-beam lithography and plasma dry etching. In contrast, bottom-up technologies involve vapour–liquid–solid nanowire growth techniques [75].

Analysis of single cells at a high resolution for a nanoscale sample of the previously undetectable cell organelles is a tedious work. In addition, determining various cellular components and their three-dimensional organisation, unravelling the nanodomains for biochemical reactions and profiling cell-to-cell variations at the cellular level are also not easy tasks. Recently, a great effort has been made in analytical methods for observing, manipulating and exploring single cells at the nanoscale level [76]. Nevertheless, it is extremely exciting to accomplish a high spatial resolution for detecting the structure at the nanoscale. It is a must to have high sensitivity and specificity with high signal-to-noise (S/N) ratio for small amounts of a compound in individual organelles. An efficient set of tools must be established in order to analyse nanometrics organelles.

Pan et al. [77] developed the single-probe mass spectrometry (MS) technology, for real-time analysis of in situ metabolomics study of single living cells. The researchers have used the single-probe to detect several cellular metabolites and the anticancer small molecules paclitaxel, doxorubicin and OSW-1 in individual cervical cancer cells (HeLa) (Fig. 3).

In the past ten years, the progress in nanotechnology has accelerated the development of nanotools in single-cell studies at the nanoscale level for small structures and compound compositions. Nanoprobes are a type of nanoscale devices designed to probe single cells with minimum intrusion [76]. These techniques have huge potentials in important cellular processes. Developments in this technology

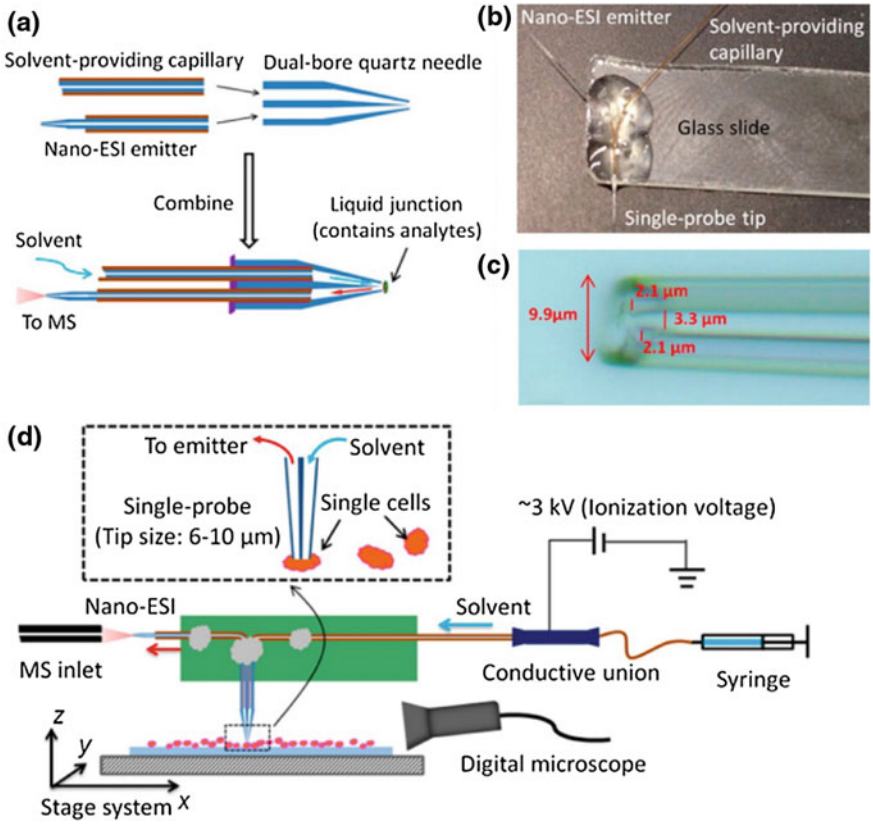

Fig. 3 Single-probe MS system from fabrication to utilisation. **a** Fabrication steps of the single-probe; **b** photograph of a working Single-probe; **c** 40× magnification of the single-probe tip with measurements obtained from the calibrated digital microscope; **d** setup schematic of a single-cell MS analysis. Reprinted with the permission from Ref. [77]. Copyright 2014 American Chemical Society

have helped in the observation and manipulation of single cells at the nanoscale level while elucidating their functions. The extensive use of high-resolution techniques can give insight in single-cell analysis at the nanoscale.

4 Recent Improvement of Sensitivity and Specificity

4.1 Mass Spectrometry (MS)

Mass spectrometry is both sensitive and fast, and therefore has a principal place in metabolomics. The requirement for simple protocols for diagnosis of human

diseases has pushed forward the development of mass spectrometry and improvements in equipment, methodology and software and databases. This has enabled metabolomics to move away from the quantitative approaches generally used. As a result, methods such as isotope labelling and tracing are being frequently used. Moreover, ambient ionization techniques such as desorption ionization and rapid evaporative ionization have permitted new MS imaging methods. Direct, real-time MS analysis has also proved as being useful [12].

Analytical chemistry has also been instrumental in the development of MS-based single-cell metabolomics, particularly those in which labelling of targeted molecules is not required and the methods are suitable for the detection of unknown molecules [12, 78, 79]. Several analytical techniques have been established that enable single-cell analyses: matrix-assisted laser desorption ionization (MALDI), desorption electrospray ionization, secondary ion MS (SIMS), laser desorption ionization, laser ablation electrospray, electrospray ionization (ESI), inductively coupled plasma (ICP) and nanostructure-initiator [12, 23, 80, 81].

Matrix-assisted laser desorption ionization (MALDI) and secondary ion mass spectrometry (SIMS) are commonly conducted in a vacuum and live cell analysis is therefore not possible. In addition to MALDI and SIMS, laser ablation electrospray ionization mass spectrometry (LAESI-MS) can also be used to analyse single cells [82]. Subcellular detection of metabolites has also been possible with LAESI-MS [83]. The use of a nanospray tip to obtain a small volume of cellular content prior to analysis by MS has also been used to analyse live cells.

Other methodologies which are useful for the analysis of single-cell metabolites include microarrays for mass spectrometry (MAMS) [84]. Whilst there were initially issues with the quality of the microarrays, meaning that direct microarrays' comparisons were difficult and required many normalisation steps to reduce experimental noise in the data, an improved MAMS fabrication process, implemented by Schmidt et al. [85] was able to enhance the quality of the data produced. This also enabled data from measurements of single cells to be amalgamated to facilitate analysis of diverse metabolic phenotypes within a population.

The investigation of cellular populations using MAMS can also be improved using Raman and fluorescence techniques. This can reveal alterations in the metabolite profile during cellular transitions, for example from a motile to a dormant state in the alga *Haematococcus pluvialis* [86]. This process also identified a metabolically unique cell, illustrating the capability to discover rare cell types using these multi-method high-throughput techniques.

4.2 MS Imaging

Mass spectrometry imaging is another useful technique to analyse the metabolome of individual cells. This technique not only provides morphological data but it also can reveal metabolites within subcellular compartments, identify them and track their spatial distribution within the cell. To produce the images, the data from mass

spectrometry is used to construct mass spectrum charts to indicate the location of various molecules within the cells. Matrix-assisted laser desorption ionization (MALDI), desorption electrospray ionization (DESI) or secondary ion mass spectrometry (SIMS) are often used to produce the images and imaging mass spectrometry has proved useful in analysing drug effects, drug screening and medicinal diagnosis [87].

The most established mass spectrometry techniques in single-cell metabolomics that can provide information on cellular morphology coupled with chemical data are probably SIMS and MALDI (Fig. 4) [88]. SIMS is a surface analysis method that can obtain chemical information from the first few nanometres of the sample surface, so it is useful in visualising membrane-localised molecules including phospholipids and other small molecules. SIMS is the most effective method to analyse samples at the sub-micron level and it also provides valuable quantitative data.

There are two SIMS methods: dynamic and static. Dynamic SIMS is generally combined with other techniques such as electron, atomic force and fluorescence microscopy, which provide high-resolution imaging [89]. It provides high sensitivity with good lateral resolution and has been used to visualise the location of protein and nucleic acids within cells. In addition, it can be used for compounds labelled with rare elements, for example in determining the cellular localisation of cancer drugs and the distribution of iron in diseased cells of Alzheimer sufferers [89]. Static SIMS is often used with other techniques such as a time-of-flight (TOF) analyser, which obtains mass spectra for each pixel. Softer ionization and higher-yield cluster ion sources have recently enhanced the utility of SIMS, increasing the availability of molecular data and molecular depth profiling. As a result, this technique is enhancing the subcellular mapping of the location of unlabelled biomolecules of interest [90, 91].

Matrix-assisted laser desorption ionization (MALDI) MS is the most versatile technique for imaging single cells, and it is well established and easy to use. This technique is highly sensitive and is able to detect analytes over a large mass range, as well as from within complex mixtures. Furthermore, it has been successfully

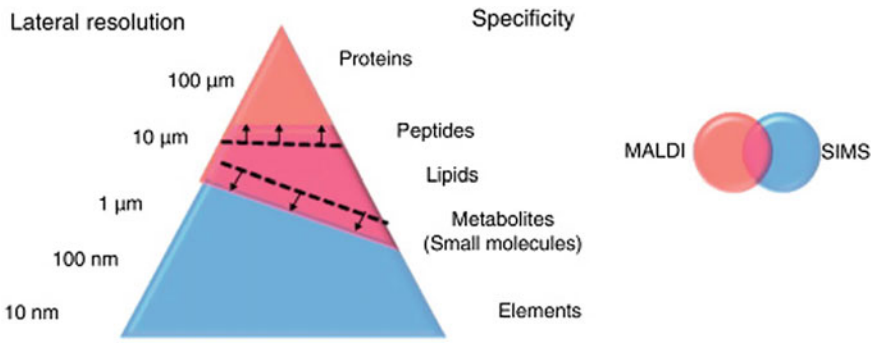

Fig. 4 The overlap of MALDI and SIMS technologies. Reprinted from Ref. [88], Copyright 2013, with permission from Elsevier

utilised in single cell and organelle profiling. Some of the challenges of MALDI-MS, including the poor spatial resolution for cellular and subcellular investigations, have been overcome in recent years to achieve a resolution between 4 and 7 μm. The use of scanning microprobe MALDI (SMALDI) enabled Spengler and Hubert [92] to obtain a resolution between 0.6 and 1.5 μm.

4.3 Capillary Electrophoresis

In the emerging field of metabolomics, CE-MS is now considered as a useful analytical technique for the polar ionogenic metabolites. Over the decades, significant contribution has been reported in metabolic profiling study using CE-MS [93]. Capillary electrophoresis (CE) mass spectrometry (MS) is one of many analytical techniques that have been used in metabolomics. CE is greater in the separation efficiency of ionic metabolites, and MS can offer detection at very high sensitivity. Therefore, the platform of CE with MS can help to improve the performance of analytical tools with high resolution, sensitivity and efficient separation of metabolites. CE-MS has been demonstrated as a superior technique for profiling polar metabolites in bacterial, plant, urine, plasma and other biological samples. CE-MS has also been used to detect ionic metabolites mostly from primary groups of metabolites. For example: amino acids, organic acids, nucleotides and sugar phosphates.

Among the separation methods, capillary electrophoresis (CE) has proven to be an efficient method for single-cells separation. Single-cell studies involve low detection limits and highly effective separation. CE with nano or picoliter sample volumes and high separation effectiveness has been shown to enhance the coverage of analyte in metabolites profiling and quantification in single-cell studies [94, 95]. A study demonstrated that CE can be hyphenated with MS for single-cell metabolomics profiling of *Aplysia californicas* the neurons. Their study served as a starting point for the advancement of single-cell analysis in terms of anionic metabolites as a complementary with cationic metabolites [31]. CE compromises the ability to separate a wide range of biomolecules from different types of samples. Lapainis et al. [94] developed a single-cell metabolomic by utilising the CE-MS method. Most of the reported works described about neuron cells. Recent trends suggested that CE analyses are being developed to help to increase the quality of compounds detected in minuscule structures [94].

Nemes et al. [34] demonstrated the capability of CE-ESI-MS in profiling and quantifying the metabolites in single cells from model organisms in neuroscience and systems biology [34]. The experimental setup designed is shown in Fig. 5. There searchers have proved that CE-ESI-MS is capable of profiling and quantifying the metabolic content of single cells from model organisms in neuroscience and systems biology. They have also successfully established the single-cell procedure to detect and characterise multiple metabolites in individual neurons collected from the *A. californica* central nervous system (CNS) and the *Rattus*

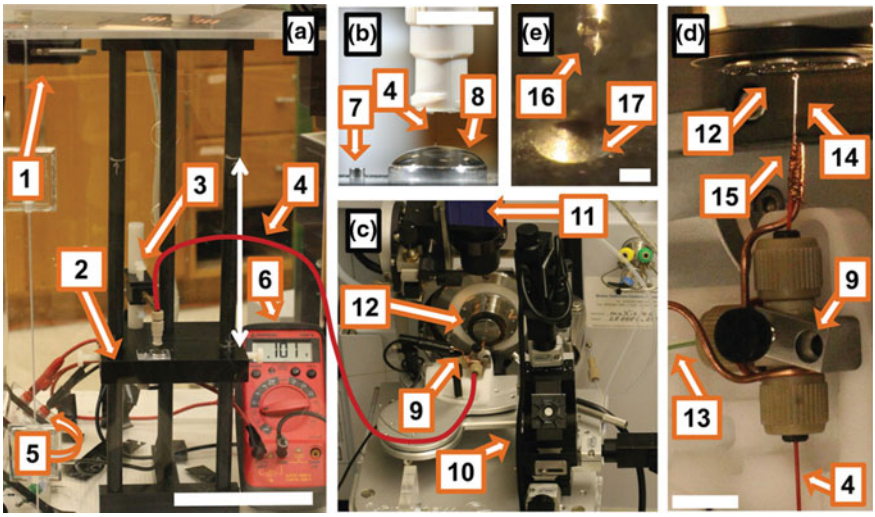

Fig. 5 Experimental setup of the single-cell CE-ESI-MS system. **a** Front view of the CE platform highlighting (1) the enclosure equipped with a safety-interlock-enabled door, (2) platform for sample loading, which can be rapidly elevated by 15 cm (see *arrow*), (3) holder allowing manual positioning of the separation capillary in three degrees of freedom, (4) separation capillary (*solid line* in *red*), (5) resistor connected in series to a stable HVPS (Figure S2) and the CE platform, and (6) digital multimeter connected in parallel measuring voltage drop on the resistor. Scale = 10 cm. **b** Magnified view of the sample-loading platform consisting of (7) the sample-loading vial and (8) electrolyte-containing vial with the separation capillary positioned 2 mm below the electrolyte meniscus. Scale = 1 cm. **c** Distant view of the CEESI-MS ion source consisting of (9) the CE-ESI interface mounted on (10) the three-axis translation stage of a PicoView nanospray source, (11) CCD camera equipped with light collimating and focusing lenses to record ES performance, and (12) a mass spectrometer equipped with a nanospray sampling plate. **d** Close-up view of the CE-ESI-MS ion source highlighting a T-union that houses fused silica capillaries for (4) CE separation and (13) ES sheath solution delivery as well as (14) a metal emitter grounded (earth) through a (15) thin copper wire. Scale = 1 cm. **e** Magnified view of (16) the stable Taylor cone formed upon operating the ES in the cone-jet spraying mode (see reflected image) in front of (17) the orifice of the mass spectrometer sampling plate. Scale = 500 µm. Reprinted by permission from Macmillan Publishers Ltd: Ref. [34], copyright 2013

norvegicus peripheral nervous system. The analytical workflow started with sample preparation, then CE-MS separation detection, and finally data analysis and quantitation. The developed protocol can be implemented in characterising the metabolome of smaller cells and/or subcellular domains.

The approaches could be implemented *in planta* by improving the experimental conditions of single-cell isolation [96]. A few studies have reported on the plant single-cells metabolite analysis. Due to the benefits and prospective of single-cell *in planta* studies, the analysis in plant single cell will be speedup. Oikawa et al. [30] demonstrated the metabolomics approach using CE-MS to explore the metabolomics of a single organelle by looking at the giant internodal cell of the algae *Chara australis* [30]. In the study, they utilised this unique cell to define the single

vacuole and cytoplasm metabolome, thus leading to the elucidation of the metabolite dissemination in a single cell.

In plant studies, single-cell analysis could be implemented to understand the changes between each de-differentiated cell to understand plant development mechanisms. Analysis of exudates from the cells could provide an insight into the chemical communication between cells [96].

4.4 Nuclear Magnetic Resonance (NMR)

NMR has been widely used for metabolomic studies in biological samples, such as in animals, plants and microbes. NMR-based metabolomics have a potential to deliver a 'complete view' of the metabolites under different treatments. NMR spectroscopy is a highly useful tool for the study of metabolites in individual bigger cells, for example; *Xenopus laevis* oocytes and *A. californica* neurons. However, NMR spectroscopy is hindered by low coverage and sensitivity. Therefore, improvements in NMR sensitivity have been accomplished with new technologies. These include small-scale NMR probes which have improved the detection limits of NMR and enable the characterisation of single-cell samples. It is possible to propose a system that could exploit NMR with fluorescent probes to observe different amount of metabolites. NMR spectroscopy has also been applied widely for the quantitative and non-invasive detection of metabolites [97]. Currently, NMR has been utilised efficiently for single-cell metabolite studies. Grant et al. [98] proved the potential of NMR spectroscopy for single-cells studies [98]. This increased the application of NMR spectroscopy from entire living organisms, isolated tissues and even down to single cells.

A study by Lee et al. [99] was intended to assess the possibility of NMR spectroscopy to explore subcellular phenomena. They have successfully recorded the first compartment-selective in vivo NMR spectra from oocytes of the frog *X. laevis* using a high magnetic field and a home-built microscopy probe. This study shows that the two cytoplasmic regions differed in their lipid contents. Their study demonstrates that NMR may be used as a tool in the study of cell biology.

Despite limitations in resolutions, this study has clearly shown metabolite localization in plant tissue by NMR signals. The study proved that NMR technique is promising for single-cells study. NMR was expected to deliver low coverage of metabolite detection due to the low sensitivity. However, as demonstrated by Krojanski et al. [100], this limitation has been improved by using a small volume of probes. This technique permits single-cell-sized detection and quantification.

5 Limitations and Challenges

In comparison to other single cell "omics", metabolomics is most challenging to measure. Whilst there have been substantial developments in metabolome coverage, there is still no analytical protocol that can investigate the entire cellular metabolome in a single measurement [12].

One of the key challenges in metabolomics is the fact that the metabolome can dynamically respond to the environment very rapidly. Therefore, the cell's metabolism needs to be paused immediately in order for it to be accurately measured. To overcome this, sample preparations need to be carefully managed, as this will also affect the information obtained. At this time, isolation of single cells and direct sampling from individual cells are still technically difficult.

Another key challenge in metabolomics is the large range of metabolites in a cell, relative to the molecules analysed in genomics and transcriptomics. These diverse unidentified molecules in the metabolome may confound the observation of other metabolites. Similarly, another issue that is not experienced with the analysis of nucleic acids is the lack of a technique to amplify the small amount of metabolites present to facilitate detection. Furthermore, the molecules in the medium in which cells are grown can be very similar to the metabolites produced by the cells, making separation of the metabolic products difficult. In all these cases, metabolic precursor concentrations may be increased experimentally and may allow the identification of formerly indiscernible metabolites. In addition, instruments to increase sensitivity of detection may need to be developed. The most common methods to measure the untargeted metabolome are mass spectrometry and nuclear magnetic resonance spectroscopy (NMR), although so far the utility of NMR for single-cell metabolomics is limited.

Other challenges of single-cell metabolomics include inadequate databases. The NIST electron ionization mass spectral library is incomplete and inconsistent and as such database comparison can be problematic. Finally, high-throughput methodologies should be progressed in order to make accurate conclusions from the data obtained from the analysis of multiple individual single cells simultaneously.

6 Future Prospects and Conclusion

Over the past few years, metabolomics methodologies have progressed swiftly and there are several valuable databases that store, manage and analyse metabolomic data. These technologies that are used to analyse the metabolites from single cells can provide valuable insights into biological interactions, which the fields of genomics and transcriptomics cannot deliver. Metabolomics at a single-cell level remains technically challenging owing to numerous fundamental limitations, including the rapid changing of the metabolome, small sampling volumes, low

quantities of metabolites, diverse range of metabolites present in the cell and inadequate sensitivity of analytical instruments.

Metabolomics at the single-cell level, however, is in its infancy. Enhancements allowing increased coverage of the metabolome, the improvement and more rapid identification of metabolites and the implementation of non-destructive measurements are expected. This will enable us to start to comprehend how biological systems interact with one another and the environment. This will therefore enable us to understand the unique properties of cells, cell–cell communications and cell-environment interactions. Large-scale single-cell metabolomics data will provide insights to permit the formation and testing of hypotheses to further understand the fundamental biological mechanisms and to address clinical issues in diagnostics and diseases. Further challenges need to be addressed pertaining to the integration of genomics, transcriptomics, proteomics and metabolomics data before a complete understanding of cellular physiology and development can be obtained. Nevertheless, current developments signpost an impending archetypal shift from analysis of tissue-scale metabolomics to the study of single-cell metabolomics, which will supplement other "omics" approaches on the path towards amalgamated systems biology of single cells.

References

1. Griffiths WJ, Karu K, Hornshaw M, Woffendin G, Wang Y (2007) Metabolomics and metabolite profiling: past heroes and future developments. Eur J Mass Spectrom 13(1):45–50
2. Hall RD (2006) Plant metabolomics: from holistic hope, to hype, to hot topic. New Phytol 169(3):453–468
3. Fiehn O (2002) Metabolomics—the link between genotypes and phenotypes. Plant Mol Biol 48(1–2):155–171
4. Tugizimana F, Piater L, Dubery I (2013) Plant metabolomics: a new frontier in phytochemical analysis. S Afr J Sc 109(5–6), 1–11
5. Kuehnbaum NL, Britz-Mckibbin P (2013) New advances in separation science for metabolomics: resolving chemical diversity in a post-genomic era. Chem Rev 113 (4):2437–2468
6. Martins BMC, Locke JCW (2015) Microbial individuality: how single-cell heterogeneity enables population level strategies. Curr Opin Microbiol 24:104–112
7. Li C, Klco JM, Helton NM, George DR, Mudd JL, Miller CA, Lu C, Fulton R, O'Laughlin M, Fronick C, Wilson RK, Ley TJ (2015) Genetic heterogeneity of induced pluripotent stem cells: results from 24 clones derived from a single C57BL/6 mouse. PLoS ONE 10(3): art. no. e0120585
8. Han Q, Bagheri N, Bradshaw EM, Hafler DA, Lauffenburger DA, Love JC (2012) Polyfunctional responses by human T cells result from sequential release of cytokines. Proc Natl Acad Sci USA 109(5):1607–1612
9. Gómez-Sjöberg R, Leyrat AA, Pirone DM, Chen CS, Quake SR (2007) Versatile, fully automated, microfluidic cell culture system. Anal Chem 79(22):8557–8563
10. Yang Q, Pando BF, Dong G, Golden SS, Van Oudenaarden A (2010) Circadian gating of the cell cycle revealed in single cyanobacterial cells. Science 327(5972):1522–1526
11. Fritzsch B, Jahan I, Pan N, Elliott KL (2015) Evolving gene regulatory networks into cellular networks guiding adaptive behavior: an outline how single cells could have evolved into a centralized neurosensory system. Cell Tissue Res 359(1):259–313

12. Zenobi R (2013) Single-cell metabolomics: analytical and biological perspectives. Science 342(6163):art. no. 1243259
13. Yang Q, Pando BF, Dong G, Golden SS, Van Oudenaarden A (2010) Circadian gating of the cell cycle revealed in single cyanobacterial cells. Science 327(5972):1522–1526
14. Jové M, Portero-Otín M, Naudí A, Ferrer I, Pamplona R (2014) Metabolomics of human brain aging and age-related neurodegenerative diseases. J Neuropathol Exp Neurol 73 (7):640–657
15. Aldridge BB, Rhee KY (2014) Microbial metabolomics: innovation, application, insight. Curr Opin Microbiol 19(1):90–96
16. Dittrich P, Jakubowski N (2014) Current trends in single cell analysis. Anal Bioanal Chem 406(27):6957–6961
17. Bendall SC, Simonds EF, Qiu P, Amir E-AD, Krutzik PO, Finck R, Bruggner RV, Melamed R, Trejo A, Ornatsky OI, Balderas RS, Plevritis SK, Sachs K, Pe'er D, Tanner SD, Nolan GP (2011) Single-cell mass cytometry of differential immune and drug responses across a human hematopoietic continuum. Science 332(6030):687–696
18. de Vargas Roditi L, Claassen M (2015) Computational and experimental single cell biology techniques for the definition of cell type heterogeneity, interplay and intracellular dynamics. Curr Opin Biotechnol 34:9–15
19. Müller S, Hübschmann T, Kleinsteuber S, Vogt C (2012) High resolution single cell analytics to follow microbial community dynamics in anaerobic ecosystems. Methods 57 (3):338–349
20. Wilson JL, Suri S, Singh A, Rivet CA, Lu H, McDevitt TC (2014) Single-cell analysis of embryoid body heterogeneity using microfluidic trapping array. Biomed Microdevices 16 (1):79–90
21. Rogers ED, Jackson T, Moussaieff A, Aharoni A, Benfey PN (2012) Cell type-specific transcriptional profiling: implications for metabolite profiling. Plant J 70:5–17
22. Tejedor ML, Mizuno H, Tsuyama N, Harada T, Masujima T (2012) In situ molecular analysis of plant tissues by live single-cell mass spectrometry. Anal Chem 84:5221–5228
23. Misra BB, Assmann SM, Chen S (2014) Plant single-cell and single-cell-type metabolomics. Trends Plant Sci 19(10):637–646
24. Tohge T et al (2011) Towards the storage metabolome: profiling the barley vacuole. Plant Physiol 157:1469–1482
25. Kajiyama K et al (2006) Single cell-based analysis of torenia petal pigments by a combination of ArF excimer laser micro sampling and nano-high performance liquid chromatography (HPLC)-mass spectrometry. J Biosci Bioeng 102:575–578
26. Amantonico A et al (2010) Single cell MALDI-MS as an analytical tool for studying intrapopulation metabolic heterogeneity of unicellular organisms. Anal Chem 82:7394–7400
27. Tejedor LM et al (2009) Direct single cell molecular analysis of plant tissues by video mass spectrometry. Anal Sci 25:1053–1055
28. Shrestha B, Vertes A (2009) In situ metabolic profiling of single cells by laser ablation electrospray ionization mass spectrometry. Anal Chem 81:8265–8271
29. Hölscher D et al (2009) Matrix-free UV-laser desorption/ionization (LDI) mass spectrometric imaging at the single-cell level: distribution of secondary metabolites of *Arabidopsis thaliana* and *Hypericum* species. Plant J 60:907–918
30. Oikawa A, Matsuda F, Kikuyama M, Mimura T, Saito K (2011) Metabolomics of a single vacuole reveals metabolic dynamism in an alga *Chara australis*. Plant Physiol 157:544–551
31. Liu JX, Aerts JT, Rubakhin SS, Zhang XX, Sweedler JV (2014) Analysis of endogenous nucleotides by single cell capillary electrophoresis-mass spectrometry. Analyst. doi:10.1039/c4an01133c
32. Tobias HJ, Pitesky ME, Fergenson DP, Steele PT, Horn J, Frank M, Gard EE (2006) Following the biochemical and morphological changes of *Bacillus atrophaeus* cells during the sporulation process using Bioaerosol Mass Spectrometry. J Microbiol Methods 67:56–63

33. Koek MM, Bakels F, Engel W, van den Maagdenberg A, Ferrari MD, Coulier L, Hankemeier T (2010) Metabolic profiling of ultrasmall sample volumes with GC/MS: from microliter to nanoliter samples. Anal Chem 82:156–162
34. Nemes P, Rubakhin SS, Aerts JT, Sweedler JV (2013) Qualitative and quantitative metabolomic investigation of single neurons by capillary electrophoresis electrospray ionization mass spectrometry. Nat Protoc 8(4):783–799
35. Schneider B, Holscher D (2007) Laser microdissection and cryogenic nuclear magnetic resonance spectroscopy: an alliance for cell type-specific metabolite profiling. Planta 225:763–770
36. Goodger JQD et al (2010) Isolation of intact sub-dermal secretory cavities from Eucalyptus. Plant Methods 6:20
37. Murata J et al (2008) The leaf epidermome of *Catharanthus roseus* reveals its biochemical specialization. Plant Cell 20:524–542
38. Li SH et al (2012) Localization of phenolics in phloem parenchyma cells of Norway spruce (*Picea abies*). ChemBioChem 13:2707–2713
39. Li SH et al (2007) Microchemical analysis of laser-microdissected stone cells of Norway spruce by cryogenic nuclear magnetic resonance spectroscopy. Planta 225(55):771–779
40. Gaupels F et al (2012) Deciphering systemic wound responses of the pumpkin extrafascicular phloem by metabolomics and stable isotope-coded protein labeling. Plant Physiol 160 (56):2285–2299
41. Brechenmacher L et al (2010) Soybean metabolites regulated in root hairs in response to the symbiotic bacterium *Bradyrhizobium japonicum*. Plant Physiol 153(57):1808–1822
42. Obermeyer G et al (2013) Dynamic adaption of metabolic pathways during germination and growth of lily pollen tubes after inhibition of the electron transport chain. Plant Physiol 162:1822–1833
43. Gou JY et al (2007) Gene expression and metabolite profiles of cotton fiber during cell elongation and secondary cell wall synthesis. Cell Res 17(60):422–434
44. Naoumkina M et al (2013) Integrated metabolomics and genomics analysis provides new insights into the fiber elongation process in Ligon lintless-2 mutant cotton (*Gossypium hirsutum* L.). BMC Genom 14:155
45. Voo SS et al (2012) Assessing the biosynthetic capabilities of secretory glands in *Citrus* peel. Plant Physiol 159:81–94
46. Jin X et al (2013) ABA-responsive guard cell metabolomes of *Arabidopsis* wild-type and GPA1 G-protein mutants. Plant Cell 25:4789–4811
47. Fridman E et al (2005) Metabolic, genomic, and biochemical analyses of glandular trichomes from the wild tomato species *Lycopersicon hirsutum* identify a key enzyme in the biosynthesis of methylketones. Plant Cell 17(67):1252–1267
48. McDowell ET et al (2011) Comparative functional genomics analysis of *Solanum* glandular trichome types. Plant Physiol 155(66):524–539
49. Schilmiller A et al (2010) Mass spectrometry screening reveals widespread diversity in trichome specialized metabolites of tomato chromosomal substitution lines. Plant J 62 (68):391–403
50. Bertea CM et al (2005) Identification of intermediates and enzymes involved in the early steps of artemisinin biosynthesis in *Artemisia annua*. Planta Med 71:40–47
51. Happyana N et al (2013) Analysis of cannabinoids in laser-microdissected trichomes of medicinal *Cannabis sativa* using LCMS and cryogenic NMR. Phytochemistry 87(70):51–59
52. Ebert B et al (2010) Metabolic profiling of *Arabidopsis thaliana* epidermal cells. J Exp Bot 61(64):1321–1335
53. Frerigmann H et al (2012) Glucosinolates are produced in trichomes of *Arabidopsis thaliana*. Front Plant Sci 3:242
54. Li CH et al (2013) Peltate glandular trichomes of *Colquhounia coccinea* var. mollis Harbor a new class of defensive sesterterpenoids. Org Lett 15:1694–1697

55. Weinhold A et al (2011) Phaseoloidin, a homogentisic acid glucoside from *Nicotiana attenuata* trichomes, contributes to the plant's resistance against Lepidopteran herbivores. J Chem Ecol 37(71):1091–1098
56. Gang DR et al (2001) An investigation of the storage and biosynthesis of phenylpropenes in sweet basil. Plant Physiol 125:539–555
57. Obel N et al (2009) Microanalysis of plant cell wall polysaccharides. Mol Plant 2 (81):922–932
58. Moussaieff A et al (2013) High-resolution metabolic mapping of cell types in plant roots. Proc Natl Acad Sci USA 110:E1232–E1241
59. Kellogs R, Tay S (2015) Noise facilitates transcriptional control under dynamic inputs. Cell 160:381–392
60. Tay S (2014) High-throughput microfluidic single-cell analysis pipeline for studies of signaling dynamics. Nat Protoc 9(7):1713–1726
61. Quake SR, Scherer A (2000) From micro- to nanofabrication with soft materials. Science 290 (5496):1536–1540
62. Haeberle S, Zengerle R (2007) Microfluidic platforms for lab-on-a-chip applications. Lab Chip—Miniaturisation Chem Biol 7(9):1094–1110
63. Khandurina J, Guttman A (2002) Bioanalysis in microfluidic devices. J Chromatogr A 943 (2):159–183
64. Roman GT, Kennedy RT (2007) Fully integrated microfluidic separations systems for biochemical analysis. J Chromatogr A 1168(1–2):170–188
65. Grünberger A, Wiechert W, Kohlheyer D (2014) Single-cell microfluidics: opportunity for bioprocess development. Curr Opin Biotechnol 29(1):15–23
66. Unthan S, Grünberger A, van Ooyen J, Gätgens J, Heinrich J, Paczia N, Wiechert W, Kohlheyer D, Noack S (2014) Beyond growth rate 0.6: What drives *Corynebacterium glutamicum* to higher growth rates in defined medium. Biotechnol Bioen 111(2):359–371
67. Cheong R, Wang CJ, Levchenko A (2009) High content cell screening in a microfluidic device. Mol Cell Proteomics 8(3):433–442
68. Cheong R, Wang CJ, Levchenko A (2009) Using a microfluidic device for high-content analysis of cell signalling. Sci Signaling 2(75)
69. Cheong R, Paliwal S, Levchenko A (2010) High-content screening in microfluidic devices. Expert Opin Drug Discov 5(8):715–720
70. Frank T, Tay S (2013) Flow-switching allows independently programmable, extremely stable, high-throughput diffusion-based gradients. Lab Chip—Miniaturisation Chem Biol 13 (7):1273–1281
71. Hung PJ, Lee PJ, Sabounchi P, Lin R, Lee LP (2005) Continuous perfusion microfluidic cell culture array for high-throughput cell-based assays. Biotechnol Bioeng 89(1):1–8
72. Hung K, Rivet CA, Kemp ML, Lu H (2011) Imaging single-cell signaling dynamics with a deterministic high-density single-cell trap array. Anal Chem 83(18):7044–7052
73. Roach KL, King KR, Uygun BE, Kohane IS, Yarmush ML, Toner M (2009) High throughput single cell bioinformatics. Biotechnol Prog 25(6):1772–1779
74. Kellogg RA, Gómez-Sjöberg R, Leyrat AA, Tay S (2014) High-throughput microfluidic single-cell analysis pipeline for studies of signaling dynamics. Nat protoc 9(7), 1713–1726
75. Kaji N, Baba Y (2014) Nanodevice-based single biomolecule analysis, single cell analysis, and in vivo imaging for cance diagnosis, cancer theranostics, and iPS cell-based regenerative medicine. Anal Sci 30:859–864
76. Zheng XT, Li CM (2012) Single cell analysis at the nanoscale. Chem Soc Rev 41:2061–2071
77. Pan N, Rao W, Kothapalli NR, Liu RM, Burgett AWG, Yang Z (2014) The single-probe: a miniaturized multifunctional device for single cell mass spectrometry analysis. Anal Chem 86:9376–9380
78. Ibáneza AJ, Fagerer SR, Schmidt AM, Urban PL, Jefimovs K, Geiger P, Dechant R, Heinemann M, Zenobi R (2013) Mass spectrometry-based metabolomics of single yeast cells. Proc Natl Acad Sci USA 110(22):8790–8794

79. Heinemann M, Zenobi R (2011) Single cell metabolomics. Curr Opin Biotechnol 22 (1):26–31
80. Trouillon R, Passarelli MK, Wang J, Kurczy ME, Ewing AG (2013) Chemical analysis of single cells. Anal Chem 85(2):522–542
81. Klepárník K, Foret F (2013) Recent advances in the development of single cell analysis—a review. Anal Chim Acta 800:12–21
82. Shrestha B, Patt JM, Vertes A (2011) In situ cell-by-cell imaging and analysis of small cell populations by mass spectrometry. Anal Chem 83(8):2947–2955
83. Li H, Smith BK, Shrestha B, Márk L, Vertes A (2015) Automated cell-by-cell tissue imaging and single-cell analysis for targeted morphologies by laser ablation electrospray ionization mass spectrometry. Methods Mol Biol 1203:117–127
84. Urban PL, Schmidt AM, Fagerer SR, Amantonico A, Ibañez A, Jefimovs K, Heinemann M, Zenobi R (2011) Carbon-13 labelling strategy for studying the ATP metabolism in individual yeast cells by micro-arrays for mass spectrometry. Mol BioSyst 7(10):2837–2840
85. Schmidt AM, Fagerer SR, Jefimovs K, Buettner F, Marro C, Siringil EC, Boehlen KL, Pabst M, Ibáñez AJ (2014) Molecular phenotypic profiling of a *Saccharomyces cerevisiae* strain at the single-cell level. Analyst 139(22):5709–5717
86. Fagerer SR, Schmid T, Ibáñez AJ, Pabst M, Steinhoff R, Jefimovs K, Urban PL, Zenobi R (2013) Analysis of single algal cells by combining mass spectrometry with Raman and fluorescence mapping. Analyst 138(22):6732–6736
87. McDonnell LA, Heeren RMA (2007) Imaging mass spectrometry. Mass Spectrom Rev 26 (4):606–643
88. Passarelli MK, Ewing AG (2013) Single-cell imaging mass spectrometry. Curr Opin Chem Biol 17(5):854–859
89. Lanni EJ, Rubakhin SS, Sweedler JV (2012) Mass spectrometry imaging and profiling of single cells. J Proteomics 75(16):5036–5051
90. Matsuo J, Okubo C, Seki T, Aoki T, Toyoda N, Yamada I (2004) A new secondary ion mass spectrometry (SIMS) system with high-intensity cluster ion source. Nucl Instrum Methods Phys Res Sect B 219–220(1–4):463–467
91. Winograd N (2005) The magic of cluster SIMS. Anal Chem 77(7):142A–A149A
92. Spengler B, Hubert M (2002) Scanning microprobe matrix-assisted laser desorption ionization (SMALDI) mass spectrometry: instrumentation for sub-micrometer resolved LDI and MALDI surface analysis. J Am Soc Mass Spectrom 13(6):735–748
93. Ramautar R, Somsen GW, de Jong GJ (2015) CE-MS for metabolomics: developments and applications in the period 2012–2014. Electrophoresis 36:212–224
94. Lapainis T, Rubakhin SS, Sweedler JV (2009) Capillary electrophoresis with electrospray ionization mass spectrometric detection for single cell metabolomics. Anal Chem 81:5858–5864
95. Buescher JM, Czernik D, Ewald JC, Sauer U, Zamboni N (2009) Cross-platform comparison of methods for quantitative metabolomics of primary metabolism. Anal Chem 81(6):2135–2143
96. Oikawa A, Saito K (2012) Metabolite analyses of single cells. Plant J 70:30–38
97. Rubakhin SS, Romanova EV, Nemes P, Sweedler JV (2011) Profiling metabolites and peptides in single cells. Nat Methods 8:20–29
98. Grant SC, Aiken NR, Plant HD, Gibbs S, Mareci TH, Webb AG, Blackband SJ (2000) NMR spectroscopy of single neurons. Magn Reson Med 44:19–22
99. Lee SC, Cho JH, Mietchen D, Kim YS, Hong KS, Lee C, Kang D, Park KD, Choi BS, Cehong C (2006) Subcellular in vivo 1H MR spectroscopy of *Xenopus laevis* oocytes. Biophys J 90:1797–1803
100. Krojanski HG, Lambert J, Gerikalan Y, Suter D, Hergenroder R (2008) Microslot NMR probe for metabolomics studies. Anal Chem 80:8668–8672

Applications of Cell-Based Drug Delivery Systems: Use of Single Cell Assay

Ranjita Shegokar, Sampada Sawant and Loaye Al Shaal

Abstract Cell-based drug delivery (CBDD) is explored widely to target particular organs (e.g., spleen, lungs, etc.) in cancer, tissue inflammation, or in bone injury. Highly mobile cells like mononuclear phagocytes (dendritic cells, sertoli cells, monocytes, and macrophages), neutrophils, and lymphocytes loaded drug nanocarriers are exploited as Trojan horses for drug delivery. Mesenchymal stromal cells and other stem cells are studied widely to deliver the drug at target site with prolonged circulation. CBDD systems serve as a biocompatible and less toxic drug delivery approach. Formulation of cell-based drug delivery is different from that of conventional drug delivery systems; the former has more formulation challenges. Nevertheless, a multifunctionalized cell system opens new perspectives for the active delivery of drugs to target sites. Single cell assay plays a potential role in identifying cellular target for nanoparticles and for CBDD. This chapter discusses different types of CBDD systems to facilitate treatments for infectious and noninfectious diseases. The potential and limitations of single cell assay in this type of drug delivery systems are reviewed along with the clinical aspects of cell-based drug delivery systems.

Keywords Cell · Diseases · Drug delivery · Nanoparticles (NP) · Cell-based drug delivery · Stem cells · Red blood cells (RBCs) · Engineered cells

R. Shegokar (✉) · L. Al Shaal
Department of Pharmaceutics, Biopharmaceutics and NutriCosmetics,
Free University of Berlin, Kelchstr. 31, 12169 Berlin, Germany
e-mail: ranjita@arcslive.com

S. Sawant
C.U. Shah College of Pharmacy, SNDT University, Santacruz (W), Mumbai, India

F.-G. Tseng and T.S. Santra (eds.), *Essentials of Single-Cell Analysis*,
Series in BioEngineering, DOI 10.1007/978-3-662-49118-8_12

1 Introduction

An increased interest in the cell-based drug delivery (CBDD) system is due to the increasing need for safe drugs, targeting, with minimal side effects. In systemic drug delivery, to achieve a required therapeutic concentration the drug has to be administered in large quantities, a major part of which is wasted in nearby healthy tissues. CBDD systems thus provide advantages of exerting pharmacological activity at the target site, using the lowest possible drug concentration and with reduced negative effects on nontarget compartments (Fig. 1).

CBDD is explored widely to target drugs to particular organs (e.g., spleen, lungs, etc.), in cancer, tissue inflammation, or in bone injury. Cell systems have emerged as interesting alternatives to biological drug carriers. Cell systems such as erythrocytes, leukocytes, platelets, islets, hepatocytes, fibroblasts, bacterial ghosts, stem cells, and dendritic cells have emerged as novel carriers for drug delivery in recent times. They demonstrate specific and sustained delivery of drugs, enzymes, peptide drugs, and genetic material to certain organs and tissues. These systems possess a number of advantages including prolonged drug delivery time, targeting of drugs to the specific cell compartments, and improved biocompatibility.

Cell systems have shown potential applications for the treatment of human immune virus/acquired immunodeficiency syndrome (HIV/AIDS), cancer, intracellular infections, cardiovascular diseases, lung diseases, Parkinson's disease, dental implants, osteogenic ailments, and in gene therapy. Carrier erythrocytes encapsulated with enzymes like L-asparaginase, hormones, or drugs such as corticosteroids, etoposide have been successfully explored in humans. Bacterial cells

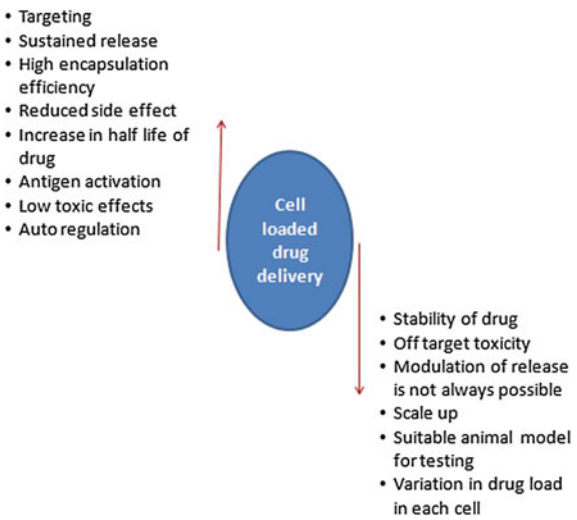

Fig. 1 Advantages and limitations of cell-based drug delivery systems

have been used in the field of vaccines and also with drugs such as doxorubicin. Genetically engineered stem cells have been tested for cancer treatment, dendritic cells for immunotherapeutic vaccines, and gold nanoparticles loaded RBCs for diagnostic imaging [1].

Overall, nanoparticles and CBDD systems are mainly used for targeting purposes, either to target specific organs or cells. Fast progress in nanoparticle research allows manipulating cell functions down to molecular levels. The quantification of drug in the form of nanocrystals, or encapsulated systems such as lipid nanoparticles, liposomes, and nanocapsules at these locations is important to predict their activity and fate. This kind of quantification is equally important for imaging and cellular therapy. At the preclinical stage, nanoparticles undergo in vitro toxicity and efficacy studies in different types of cell lines which allow scientists to get an idea of the therapeutic dose. These in vitro cell line experiments are still performed as per individual discretion; although recommendations on the use of cell type are available but no clear guideline is available on the experimental procedures [2].

Currently used methods are based on the determination of physical and bioactivity parameters from the averages of large population. The results obtained using these methods are misleading and lack correlation. The average calculations generally miss the responses from single cell, which leads to a high possibility that only the response from selective cells to stimuli or nanoparticles is being counted. Beside that, the lack of any information related to cellular heterogeneity is an equally relevant parameter to be considered in quantification of nanoparticles in cell populations. The average results of large population do not provide any information on total distribution across single cell. Other determining parameters are the total time of exposure of cells to drug or stimuli which may result in varied response, intensity of biological action, and local oxidative stress. It is a well-known fact that cells respond differently when isolated than in monolayer or cell suspension. Single cell analysis (SCA) is an innovative area for medicine, biotechnology, pharma, genomics, proteomics, and fluxomics.

Information on distribution of drug nanoparticles at cell-to-cell levels, or among different composition of cells gives scientists an idea of their distribution mechanism and particle–cell interactions. This type of direct quantification of nanoparticles in a single cell and the heterogeneity of cells might provide new insights into development of more advanced nanostructures to cure complex diseases. SCA can also provide distribution of nanoparticles at subcellular level and the similarity in performance of other cells. Single cell can be effectively employed as potential tool for target identification for nanoparticles, vaccine, and siRNA delivery. SCA can further provide information on degradation mechanisms and free radical generation at single-cell level.

Rashkow et al. found that drug concentration from the spherical titanium dioxide nanospheres (20–30 nm) determined by SCA using synchrotron X-ray fluorescence was higher than the value estimated by the traditional method of inductively coupled plasma mass spectrometry in SK-BR-3 cells [3]. Various new methods such as capillary electrophoresis (2D, 3D), polymerase chain reaction (PCR) [4], single-cell gel electrophoresis, particle in cell-3D [5], and elastography help scientists to

collate the data on cell-to-cell basis and extrapolate to the final effects. Combined use of optical and electrochemical analysis and coupled plasma mass spectroscopy, synchrotron X-ray fluorescence, microfluidics, and microreactors is employed [6]. Kann et al. explored Raman microscopy for single cell imaging and understanding drug carrier uptake [7]. Microscopy can be used along with other techniques to get synergy in analysis of single cell. Commonly used techniques such as flow cytometry (FCA) are employed to investigate the biological activity of nanoparticle at single cell level; however, the use of cell suspension makes it difficult for characterization of adherent cell and does not detect spatial location of nanoparticles within cell or interference of dye. To overcome this issue, noninvasive technique called biological microelectromechanical system was developed successfully to monitor the activity of adherent cell. On the other hand, to determine the toxicity of nanoparticles, a silicon nitride membrane cell culture chamber called micro cavity chip (0.16 mm^2) was developed for cell cultivation, which offers the detection of specific cell responses. Figure 2 depicts different analytical techniques and assays used in evaluation of nanoparticles. The validated noninvasive system allows threshold- and time-dependent analysis of nanoparticles [8]. Noninvasive single cell analysis (SCA) can be performed in a time resolved or non-time resolved manner. Furthermore, investigational possibilities are optional and can be selected based on the requirement of study, e.g., contact or contactless single-cell trapping approaches.

Current analytical technologies for chemical and biological analysis of single cells include scanning electron microscopy (SEM), transmission electron microscopy (TEM), atomic force microscopy (AFM), confocal laser scanning microscopy (CLSM), capillary electrophoresis (CE), fluorescence correlation spectroscopy (FCS), inductively coupled plasma mass spectrometry (ICP-MS), inductively coupled plasma – atomic emission spectrometry (ICP-AES) electrospray ionization (ESI), fluorescence in situ hybridization (FISH), fluorescence resonance energy

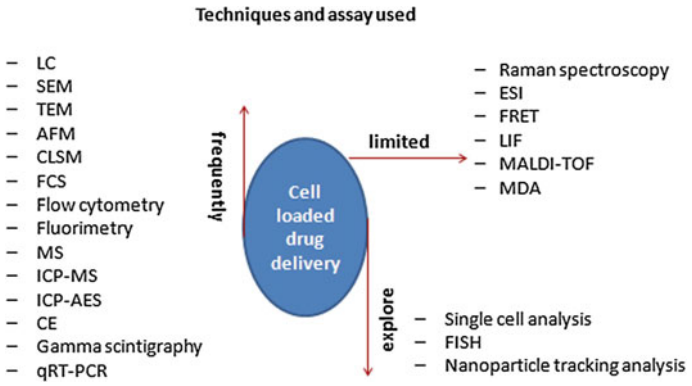

Fig. 2 Classification of in vitro analytical techniques and assays based on their popularity (limited, frequently, or exploring)

transfer (FRET), liquid chromatography (LC), laser-induced fluorescence (LIF), matrix-assisted laser desorption ionization time of flight (MALDI-TOF), multiple displacement amplification (MDA), mass spectrometry (MS), and quantitative reverse transcription polymerase chain reaction (qRT-PCR).

Reports are published on use of SCA in the investigation of drug delivery systems such as peptide targeted liposomes for vaccine formulation [9], unilamellar PEGylated liposomes containing maleimido-functionalized PEG-lipids, antisense loaded liposomes [10], use of capillary electrophoresis with laser-induced fluorescence, and FCA analysis on liposomes [11]. SCA of liposomes loaded with superoxide dismutase with microchip electrophoresis revealed that the density of liposomes and interaction-time between liposomes and cells affected the efficiency of intracellular delivery of drug [12]. Recently, polylactic glycolic acid (PLGA)-based nanoparticles have been identified at a single-cell level by synchrotron radiation fluorescence transmission infrared (FTIR) spectromicroscopy and correlation with X-ray fluorescence microscopy [13]. In other work, X-ray photoelectron spectroscopy (XPS) technique was used to track pH responsive polymeric nanoparticles [14].

The focus of this chapter is to discuss potential of cells in delivery of drugs and limitedly to discuss application of SCA in characterization nanoparticles and CBDD systems. The applications of CBDD systems in treatment of various infectious and noninfectious diseases are discussed in detail along with their production process. Risk and limitations of cell-based systems are reviewed along with clinical risks.

2 Cell Based Drug Delivery Systems

CBDD systems can either be transduced cells which express pharmacological activity and/or can deliver immunomodulatory molecules at the target site (Fig. 3). Alternatively, drugs can be loaded onto cells derived from patient under "cell carrier" platform, which allows sustained release or targeting. These types of cell carriers include use of bacterial (e.g., bacterial ghost) or human cell (macrophages, RBCs). Furthermore, the use of embryonic cell lines, pluripotent cells, and mesenchymal stem cells opens the door for treatment of complicated diseases.

In the following sections, major cell type based drug delivery systems are

2.1 Red Blood Cells (RBCs)

RBCs are the most widely studied CBDD platforms due to multiple advantages like biocompatibility, biodegradation of RBCs, ease of loading the RBCs by various methods, robust morphological, immunological and biochemical properties after

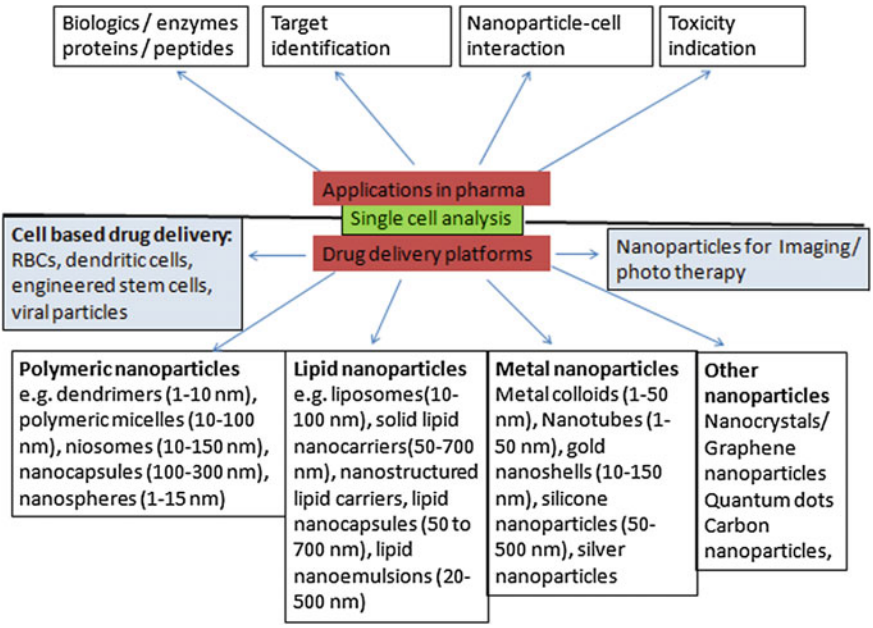

Fig. 3 Applications of single cell assays in pharma for polymeric, lipidic, metallic, and other nanoparticle platforms

drug loading, and longer life span (120 days) of the RBCs. These tiny transporters of hemoglobin and oxygen are ideal cell carriers to encapsulate drugs with a short half-life (Fig. 4).

Recently, RBCs have been explored for delivery of various plasminogen activators as biocompatible complex and showed potential in prophylactic thrombolysis. This type of CBDD approach can revolutionize the current paradigm of fibrinolytic therapy [15]. Antonelli et al. explored the possibility of encapsulated RBCs to overcome short half-life of superparamagnetic iron oxide (SPIO, Resovist,) nanoparticles (<60 nm), which can ultimately be used in magnetic particle imaging (MPI). The loaded human erythrocytes, upon intravenous injection, showed promising results in terms of higher in vivo stability and potential of RBCs in sustaining the effect [16, 17]. Other studies include encapsulation of magnetite in erythrocytes as a contrast agent for magnetic resonance imaging [18].

Various cell surface modifications have been explored either to control immune response of host, or organ distribution, or to manipulate drug release. Human erythrocyte allows modification of surface, thereby promoting autologous immunoglobulin binding and C3b deposition. This kind of deposition allows drug loaded erythrocyte recognition, uptake, and release in macrophages. Recently, surface modification of RBCs using hyperbranched polyglycerol (HPG) has been explored [19, 20].

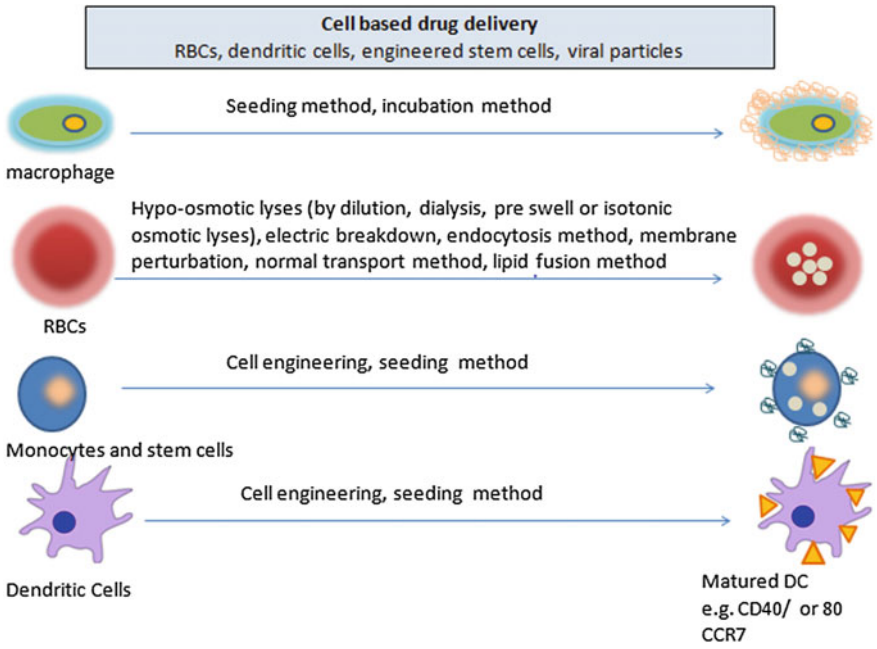

Fig. 4 Types of cells used in cell-mediated drug delivery systems and their production methods

RBCs were shown to be efficient antigen carriers for targeting dendritic cells (DCs) and could induce cytotoxic T-cell responses [21]. RBC-mediated delivery of 9-(2-phosphonylmethoxyethyl) adenine to primary macrophages showed improved activity against HIV or herpes simplex virus [22]. Similar to this study, improved drug delivery was obtained with photosensitized sickle RBCs (SSRBCs) to tumors compared to non-photosensitized SSRBCs, drug-loaded photosensitized native RBCs, and free drug [23]. RBCs loaded with antigen showed a significant contribution in application of transfusion medicine by attenuating the immunological recognition of surface antigens [24]. Recently, antisense oligodeoxynucleotides (AS-ODNs) opsonized erythrocyte ghosts (EGs) showed 4.5-fold higher levels of AS-ODN in the liver compared with unopsonized EGs ([25].

Erythrocyte-mediated delivery of enzymes such as phenylalanine ammonia lysate [26], phenylalanine hydroxylase [27], low molecular weight protamine (LMWP), and L-asparaginase-cell penetrating peptide (CPP) [28] is now being explored and has shown promising results in vitro. Other drugs encapsulated in RBCs include chlorpromazine [29], etoposide [30], and dequalinium [31]. Beside that, RBCs are effective carriers for metallic nanoparticles like silver, gold (Au), etc. The AuNP (20 nm) and gold incorporated RBCs were used in dynamic X-ray imaging [32].

2.1.1 Cancer Therapy

Cancer of the white blood cells, known as acute lymphoblastic leukemia (ALL), causes the bone marrow to produce excess immature white blood cells, called lymphoblasts, which are unable to help the body fight against infections. Regular process of hematopoiesis is inhibited resulting in a deficiency of normal white blood cells, RBCs, and platelets. L-asparaginase (ASNase) enzyme from *E.coli* hydrolyzes amino acid L-asparagine (ASN) to L-aspartic acid (AS) and ammonia. Neoplastic tissues, however, express a significantly lower level of AS, and thus have to rely solely on extracellular source of ASN to maintain protein synthesis. Systemic depletion of ASN by ASNase impairs protein biosynthesis in these cells, leads to their death through cellular and cause immunogenicity problems with high frequency of hypersensitivity reactions. Use of erythrocytes as a drug carrier for ASNase has been reported to overcome the immunotoxic reactions. ASNase loading efficiency ($\sim$4 %) and RBC loading capacity (8 IU of ASNase per 100 μL of packed RBCs) was achieved. There was no leaching or degradation of the RBC-encapsulated ASNase over a 3-day incubation period, during which the erythrocytes remained visibly intact. Preservation of both structure and functionality of the treated erythrocytes provided flexibility of replacing an unrestrictive amount of blood (or RBCs) from the patient with drug-loaded erythrocytes. ASNase-loaded RBCs were merged back with the other blood components, and finally returned to the patient for in situ drug therapy for ALL [33]. Scientists at the University of California, San Diego, have developed RBC wall wrapped nanoparticles (as camouflaged nanoparticles) of 100 nm. Preformulated PLGA nanoparticles were fused with the RBC-membrane-derived vesicles through mechanical extrusion. These wrapped polymeric nanoparticles showed stealth effect and remained in systemic circulation for almost 2 days. Polyacrylamide gel electrophoresis (PAGE) is widely used in identification of protein adsorption [34]. Protein analysis confirmed retention of protein composition of RBC membrane after extrusion. Camouflaged PLGA nanoparticles showed longer circulation and long half-life compared to PEG coated PLGA nanoparticles [35].

Biocompatible RBCs for tumor targeting are developed based on the response of light (Fig. 4). RBCs loaded with doxorubicin and albumin bound near-infrared dye were surface modified with peptide to allow efficient tumor targeting [36]. In vitro results confirmed response from near-infrared (NIR) laser-based membrane rupture and drug release, thereby allowing combined synergic therapy based on photothermal and chemotherapy approach. Use of dexamethasone (glucocortocoid class) is limited by several adverse effects such as osteoporosis and severe immunological and allergic reactions. Dexamethasone 21-phosphate loaded RBCs at a single dose (10 mg/50 ml) maintained plasma drug concentration from 15 to 50 nm for 30 days when tested in vivo. RBCs provided the necessary sustained release effect to maintain drug levels in blood. These RBCs can be used for several

therapeutic targets such as chronic obstructive pulmonary disease (COPD), cystic fibrosis (CF), and inflammatory bowel diseases (IBDs). RBCs offer delivery of fluorinated purines in cancer [37, 38]. Fluorinated purine analogs are generally used for the treatment of blood-related cancer conditions. The candidate from this class, fludarabine phosphate (9-b-D-arabinofuranosyl-2-fluoroadenine 5′-monophosphate) was loaded onto the RBCs, showed a significant cancer cell growth reduction when tested on breast cancer cell lines (MCF-7 and MDA-MB-435 cells). This confirms that RBCs loaded with anticancer drug can provide sustained release and superior functionality over conventional drug carriers.

Drug delivery of anticancer drug 5-fluoro-2′-deoxyuridine was achieved via encapsulation of prodrug 5-fluoro-2′-deoxyuridine-monophosphate in RBCs. RBCs facilitated prodrug conversion effectively, and can be used as a carrier or study models for investigation. RBCs can serve as a biological model to convert non-diffusible drugs/products into diffusible systems with the help of inhouse enzymes present in RBCs.

Furthermore, RBCs have been explored for delivery of synthetic drugs such as adriamycin (doxorubicin), methotrexate, and paclitaxel [39]. In a separate study, methotrexate-loaded erythrocytes were photosensitized by exposure to hematoporphyrin derivative. Resealed erythrocytes served as a potential carrier for photo-activable carrier system in cancer therapy [40]. Layer-by-layer (LbL) polyelectrolyte surface coated erythrocytes have been prepared for sustained release of RITC-lysozyme. LBL coating was performed using lysine hydrobromide and dextran sulfate. This type of coating can further help to fine-tune the release phenomenon [41, 42]. Surface coating of erythrocytes can help in specific drug targeting. In one of such attempts, anti-Rh antibody (IgG anti-D)–decorated autologous erythrocytes were loaded with gentamicin. In vivo studies confirmed rapid targeted drug delivery of gentamicin to RES systems [43].

Some other anticancer drugs like cytosine arabinoside (ana-C) [44] and daunorubicin [45] have been encapsulated in erythrocytes and benefited by sustained delivery. Furthermore, RBCs can be used as carrier cells for statin drugs, which mainly face bioavailability and toxicity issues and can be effectively delivered by RBCs. To overcome these challenges and to maintain controlled levels of drug in blood, pravastatin was loaded in human erythrocytes. The resealed erythrocytes maintained drug levels up to 83 % up to 23 h in phosphate buffer saline when tested in vitro; crosslinking further decreased the drug release up to 72 % [46]. Erythrocyte-based antigen delivery system was explored by Hamidi et al., by using bovine serum albumin as a model compound [47].

2.1.2 HIV and Related Complications

RBCs loaded with anti-HIV drug azidothymidine and 2′,3′-dideoxycitidine from nucleoside analog reverse transcriptase inhibitors (NRTIs) class showed enhanced antiviral potency in HIV mouse model and showed prolonged drug release. In another separate study, erythrocytes are explored as potential carriers for delivery of

reduced glutathione (GSH) for retroviral treatment with the intention to resolve pharmacokinetic issues associated with drug. In this study, GSH was loaded in RBCs in combination with AZT and in dual combination with AZT + 2,3-dideoxyinosine (DDI; Didanosine) to simulate highly activated antiretroviral therapy (HAART). In vitro analysis in murine HIV model confirmed effective delivery of GSH and AZT loaded RBCs compared to the intramuscularly administered combination. Furthermore, subsequent administration up to 10 weeks in retroviral complex LP-BM5 infected mice resulted in enhanced antiretroviral effects for both combinations and showed superior levels in brain tissue [48].

Newly synthesized nucleoside analog homo dinucleotide, di(thymidine-3′-azido-2′,3′-dideoxy-D-riboside)-5′-5′-pl-p2-pyrophosphate (AZTp2AZT) was loaded into RBCs. Encapsulated RBCs facilitated the erythrocyte-membrane protein clusterization and, furthermore, phagocytosis which resulted in targeted delivery of prodrug AZTp2AZT [49]. In other study, a potent anti-leukemic nucleoside analog called fludarabine, chemically 9-(β-D-arabinofuranosyl)-2-fluoroadenine 5′-monophosphate was loaded onto RBCs, reduced the toxic effects and facilitated the selective killing of HIV-infected macrophages. Fludarabine is converted to its active form called triphosphate derivative in RBCS [50].

Protein drugs can be successfully loaded into the RBCs, e.g., cyclosporine A (CsA) binding protein and FKBP12 as an FK506 (Tacrolimus) binding protein. Both these immunosuppressive drugs have high intra- and inter-patient pharmacokinetic variability due to low solubility and poor bioavailability. In vitro data indicated that human RBCs were loaded with 3–15 nm of FKBP12 RBC/mL and 4–16 nm of CypA RBC/mL, in a dose-dependent manner. Encapsulation of protein drugs allowed RBCs to be explored for enzyme replacement therapies and thrombolytic therapy. Several enzymes loaded into RBCs till date include aldehyde dehydrogenase, alcohol oxidase, glucose oxidase, hexokinase, galactosidase, glucuronidase, alglucerase, a modified form of the β-glucocerebrosidase, adenosine deaminase, fibrinolytic agents, urokinase, streptokinase, and L-asparaginase. In another study, liposome encapsulated clodronate (dichloromethylene diphosphonate) selectively induced apoptosis. Mice were either treated with anti-RBC antibodies or pre-opsonized, liposomal clodronate substantially decreased RBC destruction. The effect was registered by blocking and then depleting phagocytic macrophages, with action lasting for 1–2 weeks. Liposomal clodronate showed very selective effect on macrophages and phagocytic dendritic cells [51].

2.1.3 Antimalarial/Antitubercular

Pyrimethamine, an antimalarial drug was loaded on extruded erythrocytes to generate nanoerythrosomes (nE). The drug was conjugated to the nEs with the help of glutaraldehyde as a crosslinker and their performance was checked against drug encapsulated erythrocytes. nEs showed good stability at 4–37 °C. In vivo performance in albino mice confirmed controlled delivery of drug and accumulation in liver as target organ, which is an ideal target for antimalarial therapy [52].

Furthermore, RBCs are explored for sustained delivery of antitubercular drug, isoniazid [53], and for antifungal drug metronidazole [54].

2.1.4 Artificial RBCs

Artificial blood is a product made to act as a substitute for RBCs. Artificial blood is formulated for transporting oxygen and carbon dioxide throughout the body and generally has a longer shelf life (1 year or more). It can be produced using synthetic production, chemical isolation, or recombinant biochemical technology. The ideal artificial blood is safe to use and is biocompatible. It has no adverse or allergenic/immunogenic effects from other body cells and the various blood phenotypes play no role in their utility. Artificial blood can remove viruses/microorganisms and are able to transport oxygen throughout the body and release at the desired organs.

Hemoglobin-based artificial blood substitutes use hemoglobin from human, animal, and recombinant type sources. Human hemoglobin is obtained from donated blood that has reached its expiration date and from the small amount of red cells collected as a by-product during plasma donation. One unit of hemoglobin solution can be produced from 2 units of discarded blood. On the other hand, recombinant hemoglobin is mainly obtained by inserting the gene for human hemoglobin into *Escherichia coli* bacteria with subsequent isolation. The gene couch can be manipulated to obtain variant forms of hemoglobin. One unit of hemoglobin solution can be produced from 750 L of *Escherichia coli* culture.

Surface-modified hemoglobin is formulated by the conjugation of PEG molecules to surface lysine groups. PEG–conjugated hemoglobin product is being used for treatment of patients with stroke and cancer due to their size that allows them to pass through constrictions and oxygenate areas that cannot be reached by RBCs. PEGylated hemoglobin can deliver oxygen to tumor cells and increase the susceptibility to radiation or chemotherapy in cancer patients. Crosslinked hemoglobin is formed using covalently attached glycosyl bridges to dimers to create a stable tetramer. On the other hand, polymerized hemoglobin is prepared by linking surface amino acid groups using glutaraldehyde. Polymerized hemolink (24 h half-life) is formulated using affinose polymerized human hemoglobin. Use of artificial blood to carry drugs is still in infancy, and needs deep understanding of experiments. Interaction of single cell assay in artificial blood drug delivery is still in the experimental phase [55].

2.2 Stem Cells

Stem cells are the second widely studied cells for delivery of drugs. Stem cells are being explored for treatment of various diseases and have the potential application for medical therapies (Fig. 4). Stem cells are a source of replacement cells to treat

various diseases and disorders that can potentially reduce the morbidity and mortality of patients with organ failures. Some of the key problem areas where stem cells have a major role to play include Parkinson's disease, type I diabetes, arthritis, burn victims, cardiovascular diseases and congenital birth defects. Stem cells are widely used to assess the safety of newly developed drugs at the preclinical stage before testing in animal and human models.

Human pluripotent stem cells (hPSCs) have led to the option of using it as a source of cell-based therapeutic products. Numerous new hPSCs-based cell therapy products are in various stages of development in cell therapy-specialized companies and their future market is estimated to be very promising. However, the hPSCs-based therapeutic product manufacturing and their therapies have slowed down the introduction of new products and clinical applications in the market. Till date, stem cells-based delivery is explored in cancer, HIV, microbial infections, dental implants, organ targeted delivery, peptide and gene delivery.

For cancer treatment, a silica nanorattle–doxorubicin is anchored to mesenchymal stem cells (MSCs) by specific antibody–antigen recognitions at the cytomembrane interface without any cell preconditioning [56]. Almost 1500 nanoparticles were uploaded in each MSC with high cell viability and tumor-tropic ability. Increased and prolonged doxorubicin intratumoral distribution significantly enhanced tumor-cell apoptosis. On the other side, for treatment of urgent lung pathologies, such as acute respiratory distress syndrome and post-lung transplantation, CBDD is being explored. Drug delivery to small airways, terminal bronchioles, and alveoli (deep lung), especially to the lower lungs is challenging with currently available drug delivery forms. To overcome these limitations, CBDD systems are studied. Recently, isolated rat sertoli cells preloaded with chitosan nanoparticles are used to obtain a high-density distribution and concentration in mice lungs by peripheral venous vasculature route. Additionally, sertoli cells–chitosan NP were coupled with the anti-inflammatory compound curcumin. The complex upon intravenous injection in mice with deep lung inflammation showed superior activity and drug distribution throughout lung compared to the control [57].

Multipotential dental pulp stem cells (DPSCs) obtained from a connective tissue within the dental crown are useful in neural-crest-derived bone reconstruction in humans and can be used to repair body defects in low-risk autologous therapeutic strategies. DPSCs loaded onto scaffolds of collagen sponges, hydroxyapatite scaffold, chitosan scaffold, biocoral, chitosan/collagen complex, and hydroxyapatite/tricalcium phosphate HA/TCP disks are studied in bone regeneration. Human bone marrow progenitor cells known as multipotent stromal cells or MSCs differentiate into osteoblasts, chondrocytes, and adipocytes required for bone repair. Several cell types including skeletal myoblasts, MSCs (bone marrow and adipose derived), embryonic stem cells, and cardiac stem cells have been explored for cardiac regeneration. Stem cells with a specific tropism for brain tumors could be used as a delivery vehicles for nanoparticles. These cells have a natural tendency to migrate and distribute within the tumor mass and can modulate drug release.

2.2.1 Stem Cell Based Drug Delivery

Neural stem cells (NSCs) possess tumor affinities that enable their use as delivery vehicles to target enzyme/prodrug therapy selectively to tumors. Aboody et al. used cytosine deaminase (CD)–expressing clonal human NSC line, HB1.F3.CD, to develop gliomas in mice and locally converted the prodrug 5-fluorocytosine to the active chemotherapeutic 5-fluorouracil. In vitro studies showed that the NSCs have normal karyotype, tumor affinity, CD expression and were functionally and genetically stable. In vivo biodistribution studies demonstrated NSCs' retention of tumor tropism and were safe and nontoxic after intracerebral administration in nontumor-bearing and orthotopic glioma-bearing immunocompetent and immunodeficient mice. Prodrug to drug conversion related toxicities were not reported; however, no signs of pathology or tumorigenesis were noted. This research is the first clinical trial study of an allogenic NSCs-mediated enzyme/prodrug-targeted cancer therapy in patients with recurrent high-grade glioma [58].

Enzyme replacement therapy (ERT) used in the treatment of lysosomal storage diseases (LSDs) such as Gaucher disease, Fabry disease, and mucopolysaccharidosis I (MPS I) has limitations such as life-long treatment, development of antibodies, and inability to cross blood–brain barrier (BBB) resulting in failure to halt disease progression in the brain. Transplantation of hematopoietic stem cells (HSCs), bone marrow stem cells (BMSCs), and umbilical cord blood-derived stem cells (UCBSCs) offer effective solutions for the treatment of these diseases. Genetically modified stem cells were transplanted intracranially/intracerebrally as an enzyme delivery system bypassing the BBB effectively and thereby ensuring the release of enzymes to the affected CNS lesion sites. Kim 2014 has reported use of genetically modified neural stem cells encoding enzyme genes to effectively decrease the lysosomal storage with reduced pathological signs and extended life span in mouse model [59].

Stem cell-based delivery of drug loaded nanoparticles offers a promising way to overcome drug passage through the BBB. Their ability to incorporate nanoparticles and migrate throughout interstitial barriers, together with their inherent tumor affinity and synergistic antitumor effects makes them effective as combined therapy. As a novel anticancer drug carrier, drug loaded MSCs hollow silica nanoparticles was used to carry a photosensitizer drug and deliver it to breast tumors, due to the natural high tumor affinity of MSCs and inhibit tumor growth by photodynamic therapy. This new strategy for delivering photosensitizer to tumors by using tumor-affinitive MSCs addresses the challenge of the accumulation of photosensitizer drugs in tumors in photodynamic therapy [60–62].

A major limitation of cell therapies is the rapid decline in viability and function of the transplanted cells. Highly enhanced cell therapy via the conjugation of adjuvant drug-loaded nanoparticles to the surfaces of therapeutic cells is reported. Sustained pseudoautocrine stimulation to donor cells showed remarkable increase in tumor elimination in a model of adoptive T-cell therapy for cancer. This increased the in vivo repopulation rate of hematopoietic stem cell grafts with very low doses of adjuvant drugs that were ineffective when given systemically. This

approach led to augmentation of cytoreagents while minimizing the systemic side effects of adjuvant drugs. The above studies clearly suggest that stem cells are promising vectors for targeted drug delivery [63–67]. Not to mention, SCs are most preferred cells due to their selective homing, low immunogenicity, allergenic use, safety profile, easy availability, and cryopreservation.

2.3 Macrophages

Macrophages are widely studied as a cell delivery platform and are the most common targeted cells. Macrophages are ideal carriers for crossing BBB and complex cell barriers [68]. Macrophages are being explored for delivery of anti-cancer drug as well as imaging agent. Bone marrow derived macrophages (BMMs) are used to deliver indinavir nanocrystals (1.6 μm) to sustain the drug levels in body. Advanced techniques like single-photon emission computed tomography (SPECT) and tracing of labeled BMMs by T2* weighted MRI of radio- and superparamagnetic iron oxide (Feridex) were used to assess the biodistribution of cells. Indinavir loaded macrophages maintained the drug levels up to 14 days in mice, thereby exhibiting sustained HIV AIDS therapy [69, 70].

Drug-loaded macrophages are used for therapeutic enzyme delivery to brain. This type of drug delivery is highly desirable in neurodegenerative disease management. Haney et al. loaded the catalase enzyme in the polyion complex micelle ('nanozyme') in BMMs which protected nigrostriatum against 1-methyl-4-phenyl-1,2,3,6-tetrahydropyridine intoxication. Macrophages facilitated the transport of nanozyme to the brain cells via endocytosis-independent mechanisms. Recently, modified macrophages are used to encapsulate and release exosomes containing DNA, mRNA, transcription factors, and an encoded catalase protein to reduce inflammation of the brain. When tested in Parkinson's disease mouse models, macrophages-based delivery systems showed sustained release of catalase, thereby reducing the inflammation in brain [71].

Another study reports use of human acute monocytic leukemia cells to load liposomal doxorubicin (150 nm). The cells were further labeled with Qdot 800 or iron oxide (IO) and studied in subcutaneous tumor mouse model. The obtained results indicated that macrophage-mediated drug delivery system alone or in combination with a radiation can provide effective cancer treatment [72]. Macrophages were loaded with phase-change droplets composed of lipid, perfluoropentane, and doxorubicin to target hypoxic or ischemic areas in tumors. Initial experiments with RAW 264.7 macrophages (mouse leukemic monocyte macrophage cell line) showed the potential to target this area when tested for migration mobility of macrophages and antiproliferative potential [73] (Fig. 5).

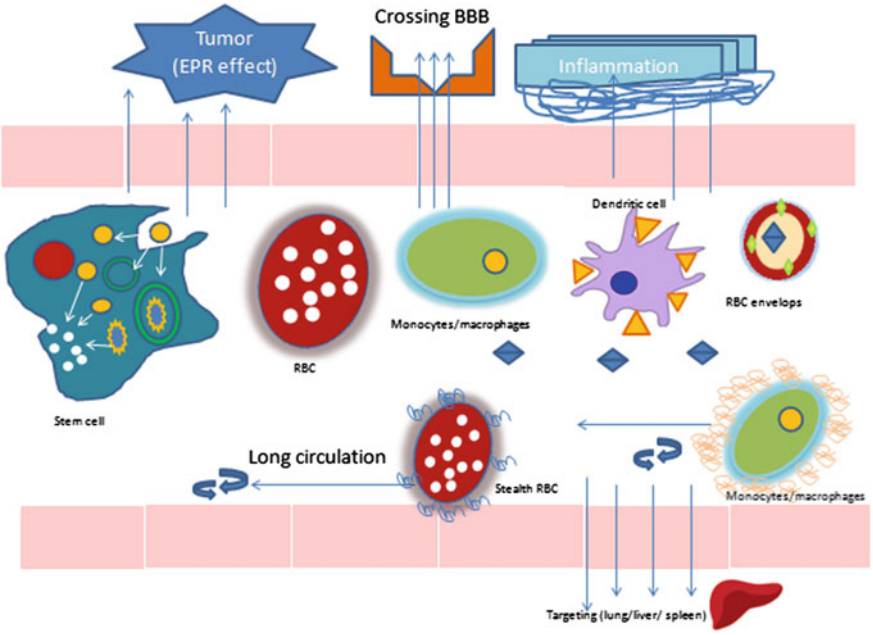

Fig. 5 Journey of cell-based drug delivery systems and the targets they can achieve

2.4 Dendritic Cells

Dendritic cells (DCs) are designated as antigen-presenting cells. Maturation of DCs is generally associated with reduced phagocytic capacity. Maturation phase results in upregulation of several molecules and thereby production of cytokines and chemokines, which is mainly necessary for optimal T-cell activation. Encapsulation of tumor-associated antigens into DCs by using bacterial or viral vectors or RNA transfection can allow effective cancer treatment options. Although several factors that include types of DCs, type and source of antigen, encapsulation efficiency, degree of maturation stimuli, activation and delivery of antigens at required time and in required dose, migration of DCs to lymphoid tissues, and lastly route of cell administration to body play an important role in the final performance of such CBDD systems. DCs serve as ideal cells for delivery of antigens, peptides, and proteins [74].

Recently, FK506 (Tacrolimus) loaded DCs have been used as targeted drug delivery carriers to achieve controlled drug release. Furthermore, use of DCs limited the adverse effects of tacrolimus compared to free form. Antigen-loaded DCs have been widely used with excellent safety profiles [74, 75].

3 Market Presence of CBDD Systems

Targeted drug delivery increases the specific drug loading in specific organs and/or cells to improve the efficacy of the drug by reducing side effects. This concept is widely studied in treatment of cancer, autoimmune diseases, neurological disorders, and pulmonary diseases where highly effective, safe, specific targeting is required. These systems often overcome mucus, BBB, osmotic barriers, and limitation by charge and varied pH. CBDD offers harmonization with body and overcomes the challenges faced by conventional drug delivery systems. Cells effectively encapsulate the drug or their nanoparticles and provide better pharmacokinetic and biocompatibility besides possibility of high drug loading with reduced toxicity leading to better patient compliance. The modulation of drug release is possible by optimal cell engineering. Cell-based drug carriers have been widely studied for many decades at various levels of research; however, their adoption at clinical levels is very low. The expensive scale-up and long-term stability might be a limiting factor for their commercial development [76]. The majority of cell-based therapeutic carriers is occupied by RBCs, while clinical research area is highly dominated by stem cells. Targeting vaccines and drugs via basic microbial cells have been studied for several years, and work on modified cell forms for effective and safer drug targeting is ongoing. Mainly, engineered erythrocytes, stem cells, bacterial ghost, magnetotactic bacteria are leading research areas and are slowly moving to clinics.

EryDel S.p.A (http://www.erydel.com/), an Italian company specialized in drug and diagnostics delivery platforms based on human red blood cells. Erydel's proprietary method allows reversible opening and closing of erythrocytes, thereby allowing encapsulation of therapeutic molecules such as peptides, proteins, nucleic acids, diagnostic agents, and nanoparticles by maintaining cells original physiological properties.

EryDel has developed an automatic, noninvasive electromedical device called Red Cell Loader. This device is based on the principle of EryDex process, in which human RBCs are loaded with marketed drug dexamethasone sodium phosphate and studies are in progress to encapsulate proteinous drugs and small molecules. EryDex system is currently developed for treatment of Ataxia Telangiectasia (a rare autosomal recessive disorder) and Duchenne Muscular Dystrophy (a fatal genetic disorder). In 2012, EryDel received the US Orphan Drug designation for EryDex for the treatment of Ataxia Telangiectasia and US IND approval in 2013. EryDel has ventured into diagnostics and targeted drug delivery (EryTargeting) market with an aim to deliver drug containers only to cells.

EryTech Pharma (http://erytech.com/home/), a French biopharmaceutical company, specialized in RBC-based cancer treatments. This company develops innovative targeting platforms based on enzymatic therapy, in particular on L-asparaginase. This ISO 9001–2008, cGMP certified company has developed a product marketed as Ery-ASP (GRASPA®), L- asparaginase loaded erythrocytes which upon delivery destroy asparagines. Ery-ASP is proven biocompatible vehicle and has a half-life of about one month after administration in the body. Its clearance

occurs via regular physiological functions performed by reticuloendothelial system (RES). Multiple clinical trials with Ery-ASP to investigate its effect in treatment of acute lymphoblastic leukemia, acute myeloid leukemia, pancreatic cancer, and solid tumors are in progress. Other platforms such as EryVAX, EryTOL, and EryMET are under development for indications such as cancer immune therapy, cancer tolerance and tumor starvation, respectively. EryTech pharma has obtained orphan drug status for Ery-ASP/GRASPA® in acute lymphoblastic leukemia, acute myeloid leukemia, and pancreatic cancer in Europe and in the US. Recently, EryTech announced successful encapsulation of a new enzyme called methionine-γ-lyase in RBCs. The industrial scale-up is planned in 2015 to enable to enter the Phase I clinical trial.

A Swiss biopharmaceutical company, Pevion Biotech AG (http://www.pevion.com), offers various virosome-based technology vaccine platforms (e.g., PeviPROTM, Inflexal®V, Epaxal®, and PeviTERTM/140–150 nm) against breast

Table 1 List of various cell-based drug delivery candidates in clinical trials

Name of the study	Name of the company/sponsor	Year
Erythrocyte-mediated drug delivery for the prevention of stent restenosis (TROY)	University of Rome Tor Vergata	2007
Erythrocytes-mediated delivery of dexamethasone 21-phosphate in steroid-dependent ulcerative colitis (Crocodex)	Casa Sollievo della Sofferenza IRCCS	2010
Vaccination with dendritic cells loaded with brain tumor stem cells for progressive malignant brain tumor	Masonic Cancer Center, University of Minnesota	2010
Treatment of multiple sclerosis and neuromyelitis optica with regulatory dendritic cell: clinical trial phase 1 b (dendritic cells loaded with myelin peptides)	Sara Varea, Fundació Clínic per la Recerca Biomèdica	2015
Vaccination with autologous dendritic cells loaded with autologous tumor lysate or homogenate combined with immunomodulating radiotherapy and/or preleukapheresis IFN-alfa in patients with metastatic melanoma	Istituto Scientifico Romagnolo per lo Studio e la cura dei Tumori	2013
Administration of allogenic red blood cells loaded l-asparaginase in cases of relapse of acute lymphoblastic leukemia (GRASPALL)	ERYtech Pharma	2009
Autologous dendritic cell-tumor cell immunotherapy for metastatic melanoma	NeoStem, Inc.	2014
Efficacy and safety of masct group' and 'non-treatment group' in patient undergone curative resection (RFA or operation) for hepatocellular carcinoma. MASCT that expresses multiple antigens specific cellular therapy, autologous immune cytotoxic of t-lymphocytes (CTL) induced by dendritic cell (DC) loaded with multiple antigens	Chonnam National University Hospital	2013

cancer, influenza, candidiasis, and tetanus using active targeted delivery approach. This virosome technology is licensed to Johnson & Johnson. Pevion has developed the second generation of stable virosomes using lyophilization and alternative formulation approaches. Pevion has out-licensed the malaria vaccine called PEV3. A number of vaccine candidates based on virosome technology are in various stages of clinical trials. Pevion has a very strong candidate pipeline with various therapeutic and prophylactic vaccines activity against infectious diseases and cancer. Two commercially successful virosome-based vaccines manufactured by Pevion are Epaxal and InflexalV, which are licensed in over 40 countries and are manufactured by Crucell, Switzerland. Table 1 lists ongoing clinical trials in this area of research.

4 Conclusion and Future Prospective

Medical science and the pharma industry are extensively studying the exact mechanism of diseases and alternations in process. This requires complete understanding of altered mechanisms in cells or nearby tissues. However, several limitations such as methods to analyze these alterations, limitations on analytical techniques for such diverse cell populations, and unavailability of in vitro cell "disease" models slows down this research. The last few decades have witnessed a strong requirement for a deep understanding of cell mechanisms with the help of cellular engineering science, which might help toward a systematic framework to understand safety, and predictably altering and regulating cellular behaviors in body as native cells or when loaded with drug. Although biologics is in high boom and has paved the way to a broad range of new targets, functional capabilities, and disease applications, scientists are still struggling to understand unknown mechanisms. New findings like use of the technique called nanofountain probe electroporation (NFP-E) boost the confidence of researchers to predict drug targeting. This technique allows creation of temporary holes in cell membranes, which promotes entry of drugs, polysaccharides, proteins, DNA hairpins, and plasmid DNA into cell. These kind of technique allows complete advantage of each cell capability in delivering drugs.

Several biologics are approved by food and drug administration (FDA) in recent years and most of them are now available in the market. However, the complexity of cell anatomy and physiology in such kind of drug delivery often requires lot of scientific data generation, animal safety data, besides very strict regulatory and associated risks, both commercial and technical. SCA will help scientists to understand deep mechanistic cell physiology, response profile, alterations after encapsulation, and ultimate fate and toxicity. All together these tiny cells are well-equipped agents that can regulate pharmacokinetics and pharmacodynamic properties and the ultimate fate of drug and enzyme encapsulation. Overall, SCA has great potential to offer in understanding of cell-to-cell behavior in presence of drug and in selection of the right drug/cell combination. The combinations of

bacterial or viral capsid with mammalian cell offer different paradigms to cell-based drug delivery systems. Each cell behaves differently to various drugs and to encapsulation methods; however, this process has not been studied in detail in cell-based therapeutics. Limitations of cell-based therapies such as stability and large-scale production and can be overcome by use of the innovative formulation and production approach.

References

1. Kaur IP, Singh H (2014) Nanostructured drug delivery for better management of tuberculosis. J Control Release Official J Control Release Soc 184:36–50
2. Shegokar R (2015) Nanotoxicity: must consider aspect of nanoparticle development, in nanoparticles' promises and risks—characterization, manipulation, and potential hazards to humanity and the environment. In: Lungu M, Neculae A, Bunoiu M, Biris C (eds) Springer International Publishing, Switzerland, pp 87–102
3. Rashkow JT et al (2014) Quantification of single-cell nanoparticle concentrations and the distribution of these concentrations in cell population. J Roy Soc Interface Roy Soc 11 (94):20131152
4. Chang YC et al (2013) Rapid single cell detection of staphylococcus aureus by aptamer-conjugated gold nanoparticles. Sci Rep 3:1863
5. Torrano AA et al (2013) A fast analysis method to quantify nanoparticle uptake on a single cell level. Nanomedicine 8(11):1815–1828
6. Fritzsch FS et al (2012) Single-cell analysis in biotechnology, systems biology, and biocatalysis. Annu Rev Chem Biomol Eng 3:129–155
7. Kann B et al (2015) Raman microscopy for cellular investigations—from single cell imaging to drug carrier uptake visualization. Adv Drug Delivery Rev
8. Kohl Y et al (2011) Biocompatible micro-sized cell culture chamber for the detection of nanoparticle-induced IL8 promoter activity on a small cell population. Nanoscale Res Lett 6:505
9. Franciscan C (2013) Single-cell analysis of specific B cell binding and uptake of peptide-targeted liposomes for vaccine formulations. https://aiche.confex.com/aiche/2013/webprogram/Paper331834.html. (poster 331834)
10. Malek AH, Khaledi MG (2003) Monitoring liposome-mediated delivery and fate of an antisense drug in cell extracts and in single cells by capillary electrophoresis with laser-induced fluorescence. Electrophoresis 24(6):1054–1062
11. Jiang Ping-Lun et al (2015) Galactosylated liposome as a dendritic cell-targeted mucosal vaccine for inducing protective anti-tumor immunity. Acta Biomater 11(1):356–367
12. Yue S et al (2006) Intracellular delivery of fluorescent dyes mediated by nanometer-liposomes Chem J Chin Univ 27(4):632–634
13. Pascolo L et al (2014) Detection of PLGA-based nanoparticles at a single-cell level by synchrotron radiation FTIR spectromicroscopy and correlation with X-ray fluorescence microscopy. Int J Nanomed 9:2791–2801
14. Lale SV et al (2015) Multifunctional ATRP based pH responsive polymeric nanoparticles for improved doxorubicin chemotherapy in breast cancer by proton sponge effect/endo-lysosomal escape Polym. Chem 6:2115–2132
15. Greineder CF et al (2013) Advanced drug delivery systems for antithrombotic agents. Blood 122(9):1565–1575
16. Antonelli A et al (2013) Red blood cells as carriers in magnetic particle imaging. Biomed Tech (Berl) 58(6):517–525

17. Markov DE et al (2010) Human erythrocytes as nanoparticle carriers for magnetic particle imaging. Phys Med Biol 55(21):6461–6473
18. Brähler M et al (2006) Magnetite-loaded carrier erythrocytes as contrast agents for magnetic resonance imaging. Nano Lett 6(11):2505–2509
19. Chapanian R et al (2012) In vivo circulation, clearance, and biodistribution of polyglycerol grafted functional red blood cells. Biomaterials 33(10):3047–3057
20. Bradley AJ et al (2002) Biophysical consequences of linker chemistry and polymer size on stealth erythrocytes: size does matter. Biochim Biophys Acta 1561(2):147–158
21. Banz A et al (2010) In situ targeting of dendritic cells by antigen-loaded red blood cells: a novel approach to cancer immunotherapy. Vaccine 28(17):2965–2972
22. Perno CF et al (1997) Red blood cells mediated delivery of 9-(2-phosphonylmethoxyethyl) adenine to primary macrophages: efficiency metabolism and activity against human immunodeficiency virus or herpes simplex virus. Antiviral Res 33(3):153–164
23. Choe SW et al (2013) Drug-loaded sickle cells programmed ex vivo for delayed hemolysis target hypoxic tumor microvessels and augment tumor drug delivery. J Control Release Official J Control Release Soc 171(2):184–192
24. Murad KL et al (1999) Structural and functional consequences of antigenic modulation of red blood cells with methoxypoly(ethylene glycol). Blood 93(6):2121–2127
25. Kim SH et al (2009) Opsonized erythrocyte ghosts for liver-targeted delivery of antisense oligodeoxynucleotides. Biomaterials 30(5):959–967
26. Rossi L et al (2014) Erythrocyte-mediated delivery of phenylalanine ammonia lyase for the treatment of phenylketonuria in BTBR-Pah(enu2) mice. J Control Release Official J Control Release Soc 194:37–44
27. Yew NS et al (2013) Erythrocytes encapsulated with phenylalanine hydroxylase exhibit improved pharmacokinetics and lowered plasma phenylalanine levels in normal mice. Mol Genet Metab 109(4):339–344
28. He H et al (2014) Cell-penetrating peptides meditated encapsulation of protein therapeutics into intact red blood cells and its application. J Control Release Official J Control Release Soc 176:123–132
29. Favretto ME et al (2013) Human erythrocytes as drug carriers: loading efficiency and side effects of hypotonic dialysis, chlorpromazine treatment and fusion with liposomes. J Control Release Official J Control Release Soc 170(3):343–351
30. Lotero LA, Olmos G, Diez JC (2003) Delivery to macrophages and toxic action of etoposide carried in mouse red blood cells. Biochim Biophys Acta 1620(1–3):160–166
31. Lizano C et al (2003) In vivo biodistribution of erythrocytes and polyethyleneglycol-phosphatidylethanolamine micelles carrying the antitumour agent dequalinium. Eur J Pharm Biopharm Official J Arbeitsgemeinschaft fur Pharmazeutische Verfahrenstechnik e.V 56(2):153–7
32. Ahn S et al (2011) Gold nanoparticle-incorporated human red blood cells (RBCs) for X-ray dynamic imaging. Biomaterials 32(29):7191–7199
33. Kwon YM et al (2009) L-Asparaginase encapsulated intact erythrocytes for treatment of acute lymphoblastic leukemia (ALL). J Control Release Official J Control Release Soc 139(3):182–189
34. Shegokar R, Sawant S (2015) Multi-dimensional electrophoresis: the march in pharma application, in nanoparticles' promises and risks—characterization, manipulation, and potential hazards to humanity and the environment. In: Lungu M, Neculae A, Bunoiu M, Biris C (eds) Springer International Pulishing, Switzerland pp 303–333
35. Hu CM et al (2011) Erythrocyte membrane-camouflaged polymeric nanoparticles as a biomimetic delivery platform. Proc Natl Acad Sci USA 108(27):10980–10985
36. Yang E et al (2015) Theranostic nanoparticles carrying doxorubicin attenuate targeting ligand specific antibody responses following systemic delivery. Theranostics 5(1):43–61
37. Rodriguez G (1994) Fludarabine phosphate. A new anticancer drug with significant activity in patients with chronic lymphocytic leukemia and in patients with lymphoma. Invest New Drugs 12:75–92

38. Biagiotti S et al (2011) Drug delivery by red blood cells. IUBMB Life 63:621–631
39. Harisa GI et al (2014) Engineering erythrocytes as a novel carrier for the targeted delivery of the anticancer drug paclitaxel. Saudi Pharm J SPJ Official Publ Saudi Pharm Soc 22 (3):223–230
40. Flynn G, McHale L, McHale AP (1994) Methotrexate-loaded, photosensitized erythrocytes: a photo-activatable carrier/delivery system for use in cancer therapy. Cancer Lett 82(2):225–229
41. Luo R et al (2012) Engineering of erythrocyte-based drug carriers: control of protein release and bioactivity. J Mater Sci Mater Med 23(1):63–71
42. Shaillender M et al (2011) Layer-by-layer microcapsules templated on erythrocyte ghost carriers. Int J Pharm 415(1–2):211–217
43. Eichler HG et al (1986) In vivo clearance of antibody-sensitized human drug carrier erythrocytes. Clin Pharmacol Ther 40(3):300–303
44. DeLoach JR, Barton C (1982) Circulating carrier erythrocytes: slow-release vehicle for an antileukemic drug, cytosine arabinoside. Am J Vet Res 43(12):2210–2212
45. Lejeune A et al (1994) Nanoerythrosome, a new derivative of erythrocyte ghost: preparation and antineoplastic potential as drug carrier for daunorubicin. Anticancer Res 14(3A):915–919
46. Harisa GEDI, Ibrahim MF, Alanazi FK (2011) Characterization of human erythrocytes as potential carrier for pravastatin: an in vitro study Int J Med Sci 8(3):222–230
47. Hamidi M et al (2007) Preparation and in vitro characterization of carrier erythrocytes for vaccine delivery. Int J Pharm 338(1–2):70–78
48. Fraternale A et al (2003) Erythrocytes as carriers of reduced glutathione (GSH) in the treatment of retroviral infections. J Antimicrob Chemother 52(4):551–554
49. Magnani M et al (1996) Synthesis and targeted delivery of an azidothymidine homodinucleotide conferring protection to macrophages against retroviral infection. Proc Natl Acad Sci USA 93(9):4403–4408
50. Magnani M et al (2003) Drug-loaded red blood cell-mediated clearance of HIV-1 macrophage reservoir by selective inhibition of STAT1 expression. J Leukoc Biol 74(5):764–771
51. Jordon MB et al (2003) Liposomal clodronate as a novel agent for treating autoimmune hemolytic anemia in a mouse model. Blood 101(2):594–601
52. Agnihotri J, Gajbhiye V, Jain NK (2010) Engineered cellular carrier nanoerythrosomes as potential targeting vectors for anti-malarial drug. Asian J Pharm 4(2):116–120
53. Jain S, Jain SK, Dixit VK (1995) Erythrocytes based delivery of isoniazid: preparation and in vitro characterization. 32:471–476(Indian Drugs)
54. Talwar N, Jain NK (1992) Erythrocytes as carriers of metronidazole: in-vitro characterization. Drug Dev Ind Pharm 18:1799–1812
55. Kresie L (2001) Artificial blood: an update on current red cell and platelet substitutes. Proc (Bayl Univ Med Cent) 14(2):158–161
56. Li L et al (2011) Silica nanorattle-doxorubicin-anchored mesenchymal stem cells for tumor-tropic therapy. ACS Nano 5(9):7462–7470
57. Kumar A et al (2011) Initial observations of cell-mediated drug delivery to the deep lung. Cell Transplant 20(5):609–618
58. Aboody KS et al (2013) Neural stem cell-mediated enzyme/prodrug therapy for glioma: preclinical studies. Sci Transl Med 5(184):184ra59
59. Kim SU (2014) Lysosomal storage diseases: stem cell-based cell—and gene-therapy. Cell Transplant
60. Andrews TE, Wang D, Harki DA (2013) Cell surface markers of cancer stem cells: diagnostic macromolecules and targets for drug delivery. Drug Delivery Transl Res 3(2):121–142
61. Greco SJ, Rameshwar P (2012) Mesenchymal stem cells in drug/gene delivery: implications for cell therapy. Ther Deliv 3(8):997–1004
62. Selbo PK et al (2012) Strongly amphiphilic photosensitizers are not substrates of the cancer stem cell marker ABCG2 and provides specific and efficient light-triggered drug delivery of an EGFR-targeted cytotoxic drug. J Control Release Official J Control Release Soc 159 (2):197–203

63. Wu H et al (2014) Prostate stem cell antigen antibody-conjugated multiwalled carbon nanotubes for targeted ultrasound imaging and drug delivery. Biomaterials 35(20):5369–5380
64. Qutachi O, Shakesheff KM, Buttery LD (2013) Delivery of definable number of drug or growth factor loaded poly(DL-lactic acid-co-glycolic acid) microparticles within human embryonic stem cell derived aggregates. J Control Release Official J Control Release Soc 168 (1):18–27
65. Flight MH (2012) Drug delivery: Encapsulation improves therapeutic stem cell action. Nat Rev Drug Discov 11(2):106
66. Zhou P et al (2010) Uptake of synthetic Low Density Lipoprotein by leukemic stem cells–a potential stem cell targeted drug delivery strategy. J Control Release Official J Control Release Soc 148(3):380–387
67. Wu DQ et al (2008) Fabrication of supramolecular hydrogels for drug delivery and stem cell encapsulation. Langmuir ACS J Surf Colloids 24(18):10306–10312
68. Haney MJ et al (2011) Cell-mediated transfer of catalase nanoparticles from macrophages to brain endothelial, glial and neuronal cells. Nanomedicine 6(7):1215–1230
69. Dou H et al (2006) Development of a macrophage-based nanoparticle platform for antiretroviral drug delivery. Blood 108(8):2827–2835
70. Dou H et al (2009) Macrophage delivery of nanoformulated antiretroviral drug to the brain in a murine model of neuroAIDS. J Immunol 183(1):661–669
71. Haney MJ (2013) Specific transfection of inflamed brain by macrophages: a new therapeutic strategy for neurodegenerative diseases. PLoS ONE 8(4):e61852
72. Choi J et.al (2012) Immunocytes as a biocarrier to delivery therapeutic and imaging contrast agents to tumors. J Nanomaterials. (Article ID 863704)
73. Lee Y-H (2011) Feasibility study of using macrophages as drug delivery carriers for drug-loaded phase-change droplets. In: IEEE International Ultrasonics Symposium (IUS), pp 1498–1501
74. Sabado RL, Bhardwaj N (2010) Directing dendritic cell immunotherapy towards successful cancer treatment. Immunotherapy 2(1):37–56
75. Orange DE et al (2013) Dendritic cells loaded with FK506 kill T cells in an antigen-specific manner and prevent autoimmunity in vivo. eLife, 2:e00105
76. Prather KJ et al (2003) Industrial scale production of plasmid DNA for vaccine and gene therapy: plasmid design, production and purification. Enzym Microb Technol 33:865–883

Applications of Single Cell Sequencing in Cancer

Kuo Ping Chiu

Abstract Single cell sequencing (SCS) was chosen as Method of the Year in 2013 by *Nature Methods*. It refers to the deep sequencing of DNA or RNA molecules of single cells for the study of genome, transcriptome, noncoding RNA, and protein sequences encompassed within the single cells of interest. SCS possesses a strong potential to exert a great impact on biological research due to its unprecedented opportunity and capability of resolving sequence composition and genetic variations on single cell basis, which can be further integrated to explain the biological phenomena at the population or organismal level. During the past few years, SCS has produced promising results in a number of fields, especially cancer research. Prior to SCS, tissue sequencing could only analyze a tumor mass or a cancer cell population as a whole. With methods for single cell isolation, further powered by molecular level resolution made possible by minute DNA amplification and nucleotide level resolution made possible by next-generation sequencing, SCS technologies are becoming robust approaches for the study of cancer genomics and transcriptomics, and the cancer–normal cell interactions in the microenvironment. SCS analyses of cancer evolution, for example, have shown the capability of being able to empirically infer the driver mutations and map the sequential mutation events during cancer development. Undoubtedly, these novel approaches will produce profound health benefits. SCS will continue to attract more attention, and further expansion of its applications in many biological fields is inevitable. This chapter focuses on SCS methodologies, its existing applications, especially its capability in reconstructing the evolutionary history of cancer progression and in profiling cancer transcriptome, and the potential applications expected to come.

Keywords Single cell sequencing (SCS) · Single cell transcriptome sequencing (SCT)

K.P. Chiu (✉)
Academia Sinica, Taipei, Taiwan
e-mail: chiukp@gate.sinica.edu.tw

F.-G. Tseng and T.S. Santra (eds.), *Essentials of Single-Cell Analysis*,
Series in BioEngineering, DOI 10.1007/978-3-662-49118-8_13

1 Introduction

A normal diploid human genome is composed of ~6 billion bp of nuclear DNA distributed in 23 pairs of linear chromosomes, forming DNA-protein complexes, or chromatins, during the interphase of cell cycle. Besides, there are thousands of copies of mitochondrial genomes (mitogenomes) per cell, each composed of 16,569 bp of deoxynucleotides forming a circular DNA structure. Together, the nuclear genome and the mitochondrial genome form the basis of the information reservoir. Through differential expression of ~26,000 protein-coding genes [1] and hundreds, or more, noncoding RNAs, they drive all the biological activities of human life. As the doctrine of the Central Dogma teaches [2], gene expression is mediated by transcription of genomic sequences to produce RNA molecules (mRNA, tRNA, rRNA, and other noncoding RNA) and translation of the protein-coding mRNA molecules.

All matter in the universe is subject to dynamic environmental impacts. There is no exception for DNA and RNA molecules. Environmental impacts, including toxic chemical compounds, radiations, magnetism, reactive oxygen species (ROS), and many others, may cause DNA/RNA damages. Aberrations in DNA/RNA sequences are then subject to selection by evolution which constantly occurs in the context of the environment. Some aberrations, either as small as single base alterations or as large as deletions or insertions of chromosomal fragments and chromosomal breakage and rearrangements, are likely to result in cell death. Some aberrations, on the other hand, may lead to tumorigenesis [3].

One of the most remarkable features of cancer is genome instability, which acts as a driving force for genetic mutation and plays a key role in wide spectrum reshuffling of the genomic material [4, 5], eventually causing a tumor mass to diversify and form a mixture of heterogeneous, aneuploid genomes. During cancer progression, genomic alterations are recorded as "mutational fingerprints," which, in theory, can be traced to reveal the cancer evolutionary history. Through gene expression, the genomic alterations are carried onto transcriptome and then proteomes, showing abnormal gene expression profile and altered proteomic state, respectively. Besides cancerous cells, tumors are also composed of infiltrating normal cells (such as fibroblasts) and immune cells (such as macrophages and lymphocytes) [6, 7]. Multiple lines of evidence indicate that the complexity of cancer cannot be fully appreciated by conventional approaches which study cancer cell population as a whole. With the advances of sequencing technologies, aberrations in nucleic acids can now be revealed and analyzed by next-generation sequencing (NGS) at a large scale [8, 9], and single cell sequencing (SCS) technologies are becoming the right choice. Then, may cancer genomes in a tumor be subdivided into subpopulations or subclones? Is SCS able to reveal the developmental history of a tumor? Moreover, since solid tumors also contain a number of noncancerous cells and the gene expression of these "normal" cells is known to be influenced by cancer cells, can SCS provide further insight into how these cells interact to foster cancer progression? From the technical point of view,

can SCS compete against other ensemble methods for early detection of cancer? How far can SCS go to straighten out these issues and help answer the questions?

To maintain cell integrity and help define the boundary of cellular activities, each single eukaryotic cell has a well-defined cell membrane, which can be directly observed under an electron microscope. Imaging-based analysis of gene expression at the single cell level by in situ hybridization followed by imaging had long preceded PCR and NGS approaches [10, 11]. Automation of Sanger sequencing together with the invention of PCR by Kary Mullis in 1980s stimulated the invention of NGS platforms during 2005–2007, which have created a sustainable state of sequencing-based biological research [12], and are now, by studying single cells [13], revolutionizing cancer research [14].

Prior to the invention of NGS technologies, tumor evolutionary histories could be studied by dissecting tumors into subregions based on phenotypical characteristics or topographical locations, followed by sequencing library preparation using tissues from subregions, sequencing, and sequence data analysis [15]. With single cell sequencing technologies, the process can be significantly simplified. Recent studies have shown that the mutational fingerprints in single cells of the same tumor, when revealed by SCS, can be interconnected to form lineages of clonal expansion and the history of cancer evolution [14, 16]. Furthermore, the temporal order of the mutational fingerprints may also indicate the driver mutations and their role in cancer progression. Recent researches have also shown that the expression of cancer-associated genes (e.g., oncogenes, tumor suppressor genes, oncogenic miRNA, hormone receptor genes, etc.) can now be better understood with single cell resolution [13, 17]. How they coordinate and interplay with one another will provide us in-depth understanding of intercellular molecular activities in a cell population.

2 Single Cell Sequencing and Its Challenges

One cannot fully appreciate the beauty of a technology without knowing the challenges it has overcome. Indeed, it is much more difficult to conduct single cell sequencing than tissue sequencing [18], mainly because of the limitation in the quantity of genetic materials a single cell can provide. Before single molecule sequencing becomes sophisticated and available for minute DNA sequencing, SCS technologies have to rely on NGS technologies for sequencing the genetic materials in single cells. Conventional NGS technologies require bulk genetic materials to sequence. However, each single cell, even for cancer cells, contains only a minute quantity (normally at picogram level), with at least three orders of magnitude less than that required for conventional NGS protocols. This gap can only be filled by DNA and/or RNA amplification using PCR-based and/or RNA polymerase-based strategies, especially the former. PCR amplification is crucial for SCS. PCR, however, may result in bias due to imbalanced amplification efficiency between amplicons and thus needs to be carefully designed. In fact, this was one of the major

barriers that hindered the progress of SCS during the past. Furthermore, because most molecules in a single cell are of low abundance and low copy number, SCS is extremely vulnerable to fluctuations which may result from genetic material loss, poor personal skill, or contamination. Thus, the experimental procedure of a SCS protocol, especially from single cell or nucleus isolation up to DNA/RNA amplification, has to be well formulated and every step needs to be carefully characterized and optimized when dealing with trace amount of DNA or RNA. Moreover, sequencing error is also an issue that needs to be taken care of. While heterozygous alleles have equal chance of being sequenced, sequencing errors are shown at relatively much lower frequency and can be corrected by sufficient fold-of-coverage, or, as demonstrated by Kim and Simon, by incorporating the probability of sequencing error into Bayesian probability test (see below) [19].

2.1 Cells Suitable for Single Cell Sequencing

SCS is suitable for the study of a number of normal and diseased cell types of both prokaryotes and eukaryotes [20, 21]. These include early-stage embryonic cells, stem cells, immune cells, rare cells, microbes that cannot be easily cultured, differentiated cells, bacteria or virus infected cells, and cancer cells at various stages. The application of SCS in the study of cancer and normal cells in the tumor-surrounding microenvironment is of particular interest because of their complexity and tight association with human disease. Cultured cancer cells are probably the most accessible cancer cells for researchers, while circulating tumor cells (CTCs) and intratumor cancer cells require reliable experimental procedure to isolate. SCS analyses will benefit the diagnosis and help in guiding chemotherapy and monitoring/following up the progress of treatment.

2.2 Methods for Cancer Cell Isolation

Depending on the conditions of the single cells, a number of methods are available for single cell isolation. The most commonly used methods are micromanipulation, flow cytometry, microdissection, single cell labeling, and cell trapping [21]. Recently, an automated system (C1 System by Fluidigm^{TM}) for single cell genome and transcriptome analyses has been made commercially available. It is relatively easy to isolate single cells from a cell culture or from the blood, because most of these cells are either already separated or can be separated easily. In this situation, single cells can be washed, diluted, and isolated by manipulation such as mouth pipetting under a microscope. Compared to flow-sorting, micromanipulation is more tedious and may not be suitable for collecting a large number of single cells. However, micromanipulation is probably the mildest and gentlest approach that can minimize the impact of harsh conditions such as high pressure produced by flow

cytometer and thus can preserve the cell integrity. As such, this method is useful for transcriptome analysis. On the other hand, flow cytometry is probably the most efficient approach [21]. As mentioned above, since high flow pressure can easily damage the cell membrane and cause leakage of the cytoplasm and cross-contamination, precaution has to be taken before using flow cytometer for whole cell isolation. A short period of cell wash and/or cell culture may be needed. Single cell trapping which uses a matrix coated with specific molecule(s) is also for isolating specific cells. It is important to pick single cells that are representative, healthy, with well-maintained cellular integrity, and free of contamination. The automated C1 System facilitates single cell genome and transcriptome analyses by increasing throughput, reducing technical variations, and easing control and comparison [22, 23]. However, its potential problem with primer dimers may result in false positive signals [22]. Moreover, its sensitivity may not be high enough to detect low abundance transcripts. How to improve these drawbacks seems to be critical issues for future improvement for the automated single cell instruments.

2.3 Methods for Single Cell Whole Genome Amplification

Whole genome amplification (WGA) is the key for single cell sequencing, no matter whether it is for exome sequencing or whole genome sequencing of the single cells. To preserve the original state of the genome by minimizing uneven amplification is essential for whole genome amplification. This is frequently done by reducing the number of PCR cycles, preventing PCR by-products, or using barcodes. Barcodes can not only minimize bias resulted from the differences in personal skills and experimental procedure, but also allow multiple small samples to be combined into a larger sample. A number of methods for DNA amplification, together with their limitations, have been reviewed previously [24]. Here, we quickly skim through the methods employed by Navin and Hou.

In 2011, Navin and colleagues adopted degenerated oligos to prime single cell whole genome amplification (DOP-WGA) [14]. Although efficient enough for the authors to generate reliable datasets for copy number variation (CNV) analysis, this approach provided only a low coverage ($\sim 6\times$), presumably due to the limitation in the size range of DOG-WGA products. In 2012, Hou and colleagues published the Multiple Displacement Amplification (MDA) method for single cell whole genome amplification. In the method, they used the Φ29 (Phi29) enzyme to amplify DNA in linear fashion [16]. The products were subsequently subjected to a fluorometry-based quantitation procedure which selected quality sequences for further analysis (see below). This seems to be an efficient approach for single cell genomic amplification for NGS. However, as drawbacks of the approach, allelic dropout and imbalanced amplification have been reported [24]. Imbalanced amplification is a common phenomenon for multiplex PCR. Previous studies have indicated that %GC is responsible for these drawbacks. GC pair is stronger than AT pair because, while AT base pairing is mediated by two hydrogen bonds, GC pairing is mediated by three

hydrogen bonds. Besides, high GC content favors Z-form conformation [25]. These properties influence the efficiency of DNA amplification, causing imbalanced PCR amplifications (especially when a significant number of primer pairs are deployed across the entire genome [26]), with allelic dropouts being the most severe cases. Kim and Simon proposed a computational approach to correct potential sequence errors which may be introduced by multiple displacement amplification to cause false discovery or allelic dropout, or by sequencing—see Fig. 3.

2.4 NGS DNA Sequencing

Besides genome amplification, next-generation sequencing (NGS), which is currently the only method able to provide sufficient coverage (sequencing depth) for

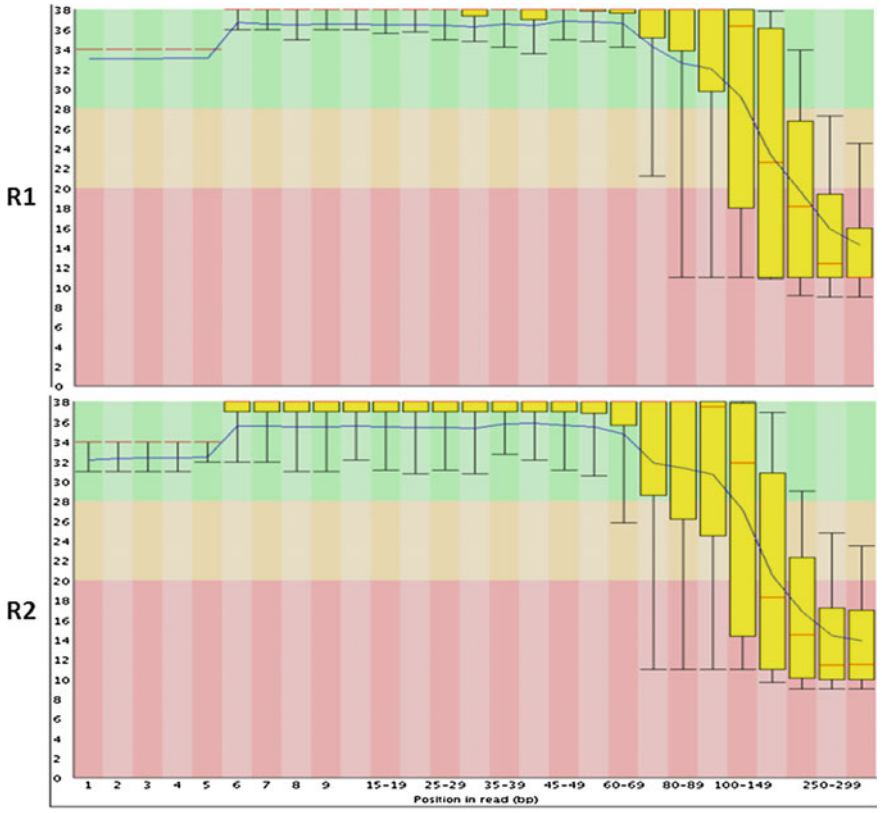

Fig. 1 Comparison between R1 and R2 QV profiles. The *M. cyclopis* mitochondrial DNA library was sequenced by MiSeq with 2 × 300 bp paired-end sequencing. The R1 and R2 QV profiles were then displayed in parallel to indicate the faster decrease in R2 quality

reliable analysis, is also essential for single cell sequencing. After years of competition since 2005, the Illumina platform has prevailed over the others (e.g., 454 and SOLiD systems) [9]. In terms of single cell sequencing, long reads would be better for at least most cases. However, R2 quality drops faster than R1, making 250 bp an evident barrier for the current Illumina sequencing technology (Fig. 1). The faster quality drop for R2 may result from cluster regeneration. Right before R2 sequencing, R1 clusters (i.e., clusters used as the templates for R1 sequencing) are replaced by their complementary clusters (i.e., R2 clusters made from the complementary strands of the R1 clusters). During the process, some templates in each cluster may get damaged or degraded, making the cluster less sufficient and thus more vulnerable to sequencing reactions. Limited read length is a natural phenomenon. By nature, reading of some templates in a cluster may go wrong in any step of the sequencing reaction. The mistakes accumulate over time, causing the quality value to drop gradually.

3 Existing Applications

3.1 Genome Sequencing of Individual Cancer Cells

Depending on the original cell type and the developmental stage, cancer cells may exist as various forms. During cancer progression, cancer cells further diversify in genomic makeup and function. The heterogeneity of cancer genome presents a challenge for cancer research. However, at the same time it also provides an opportunity for the study of intratumor substructure, cancer progression, and cancer evolution. This is made possible by single cell sequencing, a breakthrough in next-generation sequencing, of the genomes in the same tumor mass.

The report by Navin and colleagues in 2011 using single nucleus sequencing (SNS) to study the evolutionary history of human breast cancer marked a breakthrough in cancer research [14]. The experimental procedure can be outlined to include three major steps: isolation of single cancer nuclei by flow-sorting, whole genome amplification by random priming with degenerated oligonucleotides, and next-generation sequencing. The sequence reads were then analyzed to resolve genomic differences in copy number among individual cancer cells (Fig. 2).

The experimental approach was first validated by using single nuclei isolated from SK-BR-3 cell line, together with a million-cell population control from the same cell line. After genomic amplification using degenerated oligos in random priming, they obtained only a low overage ($\sim$6x) of the single cell genomes. However, such level of coverage is sufficient for CNV analysis. In terms of bioinformatics, the authors designed unique analytical approaches. For example, instead of using fixed intervals to calculate integer copy number, they used variable length bins but with uniform expected unique counts, which would correct for biases that have been reported in WGA. Pileups (over-replicated loci) were found to

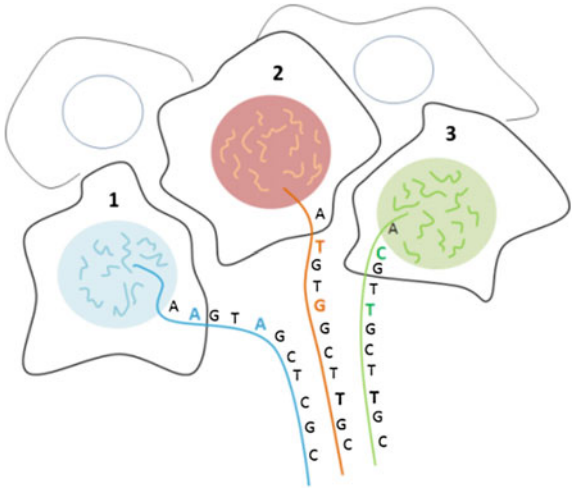

Fig. 2 Single cell genome sequencing reveals the differences in genomic sequences between single cells. Individual cells, or nuclei, are first collected in separate tubes. Genomic sequences (chromosomes) are amplified and sequenced. Sequence reads are then mapped against human genome assembly to identify their locations and sequence variations (e.g., copy number variations, insertions, deletions, single base alterations, etc.). Cross-comparison on sequence variation of single cell libraries, if isolated from the same cancer, allows us to reconstitute the evolutionary history of that cancer

be randomly distributed and sparse so that would not affect the results. In both single cells and million-cell population control, they found major amplifications in genes encoding MET, TPD52, ERBB2, and BCAS1 proteins. Deletion in DCC (deletion in colorectal cancer) gene was also detected in both single and 1-million-cell population of SK-BR-3 cells. These results generated from the SK-BR-3 cell line allowed them to move forward to study single nuclei isolated from different sections of breast tumors.

They divided a high-grade (grade III) triple negative (ER^-, PR^-, and $Her2^-$) carcinoma (labeled as T10) into six sections and analyzed 100 single cell nuclei isolated from these sections. From the study, they identified distinct clonal subpopulations in the genetically heterogeneous ductal carcinoma. The integer copy number profiles were built and analyzed to contain 63 % of normal cells and 37 % tumor cells and infiltrated with leukocytes. By calculating pair-wide distances between the 100 profiles followed by building a phylogenetic tree using neighbor joining, four subpopulations were identified, one with flat diploid profile and three with complex (advanced) genomic structures, suggesting three clonal expansions. Moreover, their method was able to detect diverse chromosome gains and losses and discern 'pseudodiploid' nuclei in diploid nuclei. Further clonal analysis allowed the authors to trace the evolutionary history of the cancer from the primary stage to the metastatic stage. The data further suggested that, differing from gradual models

of tumor progression, tumors grow by "punctuated" clonal expansion, without discernible intermediate branching.

The application of single nucleus sequencing in reconstitution of cancer evolutionary history, which suggested cancer progression mediated by punctuated clonal expansion, was reviewed [21, 27]. The drawbacks of such copy number-based approach include low coverage and being unable to reach down to the nucleotide resolution.

Following the report by Navin et al., Hou and colleagues reported an MDA-based exome sequencing of single cancer cells [16]. Deviating from copy number-based SCS analysis, this report presented a pilot study at the single cell nucleotide level. The single cell nucleotide sequencing is made possible by using multiple displacement amplification of the whole genome. MDA products are mostly of high molecular weight (>10 Kb), being able to boost genome coverage.

The MDA method was first tested with two single cells under multicell control and hg18 was used as the human genome reference. The coverage was found to be $\geq$15× (mean fold coverage = 18×), and sequences of both single cells covered more than 90 % of the reference genome, while more than 95 % of the bases in hg18 were recovered with $\geq$15× sequencing depth. WGA failure was found to be associated with GC content, with failed regions containing higher GC% than the average 41 % GC content in human genome. The ratio of allele dropout (ADO), which indicated whether non-amplification occurred in one of the alleles present in a heterozygous sample and would lead to false negative, was maintained at $\sim$11 %. ADO showed no bias relative to genomic location, and errors of MDA also showed no preferences on genes or functions.

After testing, the authors applied MDA procedure to study the genes involved in essential thrombocythemia (ET) evolution. For certain reasons, they conducted exome sequencing instead of whole genome sequencing. A total of 90 single cells from an ET patient were sequenced to a mean depth of 30×. After filtering out the single cells with <70 % coverage, 58 single cells were chosen for further analysis. These single cells have an average of $\sim$70 % of target bases at $\geq$5 depth. They considered this coverage as sufficient for population variant calling when multiple single cells have the same variant. Exome sequencing generated SMAFS (somatic mutant allele frequency spectrum) for evolutionary study. Results indicate that ET patient carries a distinct set of mutations and a monoclonal origin of ET cancer cells.

In a parallel study, Xu et al. used single cell exome sequencing to investigate clear cell renal cell carcinoma (ccRCC) by which they revealed kidney tumor-specific single nucleotide mutations [28]. Unlike reports by Navin and colleagues, no significant clonal subpopulations were identified in their ccRCC cases, presumably due to the difference in cancer type and origin. This single cell exome sequencing also revealed single nucleotide mutation characteristic of the kidney tumor.

Besides the above-mentioned reports, a computational approach for inferring the evolutionary mutation history of a cancer using single cell sequencing data has also been reported by Kim and Simon (Fig. 3) [19]. Although the quality of a library is

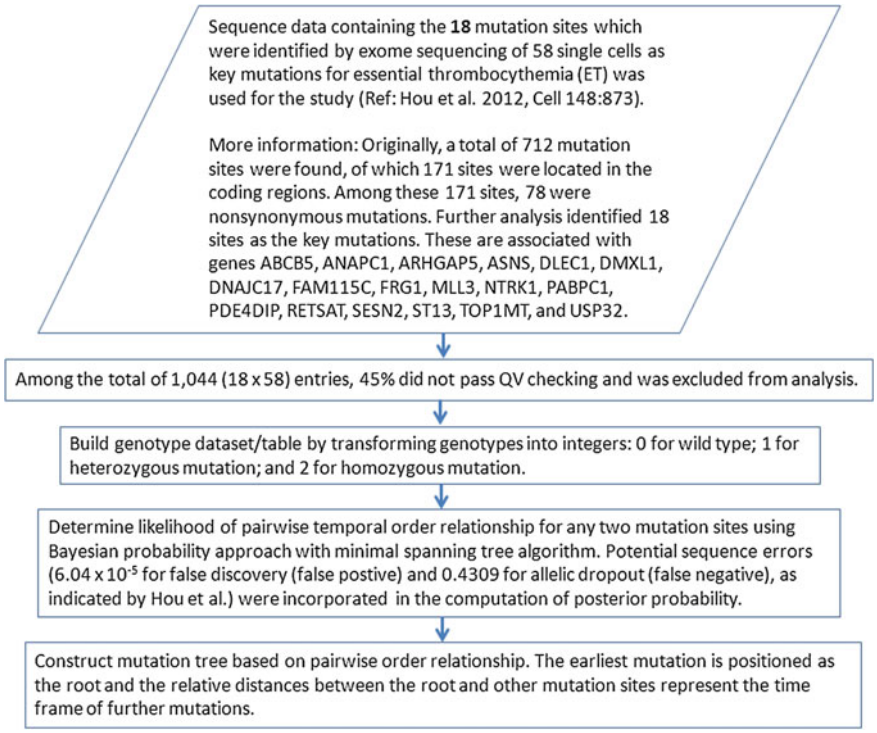

Fig. 3 Workflow for the construction of evolutionary mutation tree presented by Kim and Simon

influenced by a number of factors such as the make or design of a sequencer, personal skill, and the quality or the preparation of the material, the forefront quality control would remove the questionable reads, keeping the sequencing errors in the qualified reads at low rate, while on the other hand, heterozygous alleles remain having equal chance to be detected in the sequence reads, making these two types of sequence variations readily distinguishable from each other. The sequencing errors can be more easily detected by sufficient coverage (normally set at 30-fold or above) and then removed by programs, or by incorporating the probability of sequencing error into computation, as demonstrated by the authors.

3.2 Transcriptome Sequencing

Sometimes transcriptional information of individual cells, instead of a cell population, is desired. Obtaining such information relies on single cell transcriptome (SCT) sequencing and analysis (http://genomebiology.com/2010/11/S1/P8), which remains a great challenge for current technologies [17].

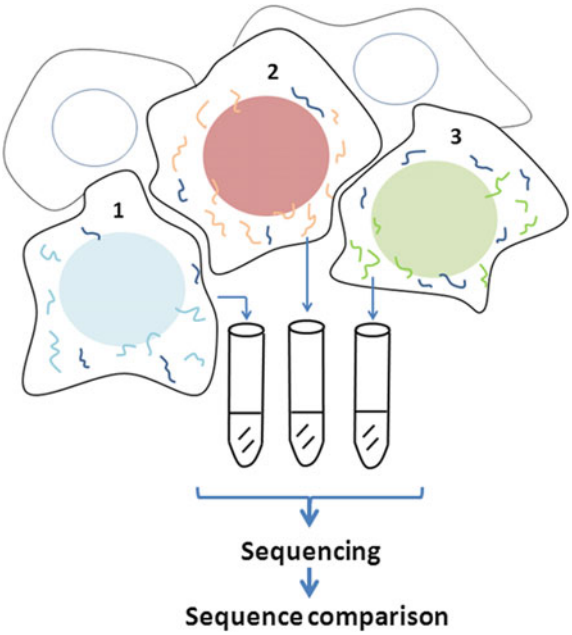

Fig. 4 Single cell transcriptome sequencing. The profiles of gene expression in single cells can now be studied by single cell transcriptome sequencing. Basically, the procedure is similar to that used for transcriptome analysis of a cell population, except that each cell has to be collected separately and then goes through cell lysis, cDNA synthesis, cDNA amplification, sequencing, sequence data analysis, and cross-library comparison. To prevent material loss, all reactions are conducted at very low volume (e.g., a few microliters or less) and wash is also minimized until the cDNA molecules have been amplified

Indeed, several lines of evidence show that stochastic gene expression is likely to be a natural phenomenon and thus the gene expression of a tumor or a tissue should be considered as a combinatorial phenomenon summarized from its constituent single cell transcriptomes. SCT sequencing is becoming the most advanced approach for studying gene expression and regulation (Fig. 4), and this line of application heavily relies on cDNA synthesis. In fact, there were methods for single cell cDNA synthesis published before NGS became a popular technology for sequencing. These include the first single cell transcriptome analysis reported by Eberwine and colleagues in 1992 [12]. Later in 2006, Kurimoto et al. published another method for microarray-mediated SCT analysis [29]. The first NGS-based single cell transcriptome sequencing was published in 2009 [13]. In 2012, Ramskold and colleagues published an elegant method for cDNA synthesis and amplification [30]. This approach has been commercialized by Clontech to make a kit called “the SMARTer Ultra Low RNA Kit.” Instead of using oligo-dT as employed by Tang et al., Ramskold and colleagues used CDS primer, which carries a VN tail (V stands for ‘non-T’ and N stands for ‘any base’) in the 3’ end of the

oligo-dT sequence, to prime the first strand cDNA synthesis. The VN tail significantly enhances the specificity of priming because the VN tail allows the prime to "hook" to the last two bases right in front of the polyA tail in the mRNA molecule. Without the VN tail, the primer would 'slip' within the polyA region, resulting in a significant amount of imprecise priming. The above-mentioned automated single cell analysis system is an efficient approach, but solely for the study of a limited number of genes or genomic regions. Similarly, primer dimer is an issue of concern [22].

Single cells are delicate entities, and thus concerns about the accuracy of SCT analysis are inevitable. Various potential factors that may cause transcriptional variations have been, and will continue to be, examined. Indeed, it can be difficult to identify the factors causing variations in single cell transcriptomes. Some variations between individual cells may be real, but some may result from differences in personal technical skills and thus need to be minimized. To minimize the influence of variability in personal technical skill, it is recommended to increase the number of SCTs and use internal controls such as housekeeping genes and previously studied expression patterns of certain genes. For example, in our study of single cell transcriptomes of MCF-7 breast cancer [31], we used the expression the *LDHB* (lactate dehydrogenase) gene, which is known to be completely shutdown in MCF-7 cells, as an internal control. As expected, its expression was not detected in all libraries (data not shown).

4 SCT Protocols Can Be Modified for Various Reasons

Protocols may need to be modified for certain reasons [9]. For example, a protocol might not have been optimized when it is published. This frequently occurs when it is published in a hurry by companies trying to catch up market demand. Besides, taking advantage of its low input requirement, one can adopt single cell sequencing protocol to generate sufficient amount of input material for a regular sequencer. As shown in the following section, we can use total RNA or mRNA, instead of single cells, as the input material for a single cell protocol. By so doing, we bypass the conventional protocol and use the single cell protocol to rescue the situation when material is not sufficient for a regular sequencer.

5 Using Different Types of Materials as the Input

Since polyA$^+$-RNA molecules in single cells are the only molecules required for double-stranded cDNA synthesis, it is reasonable to use either total RNA or mRNA to replace single cells.

The majority of RNA molecules are ribosomal RNA (rRNA) and transfer RNA (tRNA), while mRNA species constitute only ~2 % of the total RNA. The presence of rRNA and tRNA may reduce the efficiency of cDNA synthesis because of a number of reactions, including oligo-dT priming, reverse transcription, and PCR amplification. As such, it is strongly recommended to use mRNA as the starting material, if the amount of total RNA is sufficient for mRNA isolation. In fact, it has been empirically demonstrated that mRNA works better than total RNA.

Then, how do we correlate the results produced from mRNA or total RNA with cell number? Using MCF-7 as an example, each MCF-7 cell expresses about 10 pg of total RNA. Accordingly, 50 ng of total RNA is equivalent to about 5000 cells, and 50 ng of mRNA is equivalent to 250,000 (=0.25 million) single cells. One can calculate and use a certain amount of total RNA or mRNA based on the number of cells he/she wants to use in the study. Since the total amount of RNA expressed from a single cell varies across different cell types, it is strongly recommended to empirically fine-tune this value based on the cell type being used.

Completion of the second PCR amplification marks the junction where the SCT protocol and other protocols meet. Now the retrieval of mRNA molecular information from a single cell is completed and preparation of a sequencing library can be initiated. Here, one can determine what sequencing libraries to make: shotgun fragment sequencing, paired-end (PE) sequencing, or pair-end ditag (PED) sequencing.

6 Future Potential Applications of Single Cell Sequencing

We can expect many more SCS applications to be developed for cancer research in the near future. Using transcription factor binding site (TFBS) analysis as an example, there is a strong potential for us to conduct TFBS analysis at the single cell level. Currently, most cancer researches have been focused on the study of mutations in cancer-associated genes such as *KRAS*, *TP53*, *cMYC*, etc. Less attention was paid to in vivo study of how alterations in DNA motifs interact with transcription factors (TFs) and/or other intracellular proteins, and how a mutation in TF affects its DNA binding. Will it form complexes with other unexpected proteins? Or, will it bind to different locations in the genome? It would be interesting to further understand how an altered motif influence TF binding at the single cell level and how the effects at the single cell level exert a combinatorial effect at the population level. In theory, one would expect an alteration in DNA motif to result in a corresponding switch in the interacting protein(s), which may in turn play a role in tumorigenesis, angiogenesis, and/or metastasis. Empirical SCS data will help to either prove or disapprove the speculation.

7 Further Improvements

To enhance SCS data analysis and protocol design, it can be helpful to produce a virtual population profile through the integration of SCS profiles by statistical approach. By comparing the virtual population profile with the empirically produced population profile, we can evaluate and improve the SCS procedure. Conceivably, protocols for single cell experiments have to be reproducible, straightforward, and adaptable. However, many protocols do not yet meet these criteria and need to be optimized.

The progress of biological research heavily relies on the advance of biotechnologies. There is no doubt that more innovative SCS approaches will be created in the near future.

References

1. Venter JC et al (2001) The sequence of the human genome. Science 291:1304–1351. doi:10.1126/science.1058040
2. Crick F (1970) Central dogma of molecular biology. Nature 227:561–563
3. Hanahan D, Weinberg RA (2011) Hallmarks of cancer: the next generation. Cell 144:646–674. doi:10.1016/j.cell.2011.02.013
4. Negrini S, Gorgoulis VG, Halazonetis TD (2010) Genomic instability–an evolving hallmark of cancer. Nat Rev Mol Cell Biol 11:220–228. doi:10.1038/nrm2858
5. Aguilera A, Gomez-Gonzalez B (2008) Genome instability: a mechanistic view of its causes and consequences. Nat Rev Genet 9:204–217. doi:10.1038/nrg2268
6. Gerdes MJ et al (2014) Emerging understanding of multiscale tumor heterogeneity. Front Oncol 4:366. doi:10.3389/fonc.2014.00366
7. Wels J, Kaplan RN, Rafii S, Lyden D (2008) Migratory neighbors and distant invaders: tumor-associated niche cells. Genes Dev 22:559–574. doi:10.1101/gad.1636908
8. Metzker ML (2010) Sequencing technologies—the next generation. Nat Rev Genet 11:31–46. doi:10.1038/nrg2626
9. Chiu KP (2015) Next-generation sequencing and sequence data analysis, 1st edn. Bentham Science Publishers
10. Gall JG, Pardue ML (1969) Formation and detection of RNA-DNA hybrid molecules in cytological preparations. Proc Natl Acad Sci U S A 63:378–383
11. Capodieci P et al (2005) Gene expression profiling in single cells within tissue. Nat Methods 2:663–665. doi:10.1038/nmeth786
12. Eberwine J et al (1992) Analysis of gene expression in single live neurons. Proc Natl Acad Sci U S A 89:3010–3014
13. Tang F et al (2009) mRNA-Seq whole-transcriptome analysis of a single cell. Nat Methods 6:377–382. doi:10.1038/nmeth.1315
14. Navin N et al (2011) Tumour evolution inferred by single-cell sequencing. Nature 472:90–94. doi:10.1038/nature09807
15. Tsao JL et al (2000) Genetic reconstruction of individual colorectal tumor histories. Proc Natl Acad Sci U S A 97:1236–1241
16. Hou Y et al (2012) Single-cell exome sequencing and monoclonal evolution of a JAK2-negative myeloproliferative neoplasm. Cell 148:873–885. doi:10.1016/j.cell.2012.02.028

17. Tang F, Lao K, Surani MA (2011) Development and applications of single-cell transcriptome analysis. Nat Methods 8:S6–11. doi:10.1038/nmeth.1557
18. Eberwine J, Sul JY, Bartfai T, Kim J (2014) The promise of single-cell sequencing. Nat Methods 11:25–27
19. Kim KI, Simon R (2014) Using single cell sequencing data to model the evolutionary history of a tumor. BMC Bioinformatics 15:27. doi:10.1186/1471-2105-15-27
20. Shapiro E, Biezuner T, Linnarsson S (2013) Single-cell sequencing-based technologies will revolutionize whole-organism science. Nat Rev Genet 14:618–630. doi:10.1038/nrg3542
21. Navin N, Hicks J (2011) Future medical applications of single-cell sequencing in cancer. Genome Med 3:31. doi:10.1186/gm247
22. Guo G et al (2013) Mapping cellular hierarchy by single-cell analysis of the cell surface repertoire. Cell Stem Cell 13:492–505. doi:10.1016/j.stem.2013.07.017
23. Gawad C, Koh W, Quake SR (2014) Dissecting the clonal origins of childhood acute lymphoblastic leukemia by single-cell genomics. Proc Natl Acad Sci U S A 111:17947–17952. doi:10.1073/pnas.1420822111
24. Macaulay IC, Voet T (2014) Single cell genomics: advances and future perspectives. PLoS Genet 10:e1004126. doi:10.1371/journal.pgen.1004126
25. Foloppe N, MacKerell AD Jr (1999) Intrinsic conformational properties of deoxyribonucleosides: implicated role for cytosine in the equilibrium among the A, B, and Z forms of DNA. Biophys J 76:3206–3218. doi:10.1016/S0006-3495(99)77472-2
26. Mamedov TG et al (2008) A fundamental study of the PCR amplification of GC-rich DNA templates. Comput Biol Chem 32:452–457. doi:10.1016/j.compbiolchem.2008.07.021
27. Navin NE (2014) Cancer genomics: one cell at a time. Genome Biol 15:452. doi:10.1186/s13059-014-0452-9
28. Xu X et al (2012) Single-cell exome sequencing reveals single-nucleotide mutation characteristics of a kidney tumor. Cell 148:886–895. doi:10.1016/j.cell.2012.02.025
29. Kurimoto K et al (2006) An improved single-cell cDNA amplification method for efficient high-density oligonucleotide microarray analysis. Nucleic Acids Res 34:e42. doi:10.1093/nar/gkl050
30. Ramskold D et al (2012) Full-length mRNA-Seq from single-cell levels of RNA and individual circulating tumor cells. Nat Biotechnol 30:777–782. doi:10.1038/nbt.2282
31. Chiang Y-S et al (2010) Single cell transcriptome analysis upon MCF-7 breast cancer. Genome Biol 11:P8

Single-Cell Characterization of Microalgal Lipid Contents with Confocal Raman Microscopy

Rasha Abdrabu, Sudhir Kumar Sharma, Basel Khraiwesh, Kenan Jijakli, David R. Nelson, Amnah Alzahmi, Joseph Koussa, Mehar Sultana, Sachin Khapli, Ramesh Jagannathan and Kourosh Salehi-Ashtiani

Abstract The environmental impacts from consumption of fossil fuels have raised interest in finding renewable energy resources throughout the globe. Much focus has been placed on optimizing microalgae to efficiently produce compounds that can substitute for fossil fuels. However, the path to achieving economical feasibility of this substitution is likely to require strain optimization through mutagenesis screens as well as other available approaches and tools. Rapid characterization of the type of fatty acid expressed at a single-cell level can help identify screened cells with the desired lipid characteristics such as chain length and saturation status. Confocal Raman microscopy is a powerful tool for physicochemical characterization of biological samples. It enables single-cell, in vivo monitoring of various cellular components in a rapid, quantitative, label-free, and nondestructive manner. In this chapter, we describe recent advances in this method, which have resulted in remarkable enhancements in the sensitivity, specificity, and spatiotemporal

R. Abdrabu, S.K. Sharma, B. Khraiwesh and K. Jijakli—These authors contributed equally to this work.

R. Abdrabu · B. Khraiwesh · K. Jijakli · D.R. Nelson · A. Alzahmi · J. Koussa · K. Salehi-Ashtiani (✉)
Laboratory of Algal, Systems, and Synthetic Biology, Division of Science and Math, and Center for Genomics and Systems Biology (CGSB), New York University Abu Dhabi, P.O. Box 129188, Abu Dhabi, UAE
e-mail: ksa3@nyu.edu

S.K. Sharma · S. Khapli (✉) · R. Jagannathan (✉)
Division of Engineering, New York University Abu Dhabi, P.O. Box 129188, Abu Dhabi, UAE
e-mail: sdk275@nyu.edu

R. Jagannathan
e-mail: rj31@nyu.edu

M. Sultana
Center for Genomics and Systems Biology (CGSB), New York University Abu Dhabi, P.O. Box 129188, Abu Dhabi, UAE

F.-G. Tseng and T.S. Santra (eds.), *Essentials of Single-Cell Analysis*, Series in BioEngineering, DOI 10.1007/978-3-662-49118-8_14

resolution of the technique. We utilize this technique for analyzing lipid content of algal isolates obtained through a mutagenesis screen of the green alga, *Chlamydomonas reinhardtii*, for increased lipid production at the single-cell level. Our results demonstrate cell-to-cell variation in structural features of expressed lipids among the screened *C. reinhardtii* mutants, while clonal isolates show little to no variability in expressed lipids. The lack of stochasticity in expression of lipids in clonal populations of *C. reinhardtii* is a desired feature when accompanied by expression of fatty acids suitable for use as biofuel feedstock.

Keywords Algae · Single-cell analysis · Fluorescence activated cell sorting (FACS) · Raman microscopy · Lipidomics · Biofuels

1 Introduction

The unicellular alga, *Chlamydomonas reinhardtii*, is an invaluable model organism for the study of a wide range of biological questions in areas such as flagella function, photobiology and photosynthesis, as well as being an attractive bioproduction system [1–3]. In order to develop biofuels from algae, research is being conducted to find suitable strains that produce high levels of lipids, can tolerate heat and high concentrations of carbon dioxide, and are easy to harvest [4–6]. Some of these strains may be grown using bubble columns and photobioreactors in conjunction with CO_2 from flue gas emissions [4]. At the same time, research is being conducted to develop methods for genetic modification to introduce desirable traits into algae, and to develop synthetic biology approaches to reengineer algal cells [7–10]. The crux of this research is to advance the molecular biology techniques utilized for alga, and to ease the modification of the molecular systems of the species.

Technological advancements in the production of algal biofuels therefore require the development of methods to precisely and rapidly identify and quantify the lipids generated within microalgae and correlate them to the various genetic manipulation strategies and/or growth conditions [11–13]. Availability of such techniques would enable rational selection and metabolic engineering of microalgae that is necessary for the optimal production of biofuels.

Single-cell analysis (SCA) has the potential to change our understanding of whole organisms since cell lineages can be traced and heterogeneity inside an organism can be described with unprecedented resolution [14–16]. SCA has been increasingly recognized as the key technology for the elucidation of cellular functions which are not accessible from bulk measurements on the population level [14]. Thus far, SCA has been achieved by miniaturization of established engineering concepts to match the dimensions of a single cell. Today, SCA methods can be divided into invasive SCA (chemical SCA), used to quantify the intracellular compounds of a single cell, and noninvasive SCA (biological SCA), used to

quantify the responses of an intact cell [14–16]. Gene expression, in terms of both identity and quantity, can be assessed using transcriptomics. Single-cell transcriptomics using next generation sequencing (RNAseq) is emerging as a powerful approach, providing the insights of transcriptomics at a single-cell resolution [17–19]. This single-cell resolution allows the assessment of cell-to-cell variability in terms of actual expressed genes, bridging genotype to expressed phenotype [18, 20]. However, care should be given in extending mRNA expression to phenotype, especially in the case of products that are the result of complex metabolic interactions. Many studies show that currently an incomplete overlap between transcriptome and proteome exists [21–24]. This lack of overlap highlights the importance of complementing single-cell transcriptomics with single-cell phenotypic analysis methods. Combining single-cell sorting and phenotypic analysis techniques, such as live cell imaging and single-cell Raman spectroscopy, can offer a powerful single-cell phenotypic extension to single-cell genomics and transcriptomics. This is potentially a powerful combination for tracing cell lineage during development or cell differentiation, especially in conjunction with a florescent protein reporter [25, 26].

Raman spectroscopy yields information about the vibrational modes of molecules and can be applied for the analysis of biological systems on a molecular level [27]. In the toolbox of the bioanalytical chemist, it is a versatile tool to characterize biological samples with high analyte specificity and spatial resolution. It is a noninvasive technique and requires little sample preparation. Recent advances in the instrumentation and data analysis techniques enabled the application of Raman spectroscopy for performing quantitative analysis on a single-cell basis, which is useful for studying cellular dynamics [28]. Importantly, the analysis can be carried out in a label-free, nondestructive, and real-time manner. Because of these advantages, Raman spectroscopy has been extensively used in algal research [29, 30] for the analysis of various biomarkers such as lipids [31, 32] and pigments [33, 34].

Medical research has also benefitted from the use of Raman spectroscopy to analyze tissue- and cell-specific disease markers. For example, bladder cancer can be detected with high accuracy using Raman spectroscopy on peripheral blood cells from diagnostic bands in the spectral regions of 481–486, 682–687, 1018–1034, 1313–1323, 1450–1459, and 1582–1587 cm^{-1} which correspond to proteins, nucleic acids, and lipids that are abnormal in bladder cancer [35]. Microcalcification of mammary glands, an early sign of breast cancer, has been detected and resolved with Raman spectroscopic sensing of carbonate intercalation [36]. Using Raman spectroscopy to analyze lipids in a clinical setting has enabled the successful identification of hepatocellular carcinoma [37], and oral squamous cell carcinoma [38]. Raman spectroscopy has also been used to map human stem cell micropatterns with a high resolution [39].

1.1 Fundamentals of Raman Spectroscopy

In Raman spectroscopy, the sample is irradiated with high-intensity monochromatic radiation, usually a laser, and the scattered radiation is analyzed in terms of the energies (frequencies) of the scattered photons. Most of the photons are scattered elastically (i.e., without energy loss); while a small fraction of photons (about 1 in 10^6) are scattered inelastically (i.e., with a change in energy). The elastically scattered photons have the same frequency as that of the incident radiation ω_L, whereas the inelastically scattered photons contribute to the Raman component of the scattered radiation. The Raman component of the scattered radiation can be further divided into two parts, called Stokes- and anti-Stokes Raman scattering, which are observed in the spectrum at lower $(\omega_s = \omega_L - \omega_R)$ or higher $(\omega_{As} = \omega_L - \omega_R)$ frequencies, respectively, compared to the frequency ω_L of the incident radiation. Intensities of anti-Stokes bands are much smaller than the Stokes bands as the population in the excited vibration states is small at room temperature.

The observed Stokes shift $(\omega_R = \omega_L - \omega_S)$ can be identified with a rotational or vibrational molecular transition. Thus, the Raman spectrum contains information about the vibrational and rotational energies of a molecule, which could be interpreted in terms of the type of bonds, bond strength, bond angles, symmetry, etc. In general, Raman spectra are rich in information and enable the determination of chemical composition based on the "spectral fingerprints" of molecules. Typically, the intensities of Raman bands depend on the polarizability of the molecule and the frequency $(\sim\omega^4)$ as well as intensity $(\sim\mathrm{I})$ of the incident radiation. Raman and Krishnan demonstrated the Raman effect in 1928 using sunlight and filters. Today's scientists have access to high-power lasers, sensitive CCD, fast data acquisition, and processing techniques. The advances in instrumentation have significantly improved the utility of this technique. New linear Raman spectroscopic techniques (e.g., resonance Raman spectroscopy (RRS) [40], surface-enhanced Raman spectroscopy (SERS) [41], confocal Raman microscopy [42]) and nonlinear Raman spectroscopic techniques (e.g., SRS [43], CARS [44]) have been developed that provide faster and more accurate analyses. These methods overcome the limitation of conventional Raman spectroscopy, namely a signal that is often weak due to Raman scattering being a nonresonant phenomena.

1.2 Integration of Raman Spectroscopy with Mutagenesis Screening of Algae

There is significant interest in microalgae for the direct production of biofuels and valuable lipids. *C. reinhardtii* is the leading model system for studying lipid metabolism in green algae. New isolates of UV mutagenesis of existing strains (CC-503) are used here as valuable sources of desired lipid products, and deeper insight into the lipid content of each population has been obtained at a single-cell

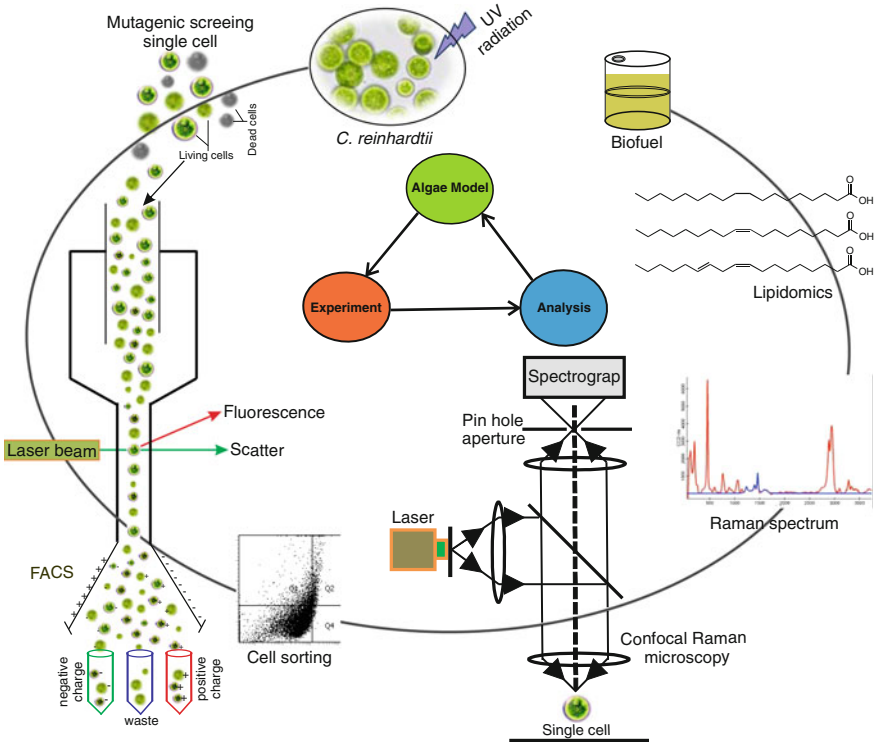

Fig. 1 Conceptual diagram of experiments undertook for mutagenic screening of algal cells for increased lipid production and their single-cell Raman characterization. *C. reinhardtii* mutants prepared by UV-induced mutagenesis lead to possible targets for lipid characterization. Mutagenized cells are then sorted by FACS, which is accomplished by electrical charge. The onboard computer determines how the cells will be sorted before the drop forms at the end of the stream. The charged drop is then deflected by charged electrodes into waiting sample tubes, and drops that contain no cells are sent into the waste tube. The number of cells in each tube is known and the level of fluorescence is also recorded for each cell. Confocal Raman microscopy is used for in vivo characterization of lipids and ratiometric analysis of Raman spectra yields information about the number of C=C bonds and the hydrocarbon chain length of the lipid molecules. These molecular traits influence the suitability of lipids for optimal production of biofuels

resolution level using Raman spectroscopy. Our approach in combining UV mutagenesis, FACS screening for increased lipid accumulation,[1] and characterization of lipid contents is summarized in Fig. 1.

[1]We note that the accumulated lipids are expected to be in the from triacylglycerides [45].

2 Experimental Methods

2.1 UV Mutagenesis and Fluorescence Activated Cell Sorting (FACS) Screening and Selection

CC-503 was grown using TAP liquid media [46]. 3.25×10^8 cells/mL were transferred to TAP agar plates exposed to ultraviolet (UV) light at a distance of 30 cm (253.7 nm, 100 μW/cm^2, 60 Hz, NuAire, http://www.nuaire.com) for 2 min under sterile conditions. The plates were subsequently kept in dark for one day to prevent photo reactivation of the DNA repair mechanism [47]. The plates were then allowed to grow under light for approximately a week [48, 49]. The resulting colonies were suspended in TAP liquid media and stained by BODIPY 505/515 for visualizing cells containing neutral lipids, which were then sorted using BD FACSAria III instrument. FACS sorts cells based on gating information provided by the user. The information given by the different channels can be visualized in two-dimensional plots combining two of the variables. Forward scatter (FSC) is normally assumed to be proportional to cell size or cell volume and side scatter (SSC) is proportional to the complexity of the cell. SSC intensity is affected by cell morphology, and especially by intracellular structures that are determined by chemical composition such as starch, and lipid content. A cell with higher level of cytoplasmic granularity will result in higher SSC intensity [50]. The highest emission intensity of the lipophilic dye BODIPY 505/515 is in the green fluorescence bandwidth range. Hence, cell complexity (SSC) was subsequently plotted against the fluorescence emission in the FITC-A and AmCyan-A channels, which correspond to green fluorescence.

2.2 Single Colony Analysis

CC-503 and the sorted cells from the fourth round of mutagenesis were grown using a TAP liquid media. The resulting single colonies were picked and suspended in TAP liquid media and stained by BODIPY 505/515 to illuminate cells containing neutral lipids, which were then analyzed using a FACS instrument. For this study, four colonies that produced highest signal were selected and expanded clonally as described below; these are annotated in this chapter as M1–M4.

2.3 Confocal Microscope Visualization

CC-503 and single colony cells from the fourth round of UV mutagenesis were grown for 4 days at 25 °C in a Photon System Instrument (PSI) growth chamber (AlgaeTron, Drasov, Czech Republic) using a TAP liquid media. Cell concentration

was measured using an automated cell counter (Cellometer Auto M10, Nexcelom Bioscience, Lawrence, MA, USA) and normalized for staining. Cells were observed with an Olympus Fluoview 1000 confocal laser scanning microscope (Tokyo, Japan) using 405, 488, 559, and 635 nm lasers to visualize BODIPY 505/515 (Schenectady, NY) stained cells. For BODIPY, the 488 nm excitation laser was used. A photomultiplier tubes (PMT) detector was used to collect the light and the spectral filter was set from 520 to 580 nm. Lipid staining was performed as follows: 1 µl of 10 mg/mL Bodipy-505/515 was added to 100 µl of cells (approximately 1×10^7/ml) and allowed to incubate at room temperature for one hour. If fluorescence quenching was too rapid to allow for imaging, cells were incubated for longer periods before microscopy.

2.4 Single-Cell Confocal Raman Microscopy

Confocal Raman Microscopy experiments were carried out using a combined Confocal Raman Imaging System, alpha 300 RA WiTec GmbH, Germany. For the green ($\lambda = 532$ nm) laser used in our experiments, the laser spot size, the theoretical (diffraction limited) lateral and axial resolutions are 0.811, 0.279 and 0.971 µm, respectively, since we used a 50× objective with 0.8 NA. Spectra were recorded in the range of 0–3400 cm^{-1} with a spectral resolution of 3 cm^{-1}. Raman single spectra, as well as spectral images, were collected using WiTec Control software and post-processed with Project FOUR software (WiTec Company, Germany) without any data smoothening. Laser power (8 mW at 532 nm) and exposure times (t = 30–75 s) were optimally chosen through a series of control experiments to ensure that the fluorescence background is minimized, at the same time ensuring that there is no laser induced damage (i.e., formation of amorphous carbonaceous char). For fatty acid standards and algal lipids, we used accumulation times ranging from 1 to 4 s and number of accumulations ranging from 10 to 25 to obtain signals with good signal-to-noise ratio [51].

3 Results and Discussion

3.1 UV Mutagenesis and FACS Analysis

Cell-to-cell analysis of variation in structural features of expressed lipids was done by assaying *C. reinhardtii* mutants screened for increased lipid accumulation. These mutants were isolated through sorting by Fluorescence Activated Cell Sorting (FACS) after each UV mutagenesis stage. *C. reinhardtii* cells were mutagenized to create populations with higher levels of intracellular lipids. Sorting of these populations by FACS allowed us to collect subpopulations enriched for lipid production. The high-lipid subpopulations were grown and subjected to UV mutagenesis

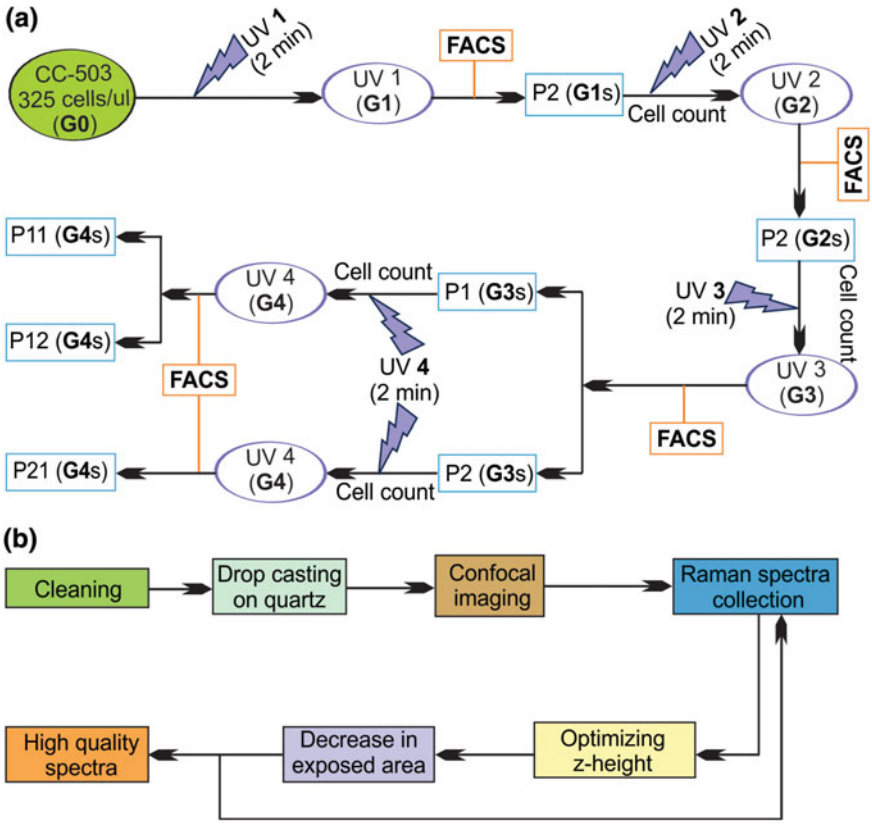

Fig. 2 **a** *C. reinhardtii* (CC-503) mutant screening using FACS instrument, CC-503 cells (G0) were exposed to ultraviolet (UV) light for 2 min (G1). Then the resulting colonies were stained by BODIPY to illuminate cells containing natural lipids that were then sorted using FACS instrument (G1s). The sorted cells were grown in a liquid TAP media, then a second round of mutagenesis (G2) and sorting (G2s) was done. The same process was done for the third and fourth rounds. **b** Flowchart schematically illustrating Raman imaging

and FACS sorting for several rounds (Fig. 2a). This technique has been shown to select for mutations in several pathways unrelated to starch metabolism [52, 53]. Using this protocol in an iterative fashion, we were able to see increases in lipid accumulation after two rounds of selection [51]. In the present study we carried out two additional rounds of mutagenesis and selection to further enrich for lipid accumulating cells. The cells selected after the fourth round were sorted again without mutagenesis to further enrich the lipid accumulating cells (refer to Fig. 2a for a summary of the process).

Recently, the use of in situ measurements of cellular lipids to monitor lipid changes within individual cells has generated attention, notably through the use of flow cytometry and lipophilic fluorescence dyes like Nile red and BODIPY 505/515 [54]. BODIPY 505/515 is useful for certain applications such as confocal imaging

and high-content screening of microalgae samples. Cooper et al. [55] successfully applied BODIPY 505/515 to monitor oil content within several microalgae species [55]. BODIPY 505/515 has a high oil/water partition coefficient, which allows it to easily cross cell and organelle membranes so that the lipid components of live cells can be distinctively labeled without killing the cells [54]. These properties allow recovery of stained cells with desired lipid content. Flow cytometry has been used successfully to select algal cells with an increased total lipid content [51, 56].

FACS allowed us to analyze lipid content on a single-cell basis (as marked by fluorescence from a lipophilic dye (see experimental methods) for millions of cells from a mutagenized population). Ultimately, after four rounds of flow cytometric cell sorting, thousands of mutant cells were screened and four different mutants were selected for further analysis. CC-503 and four different mutants from the forth round of mutagenesis (M1, M2, M3, and M4) were analyzed by FACS. CC-503 was analyzed first and two lines were drawn to indicate the maximum fluorescence emission reached. All the mutants have more cell complexity (SSC) and higher fluorescence emission in the FITC-A and AmCyan-A, indicating more lipid accumulation than the parental CC-503 strain (Fig. 3a). M1 and M3 show the highest increase in lipid content while M2 and M4 show lower lipid production but still higher than CC-503. Forward scatter, indicating cell size, was considered but has not been reported to help with distinguishing between the different mutants and the wild-type strain [52]. In order to qualitatively confirm the increase in mutants' lipid content, confocal microscopy was used for detecting fluorescent label in BODIPY 505/515-stained putative mutants. Lipid bodies in CC-503 and all four UV-induced mutants could be visualized and observed in a confocal microscope (Fig. 3b). The confocal microscope images show that all four mutants have more lipid bodies and higher lipid content than CC-503.

3.2 Raman Spectroscopy

Application of Raman spectroscopy to biological analysis is challenging due the inherently weak intensities of Raman signals. As explained earlier, the probability of spontaneous Raman scattering is quite small, i.e., about 1 in 10^6 photons. This leads to very weak optical signals. The poor signal-to-noise ratio of Raman signals is often a limiting factor in the application of Raman spectroscopy to biological analysis. This requires special consideration in algal analysis due to the presence of various pigments that can give rise to fluorescence and/or Resonance Raman spectra. Another limitation of the Raman technique in biological analysis is the complexity of biological Raman spectra due to the presence of a large number of Raman bands from the various chemical constituents of the cell. Fundamental building blocks such as nucleic acids, proteins, lipids, and carbohydrates, often give rise to overlapping Raman bands in the fingerprint region and that complicates the data analysis. Confocal Raman spectroscopy (CRM) can be used to overcome these

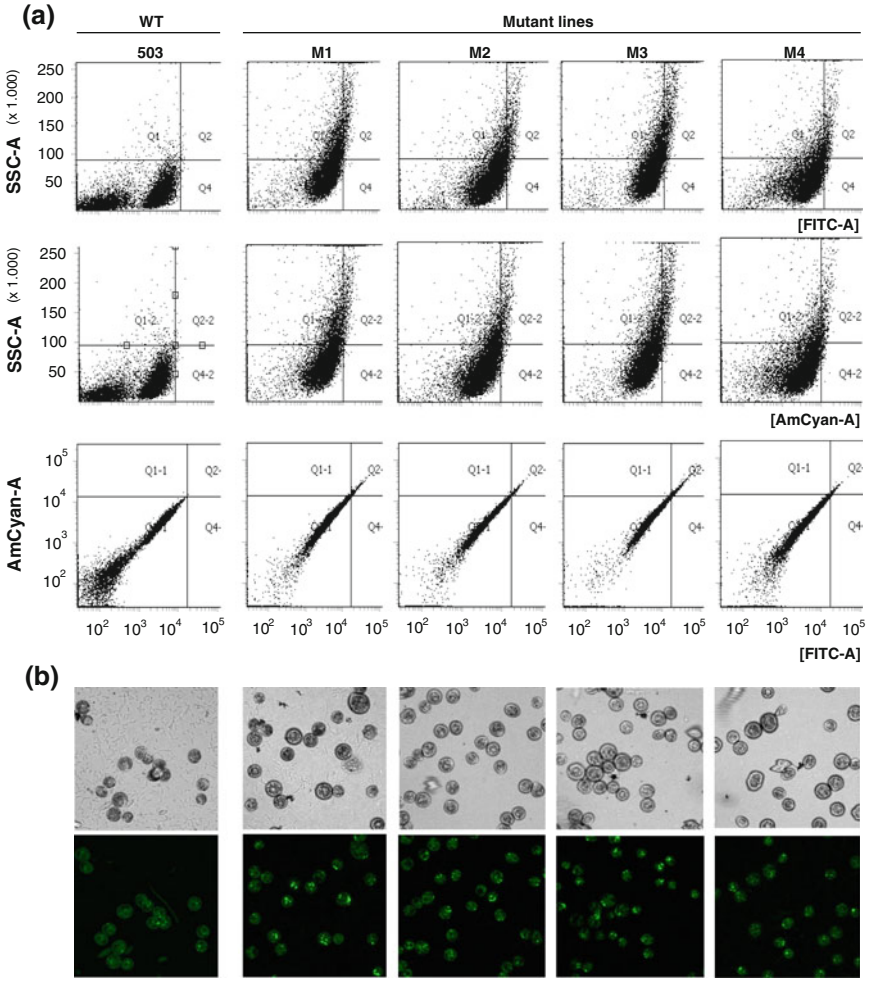

Fig. 3 **a** Dot plot relating cell size (FSC-A) with the inner cell complexity (SSC-A), SSC-A with fluorescence emission in the FITC-A and Amcyan-A channels, and fluorescence emission in the FITC-A with Amcyan-A for CC-503 wild-type and UV mutant lines (M1, M2, M3 and M4). **B** Bright-field and fluorescence microscope images of cells stained with BODIPY are shown left to right for CC-503 (wild-type) and UV mutant lines (M1, M2, M3 and M4)

limitations because it allows the acquisition of Raman spectra from a small volume (<1 μm^3) of the cell while rejecting noise from the surrounding regions.

CRM provides higher spatial resolution and sharper images, however, at the expense of reduced signal intensity. CRM is quite challenging since Raman scattering inherently produces weak signals. Recent advances in instrumentation have, however, allowed for the development of a true confocal microscope for acquisition of Raman spectra with high spatial and spectral resolutions. CRM offers the same advantages of

confocal fluorescence imaging, without using fluorescent labels. NIR (near infrared radiation) can be used for excitation in CRM for greater depth penetration in living tissue and to reduce background fluorescence in fluorescent samples. Finally, using ratiometric analysis, it is possible to obtain quantitative information on structural features of molecules such as lipids. By locating the lipid bodies in the cell and optimizing the acquisition parameters, it is possible to obtain good quality Raman spectra with high signal-to-noise ratios. We developed an effective protocol based on controlled photobleaching and hyperspectral imaging of cells to locate regions of lipid concentration. This leads to an improvement in the quality of resulting spectra and enables fast and precise quantitative characterization of algal lipids [51].

Figure 2b shows a schematic of a rapid and robust methodology for quantitative assessment of lipids through ratiometric analysis using CRM. The cells are washed thrice and resuspended in deionized water. A drop of this suspension containing microalgae cells is placed on pre-cleaned quartz substrates for analysis. Quartz is chosen as a substrate since it does not have any interfering Raman bands in the fingerprint region of lipid molecules [57]. Optical imaging is first performed using 50× objective (N.A. = 0.8) to locate the cells immobilized on the quartz surface. Cells are then photobleached by controlled exposure to radiation at $\lambda = 532$ nm. Next, approximate locations of lipid-rich regions are identified by Raman hyperspectral imaging over a scan area of approximately 25 × 25 μm at various scan depths around 10 μm. Imaging is performed at a low pixel density (10 × 10 spectra per image) for faster acquisition. Regions of high-lipid concentrations are located by mapping the integrated peak intensities of peaks corresponding to the lipid molecules. The region with highest peak intensity is then selected for further image acquisition and scanned at a low pixel density (10 × 10 spectra per image). The above procedure is repeated and the scanning area is reduced gradually until a scan area around (1 × 1) μm^2 is obtained. Spectral data acquisition and imaging are then carried out on the spot within this region by varying z-focus to maximize the lipid signal. The same acquisition parameters (integration time and laser intensity) are used to acquire high-quality data from standard fatty acids. Peak intensities are calculated by Lorentz curve fitting. For quantitative analysis, ratios of peak intensities are used since the determination of concentration from absolute intensities is not possible due to various experimental factors.

3.2.1 Raman Analysis

Fatty Acid Standards

In the present investigation, we used ratiometric analysis for quantitative assessment of lipids due to the difficulty in determining concentrations from absolute spectral intensities in Raman spectroscopy of complex samples. Specifically, for compositional analysis of lipids, the intensity ratios of integrated peak intensities at 1440 and 1650 cm^{-1}, (I_{1650}/I_{1440}), corresponding to the $–CH_2$ bending and C=C stretch, respectively, were used as the lipid markers.

We selected a set of nine pure fatty acids as calibration standards for determination of lipid composition. These fatty acids are even numbered and commonly found in microalgal lipid extracts. The difference in their aliphatic chain lengths and the number of C=C bonds is listed in Table 1.

Table 1 List of standard fatty acids used for ratiometric analysis of Raman spectra

Standard fatty acids	C-atoms	C=C bonds	$N_{C=C}/N_{CH2}$
Myristic acid	14	0	0
Palmitic acid	16	0	0
Lignoceric acid	24	0	0
Palmitoleic acid	16	1	0.08
Oleic acid	18	1	0.07
Linoleic acid	18	2	0.15
cis-11,14 Eicosadienoic acid	20	2	0.13
Linolenic acid	18	3	0.30
Arachidonic acid	20	4	0.36

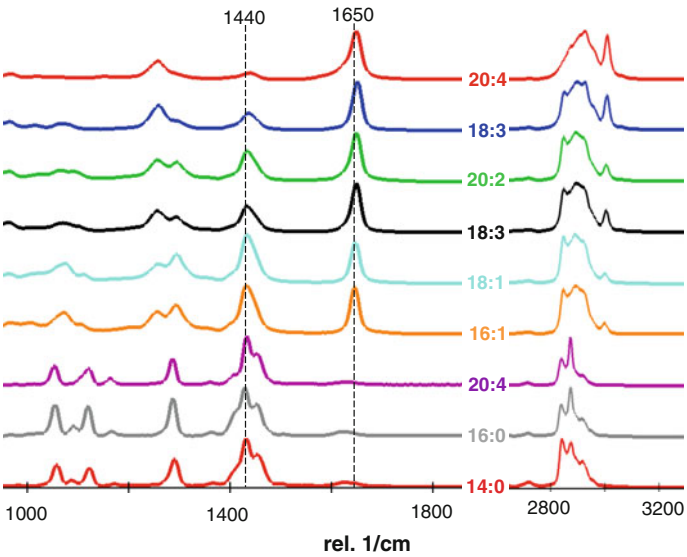

Fig. 4 Raman spectra collected for nine standard fatty acids listed with decreasing degree of unsaturation (from *top* to *bottom*). Those standards are listed in reverse order in Table 1. Raman spectra were acquired using 532 nm laser as the excitation source and show a gradual decrease in the intensity of the Raman band at 1650 rel cm^{-1} (C=C stretching mode) compared to that of 1440 rel cm^{-1} band (CH_2 bending mode) (from *top* to *bottom*). With the 532 nm excitation, the intensities of Raman bands in 2800–3000 rel cm^{-1} (CH_2 symmetric and asymmetric stretches) are orders of magnitude higher than those of the lipid characteristic bands at 1650/1440 rel cm^{-1} and are scaled down in intensity to allow visualization

The collected Raman spectra of these standards are arranged with decreasing degrees of unsaturation (top to bottom) as determined by a 532 nm laser excitation (Fig. 4).

The dominant peaks for 532 nm excitations are due to $–CH_2$ symmetric and asymmetric stretching vibrations at 2800–3000 cm^{-1}. Peaks at 1260 cm^{-1} (=C–H cis stretch), 1650 cm^{-1}(C=C stretch), and 3023 cm^{-1} (=C–H stretch) are indicative of unsaturation whereas peaks at 1300 cm^{-1} ($–CH_2$ twist), 1440 cm^{-1} ($–CH_2$ bend), and ~2800–3000 cm^{-1} (CH_2 symmetric and asymmetric stretches) correspond to the aliphatic chains of fatty acids. A gradual decrease in these markers of unsaturation is seen as the number of C=C bonds decreases from 4 to 0 (from top to bottom). For these standards, the ratio of I_{1650}/I_{1440} showed a linear correlation with both the number of C=C bonds and $N_{C=C}/N_{CH2}$, where N_{CH2} is the number of aliphatic $–CH_2–$ groups.

Figure 5a, b shows the calibration plots for intensity ratios of I_{1650}/I_{1440} recorded using a 532 nm laser excitation along with the number of C=C bonds and $N_{C=C}/N_{CH2}$ in standard fatty acids. The increase in the degree of unsaturation led to a linear increase in intensity ratio, which is in agreement with reported literature [29–34]. Fig. 5 also shows the results of ratiometric Raman analysis of five microalgal lipids (red circles).

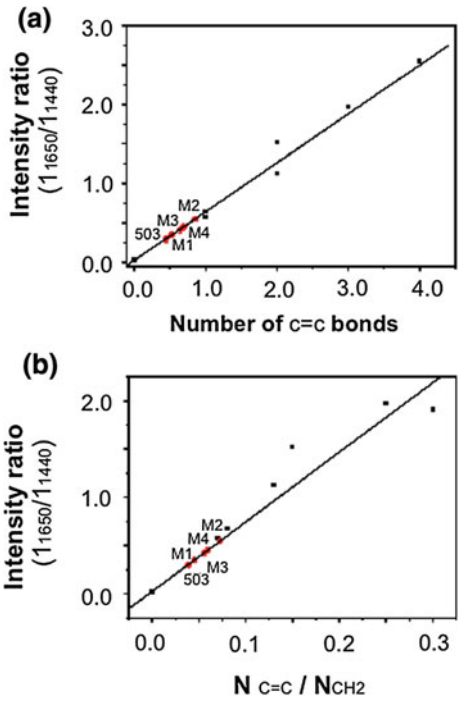

Fig. 5 Calibration plots calculated from standard fatty acids were used for quantitative assessment of extracted microalgal lipids. **a** The linear variation of intensity ratio with the degree of unsaturation (i.e., C=C bonds), **b** the linear variation of intensity ratio with $N_{C=C}/N_{CH2}$ (i.e., ratio of the number of C=C bonds with the number of $–CH_2–$ units). *Red* markers correspond to the intensity ratio measurements of algal lipids of both the nonmutated CC-503 and the four mutant populations

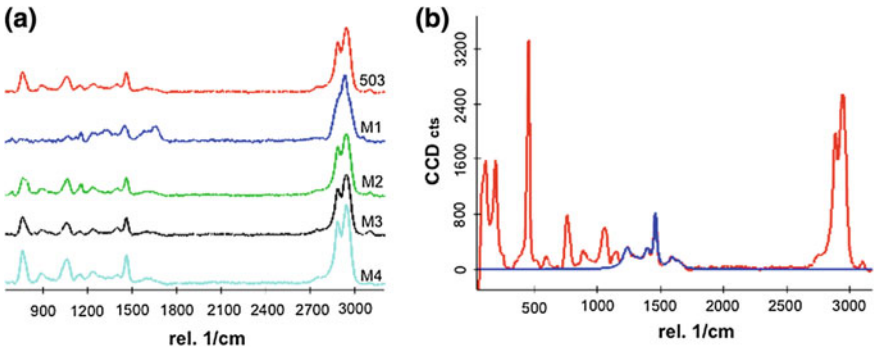

Fig. 6 **a** Raman spectra collected for various algal lipids using 532 nm laser excitation. The cells were photobleached through controlled exposure to 532 nm laser to suppress the background fluorescence and resonance Raman signals from the pigments. **b** Curve fitting of typical 503 microalgae sample (*red* curve represents the observed Raman spectrum, *blue* curve represents the best fit model)

Lipid Content Differences Between Mutant Lines and Within Clonal Populations

We examined four different mutant isolates and their clonal populations to determine if there are differences in lipid content among different isolated mutants and within their derived clonal populations. We collected single-cell Raman spectra using a 532 nm laser as an excitation source. Data was collected from more than 30 different cells individually for each of the four mutant lines and the reference unmutagenized CC-503 cells. Typical single-cell Raman spectra collected for these samples is shown in Fig. 6.

All collected spectra for the unmutagenized cells were found to be almost identical (with ±0.05 standard deviation) within each clonal population with variations not observed beyond what is expected from experimental error limits. This low observed variation within each clonal population indicates homogeneity within each population. This also indicates a lack of stochasticity in lipid expression, a desired property if the lipid content is one that is of utility and interest. In contrast to this lack of heterogeneity within each population, different measured values are observed between the four mutant lines. The variation in relative peak area for each mutant population is listed in Table 2 along with the unmutagenized strain. For the well-characterized reference strain of Chlamydomonas, CC-503, our measured values are consistent with those reported in the literature [58–61], which report the occurrence of saturated and monosaturated lipids predominantly with a variation in the relative concentration depending on the growth conditions. In contrast, the four mutant lines have a distinct saturation status as indicated by differences in their intensity ratios (Table 2).

These spectra showed significant lipid signatures (i.e., the presence of $–CH_2$ bend and C=C stretch at 1440 and 1650 cm^{-1} respectively, along with $-CH_2$ symmetric

Table 2 Intensity ratios calculated from 30 different single cells Raman spectra for 1650 and 1440 spectral peaks

Microalgae lines	Intensity ratios	C=C bonds	$N_{C=C}/N_{CH2}$	$^{a}N_{CH2}$
503	0.30	0.447	0.0387	11.6
M1	0.35	0.527	0.04532	11.6
M2	0.42	0.647	0.0554	11.7
M3	0.45	0.699	0.05942	11.8
M4	0.55	0.859	0.07252	11.8

These intensity ratios were found to be identical within (±0.05) experimental error limits
$^{a}N_{CH2}$ is the number of aliphatic carbon atoms; we note that when complex mixtures of C=C are present, accurate chain length determination becomes difficult without further analyses and curve fittings

and asymmetric stretching vibrations centered at 2800–3000). Similar to standard fatty acids, spectra recorded for algal lipids with 532 nm laser excitations were dominated by the 2800–3000 cm^{-1} stretch. These microalgae lipids also demonstrated smaller peaks around 1008 and 1520 cm^{-1}, indicative of carotenoid contributions.

4 Conclusions

UV mutagenesis can generate populations with distinct altered genotypes and phenotypes. Isolating strains with the desired improvement in phenotype can be readily achieved using FACS, and has been described and discussed here for the case of increasing lipid production in the microalgae *C. reinhardtii*. In this case, we selected four UV mutants with higher lipid accumulation than the reference CC-503 strain. Deeper insight into the lipid content of each population was obtained at a single-cell resolution level using Raman spectroscopy. Specific lipid enrichment may be valuable for applications including biofuel production. For example, monounsaturated fats like oleic acid have been shown to have superior properties compared with other lipids for biofuel feedstocks.

Raman spectroscopy has the advantage of offering a noninvasive and quantifiable assay with high sensitivity and specificity. Also, Raman spectroscopy of individual microalgal cells requires very little sample preparation which makes it ideal to screen for mutants with altered lipid phenotypes. Ratiometric Raman analysis can be used to perform quantitative analysis that yields information about molecular parameters such as chain length and degree of unsaturation in lipids. Confocal Raman microscopy thus provides a tool for rapid and quantitative lipid characterization in microalgae. High-throughput studies can be done to screen for lipids of interest, whereas in traditional lipid analysis techniques, large-scale screens are precluded by sample preparation time and labor. In the case of our screen, FACS enabled isolation and confirmation of increased lipid accumulation in the

mutants, while confocal Raman microscopy provided insight into the composition of the lipid bodies. The early rise in lipid accumulation without nitrogen starvation could explain why the intensity ratio of the mutagenized strains went up compared to the reference strain. *C. reinhardtii* is known to change its lipid composition in response to nitrogen stress [62] and this change in lipid composition, as measured by a change in intensity ratio, was observed in our Raman studies of the mutants. Thus, it is possible that a false registry of low nitrogen levels could be causing this early rise in lipids [63]. The metabolism of nitrogen in *C. reinhardtii* is tightly controlled and disruptions in any component of the regulatory network could have adverse effects on nitrogen sensing or lipid metabolism [62]. For example, a U-Box module of functioning ubiquitin E3 ligases were found to be involved in lipid metabolism [62]. U-Box modules are specific protein regulatory systems that control the protein turnover of enzymes involved in target pathways [63]. Although we have not elucidated the molecular mechanisms behind the increase in lipid accumulation of the mutants compared to the reference strains, we have indirect evidence suggesting that the lipid phenotype of the mutants is changing as if the cells were nitrogen starved.

All in all, the single-cell lipid phenotyping can be combined with single-cell genomic and transcriptomic data to offer a more complete analysis of the metabolic variability within a population and across populations.

Acknowledgments Financial support for this work was provided by New York University Abu Dhabi (NYUAD) Institute grant G1205, NYUAD Research Enhancement Fund AD060, and NYUAD Faculty Research Funds (AD060, VP012, and AD008).

References

1. Castruita M, Casero D, Karpowicz SJ, Kropat J, Vieler A, Hsieh SI, Yan W, Cokus S, Loo JA, Benning C, Pellegrini M, Merchant SS (2011) Systems biology approach in *Chlamydomonas* reveals connections between copper nutrition and multiple metabolic steps. Plant Cell. doi:10.1105/tpc.111.084400
2. Lv H, Qu G, Qi X, Lu L, Tian C, Ma Y (2013) Transcriptome analysis of *Chlamydomonas reinhardtii* during the process of lipid accumulation. Genomics 101(4):229–237. doi:10.1016/j.ygeno.2013.01.004
3. Merchant SS, Prochnik SE, Vallon O, Harris EH, Karpowicz SJ, Witman GB, Terry A, Salamov A, Fritz-Laylin LK, Marechal-Drouard L, Marshall WF, Qu LH, Nelson DR, Sanderfoot AA, Spalding MH, Kapitonov VV, Ren Q, Ferris P, Lindquist E, Shapiro H, Lucas SM, Grimwood J, Schmutz J, Cardol P, Cerutti H, Chanfreau G, Chen CL, Cognat V, Croft MT, Dent R, Dutcher S, Fernandez E, Fukuzawa H, Gonzalez-Ballester D, Gonzalez-Halphen D, Hallmann A, Hanikenne M, Hippler M, Inwood W, Jabbari K, Kalanon M, Kuras R, Lefebvre PA, Lemaire SD, Lobanov AV, Lohr M, Manuell A, Meier I, Mets L, Mittag M, Mittelmeier T, Moroney JV, Moseley J, Napoli C, Nedelcu AM, Niyogi K, Novoselov SV, Paulsen IT, Pazour G, Purton S, Ral JP, Riano-Pachon DM, Riekhof W, Rymarquis L, Schroda M, Stern D, Umen J, Willows R, Wilson N, Zimmer SL, Allmer J, Balk J, Bisova K, Chen CJ, Elias M, Gendler K, Hauser C, Lamb MR, Ledford H, Long JC, Minagawa J, Page MD, Pan J, Pootakham W, Roje S, Rose A, Stahlberg E, Terauchi AM,

Yang P, Ball S, Bowler C, Dieckmann CL, Gladyshev VN, Green P, Jorgensen R, Mayfield S, Mueller-Roeber B, Rajamani S, Sayre RT, Brokstein P, Dubchak I, Goodstein D, Hornick L, Huang YW, Jhaveri J, Luo Y, Martinez D, Ngau WC, Otillar B, Poliakov A, Porter A, Szajkowski L, Werner G, Zhou K, Grigoriev IV, Rokhsar DS, Grossman AR (2007) The *Chlamydomonas* genome reveals the evolution of key animal and plant functions. Science 318 (5848):245–250. doi:10.1126/science.1143609

4. Hannon M, Gimpel J, Tran M, Rasala B, Mayfield S (2010) Biofuels from algae: challenges and potential. Biofuels 1(5):763–784
5. Radakovits R, Jinkerson RE, Darzins A, Posewitz MC (2010) Genetic engineering of algae for enhanced biofuel production. Eukaryot Cell 9(4):486–501. doi:10.1128/EC.00364-09
6. Wijffels RH, Barbosa MJ (2010) An outlook on microalgal biofuels. Science 329(5993):796–799. doi:10.1126/science.1189003
7. Jijakli K, Abdrabu R, Khraiwesh B, Nelson D, Koussa J, Salehi-Ashtiani K (2015) Molecular genetic techniques for algal bioengineering. In: Moheimani NR, McHenry MP, de Boer K, Bahri PA (eds) Biomass and biofuels from microalgae. Biofuel and biorefinery technologies, vol 2. Springer, Cham, pp 155–171. doi:10.1007/978-3-319-16640-7_9
8. Khraiwesh B, Jijakli K, Swift J, Chaiboonchoe A, Abdrabu R, Chao P-W, Yen L, Salehi-Ashtiani K (2015) Prospective applications of synthetic biology for algal bioproduct optimization. In: Moheimani NR, McHenry MP, de Boer K, Bahri PA (eds) Biomass and biofuels from microalgae. Biofuel and biorefinery technologies, vol 2. Springer, Cham, pp 137–154. doi:10.1007/978-3-319-16640-7_8
9. Salehi-Ashtiani K, Koussa J, Dohai B, Chaiboonchoe A, Cai H, Dougherty KD, Nelson D, Jijakli K, Khraiwesh B (2015) Toward applications of genomics and metabolic modeling to improve algal biomass productivity. In: Moheimani NR, McHenry MP, de Boer K, Bahri PA (eds) Biomass and biofuels from microalgae. Biofuel and biorefinery technologies, vol 2. Springer, Switzerland, pp 173–189. doi:10.1007/978-3-319-16640-7_10
10. Koussa J, Chaiboonchoe A, Salehi-Ashtiani K (2014) Computational approaches for microalgal biofuel optimization: a review. Biomed Res Int 2014:649453. doi:10.1155/2014/649453
11. Fagerer SR, Schmid T, Ibanez AJ, Pabst M, Steinhoff R, Jefimovs K, Urban PL, Zenobi R (2013) Analysis of single algal cells by combining mass spectrometry with Raman and fluorescence mapping. Analyst 138(22):6732–6736. doi:10.1039/C3AN01135F
12. Wu H, Volponi JV, Oliver AE, Parikh AN, Simmons BA, Singh S (2011) In vivo lipidomics using single-cell Raman spectroscopy. Proc Natl Acad Sci 108(9):3809–3814. doi:10.1073/pnas.1009043108
13. Popescu G, Park K, Mir M, Bashir R (2014) New technologies for measuring single cell mass. Lab Chip 14(4):646–652. doi:10.1039/c3lc51033f
14. Fritzsch FSO, Dusny C, Frick O, Schmid A (2012) Single-cell analysis in biotechnology, systems biology, and biocatalysis. Annu Rev Chem Biomol Eng 3(1):129–155. doi:10.1146/annurev-chembioeng-062011-081056
15. Lindstrom S, Andersson-Svahn H (2010) Overview of single-cell analyses: microdevices and applications. Lab Chip 10(24):3363–3372. doi:10.1039/C0LC00150C
16. Sweedler J, Arriaga E (2007) Single cell analysis. Anal Bioanal Chem 387(1):1–2. doi:10.1007/s00216-006-0921-4
17. Lange BM (2005) Single-cell genomics. Curr Opin Plant Biol 8(3):236–241. doi:http://dx.doi.org/10.1016/j.pbi.2005.03.015
18. Saliba AE, Westermann AJ, Gorski SA, Vogel J (2014) Single-cell RNA-seq: advances and future challenges. Nucleic Acids Res 42(14):8845–8860. doi:10.1093/nar/gku555
19. Woyke T, Jarett J (2015) Function-driven single-cell genomics. Microb Biotechnol 8(1):38–39. doi:10.1111/1751-7915.12247
20. Bonke M, Turunen M, Sokolova M, Vähärautio A, Kivioja T, Taipale M, Björklund M, Taipale J (2013) Transcriptional networks controlling the cell cycle. G3: Genes Genomes Genet 3(1):75–90. doi:10.1534/g3.112.004283

21. Ghazalpour A, Bennett B, Petyuk VA, Orozco L, Hagopian R, Mungrue IN, Farber CR, Sinsheimer J, Kang HM, Furlotte N, Park CC, Wen PZ, Brewer H, Weitz K, Camp DG 2nd, Pan C, Yordanova R, Neuhaus I, Tilford C, Siemers N, Gargalovic P, Eskin E, Kirchgessner T, Smith DJ, Smith RD, Lusis AJ (2011) Comparative analysis of proteome and transcriptome variation in mouse. PLoS Genet 7(6):e1001393. doi:10.1371/journal.pgen.1001393
22. Nagaraj N, Wisniewski JR, Geiger T, Cox J, Kircher M, Kelso J, Paabo S, Mann M (2011) Deep proteome and transcriptome mapping of a human cancer cell line. Mol Syst Biol 7:548. doi:10.1038/msb.2011.81
23. Washburn MP, Koller A, Oshiro G, Ulaszek RR, Plouffe D, Deciu C, Winzeler E, Yates JR 3rd (2003) Protein pathway and complex clustering of correlated mRNA and protein expression analyses in *Saccharomyces cerevisiae*. Proc Natl Acad Sci USA 100(6):3107–3112. doi:10.1073/pnas.0634629100
24. Walley JW, Shen Z, Sartor R, Wu KJ, Osborn J, Smith LG, Briggs SP (2013) Reconstruction of protein networks from an atlas of maize seed proteotypes. Proc Natl Acad Sci USA 110(49):E4808–E4817. doi:10.1073/pnas.1319113110
25. Tang F, Lao K, Surani MA (2011) Development and applications of single-cell transcriptome analysis. Nat Methods 8(4 Suppl):S6–11. doi:10.1038/nmeth.1557
26. Hebenstreit D (2012) Methods, challenges and potentials of single cell RNA-seq. Biology (Basel) 1(3):658–667. doi:10.3390/biology1030658
27. Petry R, Schmitt M, Popp J (2003) Raman spectroscopy—a prospective tool in the life sciences. Chemphyschem: Eur J Chem Phys Phys Chem 4:14–30. doi:10.1002/cphc.200390004
28. Li M, Yang L, Bai Y, Liu H (2014) Analytical methods in lipidomics and their applications. Anal Chem 86:161–175. doi:10.1021/ac403554h
29. Pořízka P, Prochazková P, Prochazka D, Sládková L, Novotný J, Petrilak M, Brada M, Samek O, Pilát Z, Zemánek P, Adam V, Kizek R, Novotný K, Kaiser J (2014) Algal biomass analysis by laser-based analytical techniques—a review. Sensors 14:17725–17752. doi:10.3390/s140917725
30. Wei X, Jie D, Cuello JJ, Johnson DJ, Qiu Z, He Y (2014) Microalgal detection by Raman microspectroscopy. TrAC Trends Anal Chem 53:33–40. doi:10.1016/j.trac.2013.09.012
31. Wu H, Volponi JV, Oliver AE, Parikh AN, Simmons BA, Singh S (2011) In vivo lipidomics using single-cell Raman spectroscopy. Proc Natl Acad Sci USA 108:3809–3814. doi:10.1073/pnas.1009043108
32. Hosokawa M, Ando M, Mukai S, Osada K, Yoshino T, Hamaguchi H-O, Tanaka T (2014) In vivo live cell imaging for the quantitative monitoring of lipids by using Raman microspectroscopy. Anal Chem 86:8224–8230
33. Heraud P, Beardall J, McNaughton D, Wood BR (2007) In vivo prediction of the nutrient status of individual microalgal cells using Raman microspectroscopy. FEMS Microbiol Lett 275:24–30. doi:10.1111/j.1574-6968.2007.00861.x
34. Kaczor A, Turnau K, Baranska M (2011) In situ Raman imaging of astaxanthin in a single microalgal cell. Analyst 136:1109–1112. doi:10.1039/c0an00553c
35. Li S, Li L, Zeng Q, Zhang Y, Guo Z, Liu Z, Jin M, Su C, Lin L, Xu J, Liu S (2015) Characterization and noninvasive diagnosis of bladder cancer with serum surface enhanced Raman spectroscopy and genetic algorithms. Sci Rep 5. doi:10.1038/srep09582
36. Sathyavathi R, Saha A, Soares JS, Spegazzini N, McGee S, Rao Dasari R, Fitzmaurice M, Barman I (2015) Raman spectroscopic sensing of carbonate intercalation in breast microcalcifications at stereotactic biopsy. Sci Rep 5. doi:10.1038/srep09907
37. Tolstik T, Marquardt C, Beleites C, Matthäus C, Bielecki C, Bürger M, Krafft C, Dirsch O, Settmacher U, Popp J, Stallmach A (2015) Classification and prediction of HCC tissues by Raman imaging with identification of fatty acids as potential lipid biomarkers. J Cancer Res Clin Oncol 141(3):407–418. doi:10.1007/s00432-014-1818-9
38. Christian K, Johanna M, Werner A, Kathrin B, Tesfay GM, Robert H, Abbas A, Stefan W, Andreas B, Wilhelm NF, Florian S (2014) Raman difference spectroscopy: a non-invasive

method for identification of oral squamous cell carcinoma. Biomed Opt Express 5 (9):3252–3265. doi:10.1364/BOE.5.003252
39. von Erlach TC, Hedegaard MAB, Stevens MM (2015) High resolution Raman spectroscopy mapping of stem cell micropatterns. Analyst 140(6):1798–1803. doi:10.1039/C4AN02346C
40. Spiro TG (1974) Resonance Raman spectroscopy. New structure probe for biological chromophores. Acc Chem Res 7:339–344. doi:10.1021/ar50082a004
41. Kneipp K, Kneipp H, Itzkan I, Dasari RR, Feld MS (2002) Surface-enhanced Raman scattering and biophysics. J Phys: Condens Matter 14:R597–R624. doi:10.1088/0953-8984/14/18/202
42. Puppels GJ, Mul FFMD, Otto C, Greve J, Robert-Nicoud M, Arndt-Jovin DJ, Jovin TM (1990) Studying single living cells and chromosomes by confocal Raman microspectroscopy. Nature 347:301–303
43. Freudiger CW, Min W, Saar BG, Lu S, Holtom GR, He C, Tsai JC, Kang JX, Xie XS (2008) Label-free biomedical imaging with high sensitivity by stimulated Raman scattering microscopy. Science (New York, N.Y.) 322. doi:10.1126/science.1165758
44. Le TT, Yue S, Cheng J-X (2010) Shedding new light on lipid biology with coherent anti-Stokes Raman scattering microscopy. J Lipid Res 51:3091–3102. doi:10.1194/jlr.R008730
45. Merchant SS, Kropat J, Liu B, Shaw J, Warakanont J (2012) TAG, you're it! *Chlamydomonas* as a reference organism for understanding algal triacylglycerol accumulation. Curr Opin Biotechnol 23(3):352–363. doi:http://dx.doi.org/10.1016/j.copbio.2011.12.001
46. Gorman DS, Levine RP (1965) Cytochrome f and plastocyanin: their sequence in the photosynthetic electron transport chain of *Chlamydomonas reinhardii*. Proc Natl Acad Sci USA 54(6):1665–1669
47. Small GD, Greimann CS (1977) Photoreactivation and dark repair of ultraviolet light-induced pyrimidine dimers in chloroplast DNA. Nucleic Acids Res 4(8):2893–2902
48. Tillich UM, Lehmann S, Schulze K, Duhring U, Frohme M (2012) The optimal mutagen dosage to induce point-mutations in *Synechocystis* sp. PCC6803 and its application to promote temperature tolerance. PLoS ONE 7(11):e49467. doi:10.1371/journal.pone.0049467
49. Zayadan BK, Purton S, Sadvakasova AK, Userbaeva AA, Bolatkhan K (2014) Isolation, mutagenesis, and optimization of cultivation conditions of microalgal strains for biodiesel production. Russ J Plant Physiol 61(1):124–130. doi:10.1134/S102144371401018X
50. Hyka P, Lickova S, Přibyl P, Melzoch K, Kovar K (2013) Flow cytometry for the development of biotechnological processes with microalgae. Biotechnol Adv 31(1):2–16. doi:http://dx.doi.org/10.1016/j.biotechadv.2012.04.007
51. Sharma et al (2015) Biotechnol Biofuels 8:164. doi:10.1186/s13068-015-0349-1
52. Terashima M, Freeman ES, Jinkerson RE, Jonikas MC (2015) A fluorescence-activated cell sorting-based strategy for rapid isolation of high-lipid *Chlamydomonas* mutants. Plant J 81 (1):147–159. doi:10.1111/tpj.12682
53. Xie B, Stessman D, Hart JH, Dong H, Wang Y, Wright DA, Nikolau BJ, Spalding MH, Halverson LJ (2014) High-throughput fluorescence-activated cell sorting for lipid hyperaccumulating *Chlamydomonas reinhardtii* mutants. Plant Biotechnol J 12(7):872–882. doi:10.1111/pbi.12190
54. Brennan L, Blanco Fernández A, Mostaert AS, Owende P (2012) Enhancement of BODIPY505/515 lipid fluorescence method for applications in biofuel-directed microalgae production. J Microbiol Methods 90(2):137–143. doi:http://dx.doi.org/10.1016/j.mimet.2012.03.020
55. Cooper MS, Hardin WR, Petersen TW, Cattolico RA (2010) Visualizing "green oil" in live algal cells. J Biosci Bioeng 109(2):198–201. doi:http://dx.doi.org/10.1016/j.jbiosc.2009.08.004
56. Hyka P, Lickova S, Přibyl P, Melzoch K, Kovar K (2013) Flow cytometry for the development of biotechnological processes with microalgae. Biotechnol Adv 31:2–16

57. Meier M, Wokaun A, Vo-Dinh T (1985) Silver particles on stochastic quartz substrates providing tenfold increase in Raman enhancement. J Phys Chem 89(10):1843–1846. doi:10.1021/j100256a002
58. Kim S, Kim H, Ko D, Yamaoka Y, Otsuru M, Kawai-Yamada M, Ishikawa T, Oh H-M, Nishida I, Li-Beisson Y, Lee Y (2013) Rapid induction of lipid droplets in *Chlamydomonas reinhardtii* and *Chlorella vulgaris* by Brefeldin A. PLoS ONE 8:e81978. doi:10.1371/journal.pone.0081978
59. Kobayashi N, Noel E, Barnes A, Rosenberg J, DiRusso C, Black P, Oyler GA (2013) Rapid detection and quantification of triacylglycerol by HPLC-ELSD in *Chlamydomonas reinhardtii* and *Chlorella* strains. Lipids 48:1035–1049. doi:10.1007/s11745-013-3828-9
60. Msanne J, Xu D, Reddy A, Casas-mollano JA, Awada T, Cahoon EB, Cerutti H (2012) Metabolic and gene expression changes triggered by nitrogen deprivation in the photoautotrophically grown microalgae *Chlamydomonas reinhardtii* and *Coccomyxa sp*. C-169. Phytochemistry 75:50–59. doi:10.1016/j.phytochem.2011.12.007
61. Siaut M, Cuiné S, Cagnon C, Fessler B, Nguyen M, Carrier P, Beyly A, Beisson F, Triantaphylidès C, Li-beisson Y, Peltier G (2011) Oil accumulation in the model green alga *Chlamydomonas reinhardtii*: characterization, variability between common laboratory strains and relationship with starch reserves. BMC Biotechnol 11:7. doi:10.1186/1472-6750-11-7
62. Luo Q, Li Y, Wang W, Fei X, Deng X (2015) Genome-wide survey and expression analysis of *Chlamydomonas reinhardtii* U-box E3 ubiquitin ligases (CrPUBs) reveal a functional lipid metabolism module. PLoS ONE 10(3):e0122600. doi:10.1371/journal.pone.0122600
63. Bielskienė K, Bagdonienė L, Mozūraitienė J, Kazbarienė B, Janulionis E (2015) E3 ubiquitin ligases as drug targets and prognostic biomarkers in melanoma. Medicina 51(1):1–9. doi:http://dx.doi.org/10.1016/j.medici.2015.01.007

Single Differentiated Neurons from Pluripotent Embryonic Stem Cells: Motor Protein Modeling and Neurodegenerative Disease

Chih-Wei Chen, Shang-Yu Wu and Geng-Ming Hu

Abstract Protein accumulation occurs in various neurodegenerative diseases, and one hypothesis to explain this phenomenon is based on defective axonal transport powered by molecular motors. Kinesin family motor proteins and the opposing dynein/dynactin motor complex proteins are the major motor proteins for transport along microtubules in axons. The interaction and regulation of transport via subunits of kinesin and the dynein/dynactin complex and how these subunits influence motor protein structure and their transport are not yet well understood. Notably, RNA interference (RNAi) knockdown is widely used to investigate motor behavior. However, RNAi knockdown results have varied. Therefore, we have used single-cell DNA devices to improve DNA delivery accuracy for retinoic acid-induced P19 neurons under optimal conditions. In addition, a mathematical method and physical hypothesis fitting with physical parameters have been used to build models. We describe a motion model based on parameters from dynamic transport, including an anterograde state, a retrograde state, and a pausing state. The residence time between two transition points shows the ability of a motion mode to maintain its state and resist the tendency to switch. Thus, the model could explain the characteristics and influences of each subunit.

Keywords Molecular motors · Modeling · Kinesin · Dynein · Dynactin · P19 cells · RNAi · Microfluidic devices · Microchannels · Single-cell DNA delivery device

C.-W. Chen (✉)
Department of Molecular and Cellular Biology, National Tsing Hua University, Hsinchu, Taiwan
e-mail: cwwaynechen@gmail.com

S.-Y. Wu
Department of Electrophysics, National Chiao Tung University, Hsinchu, Taiwan
e-mail: loganwu@gmail.com

G.-M. Hu
Department of Physics, National Taiwan Normal University, Taipei, Taiwan
e-mail: pipipshu@gmail.com

F.-G. Tseng and T.S. Santra (eds.), *Essentials of Single-Cell Analysis*, Series in BioEngineering, DOI 10.1007/978-3-662-49118-8_15

1 Molecular Motors and Disease

Cytoskeletal molecular motors, also called motor proteins, are classified into the kinesins, dyneins, and myosins and mediate cargo transport within cells. Different cargos involved in essential neuronal functions include nucleotides, lipid organelles, and proteins that are shuttled in long distances between cell bodies and synapses in axonal transport.

Axonal transport impairment has been shown to be a feature of neuroinflammatory lesions in multiple sclerosis (MS)-like disease, and pervasive axonal dysfunction in progressive axonal degeneration could be caused by transport disturbances. Organelle arrest, such as mitochondrial accumulation, occurs in neuroinflammatory areas [1].

Abnormal protein aggregation is characteristic of many neurodegenerative diseases. Huntington's disease, Parkinson's disease, Alzheimer's disease (AD), amyotrophic lateral sclerosis (ALS), Charcot–Marie-Tooth disease, and MS-like disease studies have revealed that proteins are accumulated abnormally [2–11]. This phenomenon suggested that proteins, under some circumstances, can cause certain neurological disorders. Aggregated proteins may be because of functional defects of protein folding and motor proteins in transport systems.

Pervasive transport deficits and progressive axon loss occur in MS, but anti-inflammatory agents promote or eliminate redox that enables the reversal of structural alterations of axons, cargos, and microtubules [9]. Furthermore, mutations also could affect axonal transport and lead to axon degeneration in mice and humans; interestingly, transport affected by mutations could also cause axon degeneration [11–14]. Therefore, the recovery of transport tracks or transport deficits can decelerate the progression of axon degeneration [15].

1.1 Kinesins in Disease

Kinesin superfamily members are classified into 15 families (the kinesin 14 family consists of the 14A and 14B subfamilies), and most kinesin members are microtubule-based plus-end-directed motilities. Microtubules are the cytoskeleton in cytoplasm and axons and provide a "track" for motor proteins. The 15 kinesin families are classified as N-type, M-type, and C-type kinesins according to the region of the motor domain that contains a microtubule-binding site and converts chemical energy into mechanical work powered by the hydrolysis of ATP. N-type kinesins and C-type kinesins can bind to microtubules at the kinesins' amino acid N-terminal and C-terminal regions and move along the microtubules. M-type kinesins can depolymerize microtubules, and their functions are essential for spindle morphogenesis and chromosome segregation.

Kinesin superfamily members have different roles in mitosis, brain development, learning, and memory function and are involved in tumorigenesis and

carcinogenesis [16–19]. The kinesin-1, -2, -3, -4, -11, and -13 families have been studied in neuroscience, and all kinesin-1, -2, -3 families are involved in axonal transport. Kinesin-1 family members, including KIF5A, B, and C, are well known and important for neuronal function in the central nervous system [20]. Kinesin-3, in KIF13A (Kif13a−/− mice) experiments, have been shown to possibly be related to anxiety control and connected with transport of dense core vesicles and synaptic vesicle (SV) precursors [21]. Kinesin-1 is known to shuttle short microtubules, but KIF21A, a kinesin-4 family member, suppresses and regulates microtubule length and structure, in contrast to kinesin-1. In addition, mutation of tubulins and disturbed transport also lead to neuronal degeneration and result in neuronal disease [22–24].

1.2 Dynein in Disease

Compared with kinesin, dynein moves toward the minus end of microtubules. The two major classes of dynein proteins are cytoplasmic dyneins and axonemal dyneins, which differ according to their function and structure. Cytoplasmic dynein is involved in mitosis, cell polarization, and material transport. Axonemal dynein is involved in the ciliary and flagellar waving motion [25]. A cytoplasmic dynein family consisting of dynein-1 and dynein-2 has been identified. Dynein-1 is more abundant than dynein-2 in cells and engaged in retrograde axonal transport. Dynein-2, in contrast to dynein-1, is found only in the cilia and flagella and provides retrograde intraflagellar transport [16, 20, 26]. Dynein-1 has roles in cargo recycling and axonal retraction. Disrupted dynein-dependent trafficking resulted in retraction of the axonal cytoskeleton [21, 27]. Mutation in dynein-2 and structural defects in the cilia lead to skeletal ciliopathy, which is also referred to as primary ciliary dyskinesia (PCD) [28–32].

1.3 Motor Subunits and Adaptors in Disease

Regulators, adaptors, and proteins associated with molecular motors as well as functional interaction between motor protein subunits have been studied and reported [21, 33–36]. However, information regarding subunits is limited. Current research has demonstrated that motor adaptors and subunits affect motor function in disease.

Kinesin superfamily-associated protein 3 (KAP3) is linked to ALS. KAP3 is associated with heterotrimeric kinesin-2 motor proteins that were formed from the kinesin-2 family members, KIF3A and KIF3B [37–40]. FEZ1 mutations, engaged in FEZ1-mediated kinesin-1-based transport, cause abnormal Stx1 aggregation in the soma and axons of neurons, and further transport defects may lead to neurodegenerative disorders [40].

Dynein-1 has known regulators, such as dynactin, lissencephaly protein 1 (LIS1), and bicaudal D homolog 2 (BICD2). In a recent study, Tripathy et al. determined that dynactin could autoregulate and further interfere with dynein activity [41]. LIS1/NUDE is known to regulate cytoplasmic dynein ATPase; BICD2 acts as a motility-inducer of dynein and stabilizes dynein and dynactin complexes that attach to vesicles that transport mRNAs and nuclei [42, 43].

In *Drosophila,* LIS1 contains a WD repeat region that physically interacts with the p150 dynein light chain (DLC), a subunit of dynactin, and kinetochore on chromatids. Other evidence from yeast two hybrid assays have shown that dynein heavy chain, dynein intermediate chain, and dynamitin (p50) enable interaction with LIS1 [44–46].

Smooth brain, a brain developmental disease, is also associated with mutations in the LIS1 gene and appears as less prominent folds on the surface of the brain. When one allele of the LIS1 gene mutation, LIS1 protein expression decreased and led to lissencephaly type I disease [47].

A subunit of DLC, Tctex-1, is associated with rhodopsin function by linking dynein and rhodopsin. Tctex-1 may contribute to biochemical functions of dynein and photopigments [48].

The P50 dynactin subunit has been linked to Alzheimer's disease, and tissues from clinic patients appear to alter the expression and distribution of P-tau, PAPP, dynactin-P50, and synaptophysin [49].

P150 is the largest subunit in dynactin. P150 mutations and insufficient expression are associated with disease in cell lines, *Caenorhabditis elegans*, mice, and clinical research; low p150 expression leads to progressive loss of motor neurons because of the accumulation of autophagosomes in sporadic ALS. Recent studies by Ikenaka et al. showed that dynactin 1 was insufficient, transport of autophagosomes was disrupted, and further motor neuron degeneration was induced [50–52].

The G59S mutation in the p150 Gap–Gly domain is associated with motor neuron cell death through loss of dynein/dynactin complex function and appears as abnormal dynein/dynactin clusters in neurons in immunohistochemical analyses. In clinical investigations, family members carrying the G59S mutation have shown general clinical or electrophysiological sensory functions but an abnormal morphology of epidermal nerve fibers [53, 54].

Distal spinal and bulbar muscular atrophy (dSBMA) observed in a mouse model suggest that p150 mutation may be involved in disease progression because of the observed defects in axonal caliber and neuromuscular junctions [55].

2 Overview of Theoretical Models of Intracellular Transport by Molecular Motors

It is very interesting to study the physics of motion in a preferred direction in a highly stochastic environment. In this part, we will briefly review some physics concepts about modeling of the dynamics of molecular motor transport. We will first describe the dynamics of single motors and then describe the collective behavior of multiple motors. Finally, we will discuss bidirectional transport achieved by two teams of molecular motors.

2.1 Unidirectional Transport of Molecular Motors

The motion of a single motor proceeds through three stages: (i) transformation of chemical energy into mechanical energy and generation of a single step of motion by the motor; (ii) an effective biased random walk along the filament during a single walk; (iii) repetition of (i) and (ii) along the filament and diffusive or stationary motion when the motor detaches from the filament. To explain the above stochastic dynamics of a single motor, a simple model, named the Brownian ratchet model, was proposed by Feynman [56–58]. To perform a step walk along the filament, the motor cycles through a sequence of conformational change before returning to the initial state. To simplify the question, assume two internal states, bounded or unbounded, to model the motor as an overdamped-driven Brownian particle[1] moving in an asymmetric periodic potential $V_i(x)$.[2]

The state of motor satisfies the Fokker–Planck equation [3]

$$\frac{\partial p_i(x,t)}{\partial t} = -\frac{\partial J_i(x,t)}{\partial x}, \quad i = 1, 2,$$

where $p_i(x,t)$ is the probability density that the motor is in the state i at location x and time and $J_i(x,t)$ is the probability flux

$$J_i(x,t) = \mu_i \left[-\frac{\mathrm{d}V_i(x)}{\mathrm{d}x} - k_B T \frac{\partial}{\partial x} \right] p_i(x,t),$$

where μ_i denotes the mobility, T is the temperature in the aqueous environment, and k_B is the Boltzmann constant. If we allow the states transition in the form of a Markov process, a source term should be added to the following Fokker–Planck equations:

[1]Because the aqueous environment of a cell is highly viscous, one can treat a diffusing particle as an overdamped Brownian particle.

[2]To guarantee the motor moves in a preferred direction.

$$\frac{\partial p_1(x,t)}{\partial t} = -\frac{\partial J_1(x,t)}{\partial x} + [\omega_1(x)p_1(x,t) - \omega_2(x)p_2(x,t)],$$

$$\frac{\partial p_2(x,t)}{\partial t} = -\frac{\partial J_2(x,t)}{\partial x} + [\omega_2(x)p_2(x,t) - \omega_1(x)p_1(x,t)]$$

where ω_i denotes the transition rate in which the motor switches from one state to the other. The currents result from diffusion, interaction with the filament, and the action of the following possible external force f_{ext},

$$J_i(x,t) = \mu_i\left[-\frac{\mathrm{d}V_i(x)}{\mathrm{d}x} - k_BT\frac{\partial}{\partial x} + f_{\text{ext}}\right]p_i(x,t).$$

The above equations can be used not only to illustrate the motion of molecular motors but also to explicitly show how this motion and force generation emerges. These can be shown as follows. Define the steady-state current $J = J_1(x) + J_2(x)$, $p = p_1(x) + p_2(x)$ and $\lambda = p_1(x)/p$. Then, the current can be expressed in the following form:

$J = J_1(x) + J_2(x)$, $p = p_1(x) + p_2(x)$ and $\lambda = p_1(x)/p$. One can express the current as the form

$$J_i(x,t) = \mu_{\text{eff}}\left[-\frac{\mathrm{d}V_i(x)}{\mathrm{d}x} - k_BT\frac{\partial}{\partial x} + f_{\text{ext}}\right]p_i(x,t).$$

with an effective mobility

$$\mu_{\text{eff}} = \mu_1\lambda + \mu_2(1-\lambda)$$

and an effective potential satisfies

$$V_{\text{eff}}(x) - V_{\text{eff}}(0) = \int_0^x \mathrm{d}x' \frac{\mu_1\lambda V_1'(x') + \mu_2(1-\lambda)V_2'(x')}{\mu_1\lambda + \mu_2(1-\lambda)}.$$

If one assumes the thermodynamic equilibrium condition, the detailed balance condition[3] is satisfied

$$\frac{p_1}{p_2} = \frac{\omega_1}{\omega_2} = \exp\left[\frac{V_1(x) - V_2(x)}{k_BT}\right],$$

and as a consequence,

[3]Detailed balance means that for kinetic systems that are decomposed into elementary processes, and are at equilibrium each process should be equilibrated by its reverse process.

$$\lambda = (1 + \exp(V_2(x) - V_1(x))/k_B T)^{-1}.$$

For the symmetric potential, the potential is on a large scale, so there is no net motion in a preferred direction. However, for an asymmetric potential, the effective potential generally has a nonzero average slope on large scales. This nonzero average slope corresponds to an average force developed by the motors that are able to generate motion against a weaker external force f_{ext}: this implies that for a molecular motor to sustain a directed motion, a net positive supply of chemical energy is required to maintain the state transition rates away from a detailed balance, which is achieved by the hydrolysis of ATP.

The above discussion focuses on the motion of a single molecular motor. How do multiple molecular motors work? Let us consider the unidirectional motion of a single cargo with N of the same motors [59].

Each motor can interact with and actively pull on the cargo. However, the number of pulling motors, n, is not constant and varies with time. Assume the cargo is in the state n, the transition rate from the state n to $n + 1$ is $\omega_{n,n+1}$, and the transition rate from the state n to n − 1 is $\omega_{n,n-1}$. The probability of the cargo staying in the state n at time t is $P_n(t)$ and evolves according to the master equation

$$\frac{\partial P_n(t)}{\partial t} = -\Delta J_{n,n+1} - \Delta J_{n,n-1},$$

with

$$\Delta J_{n,n+1} = P_n \omega_{n,n+1} - P_{n+1} \omega_{n+1,n}$$

and

$$\Delta J_{n,n-1} = P_n \omega_{n,n-1} - P_{n-1} \omega_{n-1,n}$$

where $\omega_{n,n+1}$ is the binding rate of a motor attached to the cargo, and $\omega_{n,n-1}$ is the unbinding rate of a motor detached from the cargo. In the steady state, the probability distribution P_n^{st} satisfies

$$P_{n+1}^{\text{st}} \omega_{n+1,n} = P_n^{\text{st}} \omega_{n,n+1}.$$

This relationship corresponds to the detailed balance condition between state $n + 1$ and n and implicitly assume that all movements of the bound cargo particle begin and end with $n = 0$ and that every transition from n to $n + 1$ implies a backward transition at some later time. It is also implicitly assumed that the binding and unbinding rates are independent of the transition rates for stepping along the filament. By solving the master equation, one can estimate the average number (n), the average run length and velocity, and the distributions of run length and velocity in the absence of a load force. Similarly, if the cargo is under a load–force, the

transition rates will have load force dependence. We can apply similar analysis by replacing the modified transition rates [59].

2.2 *Bidirectional Transport by Molecular Motors*

In previous discussions, we only considered the unidirectional transport of molecular motors. However, in biological cells, the transport of cargo particles is usually bidirectional in the sense that the cargo particles frequently switch their direction of motion. It is natural to assume that this bidirectional transport arises from the competition of two species of molecular motors; e.g., SVs are transported by UNC-104 (KIF1A) and dynein/dynactin motors. Two scenarios of bidirectional transport have been discussed [60, 61]:

(1) **Tug-of-war**: Two species of motors pull a cargo in its own direction and perform the tug-of-war on the cargo [62–64].
(2) **Coordination**: There exists a putative coordination protein complex that prevents opposite motors from being active at the same time [65].

Here, we will only focus on the tug-of-war model.

2.2.1 Tug-of-War Model of Bidirectional Transport by Molecular Motors

According to the tug-of-war model proposed by Müller et al. [63, 64], suppose a cargo (e.g., SV) is transported along the one-dimensional microtubule via the N_+ plus-end (anterograde) moving motors (such as kinesin-3) and N_- minus end (retrograde) moving motors (such as dynein). At a given time t, the dynamics of the cargo are completely characterized by the numbers n_+ and n_- of plus and minus motors bound to a microtubule and actively pulling the cargo. For simplicity, Müller et al. assume that the motors act independently other than exerting a load on the opposite directional motors. However, some experiments suggest that this situation might be oversimplified, which implies that there might be some direct coupling between plus- and minus motors [66]. This suggests that the properties of the motor–cargo complex depend on the properties of the individual motors together with an effective load on each motor. On the other hand, when a single motor is bound to a microtubule, the velocity of a single molecular motor satisfies an approximately linear velocity–force relationship: i.e., the velocity decreases approximately linearly with the force applied against the movement of the motor.

$$\begin{aligned} v(F) &= v_f\left(1-\frac{F}{F_s}\right), \quad F \le F_s, \\ &= v_b\left(1-\frac{F}{F_s}\right), \quad F \ge F_s, \end{aligned}$$

where F is the applied force, F_s is the stall force satisfying $v(F_s) = 0$, v_f is the forward velocity of the motor in the absence of an applied force, and v_b is the backward velocity of the motor when the applied force exceeds the stall force.

The generalized model with one team of motors described above can be used to study the stochastic tug-of-war bidirectional transport between the plus and minus motors. The cargo is described by the state (n_+, n_-) where n_+ is the number of plus motors attached to the cargo and n_- is the number of minus motors attached to the cargo. The transition between binding or unbinding of a plus or minus motor leads to a random walk on the state space (n_+, n_-). This random walk is described by a master equation

$$\begin{aligned}\frac{\partial}{\partial t}p(n_+, n_-, t) = {} & \varepsilon_+(n_+ + 1, n_-)p(n_+ + 1, n_-, t) \\ & + \varepsilon_+(n_+, n_- + 1)p(n_+, n_- + 1, t) + \pi_+(n_+ \\ & - 1, n_-)p(n_+ - 1, n_-, t) + \pi_+(n_+, n_- \\ & - 1)p(n_+, n_- - 1, t) \\ & + (\pi_+(n_+, n_-) + \pi_-(n_+, n_-) + \varepsilon_+(n_+, n_-) \\ & + \varepsilon_-(n_+, n_-))p(n_+, n_-, t)\end{aligned}$$

where $\varepsilon_+(n_+, n_-)$, $\varepsilon_-(n_+, n_-)$, $\pi_+(n_+, n_-)$ and $\pi_-(n_+, n_-)$ are the binding and unbinding rates for plus or minus motors when the cargo is in the state (n_+, n_-). By solving the master equation, the average numbers of plus and minus motors, and the average velocity, run length, and velocity distribution or run length distribution can be estimated.

2.2.2 ASEP, TASEP Model

The above discussion about bidirectional transport involves a concept in stochastic dynamics called the asymmetric simple exclusion process (ASEP) [67]. Here, we briefly explain the main ideas in the ASEP model. The ASEP model is a simple particle-hopping model. In the ASEP model, a particle can hop from one lattice site to the neighboring one if it is not occupied. "Simple Exclusive" refers to the absence of multiple occupied sites, and "Asymmetric" means the motion of the particle has a preferred direction. The traffic in one dimension is more often studied for a particle that moves along a linear chain of length, L. The model is suitable for many applications, such as modeling highway traffic. If motion is allowed in only one dimension (e.g., right), it is called the totally asymmetric simple exclusion process (TASEP) [68–70]. Denote the probability of motion from site j to $j + 1$ as p. For such driven diffusive systems the boundary conditions are crucial. If we impose the periodic boundary conditions, all of lattice sites are treated equally. If we have open boundaries, then a particle can enter from a reservoir and occupy the leftmost site ($j = 1$), with probability α if this site is empty. In this system a particle

that occupies the rightmost site ($j = L$) can exit with probability β. The ASEP model has been studied extensively, and its stationary state for different dynamics can be obtained exactly. This state leads to an interesting phase diagram with a critical point $(\alpha_c(p), \beta_c(p))$, which is a prototype of a boundary-induced phase transition [71]. Three phases can be distinguished: (a) a low-density phase $(\alpha < \beta, \alpha_c(p))$ (b) a high-density phase $(\beta < \alpha, \beta_c(p))$ and (c) a maximal-current phase $(\alpha > \alpha_c(p), \beta > \beta_c(p))$. In the low-density phase, the current only depends on α, and the current only depends on β in the high-density phase.

The ASEP or TASEP model is easy to apply to computational simulations and theoretical analysis. Various models to study the phenomenon of multi-motor systems have been proposed, including motor-transport processes [72–74], motor-driven diffusive systems [74–77], cellular cargo transport [78, 79], and collective properties of interaction motors [80–82].

3 Structure and Function Investigation of Molecular Motors

The following basic properties of motor proteins are areas of active current research:

a. The number of motors active at one vesicle: minus-end-directed motors (e.g., dynein) and opposing plus-end-directed motors (e.g., kinesin) bind simultaneously to the same cargo, but not all are active and may lead to force unbalance and apparent bidirectional transport.
b. Characterization of motor proteins linked to motility; particularly, the velocity of different motors varies during the binding of motors to cargo.
c. Investigation of the effects of subunits, associated proteins, and adaptors on cargo transport.

These investigations will provide useful information related to neurodegeneration. Recent studies have revealed information about dynein, dynactin, and provided clues about subunits linked to transport ability. Allosteric changes may couple motion and are affected by subunits, adaptors, regulators, ATP, and Microtubule-binding ability [83, 84].

3.1 Dynein/Dynactin Subunits

Although motor protein functions have been investigated, the spatial structures of motor protein complexes remain unclear. For example, why and how dimeric motor proteins move forward or backward along MT-tracks with varying velocities, run

lengths, and other physical parameters are poorly understood because of the lack of structural information on motor-adaptor/regulator-MT complexes.

The migration of cell organelles and mitosis in cell division depends on cell chemistry and physical force provided by MT and motor proteins. A recent study by Tolic–Norrelykke showed that cells prefer longer MT disassembly and detached motor proteins under higher loading force [85].

An RNA interference (RNAi)-based investigation showed that the subunits of dynein/dynactin were crucial for mitotic functions of dynein [86]. Notably, dynein-dependent spindle organization did not require dynactin, but dynactin was essential for dynein recruitment with other regulators, such as Nde1/L1, which leads to both suppressed and enhanced effects of LIS1 on dynein. Dynein inhibition-like phenotypes were because of the depletion of Nde1 or NdeL1 [87–90].

Therefore, a detailed structural information regarding molecular motors and their associations is essential for understanding how motor protein behavior changes in the disease. Figure 1 shows architectures of vertebrate dynein and dynactin complex are proposed by negative-stain and cyro-EM data.

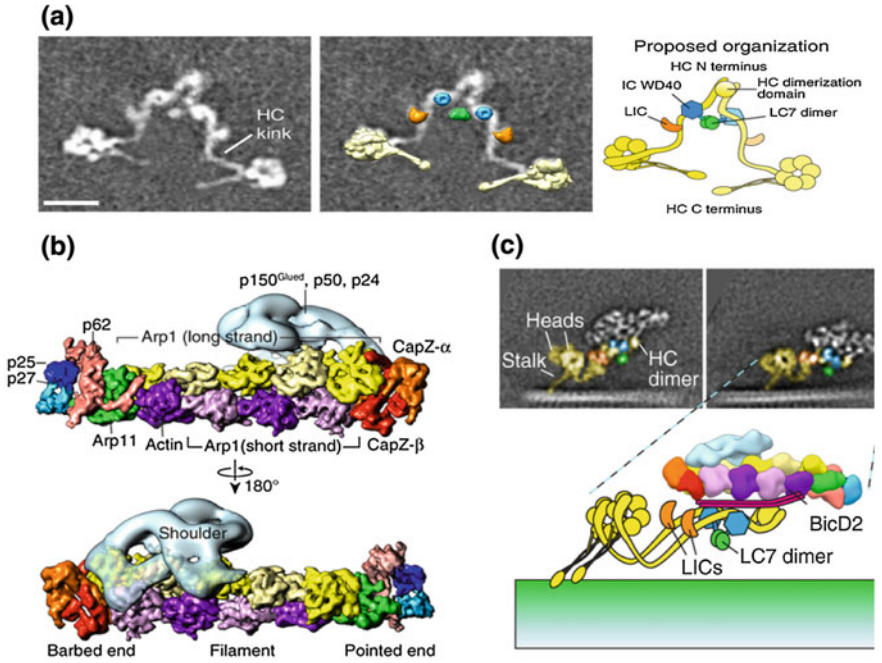

Fig. 1 Subunits in dynein and dynactin complex. **a** A created cartoon from negative-stain of purified dynein dimer represents dynein subunits including heavy chain, light intermediate chain, and intermediate chain. **b** Subunit organization of dynactin is determined by fitting the 6.5-Å cyro-EM data into the created structure from 24-Å-resolution negative-stain. **c** An intact architecture of MT-dynein-BicD2-dynactin. Scale bar, 10 nm. Reprinted by permission from Macmillan Publishers Ltd: Ref. [95] copyright 2015

In animals, the dynein/dynactin complex comprises ATP-driven heavy chain (HC, DYNC1H), light intermediate chain (LIC, DYNC1LI), and intermediate chain (IC, DYNC1I) in dynein (Fig. 1a) and comprises actin-related protein 1 (arp-1, ACTR1), arp-11 (ACTR3b), beta-actin (ACTB), actin-capping protein $\propto/\beta$ heterodimer, p150 (DNC-1, DCTN1), p50 (DNC-2, DCTN2), p22/p24 (DNC-3, DCTN3), p62 (DNC-4, DCTN4), p25 (DNC-5, DCTN5), and p27 (DNC-6, DCTN6) in dynactin (Fig. 1b) [91, 92].

In dynein structures, HC binds to LIC and IC, and IC is associated with light chains (LC), such as LC7 (roadblock, DYLRB), LC8 (DYNLL), and DYLT (tctex, DYNLT); in addition, WD40 domains act as linkers to form LC7 dimers. These associated subunits are components that form the dynein tail domain that binds to cargo [93–95].

Dynactin that has >20 subunits and forms a large structure mediates the binding between cargo, dynein, and possibly MT. The CAP–Gly domain of p150 and its extension (CC1A, CC1B, intercoiled domain, and CC2) can reach a length of almost 50 nm, and the CAP–Gly domain has been reported to interact with the tubulin acidic [96].

Kinesin has been reported to be involved in autoinhibition/autoregulation [97, 98], and dynactin p150 involvement has also been reported. The p150 coiled-coil helical domain 1B (CC1B) is associated with dynein processivity and increases the step size and forwardstep frequency of dynein but decreases microtubule detachment and lateral stepping of dynein. In addition, CC1A can physically interact with CC1B and decrease the advantages of CC1B in dynein processivity [41].

Bicaudal D2, a dynein motility-inducing cargo adaptor, interacts with dynactin and dynein (Fig. 1c). Its coiled-coil structure enables an increased interaction stability of dynein/dynactin [92].

3.2 *RNAi Knockdown at the Cellular Level and in C. Elegans, Drosophila, and Mice*

To explore the individual function of each motor protein subunit, different model organisms have been used for investigation. Primary cells, cell lines, *C. elegans, Drosophila,* and living animals have been used as models in motor protein research. Different in vivo, in vitro*, or* ex vivo approaches have been developed for motor protein studies linked to the disease [99–102].

Genetic methods, such as point mutations, genetic conditional knockout, and RNAi knockdown, are widely used in motor protein research. Particularly, RNAi is a powerful method for large-scale screening by silencing target genes; thus, a single-gene network can be characterized phenotypically and its possible functions can be inferred (Fig. 2) [103–106].

The RNAi approach is used to assess gene function in mice through small interfering RNA (siRNA) delivery or short hairpin RNA (shRNA) expression

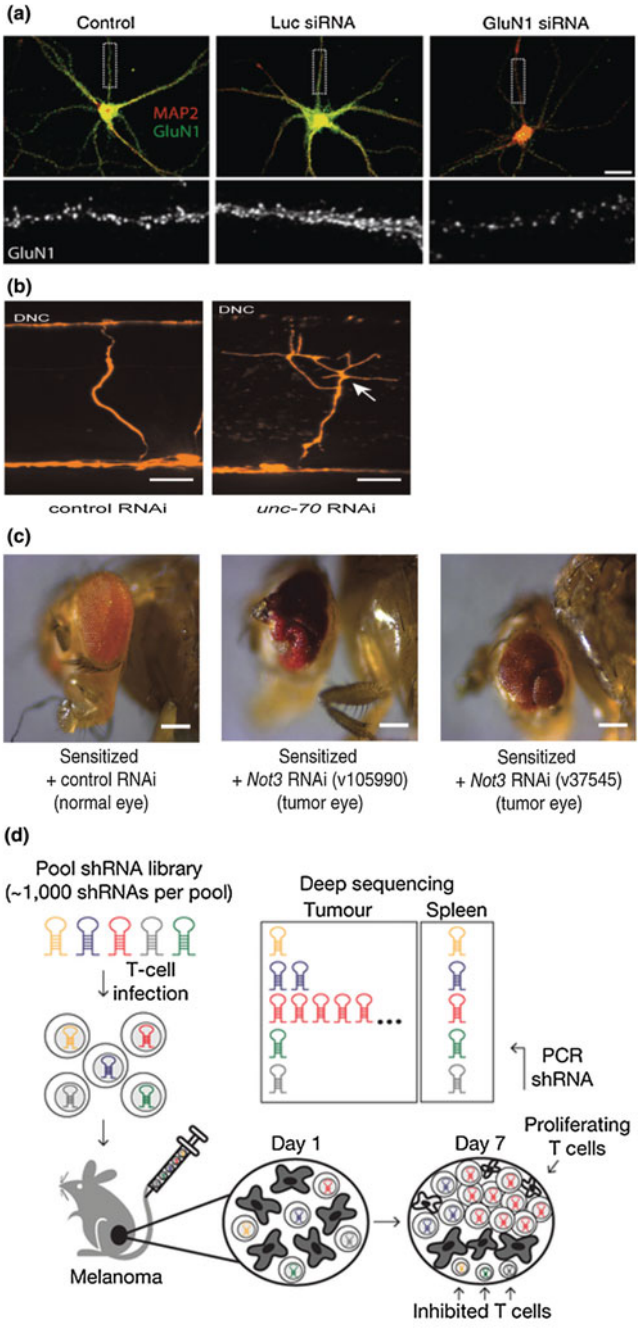
(a)
Control
Luc siRNA
GluN1 siRNA
MAP2
GluN1
GluN1
(b)
DNC
DNC
control RNAi
unc-70 RNAi
(c)
Sensitized
+ control RNAi
(normal eye)
Sensitized
+ Not3 RNAi (v105990)
(tumor eye)
Sensitized
+ Not3 RNAi (v37545)
(tumor eye)
(d)
Pool shRNA library
(~1,000 shRNAs per pool)
T-cell
infection
Deep sequencing
Tumour
Spleen
PCR
shRNA
Day 1
Day 7
Proliferating
T cells
Melanoma
Inhibited T cells

◀ **Fig. 2** The RNA interference employed from cellular level to living organisms. **a** Knockdown in cultured neurons. *Bottom images* from *dashed box* indicate dendrite area. *Right bottom image* indicating a decrease of GluN1 clusters along dendrites by GluN1 siRNA. Scale bar, 20 μm. Reprinted by permission from Macmillan Publishers Ltd: Ref. [103] copyright 2013. **b** *Unc-70* RNAi treatment leads abnormal branched processes and dorsal nerve code (DNC) degeneration in GABA commissures in RNAi-sensitive *C. elegans.* Scale bar, 10 μm. Reprinted by permission from Creative Commons Attribution 4.0 International Public License: [PLoS Genetics] [104] copyright 2013. **c** Using *Not3* RNAi in cancer research indicates that *NOT3* is a tumor suppressor in *Drosophila*. The *right image* shows a tumor eye by *Not3* knockdown. Scale bar, 200 μm. Reprinted by permission from Macmillan Publishers Ltd: [Genetics] [105] copyright 2013. **d** An *in vivo* RNAi screening is approached by shRNA library for T-cell function in mouse tumors. Reprinted by permission from Macmillan Publishers Ltd: [Nature] [106] copyright 2014

controlled by tetracycline (doxycycline)-inducible *Cre*-mediated recombination, which mediates cassette exchange for site-specific insertion. Pain relief has been achieved by siRNA delivered into the rat brain via intrathecal infusion [107]. Systemic siRNA delivery by intravenous injection in mice has been demonstrated by encoded green fluorescent protein (GFP) from pGFP-N3 and its cognate siRNA to silence GFP gene expression in various organs [108–110].

AD modeling has also been performed in *Drosophila.* RNAi-based large-scale screening was used to modify flies carrying Tau-induced toxicity, and 67 genes, including subunits of the dynein/dynactin complex, have been identified from >7000 genes. The results revealed locomotion deficits in the adult stage caused by Tau-induced detrimental effects [111]. In addition, a valuable protocol has been established for the living images of axonal transport in the brain of *Drosophila.* The protocol enables the recording of fluorescently labeled cargoes in both fast and slow axonal transport under physiological conditions [86].

Caenorhabditis elegans is also commonly used for investigations in neuronal disease. Neural map and cell lineage patterns have been well studied in *C. elegans,* which has 302 neurons, >7000 connections, and 959 somatic cells in adult hermaphrodites or 1031 somatic cells in adult males. Therefore, the neural map of *C. elegans* makes it an excellent subject for investigation of motor protein effects on neuronal physiology [112–115].

Currently, RNAi knockdown is widely used in *C. elegans* modeling. Such RNAi is triggered by double-stranded RNA introduced from shRNA or by the L4440 expression vector, an ITPG-inducible plasmid, which expresses dsRNA in the HT115 *Escherichia coli* strain carrying an RNase III deficiency. Once antisense RNA is introduced into the cells, translation of its complementary mRNA is inhibited by matching base pairs [115–120]. The CRISP/Cas9 system has also been used to knockout genes in *C. elegans* [121]. RNAi has exhibited gene suppression in various tissues, such as germ cells and somatic cells, and its effect can persist into the next generation [122]. However, low RNAi sensitivity in most neurons has been reported; therefore, RNAi-sensitive animals or RNAi importers are used for experiments in neurons [123, 124].

In RNAi technology, RNAi-sensitive strains, such as eri-1(mg366) and rrf-3 (pk1426), are significant for gene knockdown in *C. elegans* neurons by shRNA

injection or dsRNA ingestion [104, 125, 126]. In addition, SID-1, a dsRNA-selective importer, triggered by a neuron-specific promotor has also been used to achieve RNAi knockdown in *C. elegans* nerve cells and silkworms [127, 128].

Other valuable technologies for *C. elegans* enhance the utility of combined methods; for example, neuronal cell isolation and axotomy. Ex vivo approaches for neuronal cell isolation from embryos, larvae, and adults have been established for studying cell functions. These are important methods for culturing developing nerve cells from a certain time point and for identifying neurons by the expression of fluorescence markers and by a cellular appearance that includes dendrites, axons, and actin-rich growth cones. Thus, *C. elegans* isolation enables various parameters of isolated neurons to be measured in motor protein studies [129].

Laser axotomy for proteins of interest implicated in axon regeneration and fluorescence recovery after photo bleaching (FRAP), which involves fluorescent particles or dye bleached by high-powered laser, are widely used techniques for studying *C. elegans.* Thus, both techniques are used in vivo and in vitro methods to explore the candidates and collective behavior of motor proteins related to neuronal physiology [130, 131].

3.3 Microfluidic Devices and Essential Techniques for Single-Cell Motor Protein Studies

Devices for single cells and single molecular analysis are well developed and integrated with cross-field techniques, including optical science, imaging systems, material science, microfluidics, biochemistry, electronics, and engineering and are used for varying purposes, such as nucleotide sequencing, protein complex analysis, imaging, organism selection, and quantity control of delivery. The advantages of these devices are that they can facilitate streamlining of routing work, increase operational accuracy, and enable high-throughput screening. Applications of devices related to single cells, single molecules, and cell culture analyzed on-chip are used to achieve specific aims: microfluidics for living cell assays, imaging at single-molecule resolution, cell electroporation for delivery, and organism selection and immobilization (Fig. 3c, d) [132–146].

Furthermore, cultures in microchannels can influence the extension direction of neurites, and parallel channels can provide unidirectional axons from disordered neurites for measurement (Fig. 3a, b) [147–153]. Notably, material science advancements are crucial for microfluidic devices using certain materials, such as plastics, hydrogels, and elastomers. Plastic materials are cheap and common materials in laboratories, and the thermoflexible properties of polystyrene and cyclo-olefin polymers are superior [154]. Hydrogel is a porous material that contains 90 % water of the total mass and allows particles to diffuse through its internal matrix, but its disadvantage of allowing penetration by air severely limits its use

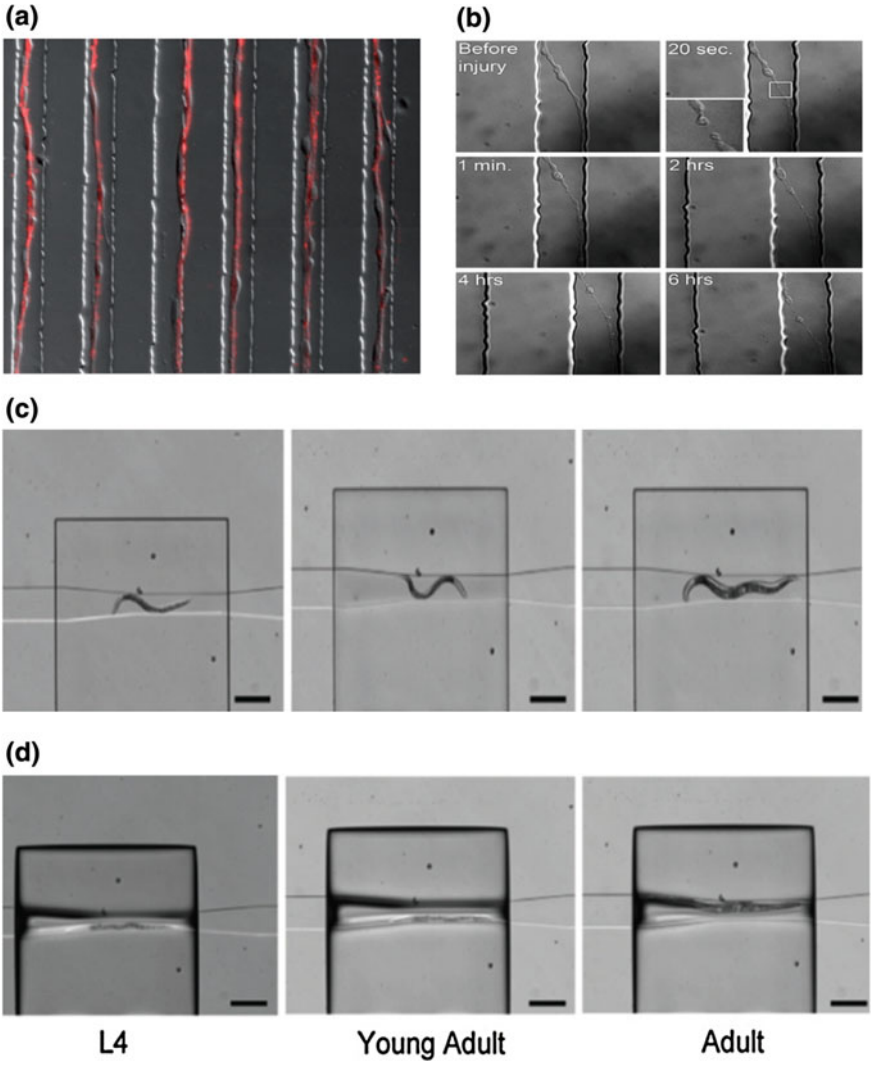

Fig. 3 Microfluidic devices for single neurons and *C. elegans*. **a** Axons of dorsal root ganglion (DRG) neurons from rat pups grow through microchannels. **b** Axon of a rat cortical neuron regenerates in a microchannel after axotomy. Reproduced (**a**) and (**b**) from Ref. [147] by permission of The Royal Society of Chemistry copyright 2009. **c**, **d** To immobilize larval stage and adult *C. elegans* by PDMS with air pressure. **c** Before immobilization. **d** During immobilization. Scale bar, 500 μm. Reproduced (**c**) and (**d**) from Ref. [146] by permission of The Royal Society of Chemistry copyright 2008

[155]. Polydimethylsiloxane (PDMS) is an elastomer that has become more popular than plastic and hydrogel as a frame material and has better optical and mechanical properties for generating scaffolding channels in bio-experiment devices. PDMS is

highly air permeable and nontoxic and can be used for skeletons, elastic membranes, and microvalves [156].

For *C. elegans, Drosophila,* and *Zebrafish* model organisms, customized microfluidic devices are widely used for neuronal transport investigations using PDMS [157]. A PDMS stamp, as its name implies, is used for microcontact printing and enables the creation of microchannels for neurite growth at nm resolution. Thus, a PDMS stamp is a convenient tool for motor protein studies for measurements of neurite length and kymograph recoding [158–160].

For motor protein studies, current approaches, such as high-throughput platforms, transferable neuronal mini-cultures, and transcriptome in vivo analysis (TIVA), are valuable tools. High-throughput clonogenic cultures and single cells are identified through computational methods, and neuronal mini-cultures transferred by microraft plates are useful for isolating neurons from a same culture pool for further use under different conditions, culture times, and reagent treatments and for observation. This array approach notably reduces culture supplies [161, 162]. Moreover, TIVA using a Swiss army knife-type tag is the first in vivo method to capture mRNA from a living cell in a cellular microenvironment that is noninvasive and nondestructive to neighbor cells; therefore, it enables the observation of motor protein mRNA changes in disease models and is effective for pre- and postsynaptic neurons [163].

In addition, optical trapping is an essential technique for single-molecule manipulation to provide physical information about motor proteins. The measurement of active transport of motor proteins in living cells and animals has been reported, particularly concerning the stepping behavior of molecular motors observed by particle tracking [164–166]. The physical parameters obtained from optical trapping provides useful information about the real-time force change between opposed motors; whether there is a stall force, velocity, or stepping dynamics that are motor-amount dependent; and how many valid motor proteins can drive a cargo.

Real-time measurement and time-lamp imaging are also indispensable methods for kymograph analysis, which provides physical parameters, such as run length, running persistence, and velocity, over a given measurement period.

Novel techniques, DNA-based autoassembling backbones, and helix-based scaffold backbones are useful for quantity control of connecting motors for one cargo. In DNA-based autonomous molecular transport devices, DNA oligonucleotides of varying numbers could be exposed to the outside of programmable three-dimensional DNA origami scaffolds. Helix-based scaffold proteins rather than DNA-based backbones have been shown to form in helix structures from myosin VI (10-nm helix), mannosyltransferase MNN4 (20-nm helix), Kelch-motif family proteins (30-nm helix), and repeat Gly–Ser–Gly sequences (60-nm helix). Thus, both methods allow control of the connecting motor type, number, and spatial distance in vitro and have revealed important results showing that the velocity and motor numbers may be unrelated during transport in ensembles of one to seven involving only dynein or kinesin, and two kinesin motors could be activated and

alternate their activities rather than help or impede each other, and motor–cargo responded sensitively to physical force from motors [167–169].

4 Combined Methods for Modeling

We established a flow chart for combined approaches involving the differentiation of pluripotent P19 cells, shRNA knockdown, and shRNA delivery by single-cell DNA delivery devices, neuron cultures in microfluidic chambers, and kymograph generation and analysis using ImageJ. Further physical modeling was performed by fitting experimental data.

4.1 Retinoic Acid (RA)-Induced P19 Neurons

P19 cells, a line of pluripotent embryonal carcinoma cells from *Mus musculus* mice, can be induced by RA (Fig. 4) or Acsl-1 to form neurons, and further neural differentiation is complete in 8 days [170–174]. Motor protein subunits knockdown in P19 neurons has been reported to identify specific roles in neuronal development [175].

The differentiated P19 neurons are suitable material for investigating motor proteins in neurodegenerative disease, and P19 neurons have been demonstrated to extend neurites and make contact with nearby neurons. Recent manipulations have shown that P19 cells could be easily transfected with dsRNA and U6 promoter-derived shRNA by ideal gene delivery approaches, including lipid-mediated lipofection, viral gene delivery agents, polyethyl-polyplexes, and Pluronic® unimers [176–180].

We have used a single-cell DNA delivery device to minimize large DNA consumption, increased cell death caused by high-voltage electric shocks, and transfer of random amounts of DNA into a cell by liposome transfection. Cells that are transfected with uncontrolled dsRNA or shRNA amounts lead to unstable knockdown efficiency. Our device enables in situ transfection with condition in 200 ng, 8 V, and 20 ms pulse and reduced variation in our RNAi knockdown results (Fig. 5) [181–183].

A plasmid carrying a U6 promotor and puromycin selection marker has been used for our investigations of motor protein subunit knockdown. After transfection, a puromycin antibiotic was used for the selection of stably transfected cells, and its titration determined the optimal condition of P19 cell survival. Interestingly, dynactin P150 knockdown exhibited condition- or state-dependent responses: one was a strong response and led to P19 neurite degeneration by puromycin treatment after neurite outgrowth because the transfected cells died under the titer conditions, and another was a gentle response at a lower titer and resulted in increased neurite length in the knockdown neurons relative to that in the control neurons. This result

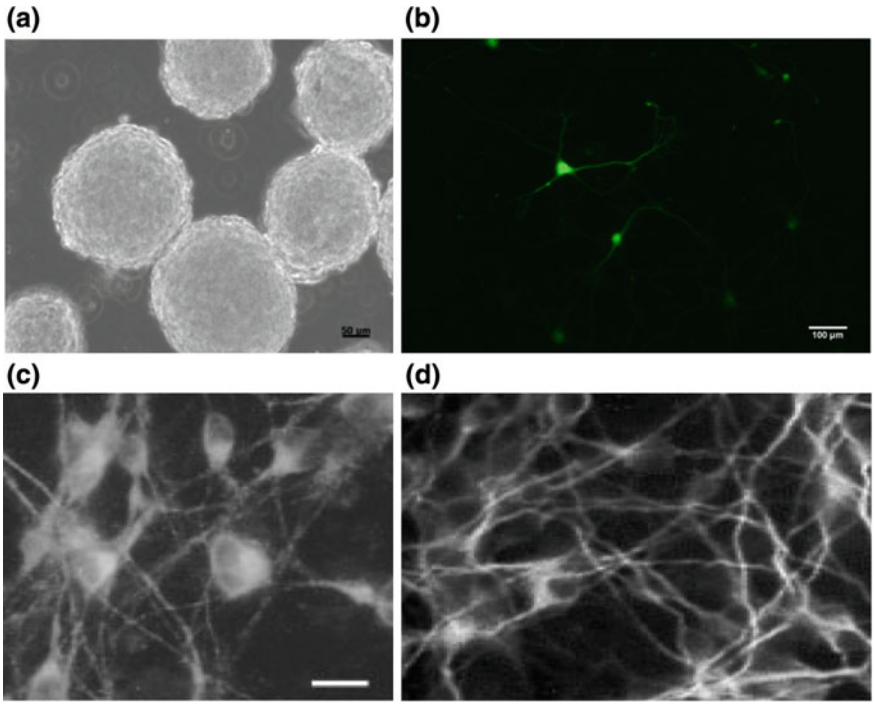

Fig. 4 P19 pluripotent cells differentiated into neurons by retinoic acid (RA). **a** Group P19 cells grown in suspension are spherical after RA induction for 2 days. Scale bar, 50 μm. **b** P19 neurons transfected with pEGFP-N3 exhibit EGFP. Scale bar, 100 μm. **c**, **d** P19 neurons on the day 8 in different rate of neurite outgrowth. **c** Sparse. **d** Dense. Scale bar, 20 μm. Reproduced from Ref. [171] by permission of John Wiley and Sons Ltd., copyright 2007

suggested that different knockdown levels of a subunit reflect the subunit's function caused by other mechanisms and functions hidden by the conditions used for neurite degeneration.

The adjustment of neuron density in culture is necessary for live imaging of axonal transport to avoid overlapping of neurites from different neurons with one another. Neuron culture at low density has been used to show that hippocampal neurons can survive and grow at densities as low as 5000 cells/cm^2 or a well area of 0.95 cm^2 in a 48-well plate [184, 185].

4.2 Growing Neurites in Microchannels

After transfection with shRNA or dsRNA, further analysis of P19 neurons using a PDMS-micropatterned culture system for neurite outgrowth was performed (Fig. 6). For the purpose of generating a kymograph using the ImageJ, a widely used free

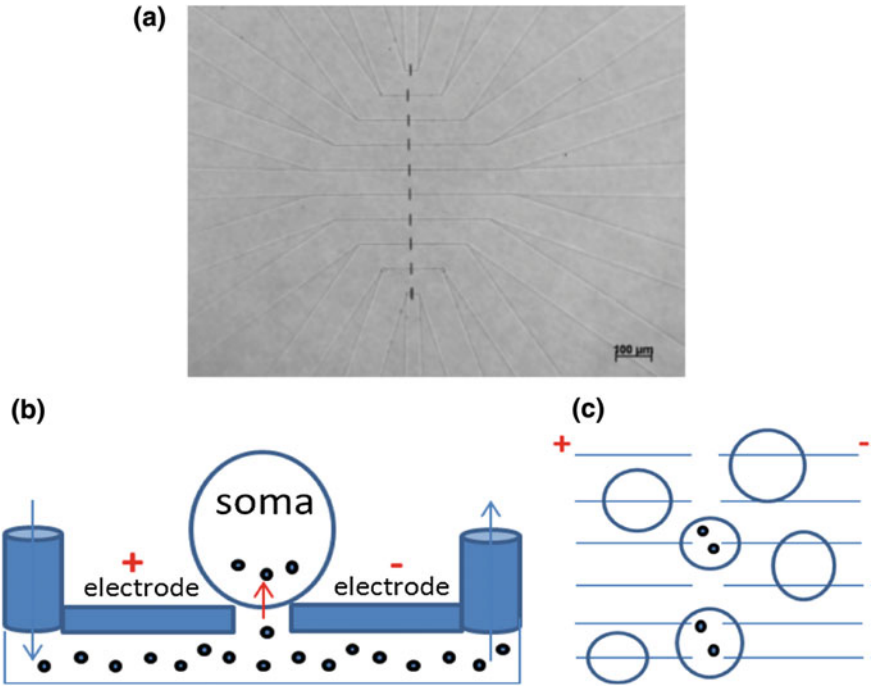

Fig. 5 A single-cell DNA delivery device. **a** The device was designed by Tuhin Santra [183] to enable cell transfection under low-voltage shorter-pulse conditions and enables *in situ* electroporation. The *dashed line* represents gaps between the (+) electrode and (−) electrode where located cells can be introduced with plasmids. Scale bar, 100 μm. **b** *Lateral view* of the device showing the local membrane opening during electric shock and foreign plasmid flow into soma by chance. Cells and the electrode array are located inside the central cup, and liquid is loaded into either cup aside. **c** Only the cells covering the gaps can be transfected by electroporation

software, and its kymograph (time–space plot) plug-in developed by Rietdorf and Seitz [159, 160].

A schema of bidirectional transport is shown in Fig. 7. The kymograph represents bidirectional transport, and individual vesicles are moving or at rest in axons. The polarity of the MT is referred to by plus (+) and minus (−) symbols, and the characteristics of transport showing anterograde transport and retrograde transport are sometimes interrupted by periodic pauses.

To make the kymographs, sequential images were recorded using 100× objectives and appropriate exposure times; for example, a time of 200–500 ms was used to track axonal transport kinetics, and then the time-lapse image was converted into a 2D time–distance graph that showed spatial position over time using a stack of linearized regions of interest (ROIs) from each image (Fig. 7a, b). When using a time–distance graph, physical parameters, such as motor velocity, run length, and pausing time, enable analysis for modeling (Fig. 7c, d).

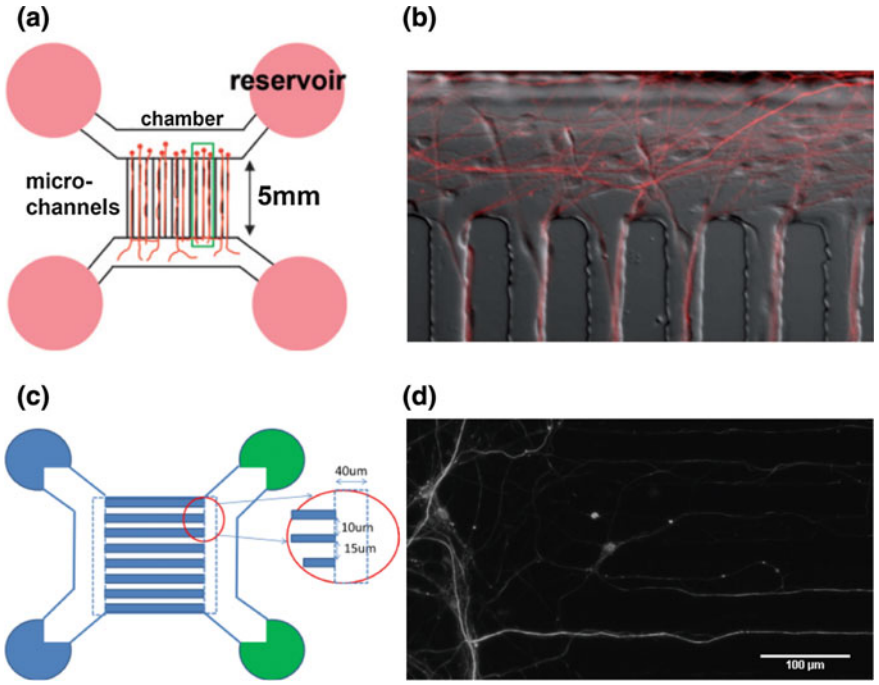

Fig. 6 Neurite extension in microchannels. **a** A schema of a microfluidic device for neurite outgrowth. **b** Axonal growth of DRG neurons through microchannels. **c** A modified chamber from the design [158] for primary cells and differentiated P19 neurons. **d** Neurites extend along microchannels. Reproduced (**a**) and (**b**) from Ref. [147] by permission of The Royal Society of Chemistry copyright 2009

4.3 ARP, A Three-States Transition Model of Cargo's Motion

The tug-of-war model and coordination model are microscopic models of cargo motion that enable studying the collective behavior of molecular motors under the assumption that motors are independent of each other. However, biological processes are always stochastic and involve complex regulation mechanisms. Previously, our understanding of cargo motion has been limited. To develop reasonable models for studying the regulating mechanisms underlying cargo motion, it is necessary to focus on some key features and simplify the methods used to describe such a system. Thus, we propose a mathematical model called the ARP three-state transition model, which simplifies the trajectories of cargo motion into the state sequence with time. Because cargo motion depends on the total effect of motors, we suppose that the direction of cargo motion is determined by the type of leading motor. The modes of single cargo motion can be simplified into three states: a mode involving kinesin is called the anterograde state (A state), the mode

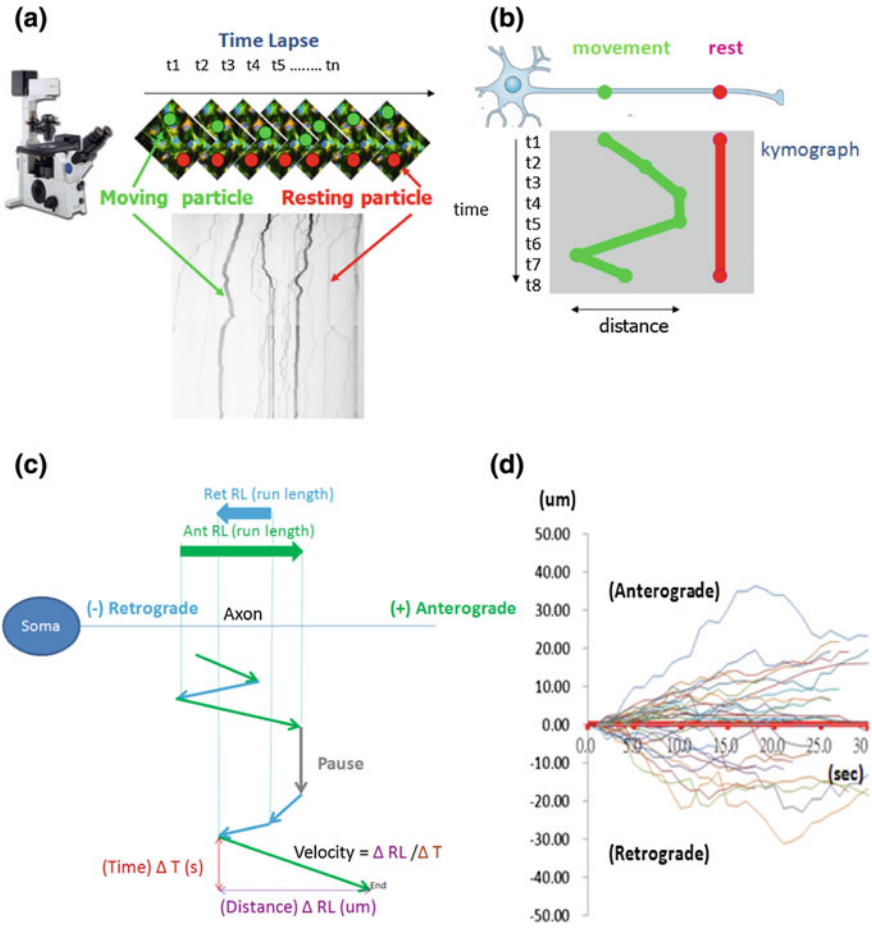

Fig. 7 Illustration of a 2D time–distance graph. **a** Time-lapse recording of motor proteins moving a single neurite and **b** creation of an region of interest (ROI) from an image stack into a 2D time–distance graph. *Green tracks* represent a moving particle and *red tracks* represent a resting particle. **c** Definitions of physical parameters used in the kymograph, including run length, running time, and velocity. **d** *Tracking map* showing the dynamics of each particle

involving dynein is called the retrograde state (R state), and the mode involving no motion is the pausing state (P state).

Figure 8 shows a cargo's trajectory divided into a time sequence of the moving state. The upper part is the trajectory of a cargo, and the lower part is the time sequence of the cargo's motion. Such a transformation can simplify a cargo's trajectory from a set position into a state sequence. Although the position and velocity information are absent in this approach, the state sequence shows moving state dynamics more clearly. Such a sequence implies a three-state transition system that represents the cargo motion in an axon. To study biological regulation

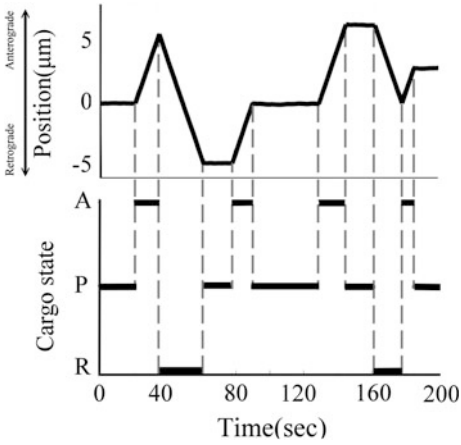

Fig. 8 Motion state transform of cargo. The *upper diagram* is the trajectory of a single cargo in which we set the anterograde direction as the positive direction. The *lower diagram* is the corresponding mode state sequence

mechanisms that could affect cargo motion, we can construct a regulation concept combined with the transition process of ARP states. A hypothetical regulation diagram would require some statistical features of the ARP sequence and fitting of the statistical properties to the experimental data so that the effectiveness of the hypothetical regulation mechanism could be tested.

Figure 9a is the cargo motion diagram in a state transition. There are three phases: cargo in the soma, cargo transport between the soma and axon, and cargo in the axon. Here we show that the cargo in the axon is described by an APR three-state stochastic transition dynamic process. In the APR dynamic process, each state has a transition rate from itself to another state.

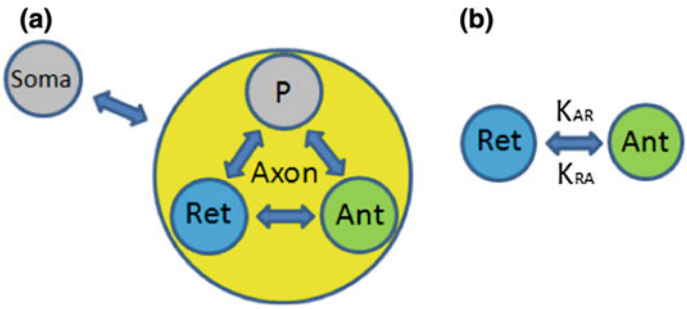

Fig. 9 ARP three-states transition system. **a** shows the diagram of a cargo's motion in a cell. **b** shows a part of the transition diagram to demonstrate the two-state transition case. The time distribution is an exponential decay type $\left((1-\mathrm{k})^{\mathrm{t}} = \mathrm{e}^{-\ln\left(\frac{1}{1-\mathrm{k}}\right)\mathrm{t}}\right)$, and a characteristic time scale is $1/\ln\left(\frac{1}{1-\mathrm{k}}\right)$, which is a measurable quantity that could be compared with experiments

Figure 9b is a simple case of only R and A state transition diagrams, and the R state has a transition rate k_{RA} to the A state, and the A state has a transition rate k_{AR} to the R state. In the stationary process, the staying time probability of the time that the R state maintain its state $\tau_R(t) = (1 - k_{RA})^t$, it is similar for A state, which is $\tau_A(t) = (1 - k_{AR})^t$. Because the staying time distribution exhibits exponential decay $\left((1-k)^t = e^{\frac{-t}{T}}\right)$, the characteristic of time scale is $T = 1/\ln\left(\frac{1}{1-k}\right)$, and it is a measurable quantity. Therefore, it could be compared with the mean staying time from experiments. For example, in stationary case, the average persistence time is 1.1 means the total transition rate k is 0.6.

The hypothetical regulation process in the Fig. 10a hypothesis involves a subunit of a molecular motor complex that may affect the transition process from cell body to axon, but that may also enhance the ARP transition. In realistic experiments, if this subunit is removed or mutated, the flux of cargo and the mean staying time of the ARP state are impaired or enhanced. Therefore, the regulation diagram can be confirmed in this way.

Figure 10b shows another hypothetical regulation diagram. M is a random factor that can enhance the transition rate k stochastically. Some subunits in a motor complex can regulate the regulation power of M. In such a system, if we remove this subunit from the motor complex, the regulation power of M to the transition rate *k* should become weaker. Under such a condition, the fluctuation in the transition rate becomes small, which also implies that the fluctuation in the residence time distribution becomes small.

The last two examples show how to create a hypothetical model to test the real regulation network of cargo motion. The use of this model-creation method may facilitate studies that provide greater insights into cargo motion and their underlying regulation mechanisms.

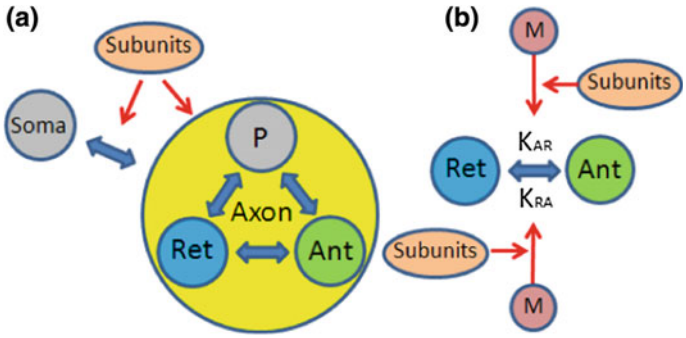

Fig. 10 Hypothetical regulation diagram. **a** shows a hypothetical regulation diagram for a subunit of a motor complex that could affect the process of cargo. **b** shows another hypothetical regulation diagram of a subunit of a motor complex that could regulate fluctuation of the transition process

5 Summary

Patients with irreversible neurodegenerative diseases suffer during their lives. Protein accumulation, particularly, is known to lead to neuron death. Therefore, greater understanding of the traffic mechanism in nerve cells is considered to be a good approach for developing treatments for these diseases. In our investigations, we combine different methods to illustrate how cross-field techniques, including the use of P19 neurons, single-cell DNA delivery devices, microchannel platforms, and kymograph data analysis for physical modeling, can enable the characterization of fundamental properties of neurodegenerative disease mechanisms.

Acknowledgments We thank Dr. Fan-Gang Tseng and Dr. Tuhin Subhra Santra for cell maintenance and cell transfection, Dr. Eric Hwang for P19 cells instruction and material support, Dr. Chien-Wen Chung for nonviral delivery instruction, King & Queen Entertainment Inc. for funding, Academic Sinica for the RNAi library, and Enago (www.enago.tw) for the English language review.

References

1. Dendrou CA, Fugger L (2014) Please mind the gap: axonal transport deficits in multiple sclerosis neurodegeneration. Neuron 84(6):1105–1107
2. Bates G (2003) Huntingtin aggregation and toxicity in Huntington's disease. Lancet 361 (9369):1642–1644
3. Bucciantini M et al (2004) Prefibrillar amyloid protein aggregates share common features of cytotoxicity. J Biol Chem 279(30):31374–31382
4. Pedersen JT, Heegaard NH (2013) Analysis of protein aggregation in neurodegenerative disease. Anal Chem 85(9):4215–4227
5. Rodolfo C et al (2010) Proteomic analysis of mitochondrial dysfunction in neurodegenerative diseases. Expert Rev Proteomics 7(4):519–542
6. Ross CA, Poirier MA (2005) Opinion: What is the role of protein aggregation in neurodegeneration? Nat Rev Mol Cell Biol 6(11):891–898
7. Selkoe DJ (2004) Cell biology of protein misfolding: the examples of Alzheimer's and Parkinson's diseases. Nat Cell Biol 6(11):1054–1061
8. Stefani M, Dobson CM (2003) Protein aggregation and aggregate toxicity: new insights into protein folding, misfolding diseases and biological evolution. J Mol Med (Berl) 81(11):678–699
9. Sorbara CD et al (2014) Pervasive axonal transport deficits in multiple sclerosis models. Neuron 84(6):1183–1190
10. Wang ZX, Tan L, Yu JT (2014) Axonal transport defects in Alzheimer's disease. Mol Neurobiol 51(3):1309–1321
11. Baloh RH et al (2007) Altered axonal mitochondrial transport in the pathogenesis of Charcot-Marie-Tooth disease from mitofusin 2 mutations. J Neurosci 27(2):422–430
12. Ebbing B et al (2008) Effect of spastic paraplegia mutations in KIF5A kinesin on transport activity. Hum Mol Genet 17(9):1245–1252
13. Hurd DD, Saxton WM (1996) Kinesin mutations cause motor neuron disease phenotypes by disrupting fast axonal transport in Drosophila. Genetics 144(3):1075–1085
14. LaMonte BH et al (2002) Disruption of dynein/dynactin inhibits axonal transport in motor neurons causing late-onset progressive degeneration. Neuron 34(5):715–727

15. d'Ydewalle C et al (2011) HDAC6 inhibitors reverse axonal loss in a mouse model of mutant HSPB1-induced Charcot-Marie-Tooth disease. Nat Med 17(8):968–974
16. Hirokawa N, Tanaka Y (2015) Kinesin superfamily proteins (KIFs): various functions and their relevance for important phenomena in life and diseases. Exp Cell Res 334(1):16–25
17. Homma N et al (2003) Kinesin superfamily protein 2A (KIF2A) functions in suppression of collateral branch extension. Cell 114(2):229–239
18. Rath O, Kozielski F (2012) Kinesins and cancer. Nat Rev Cancer 12(8):527–539
19. Iemura K, Tanaka K (2015) Chromokinesin kid and kinetochore kinesin CENP-E differentially support chromosome congression without end-on attachment to microtubules. Nat Commun 6:6447
20. Hirokawa N, Niwa S, Tanaka Y (2010) Molecular motors in neurons: transport mechanisms and roles in brain function, development, and disease. Neuron 68(4):610–638
21. Maday S et al (2014) Axonal transport: cargo-specific mechanisms of motility and regulation. Neuron 84(2):292–309
22. Franker MA, Hoogenraad CC (2013) Microtubule-based transport—basic mechanisms, traffic rules and role in neurological pathogenesis. J Cell Sci 126(Pt 11):2319–2329
23. Niwa S, Takahashi H, Hirokawa N (2013) β-Tubulin mutations that cause severe neuropathies disrupt axonal transport. EMBO J 32(10):1352–1364
24. van der Vaart B et al (2013) CFEOM1-associated kinesin KIF21A is a cortical microtubule growth inhibitor. Dev Cell 27(2):145–160
25. Roberts AJ et al (2013) Functions and mechanics of dynein motor proteins. Nat Rev Mol Cell Biol 14(11):713–726
26. Hook P, Vallee RB (2006) The dynein family at a glance. J Cell Sci 119(Pt 21):4369–4371
27. Myers KA et al (2006) Antagonistic forces generated by cytoplasmic dynein and myosin-II during growth cone turning and axonal retraction. Traffic 7(10):1333–1351
28. Blisnick T et al (2014) The intraflagellar transport dynein complex of trypanosomes is made of a heterodimer of dynein heavy chains and of light and intermediate chains of distinct functions. Mol Biol Cell 25(17):2620–2633
29. Vallee RB, Faulkner NE, Tai CY (2000) The role of cytoplasmic dynein in the human brain developmental disease lissencephaly. Biochim Biophys Acta 1496(1):89–98
30. Brown JM, Witman GB (2014) Cilia and diseases. Bioscience 64(12):1126–1137
31. Yuan S, Sun Z (2013) Expanding horizons: ciliary proteins reach beyond cilia. Annu Rev Genet 47:353–376
32. Lobo J, Zariwala MA, Noone PG (2015) Primary ciliary dyskinesia. Semin Respir Crit Care Med 36(2):169–179
33. Cianfrocco MA, Leschziner AE (2014) Traffic control: adaptor proteins guide dynein-cargo takeoff. EMBO J 33(17):1845–1846
34. Stuchell-Brereton MD et al (2011) Functional interaction between dynein light chain and intermediate chain is required for mitotic spindle positioning. Mol Biol Cell 22(15):2690–2701
35. Rao L et al (2013) The yeast dynein Dyn2-Pac11 complex is a dynein dimerization/processivity factor: structural and single-molecule characterization. Mol Biol Cell 24(15):2362–2377
36. Maier KC et al (2008) Dynamitin mutagenesis reveals protein-protein interactions important for dynactin structure. Traffic 9(4):481–491
37. Carpenter BS et al (2015) The heterotrimeric kinesin-2 complex interacts with and regulates GLI protein function. J Cell Sci 128(5):1034–1050
38. Mandelkow E, Mandelkow EM (2002) Kinesin motors and disease. Trends Cell Biol 12 (12):585–591
39. Landers JE et al (2009) Reduced expression of the kinesin-associated protein 3 (KIFAP3) gene increases survival in sporadic amyotrophic lateral sclerosis. Proc Natl Acad Sci U S A 106(22):9004–9009
40. Chua JJ, Jahn R, Klopfenstein DR (2013) Managing intracellular transport. Worm 2(1): e21564

41. Tripathy SK et al (2014) Autoregulatory mechanism for dynactin control of processive and diffusive dynein transport. Nat Cell Biol 16(12):1192–1201
42. Wang S et al (2013) Nudel/NudE and Lis1 promote dynein and dynactin interaction in the context of spindle morphogenesis. Mol Biol Cell 24(22):3522–3533
43. Neveling K et al (2013) Mutations in BICD2, which encodes a golgin and important motor adaptor, cause congenital autosomal-dominant spinal muscular atrophy. Am J Hum Genet 92 (6):946–954
44. Tai CY et al (2002) Role of dynein, dynactin, and CLIP-170 interactions in LIS1 kinetochore function. J Cell Biol 156(6):959–968
45. Vallee RB, McKenney RJ, Ori-McKenney KM (2012) Multiple modes of cytoplasmic dynein regulation. Nat Cell Biol 14(3):224–230
46. Wynshaw-Boris A, Gambello MJ (2001) LIS1 and dynein motor function in neuronal migration and development. Genes Dev 15(6):639–651
47. Vallee RB, Tsai JW (2006) The cellular roles of the lissencephaly gene LIS1, and what they tell us about brain development. Genes Dev 20(11):1384–1393
48. Tai AW et al (1999) Rhodopsin's carboxy-terminal cytoplasmic tail acts as a membrane receptor for cytoplasmic dynein by binding to the dynein light chain Tctex-1. Cell 97(7):877–887
49. Aboud O et al (2015) Aging, Alzheimer's, and APOE genotype influence the expression and neuronal distribution patterns of microtubule motor protein dynactin-P50. Front Cell Neurosci 9:103
50. Ikenaka K et al (2013) dnc-1/dynactin 1 knockdown disrupts transport of autophagosomes and induces motor neuron degeneration. PLoS ONE 8(2):e54511
51. Tanaka F et al (2012) Neuropathology and omics in motor neuron diseases. Neuropathology 32(4):458–462
52. Ikenaka K et al (2012) Disruption of axonal transport in motor neuron diseases. Int J Mol Sci 13(1):1225–1238
53. Levy JR et al (2006) A motor neuron disease-associated mutation in p150Glued perturbs dynactin function and induces protein aggregation. J Cell Biol 172(5):733–745
54. Puls I et al (2005) Distal spinal and bulbar muscular atrophy caused by dynactin mutation. Ann Neurol 57(5):687–694
55. Chevalier-Larsen ES et al (2008) Lysosomal proliferation and distal degeneration in motor neurons expressing the G59S mutation in the p150Glued subunit of dynactin. Hum Mol Genet 17(13):1946–1955
56. Feynman R, Leighton R, Sands M (1963) The Feynman lectures on physics: Chap. 46, Ratchet and pawl, vol 1
57. Bressloff PC, Newby JM (2013) Stochastic models of intracellular transport. Rev Mod Phys 85:135–196
58. Reimann P (2002) Brownian motors: noisy transport far from equilibrium. Phys Rep 361 (2):57–265
59. Lipowsky R et al (2010) Cooperative behavior of molecular motors: cargo transport and traffic phenomena. Physica E 42:649–661
60. Gross SP (2004) Hither and yon: a review of bi-directional microtubule-based transport. Phys Biol 1(1–2):R1–R11
61. Welte MA (2004) Bidirectional transport along microtubules. Curr Biol 14(13):R525–R537
62. Müller M (2008) Bidirectional transport by molecular motors, PhD thesis
63. Muller MJ, Klumpp S, Lipowsky R (2008) Tug-of-war as a cooperative mechanism for bidirectional cargo transport by molecular motors. Proc Natl Acad Sci U S A 105(12):4609–4614
64. Muller MJI, Klumpp S, Reinhard L (2008) Motility states of molecular motors engaged in a stochastic tug-of-war. J Stat Phys 133:1059–1081
65. Guerin T et al (2010) Coordination and collective properties of molecular motors: theory. Curr Opin Cell Biol 22(1):14–20

66. Driver JW et al (2010) Coupling between motor proteins determines dynamic behaviors of motor protein assemblies. Phys Chem Chem Phys 12(35):10398–10405
67. Chowdhury D, Schadschneider A, Katsuhiro NK (2005) Physics of transport and traffic phenomena in biology: from molecular motors and cells to organisms. Phys Life Rev 2 (4):318–352
68. Derrida B, Domany E, Mukamel D (1992) An exact solution of a one-dimensional asymmetric exclusion model with open boundaries. J Stat Phys 69:667–687
69. Derrida B et al (1993) Exact solution of a 1D asymmetric exclusion model using a matrix formulation. J Phys A Math Gen 26(7):1493
70. Gorissen M et al (2012) Exact current statistics of the asymmetric simple exclusion process with open boundaries. Phys Rev Lett 109(17):170601
71. Krug J (1991) Boundary-induced phase transitions in driven diffusive systems. Phys Rev Lett 67(14):1882–1885
72. O'Loan OJ, Evans MR, Cates ME (1998) Jamming transition in a homogeneous one-dimensional system: the bus route model. Phys Rev E 58(2):1404
73. Neri I, Kern N, Parmeggiani A (2011) The totally asymmetric simple exclusion process on networks. Phys Rev Lett 107(6):068702
74. Popkov V, Schutz GM (2003) Shocks and excitation dynamics in a driven diffusive two-channel system. J Stat Phys 112:523–540
75. Evans MR et al (1995) Spontaneous symmetry breaking in a one dimensional driven diffusive system. Phys Rev Lett 74(2):208–211
76. Evans MR et al (1995) Asymmetric exclusion model with two species: spontaneous symmetry breaking. J Stat Phys 80:69–102
77. Evans MR et al (1998) Phase separation in one-dimensional driven diffusive systems. Phys Rev Lett 80(3):425
78. Muhuri S, Pagonabarraga I (2010) Lattice-gas model for active vesicle transport by molecular motors with opposite polarities. Phys Rev E Stat Nonlin Soft Matter Phys 82(2 Pt 1):021925
79. Muhuri S, Shagolsem L, Rao M (2011) Bidirectional transport in a multispecies totally asymmetric exclusion-process model. Phys Rev E Stat Nonlin Soft Matter Phys 84(3 Pt 1):031921
80. Campas O et al (2006) Collective dynamics of interacting molecular motors. Phys Rev Lett 97(3):038101
81. Pinkoviezky I, Gov NS (2013) Modelling interacting molecular motors with an internal degree of freedom. New J Phys 15(2):025009
82. Teimouri H, Kolomeisky AB, Mehrabiani K (2015) Theoretical analysis of dynamic processes for interacting molecular motors. J Phys A Math Theor 48(6):065001
83. DeBerg HA et al (2013) Motor domain phosphorylation modulates kinesin-1 transport. J Biol Chem 288(45):32612–32621
84. Milic B et al (2014) Kinesin processivity is gated by phosphate release. Proc Natl Acad Sci U S A 111(39):14136–14140
85. Tolic-Norrelykke IM (2010) Force and length regulation in the microtubule cytoskeleton: lessons from fission yeast. Curr Opin Cell Biol 22(1):21–28
86. Raaijmakers JA, Tanenbaum ME, Medema RH (2013) Systematic dissection of dynein regulators in mitosis. J Cell Biol 201(2):201–215
87. Yeh TY et al (2013) Dynactin helps target Polo-like kinase 1 to kinetochores via its left-handed beta-helical p27 subunit. EMBO J 32(7):1023–1035
88. Zylkiewicz E et al (2011) The N-terminal coiled-coil of Ndel1 is a regulated scaffold that recruits LIS1 to dynein. J Cell Biol 192(3):433–445
89. Yamada M et al (2008) LIS1 and NDEL1 coordinate the plus-end-directed transport of cytoplasmic dynein. EMBO J 27(19):2471–2483
90. Huang J et al (2012) Lis1 acts as a "clutch" between the ATPase and microtubule-binding domains of the dynein motor. Cell 150(5):975–986

91. Imai H et al (2014) Dynactin 3D structure: implications for assembly and dynein binding. J Mol Biol 426(19):3262–3271
92. Urnavicius L et al (2015) The structure of the dynactin complex and its interaction with dynein. Science 347(6229):1441–1446
93. Allan V (2014) Cell biology. One, two, three, cytoplasmic dynein is go! Science 345 (6194):271–272
94. Rapali P et al (2011) DYNLL/LC8: a light chain subunit of the dynein motor complex and beyond. FEBS J 278(17):2980–2996
95. Chowdhury S et al (2015) Structural organization of the dynein-dynactin complex bound to microtubules. Nat Struct Mol Biol 22(4):345–347
96. Wang Q et al (2014) Structural basis for the extended CAP-Gly domains of p150(glued) binding to microtubules and the implication for tubulin dynamics. Proc Natl Acad Sci U S A 111(31):11347–11352
97. Moua P et al (2011) Kinesin-1 tail autoregulation and microtubule-binding regions function in saltatory transport but not ooplasmic streaming. Development 138(6):1087–1092
98. Huo L et al (2012) The CC1-FHA tandem as a central hub for controlling the dimerization and activation of kinesin-3 KIF1A. Structure 20(9):1550–1561
99. Pandey JP, Smith DS (2011) A Cdk5-dependent switch regulates Lis1/Ndel1/dynein-driven organelle transport in adult axons. J Neurosci 31(47):17207–17219
100. Karle KN et al (2012) Axonal transport deficit in a KIF5A(–/–) mouse model. Neurogenetics 13(2):169–179
101. Uchida A, Alami NH, Brown A (2009) Tight functional coupling of kinesin-1A and dynein motors in the bidirectional transport of neurofilaments. Mol Biol Cell 20(23):4997–5006
102. Godena VK et al (2014) Increasing microtubule acetylation rescues axonal transport and locomotor deficits caused by LRRK2 Roc-COR domain mutations. Nat Commun 5:5245
103. Rungta RL et al (2013) Lipid nanoparticle delivery of siRNA to silence neuronal gene expression in the brain. Mol Ther Nucleic Acids 2:e136
104. Firnhaber C, Hammarlund M (2013) Neuron-specific feeding RNAi in *C. elegans* and its use in a screen for essential genes required for GABA neuron function. PLoS Genet 9(11): e1003921
105. De Keersmaecker K et al (2013) Exome sequencing identifies mutation in CNOT3 and ribosomal genes RPL5 and RPL10 in T-cell acute lymphoblastic leukemia. Nat Genet 45 (2):186–190
106. Zhou P et al (2014) In vivo discovery of immunotherapy targets in the tumour microenvironment. Nature 506(7486):52–57
107. Dorn G et al (2004) siRNA relieves chronic neuropathic pain. Nucleic Acids Res 32(5):e49
108. Sorensen DR, Leirdal M, Sioud M (2003) Gene silencing by systemic delivery of synthetic siRNAs in adult mice. J Mol Biol 327(4):761–766
109. Kleinhammer A, Wurst W, Kuhn R (2010) Gene knockdown in the mouse through RNAi. Methods Enzymol 477:387–414
110. Leng Q et al (2009) Advances in systemic siRNA delivery. Drugs Future 34(9):721
111. Butzlaff M et al (2015) Impaired retrograde transport by the Dynein/Dynactin complex contributes to Tau-induced toxicity. Hum Mol Genet ddv107
112. Liu OW, Shen K (2012) The transmembrane LRR protein DMA-1 promotes dendrite branching and growth in *C. elegans*. Nat Neurosci 15(1):57–63
113. Sulston JE, Horvitz HR (1977) Post-embryonic cell lineages of the nematode, *Caenorhabditis elegans*. Dev Biol 56(1):110–156
114. Kimble J, Hirsh D (1979) The postembryonic cell lineages of the hermaphrodite and male gonads in *Caenorhabditis elegans*. Dev Biol 70(2):396–417
115. Felix MA (2008) RNA interference in nematodes and the chance that favored Sydney Brenner. J Biol 7(9):34
116. Fraser AG et al (2000) Functional genomic analysis of *C. elegans* chromosome I by systematic RNA interference. Nature 408(6810):325–330

117. Kim JK et al (2005) Functional genomic analysis of RNA interference in *C. elegans*. Science 308(5725):1164–1167
118. Lehrbach NJ, Miska EA (2008) Functional genomic, computational and proteomic analysis of *C. elegans* microRNAs. Brief Funct Genomic Proteomic 7(3):228–235
119. Devanapally S, Ravikumar S, Jose AM (2015) Double-stranded RNA made in *C. elegans* neurons can enter the germline and cause transgenerational gene silencing. Proc Natl Acad Sci U S A 112(7):2133–2138
120. Fischer SE (2010) Small RNA-mediated gene silencing pathways in *C. elegans*. Int J Biochem Cell Biol 42(8):1306–1315
121. Waaijers S et al (2013) CRISPR/Cas9-targeted mutagenesis in *Caenorhabditis elegans*. Genetics 195(3):1187–1191
122. Fireman E et al (1998) Predictive value of response to treatment of T-lymphocyte subpopulations in idiopathic pulmonary fibrosis. Eur Respir J 11(3):706–711
123. Kamath RS et al (2001) Effectiveness of specific RNA-mediated interference through ingested double-stranded RNA in *Caenorhabditis elegans*. Genome Biol 2(1): RESEARCH0002
124. Timmons L, Court DL, Fire A (2001) Ingestion of bacterially expressed dsRNAs can produce specific and potent genetic interference in *Caenorhabditis elegans*. Gene 263(1–2):103–112
125. Ohkumo T et al (2008) Use of RNAi in *C. elegans*. Methods Mol Biol 442:129–137
126. Kuwahara T et al (2008) A systematic RNAi screen reveals involvement of endocytic pathway in neuronal dysfunction in alpha-synuclein transgenic *C. elegans*. Hum Mol Genet 17(19):2997–3009
127. Calixto A et al (2010) Enhanced neuronal RNAi in *C. elegans* using SID-1. Nat Methods 7 (7):554–559
128. Xu J et al (2014) Establishment of *Caenorhabditis elegans* SID-1-dependent DNA delivery system in cultured silkworm cells. Mol Biotechnol 56(3):193–198
129. Zhang S, Banerjee D, Kuhn JR (2011) Isolation and culture of larval cells from *C. elegans*. PLoS ONE 6(4):e19505
130. Nix P et al (2014) Axon regeneration genes identified by RNAi screening in *C. elegans*. J Neurosci 34(2):629–645
131. Bourgeois F, Ben-Yakar A (2008) Femtosecond laser nanoaxotomy properties and their effect on axonal recovery in *C. elegans*. Opt Express 16(8):5963
132. Martins SA et al (2012) Towards the miniaturization of GPCR-based live-cell screening assays. Trends Biotechnol 30(11):566–574
133. Shen J et al (2015) A microfluidic live cell assay to study anthrax toxin induced cell lethality assisted by conditioned medium. Sci Rep 5:8651
134. DuFort C, Paszek M (2014) Nanoscale cellular imaging with scanning angle interference microscopy. Methods Cell Biol 123:235–252
135. Streets AM et al (2014) Imaging without fluorescence: nonlinear optical microscopy for quantitative cellular imaging. Anal Chem 86(17):8506–8513
136. Wei L et al (2014) Live-cell imaging of alkyne-tagged small biomolecules by stimulated Raman scattering. Nat Methods 11(4):410–412
137. Hewapathirane DS, Haas K (2008) Single cell electroporation in vivo within the intact developing brain. J Vis Exp (17)
138. Kitamura K et al (2008) Targeted patch-clamp recordings and single-cell electroporation of unlabeled neurons in vivo. Nat Methods 5(1):61–67
139. Wang HY, Lu C (2006) High-throughput and real-time study of single cell electroporation using microfluidics: effects of medium osmolarity. Biotechnol Bioeng 95(6):1116–1125
140. Wang S, Lee LJ (2013) Micro-/nanofluidics based cell electroporation. Biomicrofluidics 7 (1):11301
141. Streets AM, Huang Y (2014) Microfluidics for biological measurements with single-molecule resolution. Curr Opin Biotechnol 25:69–77

142. Wang Z et al (2014) Micro-/nanofluidic device for tunable generation of a concentration gradient: application to *Caenorhabditis elegans* chemotaxis. Anal Bioanal Chem 406 (11):2679–2686
143. Xian B et al (2013) WormFarm: a quantitative control and measurement device toward automated *Caenorhabditis elegans* aging analysis. Aging Cell 12(3):398–409
144. San-Miguel A, Lu H (2013) Microfluidics as a tool for *C. elegans* research. WormBook, pp 1–19
145. Rohde CB et al (2007) Microfluidic system for on-chip high-throughput whole-animal sorting and screening at subcellular resolution. Proc Natl Acad Sci U S A 104(35):13891–13895
146. Chokshi TV, Ben-Yakar A, Chronis N (2009) CO_2 and compressive immobilization of *C. elegans* on-chip. Lab Chip 9:6
147. Kim YT et al (2009) Neuro-optical microfluidic platform to study injury and regeneration of single axons. Lab Chip 9(17):2576–2581
148. Hosmane S et al (2012) Toll/interleukin-1 receptor domain-containing adapter inducing interferon-beta mediates microglial phagocytosis of degenerating axons. J Neurosci 32 (22):7745–7757
149. Cooper DR, Nadeau JL (2009) Nanotechnology for in vitro neuroscience. Nanoscale 1 (2):183–200
150. Hosmane S et al (2010) Circular compartmentalized microfluidic platform: study of axon-glia interactions. Lab Chip 10(6):741–747
151. Liu W et al (2013) A micropatterned coculture system for axon guidance reveals that slit promotes axon fasciculation and regulates the expression of L1CAM. Integr Biol (Camb) 5 (3):617–623
152. Peyrin JM et al (2011) Axon diodes for the reconstruction of oriented neuronal networks in microfluidic chambers. Lab Chip 11(21):3663–3673
153. Wang J et al (2009) Microfluidics: a new cosset for neurobiology. Lab Chip 9(5):644–652
154. Young EW, Berthier E, Beebe DJ (2013) Assessment of enhanced autofluorescence and impact on cell microscopy for microfabricated thermoplastic devices. Anal Chem 85(1): 44–49
155. Chung BG et al (2012) Microfluidic fabrication of microengineered hydrogels and their application in tissue engineering. Lab Chip 12(1):45–59
156. McDonald JC et al (2000) Fabrication of microfluidic systems in poly(dimethylsiloxane). Electrophoresis 21(1):27–40
157. Mondal S, Ahlawat S, Koushika SP (2012) Simple microfluidic devices for in vivo imaging of *C. elegans*, *Drosophila* and *zebrafish*. J Vis Exp 67:e3780–e3780
158. Neumann S et al (2014) Characterizing the composition of molecular motors on moving axonal cargo using "cargo mapping" analysis. J Vis Exp 92:e52029
159. Takeuchi A et al (2012) Sympathetic neurons modulate the beat rate of pluripotent cell-derived cardiomyocytes in vitro. Integr Biol (Camb) 4(12):1532–1539
160. Fujimoto K et al (2015) Dynamic formation of a microchannel array enabling kinesin-driven microtubule transport between separate compartments on a chip. Lab Chip 15(9):2055–2063
161. Gracz AD et al (2015) A high-throughput platform for stem cell niche co-cultures and downstream gene expression analysis. Nat Cell Biol 17(3):340–349
162. Niedringhaus M et al (2015) Transferable neuronal mini-cultures to accelerate screening in primary and induced pluripotent stem cell-derived neurons. Sci Rep 5:8353
163. Lovatt D et al (2014) Transcriptome in vivo analysis (TIVA) of spatially defined single cells in live tissue. Nat Methods 11(2):190–196
164. Sims PA, Xie XS (2009) Probing dynein and kinesin stepping with mechanical manipulation in a living cell. ChemPhysChem 10(9–10):1511–1516
165. Spudich JA et al (2011) Optical traps to study properties of molecular motors. Cold Spring Harb Protoc 2011(11):1305–1318

166. Brunnbauer M et al (2010) Regulation of a heterodimeric kinesin-2 through an unprocessive motor domain that is turned processive by its partner. Proc Natl Acad Sci U S A 107 (23):10460–10465
167. Derr ND et al (2012) Tug-of-war in motor protein ensembles revealed with a programmable DNA origami scaffold. Science 338(6107):662–665
168. Lin C et al (2012) Submicrometre geometrically encoded fluorescent barcodes self-assembled from DNA. Nat Chem 4(10):832–839
169. Norris SR et al (2014) A method for multiprotein assembly in cells reveals independent action of kinesins in complex. J Cell Biol 207(3):393–406
170. Dinsmore JH, Solomon F (1991) Inhibition of MAP2 expression affects both morphological and cell division phenotypes of neuronal differentiation. Cell 64(4):817–826
171. Inberg A et al (2007) Cellular processes underlying maturation of P19 neurons: changes in protein folding regimen and cytoskeleton organization. Proteomics 7(6):910–920
172. McBurney MW (1993) P19 embryonal carcinoma cells. Int J Dev Biol 37(1):135–140
173. Schwob AE, Nguyen LJ, Meiri KF (2008) Immortalization of neural precursors when telomerase is overexpressed in embryonal carcinomas and stem cells. Mol Biol Cell 19 (4):1548–1560
174. Huang HS et al (2012) Ascl1-induced neuronal differentiation of P19 cells requires expression of a specific inhibitor protein of cyclic AMP-dependent protein kinase. J Neurochem 120(5):667–683
175. Arens J, Duong TT, Dehmelt L (2013) A morphometric screen identifies specific roles for microtubule-regulating genes in neuronal development of P19 stem cells. PLoS ONE 8(11): e79796
176. Yuahasi KK et al (2012) Regulation of neurogenesis and gliogenesis of retinoic acid-induced P19 embryonal carcinoma cells by P2X2 and P2X7 receptors studied by RNA interference. Int J Dev Neurosci 30(2):91–97
177. McBurney MW et al (2002) Evidence for repeat-induced gene silencing in cultured mammalian cells: inactivation of tandem repeats of transfected genes. Exp Cell Res 274 (1):1–8
178. Subramanian V, Crabtree B, Acharya KR (2008) Human angiogenin is a neuroprotective factor and amyotrophic lateral sclerosis associated angiogenin variants affect neurite extension/pathfinding and survival of motor neurons. Hum Mol Genet 17(1):130–149
179. Aronov S et al (2002) Visualization of translated tau protein in the axons of neuronal P19 cells and characterization of tau RNP granules. J Cell Sci 115(Pt 19):3817–3827
180. Sahay G, Alakhova DY, Kabanov AV (2010) Endocytosis of nanomedicines. J Control Release 145(3):182–195
181. Potter H (2003) Transfection by electroporation. Curr Protoc Mol Biol. Chap. 9, p. Unit 9 3
182. Chen SC et al (2012) Delivery of molecules into cells using localized single cell electroporation on ITO micro-electrode based transparent chip. Biomed Microdevices 14 (5):811–817
183. Santra TS et al (2014) Nanolocalized single cell membrane nanoelectroporation. IEEE Nanotechnol 8(1):285–288
184. Brewer GJ, Cotman CW (1989) Survival and growth of hippocampal neurons in defined medium at low density: advantages of a sandwich culture technique or low oxygen. Brain Res 494(1):65–74
185. Jiang M, Chen G (2006) High Ca2+-phosphate transfection efficiency in low-density neuronal cultures. Nat Protoc 1(2):695–700